University of Nottingham
School of Civil Engineering

ON USING VIBRATION DATA TO DETECT DAMAGE IN MODEL-SCALE REINFORCED CONCRETE BRIDGES

STEVEN R. PEARSON, MEng (Hons)

Thesis submitted to The University of Nottingham
for the degree of Doctor of Philosophy, March 2003

LIST OF CONTENTS

LIST OF FIGURES

LIST OF TABLES

LIST OF PLATES

ABSTRACT

This thesis reports the findings of an investigation into the feasibility of using vibration characteristics to monitor the structural health of bridges. The study is the second part of a larger project commissioned by the UK Highways Agency into the investigation of possible monitoring methods that can be used in a pass/fail/monitor inspection programme. To this end, ten one-quarter-scale 5m span reinforced concrete bridge decks were fabricated and loaded incrementally to failure in the laboratory. The dynamic properties of the decks were investigated at each of the loading increments to evaluate their sensitivity to structural cracking using both free and forced vibration.

The results indicated that, for the specimens tested, natural frequencies were, in general, more sensitive to the damage introduced than mode shapes. It was found that the support conditions affected the dynamic behaviour of the decks, and indeterminate boundary conditions caused significant variation in the vibration characteristics. This presented several problems in the analysis of the modal properties and, when combined with the damage introduced through static loading, caused some modes to disappear and new modes to be measured, whilst a number of modes also displayed an increase in natural frequency.

The application of finite element model updating to determine reduction in flexural stiffness in the damaged areas of the deck provided a systematic method to investigate the condition of the deck. Updating was performed based on the natural frequencies of one symmetrically and one asymmetrically loaded deck, and the cracking observed under the loading, and offered results consistent with expectations.

In summary, the evidence presented in this thesis suggests that the natural frequencies of the decks are, in general, more sensitive to the damage introduced than the mode shapes and consistent trends can be observed in the natural frequency change as the damage to the deck increases. However, the application of this method to indicate the structural condition of real bridges

may be limited without further investigation as the vibration characteristics were affected by a number of factors arising from the realistic nature of the specimen, such as the three-dimensional distribution of the damage and the indeterminate nature of the support conditions.

NOMENCLATURE

a_{na}, b_{nb}, c_{nc} = coefficients of ARMAX model

A = state transition matrix

A_r = residue

$_rA_{jk}$ = residue or modal constant

B= input matrix

$C(\omega)$ = Fourier transform

C_n = coefficients of Fourier transform

COMAC(i) = co-ordinate modal assurance criterion

D = damping matrix

E = undamaged Young's modulus of concrete

E_b = Young's modulus of concrete displaying self-weight cracking

E_s = Young's modulus of slab

E_{50} = Young's modulus of concrete cracked at 50kN

E_{100} = Young's modulus of concrete cracked at 100kN

E_{150} = Young's modulus of concrete cracked at 150kN

E_{200} = Young's modulus of concrete cracked at 200kN

E_{250} = Young's modulus of concrete cracked at 250kN

E_{250a} = Young's modulus of concrete cracked at 250kN

E_{250b} = Young's modulus of concrete cracked at 250kN

E_{300} = Young's modulus of concrete cracked at 300kN

E_{300a} = Young's modulus of concrete cracked at 300kN

E_{300b} = Young's modulus of concrete cracked at 300kN

E_{300c} = Young's modulus of concrete cracked at 300kN

E_{300d} = Young's modulus of concrete cracked at 300kN

f = frequency, Hz

$f_\delta(t)$ = impulse matrix

f_s = sampling frequency, Hz

f_N = Nyquist frequency, Hz

$F(t)$ = function expressed as a Fourier series

$F_q(\omega)$ = Fourier transform of input force time history

G_x = one-sided auto spectral density function of x

$h(\tau)$ = impulse function

$h(t)$ = impulse response

$\dot{h}(t)$ = velocity

$\ddot{h}(t)$ = acceleration

$H(s)$ = Transfer function

$H(f)$ = Frequency Response function, FRF

$H_1(f)$, $H_2(f)$ = estimators of $H(f)$

$H[y(t)]$ = Hilbert transform of y

$H(\omega)$ = Frequency Response function, FRF

$H_{pq}(\omega)$ = Frequency Response function between points p and q

IRF = Impulse Response Function

k = stiffness

k_B = vertical spring stiffness

k_T = torsion spring stiffness

K = stiffness matrix

m = mass

M = mass matrix

MAC(p,x) = modal assurance criterion

R_x, R_y = auto correlation of data record x or y

R_{xy} = cross correlation between data records x and y

S_x, S_y = two-sided auto spectral density function of x or y

S_{xy} = two-sided cross spectral density function between x and y

t = time

t_1 = initial time

T = time

τ = time

$u(t)$ = input variable matrix

$x_k(t)$, $y_k(t)$ = time history record for sample k

$X_p(\omega)$ = Fourier transform of response time history

$\alpha_{jk}(\omega)$ = receptance Frequency Response function

γ^2_{xy} = coherence function between x and y

μ_x = mean value of x

ω = angular frequency, rad/s

ω_n = angular natural frequency, rad/s

ω_r = damped natural frequency, rad/s

ϕ_x, ϕ_p = mode shape vectors

η_r = structural damping

ζ_r = damping ratio

ACKNOWLEDGEMENTS

The help and guidance of the following, without whom this thesis would not have been produced, is gratefully acknowledged.

The author would like to thank Dr. John Owen of the University of Nottingham for the considerable time, assistance and knowledge provided during the period of the research project. Appreciation is also expressed to Prof. B.S. Choo of Napier University for offering important advice on the testing.

The support, assistance, expertise and motivation provided by Mr. David Allinson during the testing of the decks and processing of the considerable quantity of data is greatly appreciated.

Many thanks are given to the School of Civil Engineering laboratory technical staff; Geoff Mitchell, Brian Whitehouse, Nigel Rook, Melvyn Ridal and Bal Loyla for their assistance in all matters concerning the testing.

A special mention to Dr. Chuan Ming Tan, Dr. Toby Barnett, Dr. Daniel Ridley-Ellis and Mr. Zhongsheng Wang is also made for providing valuable encouragement during the project.

The author would also like to thank the UK Highways Agency and the EPSRC for the financial support provided for the research.

DECLARATION

I declare that, except where cited in the text, all work contained within the thesis is my own original work, under direction of my supervisors and the UK Highways Agency. The work presented herein was performed at the University of Nottingham between September 1999 and March 2003.

This thesis has not been submitted to any institution other than the University of Nottingham for the degree of Doctor of Philosophy.

CHAPTER 1

INTRODUCTION

1.1 Background

Much of the present stock of bridges in the UK was built between the early 1960s and the late 1980s, with peak construction occurring in the 1970s. Many of these bridges were constructed from reinforced and prestressed concrete, which was thought to be durable and require little maintenance (Woodward, 2000). However, a considerable amount of deterioration in the bridge stock was found during the 1980s in a study conducted by G Maunsell and Partners (1989). It is therefore apparent that it is necessary for the bridge stock be inspected at regular intervals to maintain its serviceability.

The main objectives of the inspection procedure are to ensure safety, whilst giving value for money in terms of the service provided and financial cost to the tax-payer, minimising the disruption to the road users and allowing a sustainable bridge stock (Johnstone, 2000). The inspection process is also used as a tool for prioritising the maintenance work required by several bridges. Ensuring safety of the general public consists of identifying those bridges that have an unacceptable probability of failure.

In the UK, the existing inspection procedure stipulated by the UK Highways Agency for trunk road and motorway bridges is given in BD 63/94 and the associated advice note. These documents state that there are four types of inspection that can be carried out, superficial (conducted whilst in the area), general (performed every 2 yrs), principal (every 6-10 yrs) and special (specific problem). During principal inspections, it is advised that limited testing should be carried out.

The major sources of deterioration in reinforced concrete bridges arise from four main areas:

- Cracking, where the size, pattern and stability of the cracks are an indicator of deterioration of the structure, as cracking can occur due to a number of different sources, such as alkali-silica reaction, settlement and overloading
- Corrosion of reinforcement identified by rust staining, spalling and exposed bars
- Delamination of the concrete from the steel reinforcement
- Failure of the bearings and expansion joints in the form of leakage causes corrosion of the joints, aggravated by increases in the loading and assumptions made about the density of loading occurring during traffic jams

Currently, the inspection procedure involves an engineer visiting the bridge and assessing it to a certain standard. This procedure is based on a pass or fail method, relying on the engineer to decide whether the bridge is safe or needs remedial action to be taken. This remedial work ranges from the introduction of maximum vehicle weight restrictions to strengthening or complete replacement of the bridge in the most severe cases.

1.1.1 Condition assessment

Currently, there are several testing techniques that are used for local testing, such as determining the cover to reinforcement, crack measurement and rebound hammer testing. These methods are suitable for a detailed investigation of areas that show some deterioration that needs to be further investigated. It is often the case that these types of testing are implemented on the recommendations from a principal inspection that has highlighted areas of concern. In general, these methods used for localised testing are utilised to investigate a particular problem, such as rebound hammer testing to study delamination, or material sampling to determine material properties.

However, for a bridge that has failed a traditional assessment, it may be the case that this testing needs to be applied over a large area and at frequent intervals. To use the methods mentioned above would be both time consuming and costly. Therefore, a technique that can perform continuous or semi-continuous monitoring of the whole structure is necessary.

1.1.2 The need for change

Due to the subjective nature of the inspection program, it will be the case that some remedial action is undertaken when it is not necessary, or that repair work is not carried out when it should be. This uncertainty in the actual condition of the bridge stock is further exacerbated by the maintaining agent for the bridge changing between inspections, leading to inconsistent reporting (Aktan et al, 1997).

The need for a more reliable determination of a bridge's condition has arisen from several sources. Firstly, there is an increased need for spending on bridge maintenance to be carried out more efficiently. Secondly, in recent years there has been a move towards a Design, Build, Finance, Operate (DBFO) type of procurement, meaning that the condition of the structure needs to be known when it is handed back to the Government. Thirdly, an increase in the axle weight of heavy goods vehicles allowed on UK roads has led to an extensive bridge rehabilitation programme.

The uncertainties that arise from the current inspection procedure are particularly important when the bridge inspected does not pass the assessment. Therefore, the UK Highways Agency is currently investigating the possibility of monitoring a bridge that fails a traditional assessment by a small margin and does not show any significant deterioration to obtain a more accurate evaluation of its condition and deterioration rate. This would allow a more efficient schedule of remedial action to be produced.

1.1.3 The role of dynamic testing

The use of dynamic techniques for testing systems in both mechanical and aeronautical engineering has been widely applied, and techniques for condition monitoring and damage detection are being investigated in several fields, such

as mechanical engineering (Ziebath, H and Baumgartner, 1981, James et al, 1994), aircraft testing (Shelley et al, 1993), aerospace applications (James III et al, 1998) and the offshore industry (Vandiver, 1975, Hamamoto and Kondo, 1993, Ruotolo et al, 2000). Corresponding research in the civil engineering field has been performed in the last twenty-five years, where there has been an increasing interest in using dynamic testing for the health monitoring of bridges.

These methods are based on determining the system's vibration response and relating it to a change in the structural system, often using the fact that the modal properties (modal frequency, mode shape and modal damping) are related to the stiffness of the system. Therefore, a change in the stiffness of the structure, which could arise due to deterioration, will cause a change in the modal properties.

The potential for dynamic testing has been recognised in an ISO standard, ISO/CD standard 14963 *Mechanical vibration and shock: Guidelines for dynamic tests and investigations on bridges and viaducts.* This document states that dynamic testing can be used as part of design or maintenance/rehabilitation management. It suggests that dynamic testing can be undertaken to:

- Evaluate safety of bridge structures during construction;
- Confirm after construction the values used in design;
- Evaluate dynamic characteristics for wind/earthquake analysis and live loading;
- Monitor real bridges in service and detect damage;
- Confirm reinforcement effects in bridges;
- Perform diagnosis in emergency;
- Carry out diagnostic testing as basis for condition monitoring.

Performing testing using dynamic measurements offers the opportunity to obtain information about the whole structure based on a small number of measurements, as the vibration behaviour is influenced by the whole system.

This is of particular benefit when considering structural health monitoring as the test measurements do not need to be made locally around the area of deterioration.

However, as opposed to the systems tested in mechanical and aerospace engineering, civil engineering structures are generally constructed as "one off" projects and therefore each structure is unique. There also exists the problem of construction tolerances, which are not apparent in other disciplines where dynamic testing is used, giving even more variation in the systems to be monitored.

It is also apparent that there are significant differences in the operating conditions of the structure to be tested arising from the fact that civil engineering structures cannot be isolated from external effects as effectively as mechanical or aerospace systems. The environment in which the bridge is tested can have a considerable influence on its dynamic behaviour, and changes in temperature are known to cause shifts in natural frequencies.

Therefore, in order to use dynamic testing in civil engineering applications, the sensitivity of the monitored parameters to changes in the structural system needs to be guaranteed. It is important to demonstrate that changes in the dynamic properties can be distinguished between those due to deterioration and environmental effects.

1.2 Research outline

1.2.1 Aim and objectives

The aim of this study is to investigate the feasibility of using dynamic testing for the structural health monitoring of bridges. In order to achieve this, the following objectives are required:

- Develop the previous work by extending it to more realistic specimens ?
- Evaluate the reliability of using modal methods for a complex specimen
- Compare the dynamic behaviour of the bridge deck undergoing increasing damage with finite element modelling

- Determine the behaviour of the bridge deck under two different static loading regimes and its effect on the vibration characteristics

This study is the second phase of a larger project investigating the use of dynamic testing for structural health monitoring of bridges. The previous work applied dynamic testing methods to reinforced concrete beams to investigate the feasibility of using vibration characteristics for structural health monitoring of bridges (Eccles, 1999). The study produced two key findings: the first four natural frequencies displayed a repeatable reduction with increasing damage and the beam exhibited non-linear behaviour during the vibration cycle.

The natural frequencies of the beams displayed repeatable trends as the cracking became more severe, and it was noted that the mode shapes were less sensitive to damage than the natural frequencies. A plateau region in the natural frequency change was also observed during the middle stages of loading. The non-linear behaviour was shown to be related to the amplitude of vibration, and produced a softening spring system.

1.2.2 Methodology

In order to achieve the objectives mentioned above, a series of dynamic tests is performed on a total of ten one-quarter-scale simply supported reinforced concrete beam-and-slab bridges. The scale bridge deck testing is conducted in laboratory conditions under differing damage levels caused by overloading and the results from this testing are analysed by considering both the static and dynamic behaviour.

The static behaviour of the bridge deck under two loading regimes is recorded by measuring the deflection at mid-span and plotting the cracking pattern due to incremental loading. The behaviour of the decks in terms of the static response is studied, and provides the means of a better understanding of changes in the vibration characteristics to be obtained. The results of the static loading are also compared with the ultimate load as determined by yield-line analysis.

The results from the measurements of the vibration behaviour are used to determine the modal properties of the decks and investigate the change in

natural frequencies and mode shapes as the damage to the deck increases. These dynamic properties are also used to provide the basis of a comparison with a finite element model of the decks by using the dynamic behaviour under two loading regimes to update the flexural stiffness of a model by simulating the damage to the real specimen in the form of reducing the stiffness of cracked areas.

1.3 Structure of thesis

The thesis began with a brief introduction to the current UK Highways Agency bridge inspection procedure together with a discussion of the major factors effecting a change to a pass/fail/monitor methodology. A brief summary of the potential for using dynamic testing as a monitoring method was presented.

The next chapter provides a review of the available literature in the field of dynamic testing, with particular references to structural health monitoring/damage detection and civil engineering structures in the form of bridges.

Chapter three discusses the results of the static loading of the one-quarter-scale bridge decks under three different loading arrangements. An examination of the load-deflection behaviour together with a detailed discussion of the cracking patterns produced under loading is presented. The behaviour is also compared to a yield-line analysis.

The next chapter describes the dynamic testing of the bridge decks in the laboratory. This chapter contains a discussion of the modal properties obtained and how they relate to the condition of the specimen, and investigates the sensitivity of natural frequencies and mode shapes to the damage introduced under the static loading regimes.

In the penultimate chapter, the application of finite element modelling and updating of the decks is studied. The updating of a finite element model is carried out for two of the loading regimes based on the natural frequencies of the modes found in the previous chapter to determine the stiffness change in the damaged areas of the decks.

The final chapter summarises the main findings of this investigation and provides a discussion on the shortcomings of this work and possible areas where further study is necessary.

CHAPTER 2

LITERATURE REVIEW

2.1 Introduction

This chapter presents a state of the art review of the literature concerning the use of dynamic testing as a structural health-monitoring tool for reinforced concrete bridges. A survey of selected studies into the use of vibration characteristics for condition assessment and damage detection are presented for civil engineering applications, although results from suitable studies in other disciplines are also highlighted. The conclusions of this chapter serve to indicate the current state of condition assessment in civil engineering structures and form the basis of this investigation into structural health monitoring for reinforced concrete bridges.

2.2 Background

The desire to detect damage at the earliest possible stage through monitoring is present in civil, mechanical and aerospace engineering fields. Currently, in the civil engineering field, most damage detection methods are either visual or based on localised testing, such as acoustic or ultrasonic methods or material sampling, and it is generally a prerequisite that the location of the damage is known before testing and that this location is accessible. Due to these limitations, it is only possible to identify damage that is either on or near the surface of the structure. This has given rise to a need for more global methods to be developed that can be applied to complex structures and has lead to the growth of techniques based on vibration characteristics.

The use of changes in the vibration characteristics to detect damage in the mechanical and aerospace fields has received considerable interest in the past

30 years, and attempts have been made to apply these techniques to civil engineering structures for the past 20 years. Therefore, a considerable amount of literature has been produced in this area. In this chapter, the review principally considers the application of these techniques to civil engineering structures, paying particular attention to bridges and reinforced concrete.

The fundamental idea behind the use of changes in dynamic properties to detect damage is that modal parameters, namely natural frequencies, mode shapes and modal damping, are functions of the physical properties of the structure, i.e. mass, stiffness, damping and boundary conditions. Therefore, changes in the physical properties will lead to changes in the modal properties.

It can be shown from the application of Newton's Second Law that the natural frequency of a system is a function of its stiffness and mass in the following form;

$$\omega = \sqrt{\frac{k}{m}} \qquad \text{Equation 2-1}$$

When damage occurs to a structure, it is often in the form of a reducing stiffness without a change in mass and it is therefore reasonable to assume that a change in the natural frequencies will also result, thus monitoring the natural frequency of a structure can give an indication of its stiffness.

This allows a change in the condition of the structure to be measured, and, in terms of structural health monitoring, any significant change can be used to launch a more detailed investigation.

2.2.1 Condition monitoring and damage detection

The problem of determining the condition of structures was investigated by Rytter (1993), who introduced the following classification system based on the amount of information provided about the structure:

Level 1: Identify that damage has occurred;

Level 2: Identify that damage has occurred and determine the location of the damage;

Level 3: Identify that damage has occurred, locate the damage, and estimate its severity; and

Level 4: Identify that damage has occurred, locate the damage, estimate its severity, and determine the remaining useful life of the structure.

This classification system leads to the development of ideas of condition or structural health monitoring and damage detection using dynamic testing. Condition monitoring is a term used when the objective of using changes in vibration characteristics is to satisfy level 1 of the classification by determining whether there is a change in the physical properties of the structure. Damage detection encompasses both levels 2 and 3, although most commonly only satisfies level 2 in a process known as damage identification. Level 4 is generally fulfilled by the use of fracture mechanics, fatigue life analysis or structural design assessment. In the remainder of this literature survey, only methods concerned with levels 1, 2 and 3 will be discussed as level 4 is outside the scope of this study.

2.3 Modal properties

2.3.1 Natural frequency

By far the most popular modal property used to detect damage is the natural frequencies of the structure. This is for several reasons, namely that they can be measured relatively quickly using a limited number of sensors (in fact only one is needed to measure the response of the structure) and to a high accuracy. There is also the fact that, as stated in equation 2-1, they are a function of the stiffness of the structure, which is the physical property that is most likely to change as a result of damage.

One of the first papers to propose this idea was by Cawley and Adams (1979), who gave a formulation to detect damage in composite materials from frequency shifts, forming the basis of using modal analysis for damage identification. From experimental results, the ratios between the frequency of

different modes for the undamaged and damaged cases were computed. An error term was developed to relate the actual frequency changes to those predicted by a model. The model was used to form a grid of possible damage points, modelled by a local stiffness reduction, and all possible damage mechanisms were investigated. Damage was assumed to occur at the location for which the model gave the lowest error term when compared with the experimental results. This method, however, does not allow for multiple damage sites and also requires all the possible damage mechanisms to be modelled in order to find the best entailing a considerable amount of processing time (Salawu, 1997a).

The method suggested by Cawley and Adams has seen a considerable amount of development, although the problem of determining which parameters are most sensitive to damage remains.

One of the first attempts to apply dynamic testing to damage detection in civil engineering structures was performed by Creed (1987) who conducted an investigation on a motorway bridge. It was suggested that there would need to be a 5% reduction in natural frequencies to determine damage, due to changes arising from environmental effects. It was also found that mode shapes were not reliable enough to be used with confidence, and should only be used to determine which natural frequency is associated with which mode.

Later, Wood et al (1991) investigated the changes in natural frequencies due to cutting reinforcing tendons in concrete beams, where no significant change was found confirming the observations made by Creed (1987), although it was stated that the damage did not appear to be major.

In an attempt to overcome the problems of insensitivity, Uzgider et al (1993) selected vibration modes previously determined to be sensitive to damage and used these to estimate flexural stiffness parameters. The presence of structural damage was indicated by the relative magnitudes of differences between the identified parameters and prior estimates. However, the success of this method is dependent on an accurate prior model and the identification of suitable stiffness parameters.

More work was conducted on investigating the sensitivity of natural frequencies by investigating the influence of cracking patterns (Casas and Aparicio, 1994). A verification of the dynamic parameters obtained was made using static tests and theoretical deflections. It was suggested that at least two natural frequencies are needed for damage detection, but it was not possible to relate changes to a unique damage pattern as the results are significantly affected by the bearing conditions.

A statistical approach was proposed by Brincker et al (1995) in which the natural frequencies observed were scaled according to an estimated standard deviation. The authors defined a "unified significance indicator" by summing the frequency and damping significance indicator over several modes, where it was found that the existence of damage was identified. However, the method was not able to provide information regarding the location of the damage.

Williams et al (1997) defined a new assurance criterion similar to the MAC, termed the "Damage Location Assurance Criterion" using frequency changes in a number of modes. The criterion was tested on the results of a finite element model and experimental trial, in which a 10% reduction in flexural stiffness was detected and located from data including a 0.15% error. The value of 0.15% was obtained from experimental testing of a free-free plate, although the validity of this value for civil engineering structures is questionable.

A study performed by Eccles (1999) on reinforced concrete beams revealed a tri-linear relationship between the change in natural frequency and increasing damage. It was found that an initial drop of about 12% in the natural frequencies occurred as the beams were loaded to 15% of their failure load, but remained relatively constant, reducing by 2.5% as the load increased to 80%, followed by a sharp reduction again at failure, as shown in Figure 2-1. This highlights the problems associated with the sensitivity of natural frequencies to certain types of damage. This tri-linear relationship has also been observed by Rohrmann et al (2001).

An investigation into the use of natural frequencies for damage detection in precast concrete slabs reinforced using glass fibre composite bars was

performed by Ebert et al (1999). However, the investigation into the dynamic properties of the structures was secondary to the study of the static behaviour so vibration measurements were made with the loading frame in place. It was observed that the trend of a selected three natural frequencies all reduced by between 10 and 25%, see Figure 2-2, and suggested that the natural frequencies were not only influenced by the severity, but also by the location of concentrated damage confirming the previous findings by Salawu and Williams (1995).

It was suggested by Chen et al (1999) that the application of a preload when performing dynamic tests is actually beneficial in terms of the effort required and the quality of the test data, due to the fact that cracks are kept open. It was put forward that the natural frequencies measured with and without preload could be related regardless of the level of damage.

An extension of the idea presented by Cawley and Adams (1979) was proposed by Wang et al (2001) by considering the results from both natural frequency changes and static testing. The method employed a "Damage Signature Matching" technique to compare a model simulating all damage cases with the measured results after which the severity of damage was estimated by comparing the displacements obtained from the model and experimentally, and solving for the damage extent using quadratic programming. Successful results were obtained when the method was applied to a model with a single damage location in both determining the position and severity of damage, but could not identify the locations of multiple damages. When applied to experimental data, the method successfully found the damage location, but produced a 100% error when estimating the damage extent, even though the actual damage resulted in an 87.5% reduction in Young's modulus.

The effect of corrosion of reinforced concrete beams on the modal properties was investigated by Razak and Choi (2001) in which the change in natural frequency was found to be correlated to the load carrying capacity of the beams. The potential of using damping measurements was also studied, the authors drawing the conclusion that, for specific modes, damping is related to the severity of the corrosion damage.

The regions of antiresonance were studied by Wahl et al (1999) for a number of different systems. It was suggested that from measurements taken from an arbitrarily supported structure, it is possible to determine the resonant frequencies of a structures under ideal boundary conditions. The authors also claimed that the relationship between the resonance and antiresonance frequencies could be used in the location of structural faults.

2.3.2 Mode shapes

The use of natural frequencies for the localisation of damage remains limited, however. It is thought by many researchers that it is possible to overcome these problems by using information obtained from the mode shapes of the structure, due to the fact that mode shapes are more sensitive to local damage than natural frequencies.

There are, however, some drawbacks to the use of mode shapes. Firstly, the damage may not be localised, and therefore it will not significantly affect the lower modes usually measured for civil engineering. It is also the case that the mode shapes are affected by environmental changes, such as ambient effects or inconsistent sensor positions. Another consideration is that the number of sensors and their locations will have a significant effect on the success of the damage detection process.

The effect of repairing a full-scale bridge was investigated by Salawu and Williams (1995) using natural frequencies, damping and mode shapes. Due to the localised nature of the repair, a difference was observed in the mode shapes compared using the MAC and COMAC algorithms, although they warned that the selection of mode used in the analysis was critical. They suggested that natural frequencies could only be used when significant damage has occurred. These findings had previously been observed by Salane and Baldwin (1990) in tests on a laboratory-scale model bridge.

These findings concerning the sensitivity of mode shapes to damage were supported by Das et al (1997) who concluded that mode shape measurements made on reinforced concrete beams were only useful when damage was highly localised. It was suggested this was due to the fact that when damage was more uniform, the mode shapes were similar to those from an undamaged

structure. Raghavendrachar and Aktan (1992) stated that only higher modes are suitable for indicating local damage, but also asserted that these are difficult to measure for large structures, such as bridges. It is the case that a large number of measurements are required to obtain mode shapes with confidence (Modena et al, 1999).

2.3.2.1 Mode shape-based methods

The use of mode shapes has been developed in several studies to take advantage of the spatial information obtained that is of great benefit when attempting to locate damage and to improve the sensitivity by selecting measurements other than displacement. Many damage indicators have been developed from mode shape data, such as curvature mode shapes and strain energy, and often found to be more sensitive than natural frequencies or the mode shapes themselves.

The use of curvature mode shapes was suggested by Pandey et al (1991) to be a superior method to obtain information regarding the location of damage, as modal stiffness has a direct relationship to the integral of modal curvature. It is also the case that curvature is directly related to bending moment, and is therefore sensitive to changes in flexural stiffness and any small changes in mode shape caused by damage would be more obvious when considering curvature. This method proved to be more a more sensitive damage indicator than the MAC or COMAC.

It was found by Petro et al (1997) that both natural frequencies and mode shapes did not display the necessary degree of change to detect a transverse cut half the width of an aluminium beam. However, they then demonstrated that the strain energy displayed a significant change in the vicinity of the damage and further developed a "strain energy damage index". This is due to the fact that strain energy is related to curvature, which is sensitive to changes in flexural stiffness.

Ndambi et al (2002) investigated a number of indicators based on the dynamic characteristics to assess the effect of progressive symmetric and asymmetric damage in reinforced concrete beams. They concluded that natural frequencies could detect the presence of damage and degree of damage, reducing by 15-

20% at failure, but they are not influenced by the crack location. Comparisons were also made using the MAC, COMAC, strain energy method and the flexibility method. MAC values varied by less than 3% in general and could not be related to damage location, which was explained by the effect of measurement errors on the mode shape magnitude. The use of the COMAC also proved to be difficult to detect damage in the correct location. A measure of strain energy proved more successful in locating local damage, although problems were found when the damage was distributed and in estimating the severity of damage. Identification of damage occurring was possible using changes in the flexibility matrix, but again locating the damage proved infeasible.

The use of strain energy was also studied by Kim, J-T. et al (2003), who developed both a methodology based on natural frequencies and one based on mode shapes to locate and estimate the severity of damage using only two modes. The methods were verified using data obtained from a finite element model. The damage was located by examining changes in the natural frequency and the crack size found using an algorithm based on natural frequency perturbation. When using the mode shapes, the damage location and size were found by monitoring modal strain energy. The methods, however, were verified for only one crack location. No indications of the performance of the algorithms when multiple damage locations, which is often problematic in damage location exercises, were given. It was also noted that when using the natural frequency based algorithms for locating damage not at the mid-span two locations were identified, one being a false-positive result.

2.3.3 Damping

Attempts to use measures of damping ratio as damage indicators have, in general, proved unsuccessful. No acceptable trend was found in the work carried out by Salane et al (1981), a finding subsequently supported by Salane and Baldwin (1990). Casas and Aparicio (1994) and Salawu and Williams (1995) also found that damping did not change monotonically with damage when conducting tests on reinforced concrete beams and a bridge, respectively.

In a review conducted by Williams and Salawu (1997), it was pointed out that damping is significantly influenced by the amplitude of vibration and also possesses the greatest degree of uncertainty compared to other modal parameters.

The use of damping for damage location was investigated by Modena et al (1999) with some success. Several methods were investigated based on modelling the damage as a local reduction in stiffness. Methods employing frequency change were not able to locate the damage effectively, but more success was found using modal curvature. However, the authors found that the most sensitive parameter was damping, and particular success was achieved when using modal friction damping.

2.4 Frequency domain methods

Several disadvantages exist when using modal properties as an indicator of damage. Modal data can be contaminated by measurement errors as well as modal extraction errors because they are indirectly measured test data. Completeness of modal data often cannot be met due to large number of sensors required. Using FRFs may offer advantages because they should contain fewer errors, such as those introduced by the curve fitting routine, as they are directly measured from the test and can provide a lot more information on damage in a desired frequency range than modes as these are extracted from only the data around resonance.

Law et al (1992) used the frequency response function and phase angle to identify the location and extent of damage in a one-fifth-scale reinforced concrete beam-slab bridge incrementally loaded to failure. The sensitivity of the FRF and phase to changes in the mass, stiffness and damping of a system were developed, which were solved using a recursive linear least square method.

The bridge was modelled using the grillage method and the diaphragm at mid-span was analysed by dividing it into four elements, each representing the stiffness between the longitudinal beams. It was found that when using the FRF magnitude the stiffnesses converged to stable values, until the reinforcement yielded and the results diverged, although at some load levels

the stiffness appeared to rise. No explanation for this was offered. The use of phase was not successful, which was attributed to errors arising from only performing 22 averages.

Samman and Biswas (1994a, 1994b) proposed a number of waveform recognition techniques based on the FRF measured for a laboratory-scale and a full-scale bridge. It was concluded that more than one technique should be used to detect small changes. Damage location was possible for the laboratory specimen, but this was not replicated for the full-scale bridge.

Schulz et al (1997) developed a method of detecting and locating damage based on the transmittance functions measured for a small composite beam. This method requires that the input has the same relative force level and the sensor locations are the same for each test, and the transmittance functions displaying the greatest change from the undamaged case are used to locate the damage. It was stated that small changes to a structure can be detected by using higher frequencies, in this case 600-1200Hz, and regions of non-resonance or anti-resonance are most sensitive.

Wang et al (1997) describe a method to determine both the location and magnitude of damage using an established analytical model and frequency response functions measured before and after damage. An algorithm based on non-linear perturbation equations of frequency response function data, together with appropriate weighting was proposed. For numerical data, the method identified the damage correctly even in the presence of 5% measurement errors, however, when used for experimental data the method identified elements adjacent to the actual damage. This was attributed to inaccurate modelling and a poor representation of the damage by the "stiffness reduction factor".

The appearance of frequency splitting or dispersive phenomena was observed by Zonta and Modena (2001) during tests on prestressed concrete panels. The time history of a damaged element displayed a beat that was absent in the undamaged structure, and appeared as a splitting of the resonant frequency in the frequency domain, as shown in Figure 2-3. It was proposed analytically that this corresponded to a skew-symmetric damping operator for a single-

degree-of-freedom (SDOF) system. It was suggested that the appearance of frequency splitting could be used in damage detection.

The focus of an investigation by Lee and Shin (2002) was to determine the effect of damage-induced modal coupling by proposing a FRF damage identification method for beams, by introducing a damage distribution function.

2.5 Non-linear behaviour

The presence of non-linear behaviour in damaged structures has been observed in a number of studies arising due to several factors, such as boundary conditions, material properties, excitation level and type and loading conditions. It could therefore be argued that methods based on linear modal analysis should not be applied to these structures. However, the major problem in this area is that it still lacks uniqueness of approach (Tomlinson, 1994) and several methods are still being investigated and developed.

One of the simplest and quickest methods for detecting non-linear behaviour is by a visual inspection of the FRF for distortions. A plot of the FRF in the Nyquist plane highlights non-linear behaviour in the form of a deviation from circular or near circular locus in the vicinity of resonance, although this is not always true for all types of non-linear behaviour.

2.5.1 Hilbert transform

A simple mathematical method to quantify non-linear behaviour is available in the form of the Hilbert transform (HT). The HT of a real valued function is defined from $-\infty$ to $+\infty$ as,

$$H[y(t)] = \tilde{y}(t) = \frac{1}{\pi}\int_{-\infty}^{\infty}\frac{y(\tau)}{t-\tau}dt \qquad \text{Equation 2-2}$$

This can be considered as being $\tilde{y}(t)$ is the convolution integral of $y(t)$ with $\frac{1}{\pi t}$, i.e.

$$\tilde{y}(t) = y(t) * \left(\frac{1}{\pi t}\right) \qquad \text{Equation 2-3}$$

Applying the HT to the FRF of a linear system will give the same FRF shape. For a non-linear system, the HT of the FRF will be distorted. This distortion is due to non-linearities in the system and the type of non-linearity can be inferred from the shape of the distortion (Feldman, 1997). However, this is only a qualitative measure. This difference between the FRF and its HT can be used in a pattern recognition regime, and has been investigated using neural networks to identify known non-linear behaviour (Wardle et al, 1997).

The HT of the time history data does, however, allow a single value extraction of the envelope of the signal and the instantaneous natural frequency. These in turn permit the estimation of the instantaneous dynamic properties and the elastic and friction force characteristics. The original signal and its Hilbert transform gives the concept of the Analytical signal, Y(t), where the original signal is the real part and its HT is the imaginary (Feldman and Braun (1997)).

The instantaneous frequency obtained from the Hilbert transform is only valid for asymptotic signals i.e. slowly varying amplitudes compared to the phase variations. It is possible, however, to use the instantaneous amplitude and frequency to construct a backbone curve for the system to obtain a quantitative measure of the non-linear behaviour (Staszewski and Chance, 1997). Using the Hilbert transform method also requires filtering and differentiation procedures. The HT test for non-linearity is best applied to FRFs obtained from stepped sine tests, and appears to fail for random excitation FRFs as this type of excitation tends to linearise the behaviour of the system.

2.5.2 Wavelet transform

One of the more recently developed methods for analysis of non-stationary data is that of the wavelet transform (WT). Wavelet analysis allows the power content with frequency to be determined as a function of time, giving an advantage over Fourier analysis, which cannot be used to analyse time and

frequency together (Baker, 1999). Wavelets analysis is based on the use of short duration waves, termed wavelets. A particular property of a wavelet function is that its area under the curve must be zero and the curve must tend to zero at infinity. A family of wavelet functions is formed by dilation and translation of a single wavelet, known as the mother wavelet, using two parameters, scale a, and translation b (Ljung, 1999). These wavelet functions can then be used to form a series of curves to match with the time history. As with the Fourier transform, coefficients are calculated to determine the degree of similarity between the wavelet function and the time history, larger coefficients indicating a close match (Chui, 1992a, Chui, 1992b).

A wavelet based FRF can be constructed using the ratio of the WT of the output to the WT of the input in the time-scale domain. The square of the modulus of the WT can be interpreted as an energy distribution over the time-scale plane (Staszewski and Giacomin, 1997). The energy of the signal is mainly concentrated around the ridges of the WT, i.e. stationary points, and can be related to instantaneous frequency. A representation of the WT using only the ridge distribution is known as the skeleton of the WT. The real and imaginary parts of the skeleton can be found to give the analytic signal (Staszewski and Chance, 1997).

For a fixed scale, the modulus and phase of the WT give the envelope and phase variation, respectively, in time of the signal. By selecting an appropriate frequency (scale) the modes can be isolated from each other and studied independently. If the IRF is from several points, the phase and amplitude relationships between the points can be obtained from the WT. The ith mode shape can be estimated by the WT of the IRF from all measurement points at the ith frequency (scale) and at fixed time (Fasana et al, 1997).

2.5.3 Volterra series

The Volterra series method of system identification is useful for the case of random vibration. The theory is based on Duhamel's integral for linear systems. The Volterra series assumes that the output of a system can be expressed as an infinite series and that an equivalent Duhamel's integral can be formed using the terms in the series (Crespo et al, 1996). The impulse

response function in Duhamel's integral is replaced by a function of the terms in the series and is known as the Volterra kernels. The Volterra series expansion takes the following form;

$$y(t)=y_1(t)+y_2(t)+y_3(t)+\cdots+y_n(t)+\cdots \qquad \text{Equation 2-4}$$

where

$$y_n(t)=\int_{-\infty}^{\infty}\cdots\int_{-\infty}^{\infty}d\tau_1\ldots d\tau_n h_n(\tau_1,\ldots,\tau_n)x(t-\tau_1)\ldots x(t-\tau_n) \qquad \text{Equation 2-5}$$

A frequency domain representation of the system can be formulated based on the higher order FRFs (HFRFs) or Volterra kernel transforms in the same way as that for a linear system. The HFRF is formed by a multi-dimensional Fourier transform of the kernels. The HFRFs are defined mathematically as;

$$H_n(\omega_1,\ldots,\omega_n)=\int_{-\infty}^{\infty}\cdots\int_{-\infty}^{\infty}d\tau_1\ldots d\tau_n h_n(\tau_1,\ldots,\tau_n)e^{-i(\omega_1\tau_1+\cdots+\omega_n\tau_n)} \qquad \text{Equation 2-6}$$

The FRFs for non-linear systems are termed composite FRFs as they will receive contributions from all the other FRFs (Worden, 1998). The composite FRF depends on the power spectral density of the input, and as this tends to zero, the composite FRF tends toward the linear FRF.

The procedure for using the Volterra series expansions involves obtaining expressions for the cross spectra between the input and the individual output components (Worden and Manson, 1997).

2.5.4 Auto-regressive moving average models

The most general model of the input, *u*, and output, *y*, of a system is the auto-regressive moving average with exogenous input (ARMAX) model. This

assumes the input and output can be represented by a linear difference equation, describing the next output by the previous values observed. This type of model can also introduce an equation error, *e*, which may be modelled in a number of ways. The ARMAX model can be shown mathematically as;

$$y(t)+a_1y(t-1)+\cdots+a_{n_a}y(t-n_a)=b_1u(t-1)+\cdots+b_{n_b}u(t-n_b)$$
$$+e(t)+c_1e(t-1)+\cdots+c_{n_c}e(t-n_c)$$

Equation 2-7

In the ARMAX representation, the outputs are modelled by auto-regression, the input forces are the exogenous inputs and the prediction errors are modelled using a moving average of white noise (Ljung, 1999). It is possible to not include a model of the error if it is considered that the noise in the input and output is uncorrelated (Adams and Allemang, 1999), leading to an ARX representation of the system. Many variations exist of the ARMAX model, ranging from including only the auto-regressive or moving average part, to modelling the error as an ARMA model in itself.

The coefficients of the difference equation may not necessarily be linear, giving rise to a non-linear auto-regressive moving average with exogenous inputs (NARMAX) model. NARMAX models can be solved in the same manner as linear models, using the past force and response samples to estimate the most recent sample of the response. It is most common to only use measured quantities when employing a non-linear model, i.e. NARX (Ljung, 1999).

2.5.5 Applications

Attempts have been made to utilise non-linear behaviour in performing damage detection with some success, although this has been held back by the wide variety of possible analysis methods available and it is often the case that these methods are employed as system identification techniques.

Wardle et al (1997) combined the Hilbert transform with neural networks to classify the type of non-linear behaviour exhibited by a model aircraft wing. The distortions in the FRF and the Hilbert transform were used in a compact neural network that successfully identified the delamination non-linearity present.

Several studies have been performed to investigate the non-linear behaviour exhibited by cracks. Lamonaca et al (1997) studied the instantaneous frequency of free vibration obtained using the Hilbert transform to update a finite element model with some success. Prime and Shevitz (1996) also investigated the instantaneous frequency, together with the half-cycle frequency and Wigner-Ville distribution. It was concluded that the use of non-linear behaviour due to crack opening and closing varied depending on the sensor position, and it was suggested that this indicated the potential for damage detection and location.

Further investigation into the behaviour of cracks has been performed by mathematical modelling in several studies, such as Eccles (1999), Tan et al (2000), Nield (2002) and Tan (2003).

Higher-order FRFs were determined to be highly dependent upon the size and position of a crack in a cantilever beam, according to Crespo et al (1996). The crack was simulated numerically to produce a non-linear behaviour, and several crack sizes and locations were tested and shown to influence higher-order FRFs more than the Transfer function.

Owen et al (2001) applied the ARMA modelling technique to data collected during the testing of cracked reinforced concrete beams, in which non-linear behaviour was detected. Spectral estimates for short duration records were produced in order to study their time-varying properties, from which it was concluded that the level of non-linearity depended on the cracking present.

The concept of ARX modelling in the time domain and Volterra series was used by Adams (2002) to develop a multi-harmonic estimator to relate the frequency response at each frequency to the input and output spectra within a given frequency band. The type of linear and non-linear differencing term provided a description of different types of non-linear behaviour and NARX

were shown to capture some of the amplitude dependent behaviour commonly associated with non-linear systems.

The use of wavelet transforms was investigated by Lu and Hsu (1999) to detect damage using the theoretical expression for a non-uniform string. The addition of mass distributed over small intervals was used to represent localised damage and produced vibration signals that were similar to the undamaged case. However, it was found that a significant change was induced in the wavelet coefficients, and that the maximum difference between these occurred close to the damaged region, with precision increasing with the resolution of the wavelet transform.

Fasana et al (1999) also studied the wavelet transform, and compared the method with an ARMA method, canonical variate analysis and a balanced realisation method. The data used was in an output only form collected from a highway bridge. A comparison of the natural frequencies produced by each of these methods showed good agreement, although the results of damping measurements were not as good. The results were also used to update a finite element model where similar values for the updated parameters were found.

2.6 Pattern recognition and statistical methods

An extension of using measures based on the FRFs is to apply pattern recognition techniques to the data. A considerable amount of work has been conducted in this area recently, mostly concentrating on the potential use of artificial neural networks, the basis for this approach is summarised by Mannan et al (1994).

2.6.1 Neural network based methods

The use of frequency response functions, modal properties and wavelet transform data to identify damage was investigated by Marwala (2000). In this study, the author proposed a method based on a committee of neural networks, and found that this approach was more successful than using a neural network for each parameter separately. It was also concluded that, in contrast to most other methods, the process was more effective when experimental data was

used, due to the fact that the committee approach assumes that the data are uncorrelated.

One of the major problems when using frequency response function data as input to a neural network is the amount of data. A method to solve this problem was proposed by Zang and Imregun (2001) by utilising principal component analysis, which reduces the data set by separating it in terms of its significance. The reduced set was then used as the input to a neural network to determine the condition of a railway wheel with great success, even in the presence of added noise. It was noted that the extension of neural networks to damage location is more difficult, requiring fine spatial resolution, more output nodes in the network and significantly more training cases. The application of principal component analysis for modal testing was also highlighted, as this effectively filters noise from the signals.

A method to use neural networks in the identification of the damaged area was suggested by Ni et al (2002), by using an auto-associative memory neural network to determine a novelty detector. The basis of this method is to compare the undamaged with the damaged detector using a "novelty index" which, when evaluated against a threshold value, could give an indication of damage. Two novelty detectors were created, one based on natural frequency and one on modal flexibility. It was shown that by partitioning a bridge into a set of structural regions it was possible to observe which region had suffered damage. However, it was cautioned that this method relies on sensors being present in the damaged area and measurements from both an undamaged and damaged structure. It was also noted that the warning threshold needed to be set accurately based on statistics of the data.

2.6.2 Statistical process control

The application of control charts to structural health monitoring was studied by Kullaa (2001a) who proposed a complete monitoring system. The basis of the method was to use principal component analysis to reduce the dimension of the natural frequencies and modal vectors, and construct statistical process control charts to monitor these variables. However, the method remains reliant on the choice of a feature or features that are sensitive to damage, and it is possible

that these can be significantly influenced by environmental changes, creating false positive results. A possible solution to these false alarms was to allow a certain percentage of the previous *N* results to be outliers before a warning was given (Kullaa, 2001b).

The use of statistical process control to determine the existence of damage was investigated by Sohn et al (2000). The authors first surmised that the damage sensitive parameters were the coefficients of an auto-regressive model fitted to the time series data, and applied a technique known as an "X-bar control chart". The control limits were defined based on data obtained from an intact structure, and the coefficients of new data monitored against these limits. A number of data cleansing techniques were employed, including principal component analysis, significantly improving the detection of damage. It was discussed that this method only requires one data set from the undamaged structure and one from another, unknown, case and that a key advantage was its ability to operate with minimal interaction. The authors warned, however, that a large number of outliers only indicate that the system has changed, which could be due to damage or operational and environmental conditions.

This work was extended by Fugate et al (2001) by considering the residual error terms of the auto-regressive model as the features to monitor. The method was applied to a cyclically loaded column where the control charts used indicated a change in the system for all cases except the initial state. The largest deviation from the auto-regressive model occurred at the first damage level, and it was suggested that this arose due to the non-linear behaviour of cracks opening and closing. For subsequent load levels the deviation reduced, attributed to the yielding of the reinforcement causing the cracks to remain open.

2.7 Finite element modelling

In the fields of mechanical and aeronautical engineering, it is common to produce finite element (FE) models of components. However, when the results of the models are compared to those obtained from the actual component, it is often the case that the correlation is not good enough to allow application of the model with confidence. If it is thought that the physical parameters are in

error, then the model needs to be modified in order to use the correct parameters in a process known as model updating. Due to the global nature of the vibration characteristics, these are often used to determine the required changes in the parameters. A comprehensive review of this area has been conducted by Mottershead and Friswell (1993). In recent years, the concept of FE model updating using dynamic properties has been extended to civil engineering structures and has given rise to a number of additional problems.

This concept was utilised by Eriksson (1991) to modify the Young's modulus of a pre-cast concrete floor element using a grillage model. The first three modes of vibration were used, finding that an increase of 10% in the static Young's modulus was required, and non-linear behaviour of the torsional mode due to cracking was investigated using the assumption of either fully rigid or hinge behaviour.

FE models of several reinforced concrete bridges were calibrated using the dynamic properties by Haritos (1995) as a baseline model for subsequent dynamic analyses, such as earthquake assessments, or to determine load capacity. It was noted that in some cases, modes were absent from the experimental testing due to excitation being applied near a node of the mode, or extra modes appeared in the tests that were not apparent in the model. For the modes that were correlated, results compared well with both natural frequency and mode shape, together with results from static loading.

The potential for obtaining non-unique solutions when updating FE models was studied by Fregolent et al (1996) by constructing and testing three nominally identical frame structures. Updating was based on both the frequency response function and natural frequencies to correct the stiffness matrix. In all three cases, the model was able to reproduce the experimental results closely, however, it was pointed out that the local corrections for each of the models were rather different even though they were nominally identical.

A FE model was also used in order to assess the effects of proposed strengthening to a bridge by Salawu and Williams (1997). Again it was found that the FE model produced modes that had not been found experimentally. For the first six experimental modes, the error in natural frequency was -1.4%,

although the maximum error was 8%. MAC values of the matched modes yielded good results except for modes 5 and 6, which was attributed to inaccuracy in measuring higher modes.

Model updating of a 1/150-scale suspension bridge was performed by Zhang et al (2000) using the eigenvalue sensitivity method. Selected parameters were used in the updating, found by solving a constrained optimisation problem, in which the constraints were based on the expected uncertainty. The method introduced a weighted frequency error norm and a weight perturbation norm to be used in the objective function, providing the ability to individually tune frequency errors or parameters and avoid ill-conditioning problems. The updated model predicted the first 11 updated natural frequencies within 5% of those measured.

Xia et al (2002) employed a statistical procedure to identify damaged regions of two experimental specimens using a few natural frequencies and incomplete mode shape data. The probability distributions of the stiffness parameters were formed using a Monte Carlo simulation and the probabilistic existence of damage found by comparing the distributions before and after the introduction of damage. It was found that false-positive locations due to inaccuracies in the initial model and non-linear behaviour of the damaged specimens could be reduced by the application of the probabilistic approach, and it was possible to identify damage even with an unknown undamaged state, although with a lower confidence.

2.8 Summary and discussion

It is clear from this survey of the available literature that there has been considerable interest in the use of dynamic testing in condition monitoring and damage detection. Methods based on linear modal analysis have been given the most attention, although there still remain some doubts regarding the sensitivity of these properties to various types of damage.

The non-linear behaviour of damaged structures has suggested that methods based on this may have significant possibilities in the field of structural health monitoring. Efforts in this area have, however, been hindered by the relatively

recent interest and the variety of techniques that could be employed, each possessing individual advantages and disadvantages.

More recently, there has been considerable interest in using statistical pattern recognition techniques, such as neural networks. These studies have been successful for the applications considered, although the problem of the neural networks requiring a large amount of data that incorporates the necessary damage mechanisms could prevent their use for unique civil engineering structures.

Methods that incorporate a model of the structure, usually a FE model, and attempt to update the uncertain parameters have been employed with some success and it appears possible that the technique is capable of producing rational results. However, this is reliant on the selection of suitable features that are sensitive to the damage and the parameters to be modified in the FE model.

Particular attention has been paid to concrete bridges, as a significant number of the bridges in the UK are of concrete construction, estimated at one-third of all bridges. However, it is also apparent that two-thirds of the maintenance budget is spent on concrete bridges, indicating that there is a considerable need to improve the efficiency of spending. A number of studies investigating the dynamic properties of bridges have been performed on prestressed or composite bridges. It is reasonable to suggest that due to the age and construction methods employed, deterioration is more likely to occur in bridges constructed from reinforced concrete when compared to prestressed and composite construction.

It is also true that, whilst some studies have drawn positive conclusions regarding the sensitivity of dynamic properties to damage, there remains a considerable amount of uncertainty in the results found. Many investigations performed on beams have provided useful indications of the potential applications of dynamic testing as a structural health-monitoring tool. However, the applicability of these findings to other structures requires further investigation. A number of other studies have involved testing of actual bridges, and have highlighted several issues that were not apparent from the

beam testing, and have, in general, been less successful than the simpler laboratory testing, due to the further complications introduced. This is further complicated by the fact that the effects of prestress and composite construction add more difficulties to already uncertain findings.

The relationship between the vibration behaviour and deterioration has been further obscured by variations due to environmental effects, boundary conditions and non-linear behaviour. There also exist limitations in terms of the requirement of measuring the excitation force and, in some cases, the necessity of data from a baseline structure.

It is clear that, due to the number of uncontrollable factors that affect the dynamic properties of bridges in the field, it is necessary to perform preliminary testing under laboratory conditions in order to assess the effect of damage alone on the dynamic properties. This also allows the damage to the structure to be more closely controlled and well developed testing techniques to be used to obtain good quality data. The control of damage is especially important, both in terms of the areas that are damaged and the severity of damage, as this is very difficult to achieve in field-testing.

In order to extend the previous work conducted on reinforced concrete beams to more realistic shapes, and to avoid external influences causing unnecessary uncertainty in the results, a scale model of a bridge deck should be tested. Due to the number of deteriorating reinforced concrete short span bridges the feasibility of using vibration characteristics for structural health monitoring needs to be investigated for reinforced concrete. This will also provide a platform for the study of the inherently more complicated prestressed and composite construction, whilst indicating some of the issues that will affect the reliability of the results.

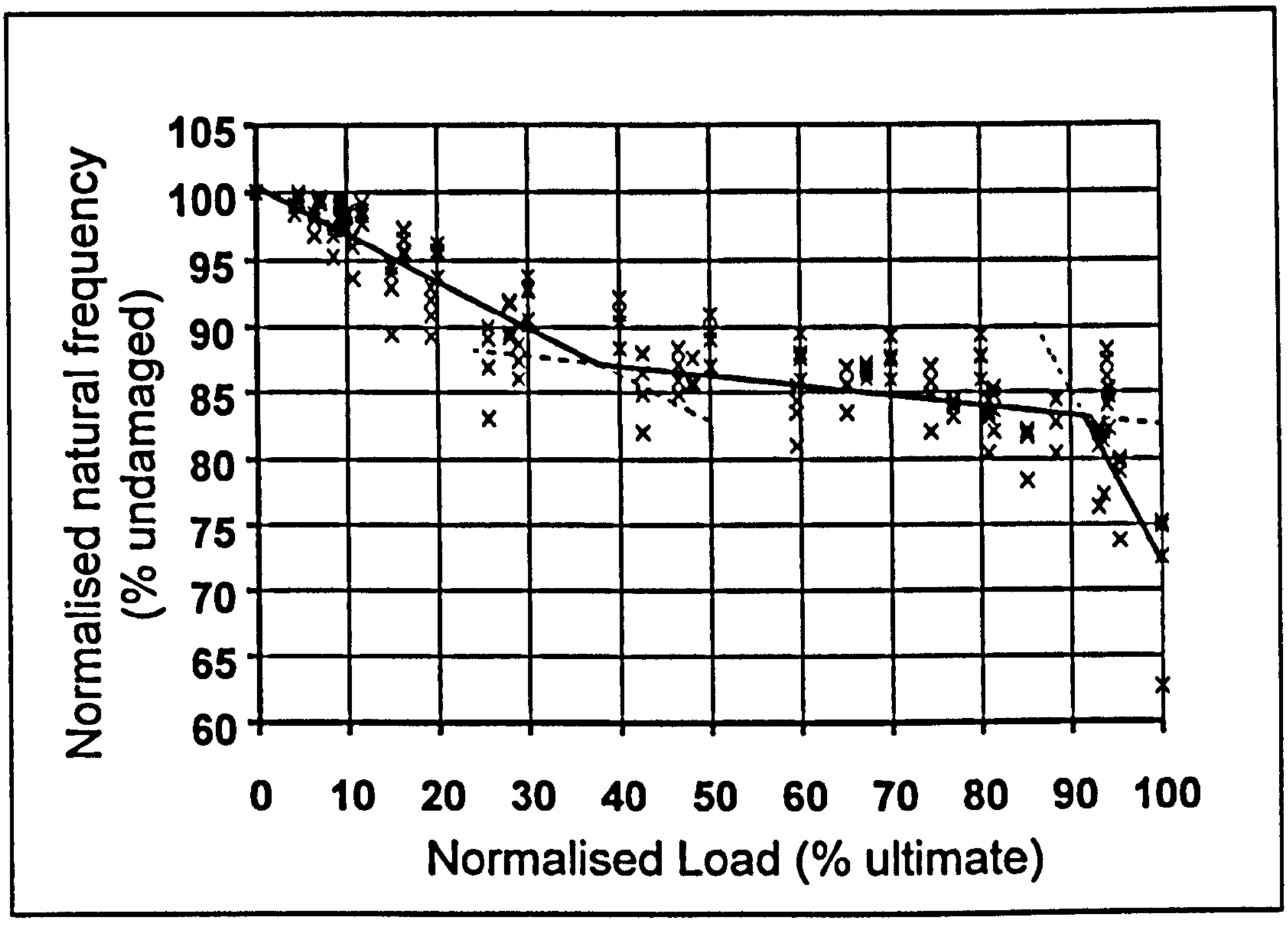

Figure 2-1: Tri-linear relationship observed by Eccles (1999)

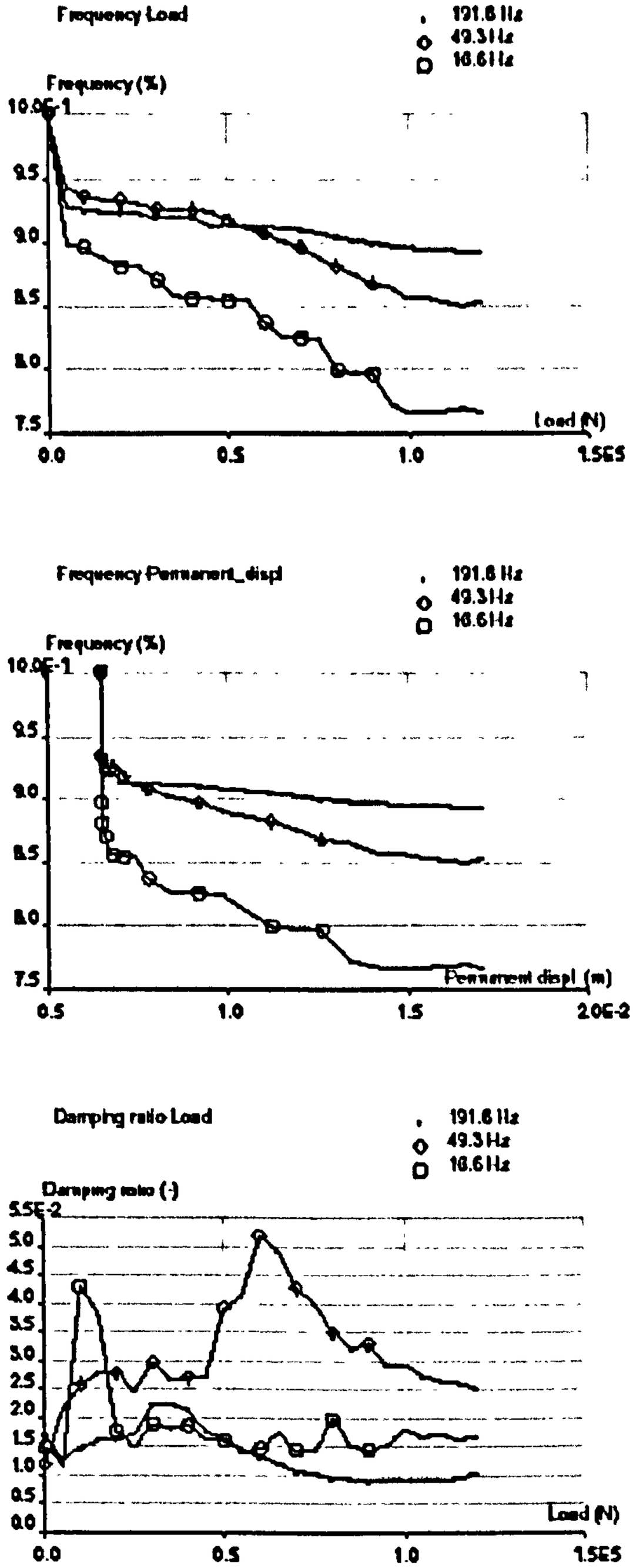

Figure 2-2: Change in modal properties of first three modes (Ebert et al, 1999)

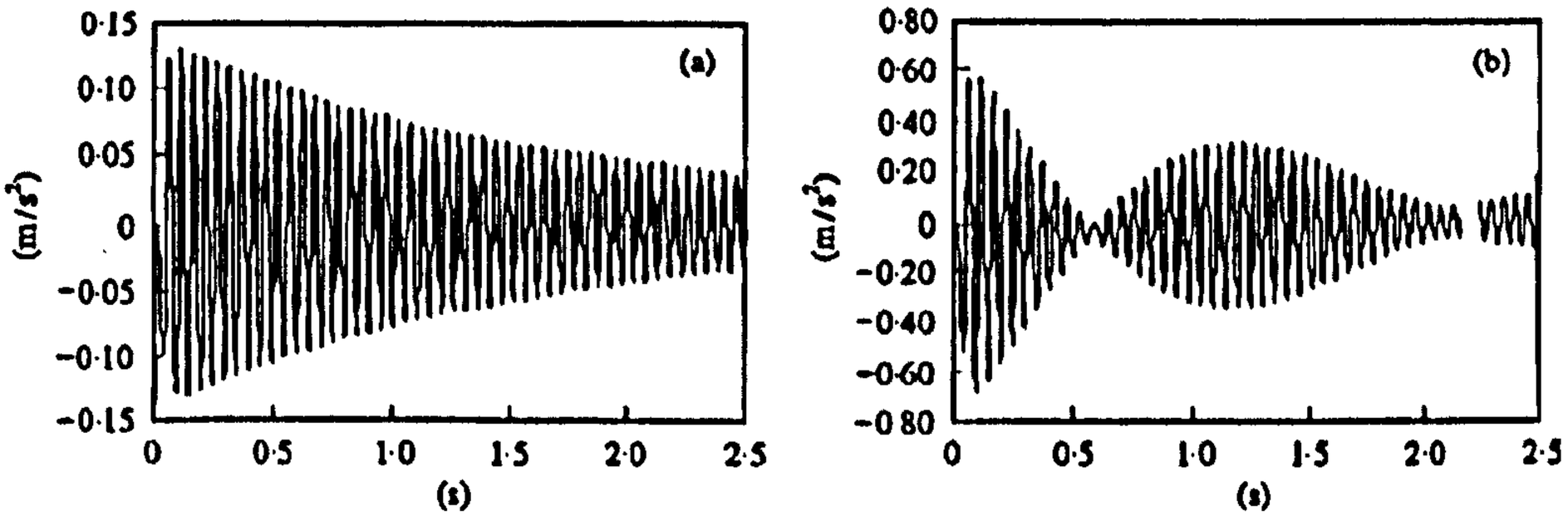

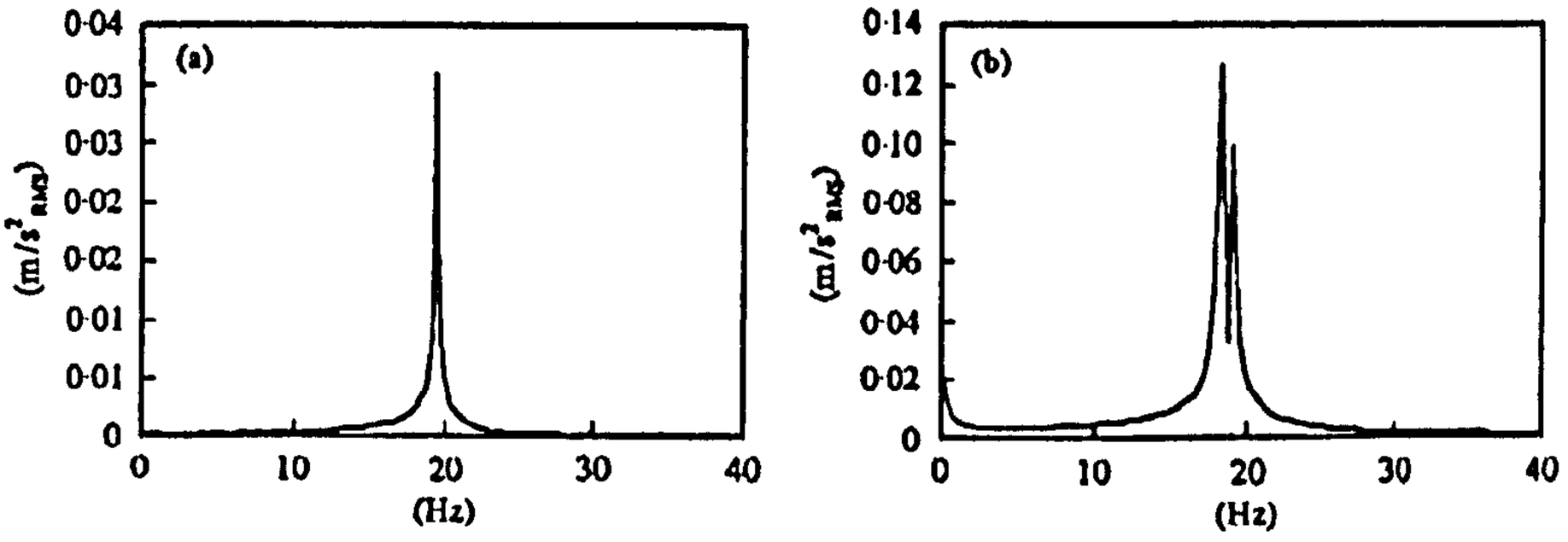

Figure 2-3: Time domain beat and frequency domain peak splitting (Zonta and Modena, 2001)

CHAPTER 3

EXPERIMENTAL DESIGN

3.1 Introduction

This chapter describes the rationale behind the experimental tests conducted to investigate the use of dynamics for structural health monitoring of reinforced concrete bridges. A study of the results obtained from the static testing is given in chapter 4, whilst chapter 5 discusses the results of the dynamic testing, in particular experimental modal analysis. Chapter 6 studies the potential for using finite element model updating as a damage detection method.

A discussion of the bridge deck specimen design and the testing procedure adopted, describing both the static and dynamic tests, is given. Also provided is a brief summary of the techniques used in experimental modal analysis and the processing of the data into meaningful quantities that could be used as structural health monitoring parameters.

3.2 Aim and objectives

The aim of this investigation is to assess the potential for using dynamic testing as a structural health-monitoring tool for reinforced concrete bridges. To achieve this, the following objectives have been identified:

- Determine the sensitivity of modal properties to changing damage levels for a realistic specimen
- Compare measured with analytical modal properties at different damage levels

- Assess the success of finite element modelling and updating as a tool to determine structural changes

In order to fulfil these objectives, a series of test have been performed. The formulation of these tests is detailed in the following sections, beginning with test methodology, then test specimen design.

3.3 Test specimen

From the literature review of the current state of using vibration characteristics as a structural health-monitoring tool for bridges, it is apparent that there is a lack of understanding in a number of key areas. Of particular relevance to the UK is the limited number of studies that have been performed on short span reinforced concrete bridges, which form a considerable number of the total bridge structures. This is also important due to the age of these bridges, as many reinforced concrete bridges were constructed in the 1960s, meaning that a large number of bridges are now suffering from significant deterioration due to poor construction methods, inadequate design and increases in loading.

Reinforced concrete bridges are generally suitable for short spans of up to 30m, and are typically constructed using a T-beam arrangement to span a motorway, trunk road or railway.

In order to maintain generality of the findings of this study, the bridge specimen tested was designed to be representative of a typical bridge and not to be a scale model of an actual bridge. One of the major concerns in laboratory scale testing is that of scale effects that cause the results to not be consistent with those found from full scale testing. This is especially important for reinforced concrete as aggregate size may affect micro-damage. In this project, the specimen scale was also dictated by constraints regarding the practicality of testing such a specimen in a laboratory. For these reasons, the bridge was designed as a one-quarter-scale reinforced concrete beam-and-slab bridge deck.

The bridge deck specimen, Figure 3-1 and Plate 3-1, consisted of five one way spanning beams in the longitudinal direction, connected to a transverse end beam at either end of the deck, covered by a slab. At full scale, this represents a span of 20m and a width of 10m, which are typical for RC bridges.

The capacity of the decks was designed to allow a number of load increments to be applied before failure. The bridge decks were cast using grade C50 concrete with a 6mm maximum aggregate size due to the scaled dimensions, further details of the mix design are given in Table 3-1, giving a concrete strength of approximately 65N/mm^2. Two reinforcement arrangements were used to allow investigation of different types of cracking and failure on the dynamic properties but also provided some interesting results regarding the static testing. The two reinforcement arrangements used were: full shear and flexural reinforcement, designated as type A; and reduced shear and full flexural capacity, type B. These arrangements are shown in more detail in Figure 3-2 and Table 3-2.

In order to retain the realistic nature of the test specimen, the bridge deck was supported on five bearings at each end, located along the centreline of the longitudinal beams under the transverse beam. The deck was supported at one end on half-round steel bearings, with a steel plate 100×100mm between the bearing and the deck, and a steel plate between the bearing and the abutment. At the other end the deck was supported on steel roller bearings, again with plates above and below, to allow for longitudinal movement of the deck. The abutments comprised five 600mm concrete cubes placed in a row at both ends of the deck.

3.4 Test methodology

The aim of this study is to investigate the suitability of using dynamic testing for structural health monitoring of bridges. This requires the bridge deck specimens described above to be tested in a manner allowing the vibration characteristics to be assessed as the deck suffers from progressively more deterioration. The most suitable method in a laboratory for causing deterioration of the decks is by applying a static load. By damaging the decks using an external load, it is possible to control the amount of cracking introduced, allowing the decks to be damaged by specific amounts, and should also cause similar damage to be exhibited by decks tested using the same regime. Applying a load to the decks also allowed the damage to be concentrated in specific areas, permitting a comparison between different

cracking patterns to be made both in terms of the static behaviour and, more importantly, the effects on the vibration characteristics, which gives an indication of the potential of the dynamic behaviour of the decks to determine the location, and possibly type, of deterioration.

As the dynamic characteristics need to be correlated with the deterioration of the decks, the load was applied in a number of increments as a proportion of the total capacity of the deck. In order to investigate the behaviour of the decks under static loading and to obtain information regarding the degree of the deterioration, the deflection of the five longitudinal beams was measured as the load increment was applied. This deflection measurement was made at the mid-span along the centreline of each beam, giving the maximum deflection of the decks under the applied load.

After each major load increment, the extent of the cracking introduced was marked on the deck to enable the crack growth to be monitored, and compared with the vibration characteristics in terms of the severity and types of cracking present. The decks were also tested to determine the vibration properties after each load increment had been applied. The damage introduced is discussed in detail in chapter 4, and its effect on the dynamic characteristics investigated in chapter 5.

3.5 Loading

Three loading arrangements were used for testing the one-quarter-scale bridge decks. The use of different loading regimes was investigated in order to study the effect of damage type on the dynamic behaviour of the decks by promoting certain types and patterns of cracking to form.

The first loading arrangement consisted of loading the central beam in a form of four-point bending, the second involving loading two of the side beams. Whilst these two arrangements are not representative of the typical loading or the most common cause of deterioration observed in real bridges, structural cracking is exhibited by real bridges.

To assess the behaviour of the bridge deck under a more realistic loading pattern and to provide more representative results than the previous loading

arrangements, a third type of loading was employed. This was designed to mimic the Highways Agency type B (HB) loading in BS5400-2 (1978), which is used to represent an abnormal load travelling on the bridge.

The load was applied to the deck by means of a hydraulic jack and an arrangement of steel spreader beams. A major concern when loading reinforced concrete is creep. For this reason, the load was applied at a rate of 6kN/min and deflection measurements taken at 5kN increments in an attempt to keep the effect of creep uniform for all decks. This equates to an approximate maximum bending stress of 0.06N/mm^{2}s, equal to the specified loading rate given in BS1881-118 (1983). A soft material was placed between the loading points and the deck surface to provide even distribution of the load as the surface of the deck was not completely smooth.

3.5.1 Type 1 – symmetrical loading

This type of loading was performed to obtain a symmetrical damage pattern. In this scheme, the load was applied at two points on the deck, via 150mm square steel plates, at a distance of 2m apart as shown in Figure 3-3 and Plate 3-2. The loading was applied to be symmetrical about both the longitudinal and transverse direction of the deck to develop damage concentrated in a single beam. The symmetrical nature of the loading and damage allowed the variation in the dynamic characteristics to be related to the progressive failure of a single beam.

3.5.2 Type 2 – asymmetrical loading

The second arrangement of loading was to load the deck in an asymmetric manner. This type of loading was designed to promote the progressive failure of two beams simultaneously, whilst introducing torsion in the remaining parts of the deck. The purpose of asymmetric loading was to produce some areas of the deck that were heavily damaged and some that were only lightly damaged and to observe the effects on the modes produced when a wider variety of cracking was introduced along with more variation around the deck.

This type of loading is more representative of the type of overloading that may be experienced by a real bridge due to one carriageway being heavily loaded,

although this is a much more simplified arrangement than would actually be applied to the bridge. It is therefore true that the general damage development observed under this loading will be more applicable to a real bridge, if it were to be damaged due to overloading.

This was achieved by applying the load to two beams and the intermediate slab section at two points 2m apart. The two beams loaded were the edge and its adjacent beam, as shown in Figure 3-4 and Plate 3-3. The load was applied via two steel square hollow sections of dimensions 150mm×150mm×745mm.

3.5.3 Type 3 – HB loading

In order to introduce more realistic damage, a third loading arrangement was designed. This type was based on the Highways Agency HB loading, used for abnormal vehicle loading. For the purposes of BS5400-2, the bridge deck was divided into two notional lanes, forming a single 2-lane carriageway.

The HB loading dimensions were reproduced at one-quarter-scale, where the variable central dimension was taken to be 6m (full-scale) to produce the most onerous loading. As stated above, the bridge deck was considered to be a single 2-lane carriageway, and the HB bogie was applied symmetrically in one lane of the bridge. For the purpose of this testing, it was decided to not include the associated HA loading as this would involve an unnecessarily complex loading scheme. The locations of the loading points used for the HB bogie can be seen in Figure 3-5 and Plate 3-4.

The HB loading was applied via 16No. 100mm square steel plates using an arrangement of loading beams designed to allow rotation at important joints to give an approximately uniform distribution of load as the deck deformed.

3.6 Dynamic testing

As stated above, the aim of this study is to further investigate the use of dynamic testing for structural health monitoring of reinforced concrete bridges. The incremental loading regime was adopted to allow an investigation into how the dynamic characteristics of the bridge decks change as a reinforced concrete bridge deck is progressively damaged. In this program, a number of

dynamic tests were performed to examine the effect of different excitation types, different bearing conditions and the presence of non-linearity. A short summary of the tests performed on the decks is given in Table 3-3, and further details are presented in the following sections.

In all cases, the data was collected using a PC running LabVIEW software and an analogue-to-digital (A/D) card. The accelerometers and force transducer were connected to the A/D card via an external connection board and signal conditioning boxes that allowed filtering and amplification of the signal. A schematic diagram of the arrangement is shown in Figure 3-6. Further details of the testing equipment used are given in Table 3-4.

3.6.1 Forced vibration testing

Due to the previously observed non-linear behaviour of cracked reinforced concrete (Eccles, 1999, Tan et al, 2000 and Nield, 2002) several tests were performed using forced vibration. This involved using an electromagnetic shaker attached to the deck at either one or two locations and measuring the response. The use of a shaker allows the input force to be controlled, thereby minimising the effect of non-linear behaviour on the resulting dynamic properties.

In all cases, the input force was measured using a force transducer positioned between the shaker and the deck, and the response recorded using accelerometers. The input signal was selected to be in the form of a sine-sweep and, after several preliminary experiments, the frequency range was selected as 5 to 300Hz. This range was chosen to compliment the impact excitation frequency range used for the first two decks to allow comparison between the results obtained.

In order to obtain sufficient frequency resolution for the accurate detection of the modes by the modal extraction routine, the time history contained 4096 samples obtained at a rate of 2000Hz, giving duration of just over 2s. The data were correspondingly filtered at 1000Hz using a Kistler Type 5134 signal-conditioning box to avoid aliasing and also amplified to utilise as much of the voltage range of the A/D card as possible to provide a high voltage resolution.

To reduce the influence of measurement noise on the output, several time histories were taken and averaged together in the frequency domain using the determined spectra. The number of averages taken was decided by examination of the coherence function (see appendix A). For decks 3 to 6, 20 time histories were taken to produce a satisfactory coherence function. Due to an improved connection between the shaker and decks 7 to 10, the number of averages taken was reduced to 10 after no significant deterioration in the coherence function after 6 records was observed.

3.6.2 Impact testing

For several of the decks, an instrumented hammer provided the excitation force. This type of excitation was chosen as it was thought to be a relatively quick and simple method to obtain the mode shapes of a structure. However, in practise, due to the large number of locations at which the mode shapes were to be measured, this proved not to be the case and the modal testing was changed to use shaker excitation for a number of decks instead.

This type of excitation provided a much better signal-to-noise ratio than the forced vibration testing, although it is not possible to accurately control the input magnitude. As a result of the anticipated non-linear behaviour, the impact amplitude was maintained at approximately 2.27kN by simply monitoring the maximum value reached by the impact. For this, it was assumed that the duration of the impulse remained constant; in practice, this duration was approximately 4ms. It was noted that the auto spectra produced using this method of control were very similar for the majority of impacts due to the use of the same stiffness hammer tip, giving substantial input in the frequency range 0 to 300Hz with minimal excitation above 500Hz.

As in the forced vibration testing, several averages of the spectra obtained were averaged to improve the coherence function to a satisfactory level. For decks 1 and 2 the number of time histories used was 20, and again this was reduced for deck 6 due to both an improved technique and time constraints.

For these tests, each time history comprised 8192 samples, again sampled at 2000Hz giving duration of slightly more than 4s. As in the forced vibration testing, the data were filtered at 1000Hz and amplified by the signal-

conditioning boxes, although to a lesser extent due to the large initial response from the impact. All the impact tests were conducted using a trigger based on the level of output from the force transducer in the hammer tip to ensure that the time history records contained similar responses.

3.6.3 Accelerometer locations

For many of the decks, seven accelerometers were used to measure the dynamic response of the deck. Examining the results of a simple finite element model and inspecting the mode shapes determined the location of the accelerometers, although this could have been done by assessing possible locations mathematically. The first ten modes were considered and positions of high response of the structure were selected as accelerometer locations. The locations chosen are presented in Figure 3-7.

The two forms of excitation chosen require the test to be carried out using different techniques. Using impact excitation involves applying the impulse at the locations the response is needed, whilst placing an accelerometer in a single position. This type of testing relies on the assumption that the structure being tested behaves in a linear manner, and therefore obeys the principle of reciprocity. For the impact testing conducted on the decks, either six or seven accelerometers were used to provide a number of independent mode shape estimates and the impact was applied at all locations, including accelerometer positions. This also allowed the validity of the assumption concerning reciprocity to be investigated.

To measure mode shapes using forced vibration, it is required that the excitation location remains fixed, whilst the accelerometers are moved to the locations where the mode shape needs to be defined. A second type of test was also performed using forced vibration to investigate the effect of changing excitation amplitude. For this test, the accelerometers were placed in the same locations as those used for the impact testing to allow for comparison between the results obtained using different excitation methods.

3.6.4 Bearing conditions

As mentioned in section 3.3, the bridge decks were supported by five bearings at each end of the deck during the static loading. For the dynamic testing, three different bearing conditions were considered. The first was to maintain the realistic nature of the specimen by conducting the dynamic tests on the bridge decks supported by ten bearings and was carried out for decks 1 and 2 and 6 to 10.

By supporting the deck at ten points, a large degree of redundancy was introduced, which may mask the effect of damage on the dynamic characteristics measured. In order to eliminate the redundancy in the deck support conditions, a number of dynamic tests were performed on the deck supported on three bearings to give a statically determinate structure. The location of the three bearings was chosen to maintain the symmetry of the deck specimen, as shown in Figure 3-8.

For decks 5 and 6, the undamaged deck was also tested under a third type of support conditions using soft bearings to replace the steel half-round and round bearings. These bearings were composed of 100mm squares of foam rubber, 40mm thick. These boundary conditions were included to allow the load on each of the supports to be more equal than the ten steel bearings.

3.7 Experimental modal analysis

The vibration characteristics were investigated by determining the modal properties of the decks, in a process known as experimental modal analysis (EMA). A brief outlined is given in this section, whilst a more detailed explanation is given in appendix A. It consists of essentially three stages: modal testing, data processing and modal parameter estimation.

3.7.1 Modal testing

This part of EMA involves the actual experimental work carried out to measure the vibration response of the system under test. In general, this requires the acceleration, velocity or displacement of the system to be measured when

subjected to some form of excitation, resulting in either forced, free or ambient vibration.

Forced vibration allows the excitation to be controlled precisely, in terms of the frequency content, amplitude and form of excitation, although the testing is more time consuming and difficult to perform, and is impractical for many civil engineering structures. Control of the excitation is particularly important when the behaviour of the system is non-linear, as applying exactly the same excitation should give the same response.

Measuring the free vibration response of the structure is often a much easier to carry out than using forced vibration, as it requires the system to be excited for only a short duration. The excitation often consists of an impact to the structure, usually by an instrumented hammer, although in some cases a quick release method is employed. This type of testing is more suited to civil engineering structures, as it can be implemented relatively simply and does not require significant interference with the structure. However, the impact force cannot be controlled to the same extent as that applied using forced vibration, and is therefore better suited to linear systems.

One of the easiest testing procedures to perform is to use ambient vibration, which, in the case of bridges, usually consists of wind and traffic excitation. As implied above, this requires no equipment to excite the structure, but it is not possible to control, or accurately measure, the excitation force. This means that there is significantly more work involved in data processing and modal extraction, as the data are often of a lower quality than that collected using some applied excitation.

3.7.2 Data processing

The response of the structure measured experimentally is in the form of a time domain signal, and usually includes a measurement of the excitation force. The data are required to be processed into a form that is then suitable for the modal extraction routines to be carried out. This processing take the form of either converting the data into the frequency domain, giving spectral functions and a frequency response function (FRF) only, or then further processing to obtain the data in the time domain to give an impulse response function (IRF).

The conversion of the time data into the frequency domain is achieved by application of the Fourier transform, itself a development of Fourier series that state that any periodic function can be represented by sine and cosine terms. Viewing the data in the frequency domain allows the contribution of the response at each particular frequency to be determined, and indicates where the natural frequencies of the system occur.

Experimental modal parameters (natural frequency, modal damping and mode shape) may be obtained from a set of FRF or IRF measurements. The FRF describes the input-output relationship between two points on a structure as a function of frequency, whilst the IRF is the inverse Fourier transform of the FRF. The FRF is the response at each frequency of the structure due to a unit impulse at that frequency, and, due to the assumptions made in calculating a FRF, the IRF is the equivalent in the time domain. It is for these reasons that the modal parameter estimation is performed on the FRF and IRF measurements, as it greatly simplifies the applied methodology.

The FRF is theoretically calculated as the Fourier transform of the output divided by the Fourier transform of the input. However, in practise, due to noise on the data, the FRF is formed by first calculating the auto- and cross-spectral density functions leading to two alternative definitions of the FRF, H_1 and H_2;

$$H_1(f)=\frac{S_{yx}(f)}{S_y(f)} \qquad \text{Equation 3-1}$$

$$H_2(f)=\frac{S_x(f)}{S_{xy}(f)} \qquad \text{Equation 3-2}$$

The use of these two definitions is also employed to calculate a measure of the quality of the data obtained by computing a coherence function. This essentially describes how much of the response can be correlated with the input excitation, by producing a value of between 0 and 1 at each frequency.

3.7.3 Modal parameter estimation

After the data have been processed into a suitable form, usually either a set of FRFs or IRFs, the process of determining the modal properties can be carried out. This involves applying a curve fit to the data to find the natural frequency, modal damping and mode shape. Several methods and algorithms exist to do this.

The methods available can be categorised by the domain of the data upon which they are applied: time or frequency; and whether they attempt to determine a single mode or multiple modes. As indicate above, the time domain methods are generally applied to the IRFs and the frequency domain methods to the FRFs. Details of several of the more common methods are given in appendix A.

3.7.4 Use of modal properties in bridge testing

For structural health monitoring and damage detection, the modal test data obtained will either be from a series of tests or from an analytical model and one modal test. In both of these cases, it is necessary to estimate the modal parameters separately for each test. This can result in a variation of the modes that are identified between the different tests. For both condition monitoring and damage identification, it is required to compare the modal properties found from the latest test to those obtained from either a previous test or a FE model. This implies a method for ensuring the correct modes are compared with each other when obtained from different sources is needed.

A popular method for comparing the mode shapes obtained is the modal assurance criterion (MAC). This utilises the two sets of mode shapes obtained and compares them in a global manner, producing a single value as a measure of the similarity between two modes. This is done for all the mode shapes that have been found from the parameter estimation routines, to give a matrix of MAC values. The MAC algorithm may be expressed as;

$$MAC(p,x)=\frac{\left|\sum_{j=1}^{n}(\phi_x)_j(\phi_p)_j^*\right|^2}{\sum_{j=1}^{n}(\phi_x)_j(\phi_x)_j^*\sum_{j=1}^{n}(\phi_p)_j(\phi_p)_j^*}$$ Equation 3-3

where ϕ_x is the measured mode shape, ϕ_p is the calculated mode shape and j is the mode number, as the MAC was originally developed for comparing experimental with analytical.

A more refined technique for comparing mode shapes is the coordinate modal assurance criterion (COMAC), which uses a point-by-point method. The COMAC algorithm compares the response at each of the measurement points and gives a value for the similarity between them. This results in a more detailed comparison to be made, but produces more data than the MAC calculation. The COMAC may be expressed as;

$$COMAC(i)=\frac{\sum_{j=1}^{n}\left|(\phi_x)_{ji}(\phi_p)_{ji}\right|^2}{\sum_{j=1}^{n}(\phi_x)_{ji}^2\sum_{j=1}^{n}(\phi_p)_{ji}^2}$$ Equation 3-4

Both of these algorithms produce a value of between 0 and 1. A value of 1 indicates that the mode shapes are in complete agreement, whereas a value of 0 implies no correlation.

In this study, considerable use will be made of the MAC algorithm to compare modes obtained from different decks, load levels and with a finite element model. It is often quoted that a MAC value of above 0.9 implies excellent agreement between the mode shapes and any MAC values less than 0.7 indicate that the modes are not the same. It should be noted, however, that the MAC suffers from a number of limitations, particularly with regard to translations in the mode shapes, which can cause a significant lowering of the MAC value calculated. This is important in this testing as the damage introduced and the support conditions often cause the mode shapes to change

slightly in orientation. This particular problem is discussed further in chapter 5 when the results of the modal analysis are presented.

3.8 Summary

The test specimen designed for this study is a one-quarter-scale model bridge deck, constructed from reinforced concrete. This specimen has been designed to be representative of a typical bridge deck of T-beam construction. A number of bridges of this type were constructed in the 1960s and are now suffering from significant deterioration. To maintain the realistic nature of the specimen, it is supported on five bearings at each end for a number of tests, and to investigate the damage only several other decks were tested supported on three bearings.

To assess the sensitivity of vibration characteristics to damage, the decks are cracked by applying a static load in increments. To investigate the effect of different types of cracking, three loading regimes are employed to produce symmetric, asymmetric damage and cracking under HB loading. After each load has been applied, the decks are tested to determine the vibration characteristics, and the natural frequency, mode shape and modal damping extracted.

The details of the results obtained from the static loading are given in chapter 4, whilst the findings from the dynamic testing are discussed in chapter 5. To better assess the use of vibration characteristics in structural health monitoring, chapter 6 discusses the use of finite element model updating when applied to the results presented in chapter 5.

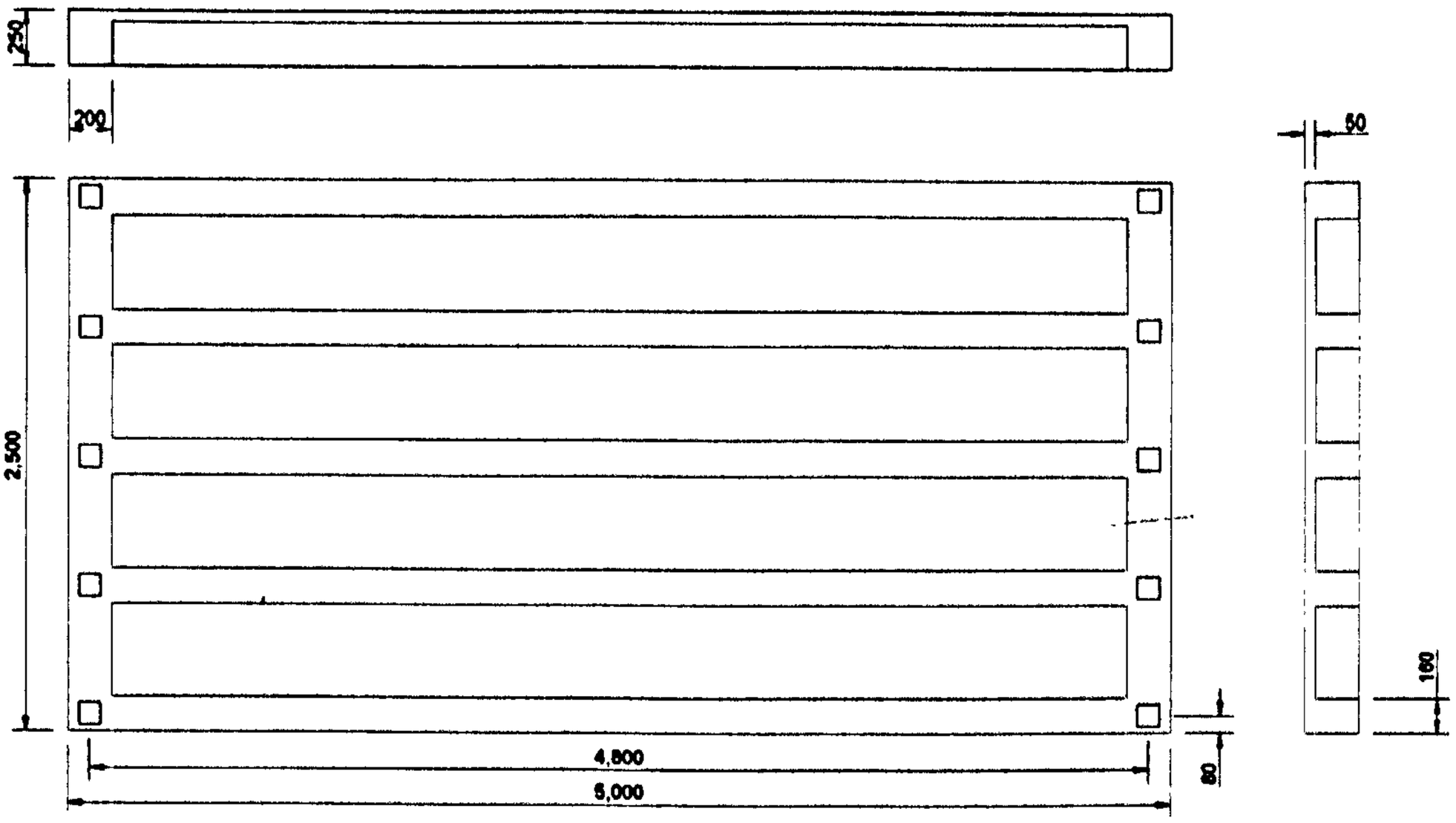

Figure 3-1: Scale bridge deck dimensions

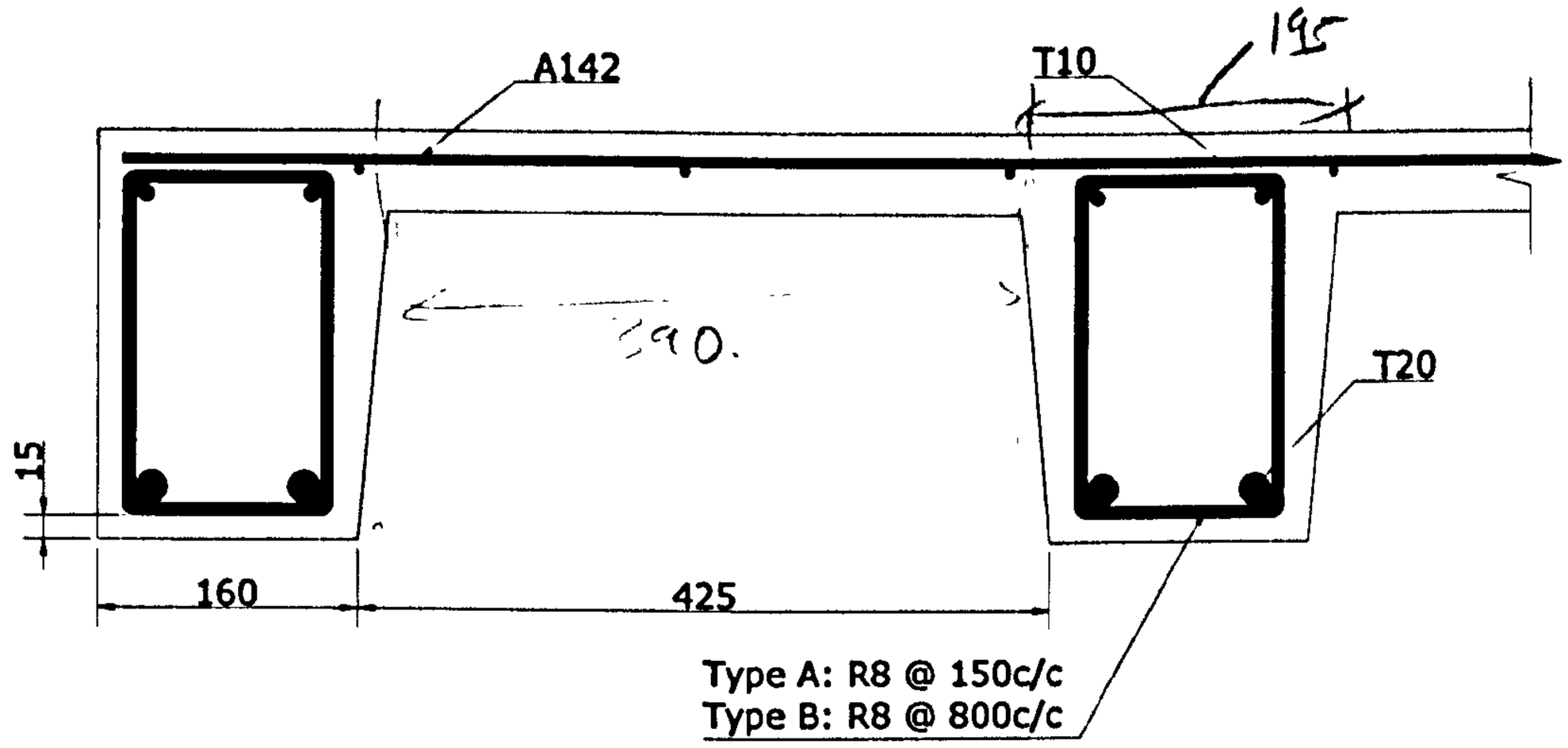

Figure 3-2: Reinforcement arrangement of type A and B decks

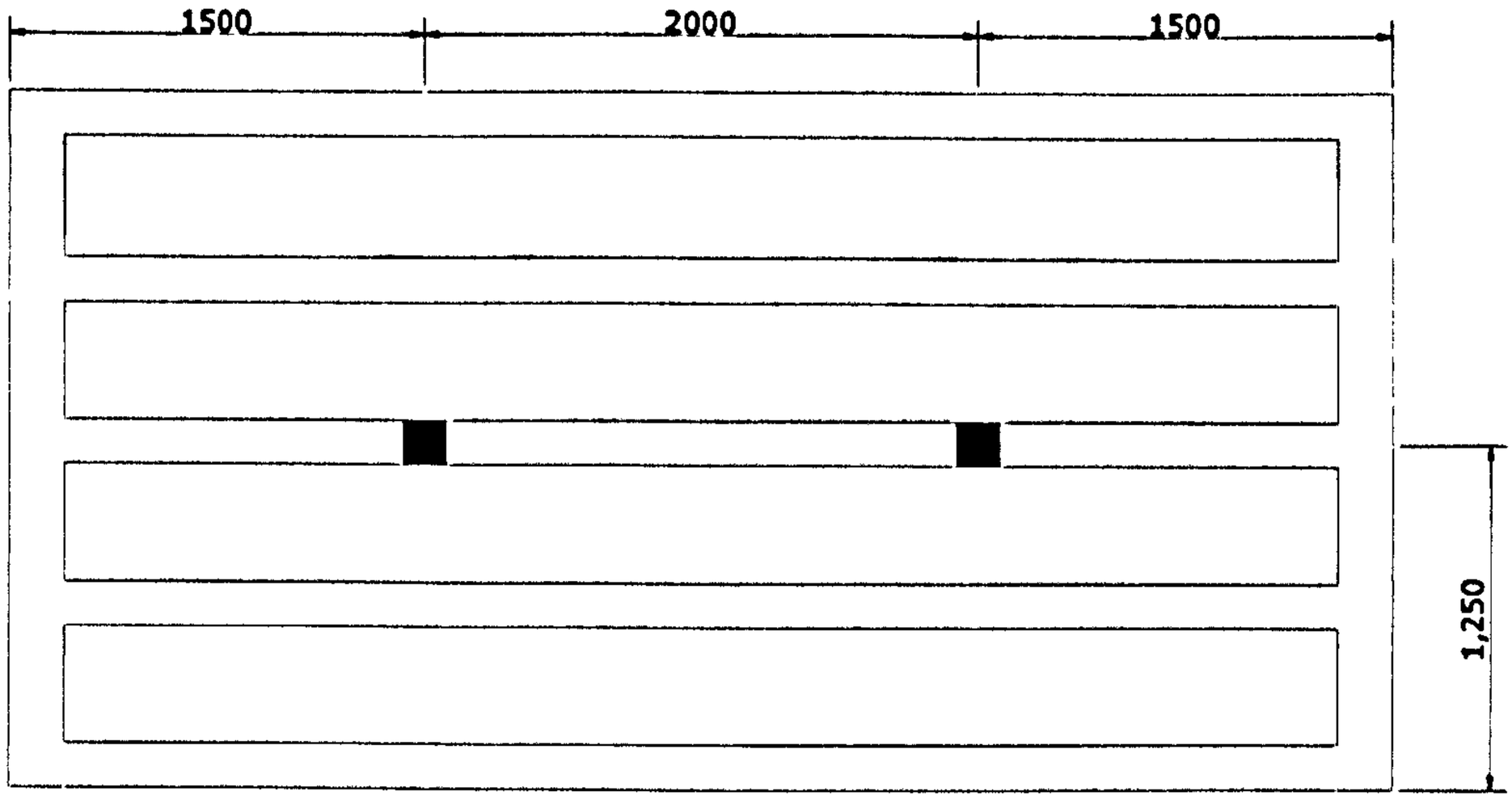

Figure 3-3: Arrangement of symmetric loading regime

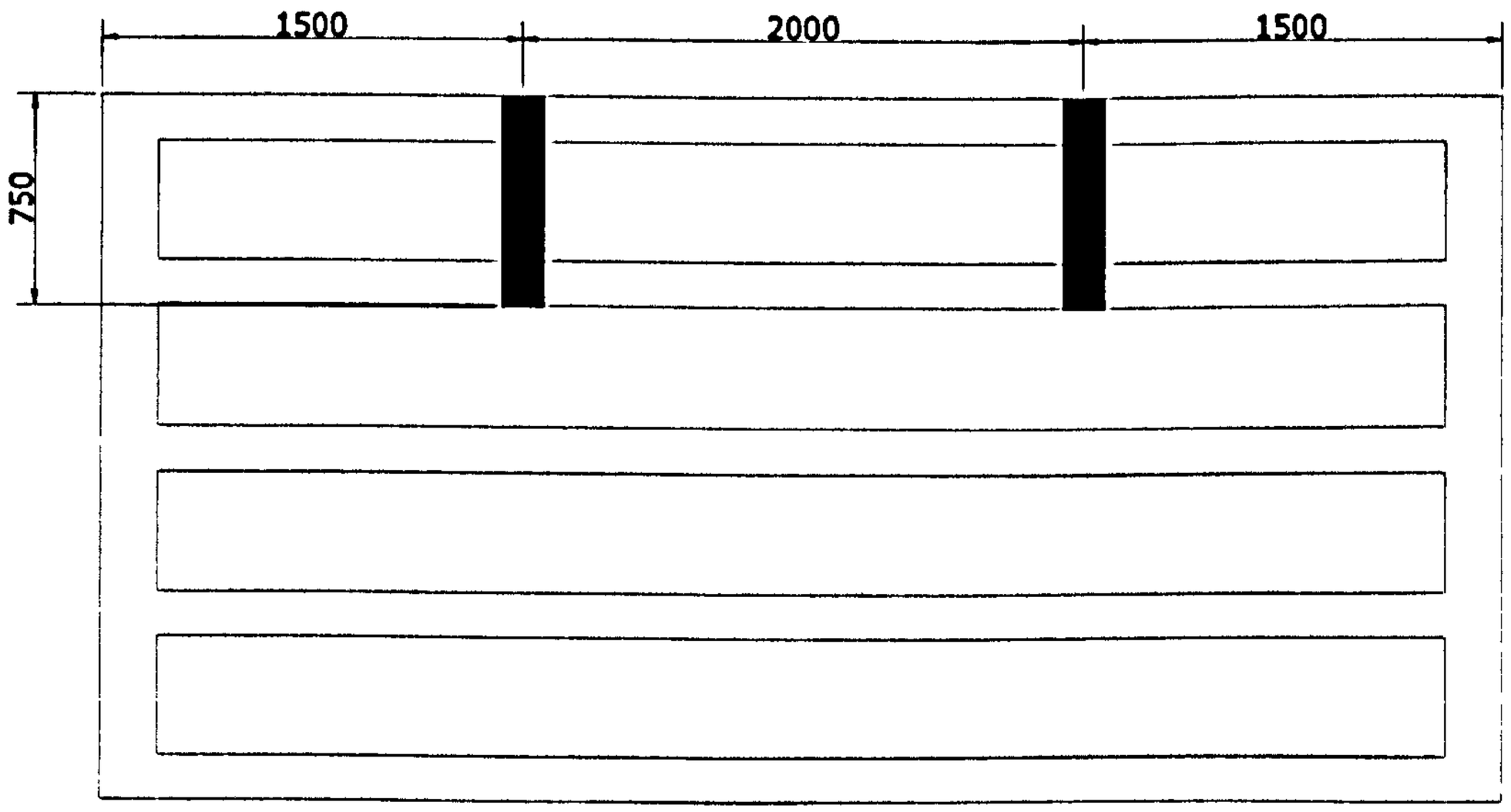

Figure 3-4: Arrangement of asymmetric loading regime

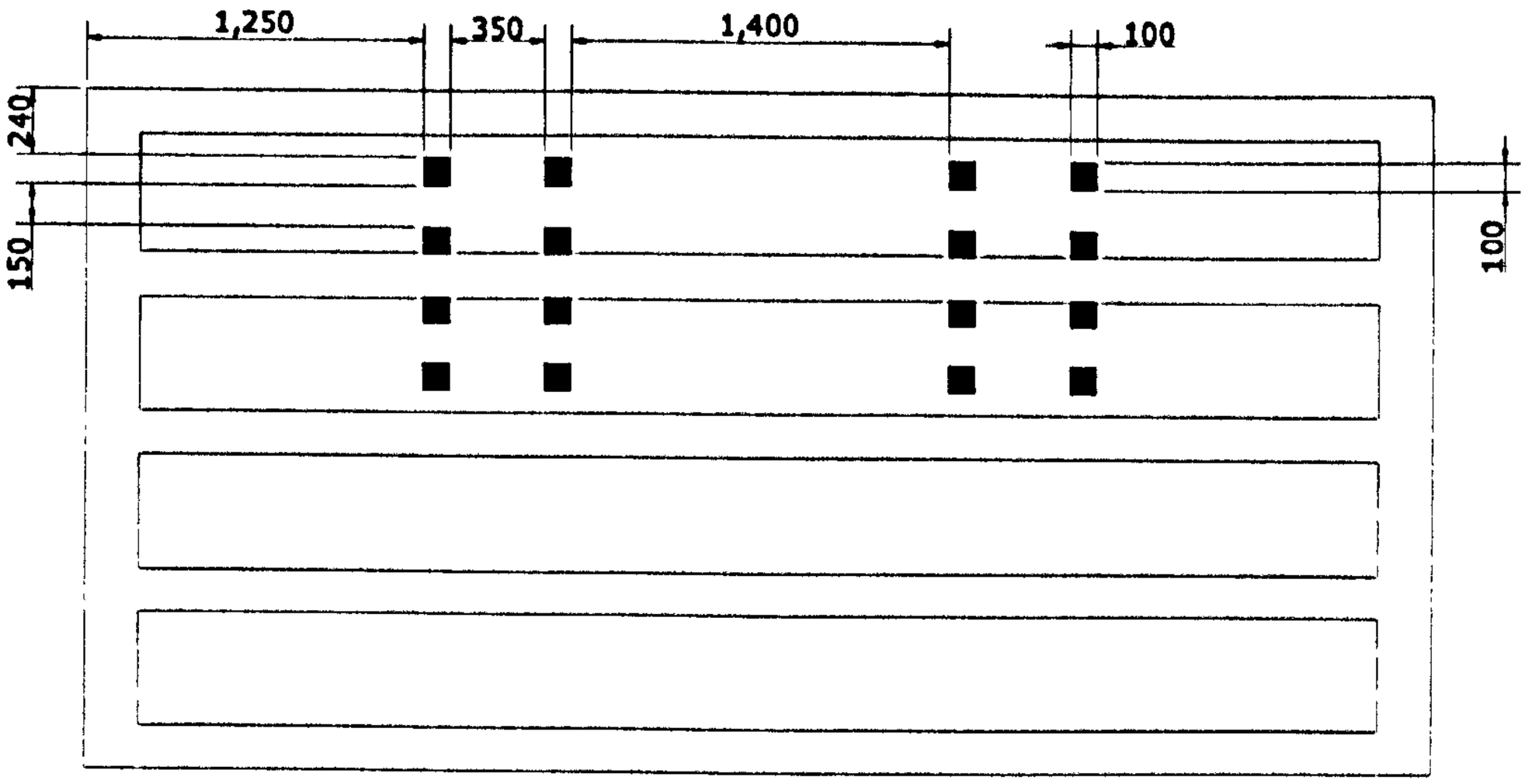

Figure 3-5: Arrangement of HB loading regime

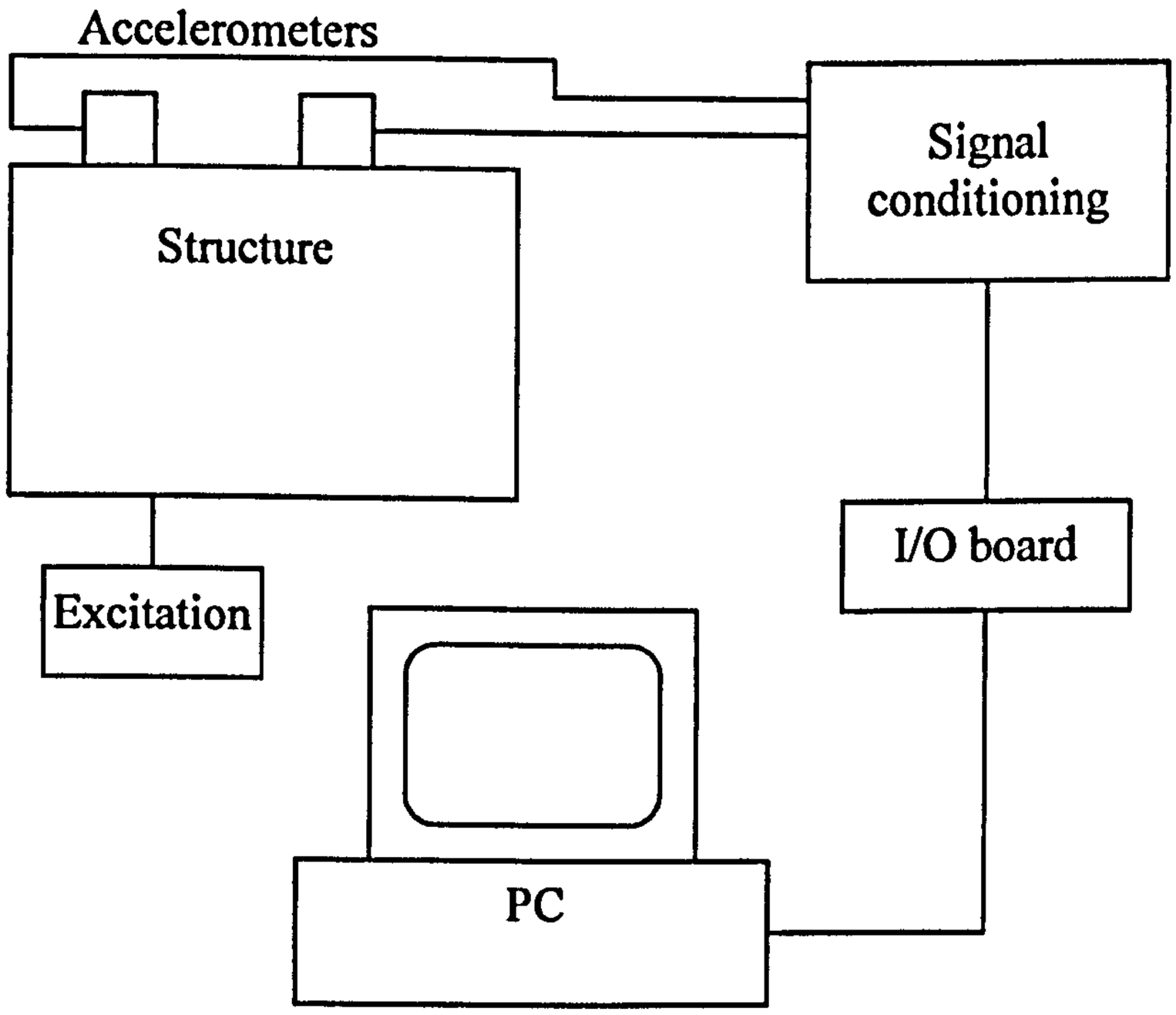

Figure 3-6: Schematic diagram of set-up for dynamic testing

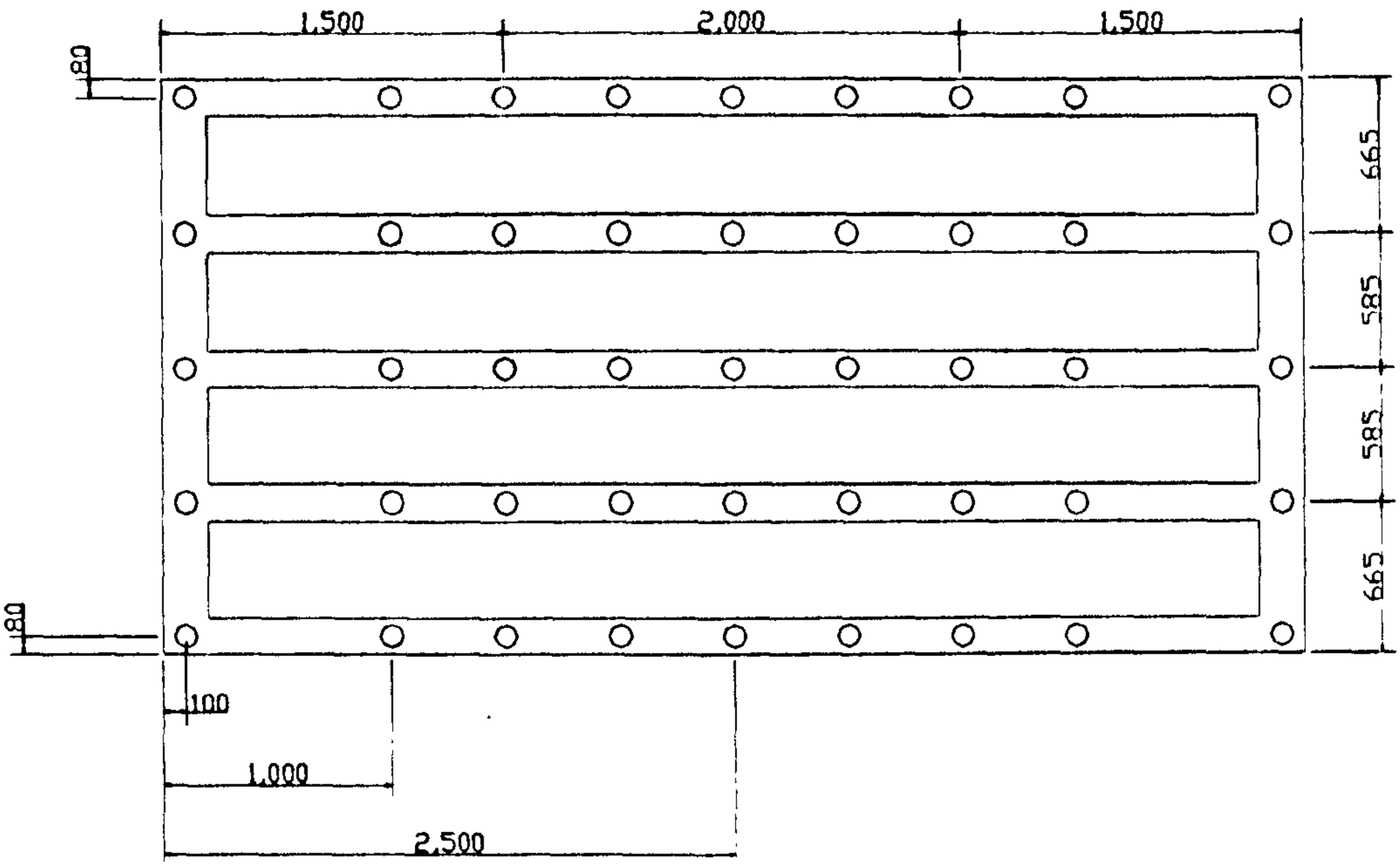

Figure 3-7: Location of accelerometers

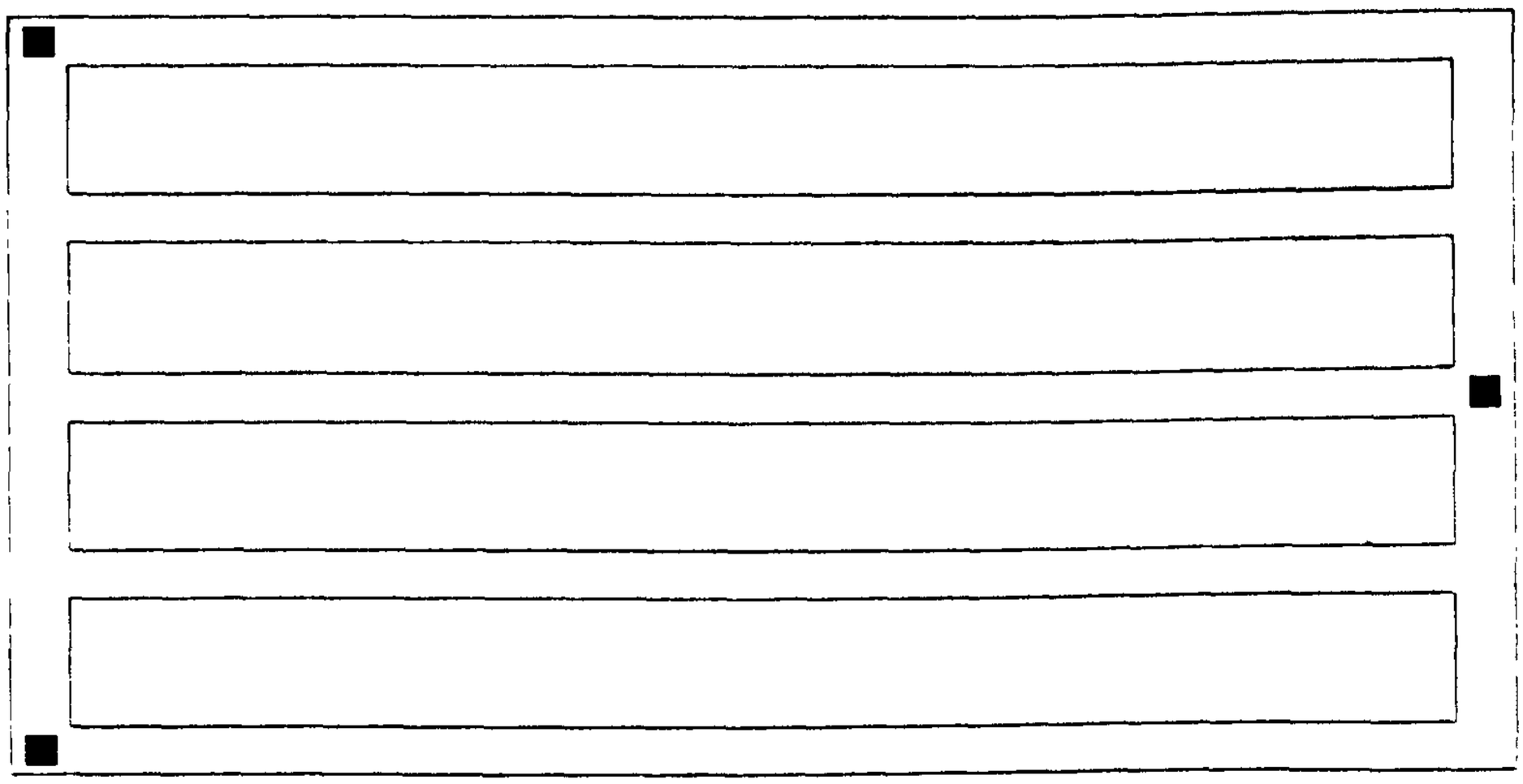

Figure 3-8: Location of supports when using three bearings

Table 3-1: Details of the concrete mix used

	SSD weights per m^3
Cement (class 52.5N)	425kg
Grade M sand	750kg
6mm aggregate	1130kg
Admixture (Sikament FF)	6.4kg
Water	183kg
a/c ratio	4.42:1
w/c ratio	0.43
s/a ratio	0.4
6mm/a ratio	0.6
admixture (Sikament FF)	1.5% by w.c.
Nominal plastic density	2494kg/m^3
Nominal workability (slump)	100mm
Nominal 28 day cube strength	65N/mm^2
Actual 28 day cube strength	61.9N/mm^2

Table 3-2: Reinforcement details

	Type A Longitudinal beam	Type B Longitudinal beam	End beam	Slab
Bottom	2T20	2T20	2T20	A142 mesh
Top	2T10	2T10	2T10	
Shear	R8 @ 150c/c	R8 @ 800 c/c	R8 @ 600 c/c	

Cover to all reinforcement = 15mm

Table 3-3: Details of the testing performed on each deck (* indicates altered loading arrangement)

			Mode shapes			
			Ten steel bearings		Three steel bearings	
Deck	Type	Loading	Hammer	Shaker	Hammer	Shaker
1	A	symm	Y	N	N	N
2	A	symm	Y	N	N	N
3	A	asymm	N	N	N	N
4	B	asymm	N	N	N	N
5	B	asymm	N	N	N	N
6	B	symm	Y	Y	Y	Y
7	B	symm	N	Y	N	Y
8	A	symm	N	Y	N	Y
9	A	HB	N	Y	N	Y
10	A	HB*	N	Y	N	Y

Table 3-4: Details of the dynamic testing equipment

Instrumentation	Manufacturer	Type	Sensitivity
Signal generator	Thurlby Thandar Instruments	TGA 1230	
Electromagnetic actuator	Ling Dynamic Systems	V406	
Force transducer	PCB Piezotronics	M221B02	52.9mV/lbF
Impulse hammer	Kistler	9728A2000	220mV/N
Accelerometers	Kistler	8630C5	1000mV/g
	Kistler	8702B50	100mV/g
Signal conditioning	Kistler	5134	

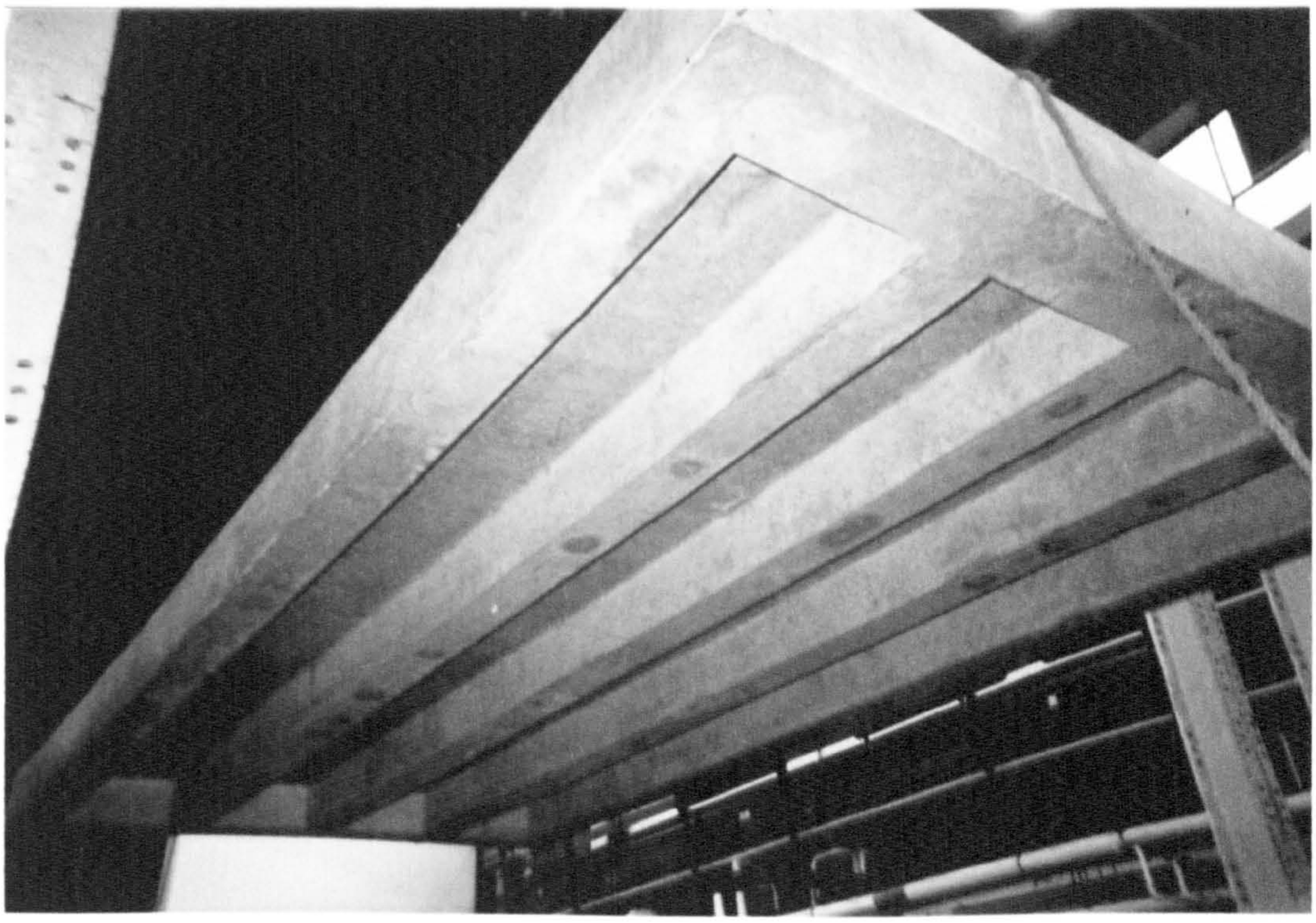

Plate 3-1: Underside of the model scale bridge deck

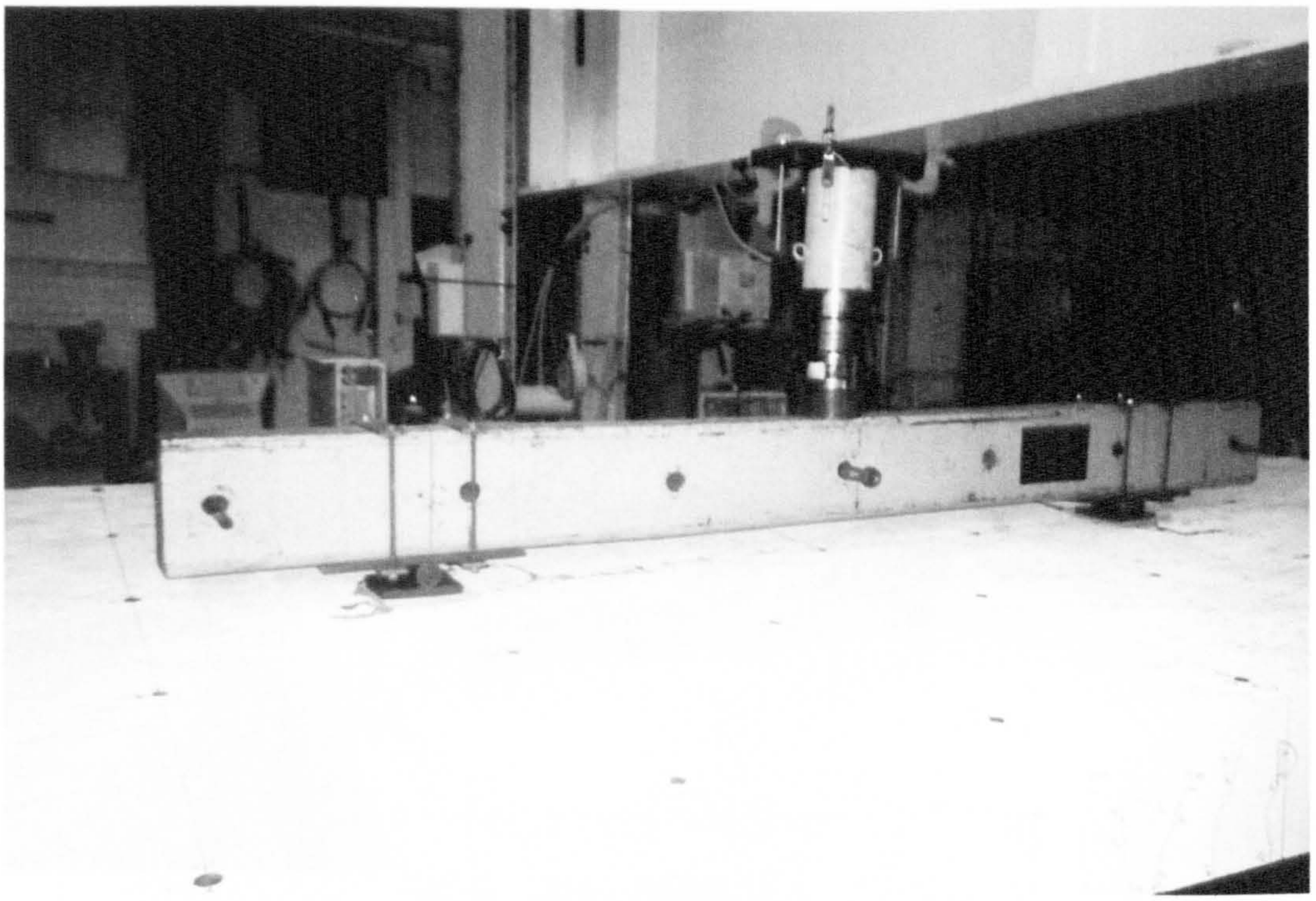

Plate 3-2: Symmetrical loading arrangement

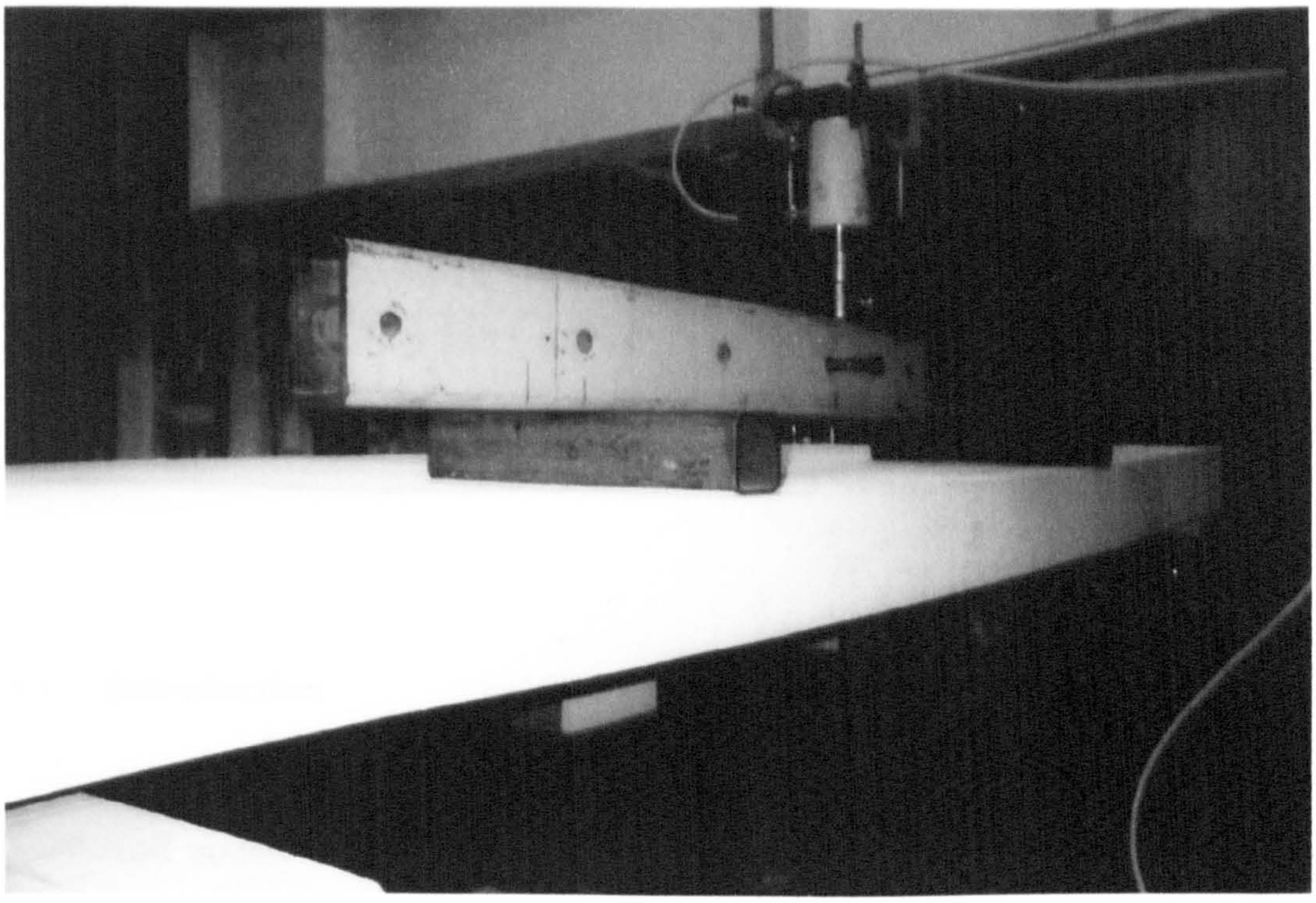

Plate 3-3: Asymmetrical loading arrangement

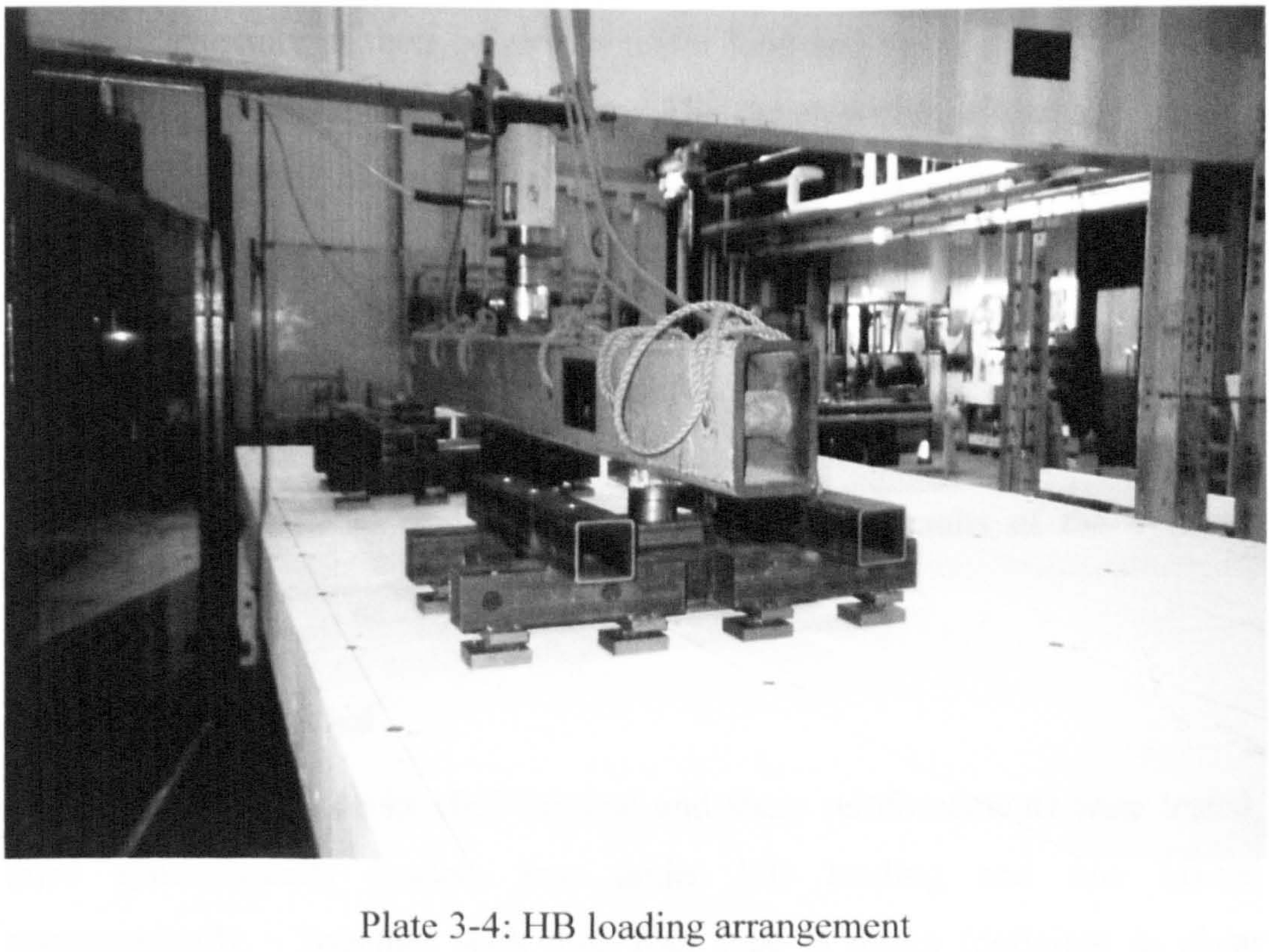

Plate 3-4: HB loading arrangement

CHAPTER 4

STATIC TESTING RESULTS

4.1 Introduction

This chapter provides a description of the testing of ten one-quarter-scale reinforced concrete beam-and-slab bridge decks under static loading. These tests were performed as a part of the investigation into the vibration characteristics of progressively damaged reinforced concrete bridge decks by facilitating a study of their behaviour under load and the cracking and failure mechanisms produced by overloading. The development of damage through the loading applied is categorised to facilitate a better understanding of the dynamic testing results by considering the effects of cracking types on the vibration characteristics of the decks. Details of the specimen design and test selection can be found in Chapter 3, whilst a discussion of the results of the dynamic testing of these specimens is given in Chapter 5. Chapter 6 details the application of finite element model updating to the results of the dynamic testing of these specimens.

4.2 Tests performed

In total, six type A decks (full flexural and shear reinforcement) were tested, three symmetrically loaded, two under HB loading and one loaded asymmetrically. Together with this, four type B decks (deficient in shear reinforcement) were also tested, two under symmetric loading conditions and two under asymmetric loading.

As stated previously, the decks were loaded in an incremental regime, as the dynamic properties were measured at certain stages throughout the deck's life. This allowed the crack development to be marked on the deck after each major

load increment and the damage to failure recorded. During each of the major load increments, the deflection was measured at the mid-span of the deck for each beam at smaller intervals.

The results of the loading will be discussed in the following sections, separated by the loading regime used in each. The discussion will concentrate on two main aspects of the static testing, namely the load-deflection behaviour and the crack development, whilst examining the nature of the progressive failure of the decks.

For the purposes of this testing, the longitudinal beams of the deck are denoted by Roman numerals for identification, as shown in Figure 4-1. A summary of the type of deck, loading regime and failure load is given in Table 4-1, together with the load levels applied to the decks in Table 4-2.

4.2.1 Initial deck condition

Initially, the decks displayed some cracking due to self-weight and shrinkage, in the form of small vertical cracks in all beams extending approximately 50-100mm. Some decks also displayed shrinkage cracking in the corners of the deck in the slab around the mesh reinforcement. This damage did not appear to be major.

Some decks also showed signs of plastic settlement. This took the form of small cracks above the reinforcement locations in the surface of the slab above the longitudinal beams. This would be due to the specimens being taken out of the moulds before the concrete had reached sufficient strength. It was also the case that several of the decks had a slight misalignment in the horizontal plane, where two opposite corners were higher that the other two. This meant that when the decks were supported on ten bearings, some needed to be packed with thin pieces of steel to ensure full contact between the support and the deck.

For all decks, each individual load increment appeared to cause a specific type of damage to be observed. This took the form of a significant amount of damage of certain types developing during the load increment, with only a

small increase in other types of damage. These stages of damage appeared to be very distinct, as discussed in the following paragraphs.

4.3 Symmetrical loading

This type of loading involves applying two point loads on the central beam (beam iii) to give a pseudo four-point bending set-up and symmetrical damage of the deck. More details of this loading regime are given in section 3.5.1.

The rationale behind loading the decks under symmetric conditions is to improve the understanding of the behaviour without complicating the results. It was anticipated that this type of loading would induce symmetric damage to the deck and allow the dynamic behaviour to be related to the damage without causing significant changes in the mode shapes produced. It was also thought that the results from this testing could be related more easily to the previous studies performed on beams.

In the following sections, the results of the application of this type of loading are discussed in terms of the load deflection behaviour and the development of cracking, together with some explanation of the results observed. This is done for both types of deck and the differences between their behaviour highlighted in the text.

This type of loading was applied to decks 1, 2, 6, 7 and 8. Decks 1, 2 and 8 are type A, whilst decks 6 and 7 are type B.

4.3.1 Crack development – Type A

As described above, the deck showed some signs of cracking before any additional load had been applied. At a load of 50kN, the initial vertical cracks grew and new cracks appeared, extending to a height of 50-150mm in the beams, which was comparable for each of the five beams. This type of damage could be termed beam flexure.

Further loading to 100kN caused the growth of this vertical cracking to approximately 170mm. At this load level, a longitudinal crack appeared along the shoulder of the central (loaded) beam in the soffit of the slab on both sides of the beam, extending for almost the full length of the deck. This damage can

be named transverse bending of the slab. This load level also promoted the development of small shear type cracks at the ends of the outer beams (i and v).

Increasing the load further to 150kN saw the vertical cracking grow to 200mm, and occupy the full height of the longitudinal beams, although this cracking did not extend into the soffit of the slab. Torsion type cracking also appeared at the ends of beams ii and iv. Shear type cracking also began to form at the ends of the central beam. At this load level, there was a difference of approximately 3.5mm in deflection between beam iii and beams ii and iv, causing the end beams of the deck to develop torsion cracking due to the deflection of the deck under the load accompanied by cracking at the ends in the top surface of the slab.

At a load of 200kN, there was very little growth in the existing cracks with only a small number of new cracks appearing in the deck.

Loading further to 250kN, the vertical cracks grew into the soffit of the slab and a number of radial cracks appeared. These radial cracks in the soffit between beams iii – iv and iii – ii emanated from the loading points and extended towards the corners of the deck, beginning the formation of a classic yield line pattern for slab failure. A longitudinal crack appeared approximately 150mm from beam iii in the soffit of the slab between beams iii and ii, extending for a distance comparable to the loaded portion (2m). The cracking in the top surface grew and spread towards the edges of the deck.

At a load of 300kN, the radial cracking in the soffit of the slab had extended to all of the deck. The shear cracks in the central beam were now significantly developed, and the torsion cracking in the adjacent beams had grown. A crack 200mm from the central beam in the soffit between beams iii and iv appeared and extended along the loaded portion of the deck (comparable to the crack at the previous load level). Four cracks appeared in the top surface, approximately symmetrical about the central beam, along the inside edges of the beams (i, ii, iv, v).

The deck was then loaded to failure, and the cracking patterns of deck 1 at 210kN is given in Figure 4-2 and decks 2 and 8 just prior to failure are given in Figure 4-3 and Figure 4-4. These figures display the deck as a development.

The ultimate failure of the deck was due to a shear type of failure in the central beam, Plate 4-1, and took the form of a combined bending and shear bond failure. Failure of the longitudinal beams caused the central beam to separate from the remainder of the deck, Plate 4-2 and Plate 4-3, creating a shear failure of the slab at the shoulders of the central beam, accompanied by cracking along the centre-line of the central beam on the top surface. The cracking on the top surface of the slab involved the growth of two new longitudinal cracks in the middle of the slab section between beams ii – i and iv – v. Transverse cracking also appeared on the top surface at the edge of the deck between beams ii – i and iv – v. The torsion type cracking in the end beams was significant.

4.3.2 Load deflection behaviour – Type A

The plots of load against mid-span deflection for decks 2 and 8 are shown in Figure 4-5 and Figure 4-6, respectively. This shows the total load plotted against the deflection measured at the mid-span of each of the five longitudinal beams. No deflection measurements were taken for the first deck, although from inspection of the cracking pattern produced it is clear that similar deflections to the other decks would have been obtained.

For deck 2, the deflection was not measured until the deck had been loaded to 100kN and the graph has been started with zero permanent deflection at this load level. Comparison with the results from other decks indicates that the permanent deflection at 100kN would cause the results to be in error by approximately 4.5mm. As with all the decks tested, the instrumentation measuring deflection was removed when 90mm of movement was recorded to avoid damage to the instrumentation. Therefore, in many cases, there is no measurement of the deflection as the deck failed.

The plots show that, as expected, the central beam (beam iii) deflects most as this is directly under load, and the other beams deflect less the further away from the load. These outer beams also behave in an almost identical manner, with approximately equal deflections. However, at higher loads, the deflected shape appears to lose the symmetry displayed at lower loads. This is most significant for the outer beams (i and v).

The first load increment displays the expected non-linear behaviour, typical when loading reinforced concrete. It is also apparent that subsequent applications of load display a generally linear relationship between load and deflection until the level of the previous load is reached, after which the curve appears to be a continuation of the previous trend. This shows that as the damage evolves, it causes a loss of the static stiffness of the deck.

It is possible to observe when the longitudinal cracks in the top surface of the slab and the longitudinal cracking at the shoulders of the beams occur by looking at the load against deflection plot. It can be seen that there are several sharp changes in the curve for the outer beams (i, ii, iv, v) as the load increases and an apparent reduction in the deflection of the beams. This occurs most noticeably when the deck is near to its failure load and the cracks in the top surface develop suddenly. As the load on each individual beam were not measured, it is unclear as to whether this is due to an actual reduction in the deflection or, as is more likely, the cracking has caused the load on the beam to reduce, thereby reducing the deflection. If a graph of the load on each beam were plotted against its deflection, this would be clearer.

The graphs show that even though the failure is in the form of a combined bending and shear bond type, the behaviour prior to failure shows significant ductility, with ultimate deflections approaching 60mm for the central beam.

The theoretical stiffness of the deck has been calculated (see Appendix C) and is plotted on the load deflection graphs. This allows some measure of the load distribution to the individual longitudinal beams to be found. From the values of the gradients, Table 4-3 and Table 4-5, it can be seen that the load is almost symmetrically distributed across the deck. Approximate values of the load on each individual beam have been calculated based on the assumption that the load taken by each beam is proportional to the resulting deflection. These are shown in Table 4-4 and Table 4-6, where it can be seen that the loads are symmetrical, as would be expected. It is also who noting that the maximum load applied to the failed beam is similar in both cases, although this is not equal to the actual failure load of the beam due to several assumptions made in obtaining this value.

It should also be noted from these plots that there is a noticeable reduction in flexural stiffness of the deck between each load step. This further reinforces the hypothesis that the natural frequencies should be able to detect a change in the condition of the structure, as they are related to the stiffness.

4.3.3 Crack development – Type B

In general, the loading of this type of deck produced similar cracking to that when loading a type A deck. However, due to the reduction in shear capacity and the dependency of the failure mechanism on the amount of shear reinforcement, this cracking developed slightly differently.

Both decks showed a considerable amount of cracking due to plastic settlement, particularly at the ends of the central beam. This cracking was more severe in deck 6 than 7.

Applying a load of 50kN to the deck caused the growth of a number of new vertical cracks, and an extension of the existing cracking to a height of approximately 100mm of the longitudinal beams. There was very little cracking towards the ends of the beams within 700-1000mm from the end of the deck. This load level also saw the development of a longitudinal crack along the outside shoulder of beam iii.

Further loading to 100kN led to the extension of the vertical cracking to a height of 150mm in the beams, and also caused the formation of shear cracking in the ends of the central beam, and the development of torsion type cracking in the adjacent beams, ii and iv. A longitudinal crack grew along the inside shoulder of beam iii, creating a symmetrical cracking pattern.

Increasing the applied load to 150kN did not produce a significant amount of growth in the vertical cracking, which extended to approximately 170mm in height. However, towards the ends of beams ii and iv, the torsion cracking extended in places into the soffit of the deck towards the central beam. This load also caused the development of torsion cracking in the outer beams, i and v and the beginning of torsion cracking in the end beams between the longitudinal beams.

When the load reached 185kN, the vertical cracking in the longitudinal beams had grown to the full height of 200mm. The torsion cracking in the end beams had also increased significantly from the previous load level. The soffit of the deck also began to display cracking typical of a yield line mechanism. Radial cracking emanating from the loading points towards the corners of the deck at approximately 45° developed in all of the soffit sections between the longitudinal beams. In the surface of the deck, longitudinal cracks grew above the inside of beams i, ii, iv and v, extending to within 1m of the ends of the decks. Cracking also developed in the slab above the central beam on both sides for 750mm at each end of the deck, together with some cracking across the central beam.

The failure of the decks was in the form of a shear failure of one end of the central beam followed by the other end, causing the beam to separate from the slab part of the deck and the loading points to punch through the slab, Plate 4-4. The shear failure formed approximately 1m from the end of the deck, and was accompanied by a shear bond failure of the concrete at the bottom of the beams extending into the end beam, Plate 4-5 and Plate 4-6.

The end of the deck failing in shear was also accompanied by the formation of transverse cracking due to a reversal of bending approximately 0.6m from the end of the deck.

At failure, a significant difference between the cracking in the surface of the decks can be seen by comparing the cracking patterns in Figure 4-7 and Figure 4-8. Deck 6 appears to have distributed the load to other parts of the deck through the slab prior to the failure of the central beam more effectively than deck 7. This can be seen in the number of longitudinal cracks that have formed in the top surface of the deck, Plate 4-7, although in both decks, the underside of appears to have developed the diagonal yield-line cracking to approximately the same degree.

4.3.4 Load deflection behaviour – Type B

The load deflection curves for decks 6 and 7 are given in Figure 4-9 and Figure 4-10, respectively.

Prior to the final load step, these two decks follow a very similar pattern in terms of their load deflection behaviour. Again it can be seen that the specimens follow the expected non-linear behaviour associated with reinforced concrete and there is a general reduction in static stiffness between each of the loading increments.

Using the measured gradients of the loading plots, Table 4-7 and Table 4-9, the load distribution across the decks can be inferred. The approximate load on each of the beams is shown in Table 4-8 and Table 4-10, where again it can be seen that the load distribution is approximately symmetrical, and the maximum load on the central beam at failure is similar in both cases. However, it should again be noted that these values are obtained using several assumptions regarding the loading and stiffness of the deck and are not equal to the actual failure load of the beams.

A small difference in the behaviour of the decks can be noticed from these load deflection plots in terms of the load distribution to each beam of the deck. It can be seen that the beams loaded directly appear to be less stiff in deck 6 than those in deck 7, whereas the opposite is true for the other beams. This can be explained by considering the amount of load that is taken by each beam, indicating that beams i and ii carry more of the load than beams iii, iv and v. This is confirmed by the cracking patterns produced, deck 6 exhibiting significantly more longitudinal cracking in the slab than deck 7 implying that the beams under direct load become increasingly more separated from the rest of the deck.

Although these were designed to be deficient in shear reinforcement, there is still some ductile behaviour prior to failure, especially when compared to a single beam with insufficient shear reinforcement, implying that there is a contribution to the shear capacity of the deck from the slab. This shows that there is significant redistribution of the load to the other beams in the deck leading to a progressive collapse. However, a major difference between these two decks is the amount of ductility exhibited.

It can be seen that deck 6 fails with a deflection of approximately 50mm, whereas deck 7 produces an ultimate deflection of 37mm. Most of this

difference in deflection occurs in the final load step. It is surprising that the more ductile deck fails at a lower load than the less ductile deck, 210kN compared with 235kN. This difference in the ductility of the structure can also be seen in the cracking exhibited by each of the decks as described in the previous section.

4.3.5 Explanation of cracking

The loading of the decks under this symmetric regime did, in general, result in symmetric crack development. However, although the deck behaved in a manner expected of four-point bending for low loads, there was significant distribution of the load through the slab to the outer beams, causing a number of different cracking types to occur. This highlights one of the major differences between testing beams and more complex structures, and is particularly important when considering the feasibility of dynamic testing for health monitoring, as discussed in the next chapter.

The development of several longitudinal cracks located above the beams was due to the fact that the beams are much stiffer in bending than the slab. The growth of these cracks caused redistribution of the load around the deck, as can be seen from the development of other cracking and the load deflection behaviour.

The torsion cracking towards the ends of the longitudinal beams forms due to the beams being effectively prevented from rotating at the very ends as a result of the connectivity with the end beams. The loading causes the outer beams to rotate, thereby causing torsion moments in the beams leading to spiral cracking near where they are restrained.

The torsion cracking in the end beams developed as a result of the differential deflection between the beams. This produces significant torsion in the end beams when the longitudinal cracking of the slab causes less load to be distributed to the outer beams. This increases the differences in the deflection of the beams, giving rise to torsion cracking of the end beams. Some decks also displayed cracking in the corners of the deck, which is an indication of significant torsion developing.

The development of longitudinal cracking in the slab between the central beam and those adjacent in the middle 2m of the deck is caused by the reduced ability of the slab to distribute the load to other beams after the formation of the cracking in the top surface. This section of the deck is loaded with the highest bending moment and the cracking allows the difference in deflection of the beams to increase to a point where the central beam fails in shear and separates from the rest of the deck.

The transverse cracking originating from the edges of the deck was an extension of the vertical cracking in the outside beams. Upon further investigation, it was discovered that this cracking in the top surface occurred directly above the transverse layer of the mesh reinforcement in the slab. The development of this type of cracking could be due to a number of factors associated with the excessive deflections produced.

The cracking may have occurred due to the large deflections causing the mesh to buckle, setting up bursting forces within the slab and causing the concrete to crack. Another cause of this cracking could be compressive membrane action. When a slab between T-beams is loaded the beams restrain the slab, which induce compression forces in the slab. At a certain load, known as the enhanced ultimate load, the confining concrete begins to crush and the load drops. At this lower load, the membrane forces change from compressive to tensile and the load increases, if enough tensile reinforcement is present, to reach ultimate load when reinforcement yields or fractures. Hon, A. et al (2001) state that tensile membrane action is only useful in preventing catastrophic failure. This is also probably the cause of the diagonal cracking in the corners of the slab.

The transverse cracking may also be the growth of existing cracks that formed due to plastic settlement but were too small to observe or were internal in the concrete until the deflection became large and caused them to open. In a few decks, some transverse cracking in the underside of the slab can be seen in the initial condition.

Although the deck was designed to fail in bending, the actual failure mechanism was a shear failure of the loaded beam. However, the development

of the crack pattern displayed predominantly flexural damage until the final load level, as can be seen by the development of a classic yield-line pattern.

Although a yield-line develops, there appears to be a significant redistribution of stresses as the deck is loaded to failure. Therefore, the yield-line analysis is not for the actual failure mechanism, as the deck appears to suffer from a progressive failure, i.e. one failure mechanism develops and fails, then the stresses redistribute to cause another failure mechanism to develop etc.

When the deck contained a deficiency in shear reinforcement, it was apparent that the same forms of cracking developed. However, due to the lower load capacity of the deck, the cracking was not able to develop to the same extent as in the fully reinforced decks.

4.4 Asymmetrical loading

This type of loading involves applying two loads to two outer beams (beams i and ii) to promote a failure of two beams simultaneously and asymmetrical damage to the deck. More details of this loading regime are given in section 3.5.2.

The rationale behind loading the decks under asymmetric conditions is to encourage the development of significant types of cracking other than those due to bending alone. This type of loading was anticipated to induce a large amount of torsion damage to the deck whilst causing considerable damage to two beams. This allows the dynamic behaviour to be investigated for other types of cracking. It is also the case that the overloading of one side of the deck is more likely to be representative of actual damage to a bridge. More details of comparisons with actual damage are presented in section 4.6.1.

This section also contains the results from the application of Highways Agency type B (HB) loading to two decks. This is discussed in more detail in section 3.5.3, but is included in this section as the behaviour under this loading is similar to the asymmetric regime. The results from this loading will give a more realistic damage pattern, without the simplifications of the asymmetric loading.

In the following sections, the results of the application of these types of loading are discussed in terms of the load deflection behaviour and the development of cracking, together with some explanation of the results observed. This is done for both types of deck and the differences between their behaviour highlighted in the text.

Asymmetric loading was applied to decks 3, 4 and 5, whilst HB loading was used for decks 9 and 10. Decks 3, 9 and 10 are type A, whilst decks 4 and 5 are type B.

4.4.1 Crack development – Type A

The initial condition of the decks is described in section 4.2.1. Upon loading the deck to 50kN, the major growth of cracking took the form of increasing the height of the existing cracks to approximately 100m in beams v, iv and iii, and 150mm in beams i and ii. There was also an increase on the number of cracks visible, although very little cracking was apparent within 500mm of the ends of the deck.

Further loading to 100kN saw an increase in crack height of approximately 50mm and again several new cracks developing. Increasing the load to 150kN produced very little growth of the existing cracks, although a number of new cracks appeared. At this load, a longitudinal crack in the soffit of the deck between beams i – ii and ii – iii developed. A crack between the soffit and the outside (S) of beam ii also grew along the length of the deck.

At the next load level, 200kN, the vertical cracking in beams v and iv grew to 170mm, whilst the remainder of the beams displayed cracking over their full height and into the soffit. A small amount of torsion cracking developed in the end beams between beams ii – iii and iii – iv. This load also caused a longitudinal crack to grow in the top surface of the slab along the inside (N) edge of beam iv, indicating that the load is approximately evenly distributed between beams i, ii and iii.

Loading further to 250kN caused the torsion cracking in the end beams to develop further, although the major cracking was still in the same locations as the previous load level. A crack grew along the inside (N) shoulder of beam ii

(as this developed second, it shows that this side is more flexible than the other, which is logical as there is only one beam on this side) together with the development of another longitudinal crack in the top surface along the outside (S) edge of beam ii in the middle section extending to 1m from the ends of the deck. The development of radial cracking towards the ends of the deck in the soffits between beams i – ii and ii – iii also began at this load level, joining with the longitudinal cracks that formed under a load of 150kN.

At a load of 300kN, there was significant growth of new longitudinal cracking in the top surface of the deck in the form of a crack above the inside edge of beam v and two cracks adjacent to the existing longitudinal crack above beam iv. This was also accompanied by more cracking towards the ends of the deck, together with torsion cracking in the end beams. In the underside of the deck, several new areas of cracking developed beneath the loading points. In general, there was only a small amount of growth in the vertical cracking causing most to cover the full height of all beams, although the shear and torsion cracking developed further towards the ends of beams ii and iii.

The failure of deck 9 was in the form of a torsion failure of beam iii, Plate 4-8, and the cracking pattern just prior to this can be seen in Figure 4-12. Both decks 3 and 10 were deemed to have failed due to excessive deflection, Plate 4-9 and Plate 4-10, when it was not possible to apply more load, however, both decks had developed significant torsion cracking of beam iii, Plate 4-11 and Plate 4-12, indicating that the ultimate failure would occur in this beam, as can be seen in the cracking patterns given in Figure 4-11, Figure 4-13 and Plate 4-13. Significant cracking in the slab had developed at this stage both in the top and the underside.

4.4.2 Load deflection behaviour –Type A

The load deflection plots are shown in Figure 4-14, Figure 4-15 and Figure 4-16 for decks 3, 9 and 10, respectively. From these graphs, it can be seen that the behaviour of these three decks is similar. However, it is also noted that there is a difference between those loaded using a HB and an asymmetric arrangement, apparent in both the ultimate load attained and the corresponding deflections.

Comparing the two loading arrangements, the load at which the longitudinal cracking occurs and the ultimate failure load appear to be related and are consistently 7-8% higher for the HB arrangement compared to the asymmetric loading. Whilst it was not possible to obtain measurements of the ultimate deflection for deck 3, by extrapolating the curves, it can be seen that this produced a significantly more ductile failure.

A major difference between the two loading arrangements is in the load distribution between the beams. As the HB loading was applied symmetrically about beam ii, both beams i and ii deflect by similar amounts due to the fact that beam i is less stiff than beam ii as there is no restraint. In the case of the asymmetric loading, beam i consistently deflects more than beam ii, even though both should be subjected to the same load.

From the load deflection plots, it is possible to draw some conclusions regarding the beams that were loaded directly and those that were not. It can be seen from a comparison between decks 9 and 10 and deck 3 that the beams i and ii deflect by a greater amount in deck 3, and beams iii, iv and v deflect less. In terms of the load distribution, this indicates that the asymmetrical loading arrangement used for deck 3 causes the two beams to separate from the remainder of the deck by a greater extent.

The gradients of the loading curves, Table 4-11, Table 4-13 and Table 4-15, are able to provide an indication of the distribution of load across the deck to each of the beams. The calculated approximate load distribution for decks 3, 9 and 10 are shown in Table 4-12, Table 4-14 and Table 4-16. From these values, it is possible to suppose that the load is distributed as would be expected, and also that the beams under or adjacent to the applied load carry most of the load. Comparing the loads at failure again reveals that the beams carry similar loads, and the values are comparable with those found under symmetrical loading.

The almost linear behaviour of beams iv and v implies that these beams do not suffer from a large amount of cracking as the load is applied and exhibit a smaller degree of hysteresis upon unloading, again suggesting only a small growth in cracking, due to the majority of the load being carried by beams i, ii

and iii. This is confirmed by the description in the previous section of the cracking patterns observed.

4.4.3 Crack development – Type B

Loading the deck to 50kN produced a growth in the existing cracking and developed new cracks that extended to a height of approximately 100mm in all beams. The number of cracks was similar in number for all five longitudinal beams even though the load was applied to one side of the deck.

Increasing the load to 100kN caused a growth of approximately 75mm in beams i and ii, and of 50mm in beams iii, iv and v. This load level also caused the development of a single longitudinal crack along the centre of the soffit between beams i and ii. The formation of shear cracking began in beams i and ii, and the development of torsion cracks began in beams iii and iv. This load step also saw the formation of torsion cracking in the end beams in the sections between beams ii – iii and iii – iv.

Further loading to 150kN saw the vertical cracking in beams i and ii grow to the full height of the beams, to 190mm in beam iii and almost no growth in beams iv and v. The vertical cracking in beams i and ii extended in places into the soffit and created diagonal cracking towards the ends of the deck in the soffit between beams i and ii radiating from the longitudinal crack that formed at the previous load level. Growth of the cracking in beam iv was in the form of torsion cracking towards the ends of the beam, which also occurred in beam iii. The torsion cracking that formed at the previous load level further developed in the end beams between beams ii – iii and iii – iv. In the surface of the slab, a single longitudinal crack formed above the inside edge of beam iii running almost the full length of the deck.

The failure of these decks was in the form of a shear failure occurring at only one end of beam i approximately 500mm from the end of the deck, Plate 4-14 and Plate 4-15. The shear cracking extended the full height of the deck and caused a small amount of separation of the beam from the slab locally. This shear failure was also accompanied by the expected shear bond failure at the bottom flexural reinforcement Plate 4-16 and Plate 4-17. Significant growth in the diagonal cracking in the soffit between beams i and ii was also observed.

Another longitudinal crack formed on the top surface of the deck above the inside edge of beam iv, extending the full length of the deck and joining with the torsion cracking in the end beams. Cracking also grew towards the ends of the deck joining the torsion cracking with the longitudinal crack from the previous load level and extending into other areas of the deck. The cracking patterns prior to failure can be seen in Figure 4-17 and Figure 4-18

4.4.4 Load deflection behaviour – Type B

The plots of load against deflection for decks 4 and 5 are given in Figure 4-19 and Figure 4-20, respectively. Both these decks were loaded using the same asymmetric arrangement and it can be seen that both attain very similar ultimate deflections and loads. Again, the behaviour is non-linear as cracking is introduced to the deck and almost linear to the level of the previous load where existing cracking is reopening.

A difference to note is that the apparent reductions in deflection due to longitudinal cracking do not appear in both plots. From the cracking produced, it is clear that the sharp change in deflection for deck 4 at a load of 155kN is due to the formation of a longitudinal crack at the shoulder in the outside of beam ii, which does not develop in deck 5.

It is interesting to note that the loading and unloading curves of beams iv and v suggest that they get stiffer at higher loads, which can be explained by considering the load distribution around the deck. The apparent increases in stiffness correspond to the appearance of longitudinal cracking in the slab of the deck, which causes the load paths to change altering the amount of load carried by each beam. The apparent increase in stiffness is therefore most likely to be due to a reduction in the load applied to the beam, rather than an actual increase in static stiffness.

Interpretation of the gradients of the load-deflection curves, Table 4-17 and Table 4-19, reveal an indication of the distribution of the applied load to longitudinal beams, as shown in Table 4-18 and Table 4-20. From the values of the approximate load distributed to each beam, it can be seen that that it is a similar pattern to the other asymmetrically loaded decks. It is worth noting, however, that the edge beam takes a larger proportion of the load than the type

A decks. Again, both decks show a similar load on the failed beams and comparable values to the other type B decks tested.

4.4.5 Explanation of cracking

The behaviour of the decks is highly dependent on the amount of shear reinforcement present in the longitudinal beams, which can be seen most clearly in terms of the ultimate failure. The decks that were fully reinforced failed in a manner consistent with a torsion failure of the central beam, whereas the decks with a deficiency in shear reinforcement failed due to a shear failure of the outer beam.

Prior to failure, several types of distinct cracking developed in stages, as was the case when the decks were loaded under symmetric conditions. The first type of cracking was due to flexure of the deck under loading. It is interesting to note that this cracking was mainly concentrated in the middle 3m of the deck and there was very little crack growth towards the ends of the deck until higher loads. This is consistent with the behaviour that would be expected from simple four-point bending of a beam.

The longitudinal cracking that formed along the shoulder and above the edge of the main beams in the slab was due to the difference in stiffness of these components. As the differential deflection between the beams increased, the low stiffness slab cracked to allow the deformed shape and load distribution to occur. As the capacity of the slab was nominally equal for all decks, the deflection at which this cracking developed was similar for all decks. However, a major difference between the longitudinal cracking in type A and B decks is apparent in their severity.

The very small growth in the vertical cracking in beams iv and v after the formation of the longitudinal cracks shows that these beams are only carrying a small portion of the total load, due to redistribution to stiffer areas.

Due to the lower capacity of the type B decks, much smaller loads and deflections were observed, thus not producing a large amount of differential deflection between the beams. This meant that the cracking was less severe,

and only developed in a small number of locations in the form of a single crack.

As expected, there was very little torsion cracking in the end beam between beams i and ii, as both beams were loaded simultaneously using the asymmetric arrangement, and beam i was more flexible as it is effectively an L-beam so could deflect by a similar amount to beam ii when loaded using the HB arrangement. In all cases, this led to the formation of a longitudinal crack halfway between beams i and ii in the underside of the slab that appeared to form a line of rotation at higher loads.

The torsion and shear cracking in the type A decks did not appear until the load was approximately 200kN, whereas in the type B decks this form of cracking was noted at 100kN. This was also the case for the torsion cracking in the end beams. This shows that the strength of the deck is extremely dependent on the beams behaving in a ductile manner by containing sufficient reinforcement to take advantage of the load carrying capacity of the slab through redistribution of loads.

The failure of the decks was very different, although similar types and stages of cracking were found for both type A and B decks. The failure of the type A decks was in the form of torsion failure in the central beam, whereas the failure of type B decks was due to shear cracking in beam i.

For the type A decks, it can be seen from the load-deflection plots that at failure, the slope in the transverse direction between beams ii and iv is approximately 3°, with a differential deflection of 60mm. This caused significant torsion forces in the central beam, which when combined with the applied shear force, produced considerable cracking and subsequent failure.

Due to the very large deflections of the type A decks at failure, several transverse cracks formed in the top surface of the deck and some diagonal cracking developed in the corners near beam v. The cause of this cracking has been discussed in the explanation of the cracking patterns of the symmetrically loaded decks in section 4.3.5.

4.5 Comparison between loading regimes

Under the symmetric, asymmetric and HB loading regimes, it was found that similar types of cracking developed. It was also noted that all the decks tested appeared to fail in a progressive collapse and there was significant redistribution of load causing a considerably higher ultimate failure load than would be expected for a T-beam bridge deck using theoretical calculations. The capacity of a single T-beam is calculated in Appendix B as 58.8kN.

The loading arrangements used appeared to cause the growth of distinct crack types during each load increment, due to flexure, shear and torsion. All the decks tested showed a degree of similarity in the longitudinal cracking, beginning with cracking along the shoulder of the beam under load and progressing to cracking in the surface of the deck in a wide arc around the loading points. This was accompanied by radial or diagonal cracking in the underside of the slab, originating from the loading points and extending towards the corners of the deck. The exact extent, severity and location of this cracking depended on the loading arrangement and the type of deck.

The four-point loading of the central beam produced a higher failure load than the asymmetric when applied to the type B decks, but similar loads were achieved when the type A decks were loaded. This appears to be related to the ability of the deck to transfer the load to the beams not directly under load.

The type B decks are not able to realise their full capacity due to the lower loads that each beam can sustain. The effect of this can be seen in the cracking patterns when loaded under asymmetric loading, where it is observed that the longitudinal cracking does not extend to the slab between beams iv and v, indicating that these two beams are not carrying much of the applied load. This implies that the deck cannot transfer load to the outer beam effectively. When the deck is loaded symmetrically, the load is distributed to all of the beams, giving a higher failure load.

It can be seen from the cracking patterns that the type A decks distribute the applied load to all beams, whether loaded symmetrically or asymmetrically. This is in contrast to the type B decks, that do not, in general, spread the applied load as effectively due to the lower shear capacity and hence lower

deflection of the individual beams. This transfer of the load to the beams not under direct load causes the failure loads of the type A decks to be very similar.

Significantly more cracking was observed during the testing of the type A decks under both loading regimes than type B, as would be expected from the smaller deflections and ultimate loads. This was particularly true for the cracking in the top surface and the diagonal cracking in the underside of the slab, and the transverse cracking at failure.

4.6 Real bridge damage

The deterioration of reinforced concrete bridges in the field has been the subject of several investigations. Ramey and Wright (1997) discussed bridge deterioration rates in terms of the durability performance, based on data available in literature and records of the Alabama Department of Transportation. From this data, it was stated that bridge decks deteriorated more rapidly than either the superstructure or substructure, and that bridge condition deteriorates with age in that older bridges deteriorate at a faster rate.

From a survey by the Organisation for Economic Co-operation and Development (OECD) conducted in 1992, the reasons for bridge closure in the UK were investigated and the frequency of occurrence estimated. It was stated that 40% of closures were due to structural inadequacy and 60% due to functional inadequacy, and further divided as shown in Table 4-21.

Cracking in concrete normally exhibits a wide variety of patterns, due to combinations of effects such as freeze-thaw damage, alkali-aggregate reactions, sulphate attack, drying shrinkage, thermal movement and corrosion of steel reinforcement, as well as the effects of externally applied loads. Some of this cracking indicates that the component is in distress, but many of the resulting cracks are of little structural significance if properly maintained (Hover, 1996).

Testing of bridge elements using non-destructive evaluation for integration into bridge management systems was discussed by Hearn (1996), in which the major areas for inspection were highlighted and possible tests indicated. Four categories were defined, tests for protection of elements, for vulnerability, for

attack and for damage. Within these categories, the cause of deterioration was indicated.

For reinforced concrete bridge elements, the aggressive agent or condition was mainly due to deicing salts, alkali-silica reaction (ASR), freeze-thaw and exposure to the atmosphere. These situations lead to deterioration of the bridge by causing corrosion of the reinforcing steel, evident by spalling, delamination, and cracking. A number of condition states for reinforced concrete beams and girders were illustrated to categorise cracking, disintegration at bearings, diagonal cracking at the stems and vertical cracking at mid-span.

A study of the bridges on the first section of the M1 opened in 1959 was conducted in 1997 by Wakeman (2001). It was found that many of these bridges were of a standard type, overbridges were uniform two-span reinforced concrete portal design, underbridges were either reinforced concrete portal frames or mass concrete three-pinned arches.

The condition of the structures was generally good, although a few highlighted concerns over durability. Recent coring produced strengths of 60Mpa. The absence of movement joints reduced the potential for leakage.

As was standard practice in the 1950s, the decks were built without waterproofing membranes, although these have subsequently been installed. However, the decks were exposed to de-icing salts, the worst areas affected are generally adjacent to low edges.

Large tapered concrete parapets were common, although no accommodation was made for movement from differential shrinkage or deflection in design and construction quality was variable. This lead to vertical cracking in the parapets, allowing water ingress causing corrosion of reinforcement and spalling concrete.

The portal structures generally incorporated a longitudinal construction joint, through which water has caused local corrosion of the bottom reinforcement and spalling of soffit concrete.

Environmental effects are the most common cause of deterioration in concrete bridges (Brown, 2000), namely reinforcement corrosion by chloride attack or

by carbonation, frost/freeze-thaw attack, sulphate attack and alkali-aggregate reactivity.

From the Maunsell report studying 200 bridges in 1989, it was found that 25 were in good condition, 114 were fair and 61 had serious defects. The most prevalent defect was inadequate reinforcement cover causing spalling or rusting, and concern was expressed regarding spalling due to corrosion from chloride attack even where the specified cover was maintained.

The observations of deterioration identified from this study were freeze-thaw damage noted particularly on parapet edge beams, minor impact damage on 18 bridges and crazing or cracking due to ASR. The commonest cause of cracking was early thermal movement or shrinkage, whilst 10 bridges had structural cracking. Minor honeycombing was frequent and was severe in one bridge. It was found that 75% of bridge deck joints studied leaked, and areas of abutments, piers and deck soffits below leaking joints became stained and contaminated with chlorides leading to severe reinforcement corrosion. Leakage and chloride contamination was also observed through some bridge decks even if decks waterproofed, which was most severe at deck joints and kerb lines. It was deduced that spray from traffic was a major source of chloride contamination, although a few bridges had uniform chloride concentrations, indicating possible chlorides in the original mix.

A study of the bridges in the Greater London area was carried out by Tajalli and Rigden (2000), using long-term inspection records collected by London Underground Limited and British Rail consisting of over 2500 observations in more than 60 years taken from over 400 bridges. The distribution of faults observed mainly from visual inspections show that 38% occurred in flexural members, whilst the lowest number was for expansion joints. This is most likely due to the types of bridges that were inspected as more than 240 of the 400 bridges comprised a single span. It was also found that nearly 450 of the 725 individual elements were constructed from in-situ concrete.

An almost equal number of the observations made were on structures exposed to mild or moderate conditions, with approximately one twelfth of this number in the severe exposure category. Analysis of 2536 observations showed that

hairline cracks were the most commonly noted fault, accounting for 33% (830 observations), with a total of approximately 1500 observations concerning cracking of various widths. Only 3.8% of the total observations found the element to be "defect free".

The defects were also rated according to the urgency of repair and compared with the exposure condition. For 4.3% of the hairline cracks, the repair urgency was shown to be "very significant", although "insignificant" and "serviceable" hairline cracks and cracks less than 1.5mm account for the majority of the data. Larger cracks (over 3mm) in the severe exposure condition totalled 8.4%, whilst severe spalling accounted for 12.5%.

However, only 4.7% of the observations recorded the cause of the deterioration, although it was stated that overloading accounted for 2.8%, impact damage 1.6% and early-age cracking 0.3%. A plot of the different types of defect against the age of the structure revealed that the number of small (less than 1.5mm) cracks falls with age, whilst the defects due to spalling increase. The number of larger cracks (greater than 1.5mm) appears to remain approximately constant, suggesting that the rate at which smaller cracks grow and the larger cracks develop to cause spalling is roughly similar.

The repairs carried out on the structures were also compared with the age of the structure, indicating that the maximum number of minor repairs is associated with structures of age 30-40 years and major repairs with 40-50 year old structures.

4.6.1 Comparison

Contrasting the type of damage induced in this testing with that experienced by actual bridges leads to some interesting conclusions. It is clear from the previous section that the major cause of reinforced concrete bridge deterioration is due to chemical processes arising from chlorides and alkali silica reaction, and from physical processes due to freeze-thaw damage. A significant proportion of deterioration arises from a decline in the condition of the bearings and joints. Approximate figures of 5-10% of bridges suffer from damage in the form of structural cracking.

The extent of cracking in bridges was specifically studied by Tajalli and Rigden (2000). Whilst the origin of the cracking was not specified in the majority of cases, it is apparent from other studies that much deterioration in bridges is due to chemical and physical processes. It would therefore appear that the damage caused in the laboratory testing is not representative of the deterioration that would be exhibited by a real bridge.

However, it can be seen that cracking is present in most bridge structures, and a large number of the elements inspected were flexural members, likely to have suffered from flexural cracking. This suggests that the cracking introduced through overloading is representative of at least some of the cracking found in real bridge structures, even though the cause may not be the same. It is also apparent that hairline cracks develop at an early age and develop into larger cracks, which in turn progress to cause spalling of the concrete. Therefore, it is advantageous to detect any cracking as early as possible, before it develops into a serious defect, regardless of the cause of deterioration.

When considering the prerequisites for most of the more common deterioration mechanisms, cracking is often necessary, such as in the case of freeze-thaw action where water penetrates cracks and subsequently freezes. It is also possible that deterioration from chemical or physical processes would lead to structural cracking, in turn causing a reduction in the remaining life of the bridge. The consequences of structural cracking developing and the bridge not being repaired could lead to considerable maintenance work being required in the future or even collapse of the bridge.

Therefore, in order to ensure that the deterioration rate is controlled, it is essential to determine the extent of cracking exhibited by a bridge, as this is often an important factor, although this cracking does not have to arise due to structural distress.

4.7 Yield line analysis

The static behaviour of the deck as it was overloaded produced a yield-line pattern of cracking often seen for slabs. The following section describes the application of yield-line theory to the decks tested in the laboratory under symmetric loading.

The cracking pattern described in section 4.3.1 is typical of a reinforced concrete slab failing by forming yield-lines. For the application of yield-line analysis, the cracking is to be approximated to that shown in Figure 4-21. It should be noted that this is not the same as the cracking pattern observed at complete failure due to the fact that the deck appeared to fail in a progressive collapse manner. This means that a yield-line pattern will develop and fail, then the stresses will redistribute to form another pattern that will fail and redistribute the stresses again until ultimate failure.

The yield-line pattern to be analysed is that which is observed to develop first, as it is not possible to accurately analyse the progressive collapse of the deck due to the fact that a yield-line pattern gives an upper-bound solution. It is therefore required that the yield-line pattern giving the lowest failure load is found, which in this case will be one of the initial stages in the progressive collapse. It should also be noted that the final failure of the deck was not due to a yield-line failure, but a shear failure of the central beam.

A major criterion for the application of yield-line analysis is that the reinforced concrete should display sufficient ductility to allow the use of plastic methods. From the measurements of deflection, it is clear that there is considerable ductility in the behaviour of the deck prior to failure, and that the application of plastic theory is valid.

The load calculated for this mechanism is 293kN (see Appendix D). This value is significantly lower than the failure loads observed in the laboratory testing, which may be due to several reasons, such as membrane action and the steel reinforcement. It has been suggested by Moy, S.J. (1996) that an increase of 30% in the calculated value due to membrane action and a further 10% due to the contribution from the strain hardening of the reinforcement can be expected. The effects of compressive membrane action have also been investigated by Hon, A. et al (2001) for reinforced concrete T-beam bridge decks in flexure. Compressive membrane action (arching) occurs as a result of in-plane restraints that restrict the horizontal expansion of the bridge deck as it deflects vertically. This induces a compressive force within the deck, enhancing the stiffness and ultimate flexural strength. Compressive membrane

action arises in two situations: transversely across the deck due to the stiffness of T-beams and adjacent panels; end conditions giving longitudinal action.

Taking these two factors into account, the calculated value could increase by approximately 33%. This means that the value for the failure load that was calculated by yield-line analysis could be increased to give a value of 389kN. This is almost the same as the failure loads measured in the laboratory testing. However, the yield-line pattern investigated here is not the final cracking pattern that developed so it is probable that the load calculated should be lower than that observed in the laboratory. This is due to the amount of redistribution of load that occurs as the cracking develops.

4.8 Conclusions

The static loading of the decks was performed as a part of the investigation into the feasibility of using dynamic testing as a structural health-monitoring tool. The main objective of loading the decks was to introduce damage in a controlled manner so the vibration characteristics could be investigated for different levels of cracking.

Three loading regimes were used to promote the growth of certain types of cracking and investigate the static behaviour of the decks as described above. The main conclusions of this study are:

- The different loading regimes produced distinctive cracking patterns and load-deflection curves
- The different types of cracking appeared to grow in several stages, indicating that the deck failed in a progressive collapse
- There is a general reduction in static flexural stiffness as the load increments are applied
- The slab of the deck contributed significantly to the ultimate load capacity and ductility by spreading the load applied to all the longitudinal beams

- The behaviour of the type A decks was considerably more ductile than the type B decks, although some ductility was exhibited by the type B decks due to the slab
- Type A decks exhibited cracking consistent with flexural failure of the beams until application of the final load increment, when failure was by shear, torsion or excessive deflection
- Type B decks displayed some flexural cracking, but ultimate failure was due to insufficient shear reinforcement causing a sudden shear or torsion failure
- Cracking patterns produced by loading the type A decks were consistent with yield-line patterns found in slabs
- Application of yield-line theory to a type A deck damaged symmetrically produced a good correlation when membrane action was taken into account

The integration of the results of the static loading with the investigation of the vibration characteristics is presented in chapter 5. Using finite element model updating based on the cracking patterns observed and the modal properties found to determine the structural changes in the decks as they are incrementally loaded is examined in chapter 6.

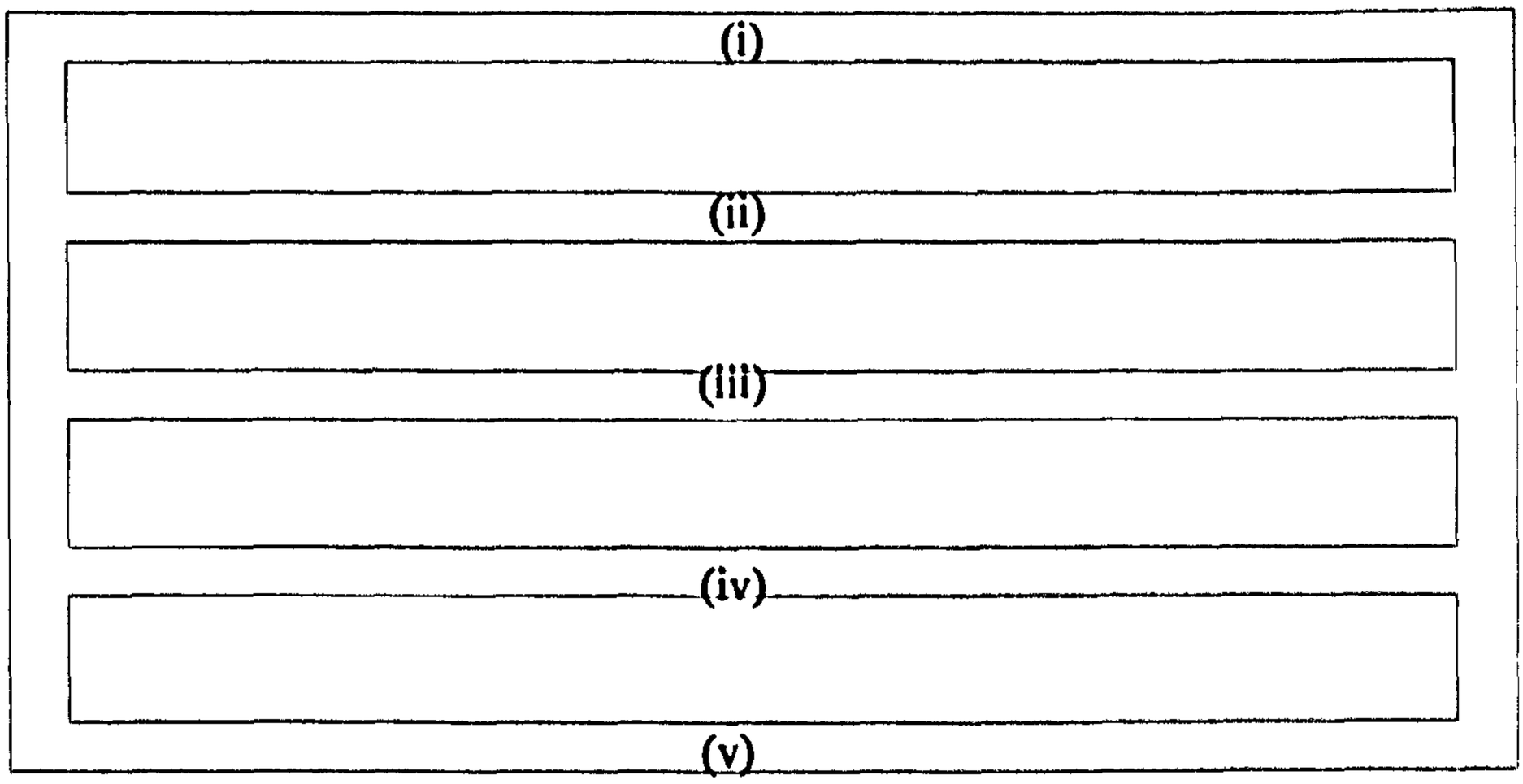

Figure 4-1: Labelling of longitudinal beams

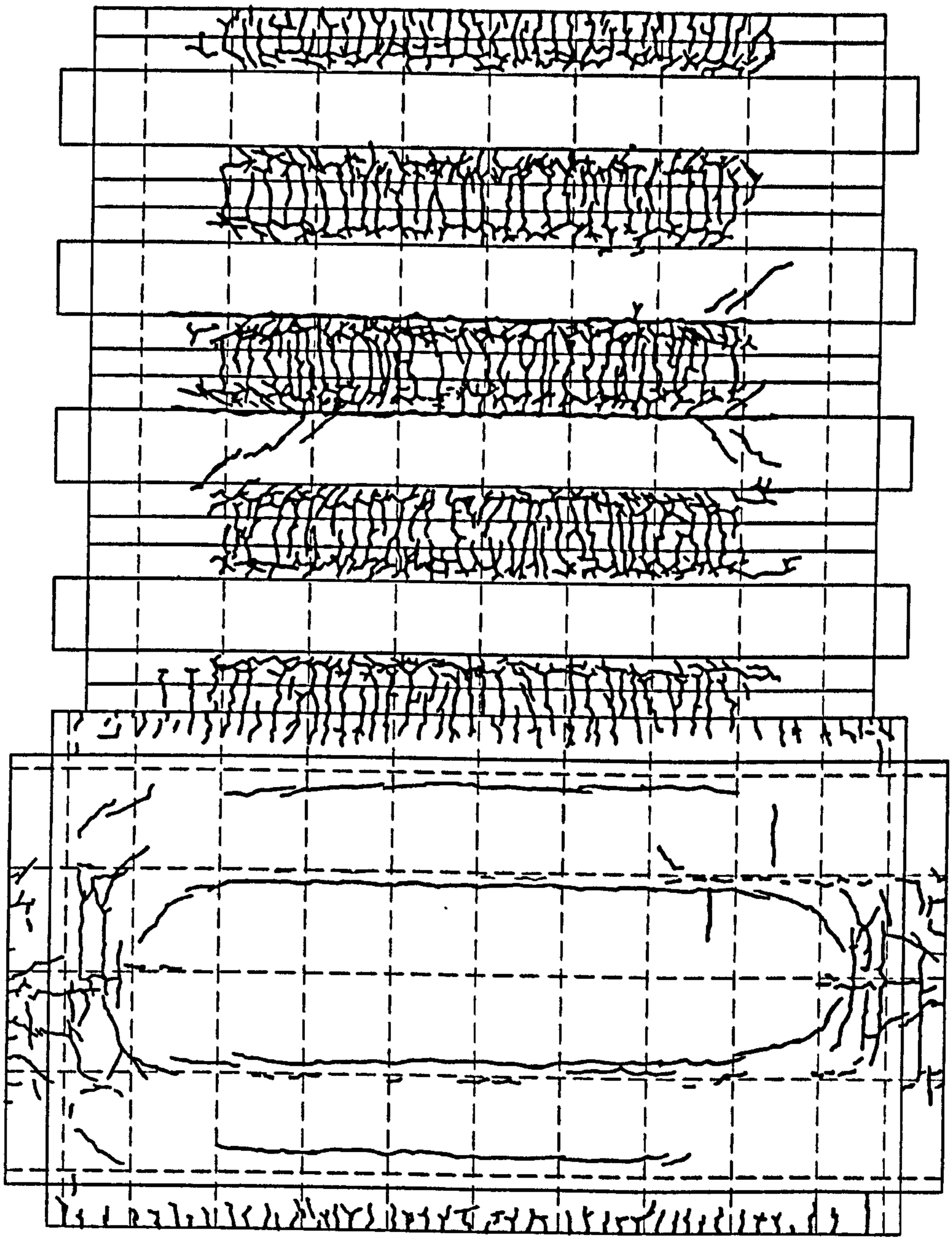

Figure 4-2: Cracking pattern of deck 1 at 210kN

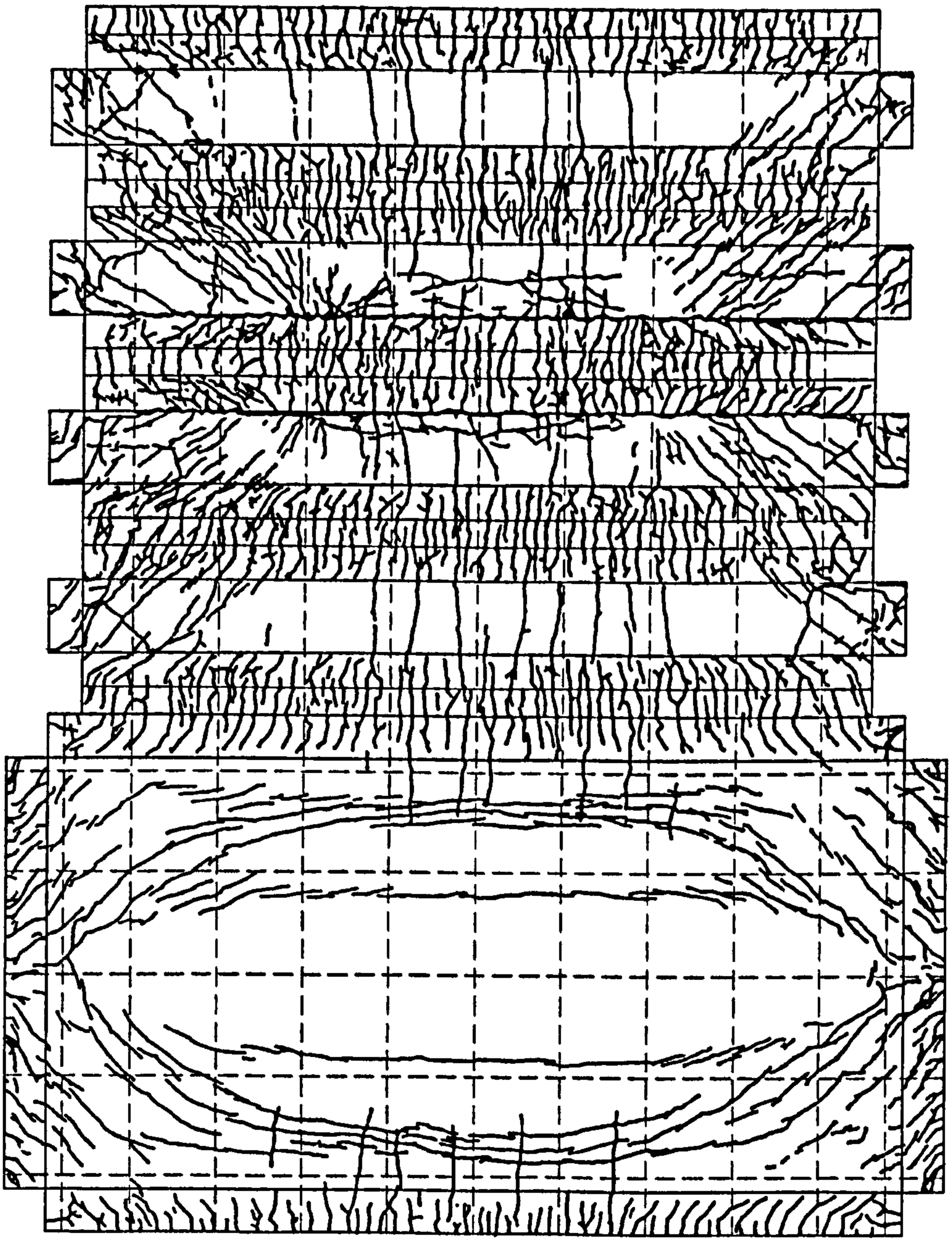

Figure 4-3: Cracking pattern of deck 2

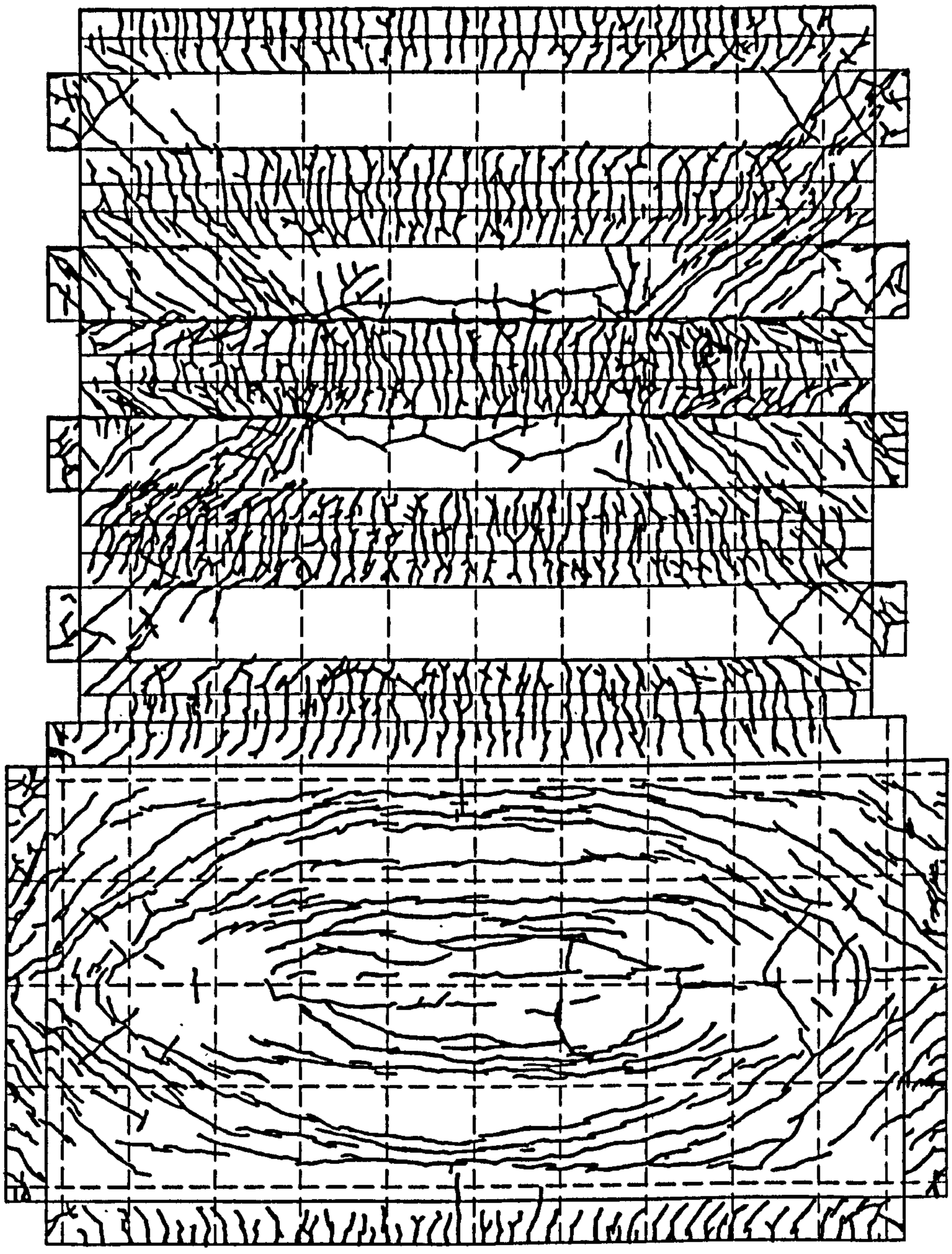

Figure 4-4: Cracking pattern of deck 8

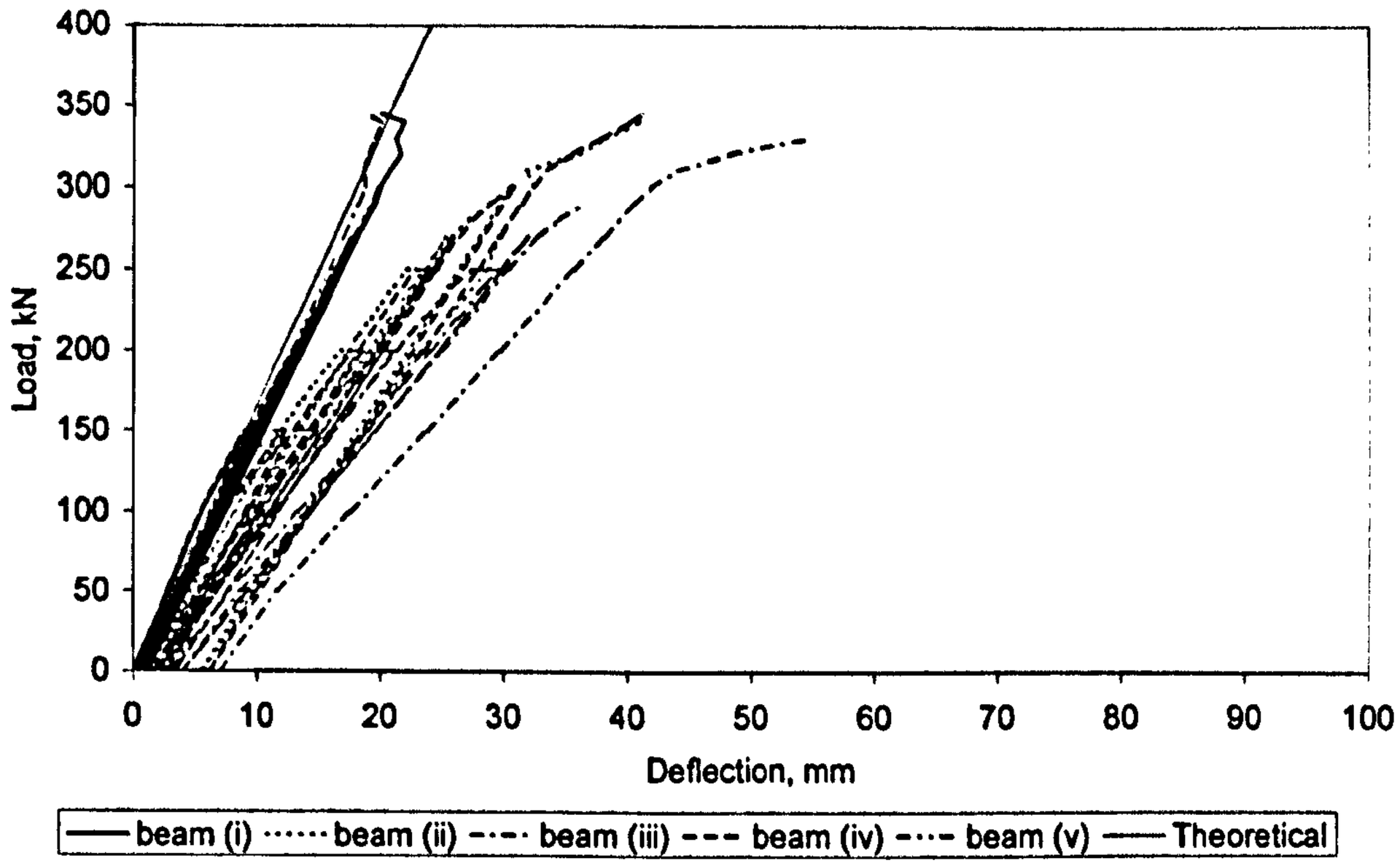

Figure 4-5: Load against mid-span deflection plot for deck 2

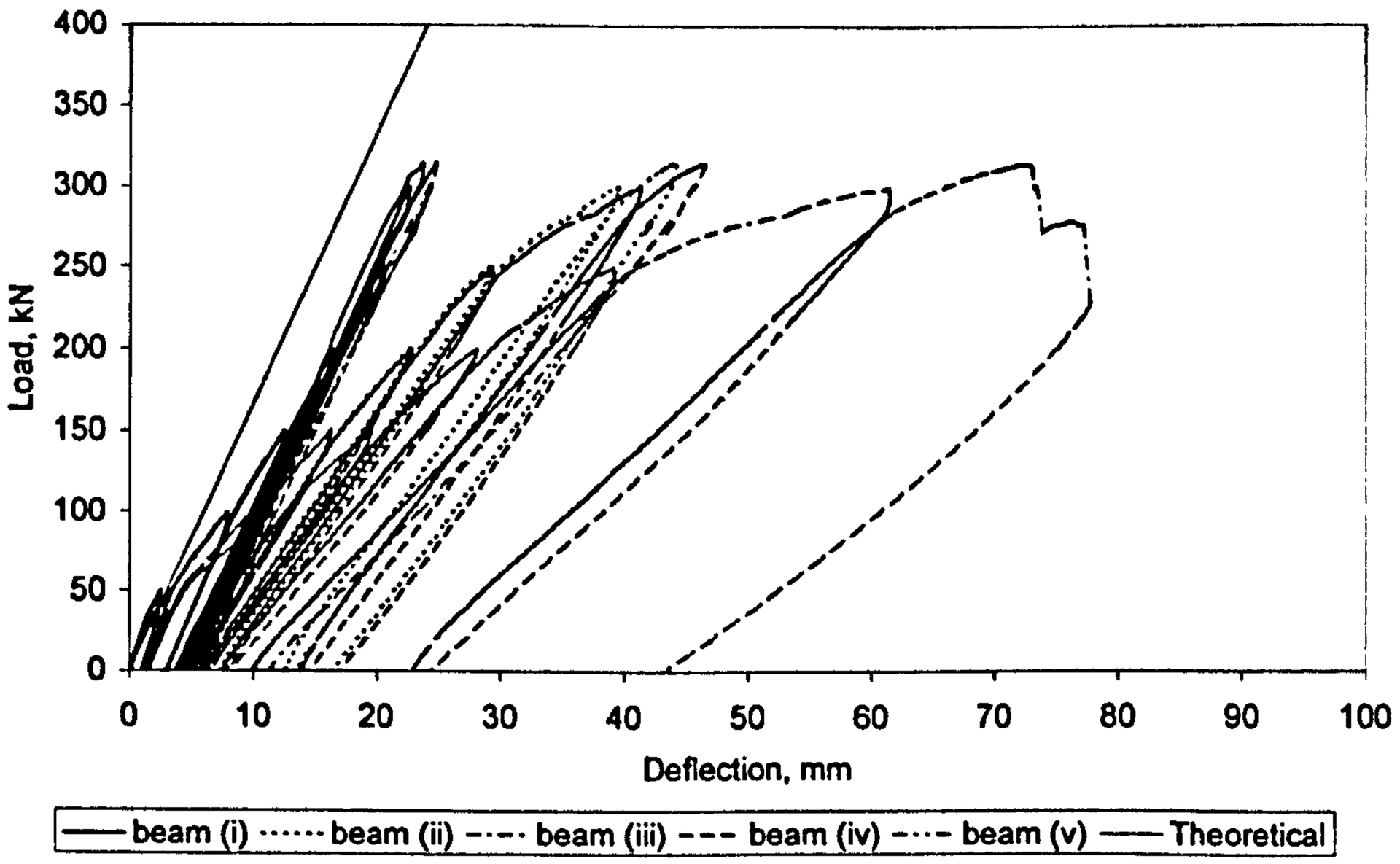

Figure 4-6: Load against mid-span deflection plot for deck 8

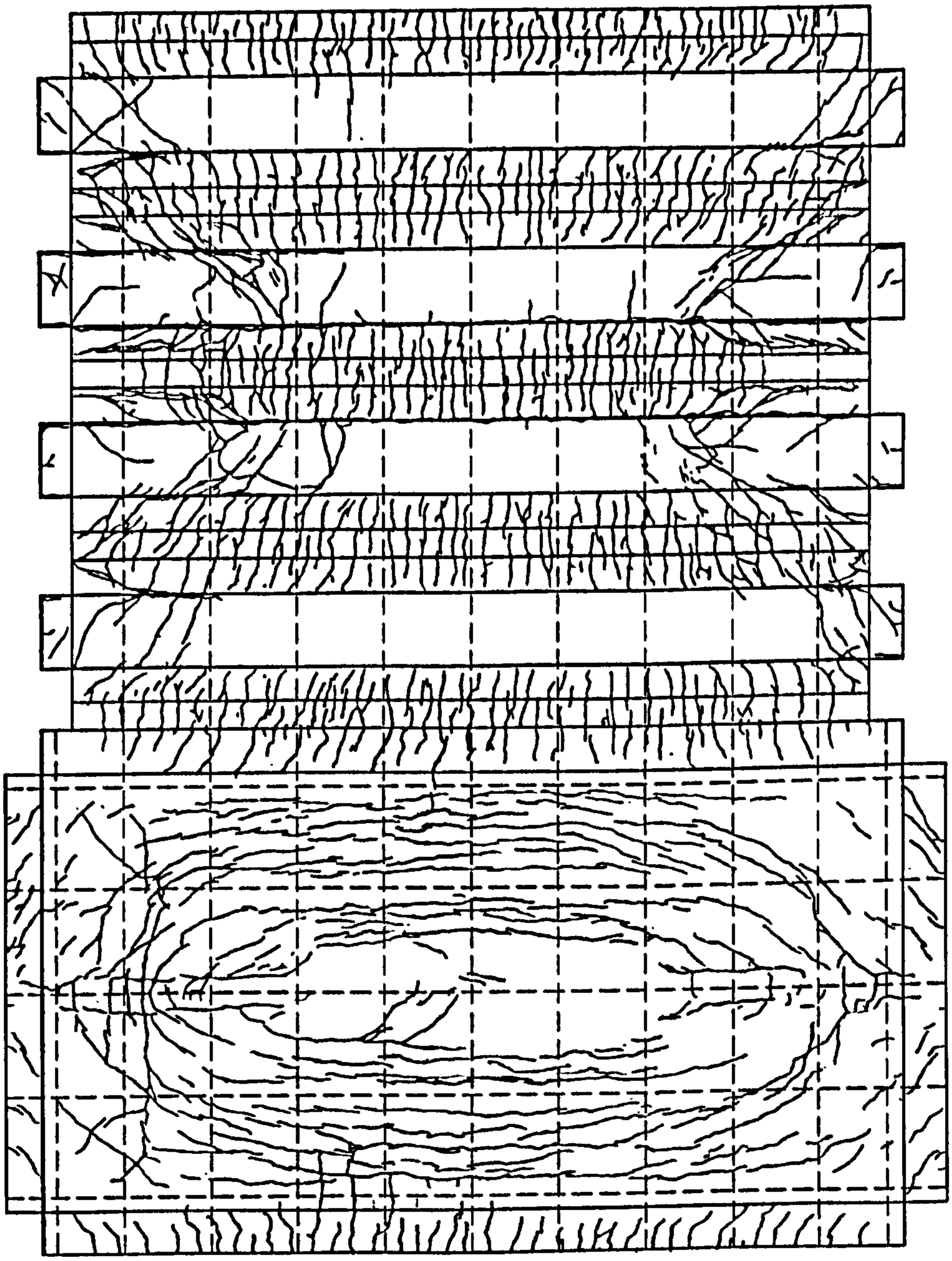

Figure 4-7: Cracking pattern of deck 6

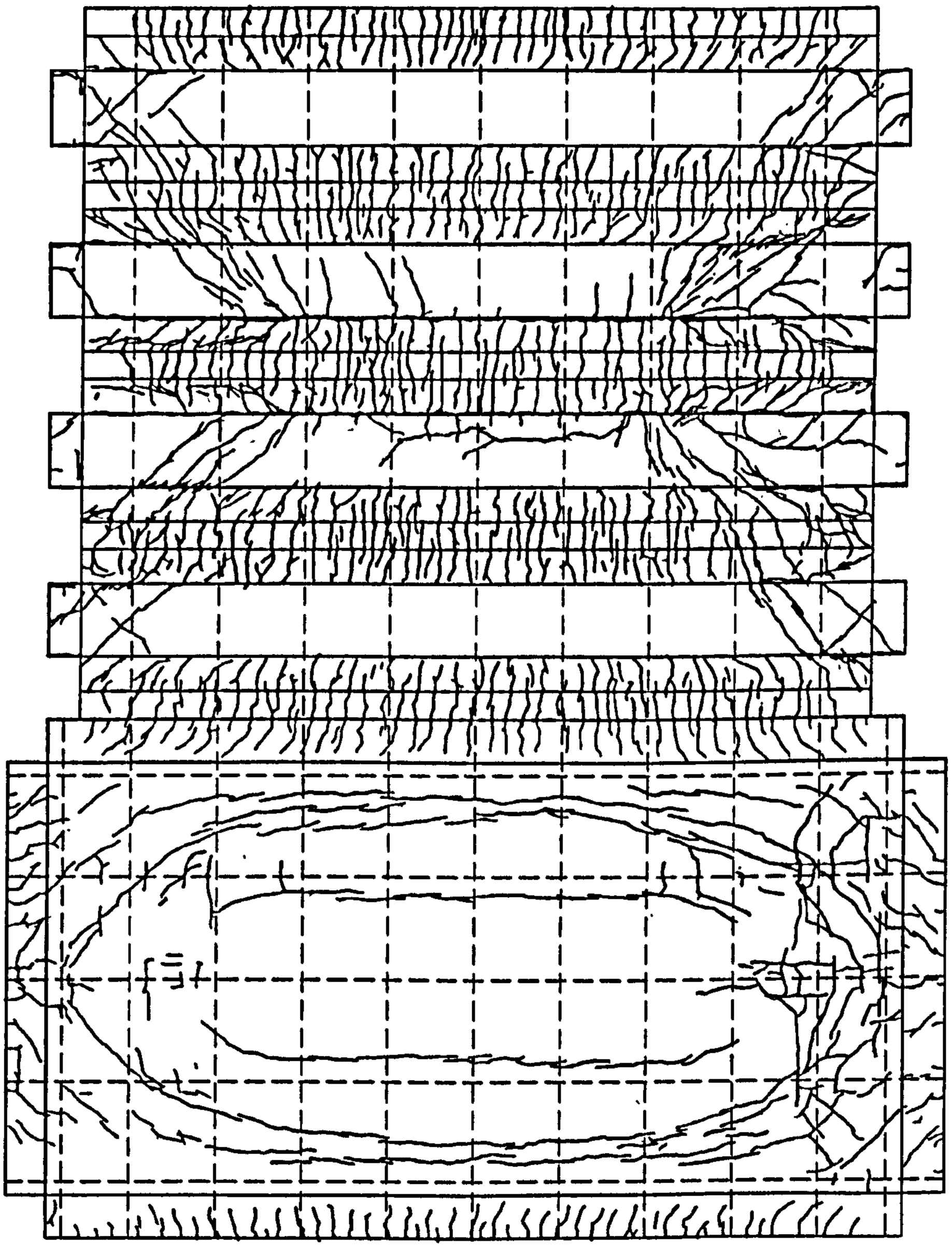

Figure 4-8: Cracking pattern of deck 7

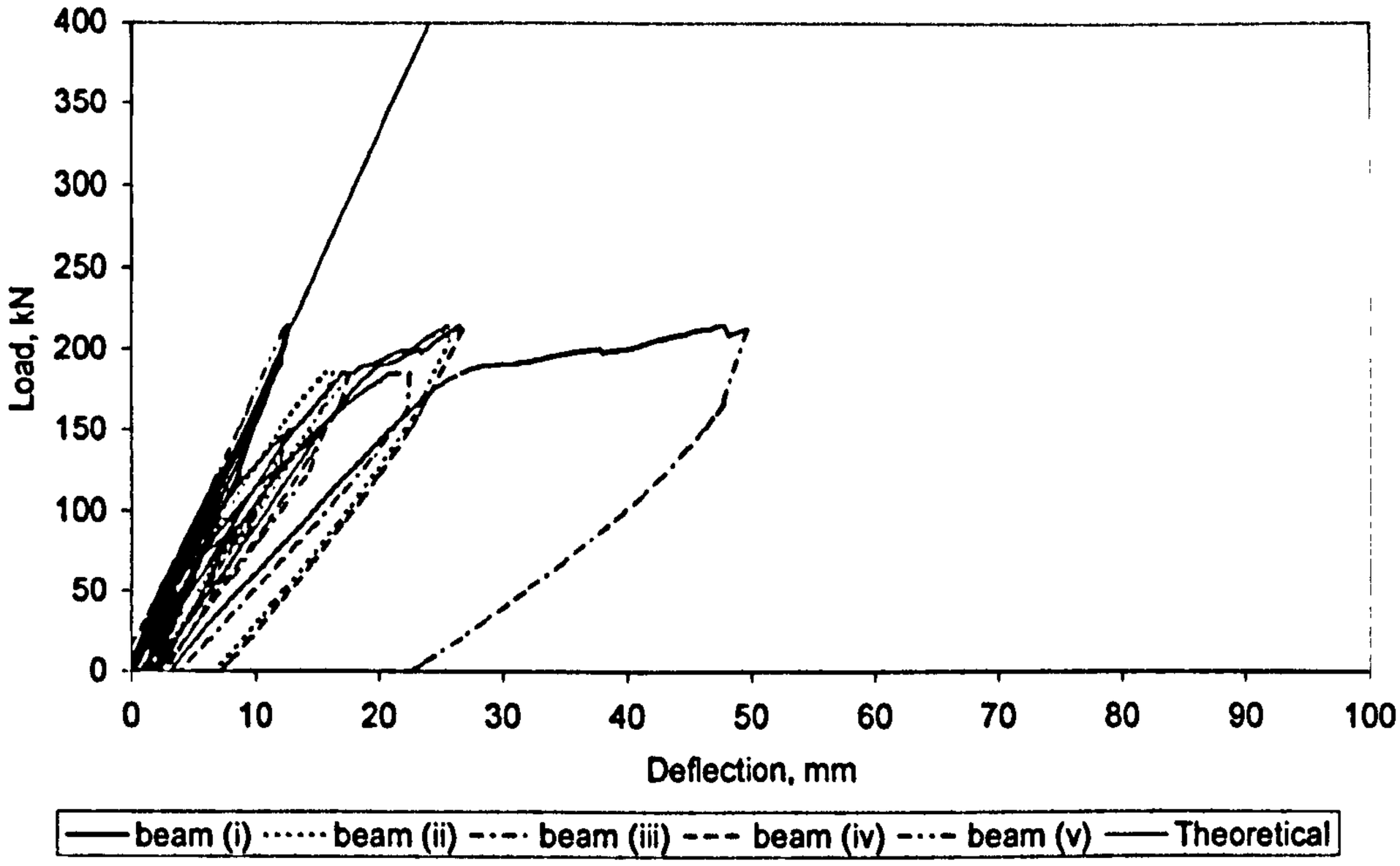

Figure 4-9: Load against mid-span deflection plot for deck 6

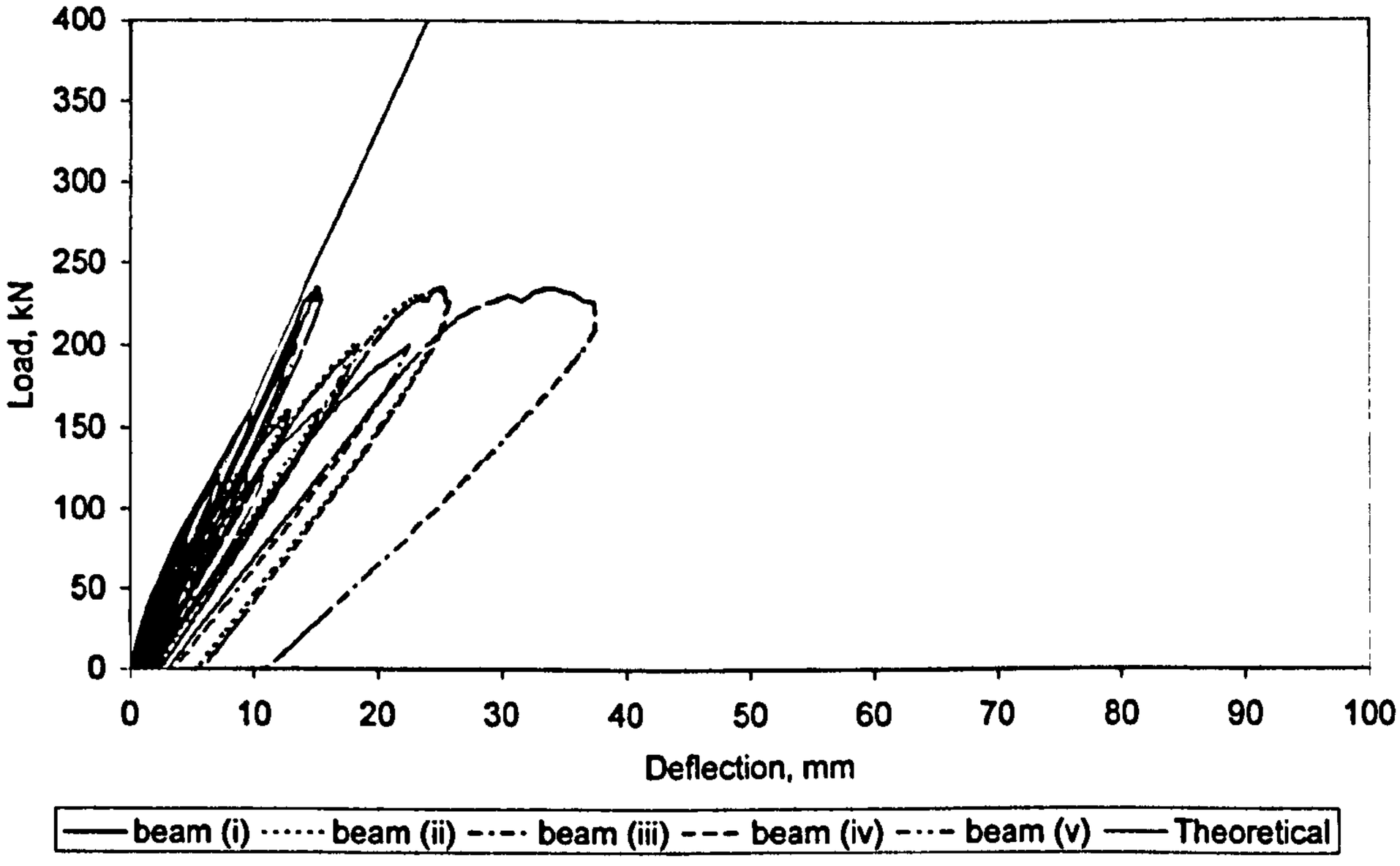

Figure 4-10: Load against mid-span deflection plot for deck 7

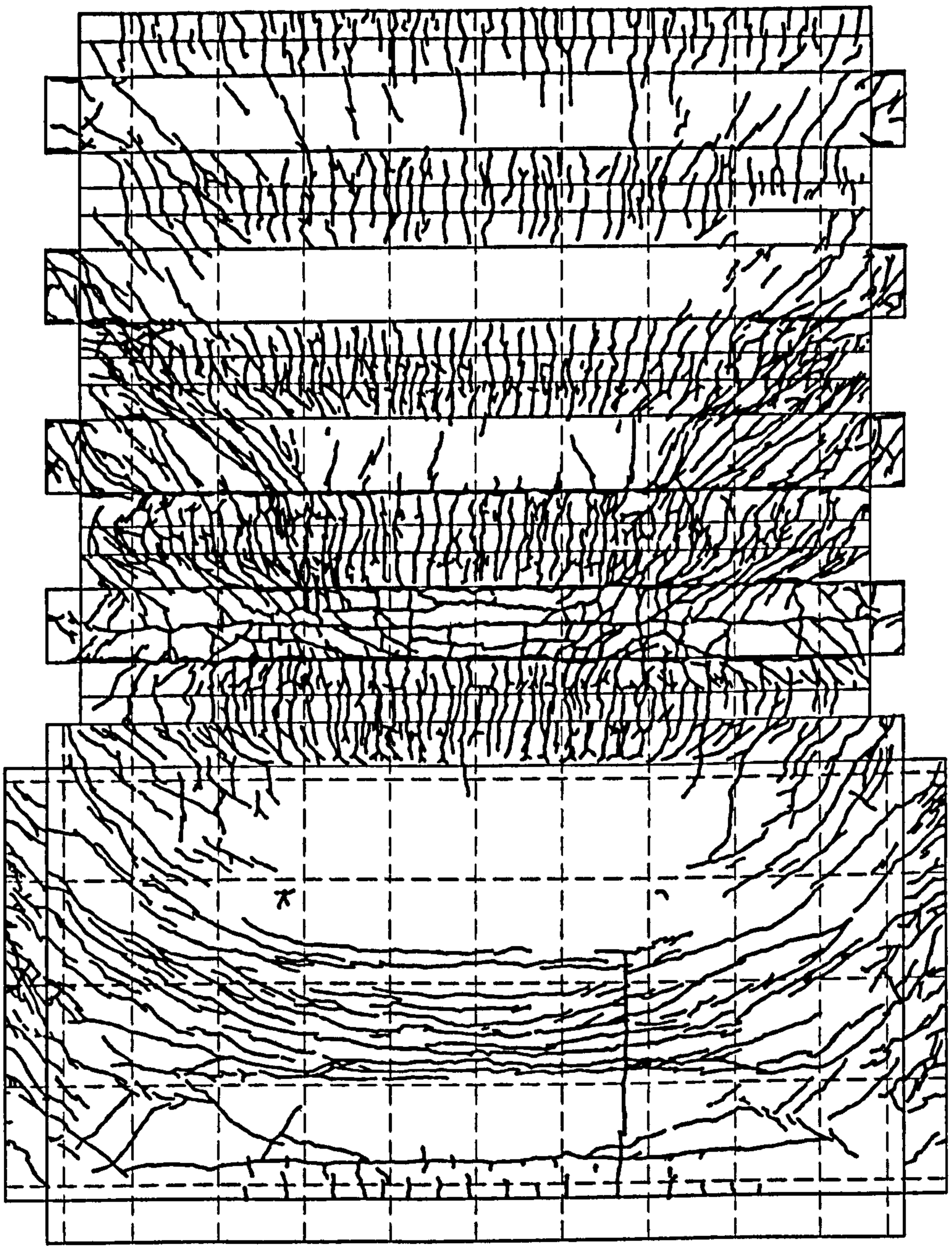

Figure 4-11: Cracking pattern of deck 3

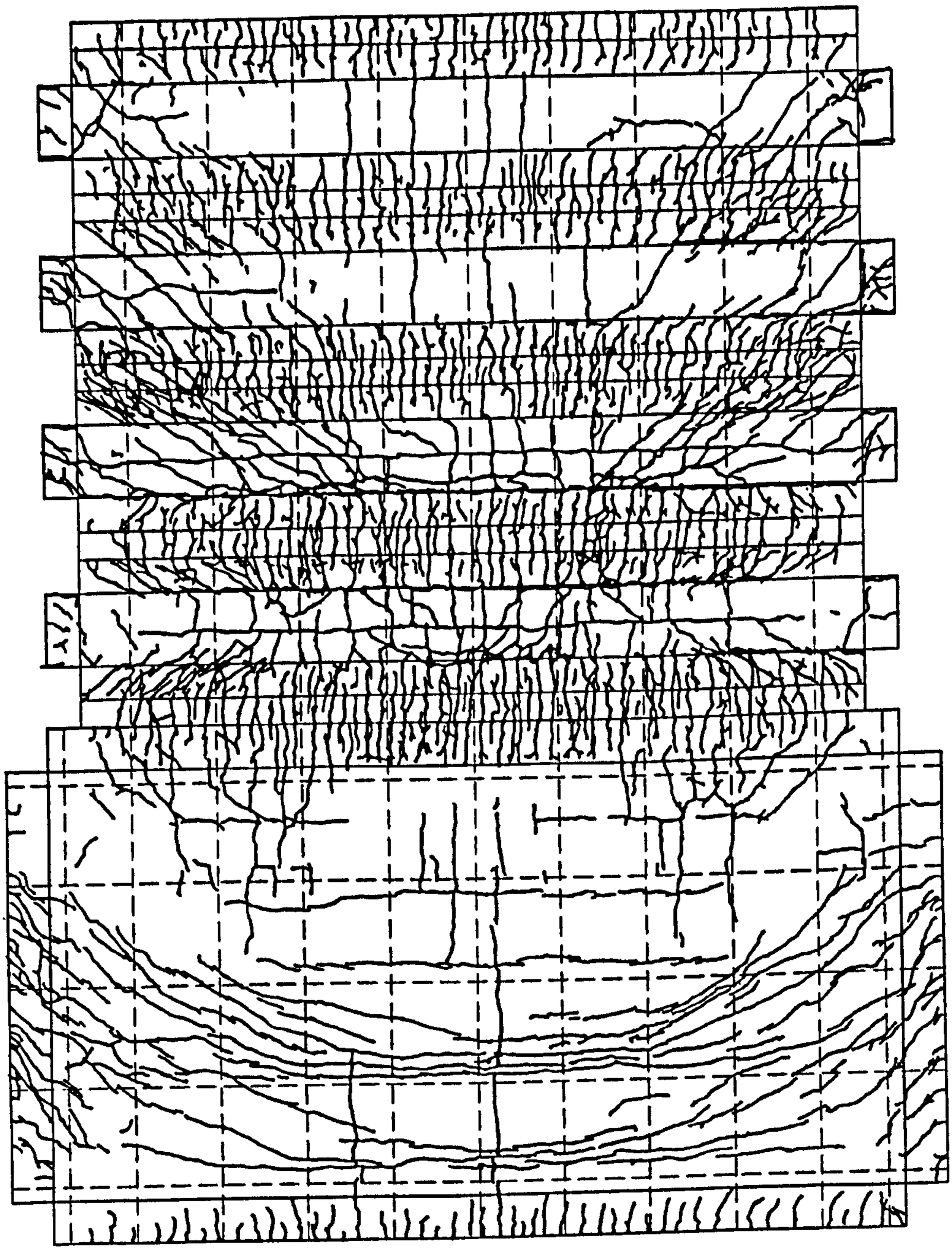

Figure 4-12: Cracking pattern of deck 9

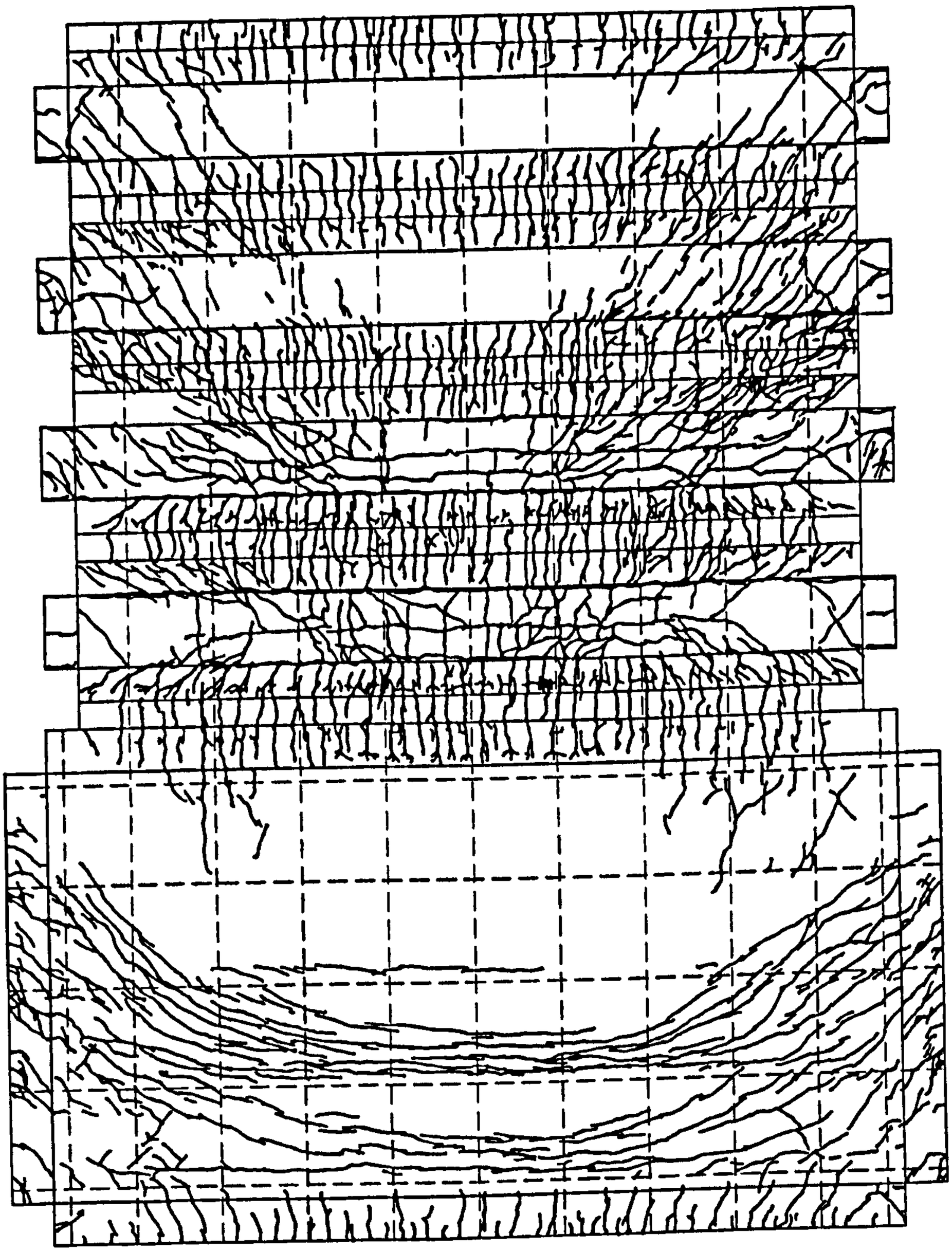

Figure 4-13: Cracking pattern of deck 10

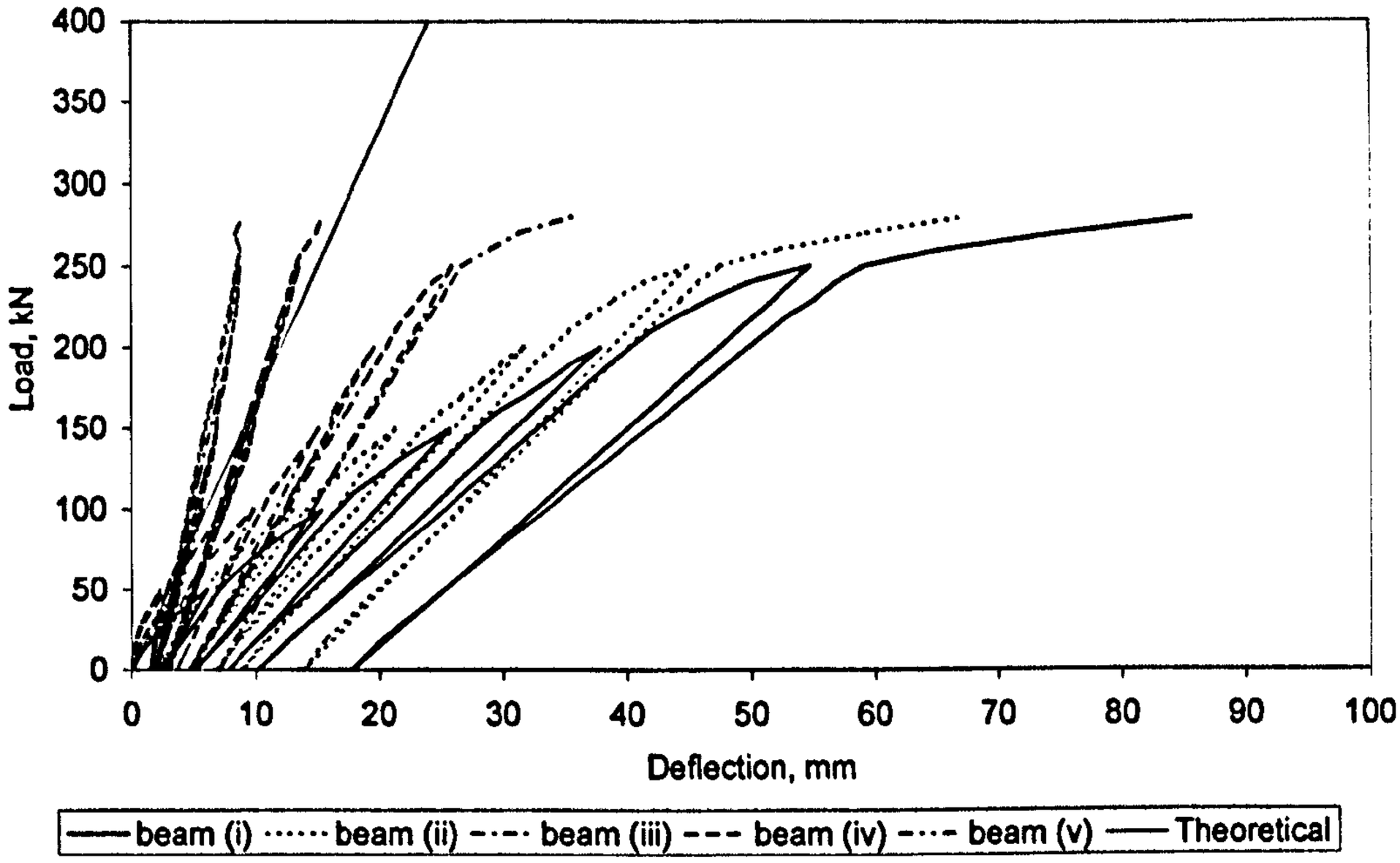

Figure 4-14: Load against mid-span deflection plot for deck 3

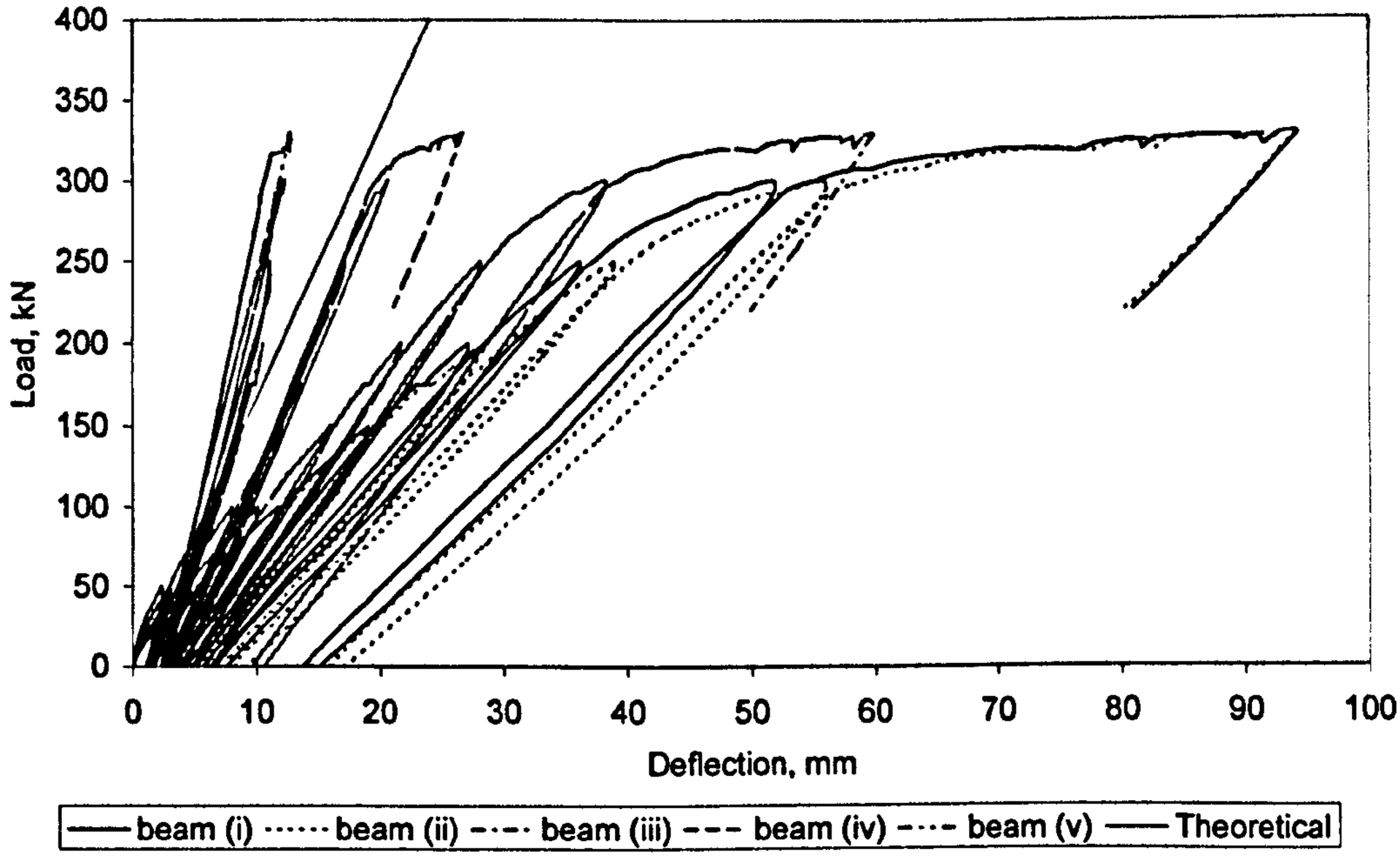

Figure 4-15: Load against mid-span deflection plot for deck 9

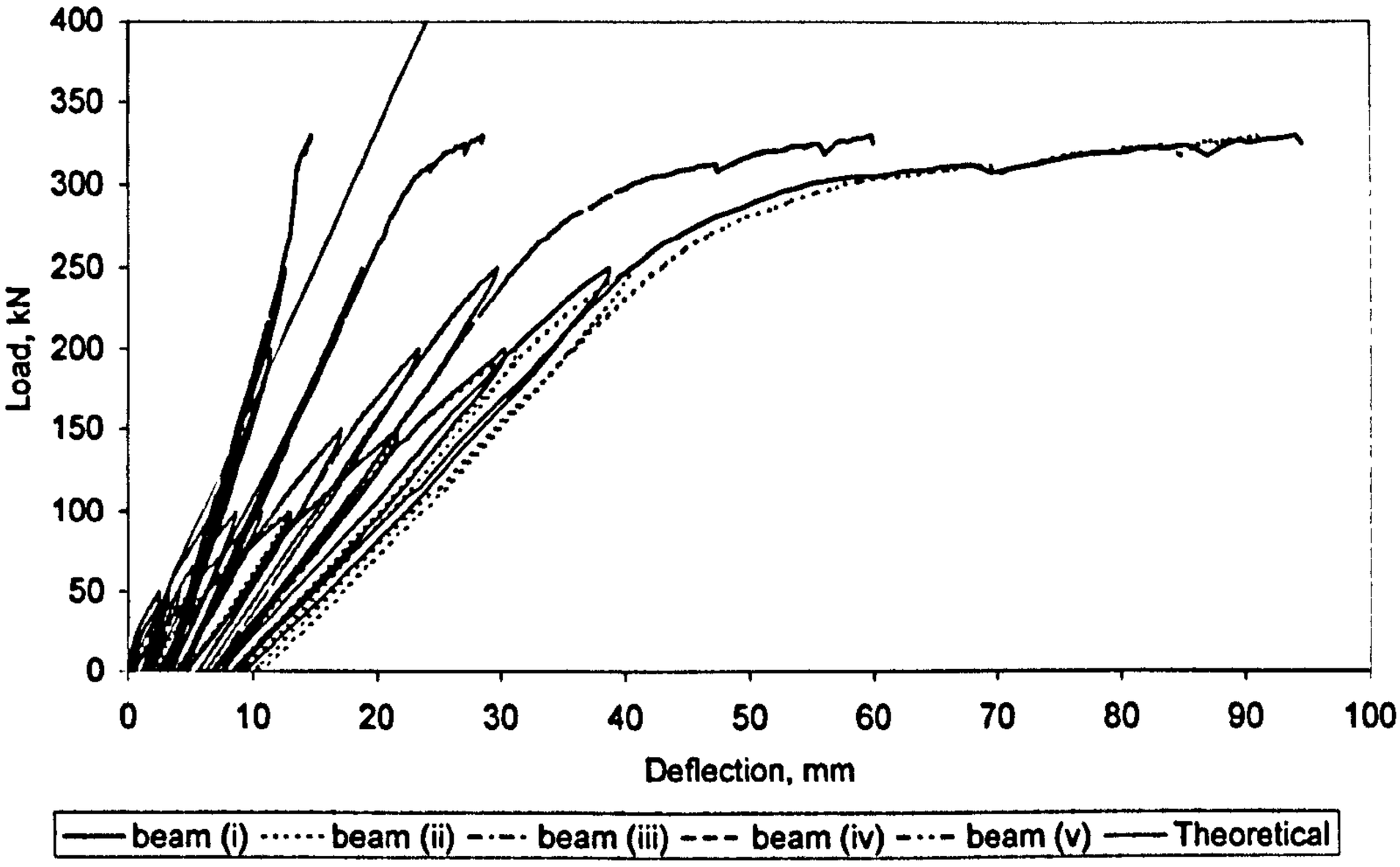

Figure 4-16: Load against mid-span deflection plot for deck 10

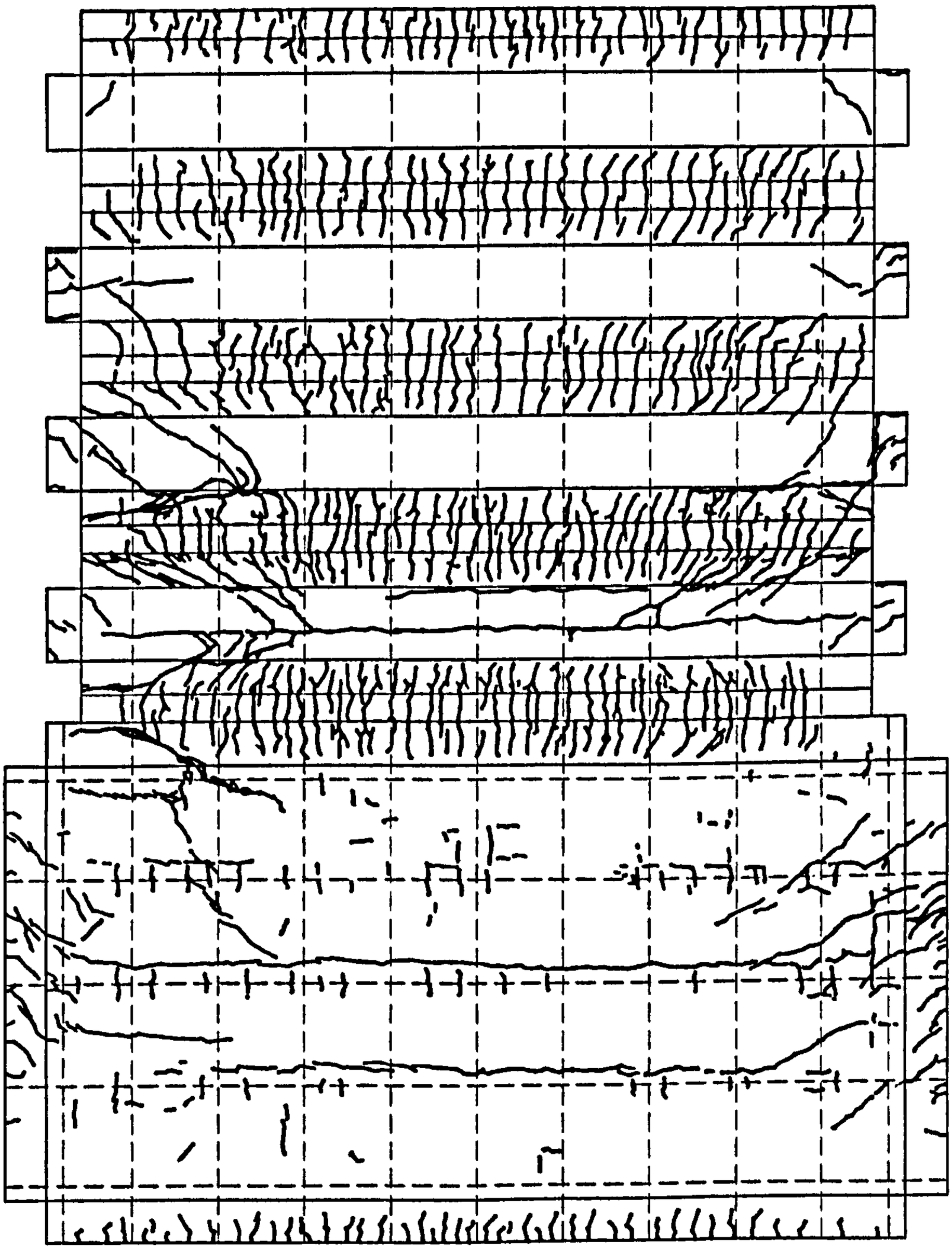

Figure 4-17: Cracking pattern of deck 4

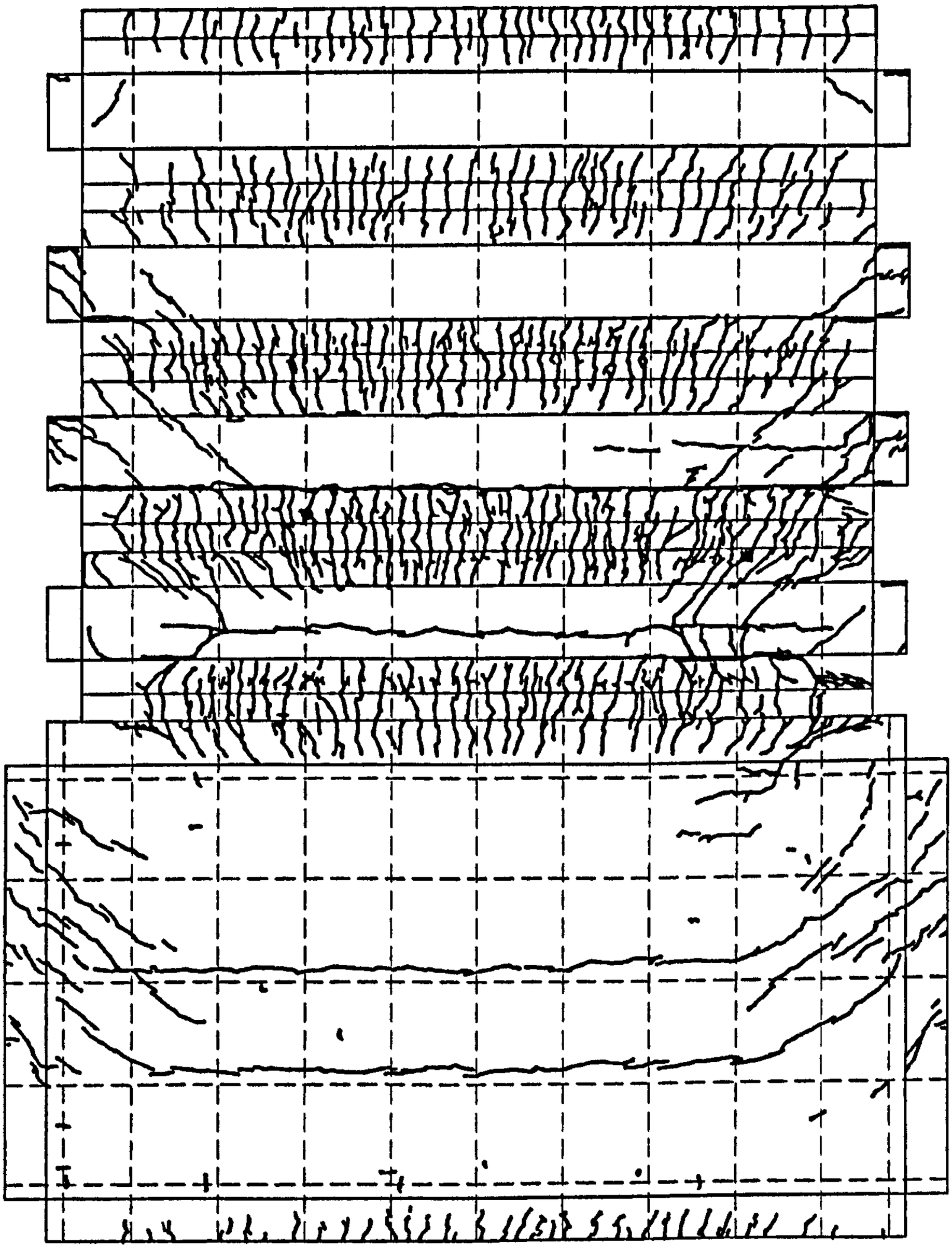

Figure 4-18: Cracking pattern of deck 5

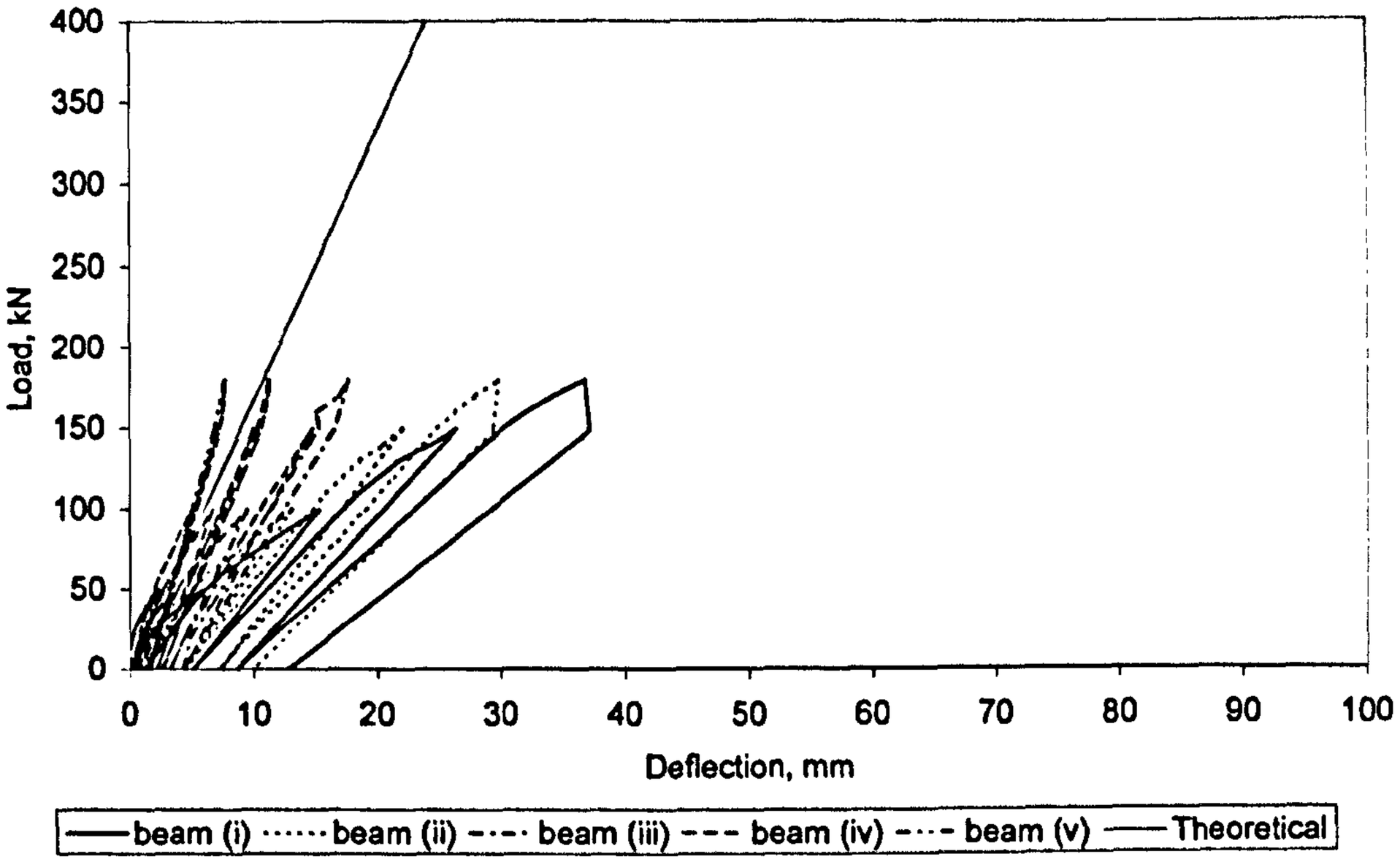

Figure 4-19: Load against mid-span deflection plot for deck 4

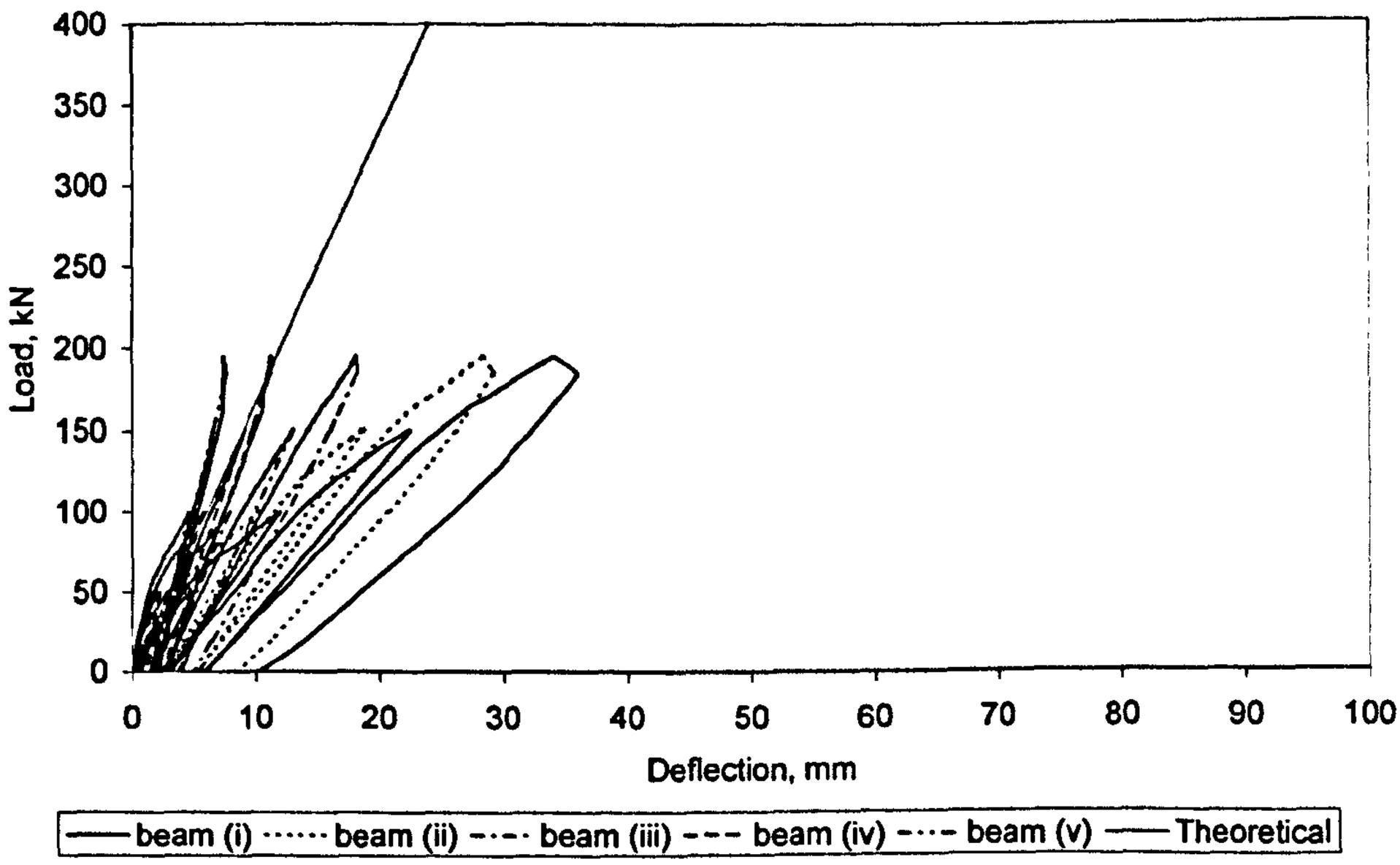

Figure 4-20: Load against mid-span deflection plot for deck 5

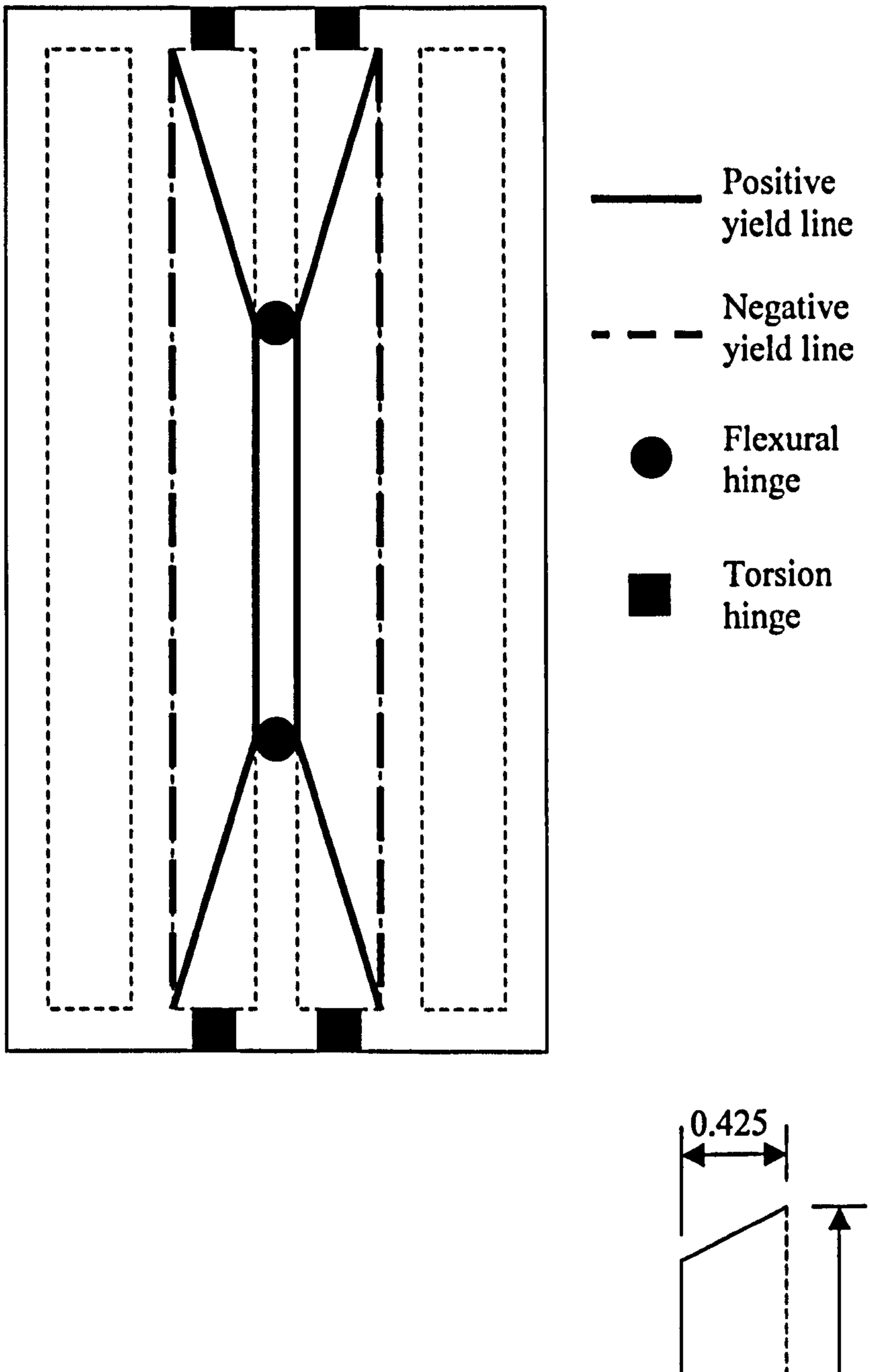

Figure 4-21: Yield-line pattern for symmetrically loaded deck

Table 4-1: Details of static testing performed (* deck not loaded to failure)

Deck	Type	Loading	Failure load
1	A	symm	210*
2	A	symm	345
3	A	asymm	316
4	B	asymm	180
5	B	asymm	200
6	B	symm	210
7	B	symm	235
8	A	symm	315
9	A	HB	337
10	A	HB	340

Table 4-2: Load increments applied to decks

Deck	Load increments, kN											
1	0	10	20	30	40	50	60	70	80	90	105	125	210
2	0	50	100	150	200	250	300	345					
3	0	50	100	150	200	250	316						
4	0	50	100	150	180								
5	0	50	100	150	200								
6	0	50	100	150	185	210							
7	0	40	80	120	160	200	235						
8	0	50	100	150	200	250	300	315					
9	0	50	100	150	200	250	300	337					
10	0	50	100	150	200	250	340						

Table 4-3: Approximate initial linear gradient of deck 2 (kN/mm) under increasing load increments

		beam (i)	beam (ii)	beam (iii)	beam (iv)	beam (v)
Load, kN	150	18.0	15.2	13.4	14.5	18.6
	200	16.2	13.4	11.5	13.4	16.8
	250	15.5	12.3	10.3	12.5	15.8
	300	15.4	11.7	9.6	11.9	15.8
	345	15.9	12.4	8.5	11.4	16.7

Table 4-4: Approximate load (kN) on individual beam for deck 2

		beam (i)	beam (ii)	beam (iii)	beam (iv)	beam (v)
Load, kN	150	23.2	32.7	37.1	34.5	22.5
	200	30.6	44.1	51.5	44.1	29.6
	250	36.8	55.7	66.4	54.8	36.3
	300	42.7	67.2	82.2	66.2	41.7
	345	46.6	71.5	104.6	78.0	44.4

Table 4-5: Approximate initial linear gradient of deck 8 (kN/mm) under increasing load increments

		beam (i)	beam (ii)	beam (iii)	beam (iv)	beam (v)
Load, kN	50	39.5	25.3	22.9	25.8	33.0
	100	23.8	18.3	17.0	18.7	23.2
	150	17.8	14.5	12.0	14.1	18.5
	200	16.4	12.7	10.3	12.6	16.6
	250	15.9	11.8	9.5	11.6	15.7
	300	16.1	11.0	8.2	10.9	16.0
	315	17.4	10.8	7.3	10.6	17.3

Table 4-6: Approximate load (kN) on individual beam for deck 8

		beam (i)	beam (ii)	beam (iii)	beam (iv)	beam (v)
Load, kN	50	6.3	11.7	13.0	11.5	7.5
	100	14.8	22.9	24.6	22.5	15.2
	150	22.4	32.7	39.8	33.6	21.6
	200	28.6	44.1	54.3	44.7	28.3
	250	34.4	55.4	69.1	56.2	34.9
	300	38.1	66.5	89.9	67.2	38.3
	315	36.0	69.6	102.4	70.8	36.3

Table 4-7: Approximate initial linear gradient of deck 6 (kN/mm) under increasing load increments

		beam (i)	beam (ii)	beam (iii)	beam (iv)	beam (v)
Load, kN	50	28.4	22.2	19.8	23.1	29.6
	100	22.6	17.9	16.4	18.7	23.2
	150	18.4	14.5	12.1	14.3	18.8
	200	16.2	12.5	10.0	12.2	16.5
	210	15.9	11.2	8.2	10.9	15.8

Table 4-8: Approximate load (kN) on individual beam for deck 6

		beam (i)	beam (ii)	beam (iii)	beam (iv)	beam (v)
Load, kN	50	7.5	11.5	12.8	11.0	7.2
	100	15.3	23.0	25.0	22.0	14.8
	150	21.9	33.3	39.8	33.6	21.5
	200	28.4	44.1	54.7	44.9	27.9
	210	27.1	45.9	62.5	47.1	27.4

Table 4-9: Approximate initial linear gradient of deck 7 (kN/mm) under increasing load increments

		beam (i)	beam (ii)	beam (iii)	beam (iv)	beam (v)
Load, kN	40	30.0	23.6	21.0	21.6	25.9
	80	29.5	21.7	19.0	19.8	23.4
	120	21.7	16.1	14.2	15.8	19.9
	160	18.2	14.3	12.0	13.8	17.7
	200	16.9	13.0	10.7	12.7	16.8
	235	17.8	12.0	9.6	11.6	16.0

Table 4-10: Approximate load (kN) on individual beam for deck 7

		beam (i)	beam (ii)	beam (iii)	beam (iv)	beam (v)
Load, kN	40	7.5	8.2	9.2	8.9	6.2
	80	14.9	16.2	18.5	17.8	12.6
	120	21.8	25.6	29.1	26.1	17.4
	160	29.1	33.6	40.0	34.7	22.6
	200	36.2	42.1	51.1	43.2	27.4
	235	42.7	49.0	61.5	50.9	30.9

Table 4-11: Approximate initial linear gradient of deck 3 (kN/mm) under increasing load increments

		beam (i)	beam (ii)	beam (iii)	beam (iv)	beam (v)
Load, kN	50	10.8	13.3	18.4	28.1	38.9
	100	11.0	13.5	18.8	27.8	45.0
	150	8.8	10.6	14.6	21.0	29.3
	200	7.5	9.0	13.2	21.6	31.4
	250	6.6	8.0	12.9	22.7	32.9
	316	6.0	7.4	12.6	24.9	38.4

Table 4-12: Approximate load (kN) on individual beam for deck 3

		beam (i)	beam (ii)	beam (iii)	beam (iv)	beam (v)
Load, kN	50	14.7	14.2	10.3	6.7	4.1
	100	29.5	28.7	20.7	13.9	7.2
	150	42.8	42.4	30.7	21.3	12.8
	200	60.3	59.7	40.7	24.9	14.4
	250	79.0	78.7	48.7	27.7	16.0
	316	105.8	102.9	60.1	30.6	16.6

Table 4-13: Approximate initial linear gradient of deck 9 (kN/mm) under increasing load increments

Load, kN	beam (i)	beam (ii)	beam (iii)	beam (iv)	beam (v)
50	19.9	19.2	23.1	32.9	65.1
100	14.0	14.0	17.0	22.6	29.4
150	11.3	11.0	13.3	17.9	24.3
200	9.8	9.7	12.2	16.9	24.4
250	8.8	8.5	11.3	17.5	26.6
300	8.3	7.8	11.0	18.4	30.7
337	7.6	7.3	10.5	19.6	36.6

Table 4-14: Approximate load (kN) on individual beam for deck 9

Load, kN	beam (i)	beam (ii)	beam (iii)	beam (iv)	beam (v)
50	11.6	14.4	12.0	8.4	3.6
100	22.7	27.1	22.4	16.9	10.9
150	33.6	41.3	34.1	25.3	15.6
200	47.0	56.5	45.1	32.5	18.9
250	60.8	75.7	56.7	36.6	20.2
300	75.6	95.3	68.1	40.6	20.4
337	89.3	111.1	76.8	41.3	18.5

Table 4-15: Approximate initial linear gradient of deck 10 (kN/mm) under increasing load increments

Load, kN	beam (i)	beam (ii)	beam (iii)	beam (iv)	beam (v)
50	16.5	18.1	23.9	37.8	66.0
100	12.9	13.4	16.2	21.4	28.8
150	10.3	10.5	13.0	17.0	22.8
200	9.3	9.4	12.0	16.3	23.0
250	8.6	8.4	11.2	17.1	25.3
340	8.0	7.7	10.6	17.1	27.3

Table 4-16: Approximate load (kN) on individual beam for deck 10

Load, kN	beam (i)	beam (ii)	beam (iii)	beam (iv)	beam (v)
50	13.6	14.8	11.2	7.1	3.4
100	23.4	27.0	22.3	16.8	10.5
150	34.8	41.0	33.1	25.3	15.8
200	47.6	56.4	44.1	32.5	19.3
250	61.4	75.0	56.0	36.8	20.8
340	85.4	105.2	76.7	47.7	25.0

Table 4-17: Approximate initial linear gradient of deck 4 (kN/mm) under increasing load increments

		beam (i)	beam (ii)	beam (iii)	beam (iv)	beam (v)
Load, kN	50	13.2	15.6	21.7	29.4	33.3
	100	10.3	12.1	16.2	22.4	29.4
	150	8.2	9.6	13.4	19.2	26.1
	180	6.9	8.4	14.8	18.6	26.6

Table 4-18: Approximate load (kN) on individual beam for deck 4

		beam (i)	beam (ii)	beam (iii)	beam (iv)	beam (v)
Load, kN	50	13.7	13.7	9.9	7.3	5.4
	100	27.2	27.6	20.6	14.9	9.6
	150	42.0	42.7	30.7	21.4	13.2
	180	55.6	54.3	31.0	24.6	14.4

Table 4-19: Approximate initial linear gradient of deck 5 (kN/mm) under increasing load increments

		beam (i)	beam (ii)	beam (iii)	beam (iv)	beam (v)
Load, kN	50	16.4	20.9	28.1	47.0	62.0
	100	12.0	13.7	19.5	26.9	36.2
	150	9.6	11.6	16.3	21.8	29.2
	200	8.0	9.8	14.6	20.7	30.8

Table 4-20: Approximate load (kN) on individual beam for deck 5

		beam (i)	beam (ii)	beam (iii)	beam (iv)	beam (v)
Load, kN	50	15.1	14.1	10.5	6.3	4.0
	100	27.5	28.7	20.2	14.6	9.1
	150	42.2	41.8	29.8	22.3	13.9
	200	59.7	58.2	39.1	27.6	15.5

Table 4-21: Reasons for bridge closure in Great Britain (OECD, 1992)

Structural inadequacy (40%)	
Design/construction	20%
Repair impossible	20%
Environmental actions (salt, frost)	10%
Catastrophic failure (collapse)	10%
Traffic on bridge	15%
Impacts under the bridge	5%
Maintenance faults	20%
Total	100%

Functional inadequacy (60%)	
Road/canal widening	50%
Heavier traffic	10%
Bottleneck: clearance	10%
Bottleneck: loads	10%
Road set out of service	20%
Total	100%

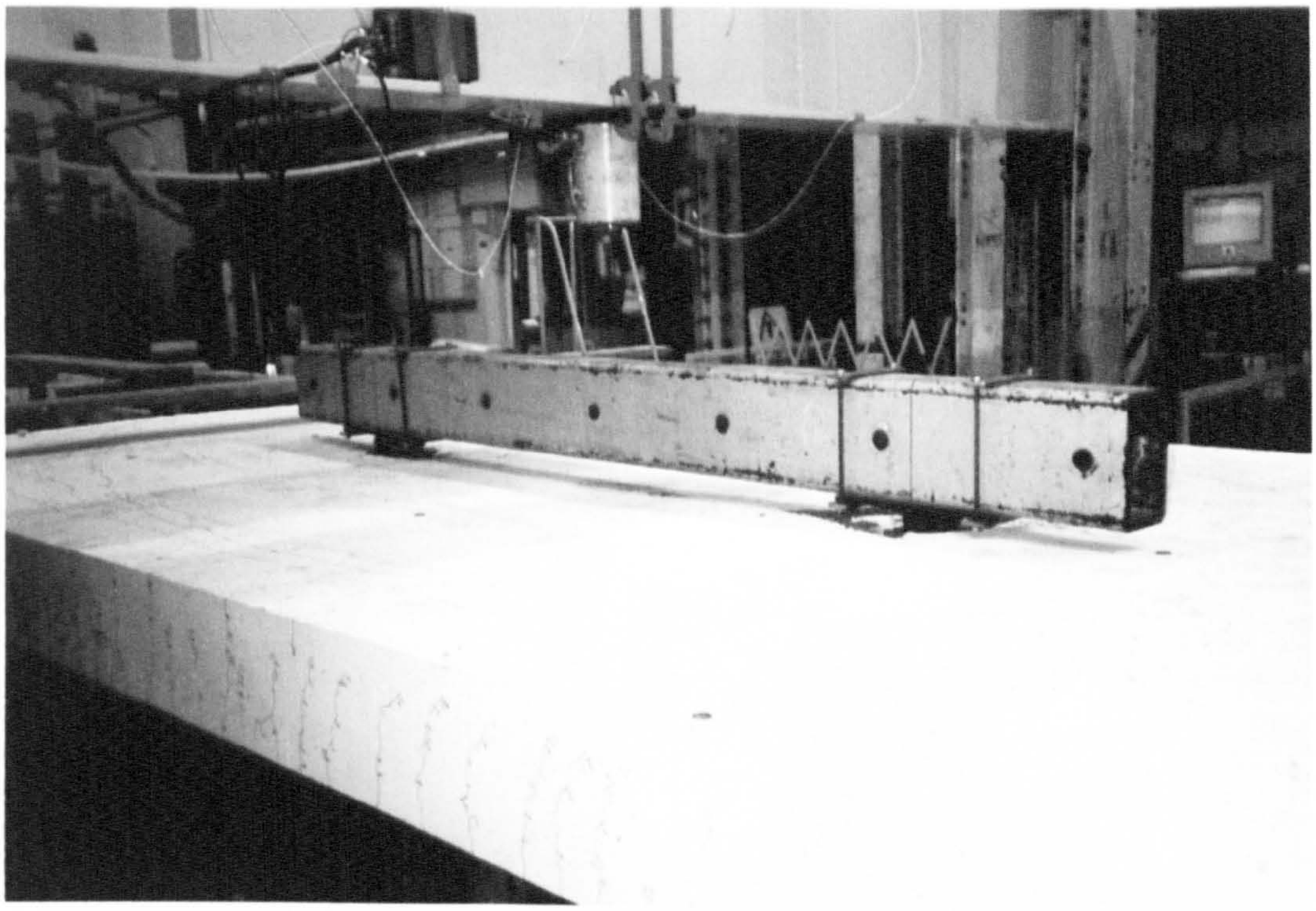

Plate 4-1: Deck 2 punching of loading points through slab

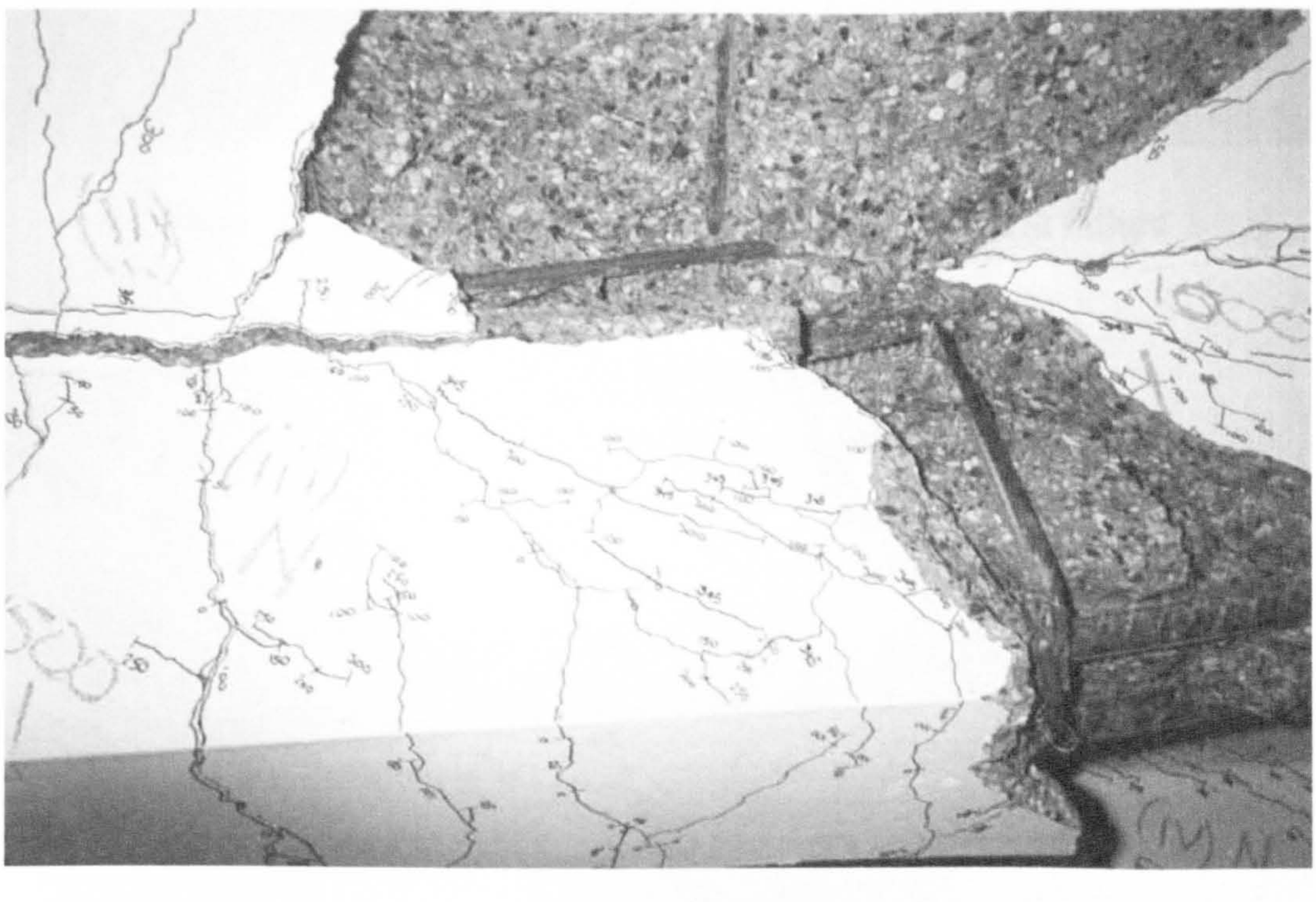

Plate 4-2: Deck 2 shear failure of beam iii and separation of beam from slab

Plate 4-3: Deck 2 showing damage to slab and beam at failure

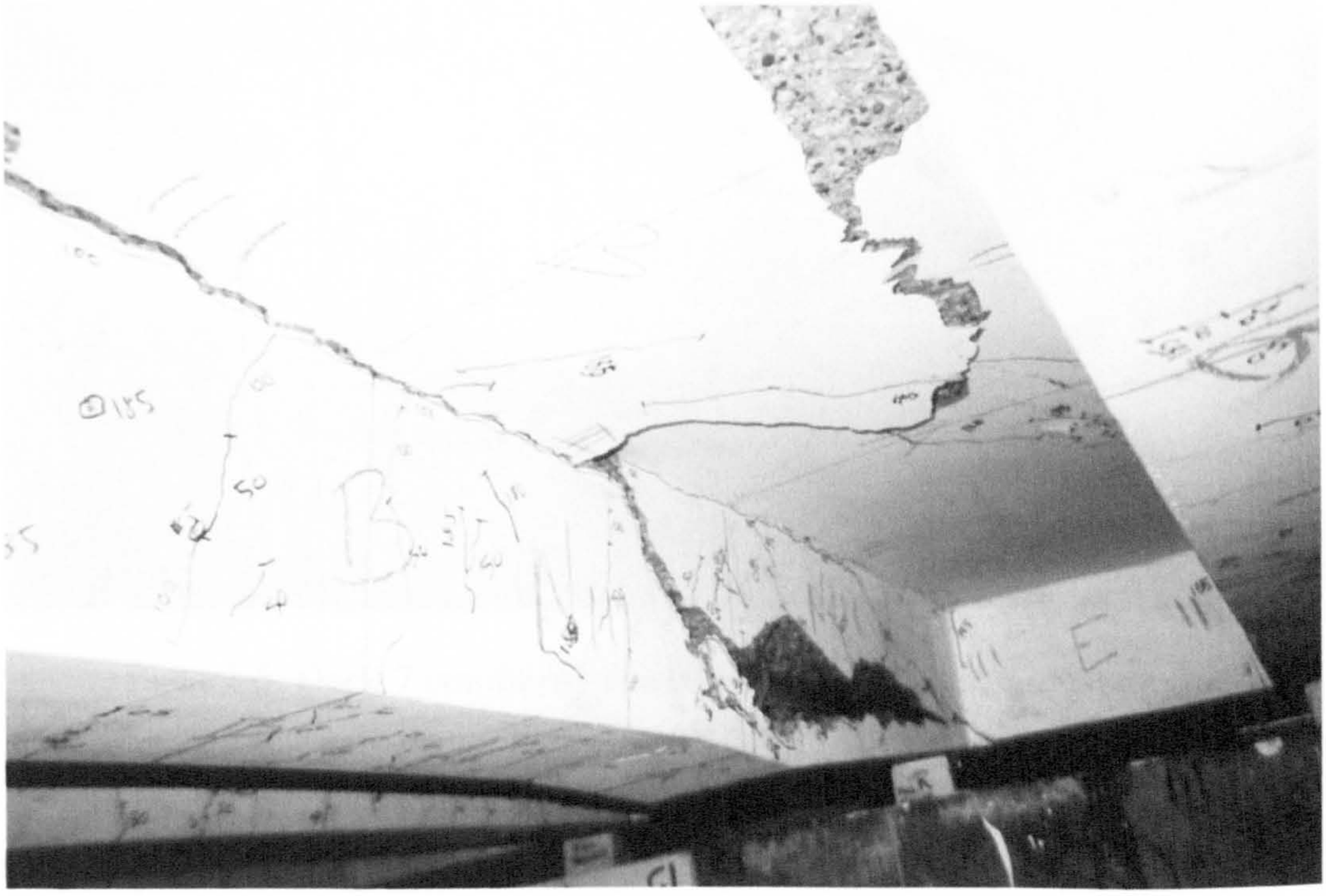

Plate 4-4: Deck 6 combined shear and bending failure in beam iii

Plate 4-5: Deck 6 combined shear and bending failure in beam iii

Plate 4-6: Deck 7 combined shear and bending failure in beam iii

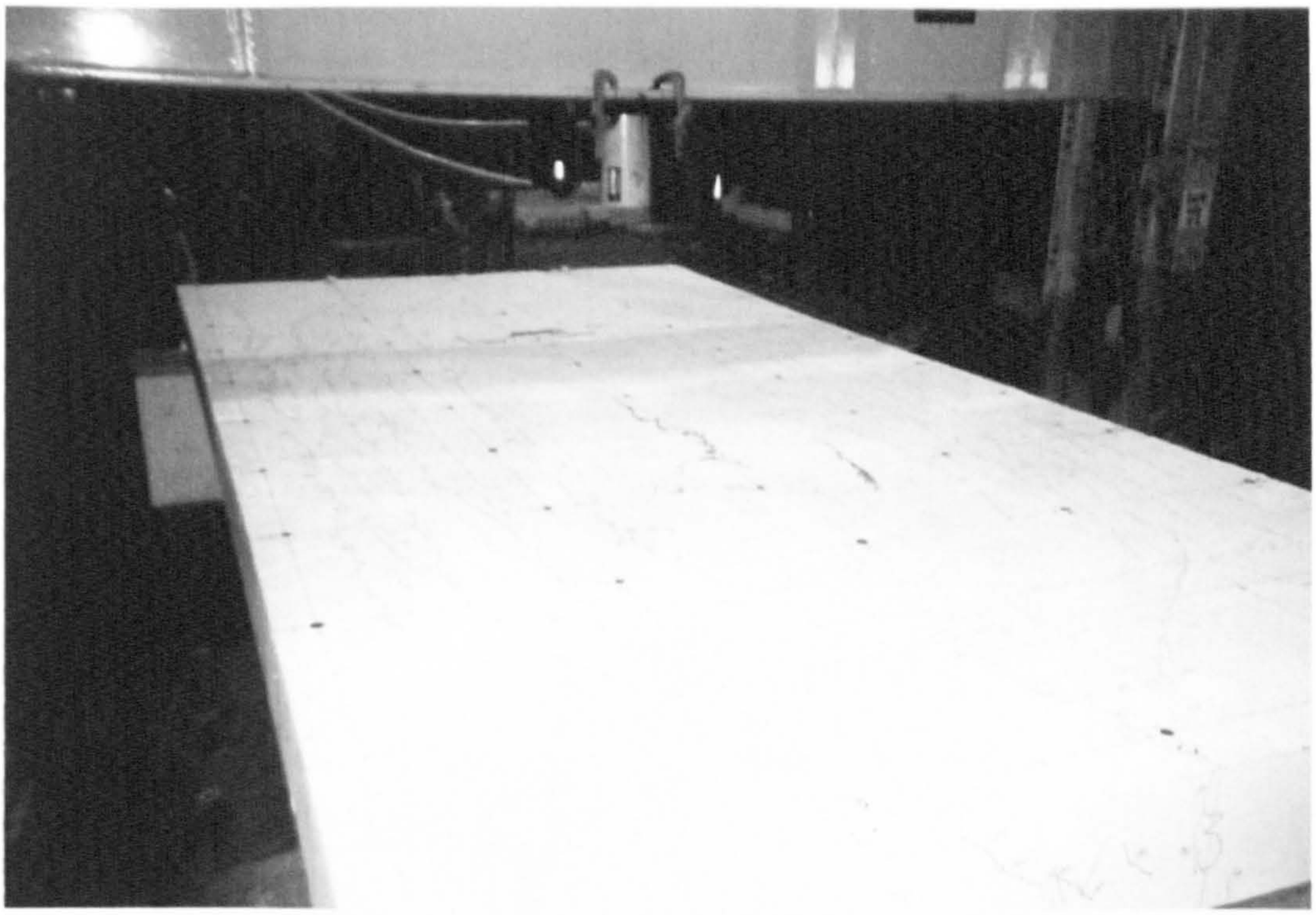

Plate 4-7: Deck 6 top surface cracking

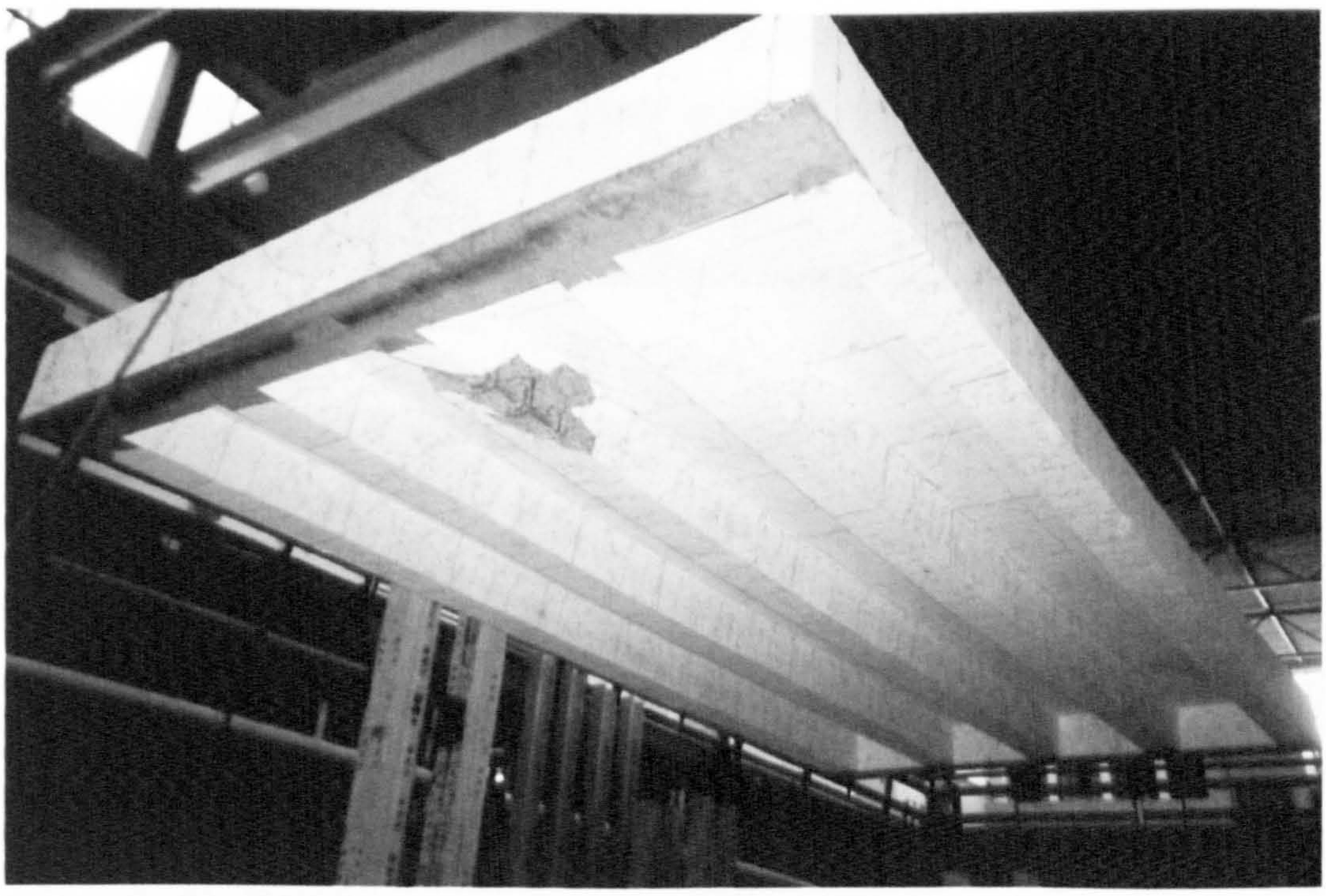

Plate 4-8: Deck 9 torsion failure in beam iii

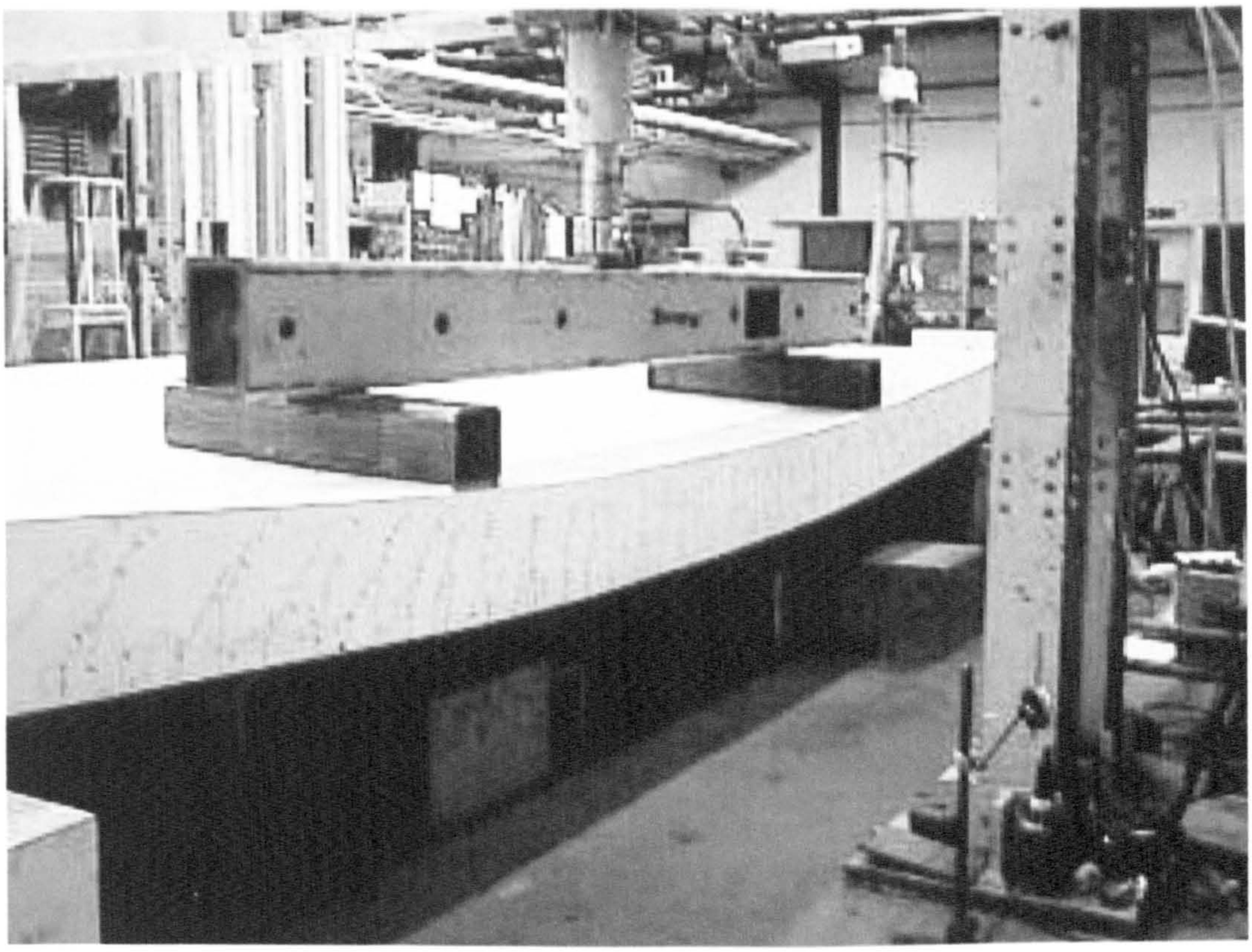

Plate 4-9: Deck 3 failure due to excessive deflection

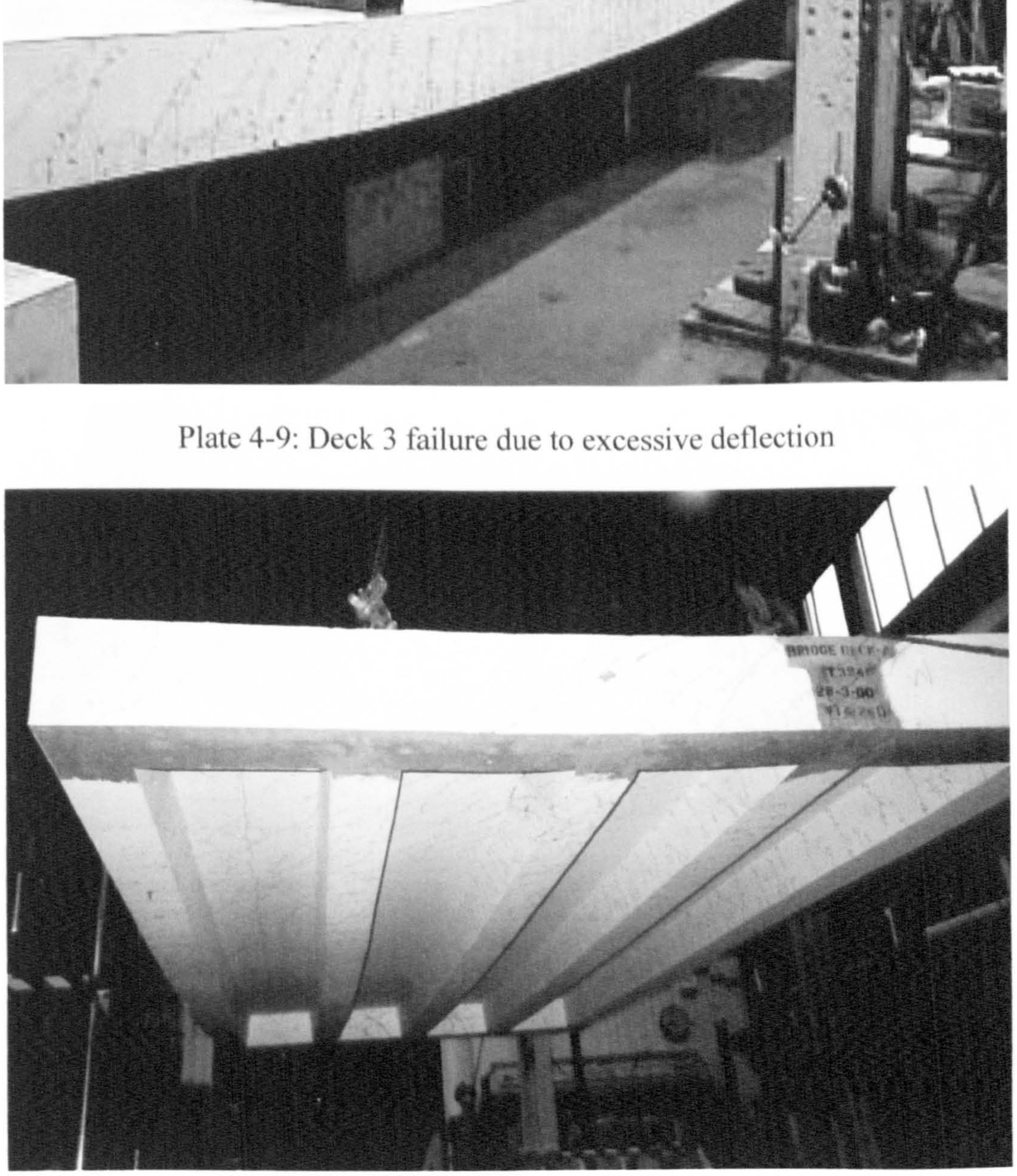

Plate 4-10: Deck 3 failure due to excessive deflection

Plate 4-11: Deck 10 torsion cracking in beam iii

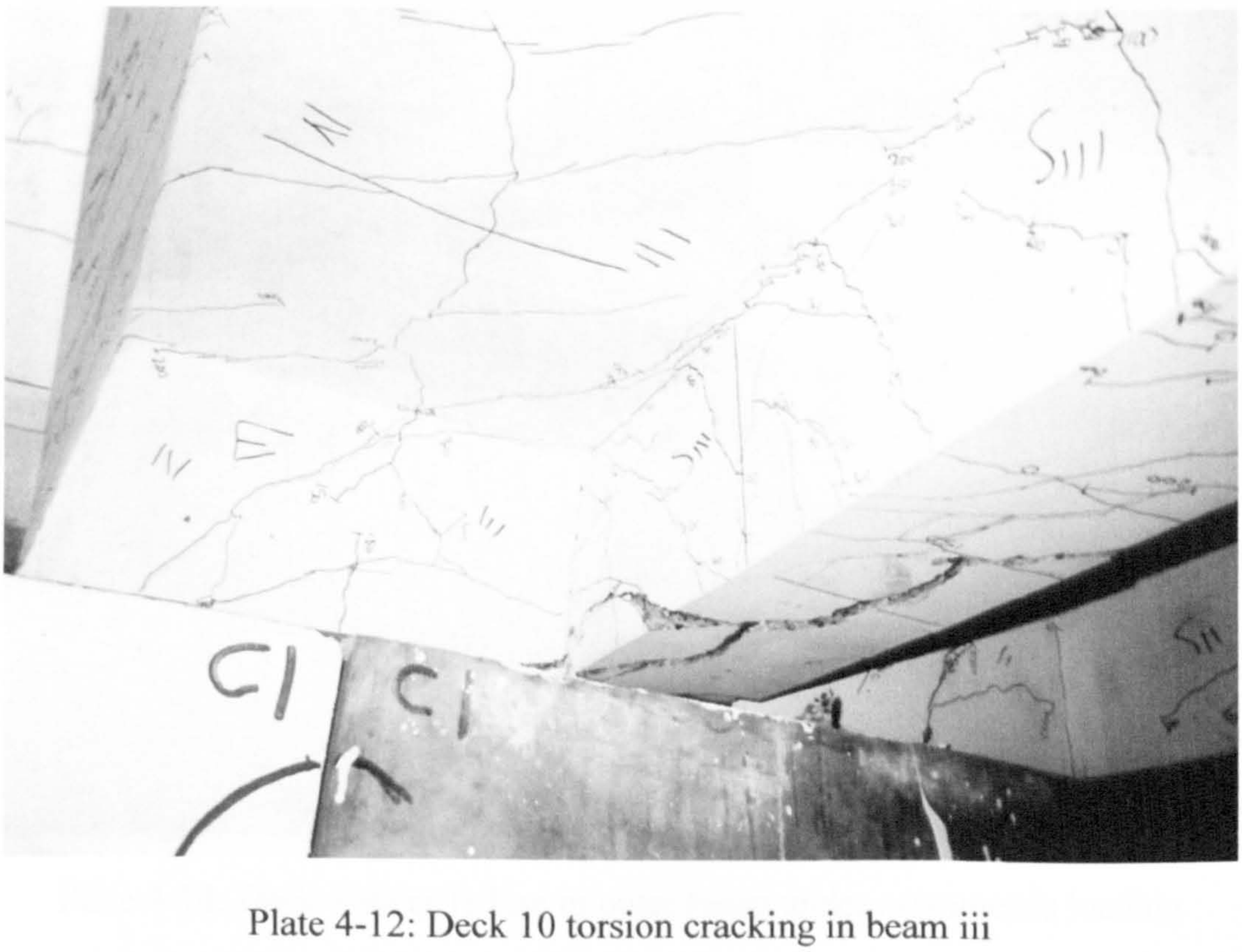

Plate 4-12: Deck 10 torsion cracking in beam iii

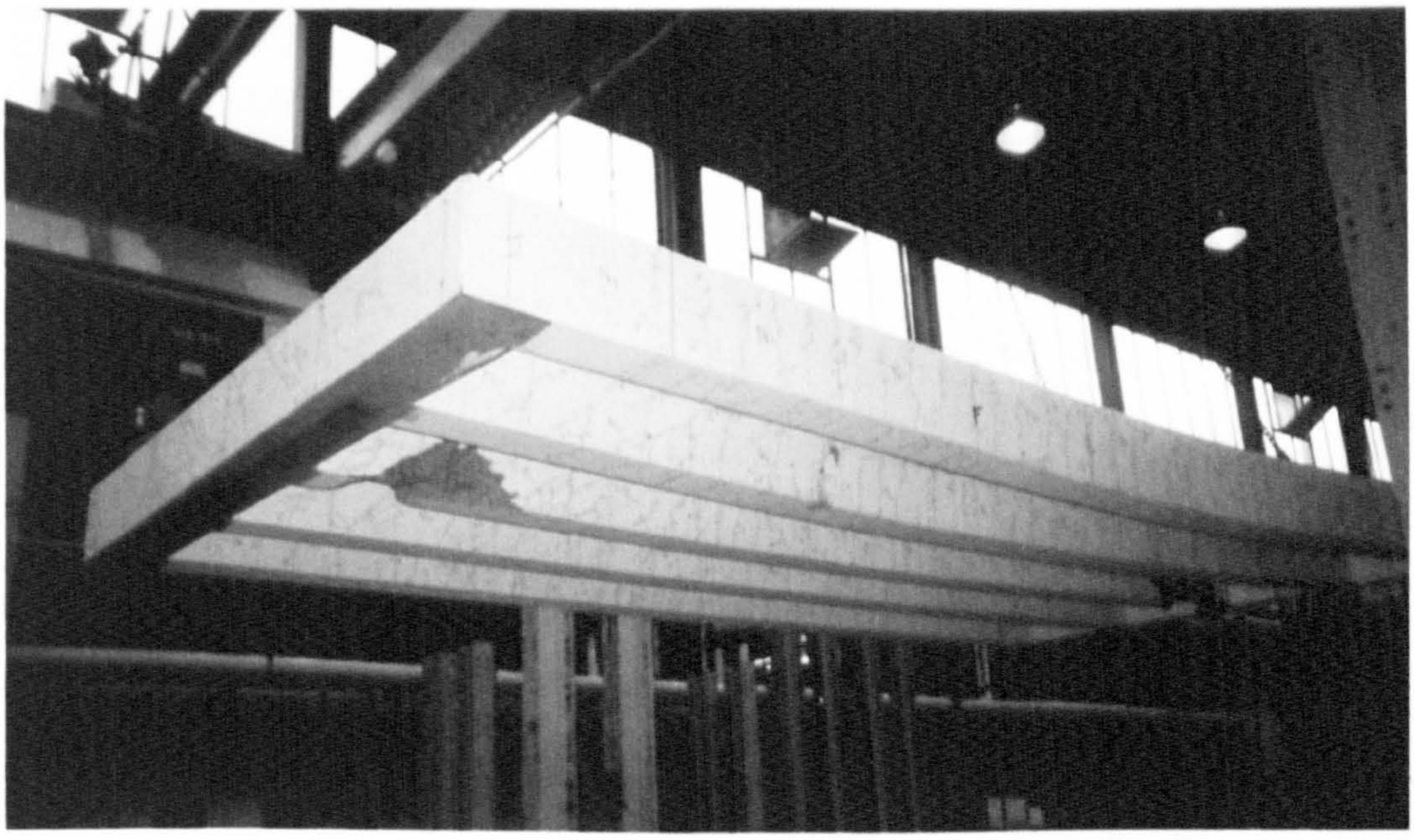

Plate 4-13: Deck 10 torsion failure at ends of beam iii

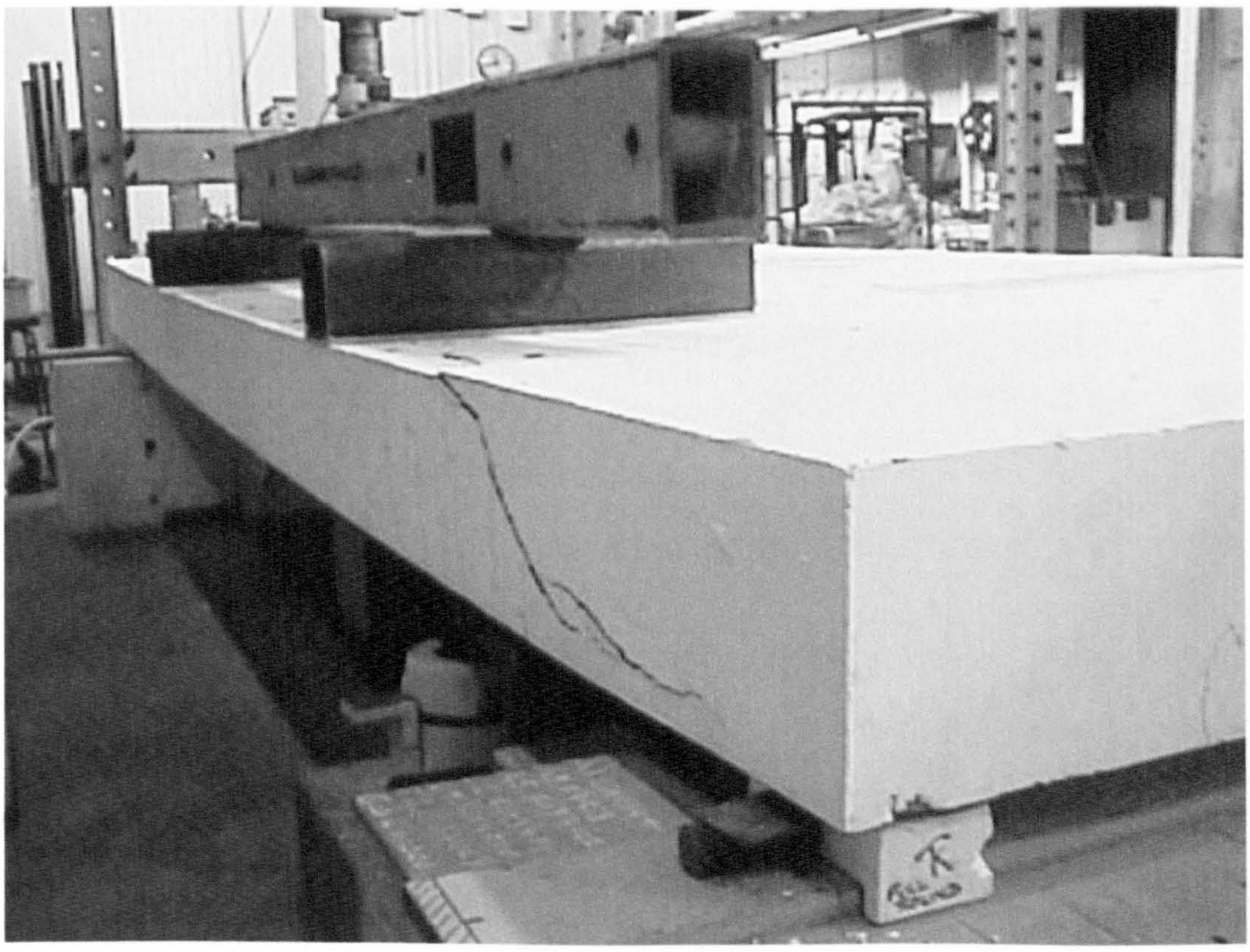

Plate 4-14: Deck 4 shear failure in outer beam under asymmetric loading

Plate 4-15: Deck 5 loading and cracking

Plate 4-16: Deck 4 shear cracking at failure in beam i

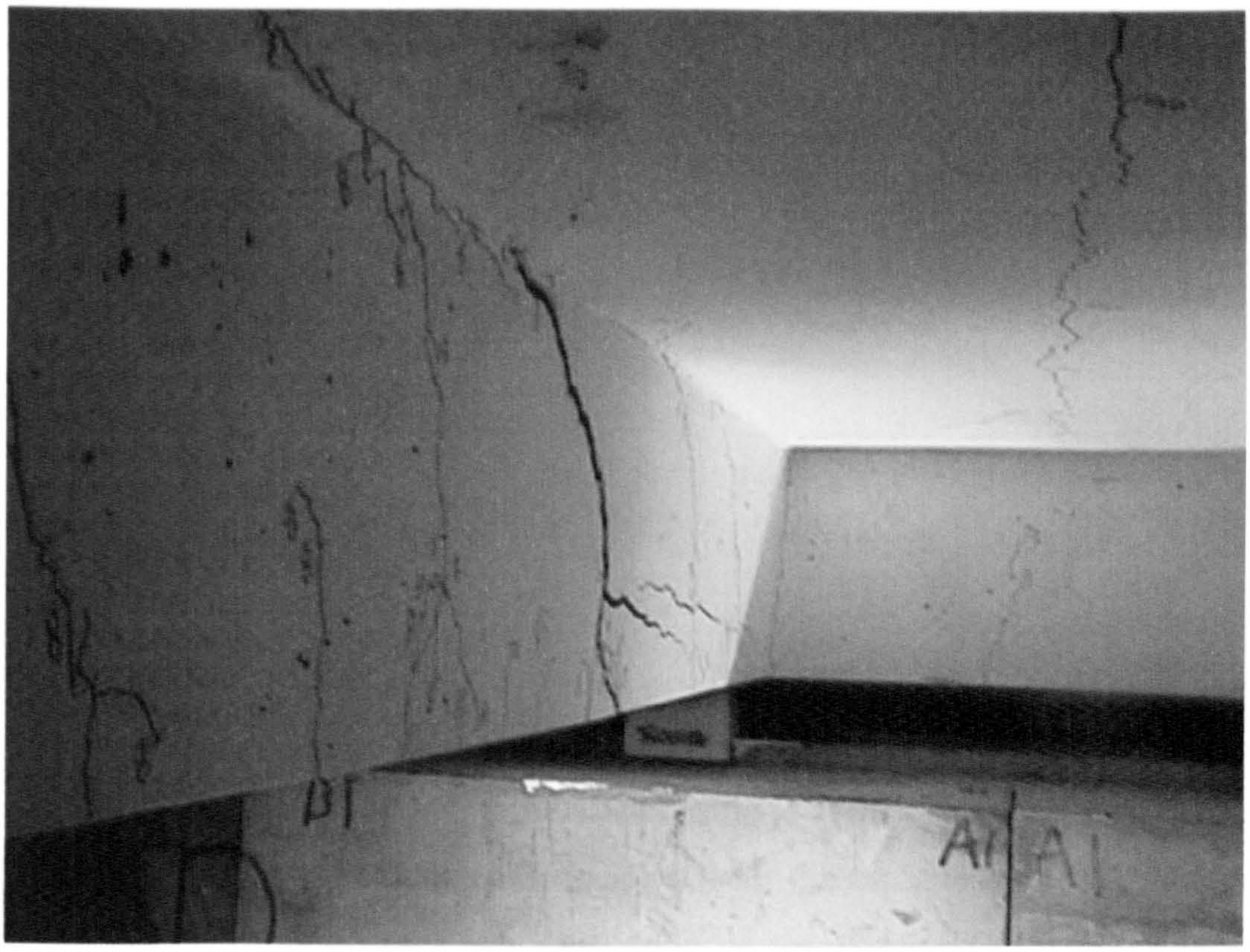

Plate 4-17: Deck 4 shear cracking at failure in beam ii

CHAPTER 5

DYNAMIC TESTING

5.1 Introduction

This chapter provides a description of the dynamic testing of ten one-quarter-scale reinforced concrete beam-and-slab bridge decks. These tests were performed on the same deck specimens used for the static testing described in chapter 3. In this chapter, the processing of the vibration data into modal properties is described and the results discussed. These tests were carried out to investigate the feasibility of using vibration characteristics for structural health monitoring of bridges and seek to extend the studies performed on beam structures by testing a more realistic specimen. The application of finite element model updating to the results of this dynamic testing is described in chapter 6.

A brief explanation of modal testing is given to provide the foundation for a discussion of the variation of modal properties with the changing state of the bridge decks. The natural frequencies and mode shapes are compared when the bridge decks are subjected to an increasing overload. A discussion of the boundary conditions is included and the results from using two different support arrangements are given and compared. The undamaged bridge decks are compared to a finite element model, which was then updated based on the modal data collected. A discussion of the quality of the correlation between the experimental data and finite element model is presented.

5.2 Modal analysis

This section gives an explanation of the techniques used for the processing of the data collected from the modal testing into the required modal properties. Details of the modal testing procedure are given in chapter 3.

The data was processed to obtain the frequency response function (FRF) for all the time histories collected as detailed in section 3.7.1, and an average FRF found for each measurement location. These averaged FRFs were then used to find the modal properties of natural frequency, mode shape and modal damping using the rational fraction polynomial curve fit routine described in appendix A.

The routine used was part of the DIAMOND toolbox (Doebling et al, 1997) developed for Matlab by Los Alamos National Laboratory especially for use in health monitoring and damage detection. The routine was adapted to allow it to be run automatically without the need to enter the lower and upper boundaries of the curve fit window using the cursors and the GUI.

In this method, a lower and an upper value of the curve fit need to be defined, and the number of modes to fit within this window and an account for the out-of-band modes selected. These values should be based on knowledge of the locations of the modes of the system and in this investigation, approximate values of the natural frequencies were identified using the complex mode indicator function (CMIF), Ewins (2000).

$$[CMIF(\omega)]_{p\times p} = [\Sigma(\omega)]^T_{p\times n}[\Sigma(\omega)]_{n\times p} \qquad \text{Equation 5-1}$$

where

$$[H(\omega)]_{n\times p} = [U(\omega)]_{n\times n}[\Sigma(\omega)]_{n\times p}[V(\omega)]^T_{p\times p} \qquad \text{Equation 5-2}$$

This indicator function results in a similar plot to an FRF, but uses principal components to determine where the major contributions are in the FRFs measured at different locations and displays these as a series of lines. This indicator function combines all the measured FRFs into a single plot where the

approximate frequencies of possible modes are given by peaks. The plot contains lines of reducing magnitude, displaying the most important contributions with a larger magnitude and the least important with low magnitude. This essentially removes most of the noise from the signals as this is displayed with the lowest magnitude.

The CMIF is particularly good at distinguishing closely spaced modes, provided the structure was tested using multiple excitation locations. This, however, means that it is not particularly useful for the shaker testing conducted as there is only one FRF collected at each location, as compared to the hammer testing where seven "independent" mode shape sets can be produced from the seven accelerometers used. For the shaker testing, the CMIF consists of only one line but, in fact, makes identifying the peaks easier than using all 45 FRFs, although an indication of locations of modes could also be obtained by averaging of all the FRFs measured.

From the frequencies of possible mode locations identified using the CMIF, a fit was performed around each of these values. The rational fraction polynomial method performs a fit between a lower and an upper value to identify a given number of modes using all the FRF data available, and includes terms representing the out-of-band modes. The algorithm performs a two step fit, first identifying the natural frequencies and damping values, then performing a second stage to determine the mode shapes.

The data collected from the decks consisted of 45 measurement locations as shown in Figure 3-7, each containing 4096 frequency points. The ideal method of extracting the modal parameters would be to perform a curve fit over the whole frequency range measured and estimating the number of modes contained in this range. However, due to limitations on computing power, it was not possible to perform a curve fit on the complete data set in a single pass. Instead, it was decided to perform a series of small fits around modes that were close to one another.

From a number of investigations, a difference between modes of at least 10Hz meant that they were sufficiently separated to permit the curve fit to be performed individually and still obtain satisfactory results. For modes closer

than this, a multiple degree-of-freedom fit was performed. The upper and lower values of the curve fit window were decided to be 20 data points above and below the highest and lowest frequency to be fitted respectively. This was kept constant for all the modes estimated and the values were selected to allow no overlap between subsequent curve fits, as this appeared to distort the modal parameters found. The modes extracted were in the region of 0 to 300Hz for all tests due to the hammer impact providing limited excitation above 300Hz.

5.3 Dynamic properties of the initial decks

In order to maintain the realistic nature of the one-quarter scale deck specimens, the dynamic properties were found when the decks were supported on ten steel bearings, as discussed in section 3.6.4. This, however, creates a large degree of redundancy in the boundary conditions that may change due to loading and induce changes in the dynamic properties that may mask the influence of damage. For this reason, a number of different boundary conditions were investigated.

To remove the structural indeterminacy associated with ten bearings, some of the decks were supported on three of the original ten steel bearings to produce a consistent degree of support given by each location. This was done to eliminate most of the effects of changing boundary conditions on the dynamic properties of the deck, allowing the consequence of structural damage to be investigated in isolation.

A third type of bearing condition was investigated by using ten rubber blocks. This essentially maintains the realistic support conditions whilst allowing the small discrepancies in the profile of the deck to be accommodated without the need for packing with steel shims. It was though that these types of supports could be more realistic than steel, but, due to the amount of deviation in the deck, it was necessary to use a very soft rubber that allowed large deflections, which is not representative of the elastomeric bearings used in actual bridge construction. It would also have been necessary to replace all the bearings between each increment, as it was not possible to load the deck when supported on soft rubber and the bearings themselves suffered from a significant amount of permanent deformation, which would again cause changes in the boundary

conditions. For these reasons, this type of bearing was only employed for two decks and for the modal survey of the initial condition of the decks.

The testing of decks 1 and 2 did not include measurements of the response at locations above the bearings, so only 35 points in a grid were measured as very little movement was expected at the bearings. However, upon further inspection, it was found that this was not the case and the modal surveys on subsequent decks that were performed used 45 measurement points including above the support locations. Deck 1 is not included in the comparison of the initial modal properties extracted, as the boundary conditions were not the same as the other decks. In all cases, when 35 or 45 measurement locations were used, the mode shapes were plotted by performing a cubic interpolation between the measured points. The results of the modal surveys performed on the decks when in an initial undamaged condition are discussed in the following sections.

5.3.1 Ten supports

A comparison of the FRFs obtained from each of the decks reveals that there are several inconsistencies between the curves. Typical plots of the FRFs obtained are given in Figure 5-1, Figure 5-2 and Figure 5-3. Although many of the FRFs display similar magnitudes in general, there are significant differences in the number and locations of the resonant peaks. This indicates that, even though the decks should be nominally identical in the undamaged state, there are considerable deviations in their dynamic behaviour.

Attempting to apply the MAC to the mode shapes using a threshold value of 0.8 resulted in approximately 3 modes that could be determined to be the same, however, this situation is improved slightly if the MAC does not include the measurements taken above the support locations. This indicates that the support locations have significant influence on the dynamic behaviour of the decks, and the amount of movement at these points can vary considerably between the decks tested. This is due to the fact that the decks did not possess a flat profile and required the bearings to be packed with thin pieces of metal to ensure a tight fit and small differences in the support conditions can cause the deck to be less supported in certain areas.

Lowering the threshold MAC value to 0.6 still appears to match modes that possess the same general shape, although according to the low MAC value these modes should not be taken to be the same. Again, discounting the measurements taken above the support locations produces more modes that are correlated between the decks. Using a MAC value of 0.6 correlates approximately 8 modes between the decks.

Due to the change in mode shapes between the decks, the corresponding natural frequencies are different for modes that are apparently similar, as would be expected.

5.3.2 Three supports

In general, the testing of the decks on three supports produced much clearer results when compared to using ten supports. In all cases, the FRFs obtained appeared to be consistent, displaying a comparable number of resonant frequencies in the approximately the same locations, as can be seen in Figure 5-4, Figure 5-5, Figure 5-6 and Figure 5-7 of typical FRF results.

Much of this testing produced consistent results, both with regard to the mode shapes found and their corresponding natural frequencies and it was often the case that similar modes were found for most of the decks tested, as can be seen in Figure 5-8 and Figure 5-9. In this case, the threshold MAC value was defined as 0.8, indicating that the mode shapes produced when testing the decks on three supports produces much better results than the other boundary conditions, as would be expected.

Approximately 15 modes were found to match between the different decks, although it was not always the same modes that produced good MAC values. Deck 7 did not appear to produce as good a match when compared to the other decks, but upon further inspection, it was noted that one measurement location was in error, distorting the mode shapes sufficiently to give considerably lower MAC values.

The natural frequencies found for the modes with high MAC values were very similar, and in general retained the relationship between the frequencies.

5.3.3 Rubber supports

The results from the modal extraction process when the decks were tested supported by ten rubber supports highlight some of the problems when using unknown material stiffness. Due to the irregularities in the deck profiles, when the decks were supported on soft rubber, the differential height in the supports was equalised across each of the five bearings causing some to be compressed to a higher degree than others. This difference in the amount of compression for each of the supports produces a variation in the stiffness of the rubber, creating unknown boundary conditions.

This variation in the boundary conditions can be seen in the FRFs produced, Figure 5-10 and Figure 5-11, and in the results for the mode shapes. The mode shapes of Deck 4, given in Figure 5-12, are not symmetrical, as would be expected if the supports were identical, and the differences in the amount of movement above the support locations distorts the mode shape considerably. Deck 5, however, produces mode shapes that are almost identical to those predicted analytically, see Figure 5-13. It can be seen that each of the bearings is providing almost the same support to the deck, and in fact gives better mode shapes than the other support conditions tested. The modes clearly indicate that the longitudinal bending modes have been excited sufficiently, which is not the case for the other supports investigated.

However, whilst the results from one deck show that high quality modes can be obtained when using rubber supports, the differences observed between the two decks indicates that it would not be possible to control the boundary conditions for different decks. When the bearings were removed, it was noted that there was a significant amount of deformation of the rubber due to self-weight of the deck that could not be reversed. Furthermore, it is not possible to load the decks whilst they are supported on the rubber bearings, as this causes significant compression, so they would need to be replaced after each load increment, again giving a possible source of variation in the results. For these reasons, the remaining decks were tested on steel supports.

5.3.4 Discussion of support conditions

This study of the undamaged decks when supported on different bearing arrangements indicates several important factors that need to be considered prior to testing a full scale bridge.

Small changes in the boundary conditions, particularly when the supports are indeterminate, can have a significant effect on the vibration characteristics of the decks. This is demonstrated by the small number of modes that formed the same mode shapes for nominally identical decks when supported on ten steel bearings.

The use of softer bearings caused the mode shapes of one deck to become almost the same as those predicted by theory, but the mode shapes of the other deck were distorted, probably due to the initial imperfections in the profile of the deck. This caused some of the bearings to be stiffer than others as they were compressed more giving non-uniform boundary conditions.

Supporting the deck on three steel bearings provided a determinate structure and allowed the boundary conditions to be essentially identical for each deck. This means that the variation in the results obtained from this testing should be due to factors other than the bearing conditions, such as differences in the material properties of the concrete and errors in dimensions. It is also likely that some of the variation will arise due to changes in the environmental conditions, experimental error and errors in the modal extraction routine. It should be noted that even though the support conditions should be identical, there remains some variation in the vibration characteristics and modal properties. The reliability of measuring the dynamic behaviour of structures requires further investigation before the method can be employed on real bridges, particularly with indeterminate boundary conditions.

A positive effect of the variation in the vibration characteristics due to different support conditions is that the dynamic behaviour is clearly extremely sensitive to changes in the bearings. As deterioration of the bearings is a common source of decline in real bridges, it may be worthwhile pursuing this area further to monitor bearing deterioration.

5.4 Frequency change and damage

5.4.1 Mode matching

In order to assess the sensitivity of natural frequencies to damage, it is necessary to be able to determine which natural frequencies belong to the same modes when the system has been changed. In simple structures where modes are well separated, it is possible to assume that the mode shape itself and the order of the modes will not change as the structure becomes more damaged. However, for more complicated structures, this assumption is no longer valid as the modes are generally more closely spaced and some switching of the order of the modes may arise due to damage and, depending on the severity of the damage, the modes of the structure can no longer be considered to be the same. Therefore, the modes must be correlated using some other means, usually involving a comparison of the mode shape, either visually or by using the MAC algorithm.

The process of matching modes between load levels in this study involves a combination of both the MAC value and a visual inspection of the mode shapes. The two main factors that caused changes in the mode shapes were the damage induced by overloading and the bearing conditions. In many cases, these two variations caused the mode shape to translate in the longitudinal or transverse direction, or to make local regions of the deck less stiff than the previous load level. This caused the local maxima and minima of the mode shape to increase in size and spread, which in turn produced relatively low MAC values. For this reason, the threshold of the MAC value defining a well matched mode was reduced to 0.7, and could be as low as 0.4.

If the MAC value is greater than 0.7, the modes are assumed to be the same mode. For two modes matching the same mode, the pair with the largest MAC value is taken. If the MAC value is less than this, a visual inspection between the plots of the mode shapes was carried out, provided that the MAC value is greater than 0.4. Visual inspection based on general shape of mode, i.e. the location of the maxima and minima, and the natural frequencies of the two modes. This was necessary due to the limitations of the MAC algorithm – if the mode shape was translated in the longitudinal/transverse etc. direction, then

there could be a significant difference between the magnitude of the mode shapes at each location, even though they have a similar general shape. This is particularly noticeable for the specimens tested as changes in the bearing conditions between load levels could change the mode shapes. This change in the bearing conditions could be due to the resetting necessary when the decks had been tested on three supports and then placed back on ten, or due to the permanent deformation of the deck after it had been subjected to loading, or due to the change in the stiffness of the deck in the end beam above the bearing.

5.4.2 Natural frequency variation with damage

One of the most common measures used in dynamic testing for condition assessment is to monitor the variation of natural frequencies, discussed in section 2.3.1. In this section, the natural frequency change is correlated with the load level applied to the deck to provide the basis for a structural health monitoring of the decks tested.

The discussion in this section is based on plots of natural frequency against load level, which are given in Figure 5-14 to Figure 5-29. In these plots, the natural frequencies have been normalised with respect to the natural frequencies of the undamaged deck due to the range of frequencies that were included in the modal extraction routine, 5 to 300Hz.

The trend in many of the plots shows that the natural frequency is sensitive to the damage introduced in the form of cracking. Whilst there are some inconsistencies in the trends observed, it can be seen that many of the natural frequencies reduce as the damage increases, although the form of the reduction appears to be unclear and possesses significant variation between the decks. However, the general trend is in the form of a relatively constant reduction for many of the load levels until the final load application leading to failure, which produces a sharp reduction in the natural frequencies, with only a small number of modes being consistent between the penultimate and final load level.

There are some significant variations between the results from the decks tested when supported on ten and on three steel bearings, although, in general, the natural frequency demonstrates a similar reduction as the load level increases.

The trends appear to display a comparable constant drop until the final load level, where there is a similar sharp reduction. The differences between the dynamic properties of the decks when supported on ten or three bearings are marked, and these features are discussed in the following sections.

5.4.2.1 Three supports

Supporting the decks on three bearings was intended to eliminate the effect of uncertain boundary conditions from the modal properties extracted and enable a direct correlation of the natural frequency variation with increasing damage in the form of cracking. It can be seen from the plots of normalised natural frequency against load level, Figure 5-14 to Figure 5-22, that the frequencies generally reduce as the damage increases. This is also seen in the average change of all modes, Figure 5-30.

For all the decks, however, there are a small number of modes that show an apparent increase in the natural frequency for a few load levels. Due to the consistent boundary conditions, this effect must arise from other sources. The most likely reasons are due to actual changes in the modal stiffness due to the cracking induced in the decks, inconsistencies in the mode tracking routine and errors in the natural frequency extracted.

A change in the modal stiffness may occur when the deck is subjected to dynamic testing supported on three bearings, as the decks were all loaded on ten bearings. This change of bearing conditions could cause some cracking introduced due to overloading to have less influence on the dynamic behaviour as more cracking is introduced changing the stress distribution, due to the facts that when the deck is supported on three bearings, the region between the two supports at one end is under a greater sagging moment due to self-weight than when it is supported across its width. At the opposite end, where the deck is only supported in the centre, the deck suffers from a greater hogging moment across the end beam. This change of the boundary condition will also cause the stress distribution in the rest of the deck to alter, causing some cracking to close and some to open more than when supported on ten bearings. The effect of the asymmetry in the support conditions will also cause the damage to become asymmetric, as cracks close due to the change in bending, and in

particular the symmetrical cracking introduced by the four-point bending loading arrangement to be converted into asymmetric damage.

It can also be seen in the plots that some apparently new modes are introduced and others seemingly disappear at certain load levels. Due to the changing condition of the deck as they are loaded, it could be argued that the modes extracted from one load level can not be the same as modes extracted from another level, even if all other factors influencing the dynamic behaviour of the deck remain constant. This view is supported by the appearance and disappearance of modes through the loading history, even when the deck is supported on the structurally determinate three supports.

The appearance and disappearance of modes may be due to an actual change in the modes exhibited by the damaged deck or existing modes changing to such a degree that the MAC value between the current and previous load level denotes that they are no longer the same mode. It is most likely that the reason is due to the existing modes becoming increasingly distorted by the damage introduced and changes in the boundary conditions, resulting in apparently new modes.

If particular areas become damaged more severely than others as the load increment is applied, a change in the mode shapes will result. For modes that are particularly sensitive to the stiffness in this region, the change in the mode shape could be significant causing a low MAC value when compared to other load levels. It is also possible that the damage could cause the introduction of new modes due to changes in the structural system or increased excitation of the mode. However, it should be remembered that the MAC algorithm suffers from a number of limitations, particularly with regard to translations in mode shapes, where maxima or minima move slightly away from their previous location.

It is interesting to note that the change in the natural frequencies is different for each mode extracted. It is also apparent that the amount of spread in the natural frequencies appears to increase as the damage increases, confirming that different modes have different sensitivities to the damage introduced, as would be expected. This indicates that there is a correlation between the

natural frequency of a mode and the damage distribution that could be employed in a damage location procedure, or to give more information regarding the damage before a more detailed inspection is instigated, allowing the investigation to be concentrated in the areas identified.

5.4.2.2 Ten supports

When the decks are supported on ten bearings, the variation in the natural frequencies becomes less clear, as can be seen in Figure 5-23 to Figure 5-29. It can be seen that some modes apparently increase in natural frequency, implying that the deck has become stiffer, even though it has been overloaded to a higher degree. It can be seen that not all mode shapes can be traced through the loading history, and that some apparently new modes appear at certain load levels. These modes were normalised by assuming that the ratio between the new and its adjacent natural frequencies remained constant and was of the same form when the deck was under no load.

This trend of increasing natural frequency can also be seen in the average of all the modes found, Figure 5-31. Considering each type of deck separately reveals the inconsistencies introduced when supporting the decks on ten bearings, as the trends are no longer as consistent as when the decks were supported on three bearings, although it should be noted that decks 6 and 7 displayed differences in the static behaviour.

The increase in natural frequencies can arise due to a number of factors associated with the distribution of damage and the indeterminate nature of the boundary conditions. Although some increases in natural frequency were found when the decks were supported on three bearings, the number and degree of modes increasing in frequency is much greater when supported on ten bearings.

An increase in the natural frequency of the decks supported on three bearings was attributed mainly to the effects of changes in the modal flexibility arising from the cracking distribution and errors in the natural frequency measurement and extraction. These factors will remain to be causes of the same behaviour when supported on ten bearings, although the increased significance of the changes appears to be due to the boundary conditions. However, it should be

noted that the changes in the natural frequencies for particular modes cannot be compared directly to ascertain the effect of changing boundary conditions due to the fact that the mode produced by one support condition are not the same as those found from another, even though the mode shapes may be similar.

A visual comparison of the change in natural frequency of the modes extracted from decks supported on both ten and three bearings reveals that the general trend of the reduction in natural frequency with increasing load level is similar. This indicates that the natural frequency is influenced by common factors regardless of the support conditions, and should therefore be mostly influenced by the cracking introduced by overloading.

When the number of new modes appearing and existing ones disappearing is compared between decks supported on ten and three bearings, it can be seen that it occurs much more frequently when the decks are supported on ten bearings. The fact that modes appear and disappear even when the deck is supported on three bearings shows that it is not totally due to changes in the boundary conditions between the load levels. However, the fact that the frequency of occurrence increases when the deck is supported by ten bearings indicates that the boundary conditions have a significant effect on the dynamic behaviour of the deck. It is evident from these findings that the bearing conditions are unlikely to be consistent for each dynamic test at different load levels.

The change in bearing conditions could arise from a number of sources. It may be the case that the cracking of the deck caused the load to be distributed in a different manner, introducing a change in the amount of load on each of the bearings and altering the degree of support provided by particular bearings. The cracking in the deck could also have reduced the stiffness of the end beams between the supports, again changing the portion of the load distributed to each of the bearings. The decks tested on both ten and three bearings were lifted off the bearings in order to change to support conditions for the dynamic tests and were loaded on ten supports. They were reset using the same packing shims used at the previous load level in an attempt to maintain constant boundary conditions, although this procedure could have introduced deviations in the support conditions.

5.4.3 Correlation with deck and damage type

Whilst correlating the change in natural frequencies with the load applied to the decks is useful in terms of predicting the remaining capacity of the structure in a health monitoring sense, it is only possible in this study as the failure load of the decks is known. A more valuable measure of the bridge deterioration may be gained from investigating how the natural frequency changes are related to the damage suffered by the structure, in this case due to the cracking introduced by overloading. In the following sections, the cracking observed at each load increment is compared with the reduction in the natural frequencies in terms of the overall trend. This was possible due to the loading increments appearing to cause specific types of cracking to develop.

However, it should be noted that the objective of the whole study is to investigate the feasibility of using dynamic testing for structural health monitoring applications, meaning that the method should be able to detect that there has been a change in the structural system in order to conduct further, more detailed, investigations or to monitor the rate of deterioration of the structure to plan maintenance of a problem identified through a previous inspection. The method is not required to be able to determine the location or severity of the actual damage that is present, although an indication of the general region that is thought to be deteriorating could be beneficial in the instigation of further inspections and in confirming the area deteriorating.

5.4.3.1 Symmetric loading

The decks tested under a symmetric loading arrangement were 1, 2, 8 (type A) and 6 and 7 (type B). Plotting the variation in normalised natural frequency for all the decks tested under a symmetric loading regime, as seen in Figure 5-32, reveals some interesting findings. (It should be noted that, due to the testing performed, these results are from decks tested on ten bearings, and as discussed in the previous section these findings are less clear than when tested on three bearings).

It can be seen that the changes in natural frequency appear to follow similar trends as the damage increases, although there are some variations in the results for each deck. Many of the decks show a change in natural frequencies

in the first load increment, then a larger reduction that become less as the decks approach failure, which is accompanied by a sharp drop.

The changes in the natural frequencies obtained from the type A decks follow very similar trends, although it is clear that deck 8 contains a larger spread in the results than deck 2. The corresponding plots for the type B decks also display similar changes to each other. However, it can be seen that the natural frequencies for deck 6 reduce by a larger amount than those for deck 7, and some frequencies of deck 7 appear to increase, but this is most likely due to inconsistencies in the bearing conditions. A similar plot can verify this when the decks were supported on three bearings, showing only a small increase in some natural frequencies and a much clearer general reduction. Still it can be seen that the results for deck 6 are lower than those for deck 7, which corresponds to the considerably greater amount of cracking exhibited by this deck.

The shallow gradient of the curve for the two type A decks between 150kN and 200kN appears to correspond to the load increment that produced very little growth in the cracking, which is reinforced by the observation that almost all the natural frequencies reduce. The increase in some natural frequencies from their values at 200kN to those at 250kN may be explained by the formation of asymmetric longitudinal and radial cracking causing an increase in the modal stiffness of particular modes due to changes in the modal curvature. However, it may be the case that this is accentuated by variations in the bearing conditions.

The more ductile failure of decks 2 and 8 can be compared to the sudden, brittle, failures of decks 6 and 7 through the changes observed in natural frequency. The trends for the type A decks demonstrate a noticeably greater reduction in the final two load steps than the type B decks due to considerably more cracking occurring over a longer period. However, it can be seen that there is a difference in the amount of reduction in the final load step for the same type of deck when loaded under the same regime. This may be due to a highly localised failure causing only a significant loss of stiffness in a small area, whilst the remainder of the deck suffers from only a small increase in cracking. This leads to a large change in the mode shape in the less stiff

region, providing enough distortion of the mode shape for it to not produce an acceptable MAC value when compared to the previous load level, meaning that only a few of the modes can be followed through to failure. Due to the large amount of damage that occurs at failure, it is questionable as to whether the mode can be considered to be the same, as the system will have changed significantly.

It appears from the generally lower natural frequencies that the stiffness of the type B decks reduces by a much greater extent than type A decks even though the cracking introduced is of a similar nature. This is especially true of deck 6, which displayed significantly more cracking than deck 7, corresponding to the larger reduction in natural frequencies observed.

The consistency of these results indicates that there is a degree of repeatability in the trends of the normalised natural frequencies when compared to the amount of damage caused to the deck. However, there are some significant differences in the results, some of which correspond to the differences in the cracking introduced and some to inconsistencies between the decks.

5.4.3.2 Asymmetric cracking

The decks tested under an asymmetric loading arrangement were 3, 9, 10 (type A) and 4 and 5 (type B). The natural frequencies of all these decks were found when they were supported on three bearings, and the plot of these normalised natural frequencies against applied load is shown in Figure 5-33 and Figure 5-34.

This figure indicates that these decks appear to behave in a similar manner to one another in terms of the change in natural frequency when compared to the initial values. The type A decks, 9 and 10, tested under HB loading with the first load increment causing a small reduction in natural frequencies, followed by a greater drop in the next increment. Interestingly, both decks then show some modes increasing slightly in frequency at a load of 150kN, before an almost constant amount of reduction until a sharp drop at failure. This increase in natural frequencies at a load of 150kN appears to correspond to the formation of a large amount of asymmetrical cracking in the form of longitudinal cracking in the soffit, with very little growth in the vertical

cracking. This agrees with the findings in the previous section, where it was noted that an increase in frequency was observed when there was little growth in the vertical cracking, but other cracks formed that were asymmetric.

The plots of natural frequency against damage for decks 9 and 10 display a slightly different trend with regard to the amount of spread in the natural frequencies as damage increases. After the decks have been loaded to 150kN, the sensitivities of the natural frequencies change, causing them to reduce to a similar ratio of the original frequency, effectively reducing the amount of spread.

Comparing these curves to that observed for deck 3, which was tested under asymmetric loading, reveals a very different trend. The behaviour in the first two load increments is similar, although deck 3 experiences a much greater reduction in most natural frequencies. The next load level produces a large increase in the natural frequency of many modes to values that are comparable to the previous load level. This increase in some modes continues for the next load increment, although to a smaller extent, followed by a reduction in the final two load levels to failure. This may be due to the greater degree of asymmetry in the cracking pattern for deck 3, where the two beams under load suffered more damage than those in decks 9 and 10 and the beams not under direct load were less damaged. From this, it may be possible to identify how the cracking develops in real bridges.

Decks 4 and 5 both appear to display similar trends when plotted against load increment, possessing comparable reductions in natural frequencies at each load level. However, it can be seen that the amount of spread in the results found is larger for deck 4 than deck 5. This may be due to differences in the initial deck, as deck 4 appeared to have suffered from a large amount of plastic settlement, causing considerable cracking in the deck. This would also be a possible explanation for the increase in some modes occurring in the first load step where the stiffness distribution would be altered, particularly as much of this cracking was in the top surface of the deck.

In general, there is an almost constant reduction in the natural frequencies of the decks, corresponding to the growth of cracking present in all the loading

increments producing a steady reduction in stiffness. The effects of the asymmetric nature of the cracking can be seen in the increase in frequency of some modes at certain load levels, which, as the decks are supported on three bearings, is mainly due to the damage caused to the decks.

The effect of the symmetry of the damage appears to produce different trends in the variation of natural frequency. The increase in some natural frequencies seems to correspond to the growth of longitudinal cracking in the soffit of the deck, which increases the asymmetrical nature of the damage by promoting the separation of the loaded beams from the remainder of the deck.

5.4.4 Natural frequency variation with deflection

Whilst it is useful to discuss the employment of a structural health monitoring procedure in terms of the ultimate load carrying capacity of the structure, it is perhaps more important to relate the modal properties to the damage that the structure exhibits. However, from the previous section, it is clear that whilst some general statements regarding the effects of particular types of cracking can be made, it is not possible to associate changes in natural frequencies directly to the actual damage that has occurred.

Another measure of damage is by the use of deflection, which should give an indication of the severity of the damage introduced into the deck and provide a more accurate description of the state of the deck than applied load. The maximum deflection under the applied load is used as this should be related to the amount of cracking that formed during each loading increment.

It should be noted that in some cases, most of the deflection of the decks occurs in the load step leading to failure, especially for the type A decks where the failure was in a ductile manner. Due to the similar behaviour of the decks under static loading, as discussed in chapter 4, the general trends of the variation in natural frequency with increasing damage remain comparable with each other. However, the natural frequency values no longer appear at uniform spacing.

The plots of natural frequency against deflection are given in Figure 5-35 and Figure 5-36 for the decks supported on ten bearings and three bearings, respectively.

5.4.5 Natural frequency variation with mode

Whilst changes in the natural frequencies alone provide a clear trend with regard to the damage level, it is possible to expand the potential by considering the associated mode. This may provide valuable information concerning the damaged location and better equip the engineer monitoring the bridge in determining the condition of the structure.

Investigating the changes in the natural frequencies of particular modes requires the mode to be present throughout most, if not all, of the loading history, which, as discussed in the previous sections, is not always the case due to a number of factors. However, the results from the decks supported on three bearings provide more consistent results than those supported on ten, and the effect of mode on the natural frequencies is investigated first for these decks, then expanded to those supported on ten bearings.

The change of the second natural frequency, corresponding to the first longitudinal bending mode, is shown in Figure 5-37, together with the typical mode shape in Figure 5-38. From these figures, it is possible to see that there does not appear to be any significant difference in the second mode due to symmetric and asymmetric damage introduced to the decks. This is probably due to the mode shape being most sensitive to the flexural stiffness of the decks, and because of the amount of flexural reinforcement provided, the flexural cracking is approximately similar. A plateau region is apparent in the load levels between 100 and 250kN, again due to the small amount of flexural damage caused in these load increments as described in chapter 4. The observation of this plateau region in the middle range of the loading history compares well with the results found in the work by Eccles (1999) and Rohrmann et al (2001).

Considering the change in the natural frequency of the third mode, Figure 5-39, essentially the first torsion mode of the deck, Figure 5-40, it can be seen that there is very little transverse bending of the mode, meaning that the mode is

unlikely to be sensitive to longitudinal cracking. The effect of this can be seen in the smaller reduction in the natural frequency when compared to the other modes, prior to the final load increment. It should also be noted that both type A and B decks exhibit similar changes in this mode, indicating that it is not sensitive to the formation of shear and torsion cracking.

The modes involving the first bending mode in the transverse direction, presented in Figure 5-42, Figure 5-44 and Figure 5-46, display consistent trends with regard to the natural frequency variation as damage increases, shown in Figure 5-41, Figure 5-43 and Figure 5-45. The natural frequencies appear to decrease in an almost linear manner until the final load step. When compared to the natural frequency change for mode 2, it can be seen that the modes involving both transverse and longitudinal bending are sensitive to the damage introduced, and a particular difference is noted in the load levels leading to the formation of longitudinal cracking in the slab and between the beams.

The natural frequency, Figure 5-47, of the mode comprising first longitudinal bending and second transverse bending, Figure 5-48, displays more spread than the modes involving only the first transverse bending, and in some decks appears to be more sensitive to the cracking. The variation in the natural frequencies could be explained by considering that this mode shape has a higher curvature in the regions where the longitudinal cracking formed, and as this varies between the different decks and loading regimes, more spread results.

Projecting the observations for three bearings to the decks supported on ten bearings reveals some similar findings, although it should be noted that the natural frequencies contain more variation, as discussed in section 5.3.4. The trend in the natural frequency change of the first longitudinal bending mode, shown in Figure 5-49 and Figure 5-50 compares well with that from the deck supported on three bearings, displaying the relative insensitivity to the damage introduced 100 and 250kN.

Although the frequency variation is somewhat masked by the spread, it can be seen that the natural frequency change displayed in Figure 5-51 for the first

torsion mode, Figure 5-52, that again this mode is less sensitive to the cracking introduced. The findings of natural frequency change, Figure 5-53, for a mode involving transverse bending, Figure 5-54, appear to follow a similar trend to the results of the first bending mode at lower load increments, displaying a plateau region between 100 and 250kN. This may be explained by the smaller amount of transverse bending when compared to the deck supported on three bearings, meaning that the mode is less sensitive to the longitudinal cracking due to the deck being supported across the full width.

The investigation into the natural frequencies, shown in Figure 5-55, of a mode comprising the first longitudinal bending mode and the second transverse bending mode, Figure 5-56 reveals a similar trend to that of the first bending mode also. It appears from these results that one of the effects of supporting the deck using five bearings across both ends is to reduce the influence of the longitudinal cracking on the natural frequencies, meaning that it is much more difficult to determine what damage has occurred by studying the natural frequencies and mode shapes. The situation may be improved if modes involving higher transverse bending modes are also considered, although the practicality of this for real bridges excited by ambient vibration could exclude consistent measurement of these modes.

5.4.6 Mode shape change

From previous studies, it has been found that the mode shape can also reveal information regarding the state of the structure. However, it should be remembered that, at this stage of the investigation, the feasibility of using dynamic testing for health monitoring is being studied, rather than its use as a damage detection tool as it is to be implemented as a monitoring method to be used on bridges that have known "suspect" areas.

It would be expected that the mode shape becomes distorted from the initial shape due to the presence of cracking, giving less stiff areas. Attempts at using the MAC value as a measure of the deterioration of the mode shapes proved to be unsuccessful in determining consistent changes, as can be seen in the typical plots Figure 5-57, Figure 5-58 and Figure 5-59. This is due to the limitations

of the MAC algorithm in detecting small changes in the mode shapes and also the accuracy with which the mode shapes can be measured.

However, it has been noted in the previous sections that tracing the natural frequencies through the loading history is difficult due to low values produced by the MAC algorithm, suggesting that there is a change in the mode shapes as the decks become increasingly more damaged. It is also apparent that new modes are found as the damage is introduced to the decks, again suggesting that the cracking causes changes in the mode shapes that are significant enough to create previously unobserved modes of vibration. In general, as the load level increases, the number of modes that can successfully be correlated with those from the previous load step becomes less, again implying that there is a consistent degradation of the mode shape as the damage becomes greater, although this trend is based on the results of applying a MAC algorithm so its limitations also apply. Whilst this general trend can be observed in the results, it does not appear to be possible to correlate the degradation in mode shapes to the damage introduced to the decks.

From visual inspection of the mode shapes, it does not appear that the cracking introduced has a significant influence on the shapes of the modes found. This supports the findings of other studies (Eccles, 1999, Das et al, 1997) in that the distribution of the stiffness change in the structure affects the mode shape, such that evenly distributed damage does not cause a significant change in the general shape of the modes of vibration.

Again, in accordance with the results from other studies, the effect of local damage can be seen in the mode shapes, Figure 5-60 to Figure 5-65, for both the symmetric and HB loading regimes. At failure, many of the decks loaded symmetrically failed by a highly localised shear of one beam, often accompanied by the loading points punching through the slab part of the deck. This caused a large reduction in stiffness in a highly localised area, which can be seen clearly in the magnitude of the mode shapes involving transverse bending at failure, Figure 5-62. Considering the asymmetric damage pattern, the effects of a variation in stiffness across the deck can be seen in the changes of the sixth mode shape, again involving some transverse bending of the deck, Figure 5-65, that cannot be easily distinguished in other modes.

There is often a large drop in the MAC value between modes in the load increment prior to the mode disappearing, indicating that the mode undergoes a considerable change in shape. This also occurs during the final load step, when there is a significant reduction in the number of modes matching and the MAC values found. This confirms the findings of the visual inspection indicating that localised damage is often the cause of significant changes in the mode shapes.

5.5 Discussion of variation in modal properties

From the results presented in the preceding sections, it is clear that there are significant problems in applying dynamic testing to realistic bridge deck type structures, and using the modal parameters obtained in a structural health monitoring procedure. Many of the problems arise from inconsistencies in the data when attempting to track modes through a loading history of a deck and from the differences found in the results obtained from nominally identical specimens loaded under the same regime, allowing only general trends to be observed.

There are several possible sources of these discrepancies in the results, some of which have been discussed in the previous sections. One of the most important factors affecting the modal properties of the decks is the bearing conditions, as identified by the testing of a number of decks on both ten and three steel bearings and discussed in section 5.3.4, the differences mainly due to distortion of the deck profile requiring the bearings to be packed using thin pieces of steel and lifting some of the decks to change between ten and three bearings.

Although the testing was carried out under laboratory conditions, variations in the behaviour observed will result from differences in the material properties. Concrete develops strength throughout its entire life that will cause the stiffness change depending on the age of the concrete tested, resulting in differences in the dynamic properties exhibited by the decks. This should not cause a large discrepancy in the natural frequencies observed as the concrete used developed high strength rapidly, which led to the shrinkage cracking present in the decks, and would therefore reach its 95% of its maximum

strength in 28 days, so only a small increase in strength would be found in the decks tested after this time.

Normalising the natural frequency data was performed in an attempt to eliminate the effects of small differences in the initial condition of the decks, although it is possible that these variations in the decks could cause different behaviour under subsequent loading.

It is known that the environmental conditions, in particular temperature, can have an effect on the dynamic properties of a structure. This was investigated for a number of the decks tested in this study, where it was found that the temperature did not vary significantly enough to cause a change in the natural frequencies measured.

The collection of the dynamic test data was carried out according to the procedure set out in chapter 3. Standard techniques were used to ensure the quality of the data obtained was sufficient for the extraction of modal properties, such as taking an adequate number of averages to produce good coherence.

However, it should be remembered that the use of natural frequencies in condition monitoring have been found using a curve fit routine, which will introduce errors, on data that already contains errors. This propagation of errors could be significant if the process is not done with care and the results investigated thoroughly.

Even though the testing regime of the decks was repeated to give some indication of the variation in the results obtained, the differences due to factors other than the cracking introduced in the deck appear to cause considerable deviation in the trends found.

5.6 Conclusions

The results of performing a number of modal surveys on ten one-quarter-scale bridge decks that are loaded incrementally to failure indicate some repeatable trends with regard to the natural frequency and mode shape change, and also appeared to be related to the loading regime employed.

- The process of experimental modal analysis of a more realistic structure is not simple, and requires significant input to ensure satisfactory modes are identified
- The natural frequency appeared, in general, to reduce as the applied load increased due to the decrease in stiffness of the deck as cracking formed
- The trend contained significant variation in the results obtained for nominally identical decks tested under the same loading regime
- It was identified that the indeterminate boundary conditions of a typical deck can cause significant variation in the modal properties obtained
- A number of the decks tested supported by three supports showed much less variation than those from decks supported on ten bearings
- Some of the deviations attributed to the indeterminate supports remained, such as increasing natural frequencies with higher load, indicating that these are due to changes in the deck behaviour and other factors
- The boundary conditions have a significant influence on the dynamic characteristics of the bridge. In some cases, the differences in the dynamic response due to changes in the bearings were greater than those due to the induced damage
- The high sensitivity to the boundary conditions indicates both an advantage and disadvantage of using the dynamic properties as the bearings are a major source of deterioration but are not safety critical.
- It was possible to relate the natural frequency change to the actual damage introduced to the decks, and it was found that the change in natural frequency could be related to certain types of cracking that formed
- Different trends in natural frequency reduction were found depending on whether the deck had been loaded under a symmetric or asymmetric arrangement

- The changes in the mode shapes did not appear to be correlated with the damage introduced to the decks, although there was a consistent degradation of the number of modes that could be matched using the MAC algorithm as the load level increased
- When the failure was of a highly localised nature, a significant change in the magnitude of the mode shapes in this area was found, confirming the findings of other studies
- The changes in the natural frequencies of certain modes appeared to be related to the locations of the damaged areas, although some of this influence was reduced when the decks were supported on ten bearings
- Many of the modes displayed a relatively low sensitivity to the damage introduced in the 100 to 250kN range, consistent with previous studies

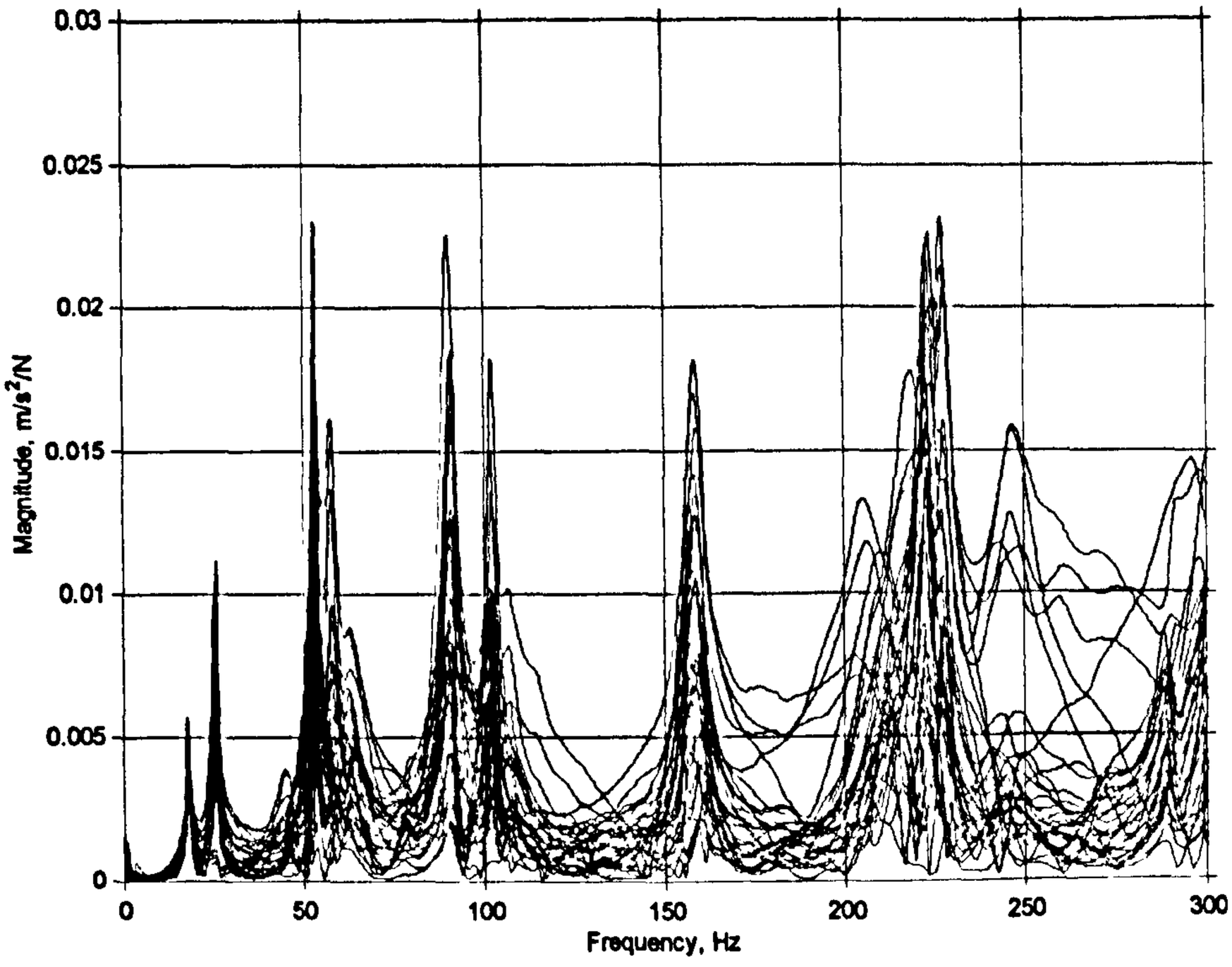

Figure 5-1: FRFs for deck 2

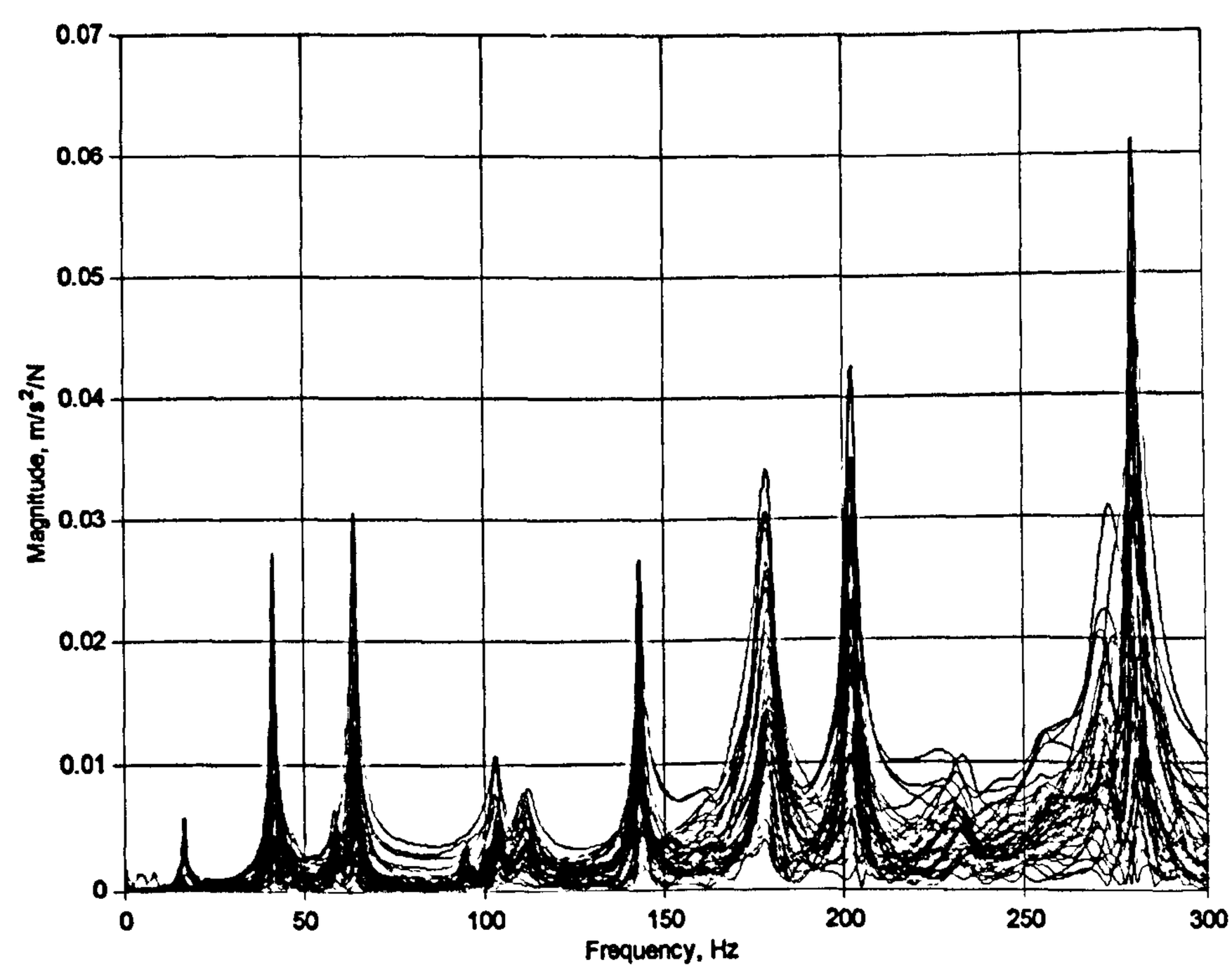

Figure 5-2: FRFs for deck 4

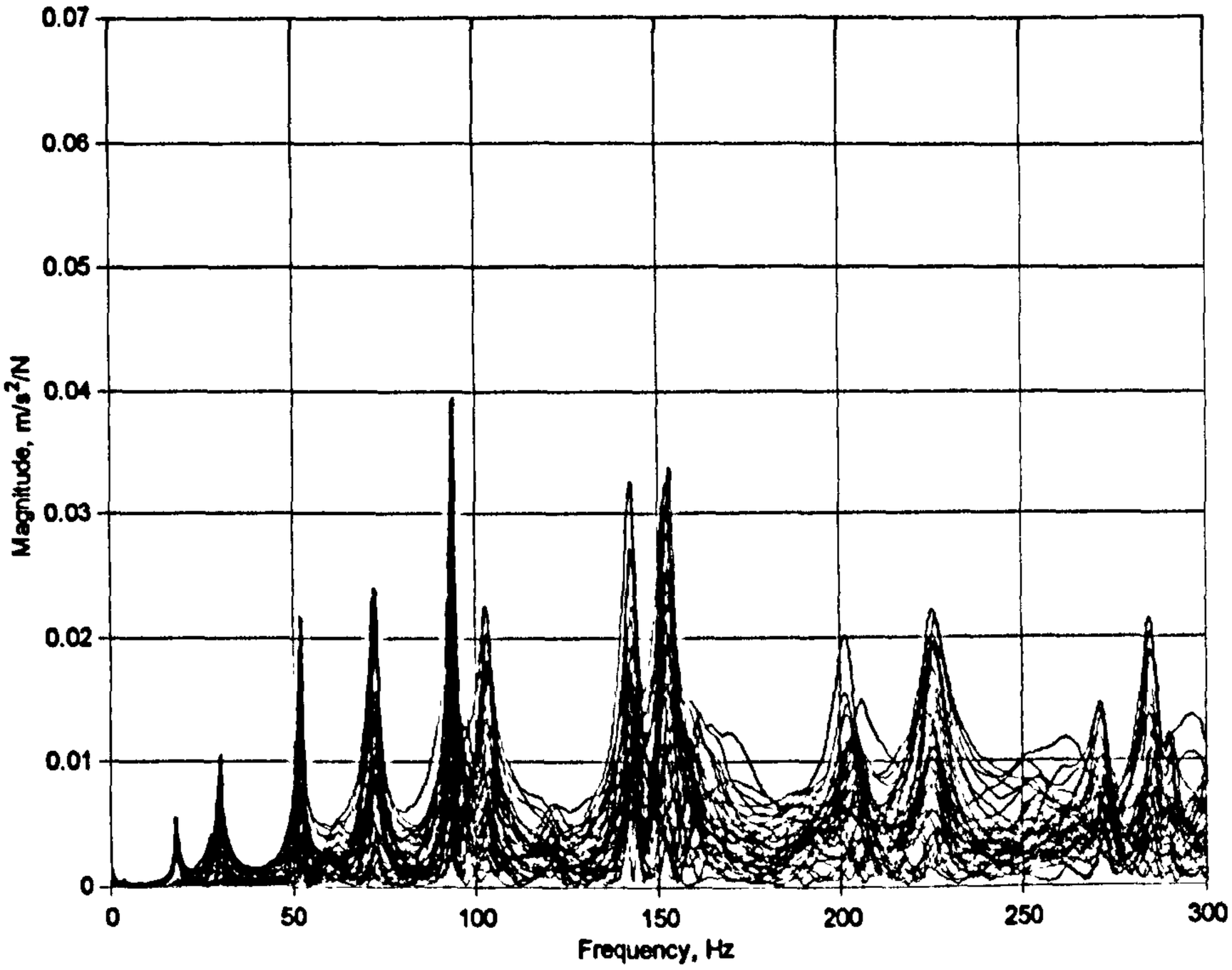

Figure 5-3: FRFs for deck 5

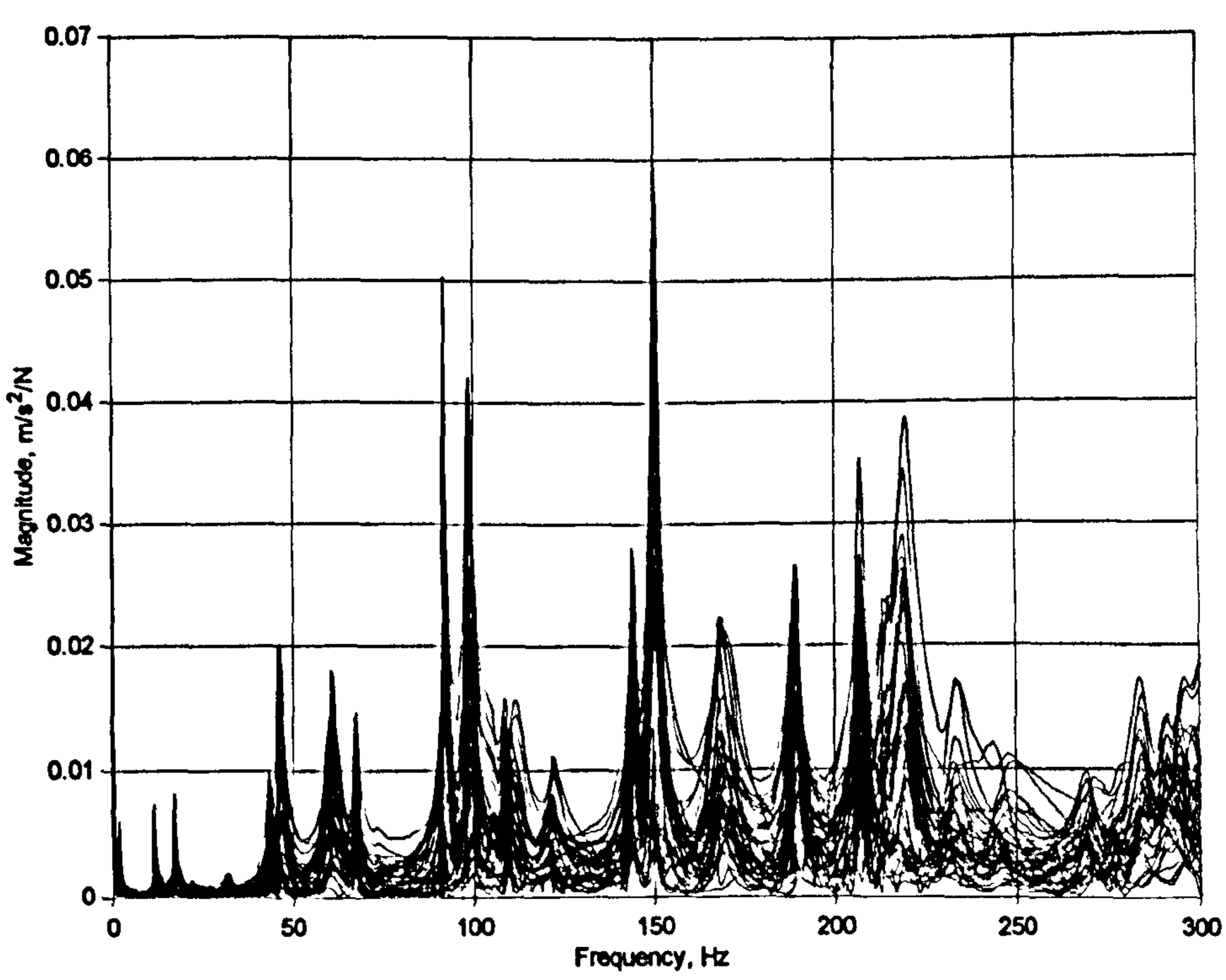

Figure 5-4: FRFs for deck 6

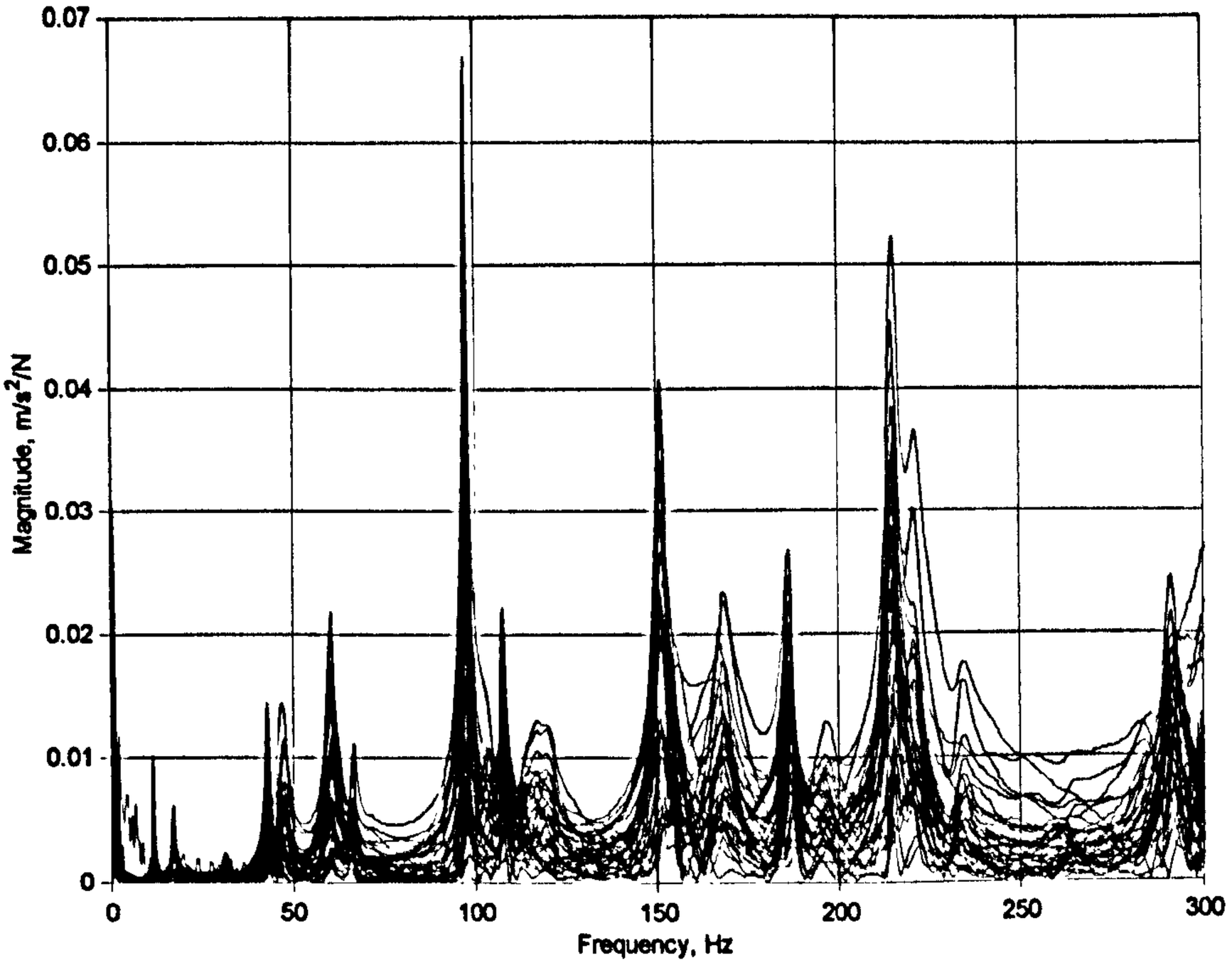

Figure 5-5: FRFs for deck 7

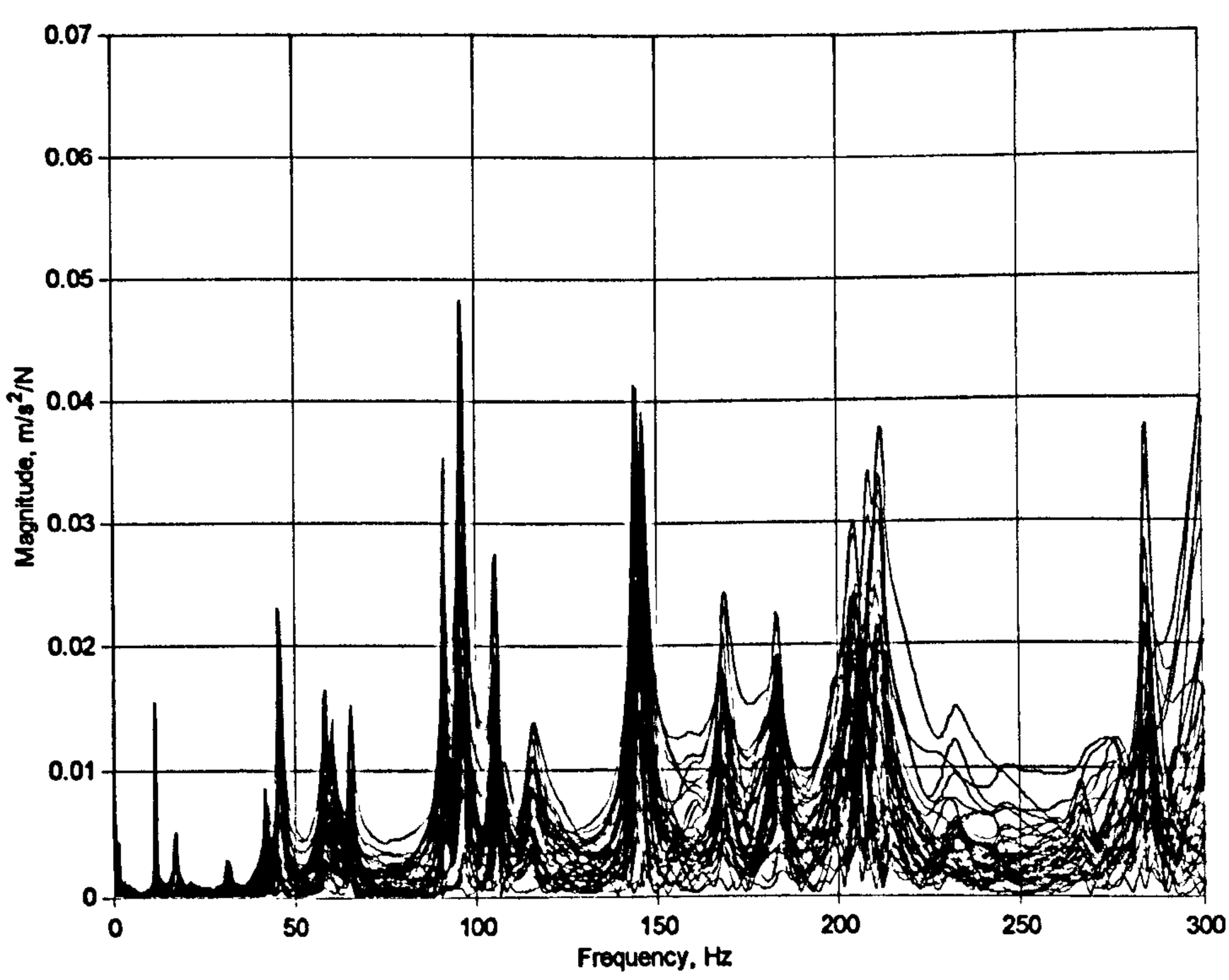

Figure 5-6: FRFs for deck 8

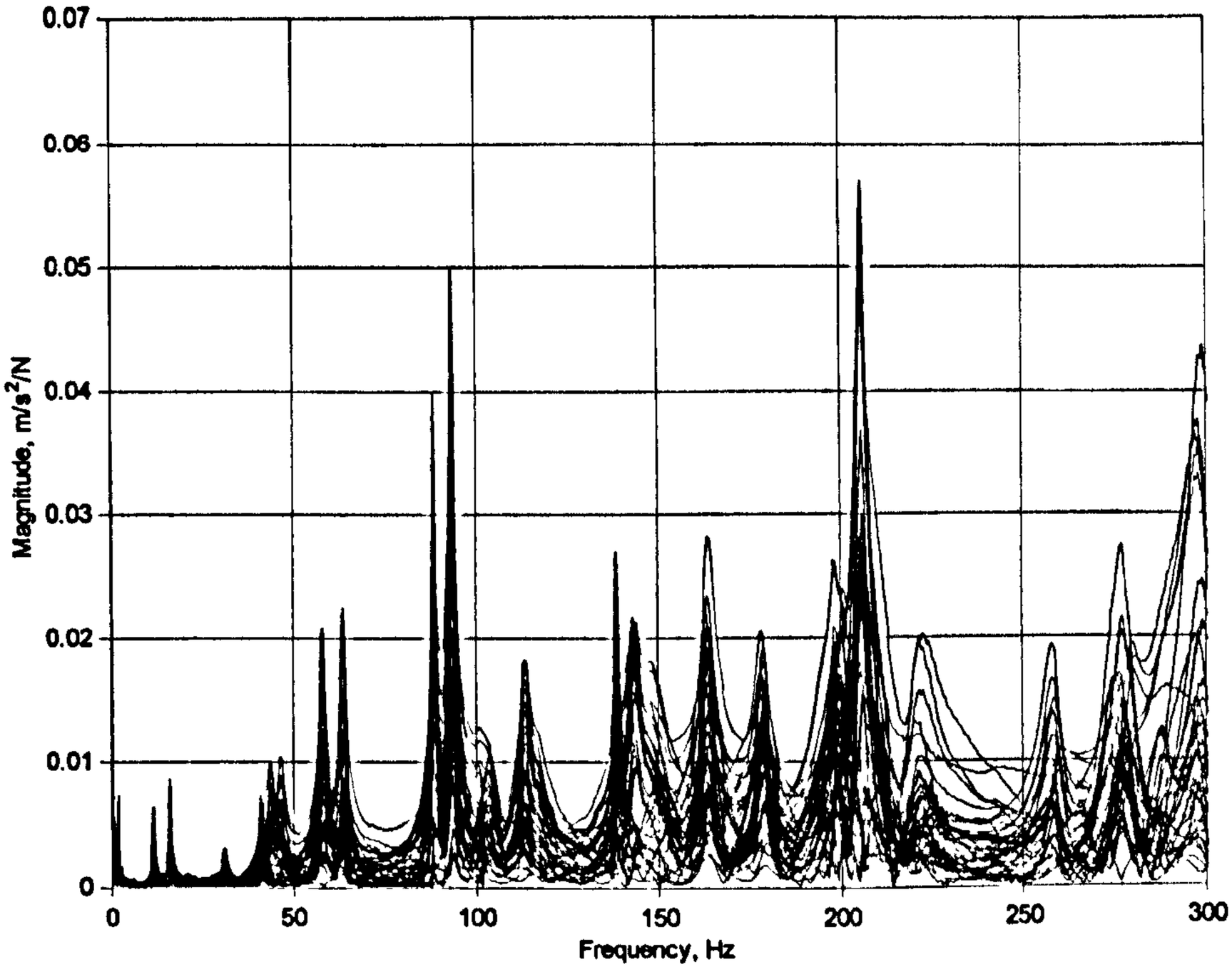

Figure 5-7: FRFs for deck 9

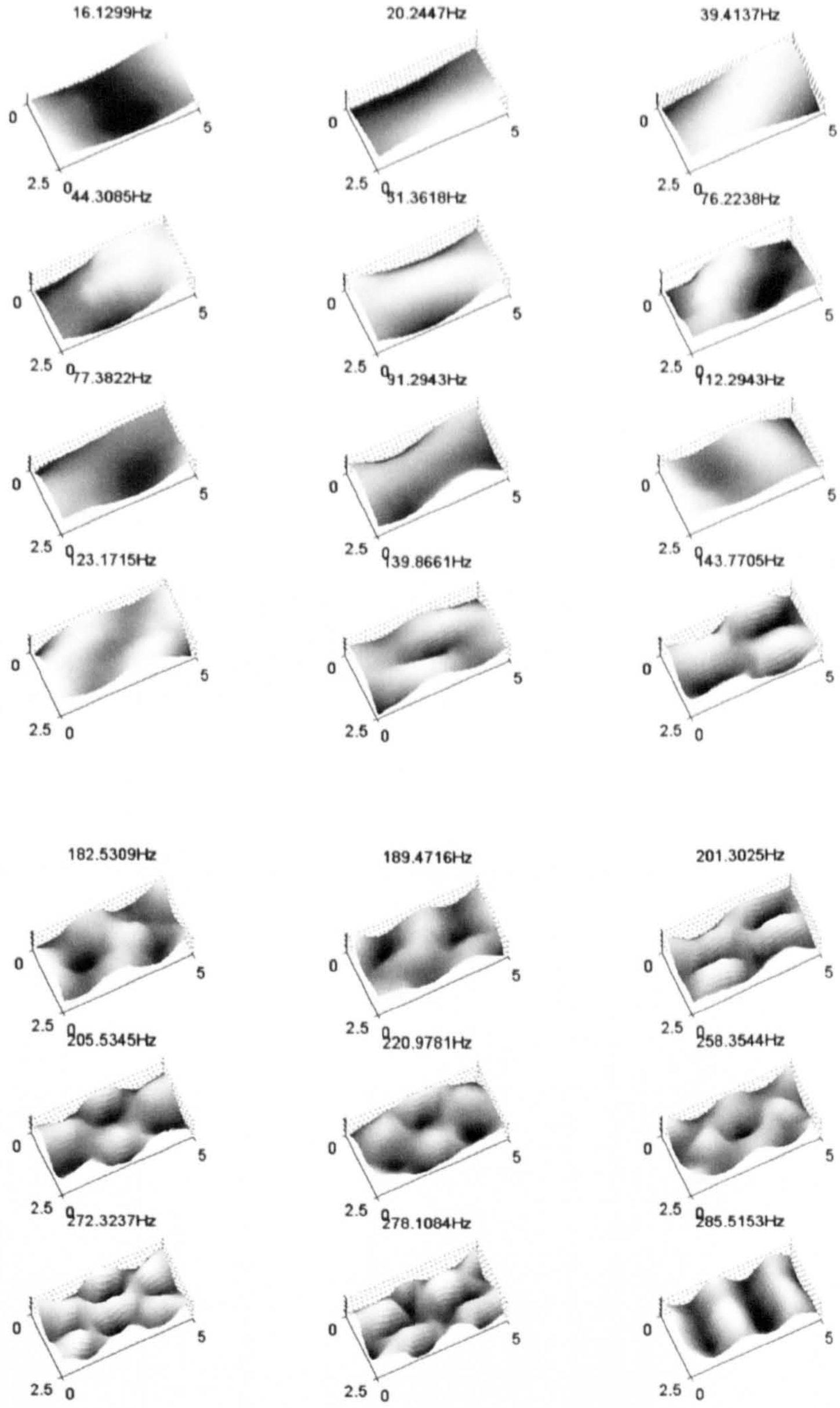

Figure 5-8: Mode shapes of deck 4

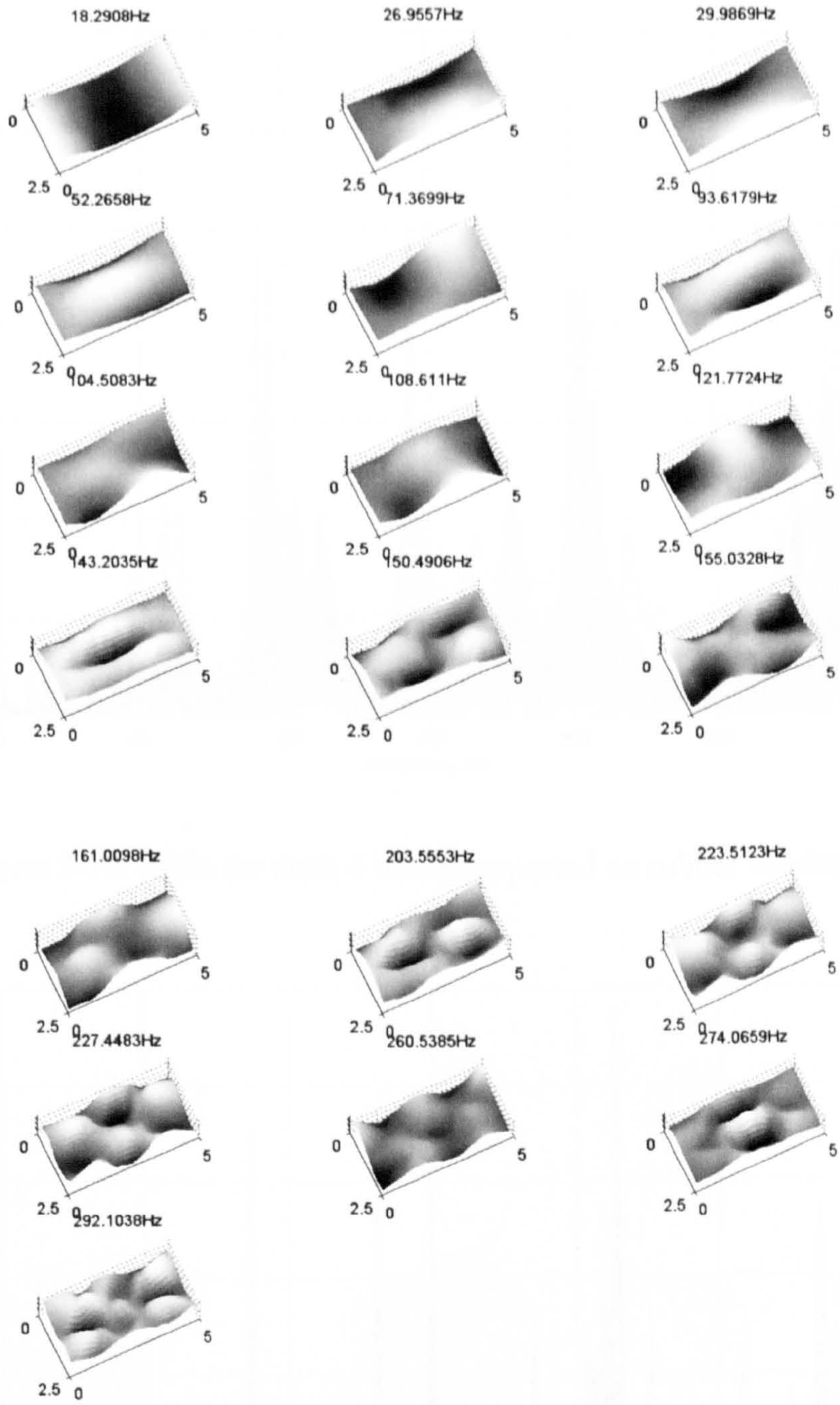

Figure 5-9: Mode shapes of deck 5

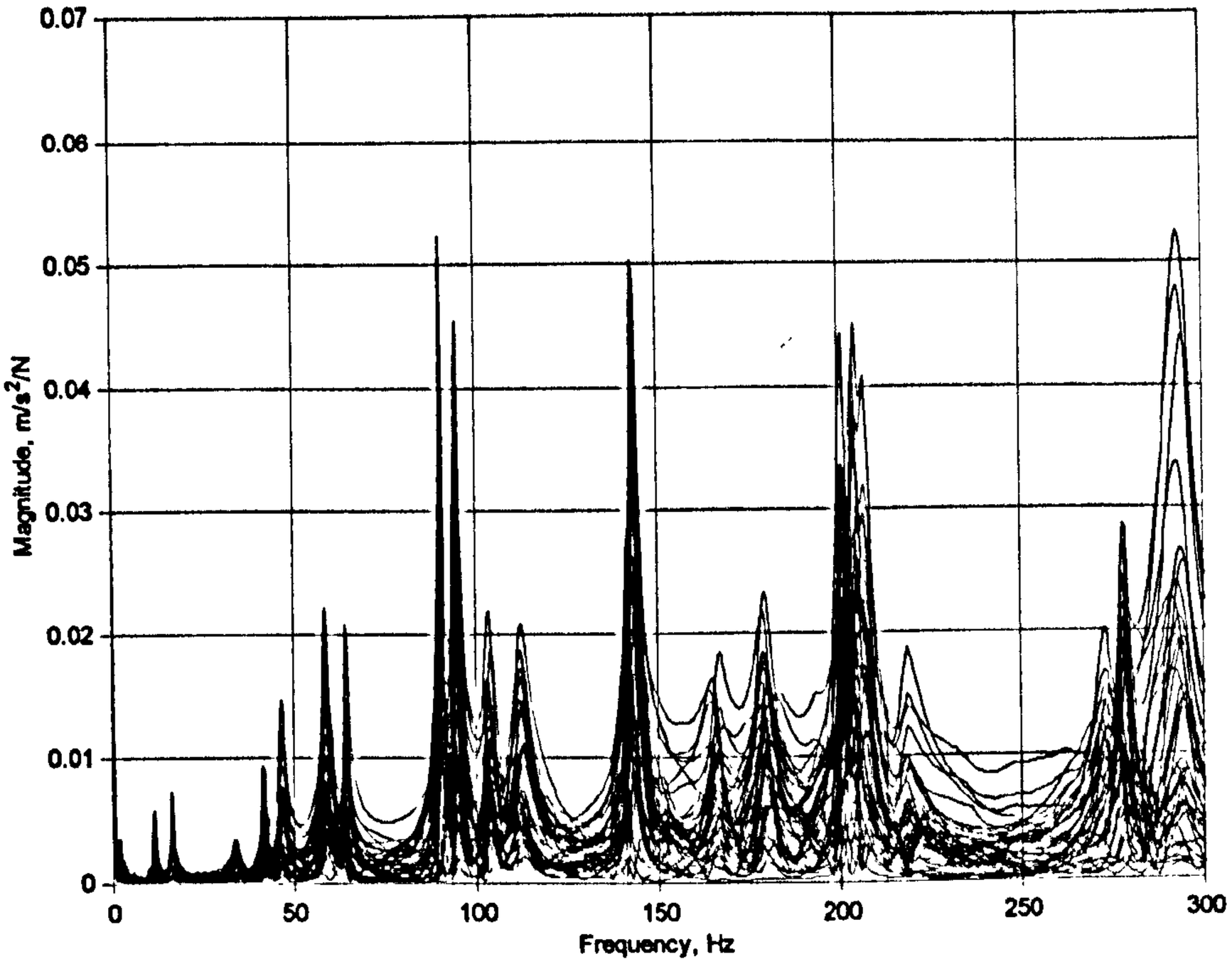

Figure 5-10: FRFs for deck 4 when supported on rubber bearings

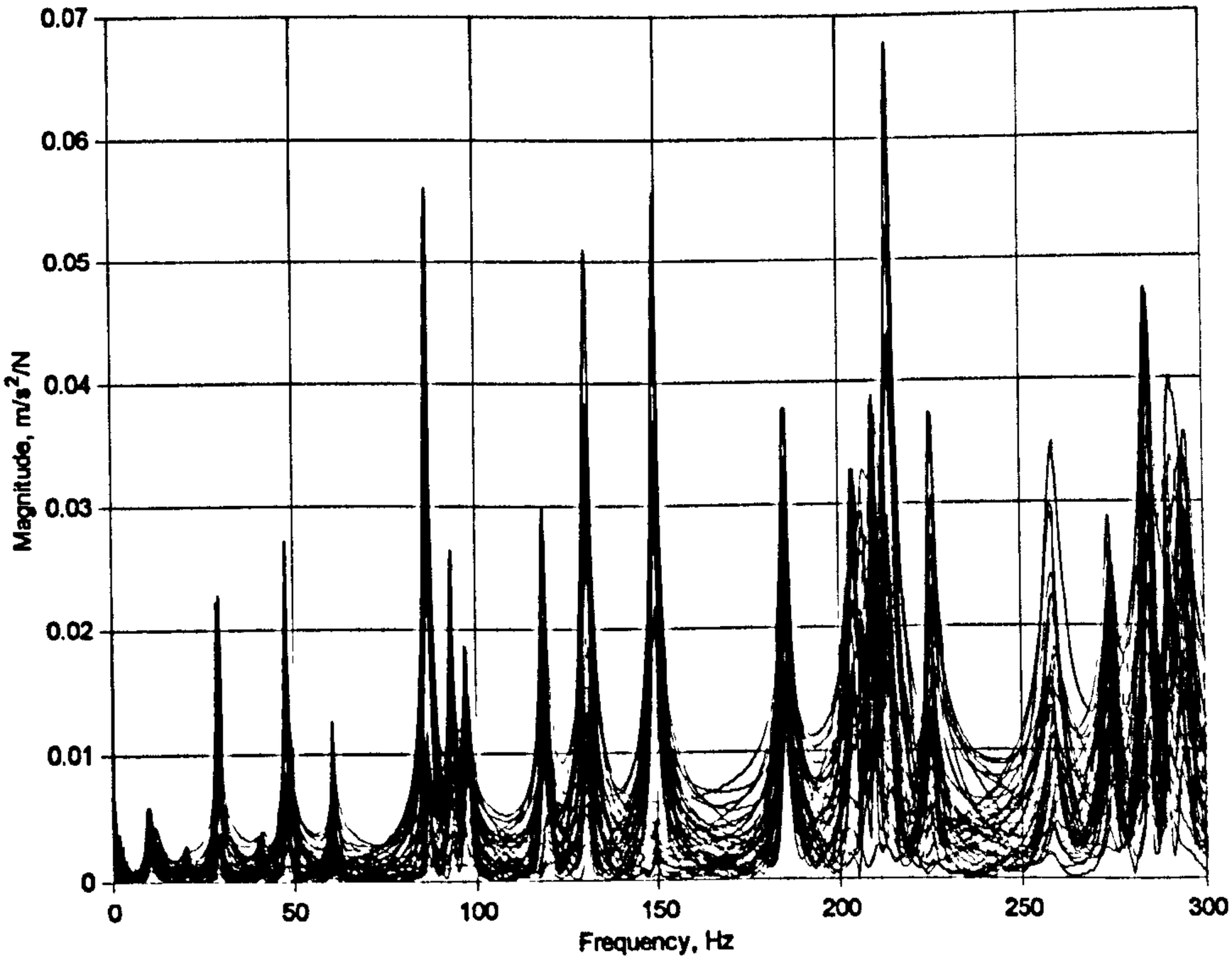

Figure 5-11: FRFs for deck 5 when supported on rubber bearings

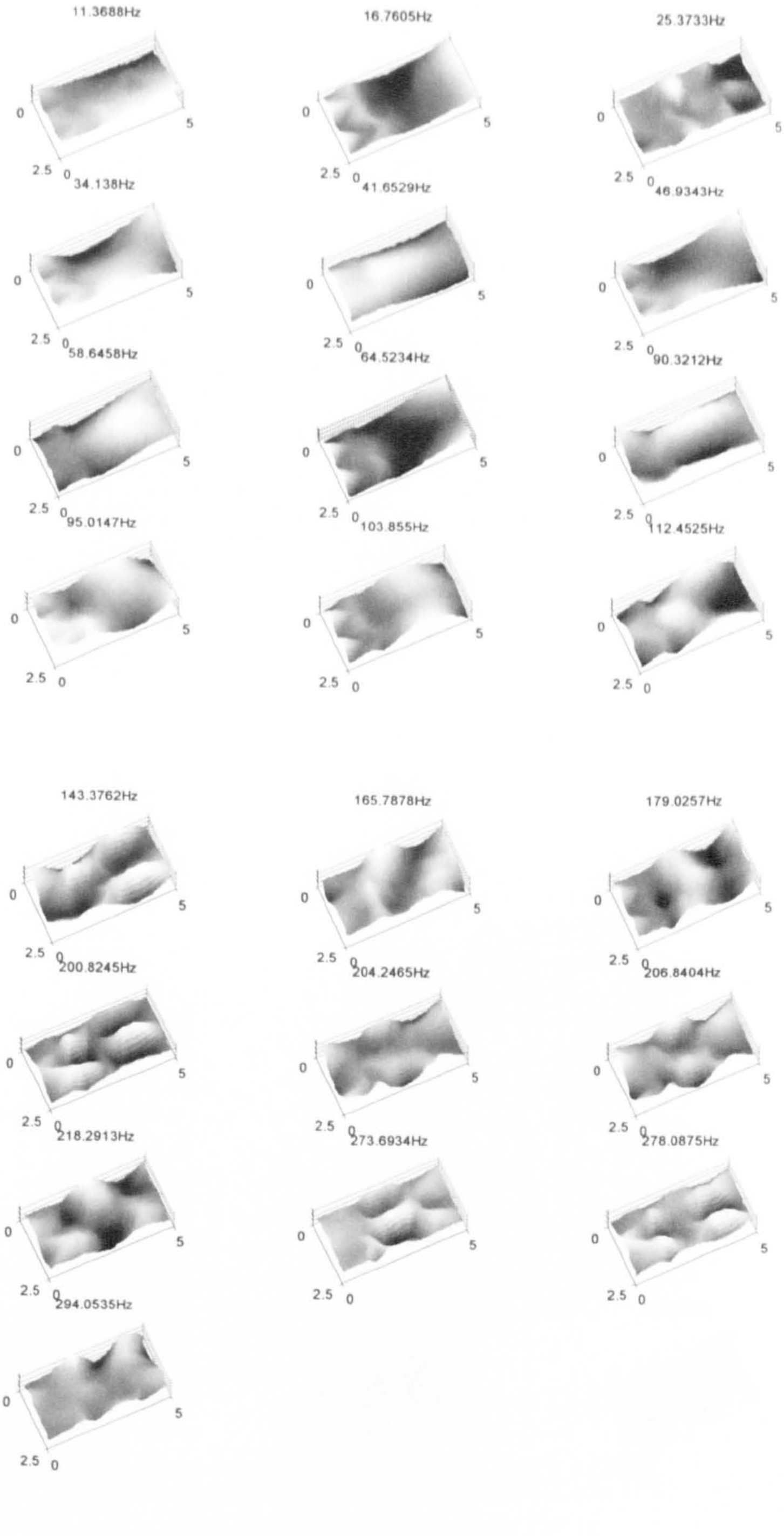

Figure 5-12: Mode shapes of deck 4 supported by rubber bearings

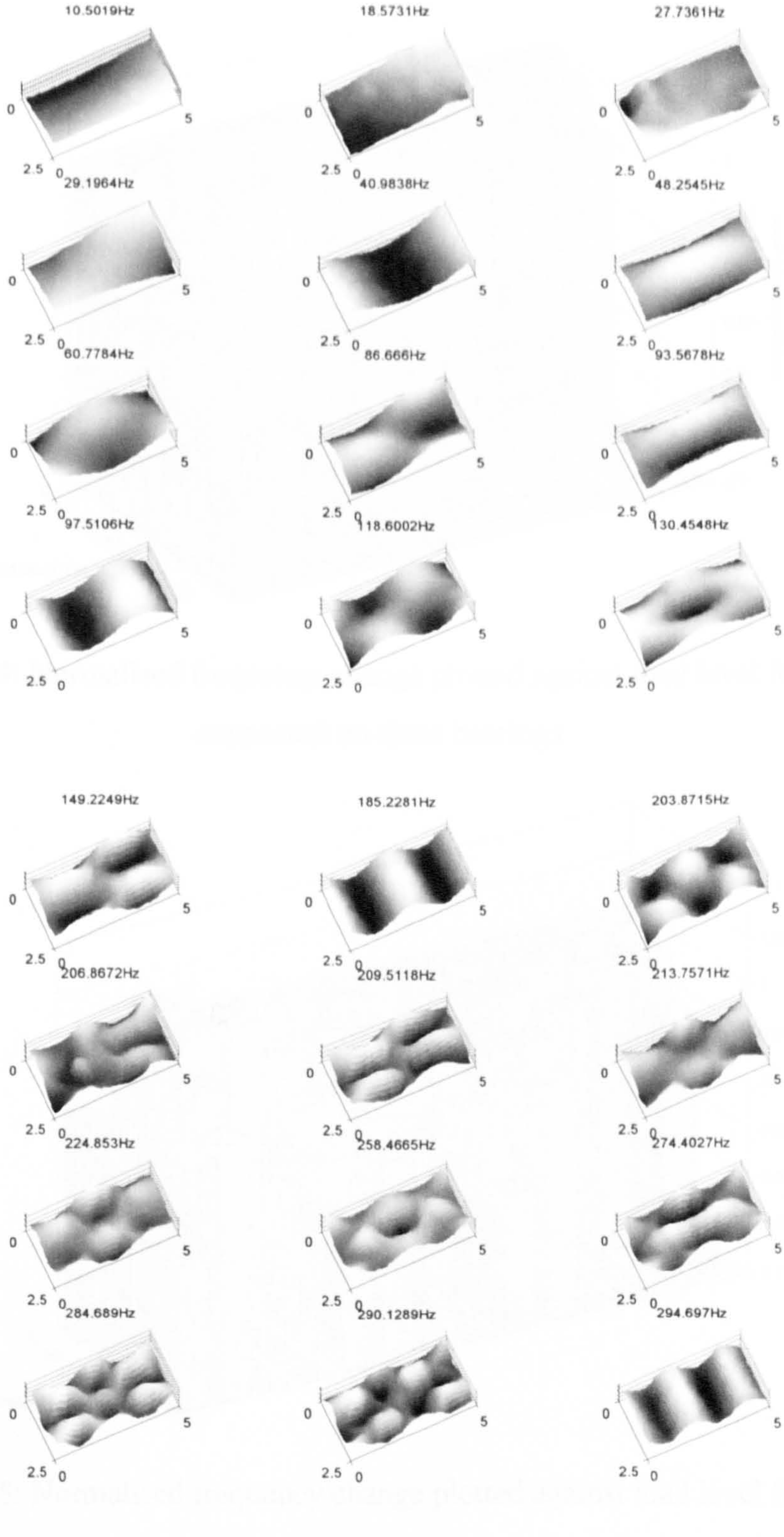

Figure 5-13: Mode shapes of deck 5 supported by rubber bearings

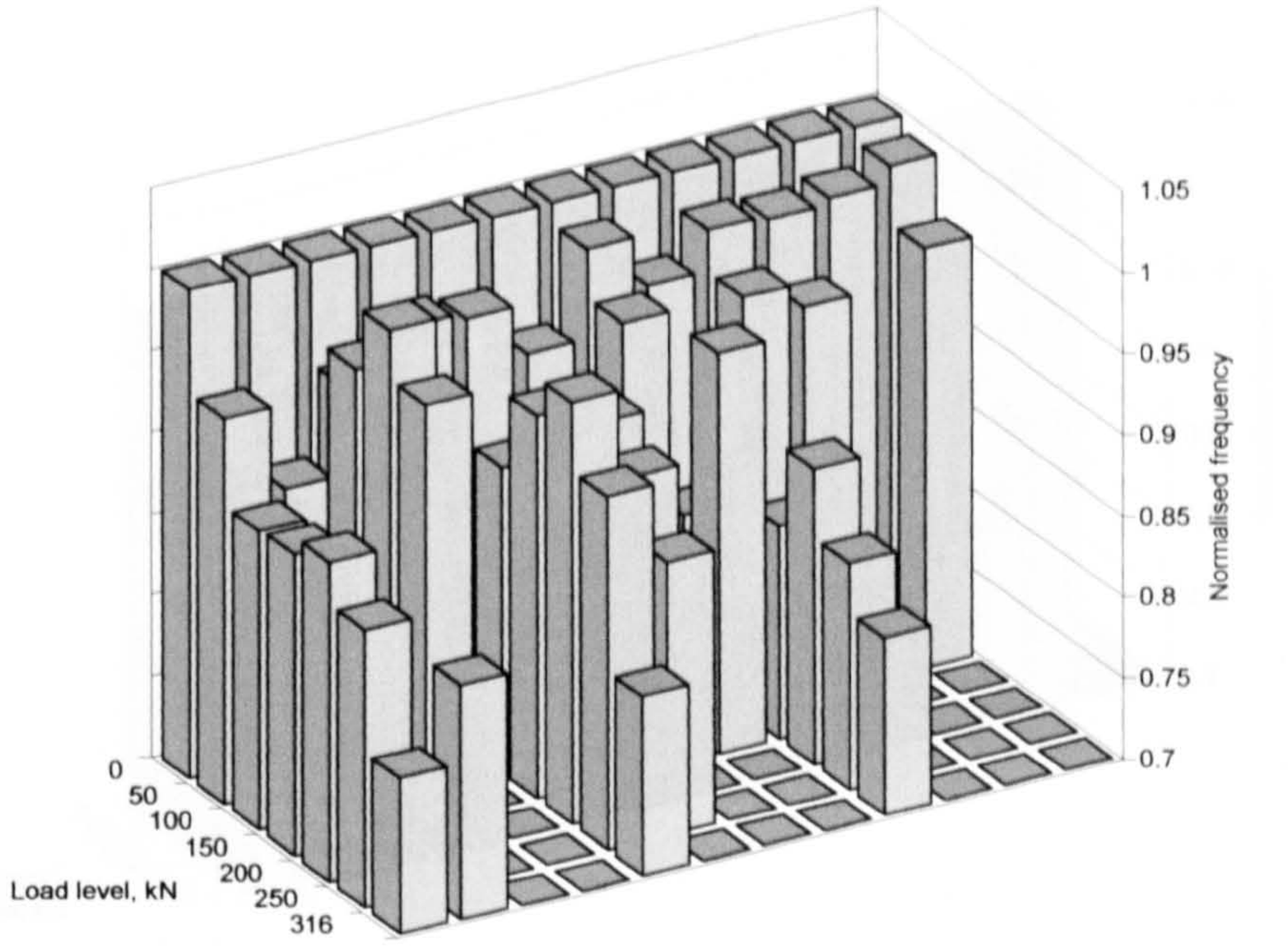

Figure 5-14: Normalised frequency change plotted against load level for deck 3 supported on three bearings

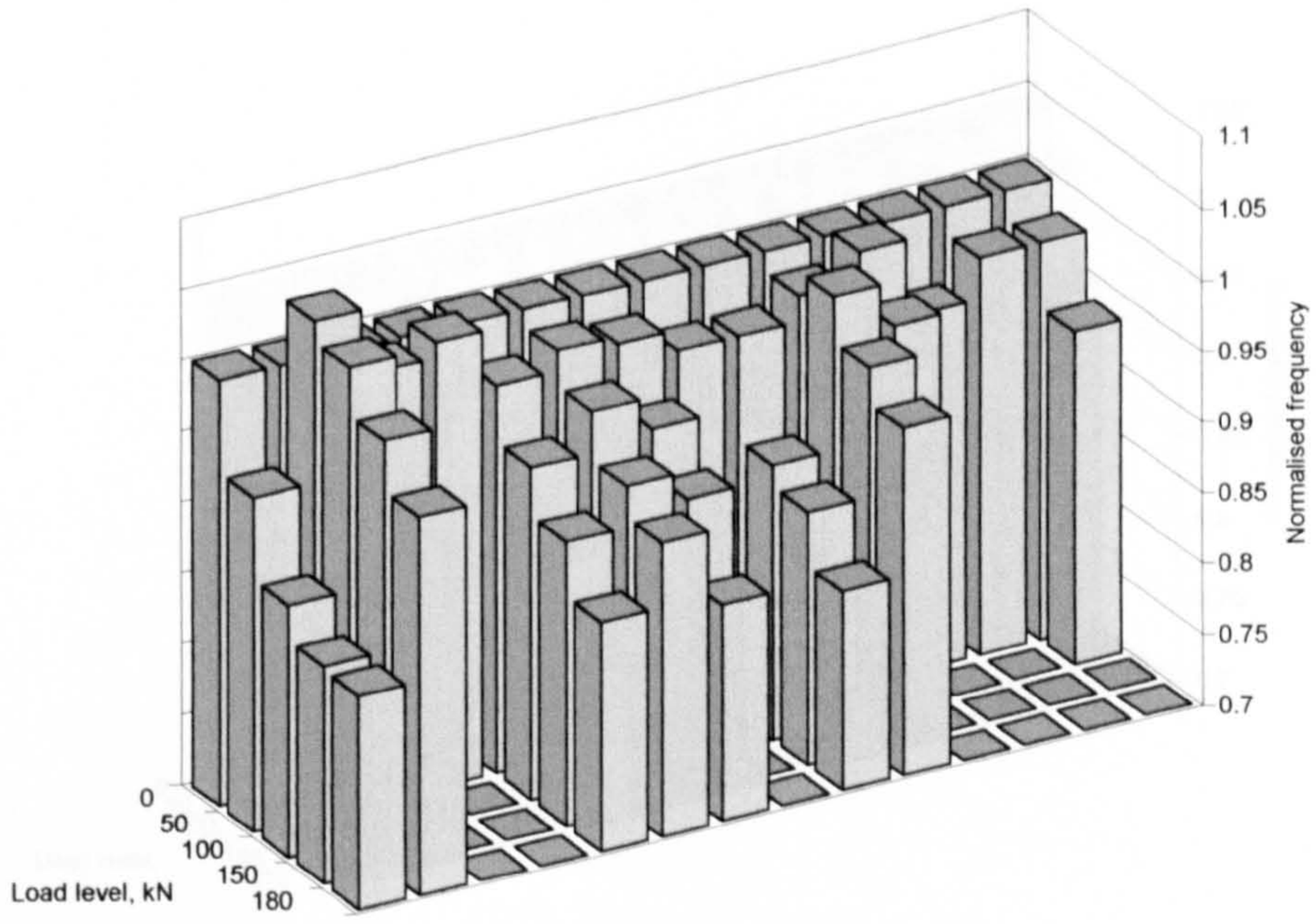

Figure 5-15: Normalised frequency change plotted against load level for deck 4 supported on three bearings

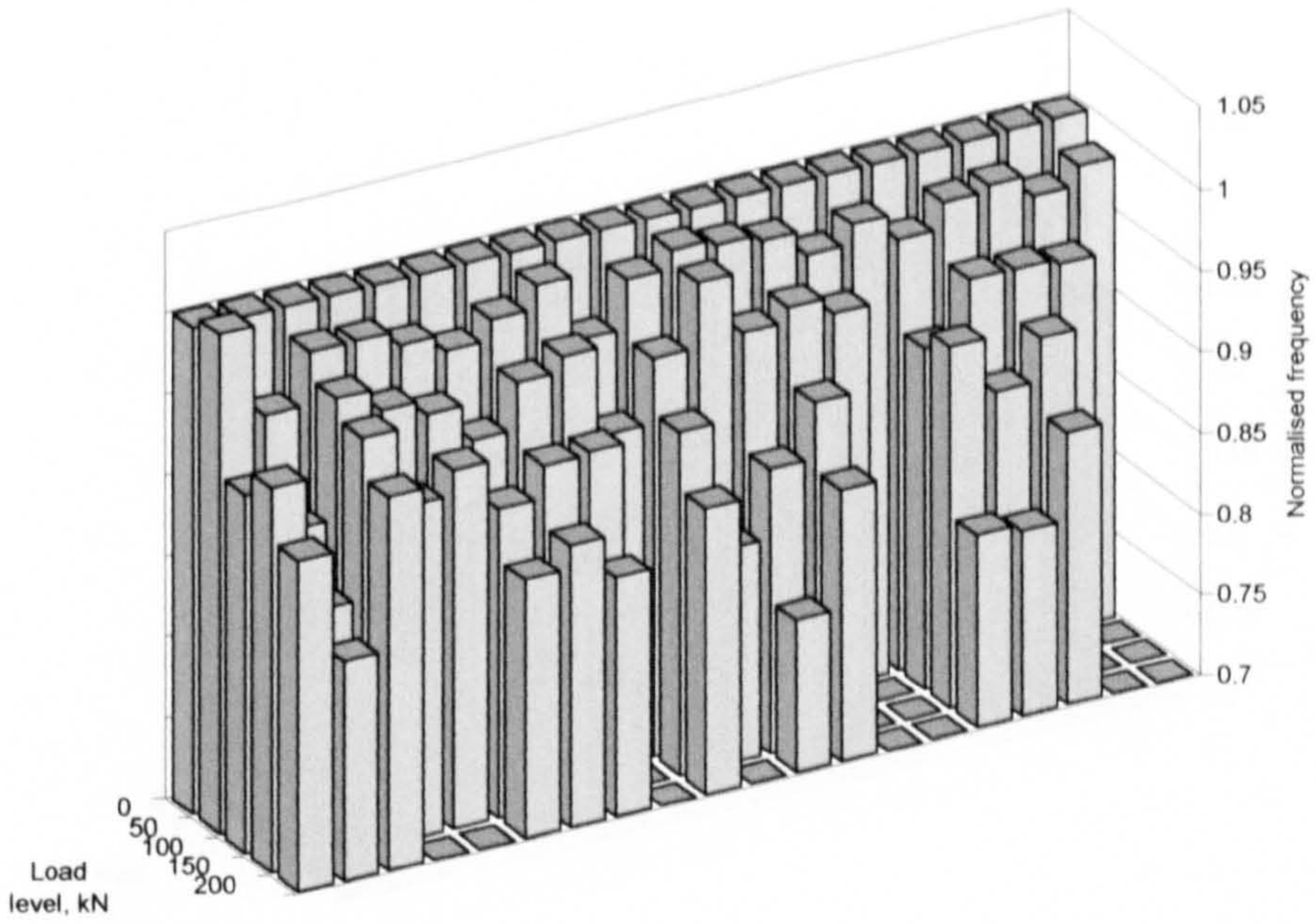

Figure 5-16: Normalised frequency change plotted against load level for deck 5 supported on three bearings

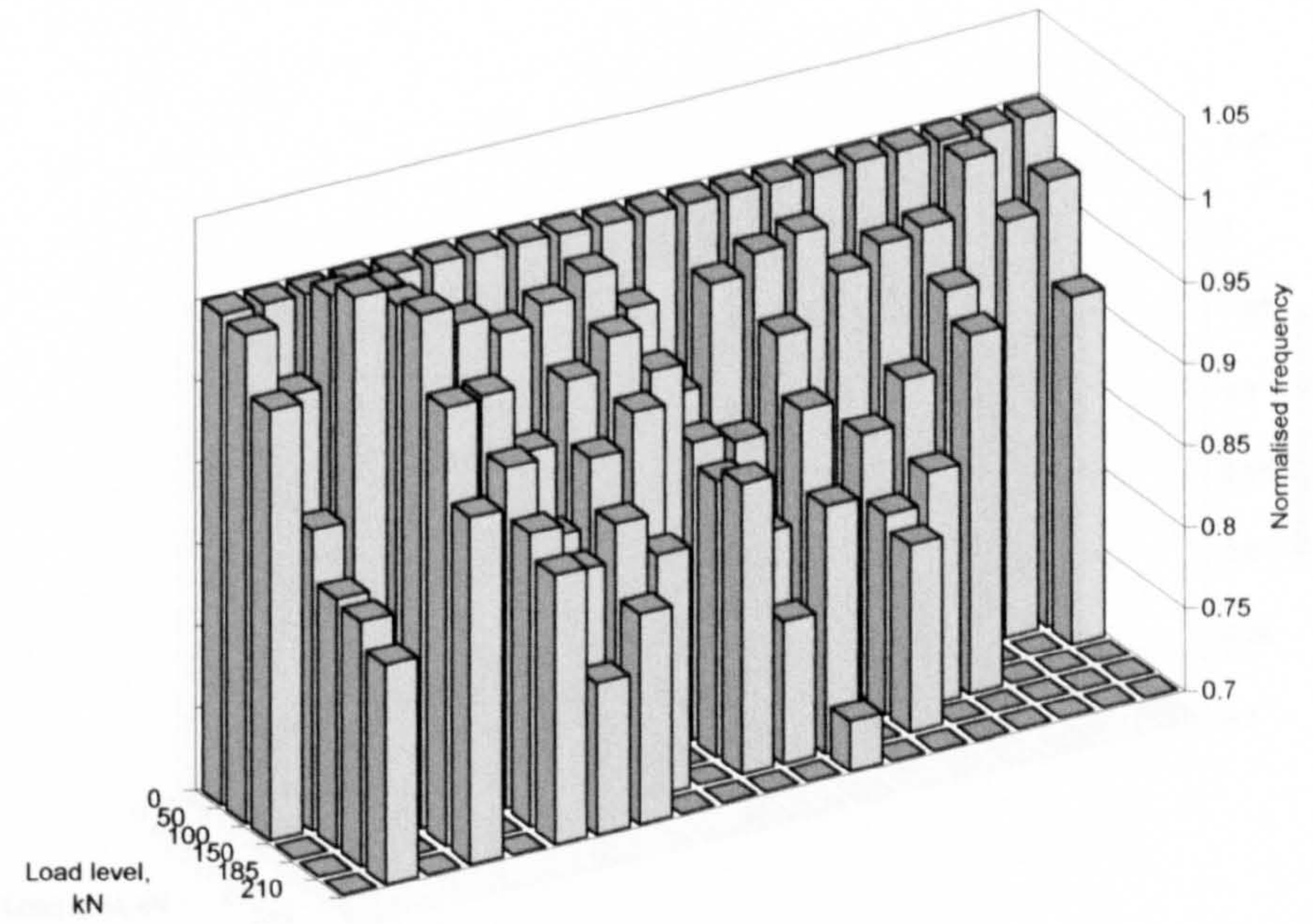

Figure 5-17: Normalised frequency change plotted against load level for deck 6 supported on three bearings

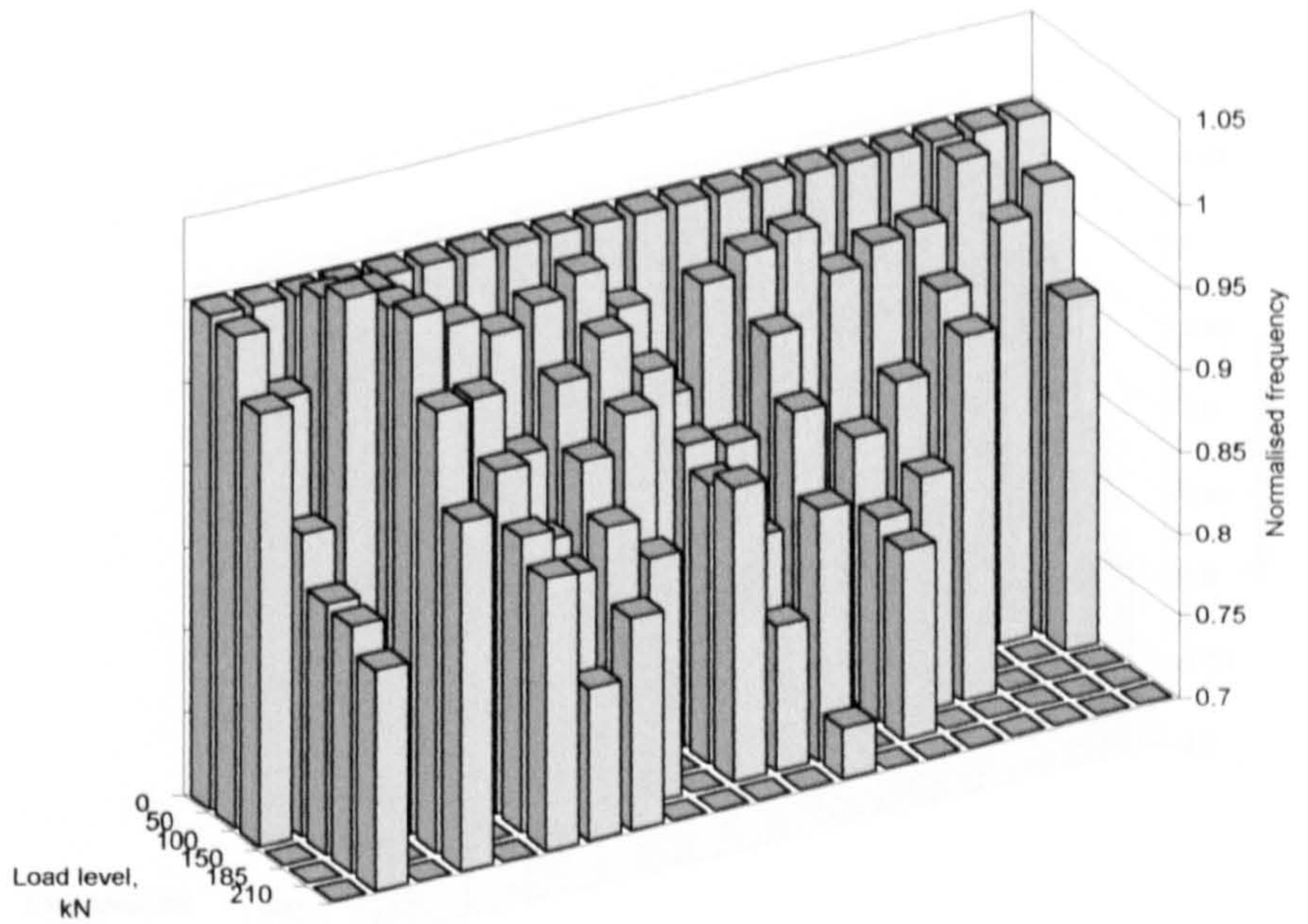

Figure 5-18: Normalised frequency change plotted against load level for deck 6 supported on three bearings obtained from impact testing

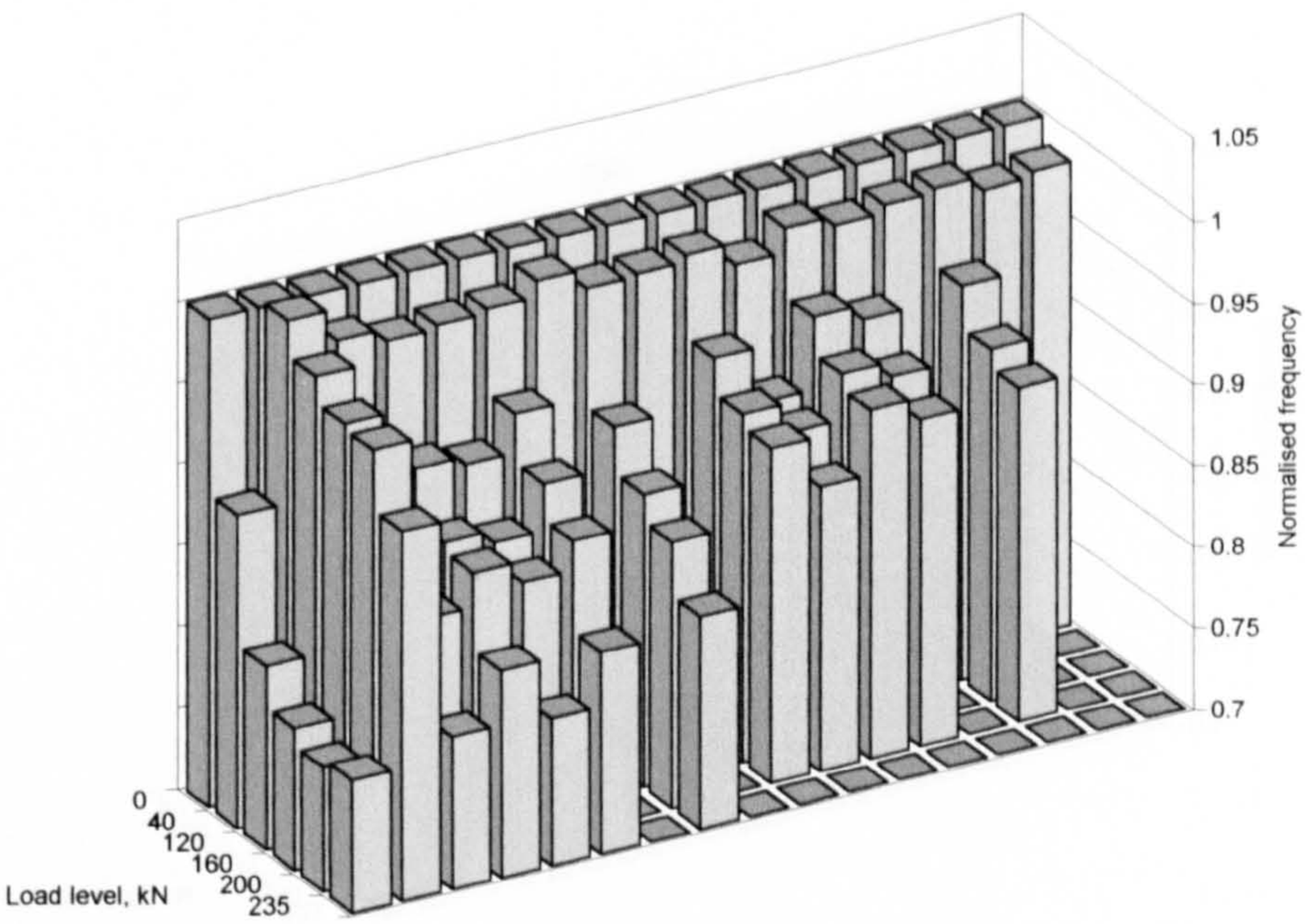

Figure 5-19: Normalised frequency change plotted against load level for deck 7 supported on three bearings

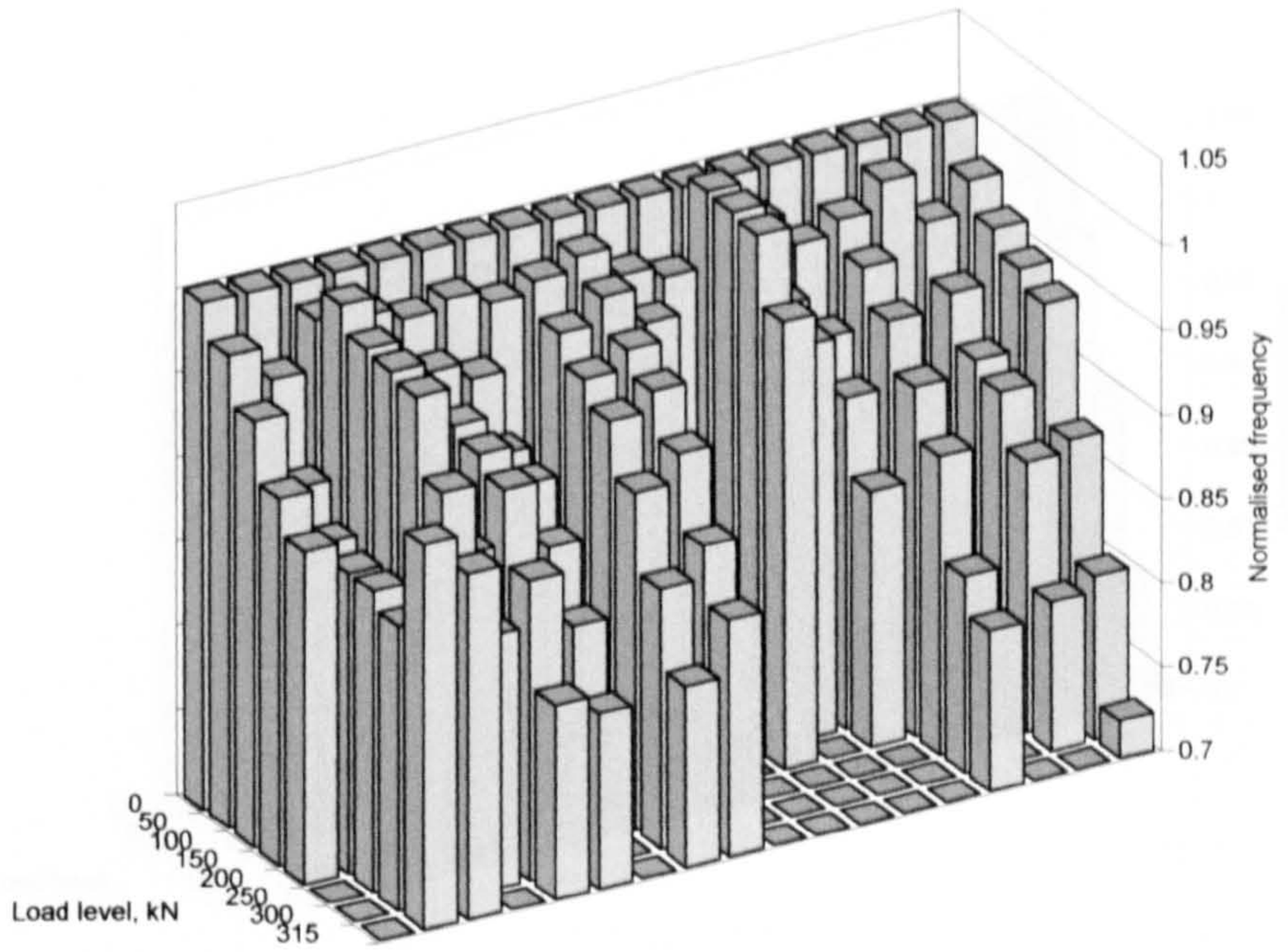

Figure 5-20: Normalised frequency change plotted against load level for deck 8 supported on three bearings

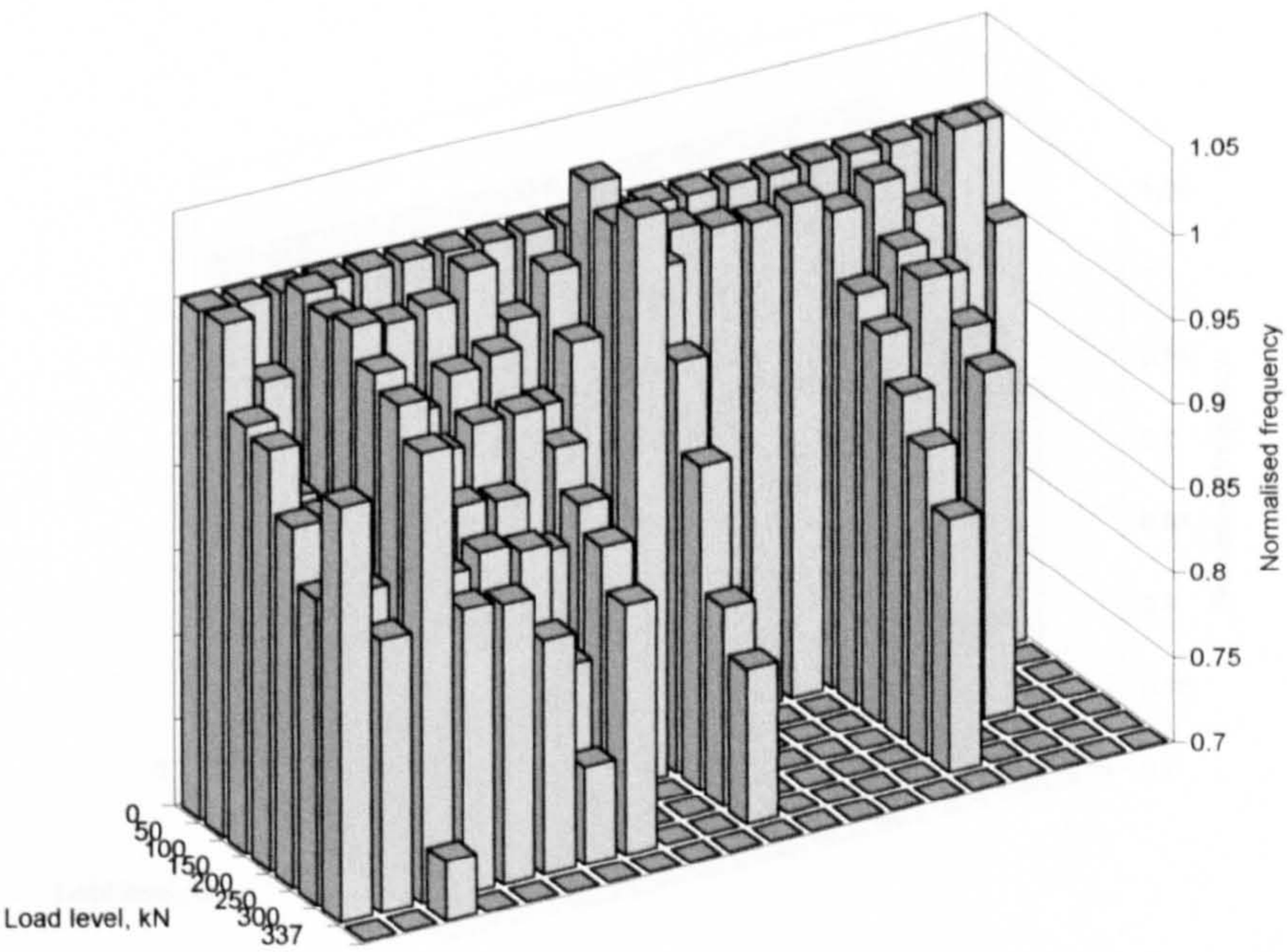

Figure 5-21: Normalised frequency change plotted against load level for deck 9 supported on three bearings

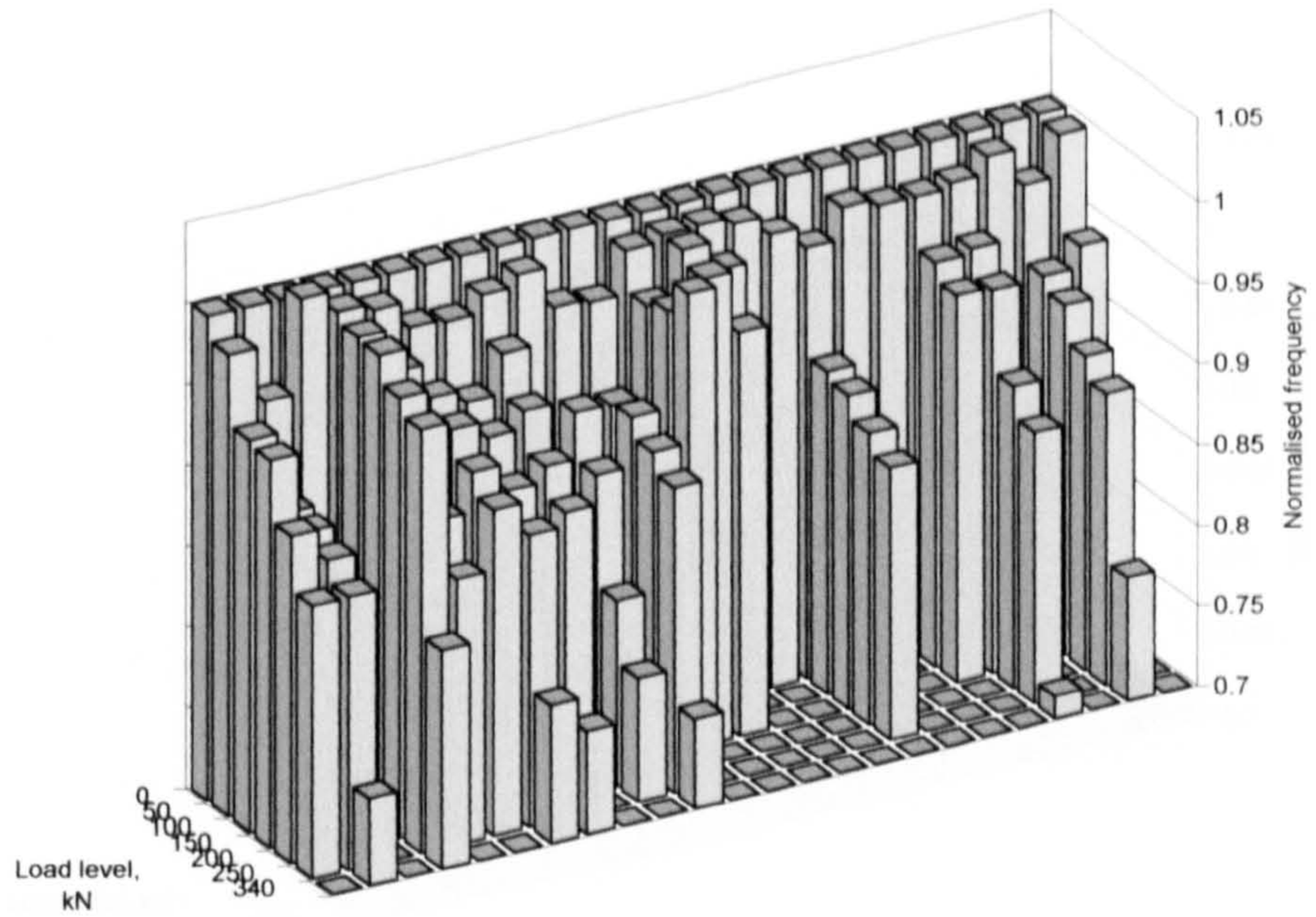

Figure 5-22: Normalised frequency change plotted against load level for deck 10 supported on three bearings

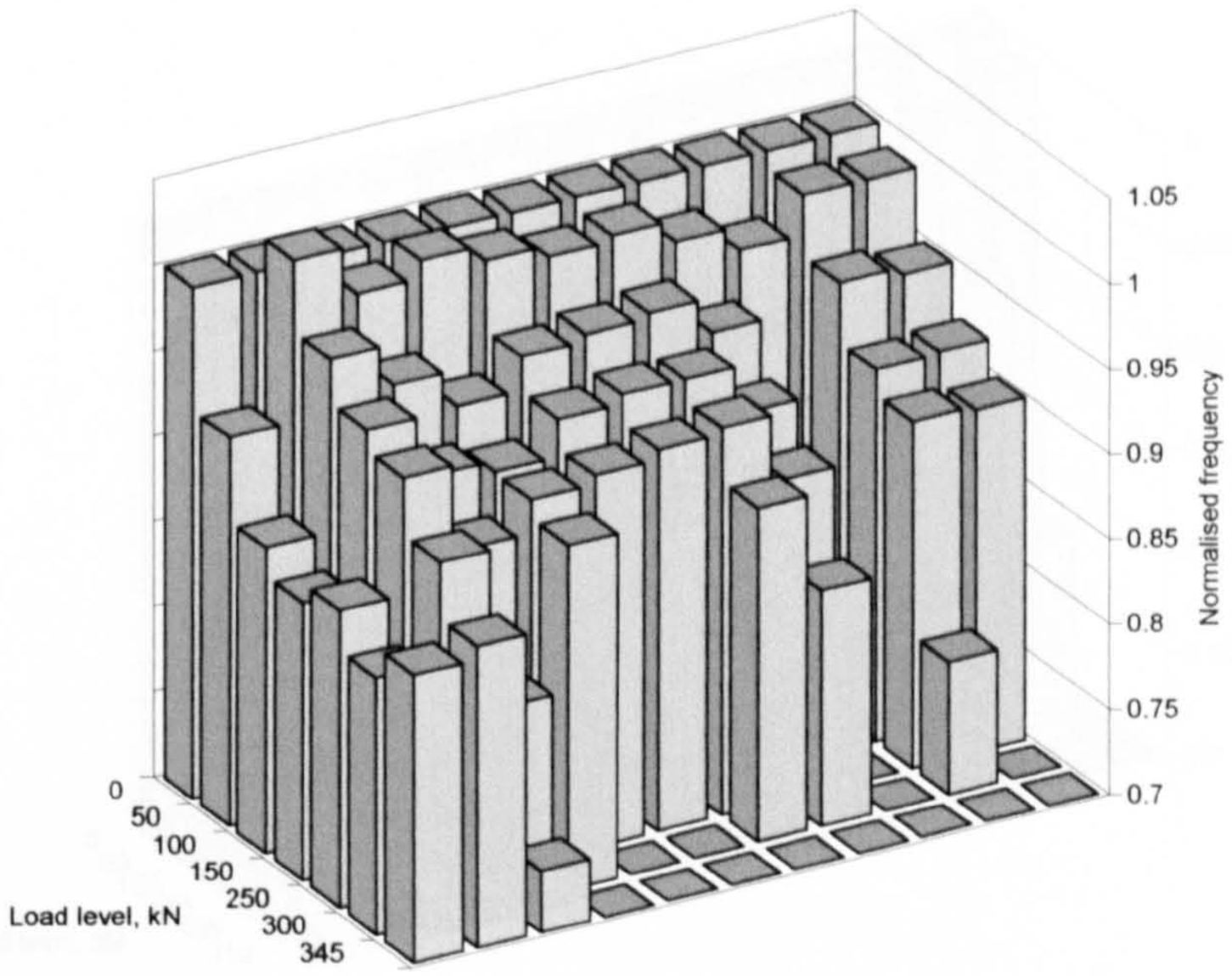

Figure 5-23: Normalised frequency change plotted against load level for deck 2 supported on ten bearings

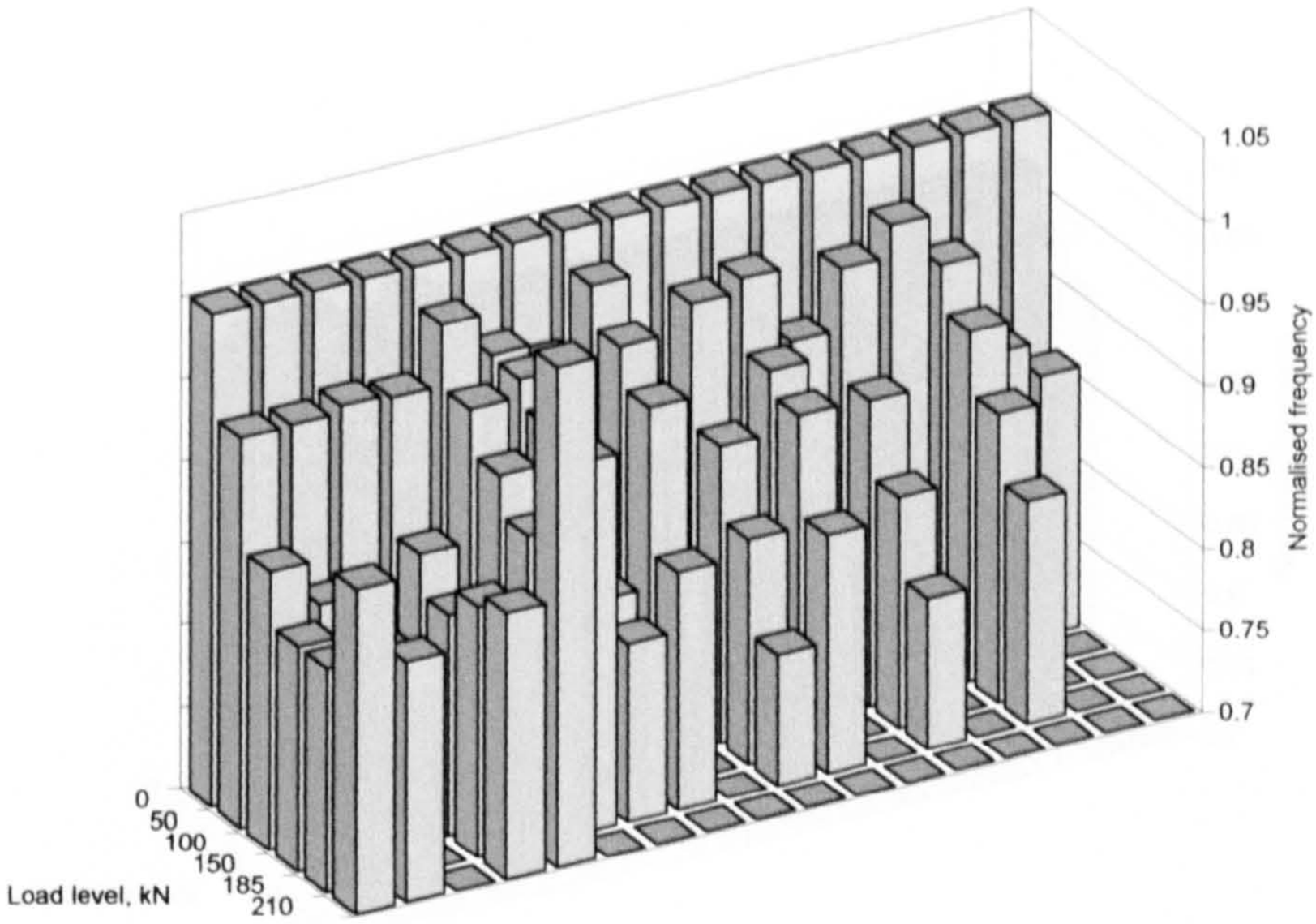

Figure 5-24: Normalised frequency change plotted against load level for deck 6 supported on ten bearings

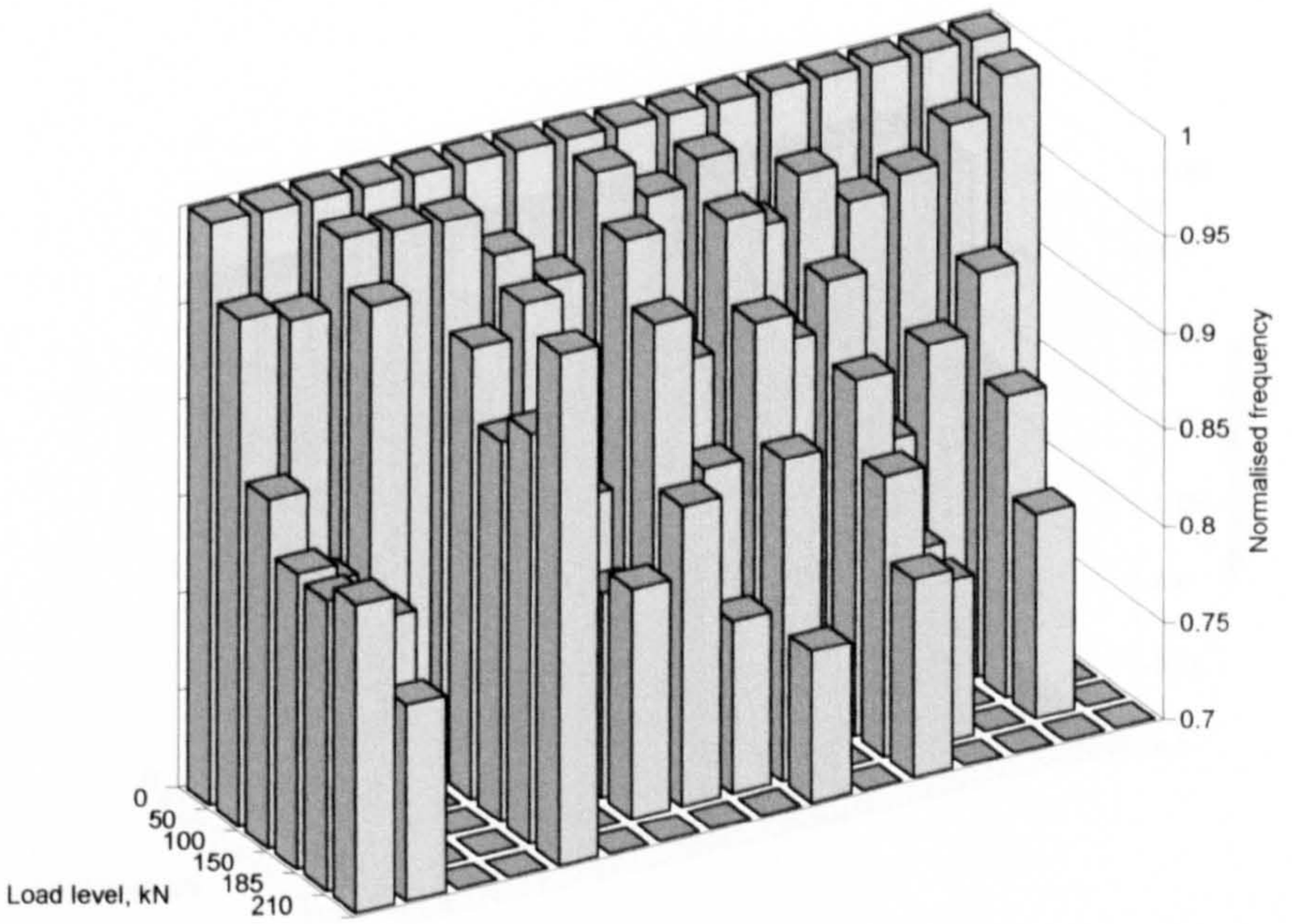

Figure 5-25: Normalised frequency change plotted against load level for deck 6 supported on ten bearings obtained from impact testing

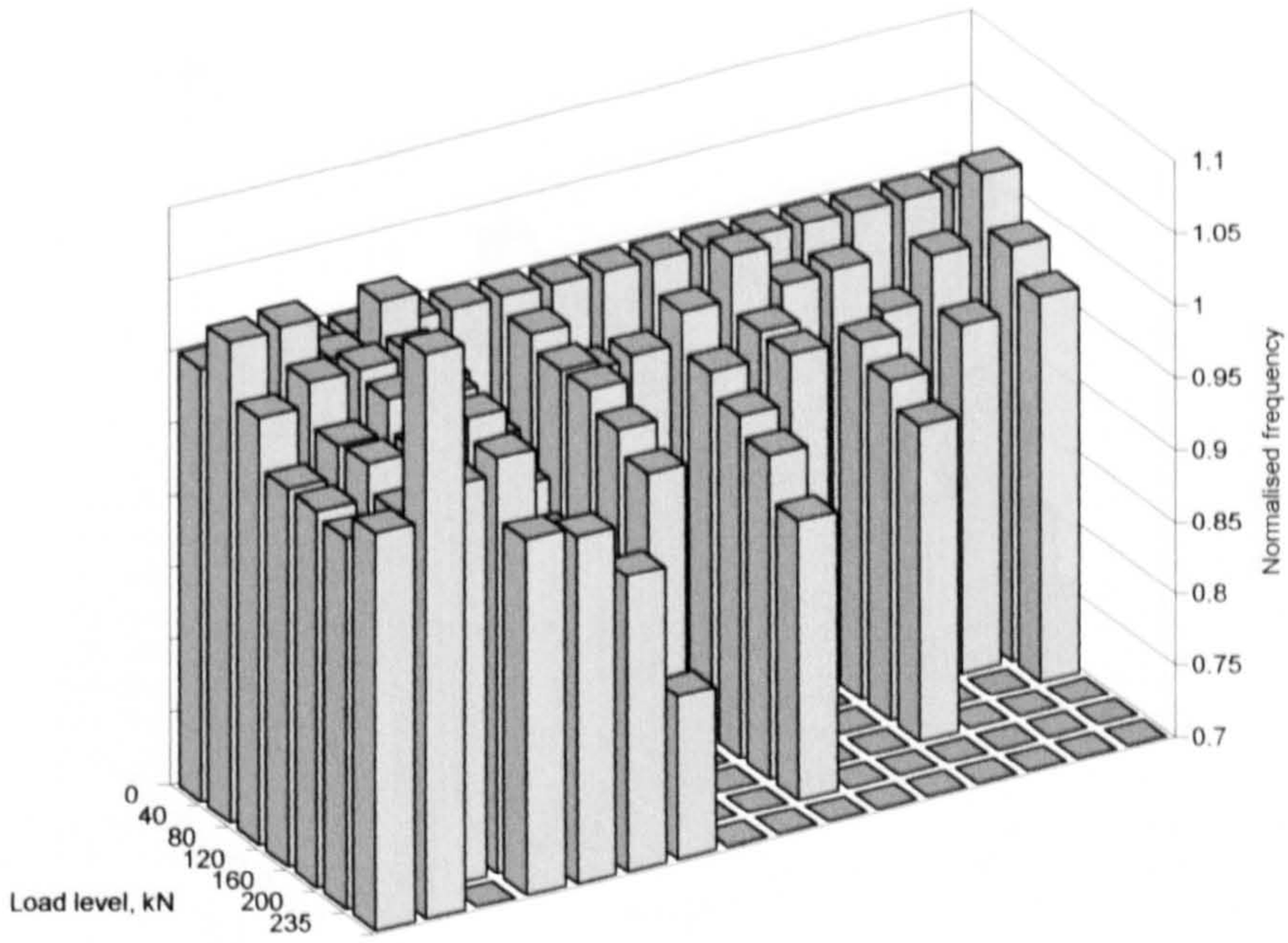

Figure 5-26: Normalised frequency change plotted against load level for deck 7 supported on ten bearings

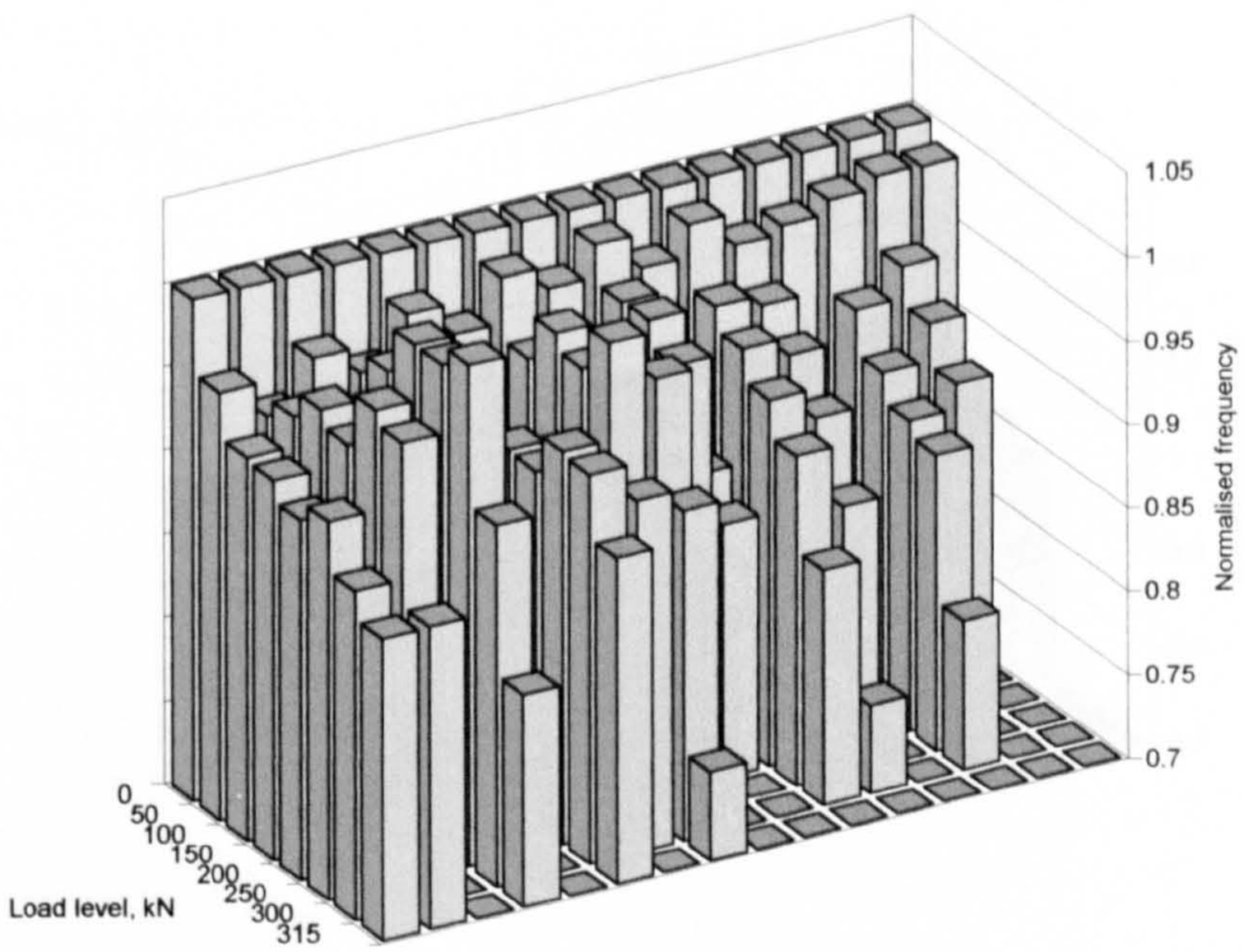

Figure 5-27: Normalised frequency change plotted against load level for deck 8 supported on ten bearings

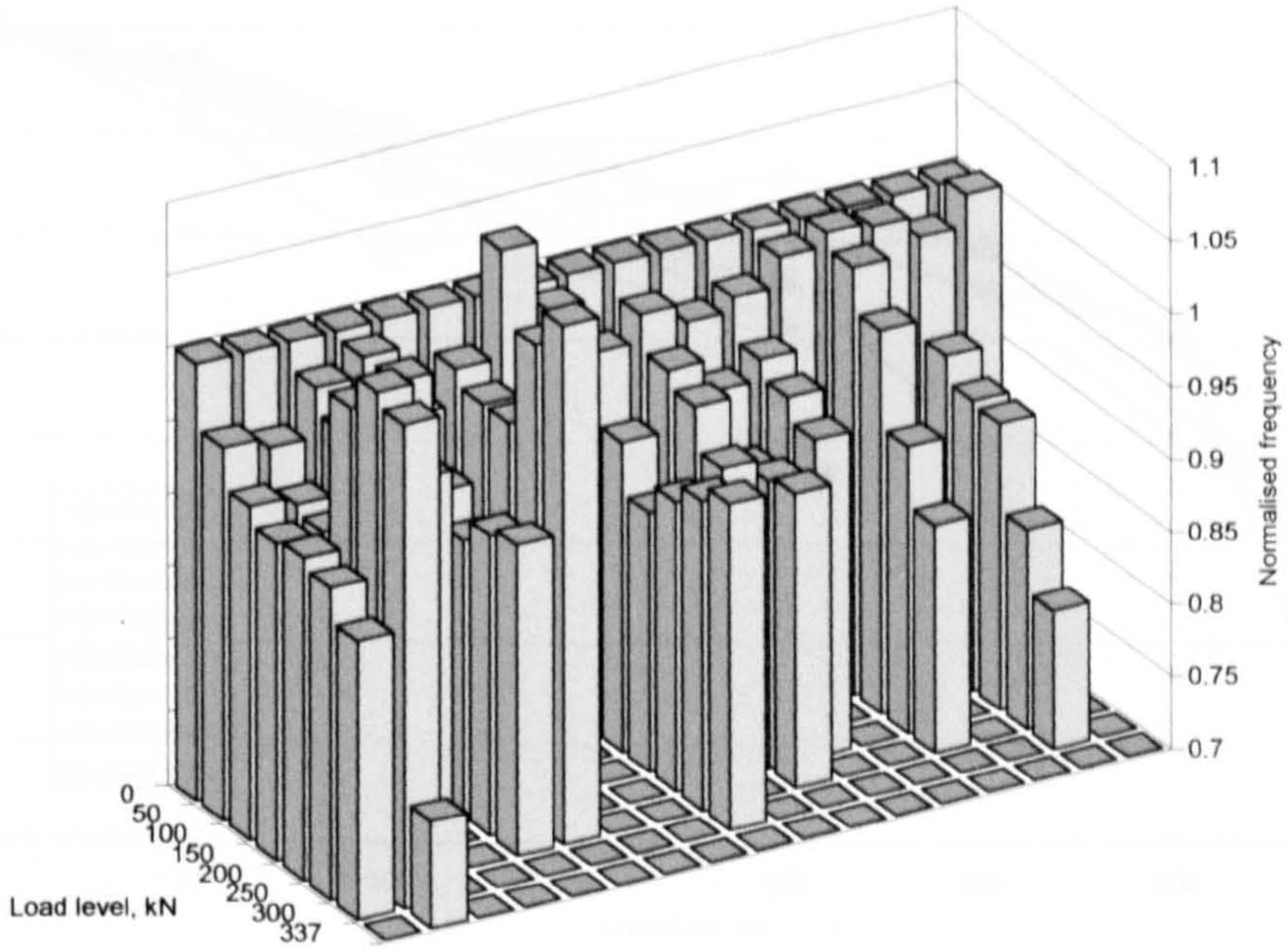

Figure 5-28: Normalised frequency change plotted against load level for deck 9 supported on ten bearings

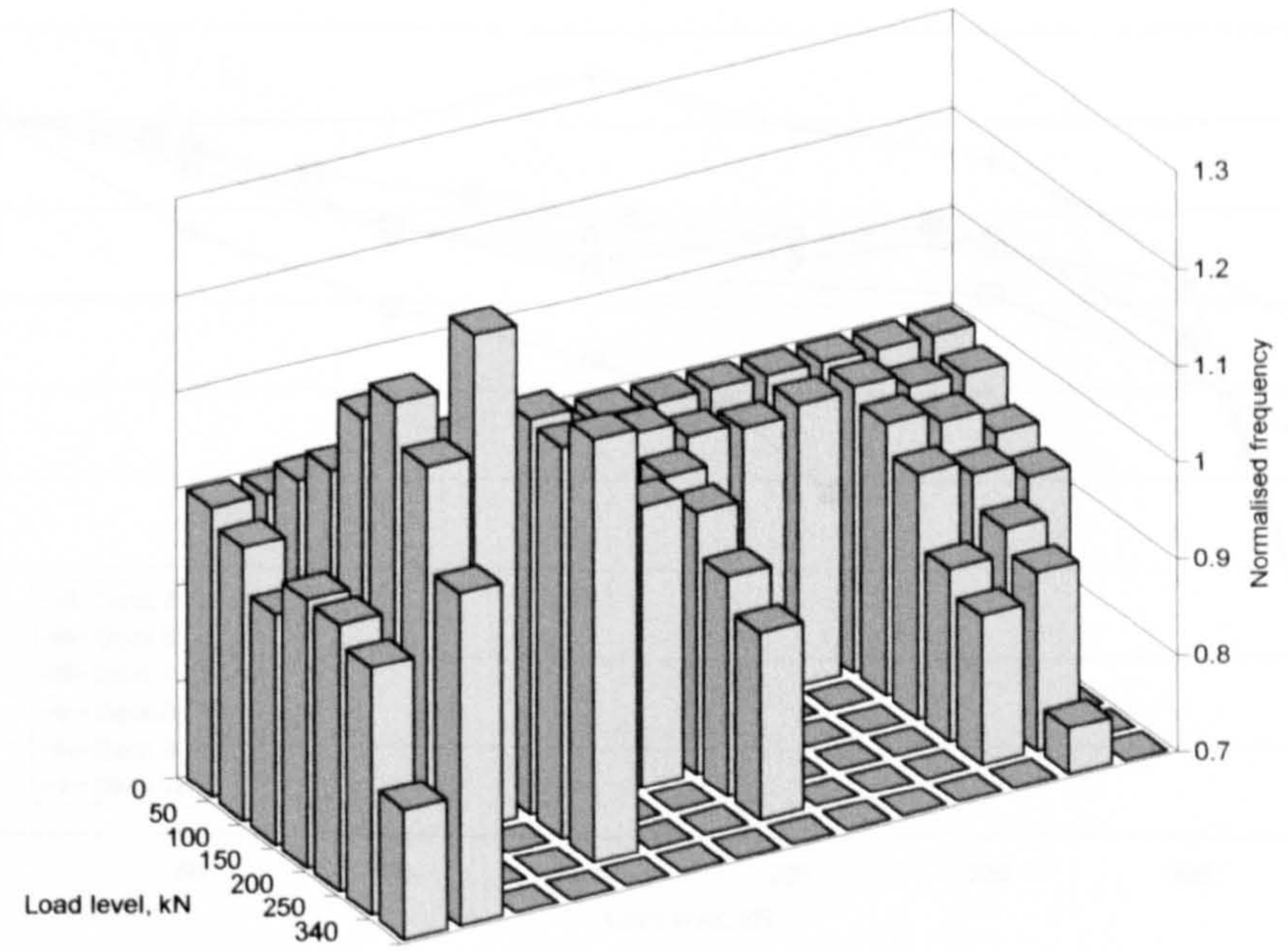

Figure 5-29: Normalised frequency change plotted against load level for deck 10 supported on ten bearings

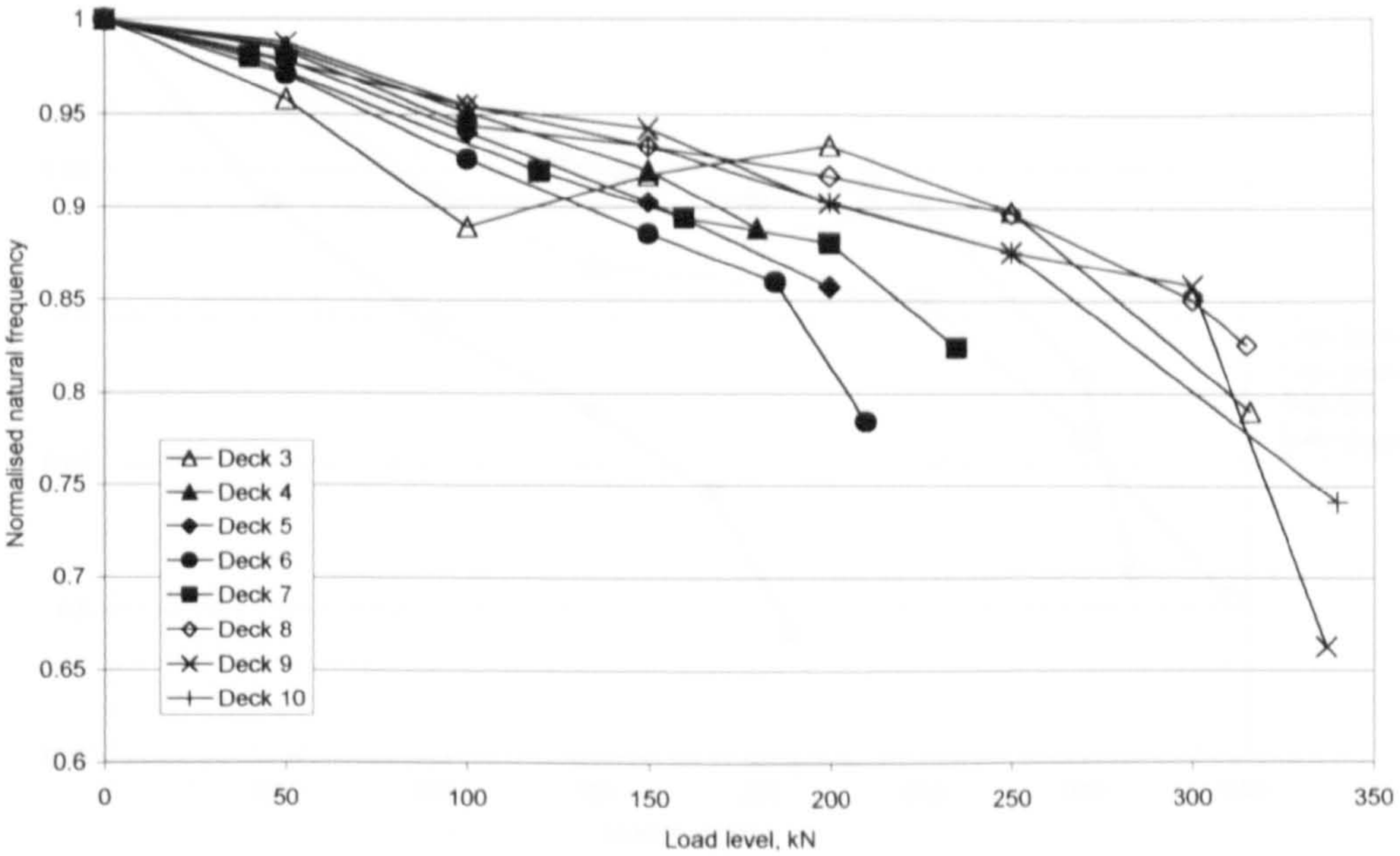

Figure 5-30: Average change in natural frequency in all modes for decks supported on three bearings

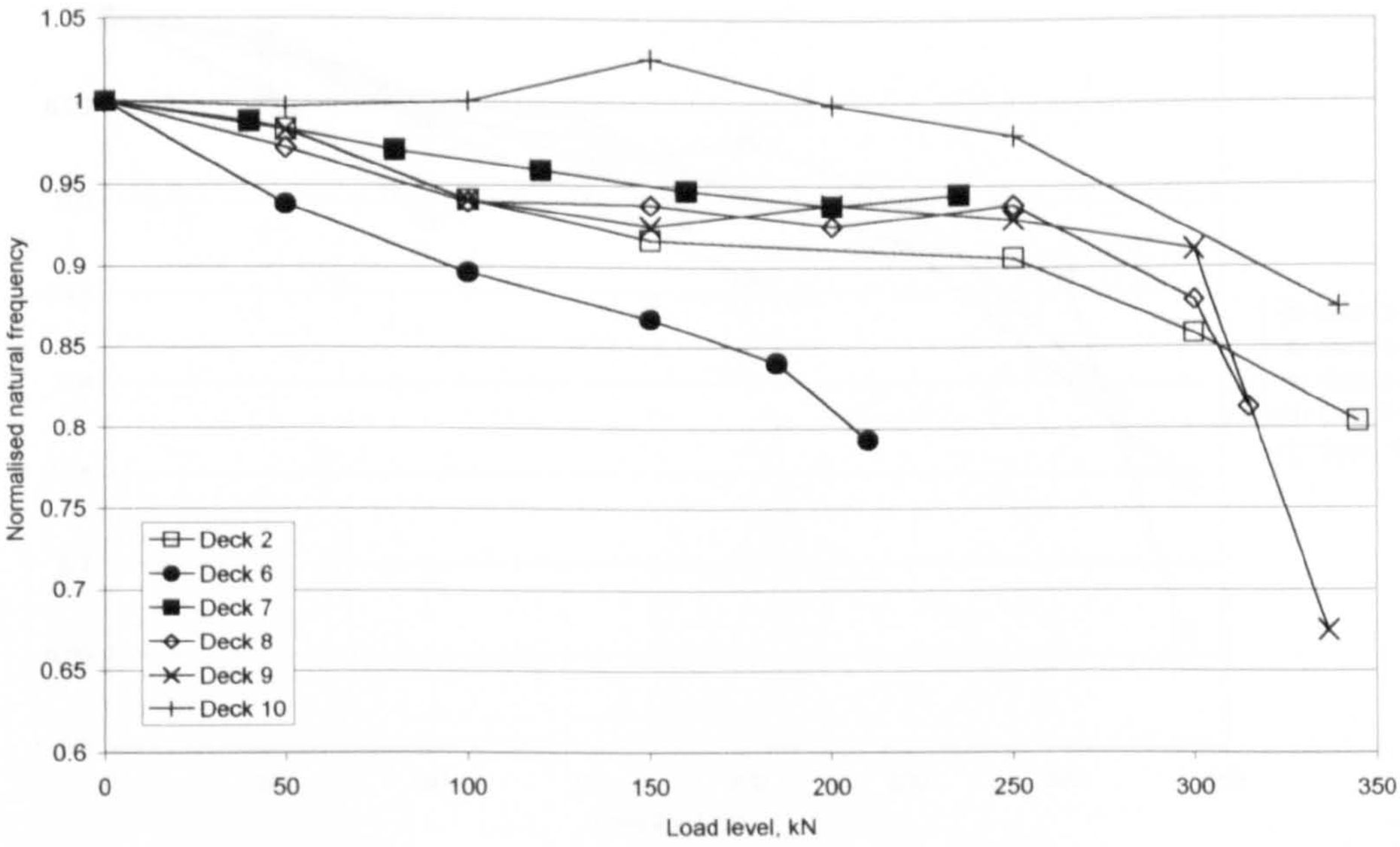

Figure 5-31: Average change in natural frequency all modes for decks supported on ten bearings

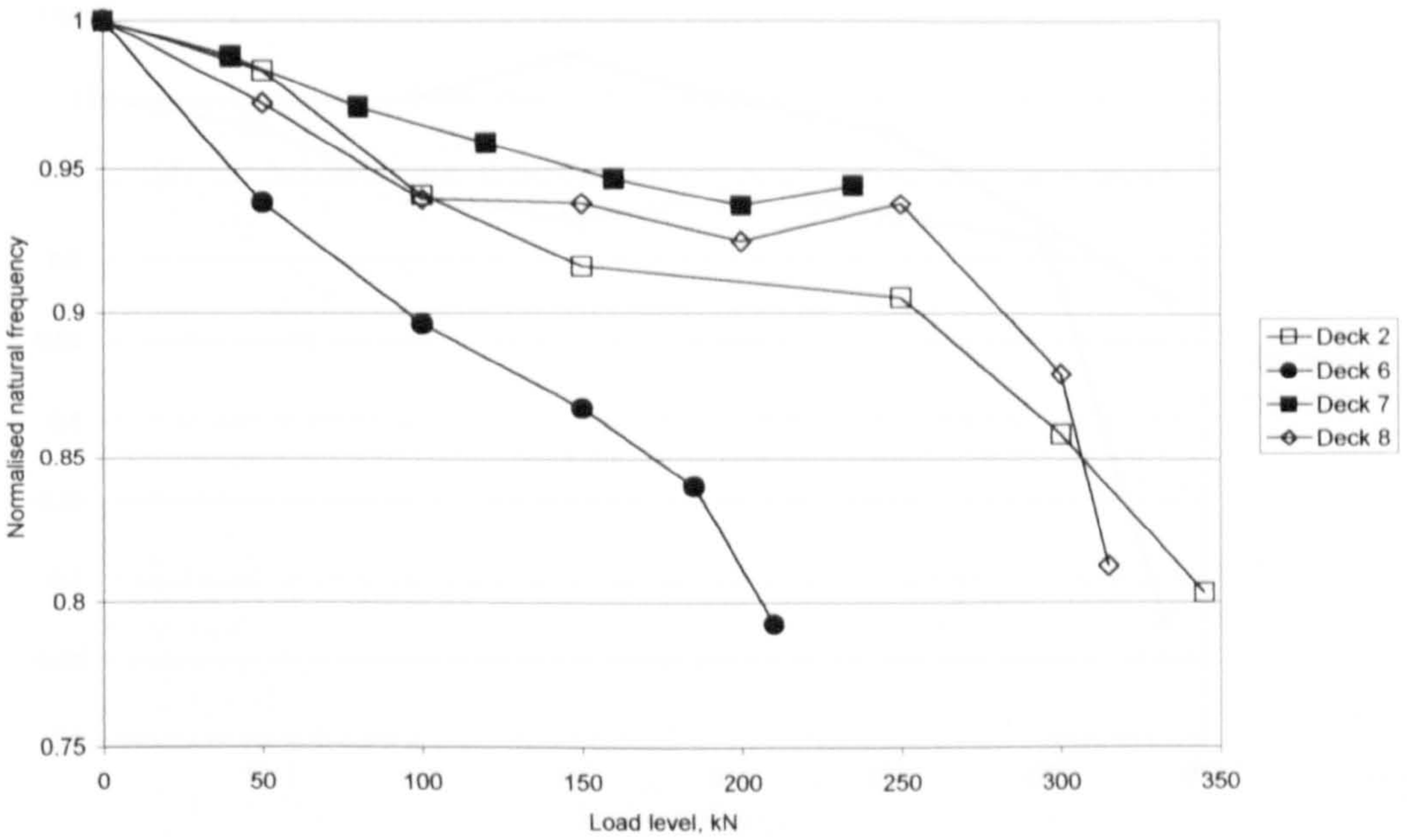

Figure 5-32: Average change in natural frequency of all modes for decks supported on ten bearings under symmetric loading

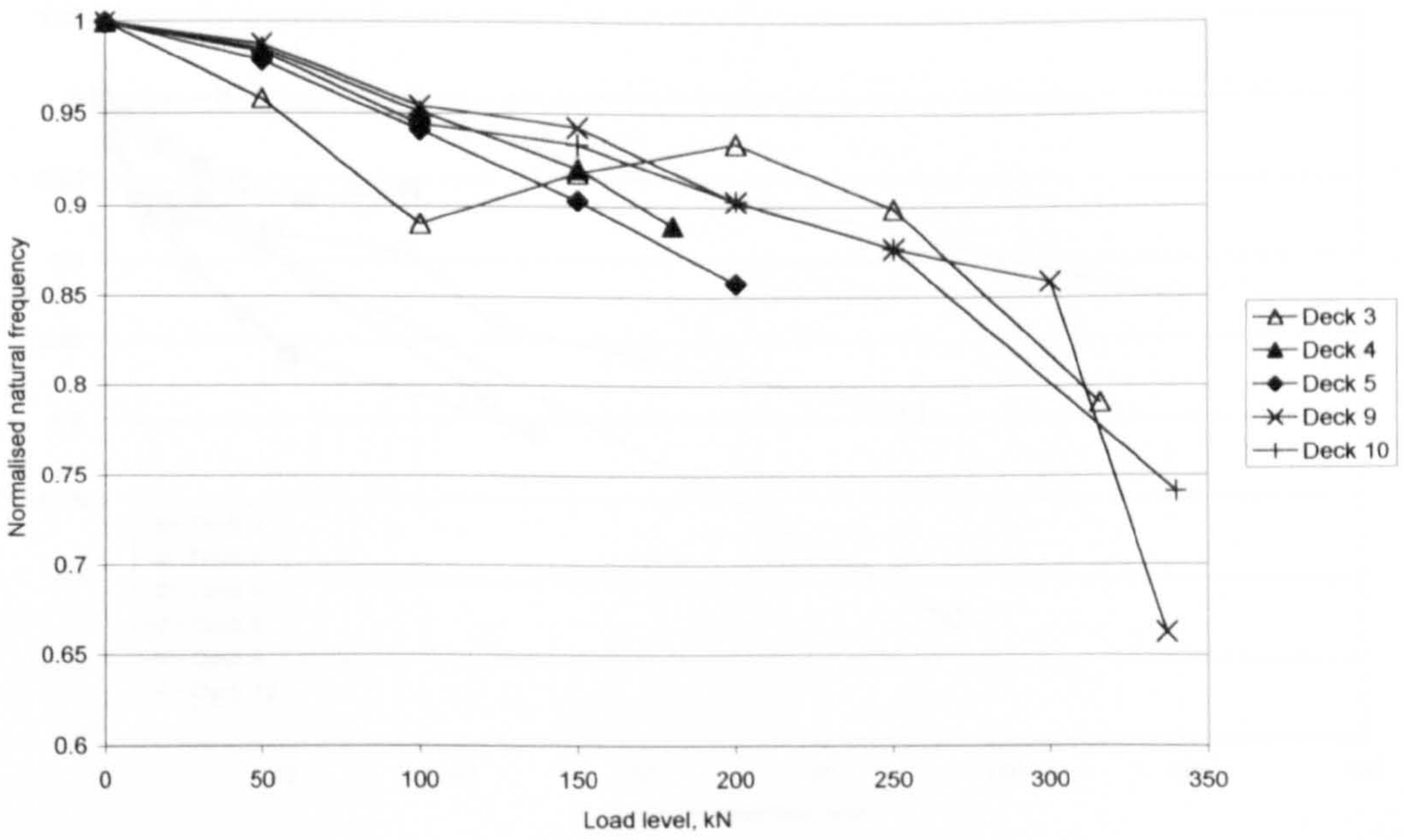

Figure 5-33: Average change in natural frequency of all modes for decks supported on three bearings under asymmetric loading

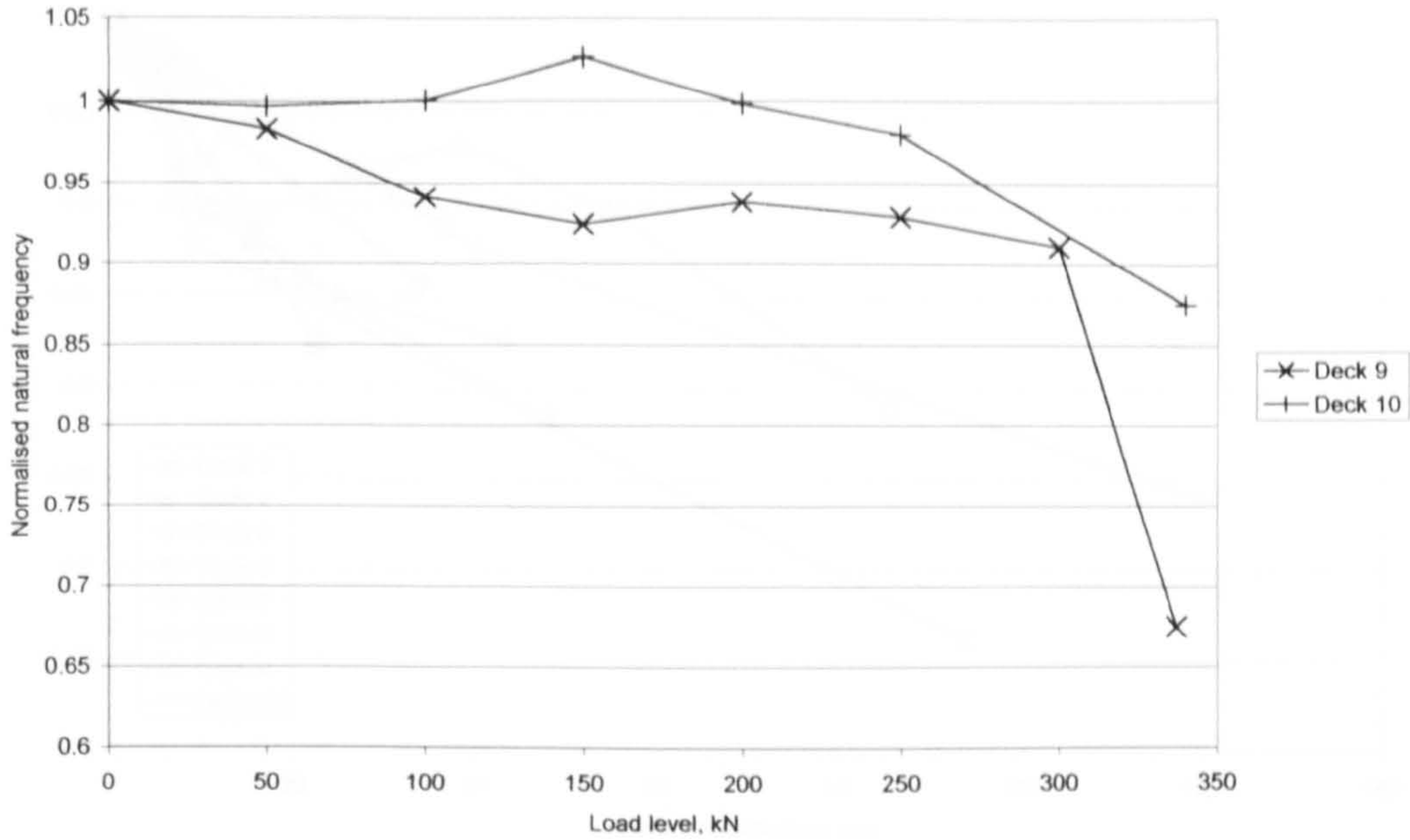

Figure 5-34: Average change in natural frequency of all modes for decks supported on ten bearings under asymmetric loading

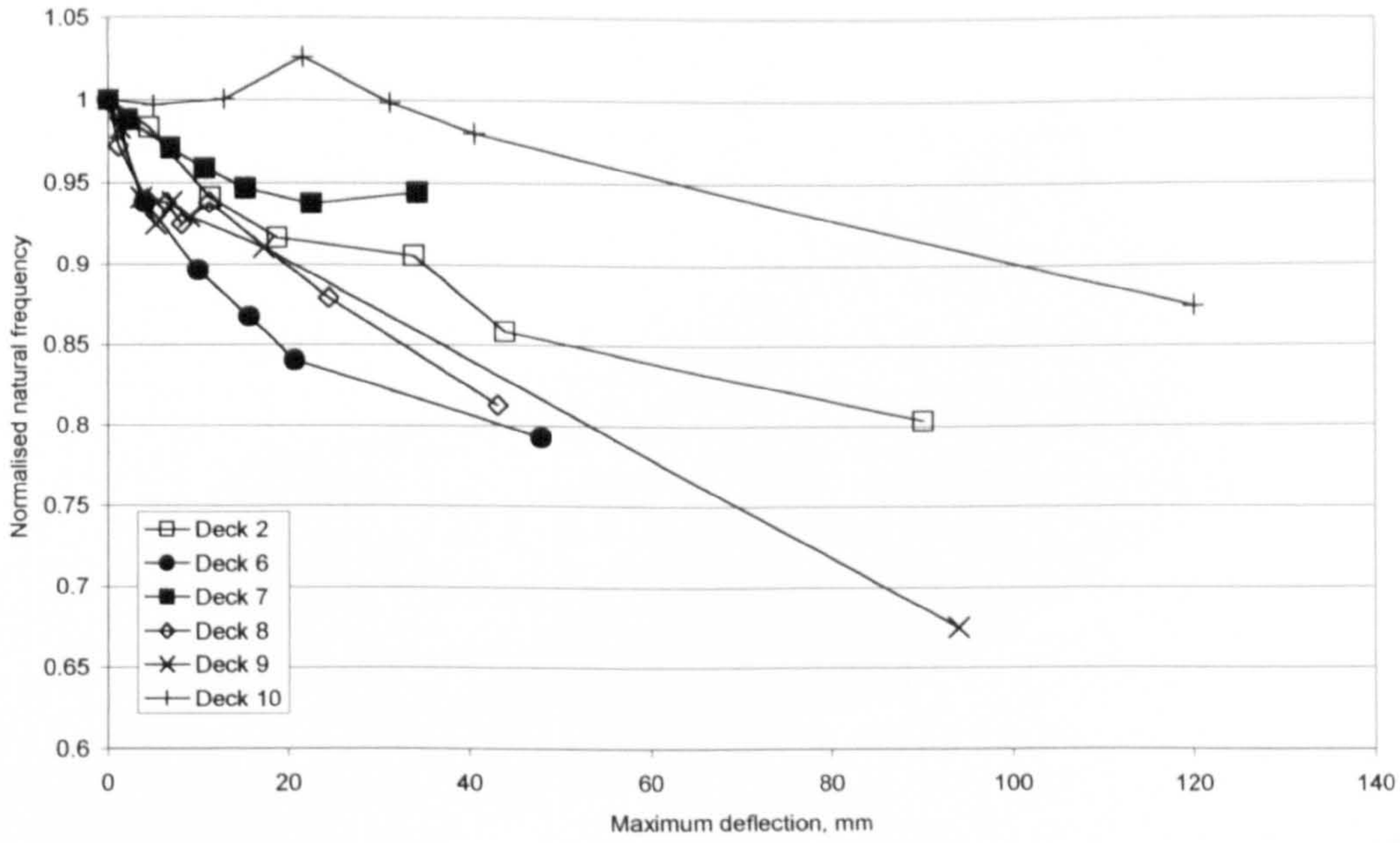

Figure 5-35: Average change in natural frequency of all modes supported on ten bearings plotted against mid-span deflection

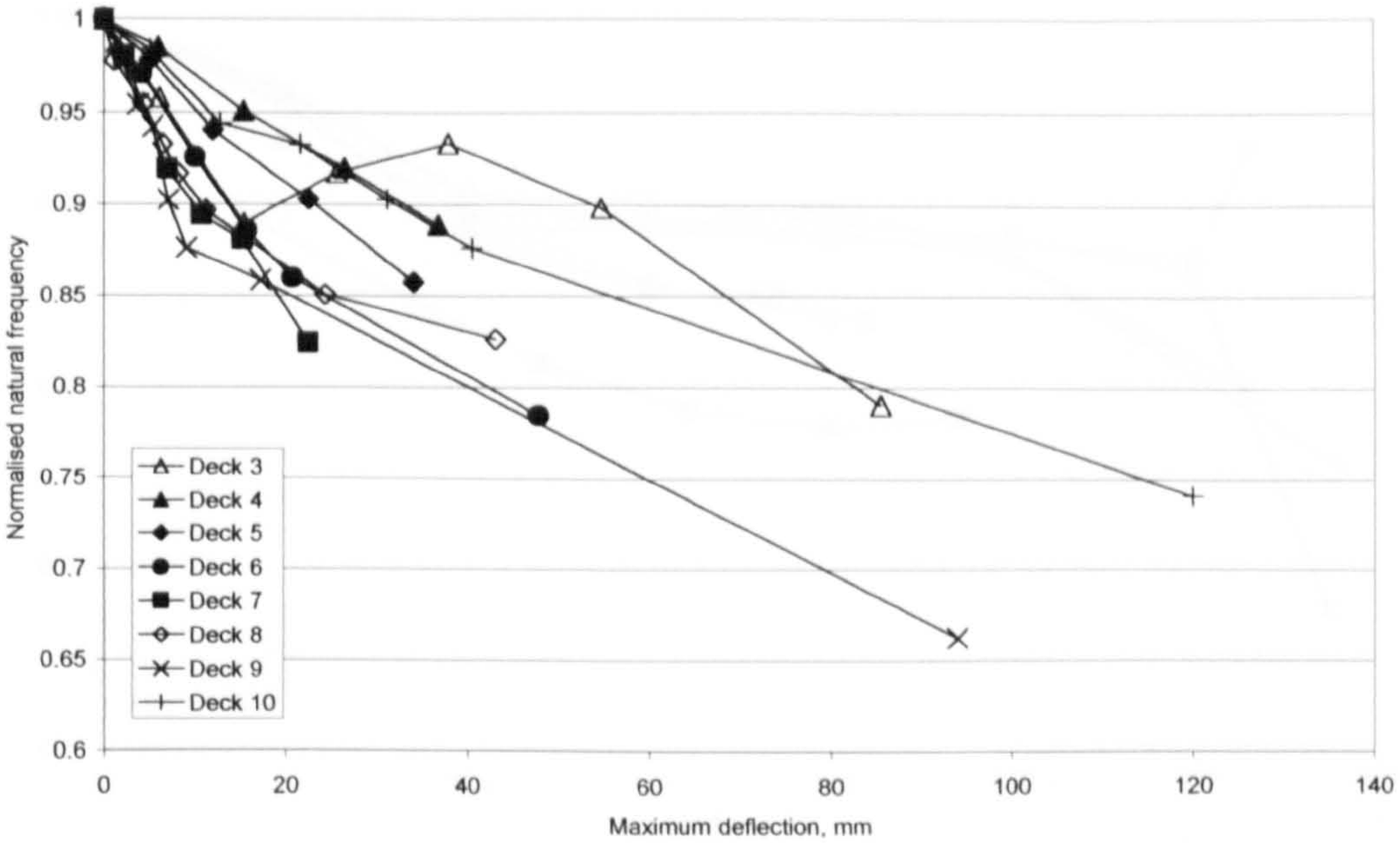

Figure 5-36: Average change in natural frequency of all modes supported on three bearings plotted against mid-span deflection

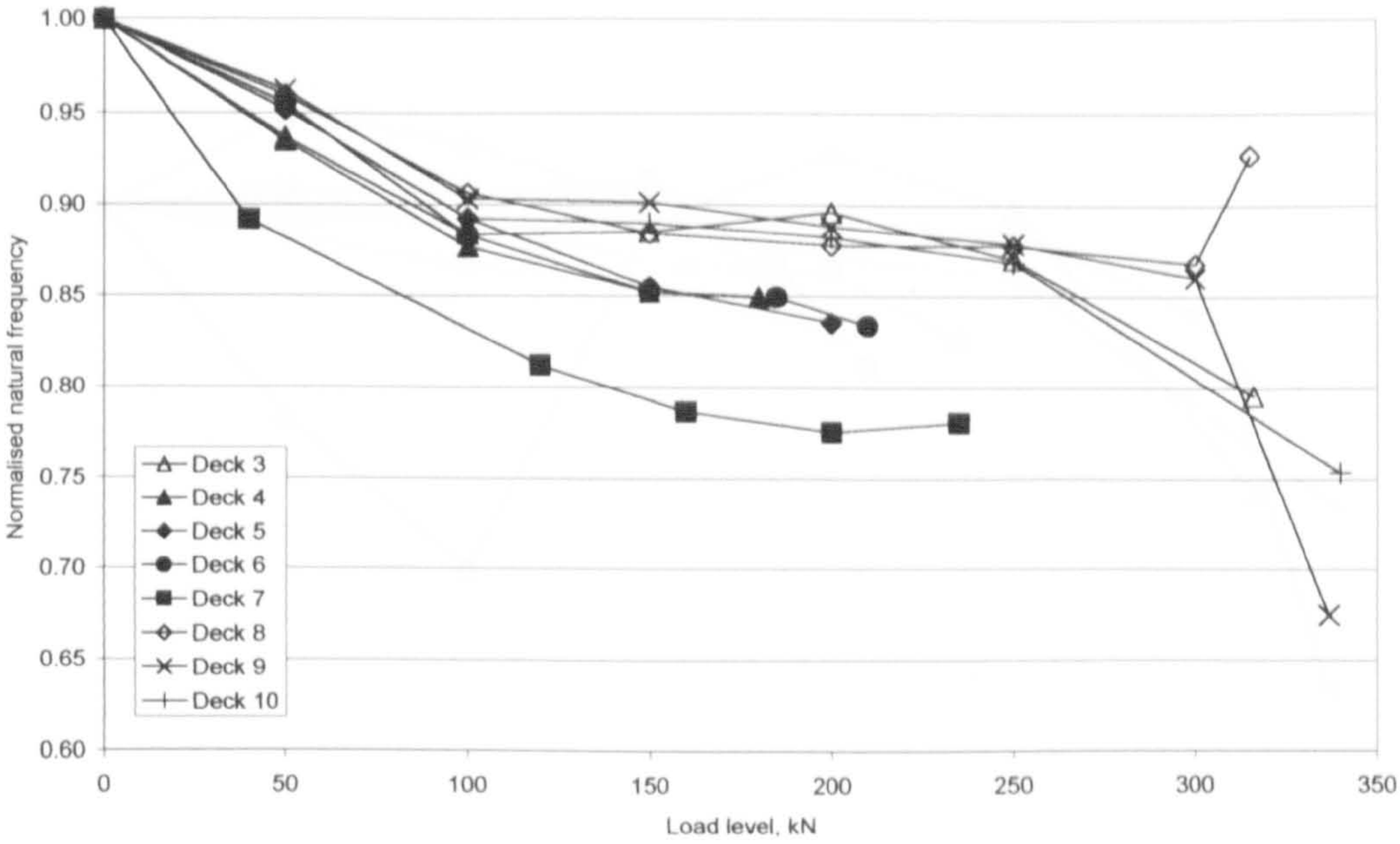

Figure 5-37: Average change in normalised natural frequency of mode 2 for all decks supported on three bearings

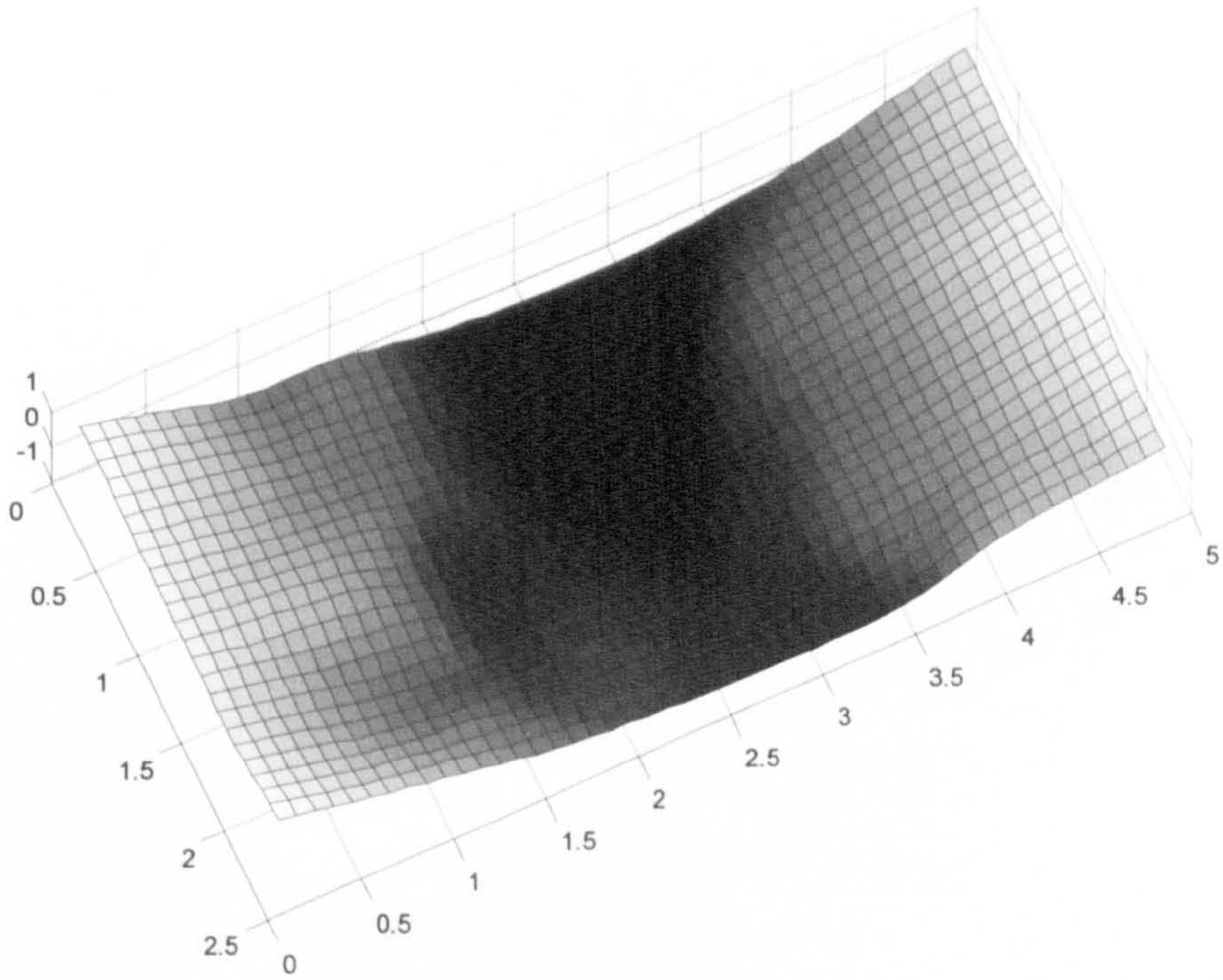

Figure 5-38: Typical mode shape for mode 2

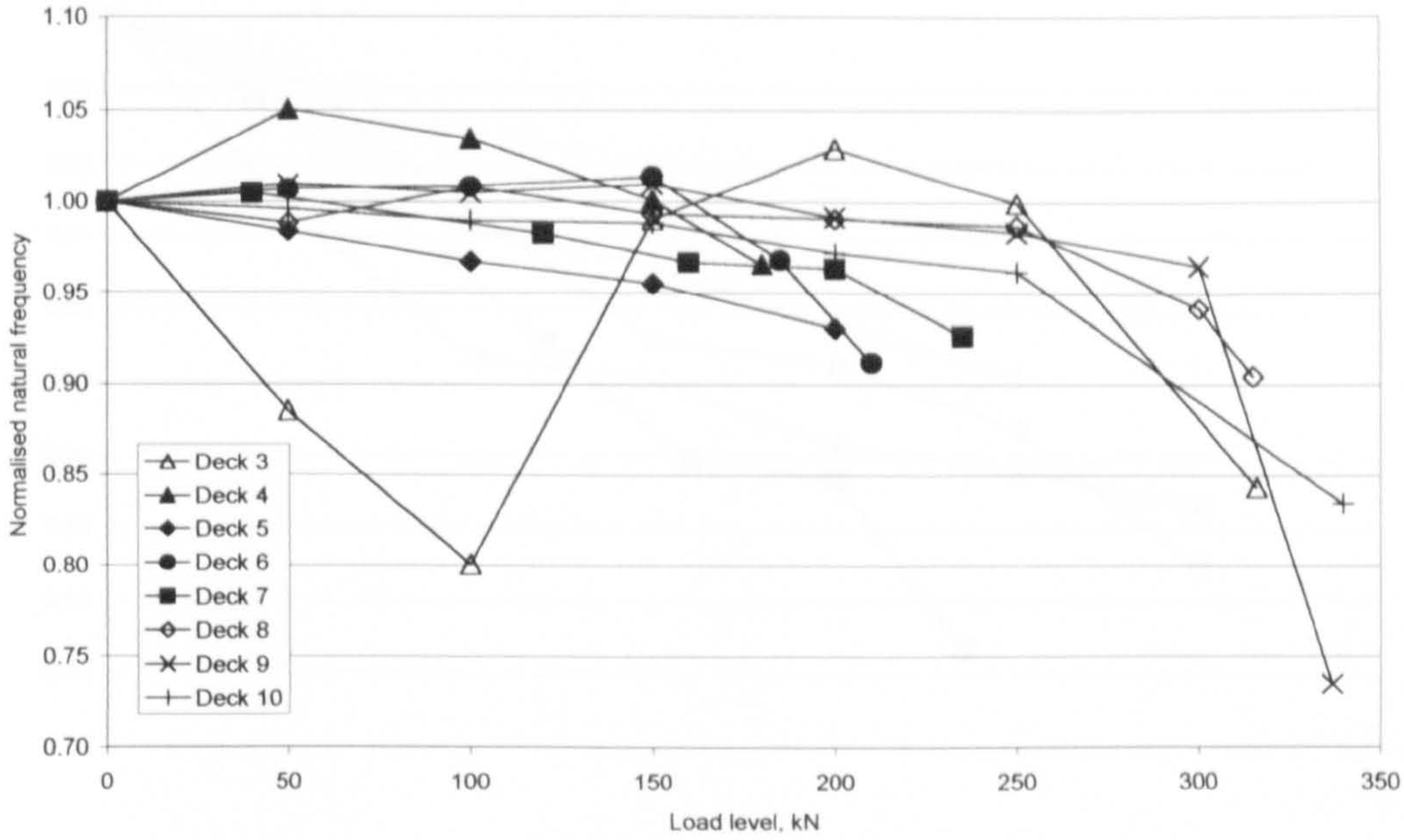

Figure 5-39: Average change in normalised natural frequency of mode 3 for all decks supported on three bearings

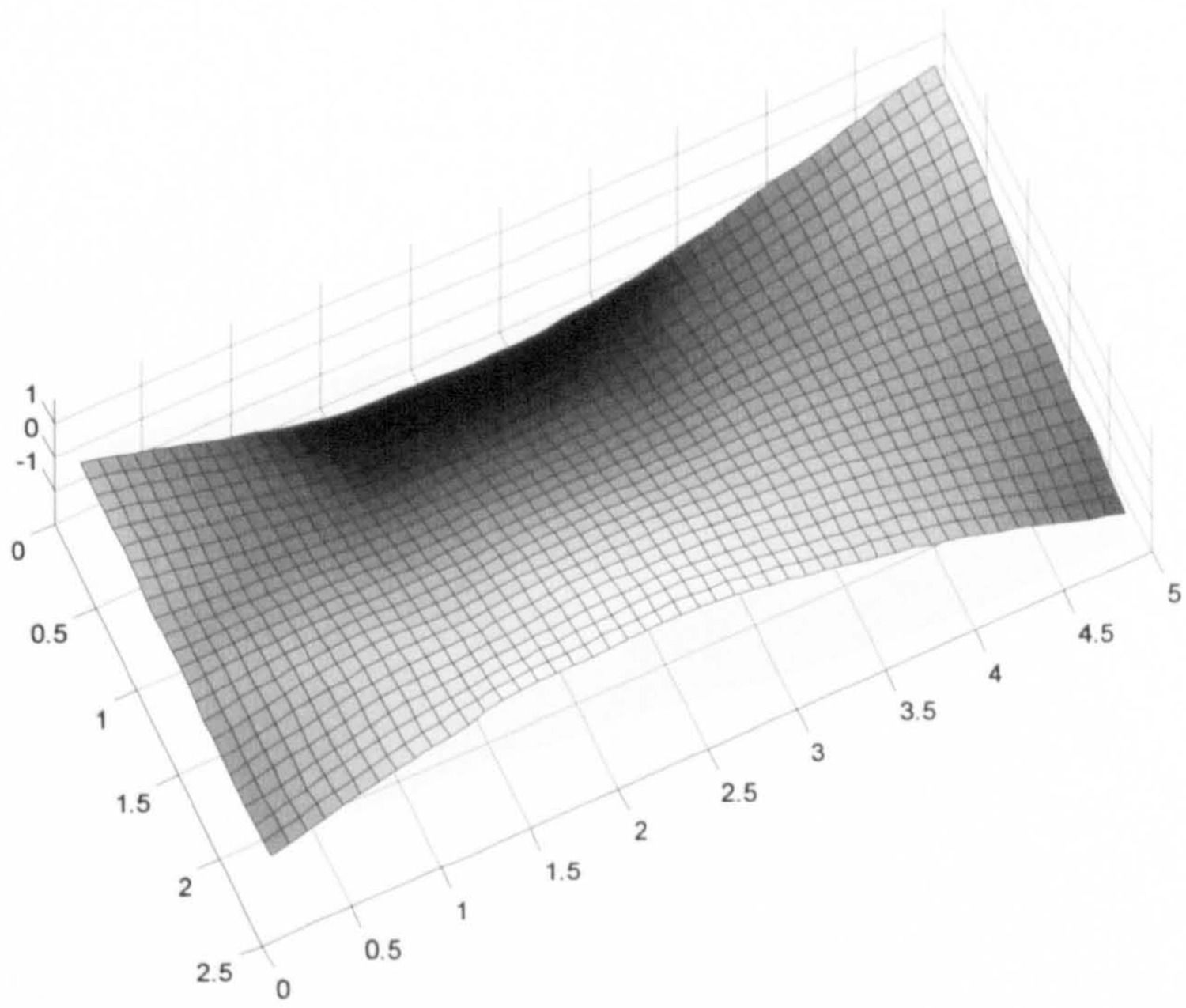

Figure 5-40: Typical mode shape for mode 3

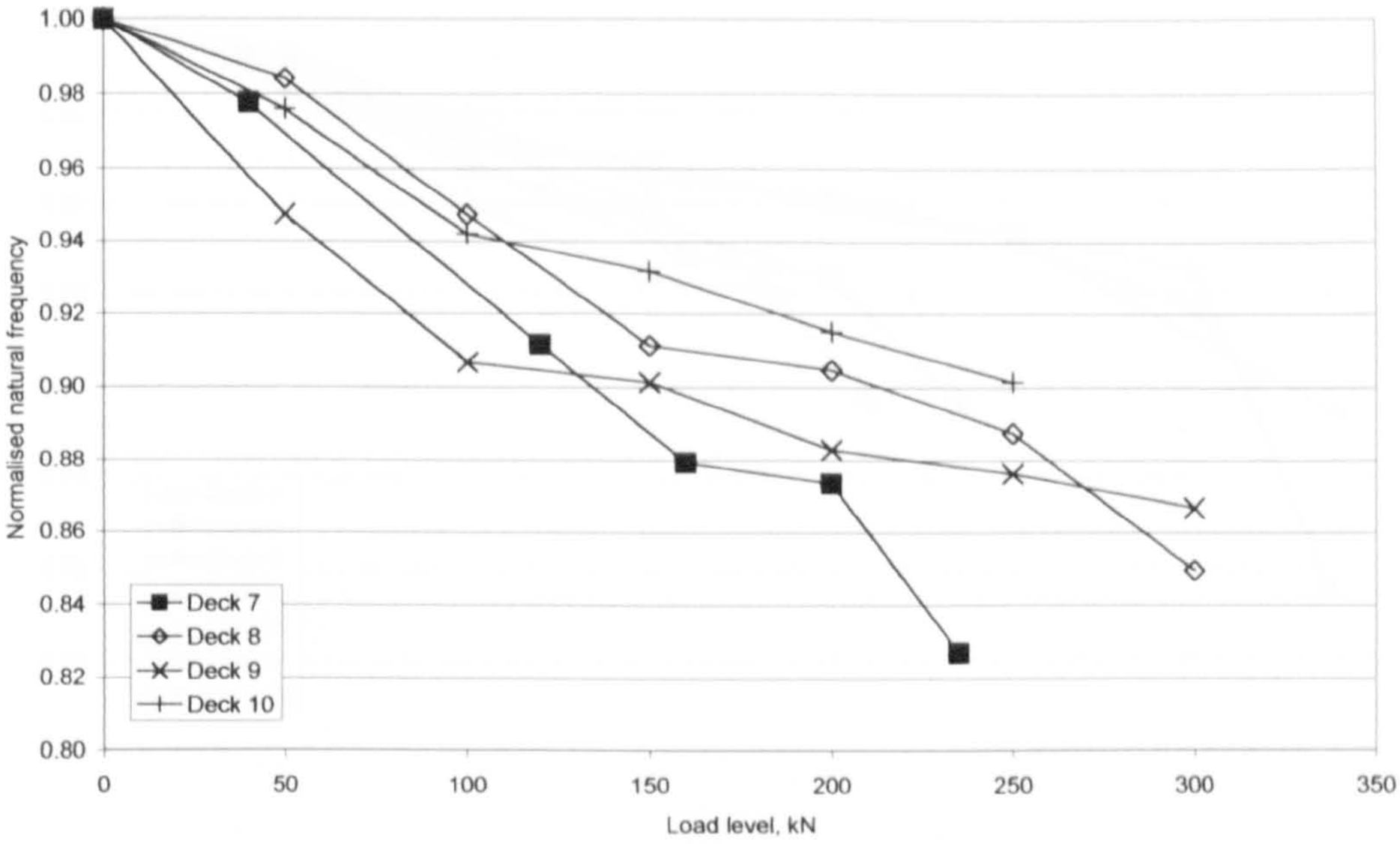

Figure 5-41: Average change in normalised natural frequency of mode 4 for all decks supported on three bearings

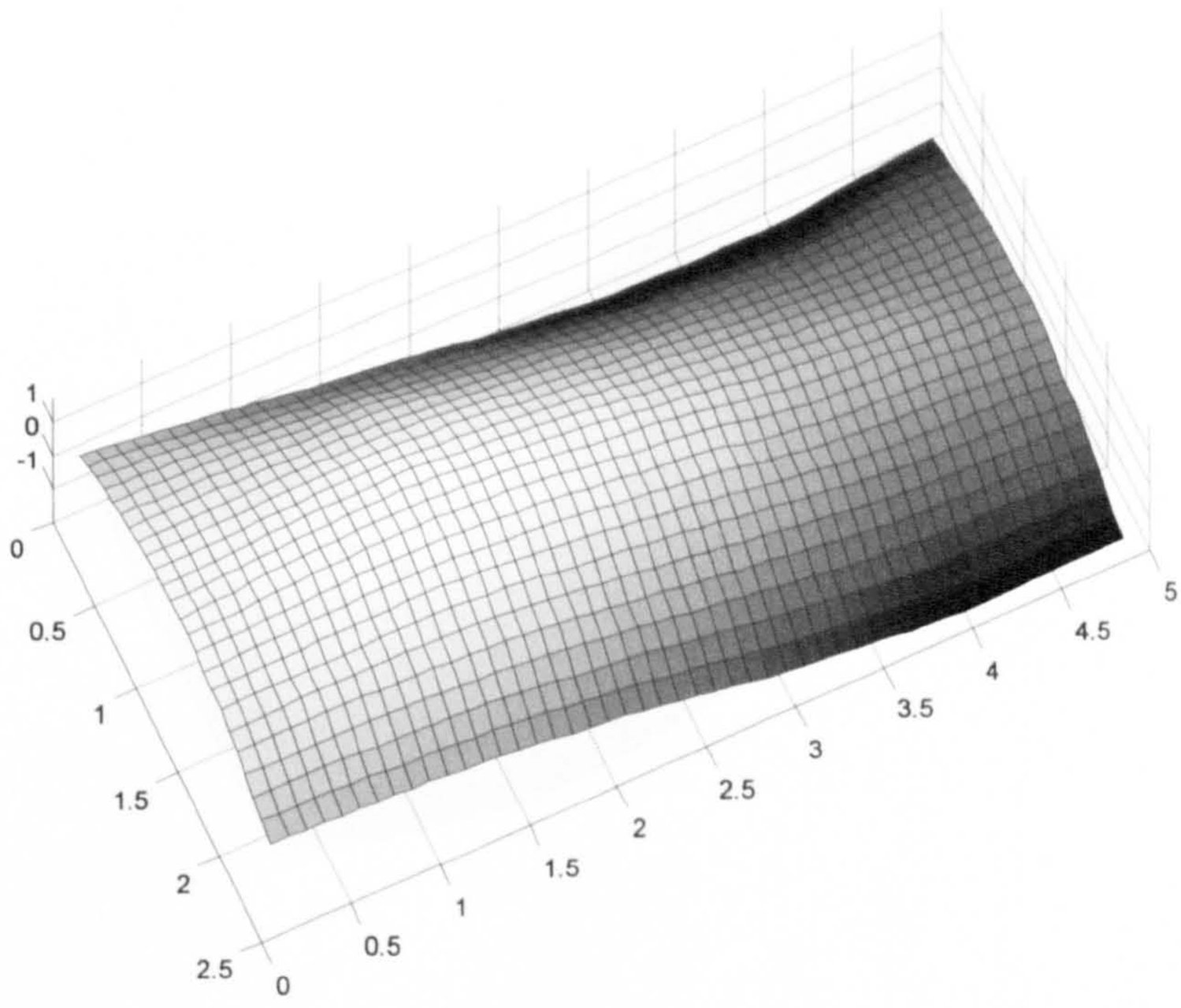

Figure 5-42: Typical mode shape for mode 4

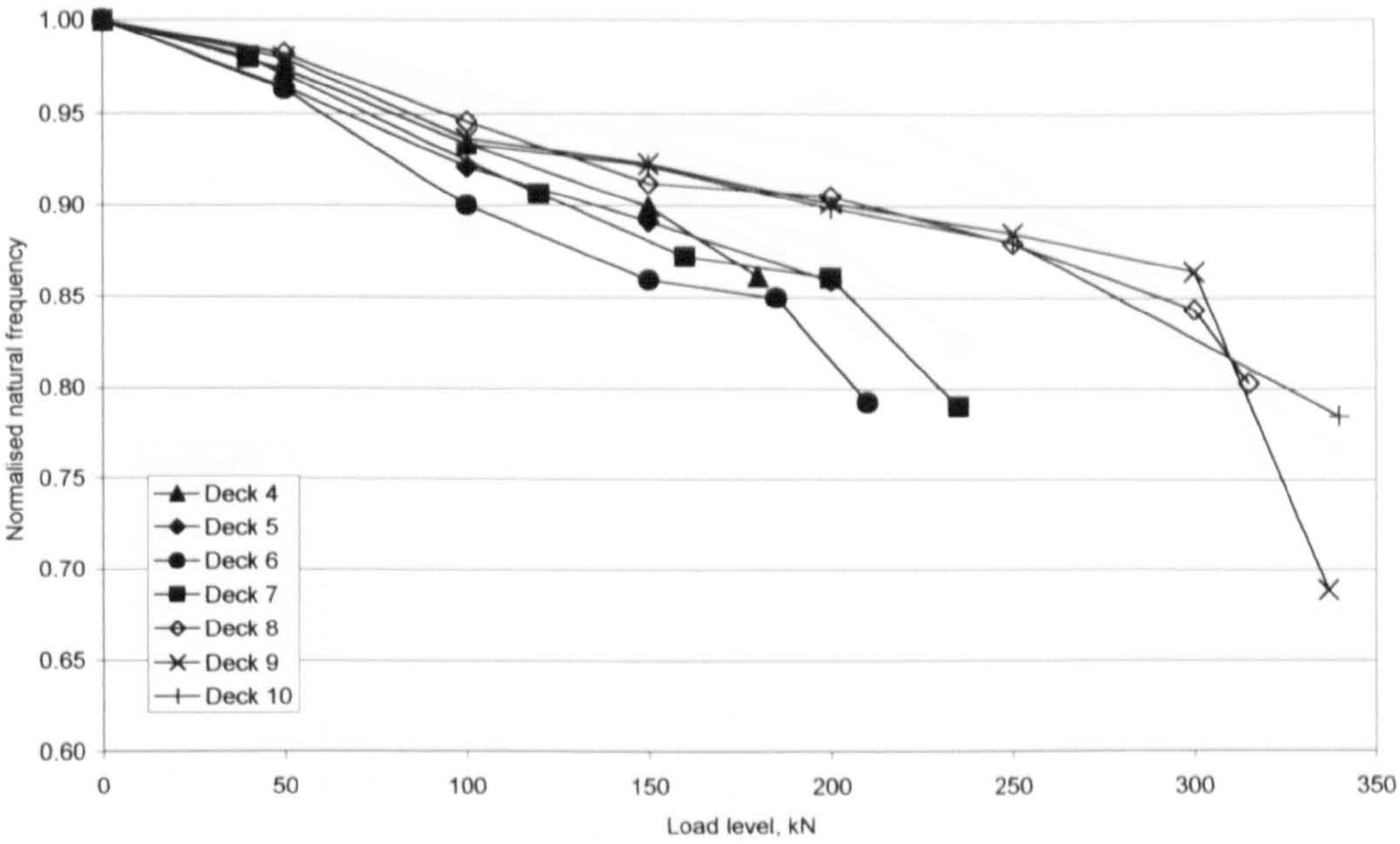

Figure 5-43: Average change in normalised natural frequency of mode 6 for all decks supported on three bearings

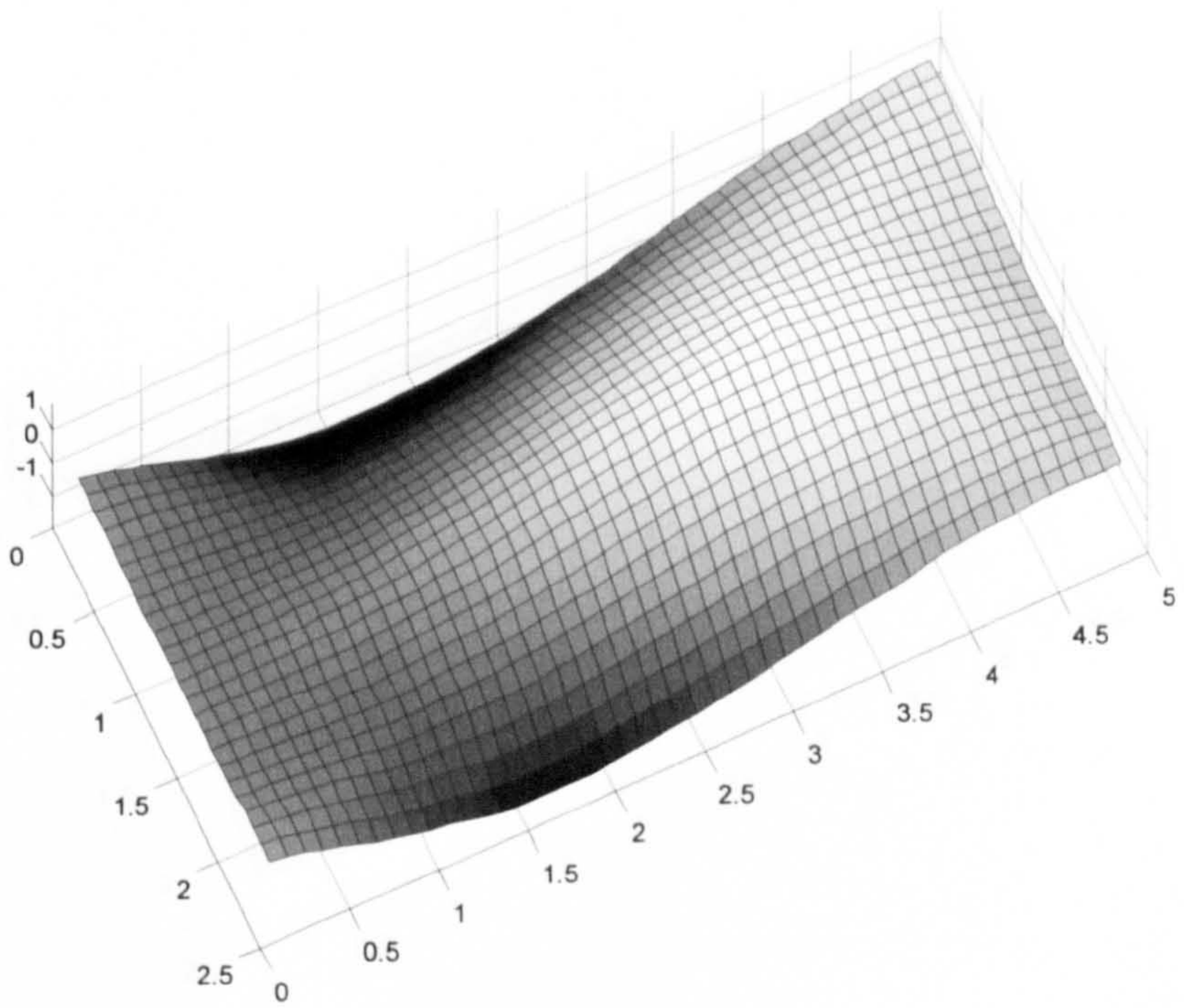

Figure 5-44: Typical mode shape for mode 6

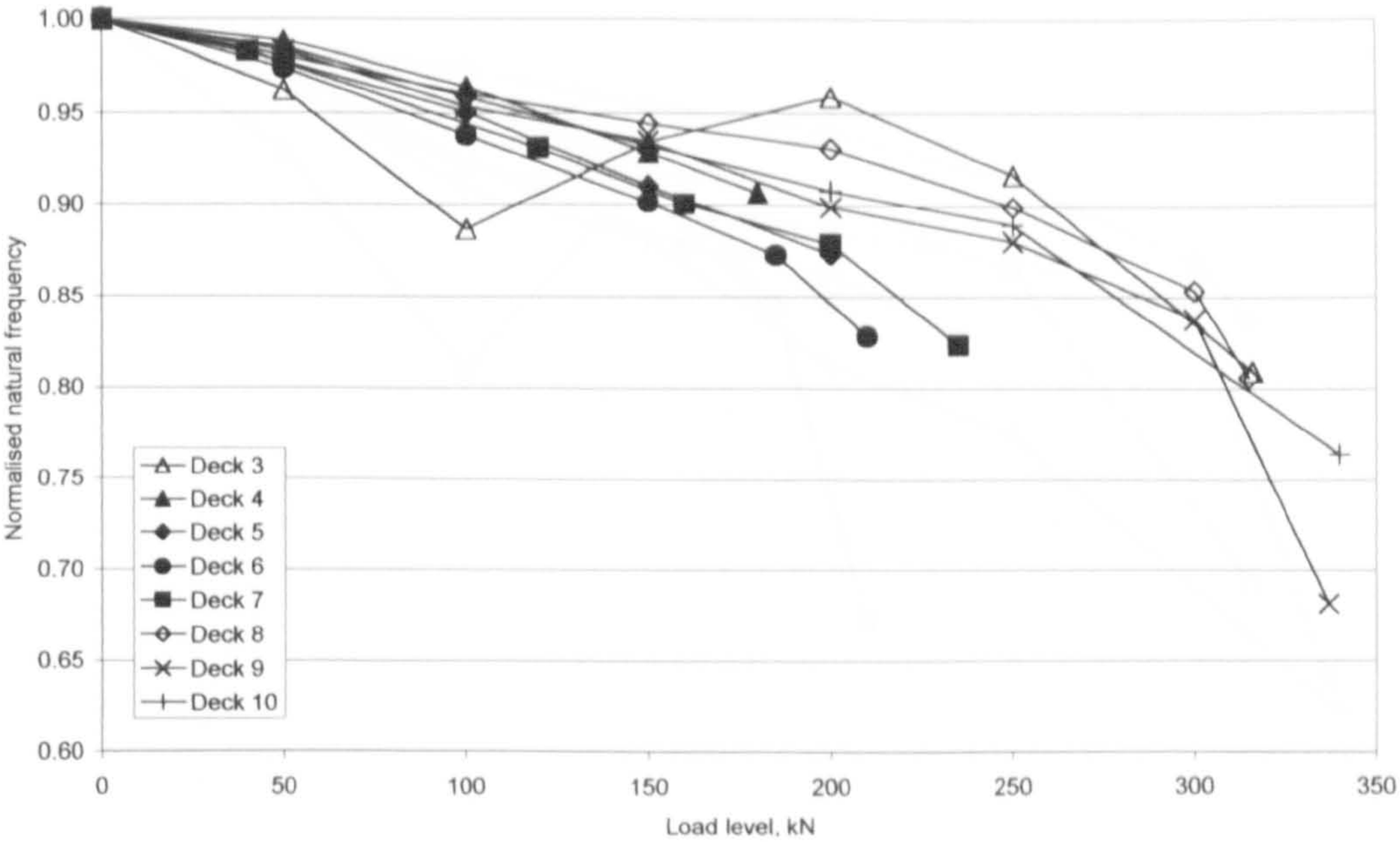

Figure 5-45: Average change in normalised natural frequency of mode 8 for all decks supported on three bearings

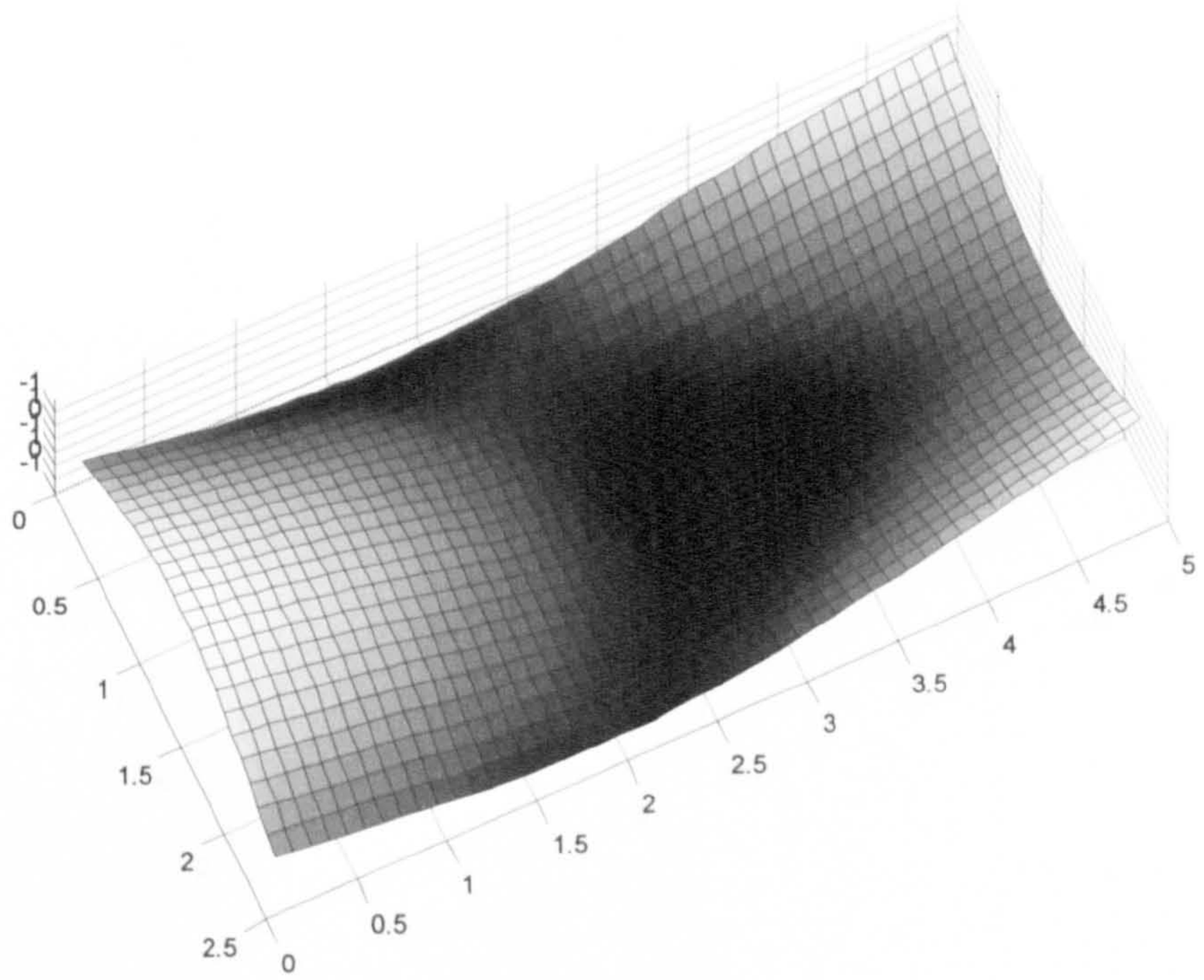

Figure 5-46: Typical mode shape for mode 8

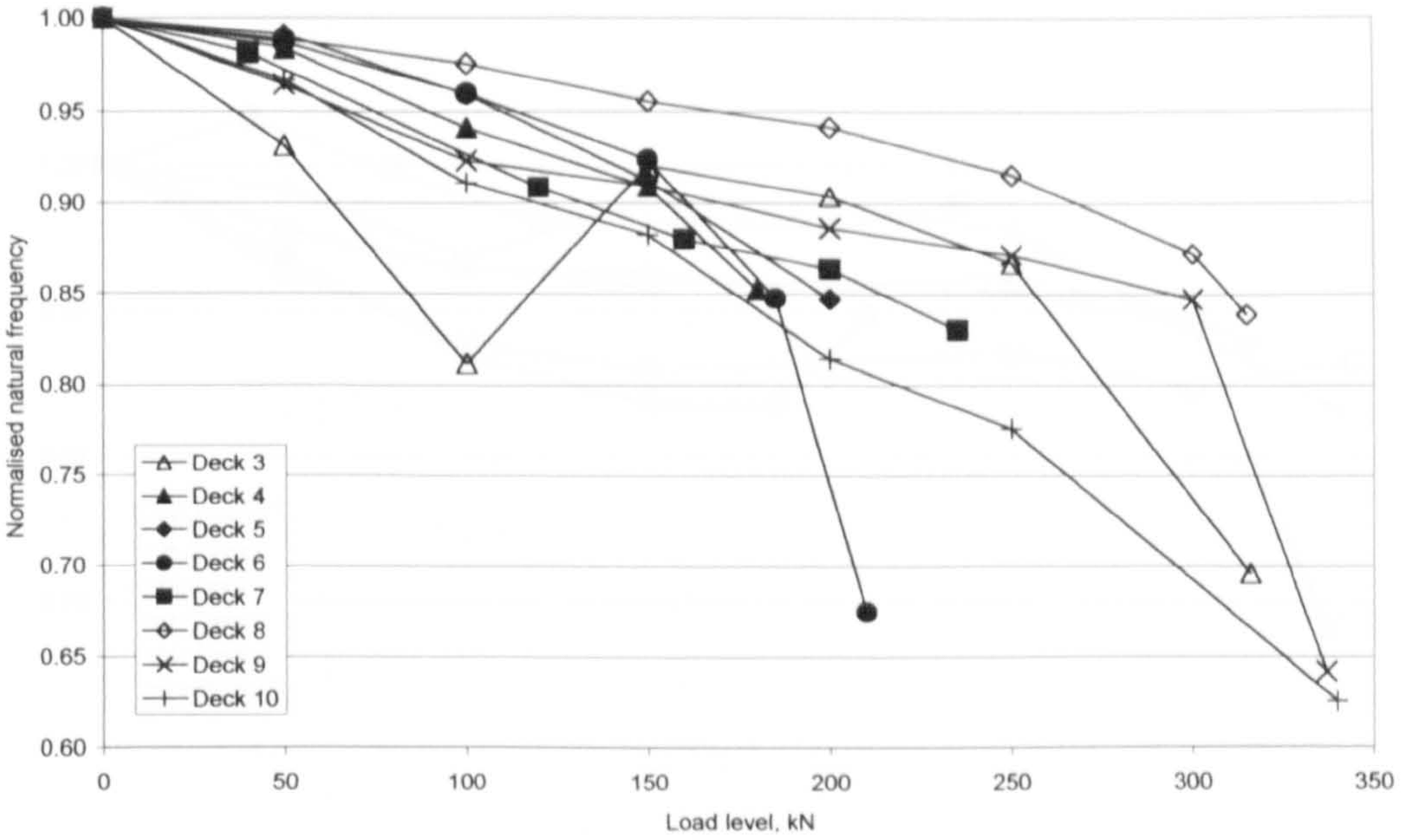

Figure 5-47: Average change in normalised natural frequency of mode 9 for all decks supported on three bearings

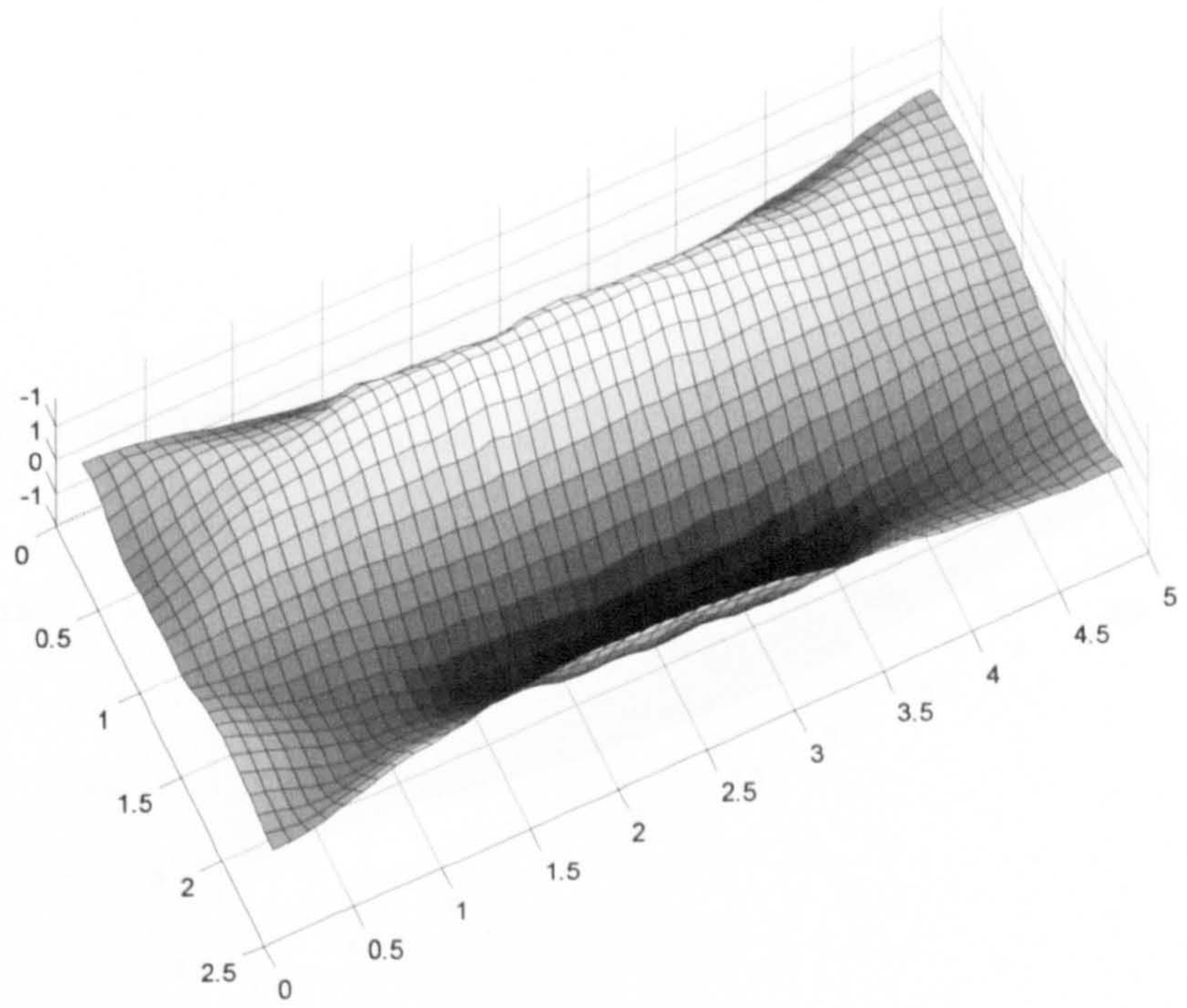

Figure 5-48: Typical mode shape for mode 9

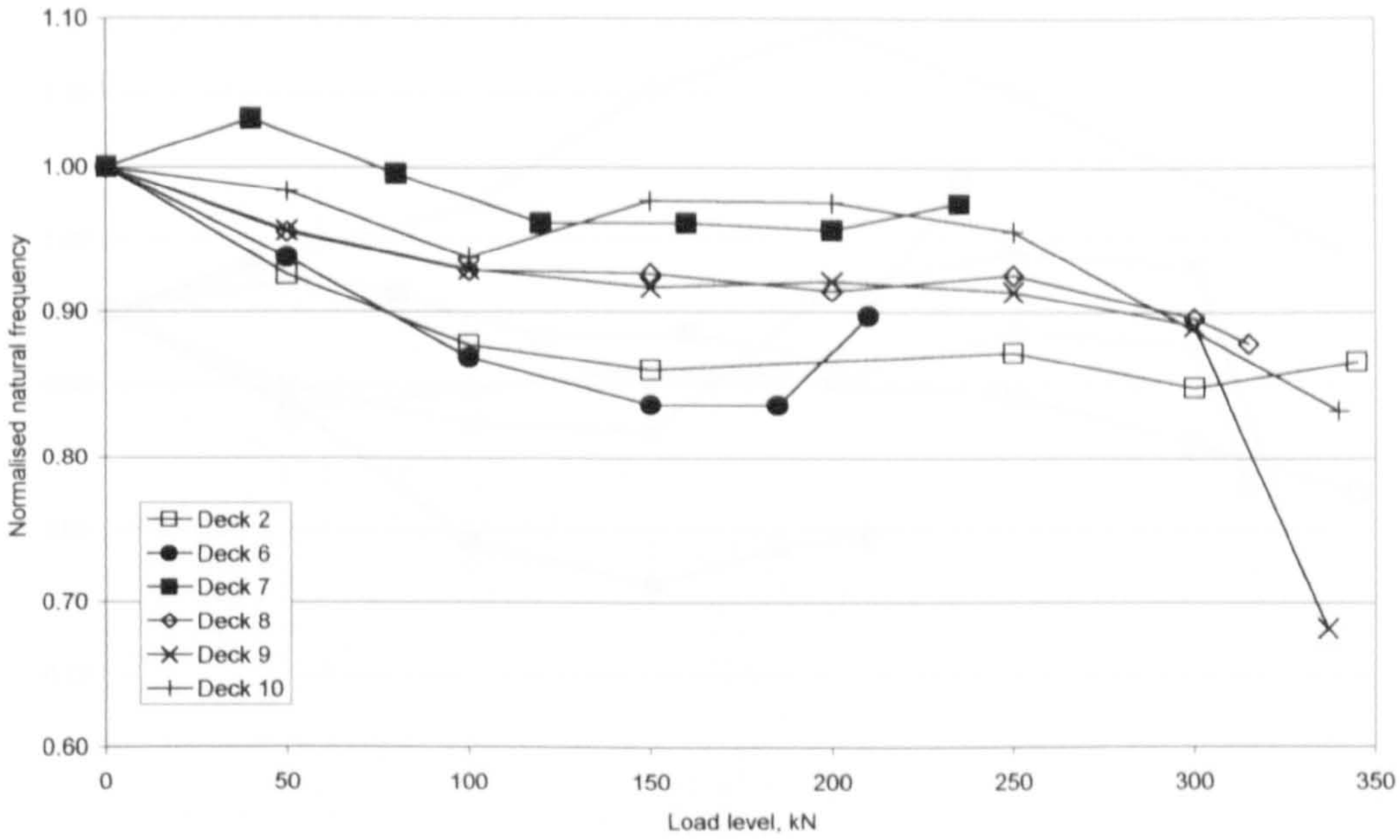

Figure 5-49: Average change in normalised natural frequency of mode 1 for all decks supported on ten bearings

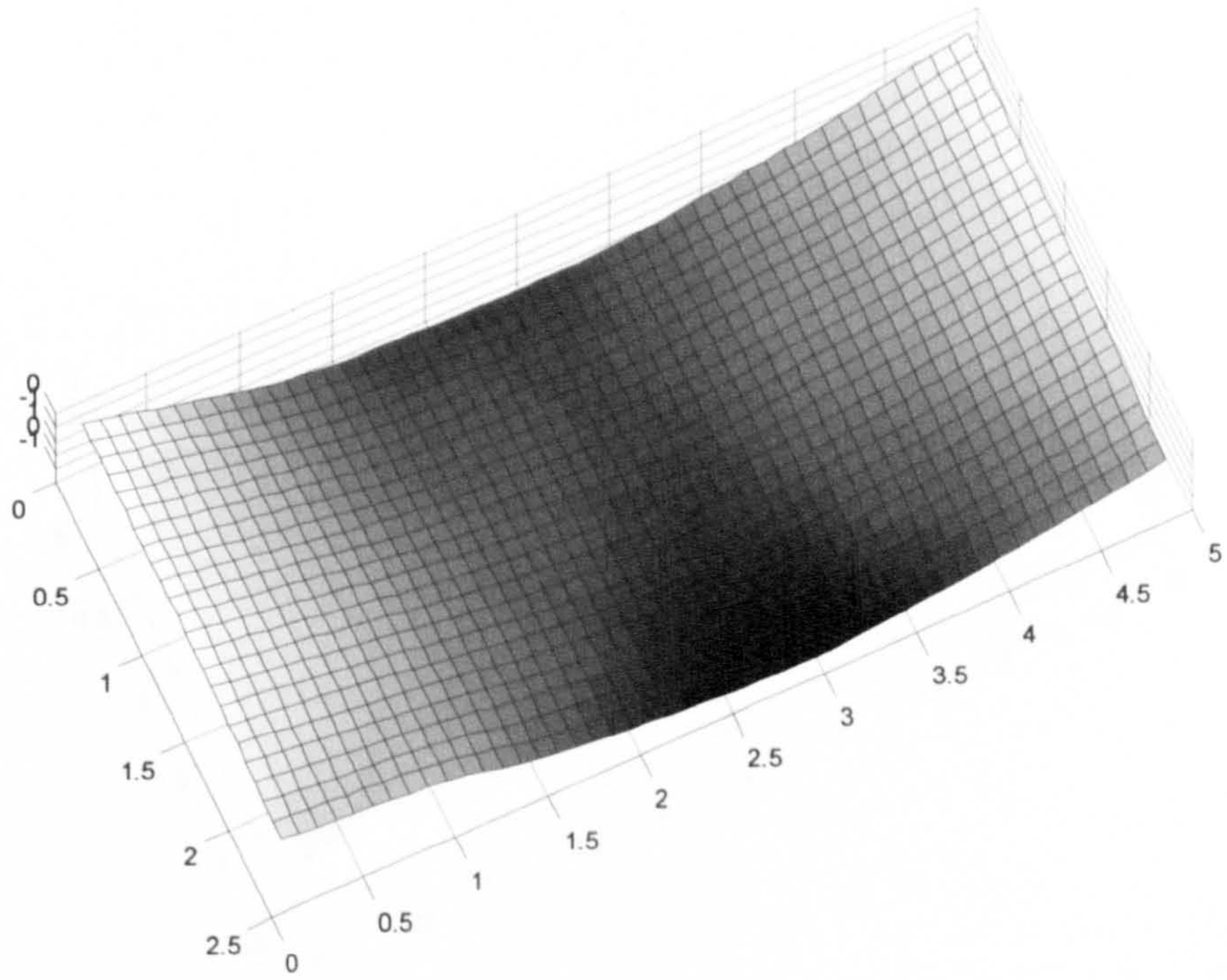

Figure 5-50: Typical mode shape for mode 1

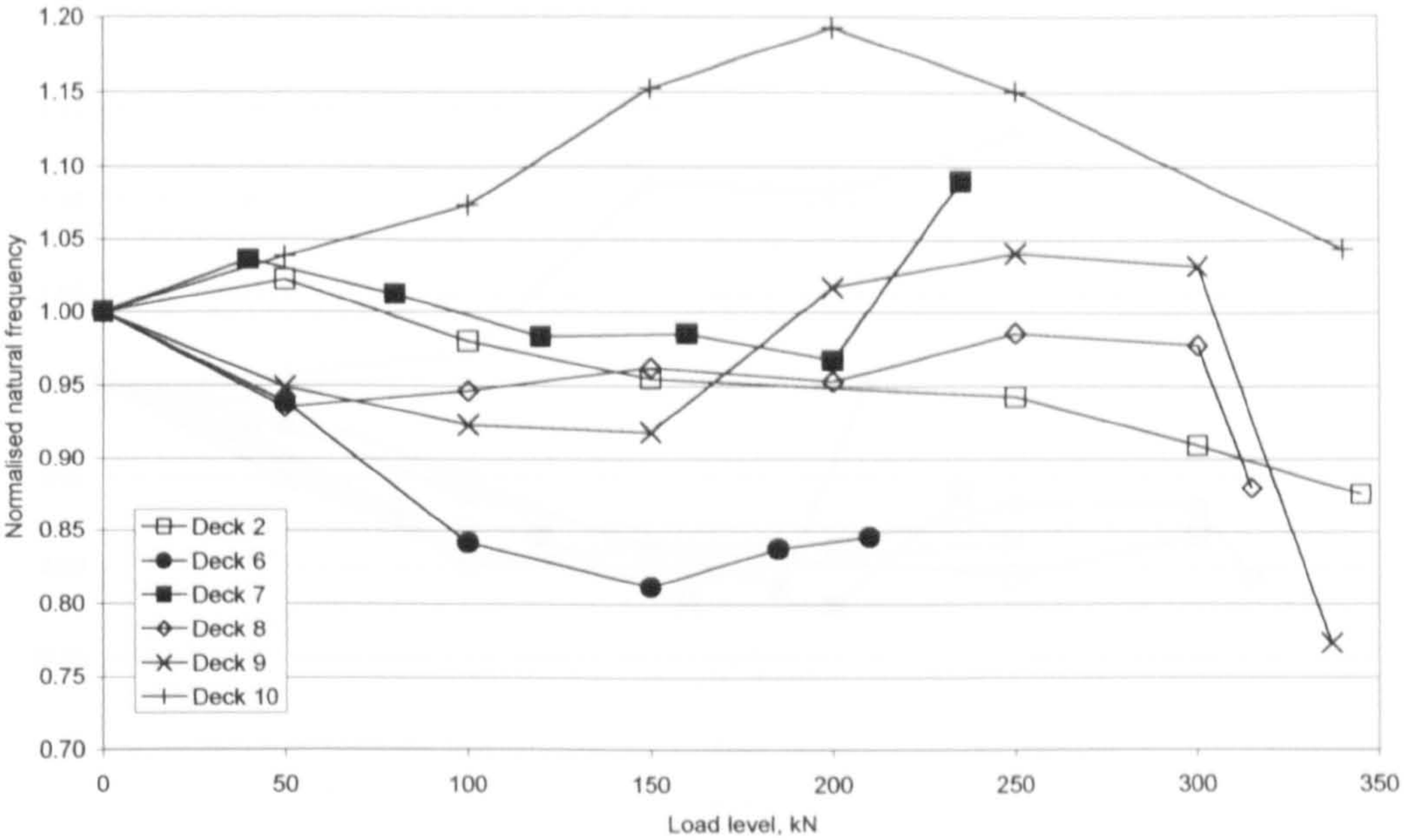

Figure 5-51: Average change in normalised natural frequency of mode 2 for all decks supported on ten bearings

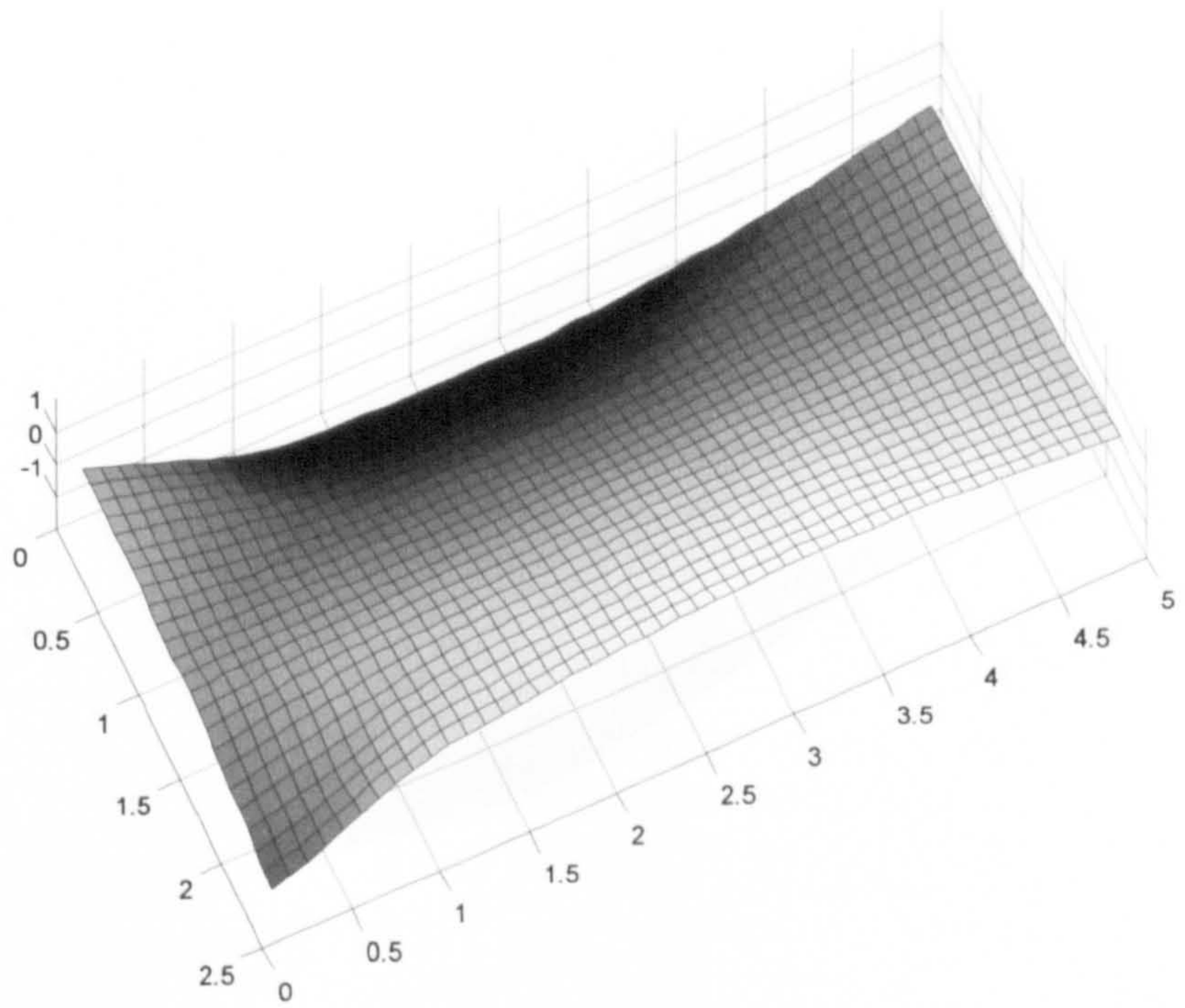

Figure 5-52: Typical mode shape for mode 2

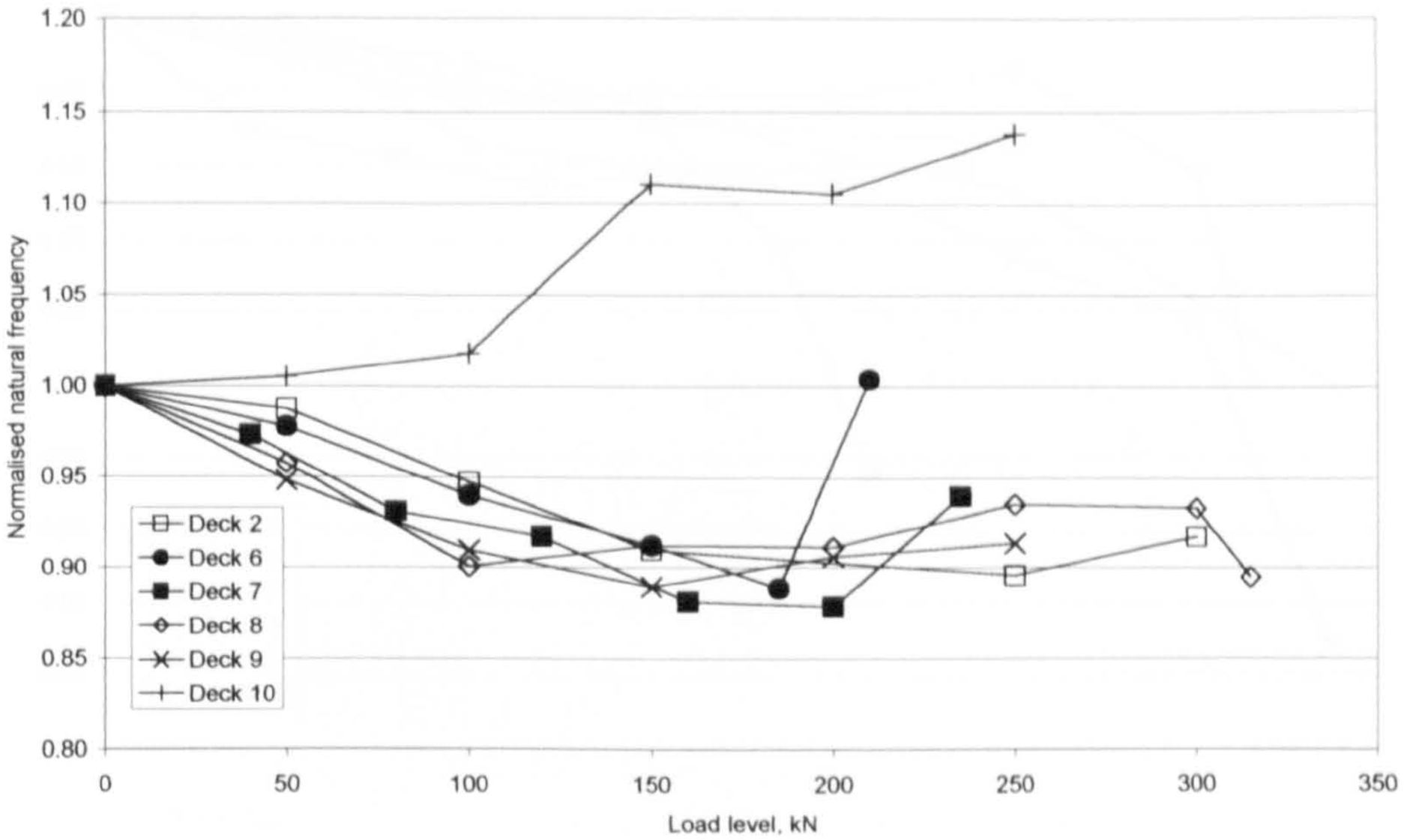

Figure 5-53: Average change in normalised natural frequency of mode 5 for all decks supported on ten bearings

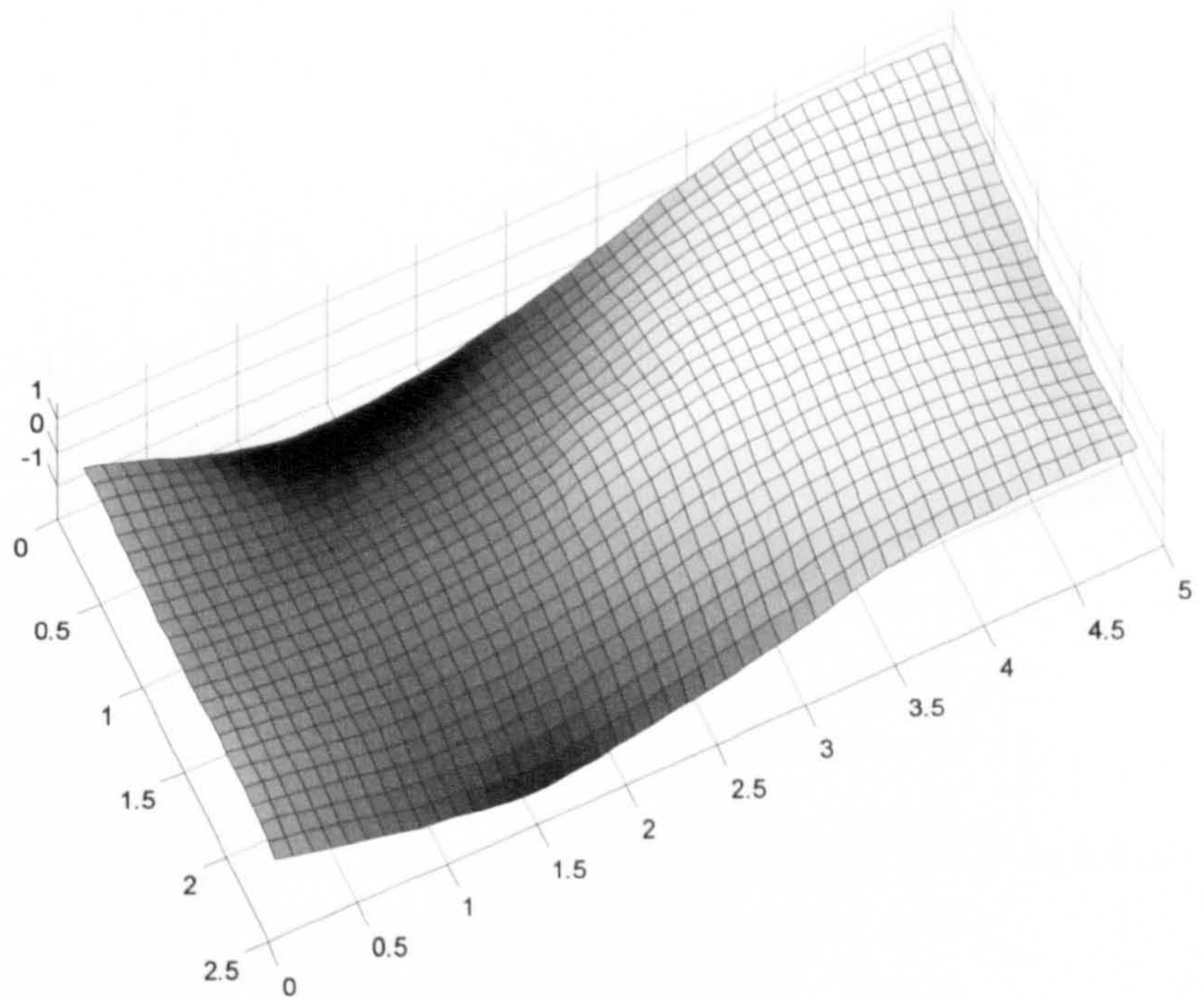

Figure 5-54: Typical mode shape for mode 5

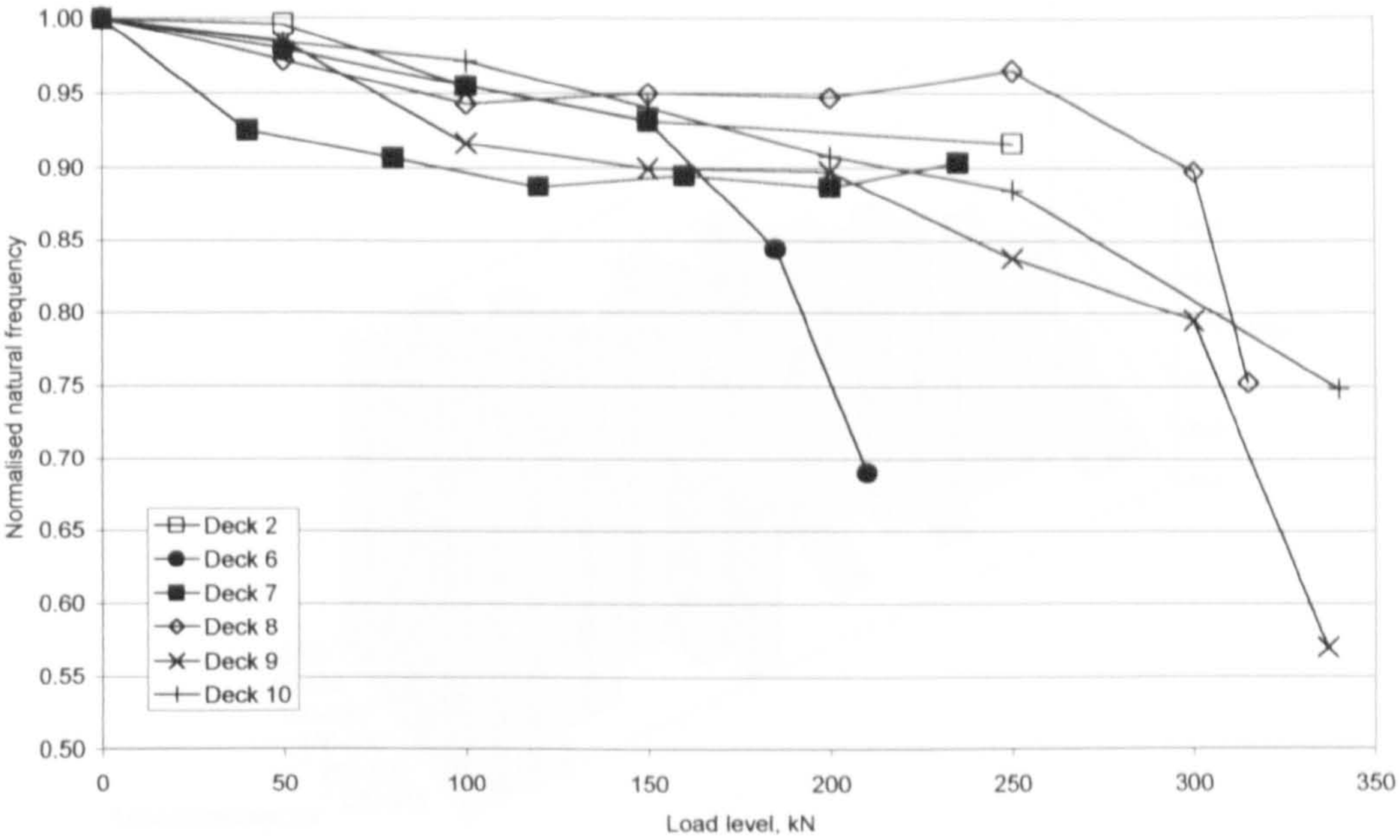

Figure 5-55: Average change in normalised natural frequency of mode 8 for all decks supported on ten bearings

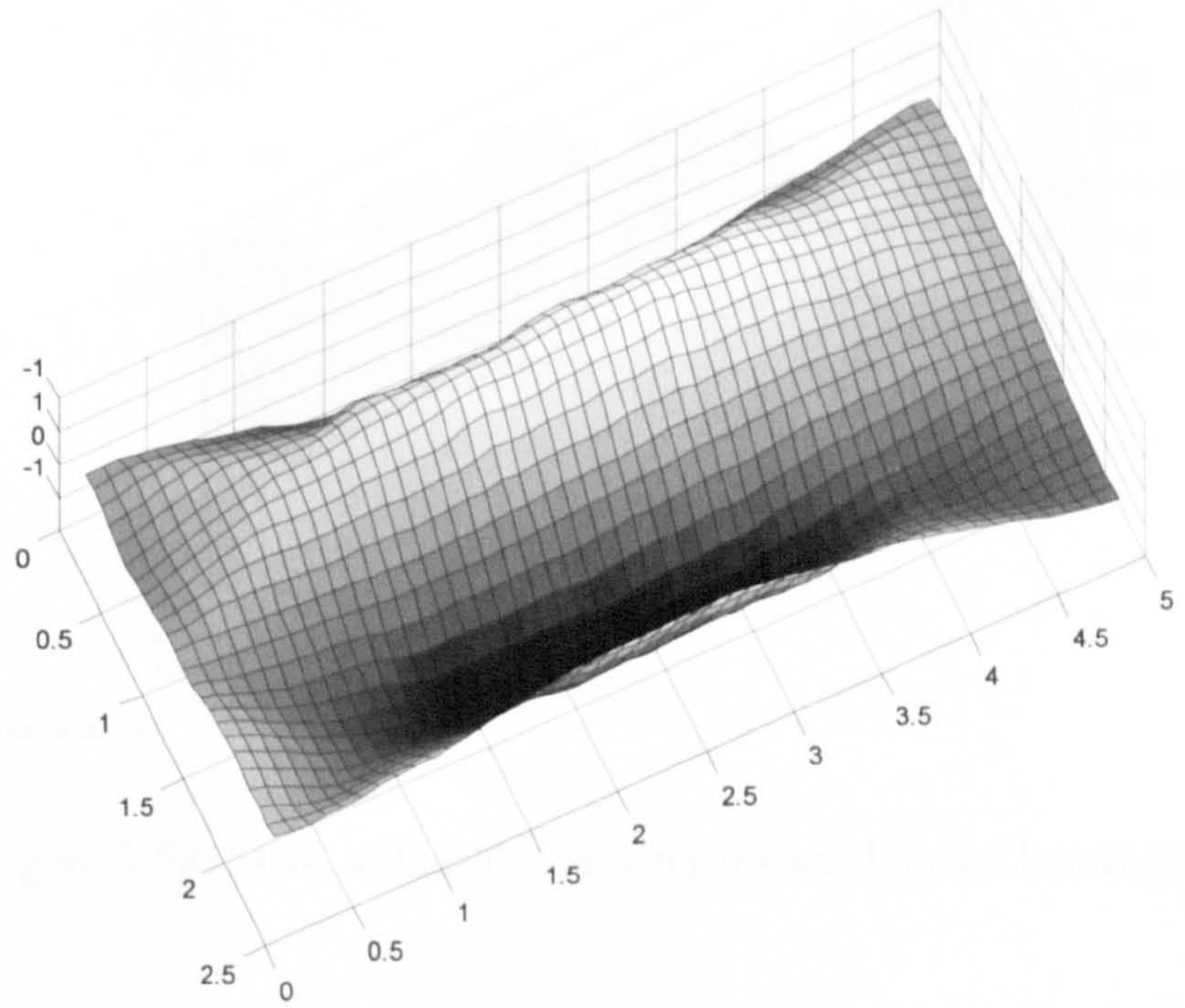

Figure 5-56: Typical mode shape for mode 8

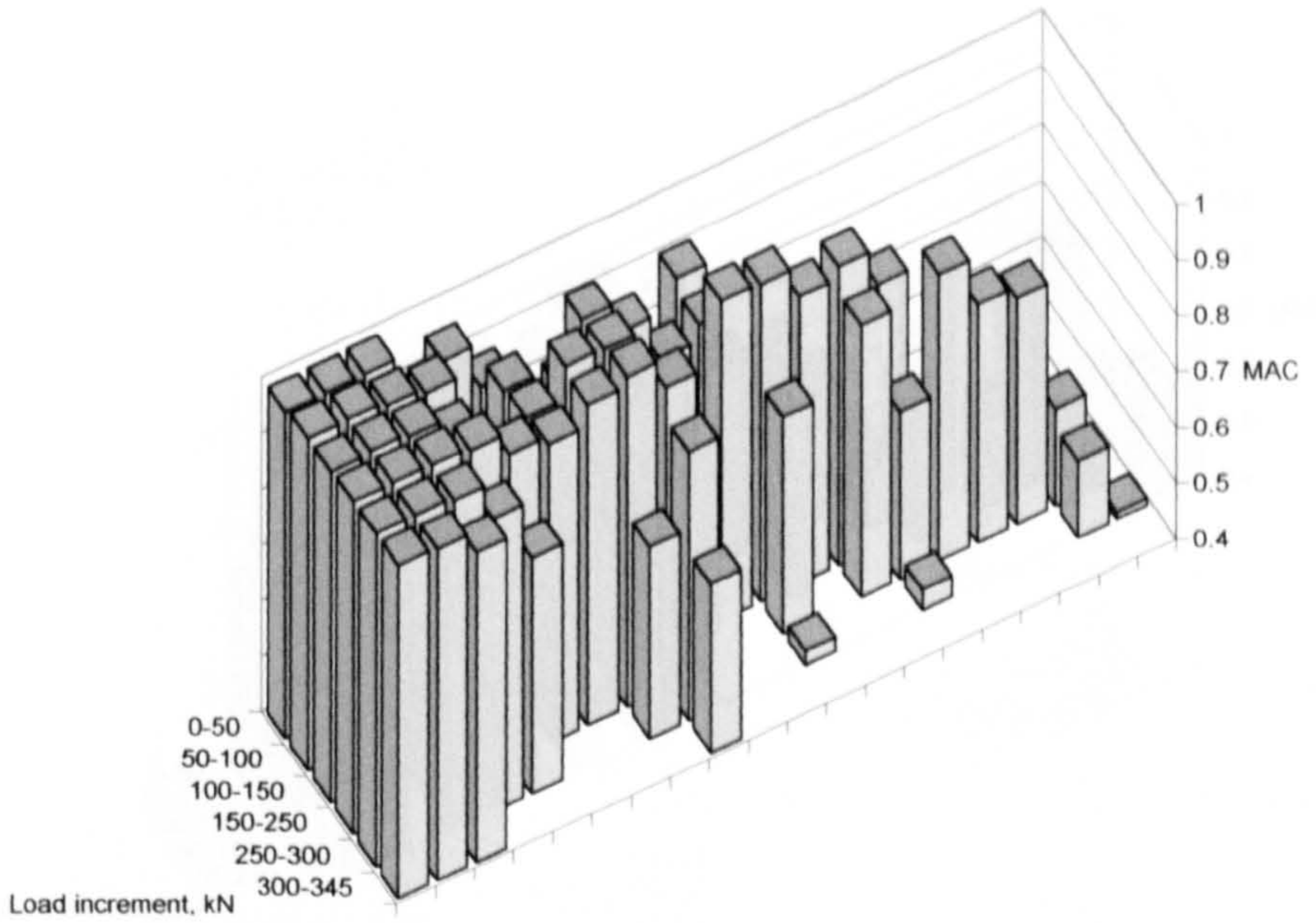

Figure 5-57: MAC values for deck 2

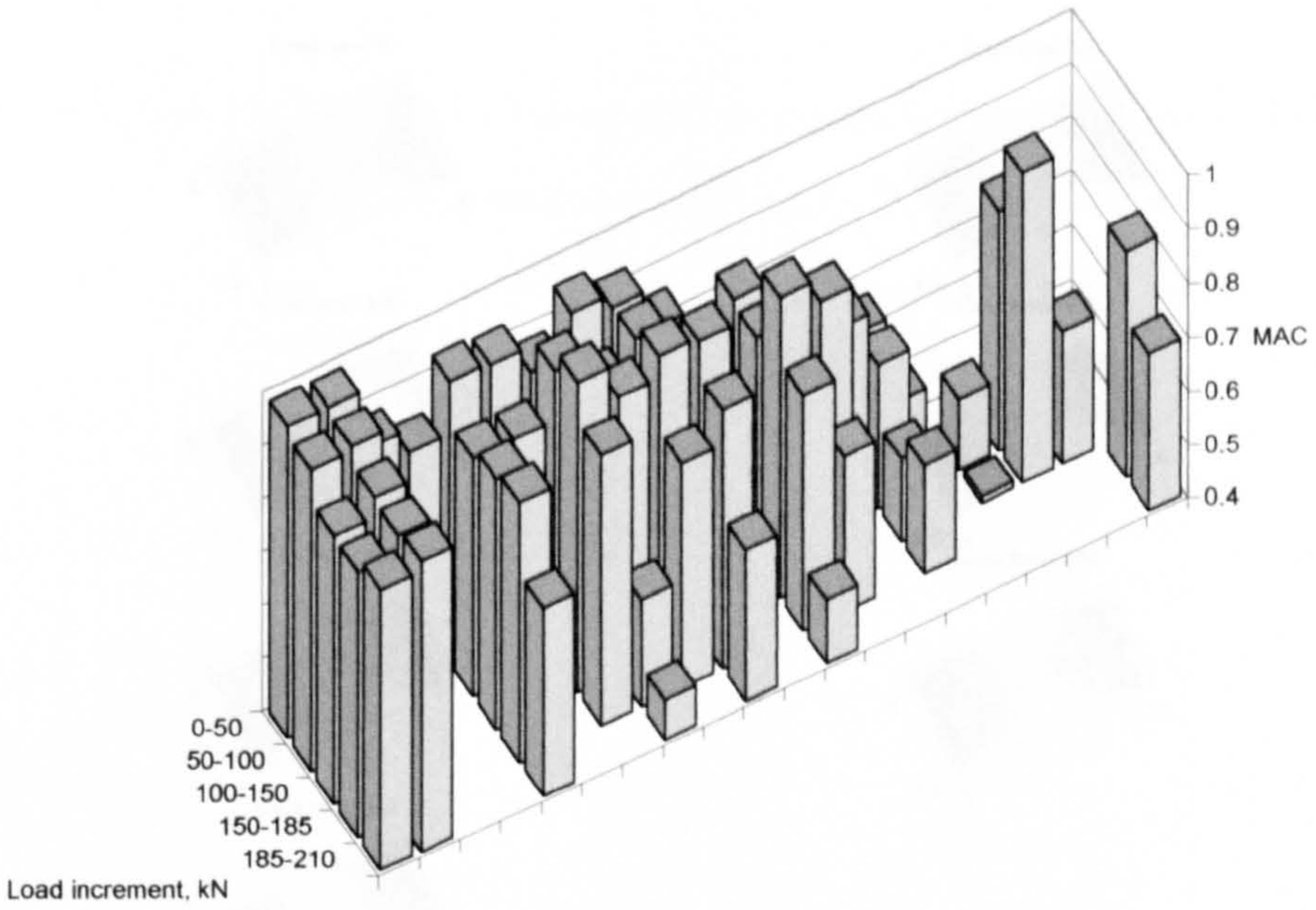

Figure 5-58: MAC values for deck 6 supported on ten bearings

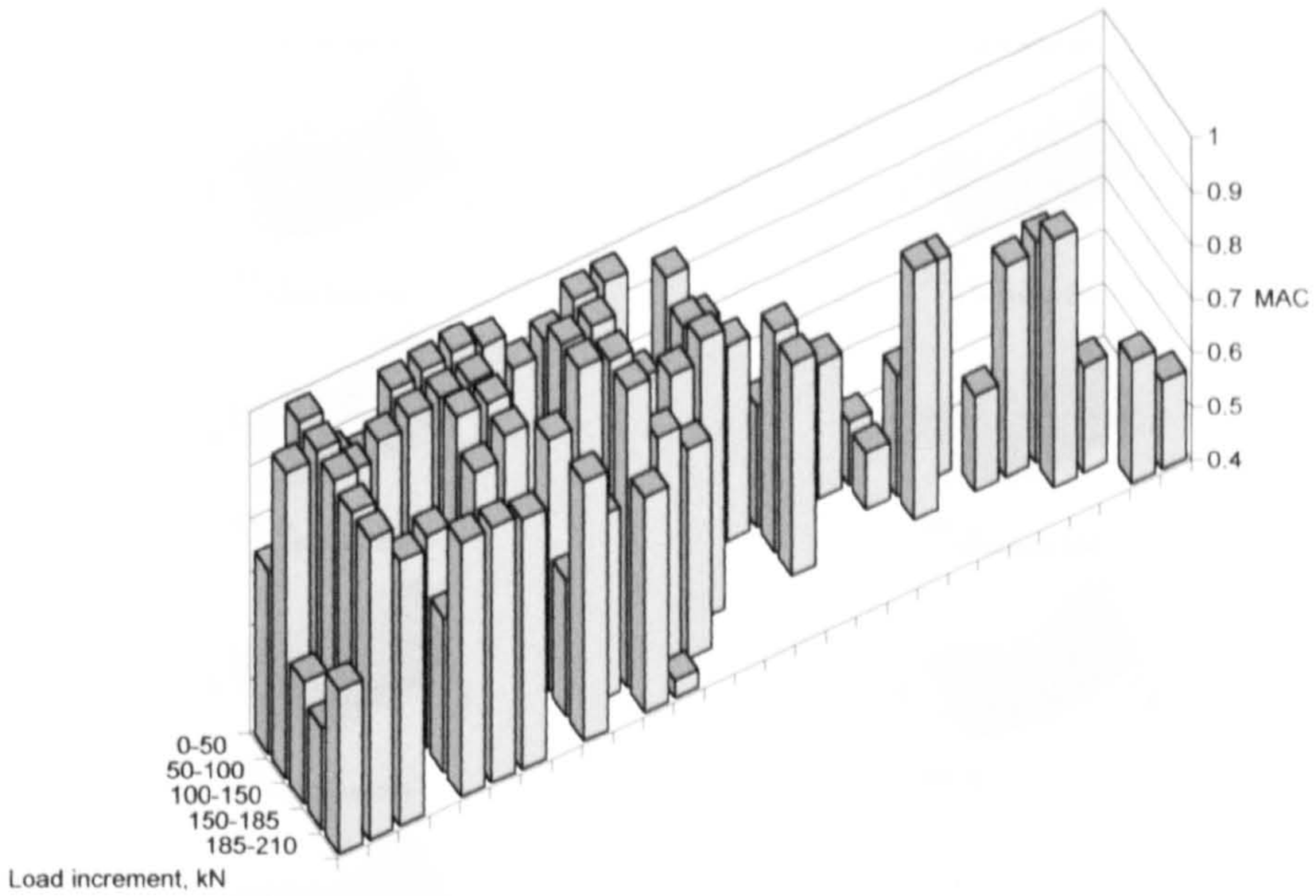

Figure 5-59: MAC values for deck 6 supported on three bearings

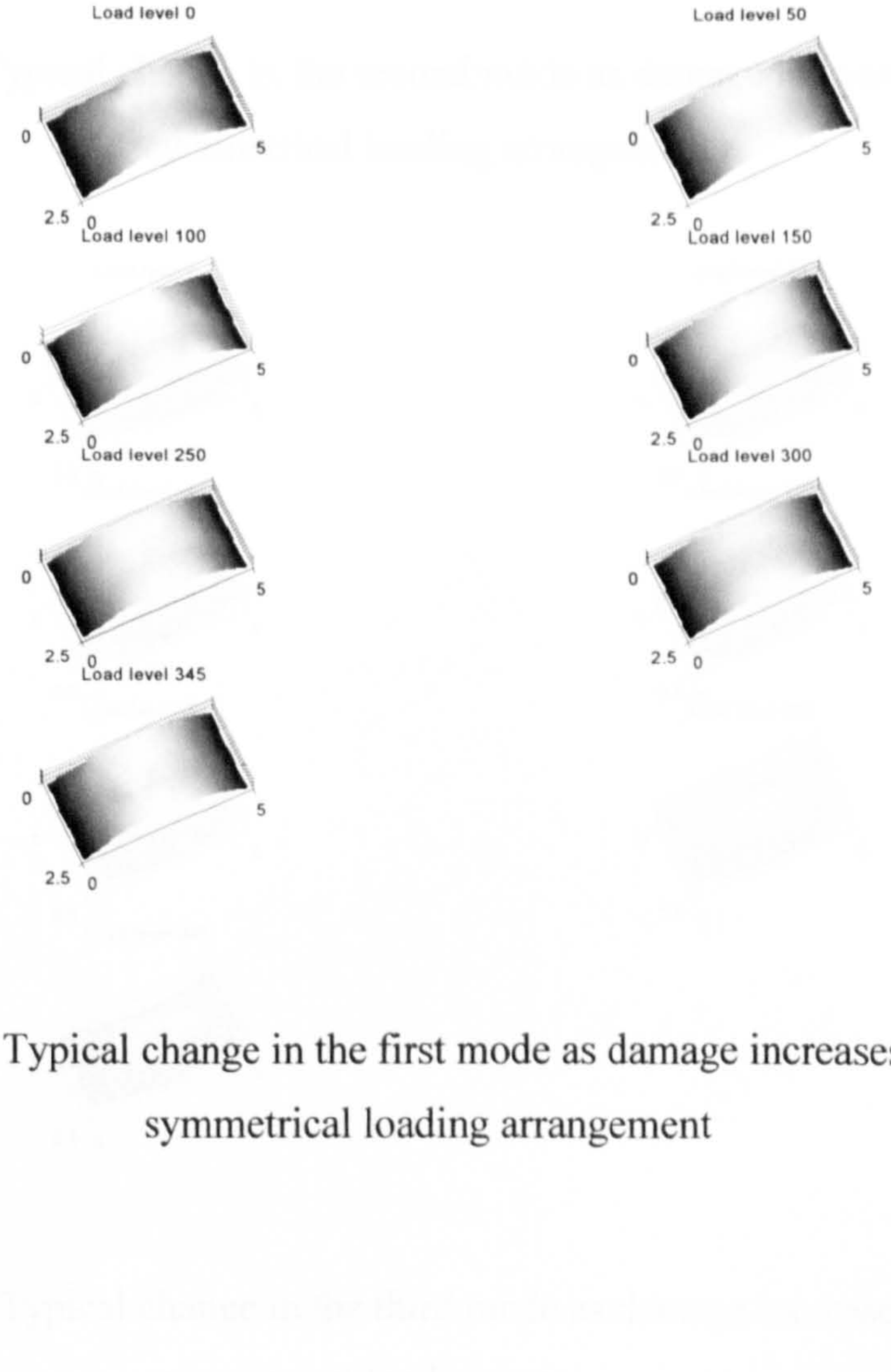

Figure 5-60: Typical change in the first mode as damage increases under the symmetrical loading arrangement

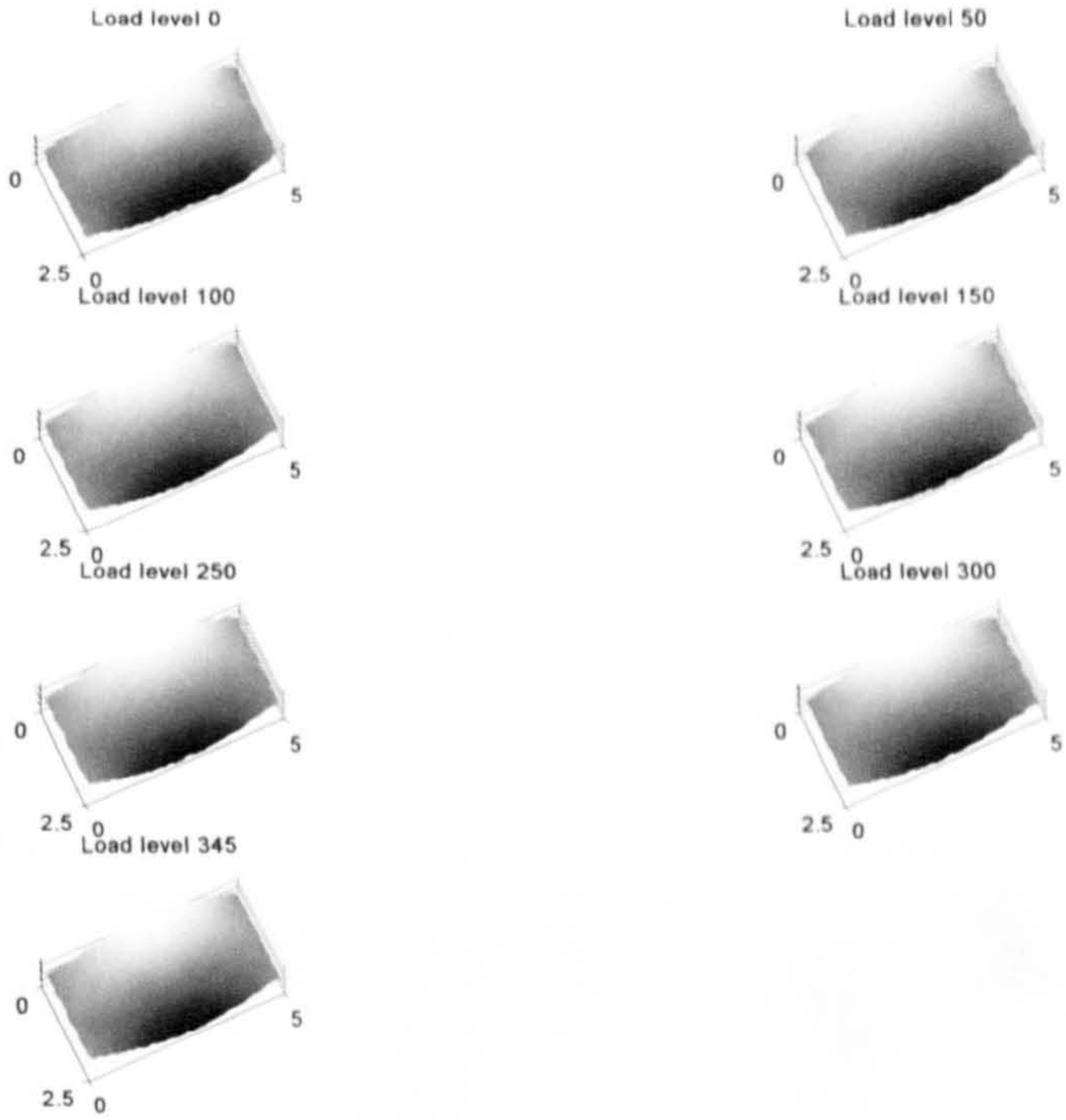

Figure 5-61: Typical change in the second mode as damage increases under the symmetrical loading arrangement

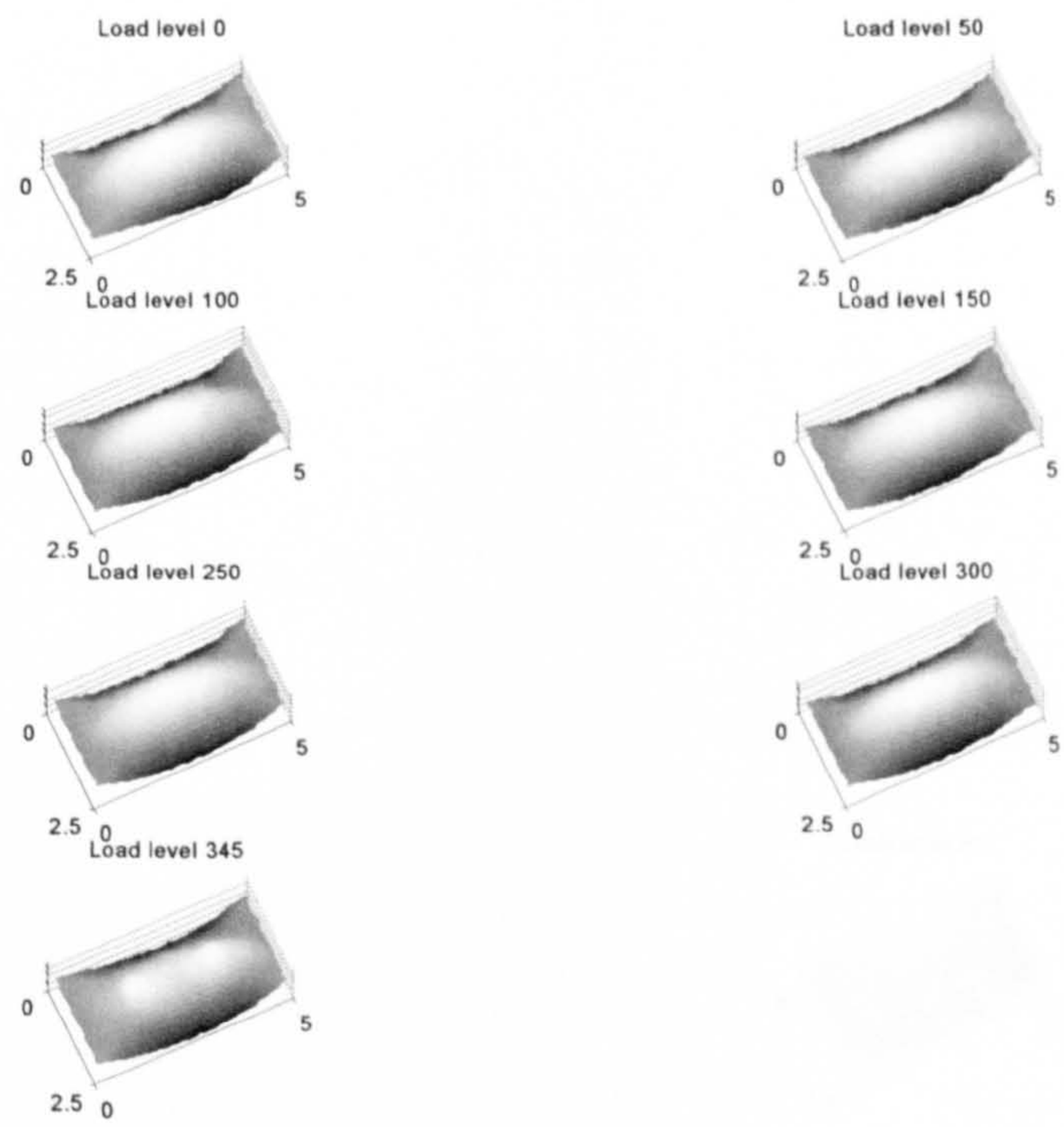

Figure 5-62: Typical change in the third mode as damage increases under the symmetrical loading arrangement

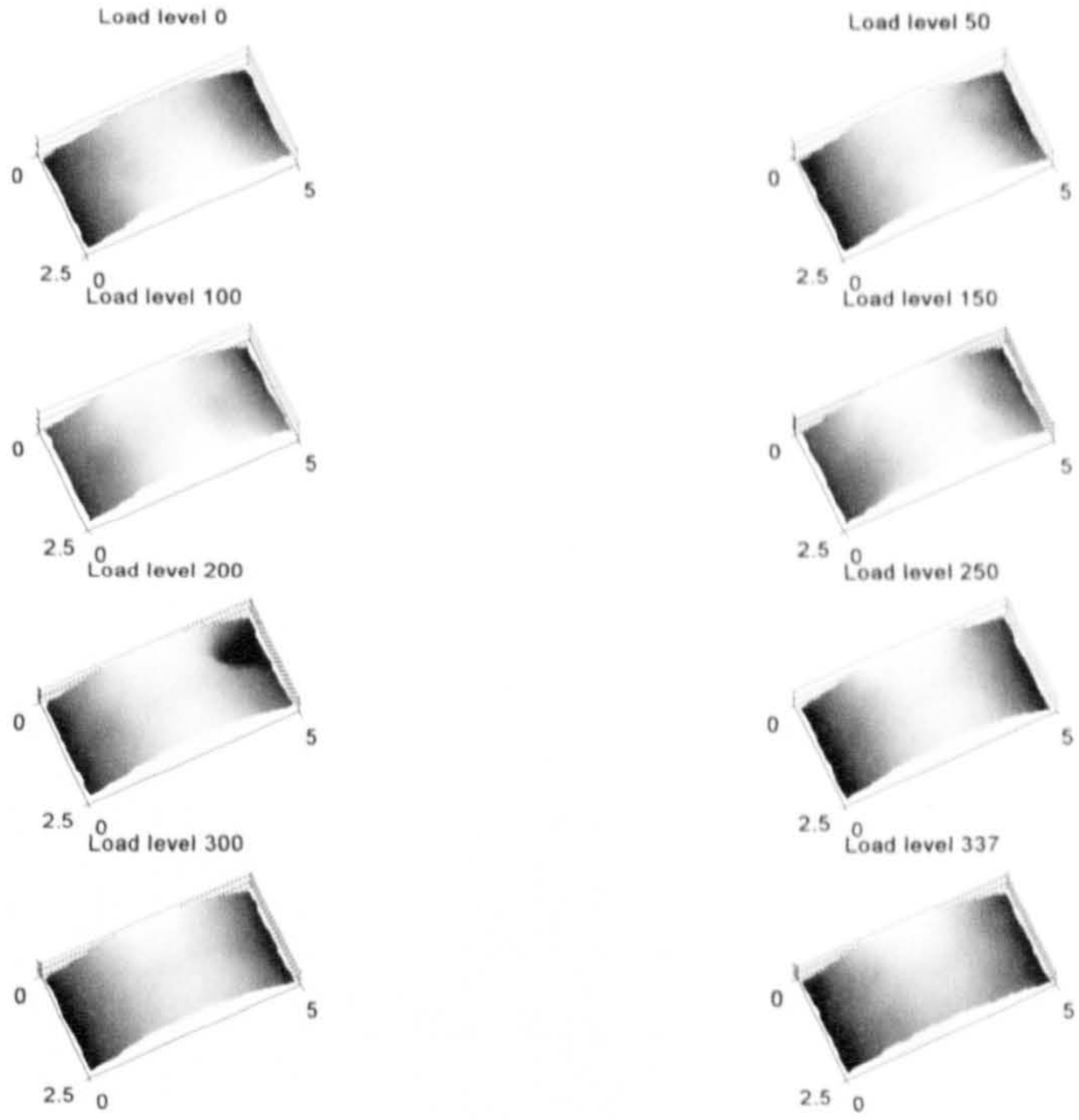

Figure 5-63: Typical change in the first mode as damage increases under the HB loading arrangement

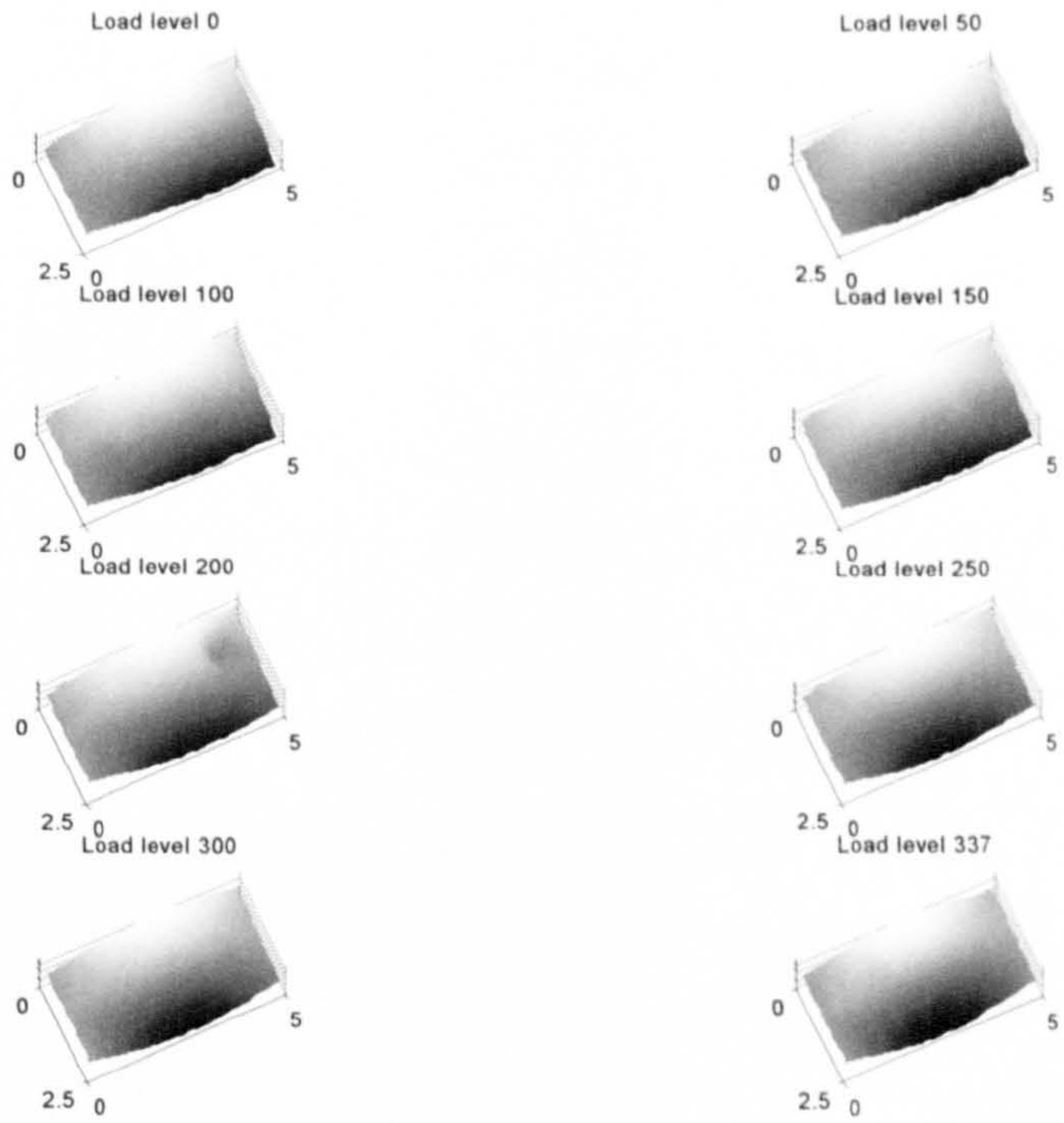

Figure 5-64: Typical change in the second mode as damage increases under the HB loading arrangement

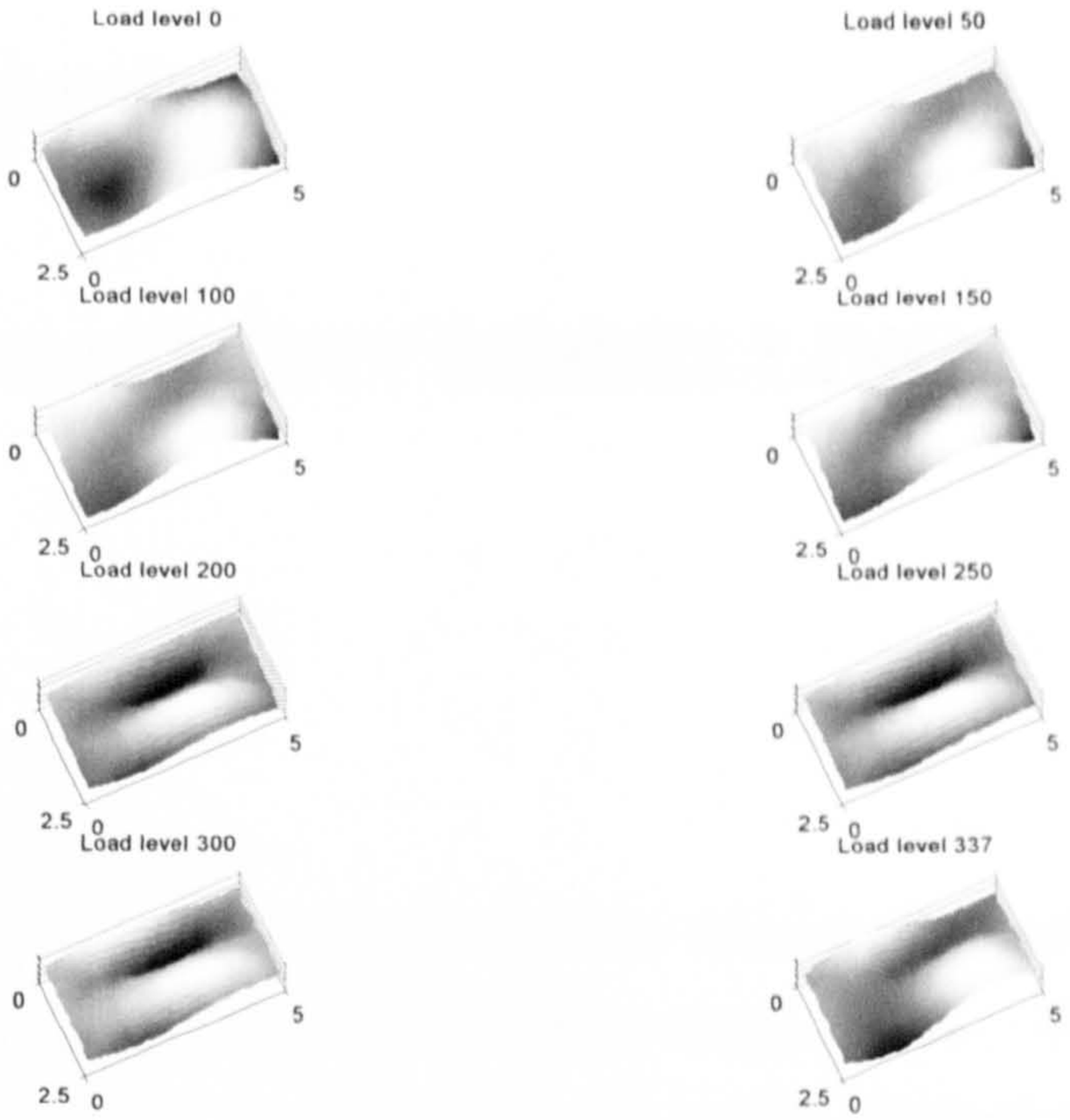

Figure 5-65: Typical change in the sixth mode shape as damage increases under the HB loading arrangement

CHAPTER 6

FINITE ELEMENT MODELLING

6.1 Introduction

This chapter contains the application of finite element (FE) model updating to two one-quarter-scale reinforced concrete bridge decks. The decks are modelled to perform comparisons with the results obtained experimentally from the dynamic testing. Details of the specimen design and test selection can be found in Chapter 3, whilst a discussion of the results of the static testing of these specimens is given in Chapter 4. Chapter 5 details the dynamic testing of these specimens and the investigation of modal properties.

An outline of FE modelling and the model updating technique are given, concentrating on the sensitivity-based approach and procedure. The application of this method is then described and two FE models updated to correlate analytical and measured natural frequencies. The method is used to determine the change of Young's modulus due to cracking that developed under static overloading for a symmetrical and a Highways Agency HB loading arrangement. The values determined by the FE models are discussed and compared with the observed behaviour of the decks.

6.2 Finite element modelling

FE modelling is a popular method used to analyse complex systems that would otherwise require considerable simplifications and assumptions to be made. The basis of FE modelling is that the system is split into a mesh of finite sized elements whose behaviour is assumed to be given by applying mathematical expressions. Within each element, the variation of displacement is assumed from simple polynomial shape functions and nodal displacements. Equations

for the strains and stresses are developed in terms of the unknown nodal displacements, allowing the equations of equilibrium to be assembled in matrix form and solved easily by computer. After the application of boundary conditions, the nodal displacements are given by the solution of the matrix stiffness equation. This then allows the element stresses and strains to be calculated based on the nodal displacements.

An important part of any experimental test is a comparison with expected results obtained from some form of numerical or analytical model. For complex problems, where the development of theoretical models is not possible, it is common to construct a FE model, which provides the required analytical solution.

In many civil engineering applications, FE models are used to predict the behaviour of structures when subjected to various loading and displacements that would otherwise be difficult to determine. It should be noted, however, as with any model it is necessary to perform some verification of the model before the results can be used with confidence. Once one model has been verified, small modifications can be made without the need for further experimental work to be carried out, allowing a great saving in time and cost.

The use of dynamic properties in the verification of FE models became popular due to the global nature of the vibration characteristics, effectively allowing the whole model to be verified based on a small number of tests, offering significant advantages over using static testing. The process of obtaining the dynamic properties from a FE model involves extraction of the eigenvalues of the system. This is achieved by, after describing the variation of displacement within each element, calculating the kinetic and potential energy of the structure to find the natural frequencies (eigenvalues) and mode shapes (eigenvectors) through solving an eigenvalue problem in terms of mass and stiffness matrices. A large number of methods can be used to find the eigenvalues and eigenvectors, such as the power, subspace and Lanczos methods.

Due to the effectiveness of dynamic testing and the increased use of FE models, it is common to determine the material and geometric properties of the

structure in a process known as FE model updating using the dynamic behaviour of the structure, discussed in more detail in section 6.4.

FE model updating using dynamic properties offers several advantages over other methods. The dynamic properties of a structure are global properties, allowing the behaviour of the whole structure to be investigated from a small set of results, and permitting only a relatively small number of measurement locations to be made. The use of vibration properties also dispenses with the need to perform destructive testing in order to determine the material properties of the structure, due to the relationship between the dynamic properties and the mass and stiffness of the system.

In this study, a FE model was constructed and updated based on the dynamic properties to determine the material properties of the decks tested in the laboratory. The aim of the FE modelling is to construct a model to represent the decks at each of the load levels to investigate the changes in the material properties due to the damage introduced by overloading by correlating the natural frequencies obtained.

The updating procedure was applied only to decks 8 and 9, as these were loaded using symmetric "4-point bending" and asymmetric HB loading, respectively. This should give an indication of whether the damage location can 1) be modelled by looking at the damage to the actual deck successfully in the FE model and 2) affect the natural frequencies in the same manner as the observed trends.

6.3 Construction of the finite element model

The FE model of the deck was constructed using "ANSYS" software, and was based on the dimensions given in the drawings. The model was created using brick elements (ANSYS element reference: 8-noded solid 42) to model the whole deck and no attempt was made to model the steel reinforcement separately as it was assumed that it would not cause a significant change in the model behaviour. The material properties were defined as linear isotropic parameters.

A modal analysis was performed to identify the first 30 modes covering the range 0 to 300Hz to match those extracted from the experimental testing using the subspace method. The mode shapes were defined at the same locations as the measurement points in the vertical direction only. This meant that there was no mode shape expansion of experimental modes and the magnitude of the mode shapes were compared using only those values obtained from the laboratory testing.

Of particular concern was the fineness of the FE model and a simple sensitivity analysis was performed on the number of elements used to obtain a model that was sufficiently accurate but did not take a long time to solve. This analysis was limited by the constraint that the number of elements across the width of all beams should be the same, and had to contain a node at the centre. If this was not the case, the natural frequencies and mode shapes were distorted for modes that involved transverse bending. Therefore, it was only possible to try certain numbers of elements (also constrained by limitations on the number of elements and nodes allowed in this version of Ansys) that satisfied this constraint. The results obtained for each model created were plotted against the first 30 natural frequencies normalised with respect to the finest model, and are given in Figure 6-1, together with the average error in Figure 6-2. The coarsest mesh that still gave reasonable answers for the natural frequencies was selected, and consisted of three elements across the width of the beams and five in the height of the deck, as shown in Figure 6-3. This gave a total number of elements of 3270, which gives an average error of approximately 1% in the natural frequencies of the first thirty modes. This also meant that the slab portion of the deck was composed from only one element depth, although a simple sensitivity analysis on a cantilever showed that the difference in the results obtained was negligible. Therefore, it was decided to model the slab part using one element depth in order to not slow down the solution time.

6.4 Finite element model updating

There exist many ways in which to correlate a FE model with measured data. Early techniques were based on updating the mass and stiffness matrices of the model to reproduce the measured data by changing the stiffness or mass matrix

as little as possible. However, there exists a number of problems with these methods, such as no guarantee that the resulting matrices will be positive definite, or that forcing a model to exactly match experimental results does not allow for errors in the data. Mode shape expansion further increases the errors, as the data will not be available at all the degrees-of-freedom present in the model.

A further limitation of these methods is in the situation where only a small number of the sites are damaged, requiring only a small number of the matrix elements to change. However, in general, due to the minimum norm optimisation in the updating method, all the matrix elements are to be changed by a small amount rather than a few elements changed significantly. This does not allow the location of the damage to be identified. The methods seeking to update the whole mass or stiffness matrices have significant disadvantages and it is unlikely that they will be useful in the majority of structural health monitoring applications (Friswell and Penny, 1997).

The most common methods used in model updating are based on a parametric model of the structure. The updating procedure minimises the residuals based on the modal properties, or the error in the frequency domain.

It is usual in these methods to reduce the number of parameters to be updated to only those that are thought to be in error. It is, however, possible that a large number of potential parameters may be generated, which would likely lead to these parameters not being identified to obtain a unique solution, in which case regularisation would need to be applied. Regularisation generally applies extra constraints to the parameters estimation problem to ensure a unique solution, such as applying weighting to the parameter changes.

This leads to the problem known as forward identification, which is essentially that of damage location. The major difference between this and model updating is that only a limited number of parameters are likely to be in error in damage location. If only these parameters are chosen for updating, then the problem is over determined and solvable in a least-squares manner. When considering damage location for a real structure, it is unusual that these parameters will be known, and therefore they must be determined.

It is often assumed that only a limited number of sites will be damaged, and the model can be updated based on this reduced set of parameters. This process may be repeated for several combinations of damage site, and the results from the model that best compares with the data selected (Cawley and Adams, 1979; Wang, 2001). The major problem with these methods is that a number of model updating runs have to be performed before it can be assumed that the best, or at least satisfactory, model has been found.

A number of other techniques have been suggested as alternatives to FE model updating, such as genetic algorithms and neural networks.

The use of genetic algorithms may be useful in some circumstances, although they do not address the cause of the problem i.e. that the important decision is what to optimise, not how to optimise it. These methods are good at finding a global minimum in difficult optimisation problems, which may be useful in damage location. However, they still require the dynamic properties of the structure to change sufficiently and in a predictable manner for the solution to be meaningful.

Neural networks possess the ability to treat damage mechanisms implicitly, and it is therefore not required to model the structure in such great detail. These methods are also capable of dealing with non-linear behaviour easily. However, the major problem with these methods is that a large amount of data is required for the training of the neural network before it can be used, and that this training data contains the essential features of the damaged structure to which it applied.

6.4.1 Sensitivity based model updating

The model updating procedure can be classified according to the modification of the system matrices. Iterative (local) methods are based on corrections to the local physical parameters of the FE model, and therefore the resulting model has physical significance. One-step (global) procedures directly reconstruct the updated global mass and stiffness matrices from the reference data and do not possess physical meaning.

Some of the most effective and popular FE model updating methods are based on sensitivity analysis. In this formulation, the experimental results, such as natural frequencies or mode shapes, are expressed as functions of the analytical responses, structural parameters and a sensitivity matrix, in terms of a first-order Taylor series:

$$\{R_e\} = \{R_a\} + [S](\{P_u\} - \{P_o\}) \qquad \text{Equation 6-1}$$

or

$$\{\Delta R\} = [S]\{\Delta P\} \qquad \text{Equation 6-2}$$

where $\{\Delta R\} = \{R_e\} - \{R_a\}$, $\{R_e\}$ and $\{R_a\}$ are the experimental and analytical response values, respectively, $\{\Delta P\} = \{P_u\} - \{P_o\}$, $\{P_u\}$ and $\{P_o\}$ are vectors of the updated and current parameter values, respectively, and $[S]$ is the sensitivity matrix. For all selected responses, the sensitivity matrix can be computed by;

$$[S]_{ij} = \frac{\partial R_i}{\partial P_j} \qquad \text{Equation 6-3}$$

where R_i and P_j represent a structural response and parameter, respectively. The subscript $i = 1,\ldots,N$ for N responses and $j = 1,\ldots,M$ for M parameters. The matrix may be computed using direct derivation or perturbation techniques. If different types of parameters are to be used, such as material, geometrical or boundary properties, then equation 6-3 should be multiplied by the relevant parameter to obtain the absolute sensitivity. It is also possible to normalise the absolute sensitivity with respect to the response value by pre-multiplying by the inverse of the relevant structural response. This gives a normalised sensitivity matrix, defined as;

$$[S_n]_{ij} = [R_i]^{-1}\left[\frac{\partial R_i}{\partial P_j}\right][P_j] \qquad \text{Equation 6-4}$$

The solution to equation 6-3 may be determined, over- or under-determined, depending on whether N is equal to, greater than or less than M. The parameter change may be solved using the pseudo-inverse technique;

$$\{\Delta P\} = [S]^{+}\{\Delta R\} \qquad \text{Equation 6-5}$$

where $[S]^{+}$ is the pseudo-inverse matrix of the sensitivity matrix, given by;

$$[S]^{+} = \begin{cases} [S]^{-1} & \text{for } N = M, \\ \left([S]^{T}[S]\right)^{-1}[S]^{T} & \text{for } N > M, \\ [S]^{T}\left([S][S]^{T}\right)^{-1} & \text{for } N < M. \end{cases} \qquad \text{Equation 6-6}$$

The pseudo-inverse may be found using Bayesian estimation or singular-value decomposition techniques.

Due to the fact that the Taylor series is truncated after the first term, the neglected higher-order terms necessitate several iterations, especially when $\{\Delta R\}$ contains large values. It is also important to note that when too large a discrepancy exists between the experimental and analytical models, the Taylor series truncation is no longer valid and the iterative process is prone to divergence. The practical consequence of this is that the initial FE model prior to any updating should be relatively close to the measured behaviour.

The formulation of a FE model to be used in an updating procedure requires consideration of some additional factors not normally taken into account when constructing a FE model. The aim of model updating is the modification of uncertainties or inaccuracies in the structure, which must be expressed in terms of parameters that can be assessed qualitatively. It is therefore vital that the

discrepancies between the FE model and the actual structure are included in the model as quantitative parameters as far as possible.

It is usually the case that damage reduces the structure geometrically and/or physically. This reduction can be represented in the FE model by incorporating 'weak' elements at specific locations, although the determination of the parameters and locations of these elements is subjective, relying on the damage condition. As long as these parameters are updated, then the values will represent the extent of the damage.

A major problem encountered in FE modelling is the selection of the boundary conditions. This can be overcome by simulating the boundary conditions using springs, where their elastic stiffness after updating will approximate the real boundary conditions (Brownjohn et al, 2001). This is of particular concern in civil engineering applications as the boundary conditions are often unknown and more complex than in other disciplines.

6.4.2 Updating procedure

Model updating normally consists of three steps. Firstly, the responses, natural frequencies, mode shapes etc. to be used to correlate the FE model with the experimental data need to be selected. Second, the parameters to be updated need to be selected. These must be sufficiently sensitive to the selected responses. Thirdly, the model is updated in an iterative process to modify the parameters selected based on the response data.

The selection of the parameters to be updated is critical to the success of the FE model updating procedure and which parameters to update is made based on the physical properties of the structure, as they must be uncertain in the model. If it is attempted to update too many parameters, the problem may appear to be ill-conditioned or under-determined due to the limited number of observations made in the vibration testing. To obtain a well-conditioned problem, the number of parameters to be updated should be kept small and cover most of the uncertainty within the model.

Due to problems with finding a satisfactory solution when the initial parameter estimates are not relatively close to the actual values, it is common to perform

some manual updating. This manual updating, or 'macro-updating', is used to provide a suitable starting point for the "automated" updating to proceed. This is usually achieved by the use of engineering judgement or some preliminary estimation.

The object of model updating based on parameters is to obtain a physically meaningful solution for the structure. This may require upper and lower bounds to be imposed on the parameters that are being updated to prevent physically implausible values being obtained. However, it is possible that when these constraints are applied, the model cannot converge, and it is therefore necessary to compromise between the required accuracy of the model and its physical significance.

The main limitations when using FE model updating are due to the ability of the FE model to accurately represent the true behaviour of the structure, and to identify enough modal properties with the required precision. Manual tuning involves not only a manipulation of the updating parameters, but also judgement regarding the level of detail and assumptions made in the FE model. When comparing the results with those obtained from experimental modal analysis, it must be remembered that the field conditions will limit the accuracy and resolution (spatially or temporally) of the measurements and statistical uncertainties will propagate through to the final updated parameter estimates.

6.5 Preliminary model updating

The FE model updating is based on a sensitivity approach. This involves determining the sensitivities of the values to be updated due to changes in each parameter in the FE model. In this study, the FE model is to be updated to correlate the natural frequencies only by making changes to the stiffness of the elements. No attempt to correlate the mode shapes was made other than using the MAC to determine which modes from the FE model and experimental testing should be compared in terms of the natural frequencies. The updating was based on the natural frequencies only for two main reasons. Firstly, in order to correlate the mode shapes, it would be necessary to introduce a large number of parameters to be updated as there needs to be a spatial variation around the deck. It would not be possible to update all these parameters based

on a limited number of mode shapes in a least squares manner and obtain satisfactory solutions. Secondly, it is typical that the amplitude of the mode shapes of a lightly damped mechanical structure can be in error by as much as 10% (Friswell & Mottershead, 1995), whereas the natural frequencies are expected to be in error by 0.1%. This situation is likely to be even worse for civil engineering structures, where materials are unlikely to be homogeneous and the properties uniform. It is common practise to not explicitly update FE models based on mode shape magnitudes as well as natural frequencies.

As stated above, the model updating used the sensitivity approach. In this investigation, the sensitivities were obtained by introducing a small perturbation in the parameters to be updated, rather than composing an analytical expression. This was achieved by solving the model with each parameter decreased by 5% in turn as the effects of changing the parameters are assumed to be constant over the parameter-space when changed by only a small amount.

The sensitivities were found by comparing each FE model with the original as the changes in the parameters could cause some modes to change order. The sensitivities were calculated by obtaining the difference in the modal natural frequency divided by change in parameter. The updating routine used involved a least squares approach that required both the sensitivity to the change in natural frequencies and to the square of the frequencies. It is important that the sensitivities are normalised to give all modes equal weighting, as this ensures that the higher modes do not dominate the least squares solution.

The initial model was created to model the deck in its initial state as received in the laboratory. As described in Chapter 4, the deck displayed a small amount of cracking due to self-weight and shrinkage prior to being loaded statically. In an attempt to model this damage, the deck was divided into regions and each assigned a separate material property, which would then be updated in terms of the Young's modulus, in the areas where the cracking was observed.

The regions created were to describe the stiffness of the slab and the cracking in the bottom of the beams. It was not possible to observe any differences in the material condition to enable other updating parameters to be selected that

would improve the mode shape match. It may be useful to use the COMAC values to identify which locations were consistently in error and assign a different material property in this region. However, due to the number of modes actually matching with the FE model, the number of parameters that could be updated successfully using a least squares approach was three or four. The problem of a large number of parameters could be solved by using a multi-stage process, but this would introduce more errors as the order in which the parameters were updated would affect the values produced and also require a lot of updating runs to be performed to ensure that the optimum solution for all parameters has been found. However, as stated above, the measured mode shapes could be expected to contain an error in the amplitude of 10%, so the inclusion of parameters based on the mode shapes would need to be used carefully.

In the FE model, the top row of elements was designated as the slab stiffness based on a Young's modulus (E_s), the bottom row of elements defined as the cracked beam stiffness (E_b) and the remainder as uncracked concrete with stiffness E. The density of the material was assumed to be constant, and assigned a value of 2430kg/m^3, based on the average of the cube test results from the decks performed by the manufacturers, and Poison's ratio taken as 0.2.

6.5.1 Boundary conditions

Due to the decks being supported on a total of ten bearings, a considerable amount of effort went into modelling the boundary conditions correctly. .For this purpose, several models were created using a number of different boundary conditions. The first assumed that the decks were supported equally on all the bearings and the bearings were rigid by applying zero displacement constraints at the ends of the beams to model the round and half-round bearings used.

The mode shapes obtained from the FE model were compared with the results found experimentally using the MAC comparison. For this model, the MAC values produced indicated that only a small number of modes calculated by FE modelling were correlated with the experimental modes. A visual inspection of the experimental mode shapes revealed that there was significant movement

above the supports, causing many of the mode shapes to produce poor MAC values when compared to the FE model.

6.5.1.1 Linear springs

A second FE model was created using linear springs to model the stiffness of the support material, denoted as k_B. This was calculated based on the transverse stiffness of a cylinder;

$$k = \frac{3\pi r^4 E}{4L^3} \qquad \text{Equation 6-7}$$

where r is the radius of the cylinder, E is the Young's modulus of the material and L is the length of the cylinder. From this, the stiffness was found to be 6.29×10^7N/m, providing an initial value for the spring stiffness. This model was then compared to the experimental results again using a combination of the MAC and a visual inspection of the mode shapes.

This model was updated for a number of decks by changing the parameters E, E_s, E_b and k_B. In this updating, the bearing stiffness, k_B, was assumed to be the same for all the bearings. This model was successful for some decks but not others and, in general, required a two or three step updating procedure, although this often produced a negative value for one of the parameters. This was particularly true for the bearing stiffness parameter, and this could often not be updated.

A comparison between the updated frequencies and the experimental frequencies showed that modes 1 and 2 were often in error by greater than 10%, even when the model had been updated several times and all other modes were within 5% of the experimental values, as shown in Figure 6-4. Mode 1 is the first bending mode of the deck; mode 2 is the first torsion mode. It was thought that the second mode could not accurately be modelled using these bearing conditions, as it involved a considerable amount of differential movement of the supports.

6.5.1.2 Constraint equations

The ideal method to model the boundary conditions would be to allow each linear spring representing one support to vary independently of the others. However, this would create a highly non-linear problem, and could not be solved using the sensitivity based model updating, as the effects of changing the bearing stiffness at either end of the deck would have the same effect.

It was therefore decided to create a third model to incorporate the movement of the supports in the second mode. This was modelled by introducing a torsional spring into the model. As before, the vertical bearing stiffness was modelled using a linear spring with stiffness k_B. However unlike the previous attempt, this is the total stiffness of the bearings at each end of the deck. A parameter k_T is introduced to represent the torsional stiffness of the bearings, in the form of a torsional spring. Several constraint equations were used in Ansys to link the displacements and rotation of the deck to these linear and torsional springs, as shown in Figure 6-5. The first type of constraint was that the average displacement of the nodes at the bearing locations should be the same as that of the linear spring. The second equation stated that the rotation at the bearing locations is the same as that of the torsional spring. The same longitudinal and torsional spring stiffness was used for both ends of the deck.

Due to unsatisfactory results when updating all the parameters at the same time, the updating was performed in a multi-stage process. Firstly, the bearing parameters (k_B, k_T) were updated once, then the cracked concrete and slab Young's modulus (E_b, E_s) and then the concrete Young's modulus (E). This process was repeated until most of the FE model natural frequencies were within 5% of the experimental frequencies. However, after several updating runs, it was noticed that updating the bearing parameters only affected the first two modes significantly, whilst updating the concrete parameters made little change to the first two modes. It was therefore decided to change the updating procedure to take advantage of the apparent independent nature of the first two modes and the parameters to be updated.

6.5.2 Methodology

The procedure used was to again update the parameters in several stages. The first step is to update only the bearing parameters (k_B, k_T) to obtain a good match between the first and second modes measured experimentally and calculated by the FE model. Then, after these natural frequencies were closely matched, the concrete parameters were updated. Again this had to be done in two steps; firstly update the cracked and slab stiffness; then the concrete stiffness.

6.5.3 Considerations

The updating parameters used were all based on the stiffness of the deck assumed in the FE model to be incorrect. In the case of the concrete, the change in stiffness is modelled by reducing the Young's modulus of certain elements. This means that all the error in the dynamic stiffness is concentrated in the Young's modulus values, and there is no reduction of the second moment of area that would correspond to the section being cracked. Therefore, the total reduction in Young's modulus of the concrete is probably due to both a reduction in stiffness and second moment of area.

It is noted that, in some cases, the updated FE model of the undamaged deck still predicts some natural frequencies with an error of almost 5%, whilst the actual natural frequencies at the next load level change by less than 5%. Therefore, it could be questioned as to whether it is possible to update the model for the damaged deck when the change in the measured natural frequencies is smaller than the error between these and the analytical frequencies.

The objective of subsequent FE model updating at other load levels is to match the natural frequencies at this load accurately. However, when the original error is taken into consideration, this becomes more difficult. Due to the error in the initial model, it is debateable whether the FE model at the next load level should be updated based on the absolute values of the natural frequencies. It may be of more use to update the model based on the change in the natural frequencies, so that the frequencies produced by the FE model change by the same percentage as those measured for the deck. This would then make the

5% error in the initial model less significant when updating subsequent load steps. However, it would then be difficult to allow for modes that appear due to the damage, as their frequency change is not known.

Due to the non-linear sensitivity of the natural frequencies to changes in the parameters, the success and speed of the updating procedure depends very much on the initial values of the parameters used in the updating. A change of 5% in each parameter is used to determine the sensitivities of the natural frequencies, and any change larger than this or updating more than one parameter will result in the sensitivities becoming invalid. Therefore, a close estimate is needed for the initial values to enable the model to converge quickly. However, this will only yield a satisfactory solution if the updated parameters have a unique solution and a global minimum of the residual can be found.

6.6 Updating a symmetrically loaded deck

6.6.1 Load 0

The deck to be updated for all load levels was deck 8. The procedure for updating the FE model to correlate with the initial deck is outlined in the following. Firstly the bearing stiffnesses, k_B and k_T, were updated to match the first two modes as closely as possible. These values were updated to the point where the sensitivity was not significant enough to update parameters further, and would require large unrealistic changes to be made. The concrete parameters were then updated as described above. The fully updated model matched the natural frequencies of modes with MAC>0.6 between the FE model and experimental to within 5%, other modes with MAC>0.4 were within 10%. The apparently low MAC values were used as the MAC is not good for comparing the mode shapes produced by the FE model and experiment, as the FE modes are symmetric and the experimental modes were not. Therefore, a small change in the orientation of the mode shape could give an apparently low MAC value, but upon visual inspection be the same mode.

The model was solved using initial values of the parameters of $5\times10^{10}N/m^2$, $3\times10^{10}N/m^2$, $1\times10^{10}N/m^2$ (E, E_s, E_b) and $3.48\times10^{8}N/m$, $3.23\times10^{12}Nm/radian$

(k_B, k_T) based on previous updating runs for a number of the decks and knowledge of the deck condition and cracking. The calculated value of the vertical bearing stiffness gave 3.145×10^8N/m based on the transverse stiffness of a cylinder. Table 6-1 contains the updated parameter values, whilst the areas assigned different material properties are shown in Figure 6-6.

An estimate of the undamaged concrete Young's modulus was 4.2×10^{10}N/m^2 found using a PUNDIT test on the deck specimen. The updated value of the undamaged concrete is 22% higher than the estimated value. The updated model resulted in a significantly lower value for the cracked concrete than the undamaged estimate, reducing by 69%. This is consistent with the cracked concrete at bottom of beam. The 25% lower value of the slab stiffness could be due to a number of reasons, such as incorrect modelling of the thickness. It was noted by inspection of the specimen that there were small variations in the profile of the deck surface, which would lead to some areas being slightly thicker than others. A simple calculation based on equation 2-1 suggests that if the thickness is underestimated by approximately 6.3%, the stiffness will be underestimated by 40%. The changes in the error of the FEM for the matched modes is presented in Figure 6-7.

Comparison of the measured FRFs and those predicted by the updated FEM can be found in Figure 6-8. A visual inspection of this plot reveals that, for a number of modes, the FRFs produce a similar peak. The problem of unmatched modes between the measured and FEM can clearly be seen, as it was not possible to update these natural frequencies, in the discrepancies between the FRFs. It should be noted that the magnitude of the measured and predicted FRFs is similar.

6.6.2 Load 50

The natural frequencies produced by the FE model show very low sensitivity to changes in both the vertical and torsional bearing stiffness. In fact the frequencies obtained for the current bearing stiffnesses are close to those found when using fixed supports. Therefore, it is not possible to update these parameters to match modes 1 and 2 more closely with any confidence due to the large unrealistic changes required.

The majority of damage in the first load level is in the form of an increase in the number and length of the vertical cracks in the beams due to increased bending and are concentrated in the middle 2m of the deck between the loading points. The FE model was modified by changing one layer of elements and the middle 3m of the next layer to simulate the growth in cracks. These modified elements were assigned a separate stiffness, denoted E_{50}. The reduction in stiffness required to match the natural frequencies found at 50kN is to be obtained from the new stiffness, E_{50}, and the cracked concrete stiffness, E_b. A constraint on the cracked concrete stiffness, E_b, is that it cannot rise above the value it was previously updated to in the undamaged case. It is possible to update both parameters together and obtain sensible results. Both parameters converged, and a final update was done on the concrete stiffness. The values obtained from this updating are given in Table 6-1.

The cracked concrete stiffness has changed by a further 25% reduction (now 19% of original E) and E_{50} has reduced by 10% compared to the previous value of E. The final update on the undamaged concrete stiffness caused a reduction of 5.5%. This final update on the concrete stiffness was included to allow for the fact that not all the damage was concentrated in E_b and E_{50}.

The updated FE model does not appear to be as successful as that for the initial deck, as no modes are within 1% of the actual values, and a MAC value of greater than 0.4 was used, so the modes do not match as well as in the previous model, as shown in Figure 6-9. This is to be expected, as the mode shapes will change due to the unsymmetrical nature of the damage and deck, as demonstrated in the undamaged deck updating, although if the damage was modelled correctly the updated decks should produce more matching mode shapes. However, as the damage is modelled as being symmetric, there is little change in the mode shapes found.

The updated values of the stiffnesses are sensible, as the bottom of the beam should reduce in stiffness due to more cracks appearing and the cracking is most dense in this region of the deck. The E_{50} stiffness should be less than the uncracked concrete and a small reduction in the overall stiffness of the concrete is expected, as the damage is not concentrated in just the locations selected.

6.6.3 Load 100

At this load level, the main type of damage was in the form of the cracks growing slightly and increasing in density and the formation of a longitudinal crack at the shoulders of the central beam. This damage is to be modelled by reducing E_{50} and E_b, and defining a new material property for the elements in the slab adjacent and above the central beam along the length of the deck. This gives a region 635mm wide, centred about the central beam. The Young's modulus of this section is denoted as E_{100}.

It was not possible to update all of these three parameters during a single updating run, as this caused the parameter E_b to increase above its previous value, which is unrealistic. It was chosen to update E_{50} and E_{100} at the same time, and attempt to obtain convergence of these parameters before updating E_b and E. This is due to the fact that most of the change in natural frequency is assumed to be due to the growth of vertical cracks and the formation of the longitudinal crack.

The values of the updated parameters are given in Table 6-1. As expected, the most significant change in the parameters occurred for the two regions described by E_{50} and E_{100}, where the majority of damage was observed in the actual decks, and also a small reduction in the "uncracked" concrete Young's modulus as would be expected by the distributed damage. However, there is a 5% increase in the Young's modulus of the cracked concrete at the bottom of the beam. This is most likely due to errors in the current and previous model, rather than an actual increase in the stiffness of the material. The error in the FEM for the updating performed is given in Figure 6-10.

6.6.4 Load 150

This load level caused the cracks in the beams to extend to approximately 200mm (i.e. the full height of the beam), modelled in the FE model by assigning a new stiffness to the remainder of the beam elements. The model was firstly updated to find new values of E_{50} and E_{150} as all the stiffness reduction is assumed to have taken place in the beams. A final update was attempted for the remaining materials, but these produced an increase in stiffness, which is not realistic. However, as the natural frequencies predicted

by the updated model were within 10% of the experimental values, Figure 6-11, this final update was ignored. The parameters found are given in Table 6-1.

6.6.5 Load 200

This load level did not produce any new crack locations, and instead caused an increase in the number and length of cracks in the regions already cracked. No new materials were defined in this model, and the model was updated to find new values of Young's modulus for the existing cracked regions.

The change in the parameters is given in Table 6-1. A small reduction was found for E_{50}, corresponding to the small growth in vertical crack length. E_{150} reduced by a considerable amount, and became lower than the Young's modulus of E_{50}, due to the amount of cracking of the beams in shear and torsion (included in this material region) that was more severe than the damage in the central section, confirmed by observations of the cracking. Therefore, this large reduction to a value lower than the rest of the beam is not unexpected. The error of the FEM for the matched modes is presented in Figure 6-12.

6.6.6 Load 250

There was a particular increase in the number and length of shear cracks at each end of the central beam and in the torsion cracking in the outer beams, together with the development of four longitudinal cracks in the top surface and several radial cracks in the underside of the slab. The longitudinal and radial cracking was modelled by reducing the stiffness of elements in the slab in a pattern similar to the actual cracking. The same Young's modulus was used for both these types of cracking, denoted as E_{250}.

At this load level, the Young's modulus for the slab was updated together with E_{250}, as not all the cracking was concentrated in the new areas defined. The values of E_{50} and E_{100} were also updated corresponding to the growth of cracking in the beams. The values obtained for these parameters are given in Table 6-1.

As expected, the largest reduction in material stiffness occurred for the elements representing the new cracking, reducing the Young's modulus in this area by 56%, to a value similar to that found for the previous longitudinal cracking at a load of 100kN. This previous cracking also reduced in stiffness by a further 14%. This is in accordance with the degree of cracking observed during the static testing.

However, the updating also caused some material stiffnesses to apparently increase. A small increase in the slab concrete stiffness was indicated, although this may be due to one or both of E_{100} or E_{250} reducing to values that are too low, requiring the stiffness of the remaining slab parts to increase to compensate. The stiffness of the concrete at the mid-height of the beams increased by a larger amount, 6%, perhaps again due to the model underestimating some material properties, as it is unlikely that this happened in the actual deck. The change in the error in natural frequencies between the FEM and measured values is given in Figure 6-13.

6.6.7 Load 300

At this load level, there were a number of severely cracked areas, due to the fact that the deck was almost at its ultimate capacity. The torsion cracking in the end beams had now become considerable, and was modelled as two vertical columns of elements with reduced stiffness, E_{300a}, in the four sections of end beam between the longitudinal beams. A significant amount of new longitudinal cracking had also developed in the top surface of the deck, together with more radial cracking in the underside, modelled in the same manner as the previous load level, but with a Young's modulus of E_{300b}. Shear and torsion cracking was now fully developed at the ends of the longitudinal beams, and was modelled by assigning a new material to 0.8m at each end of the beams, denoting the stiffness as E_{300c}, as shown in Figure 6-14.

The updating at this stage was performed for all material stiffnesses by applying constraints to the maximum and minimum values in order to maintain physical significance of the model. The maximum value was defined as the value obtained from the updated model at load 250, and a minimum value assigned as $0.5\times10^{10}N/m^2$. A final manual update was made to the values of

E_{50}, E_{300a} and E_{300c} due to poor convergence of the least squares routine. The values of the updated parameters are given in Table 6-1, and the error in the FEM for the updating performed is presented in Figure 6-15.

As expected by the progressive collapse of the deck, there were no significant changes to the parameters defined to model the cracking from load 0 to 100kN, although the value of E_{50} that had previously increased reduced to slightly lower than the value obtained at a load of 200kN.

The cracking in the top of the beam caused the Young's modulus to reduce to the minimum value permitted, due to the development of the separation of the beam from the slab that fully developed at failure. The stiffness used to model the torsion cracking in the ends of the longitudinal beams reduced to 31% of the uncracked concrete stiffness. The longitudinal cracking in the slab, modelled by E_{100}, E_{250} and E_{300b}, did not reduce further than the values at the previous load level. This indicates that the load has redistributed to promote failure of the longitudinal beams and no longer caused significant cracking in the slab. This corresponds to the ultimate failure mechanism that was observed in the experimental testing of the deck.

It was decided not to update the FE model for the final load step, as the model can no longer represent the failed deck accurately. This is due to the significant loss of stiffness and material at the ends of the central beam and the separation of the central beam from the remainder of the deck. The modes found for the deck in this condition are also significantly changed from those at the previous load, with only a few of the modes appearing to be the same.

6.7 Updating asymmetrically loaded deck

6.7.1 Load 0

The deck used for this updating was deck 9. As for the previous deck, the FE model to be updated for the initial case contained materials corresponding to the uncracked concrete stiffness, the slab stiffness and the cracked concrete at the bottom of the beams, together with the bearing stiffness in the form of a vertical and torsional spring. The same procedure used for the initial symmetrically loaded deck was followed for this deck also. The updated

parameters of E, E_s, E_b, k_B and k_T are given in Table 6-2 and are shown in and Figure 6-16.

Comparing these parameters with those obtained for deck 8 demonstrates that the condition of the initial decks was very similar, as would be expected for nominally identical decks, although all the parameters obtained for this deck are slightly lower. The error in the natural frequencies of the matched modes is given in Figure 6-17.

A plot of the both the measured FRFs and those predicted by the updated FEM can be found in Figure 6-18. From this plot, it is possible to see that, at certain modes, there is a very good match between the measured FRFs and the predicted FRFs. Again, it can clearly be seen which modes could not be included in the updating procedure, producing a discrepancy between the FRFs plotted. In general, it appears that many of the modes have been successfully updated in terms of their natural frequencies. For many modes, the magnitudes of the FRFs are similar.

6.7.2 Load 50

At this load, the cracking developed in the form of a growth in the vertical cracking in the longitudinal beams. Due to the asymmetrical nature of the loading, the cracking was more significant in beams i, ii and iii, in which the cracking was modelled as two elements deep, with stiffness E_{50}, in the central 3m, reducing to one element depth 1m from the ends of the deck and in beams iv and v.

The updating of this model was performed by modifying the values of the cracked concrete stiffness, E_b, and the new stiffness, E_{50}. The updated values of these stiffnesses is given in Table 6-2. This model produced natural frequencies that were all within 5% of the experimental, except one that was within 10%, see Figure 6-19. The values of the Young's modulus of the materials again appear to be probable, producing a decrease in the stiffness of the bottom of the beams and reducing the newly cracked regions by 14% and 8%, respectively.

6.7.3 Load 100

The major increase in damage at this load level was in the form of growth of the vertical cracking, modelled by defining a separate stiffness, E_{100}, to increase the height of the cracking by one element in all beams. This model was updated by changing the stiffness of E, E_b, E_{50} and E_{100}, to give a model that predicted all the natural frequencies within 7%, and half within 1%, of the measured frequencies, Figure 6-20, using the values given in Table 6-2.

In accordance with the observed areas of crack growth, the major reduction in stiffness was attributed to E_{50} and E_{100} that decreased by 10% and 6%, respectively. This shows that the existing cracking developed more than the new cracking, which is supported by the progressive growth of damage to the deck.

6.7.4 Load 150

This load level did not appear to promote significant growth of the existing cracking or any new regions of cracking. Instead, the increase in damage arose from the growth of cracking within the existing damaged areas, increasing the number of cracks. No new material stiffnesses were assigned to model this damage, and the updating was performed assuming a reduction in the existing stiffnesses.

The updated values of these parameters are given in Table 6-2. According to the updated model, which calculated the natural frequencies within 4% for all modes except the first (within 6%), Figure 6-21, the majority of the damage occurred in E_{100} with a reduction in stiffness of a further 36%. A smaller reduction of 7% was found for E_{50}. In physical terms, this indicates that the top of the beams has become less stiff than the mid-depth. This appears possible as the cracking grew into the soffit of the deck and could be a precursor to the longitudinal cracking that developed fully at the next load step.

6.7.5 Load 200

When the load was increased to 200kN, several cracks developed in the slab of the deck in the form of longitudinal cracking at the outside shoulder of beam ii

and in the soffits between beams i – ii and ii – iii. A single longitudinal crack also developed above inside edge of beam iv. All of this cracking was modelled as a material with stiffness E_{200}.

Due to the insignificant crack growth in all areas except where new cracking developed, the updating at this load level was performed by modifying E_{200} only, resulting in the error shown in Figure 6-22. The new material properties are given in Table 6-2, from which it can be seen that the stiffness of the longitudinal cracking in the slab is less than half, 47%, of the uncracked concrete stiffness. At the same load, the stiffness of the longitudinal cracking in deck 8 has reduced to a comparable fraction of the slab concrete stiffness, 48%, showing that there is considerable similarity between the degree of damage to the decks and that cracking to the slab causes a consistent loss of stiffness.

At this load, it should be noted that the second mode measured experimentally actually increased in frequency by approximately 11%, and is therefore in considerable error when compared to the natural frequency obtained from the FE model. A discussion concerning the apparent increases in natural frequencies is given in section 5.4. However, the updated material stiffnesses appear to compare well with previous models and with expectations based on the cracking patterns.

6.7.6 Load 250

At this load, a longitudinal crack in the opposite shoulder of beam ii developed together with a crack in the top surface of the deck above the outside of beam ii, assigned a stiffness E_{250}. This load level also caused some torsion cracking to form in the end beams, however, this could not successfully be incorporated into the updating of this model due to the insensitivity of the natural frequencies to this damage, this was justified by the relatively minor nature of the cracking.

The parameters that were updated at this load were E_{50} and E_{250}, and the updated values are given in Table 6-2, whilst the error in the natural frequencies of the updating performed and the measured values is presented in Figure 6-23. It can be seen that there is a small reduction in the stiffness of the

middle section of the longitudinal beams, due to some growth in the number of cracks extending to this height. The reduction in stiffness of the newly formed longitudinal cracking is again comparable with the previous longitudinal cracking, decreasing to 49% of the slab concrete stiffness.

6.7.7 Load 300

This load level caused the development of cracking in several new areas. The torsion cracking observed at the previous load level was now significantly more developed and was modelled as two vertical bands in the end beams between beams ii – iii and iii – iv, with stiffness E_{300a}. New longitudinal cracking grew in the top surface of the slab between beams iii – iv, creating a number of parallel cracks adjacent to the previous cracking with element stiffness E_{300b}. A significant difference between the slab near the loading points and the other parts was noticed, with the development of several new cracks in this region. This part of the slab between beams ii – iii and half way between beams i – ii was assigned a new stiffness of E_{300c}. At this load, much of the growth in cracking was seen to form at the ends of beams i, ii and iii in the form of shear and torsion cracking. This region within 1m of the ends of the deck was given a separate stiffness of E_{300d}, as shown in Figure 6-24 and Figure 6-25.

The updating of the FE model was performed in a similar manner to the final model of deck 8 by updating all parameters and incorporating constraints on the upper and lower values of Young's modulus. A number of manual modifications of the values used in the model were made to encourage faster convergence of the natural frequencies, based on previous iterations. The updated values are shown in Table 6-2 and the changes in the error in the natural frequencies are given in Figure 6-26.

It can be seen from the new values of Young's modulus that there is very little change in the parameters defined to model the cracking appearing in the load levels 0 to 200kN. This illustrates the progressive failure of the deck, in that one cracking mechanism develops to near its capacity, causing the load to redistribute and promote another cracking pattern to develop. At this load

level, it is only the parameters that correspond to the recent cracking that cause the deck to reduce in stiffness.

From the updated material stiffnesses, it can be seen that there are again similarities between these and the values obtained previously. The stiffness of the longitudinal cracking again reduces by an amount comparable to that of the other longitudinal cracking, 43%. This is slightly less due to the fact that this cracking is an extension of the cracking that developed at a load of 200kN and the deck is close to ultimate failure. The significant cracking beneath the loading points causes a significant reduction to the stiffness, as would be expected from the concentrated cracking evident in this region. However, it should be noted that part of this region was previously included in the parameters E_{200} and E_{250}, and the reduction by 89% in stiffness is compared to the uncracked concrete stiffness, not the stiffness at the previous load level.

The stiffness of the concrete due to the torsion cracking in the end beams reduced to the lower value permitted, $0.5\times10^{10}N/m^2$, indicating that this was significantly developed at this load level. The Young's modulus found for the region representing the torsion and shear cracking at the ends of the beams reduced to lower than the stiffness of the mid-height section of the beams, E_{50}, although was slightly higher than the stiffness of the top of the beams, E_{100}. This is not unexpected, as the stiffness of the top of the beams would be reduced by the cracking in the slab connected to the beams, although the ultimate collapse of the deck was due the development of a torsion failure in the beams this may not have developed fully until the final load step. Again, no update was performed for the final load step due to the significant changes required in the modelling to account for the considerable amount of cracking exhibited at ultimate failure.

6.8 Comparison of experimental and analytical behaviour

FE models also offer the opportunity to predict the behaviour of structures for modifications other than those they have been verified for. In this study, the updated models are investigated to determine the behaviour of the bridge decks at intermediate load levels that were not tested in the experimental work. This is done by assuming that the change in stiffness over the load increment

applied is linear and interpolated between the Young's modulus values obtained by performing the updating. From this, a number of points raised in chapter 5 concerning the dynamic behaviour of the decks can be investigated further.

The problems encountered in the experimental work were mainly due to the confidence with which modes can be tracked through the loading history when the damage causes the mode shapes to change. This includes the appearance and disappearance of modes and also the apparent increase in some natural frequencies. Some of these problems were attributed to the support conditions, which are also studied using this FE model.

6.8.1 Loading of deck

The natural frequencies of this deck were found for the first thirty modes, and traced through the loading history up to 300kN, as shown in Figure 6-29. It should be noted that the increase in natural frequencies between 250kN and 283kN is due to a change in the FEM used to model the damage at these loads.

It can be seen from this figure that the modes possess different sensitivities to the parameter changes made, and in some cases cause the modes to change order. It is also apparent from this figure that some modes do change significantly enough to effectively disappear according to the MAC values produced, and this is particularly evident for the higher modes.

Figure 6-30 shows the equivalent natural frequency change for the asymmetrically loaded deck. From this figure, it can clearly be seen that the disappearance of modes is more common than in the symmetrically loaded deck. The disappearance of modes also occurs for some of the lower modes, as well as the higher modes.

A comparison of the natural frequency changes with increasing damage between the FEM predictions and the actual results is presented in Figure 6-31. From this figure, it can be seen that the prediction by the FEM is reasonable until the load reaches 150kN, beyond which the two sets of results diverge. It is important to note that the FEM results plotted on this graph are the average of all modes, which may explain why the trends are less good at higher loads as

the models are based on the FEM updating detailed in sections 6.6 and 6.7 where only a small number of modes were used due to poor MAC values.

6.8.2 Boundary conditions

The effects of the bearings not contributing fully to the support of the deck were investigated by modelling the deck supported on sets of linear springs. Whilst this does not produce the correct results with regard to the experimental testing, the effect on the natural frequencies and mode shapes of the modes found can be seen, and would be, in general, similar to the effects on the actual modes.

A range of different bearing configurations were investigated, as detailed in Table 6-3, where a negligible stiffness is equal to $1N/m^2$. The results of the modified bearing arrangements are compared with a fully supported model, configuration A, and the percentage change in the natural frequencies of matching modes are presented in Figure 6-32.

In this figure, it can be seen that there are a large number of modes that disappear due to poor MAC values, and that this occurs for almost all the modes extracted. This is in contrast to the effects of damage investigated in the previous section in which mainly the higher modes were affected by poor MAC values.

From this figure, it is also possible to see that some modes increase in frequency, even though the bearing stiffness has been reduced. This finding indicates that the apparent increases in natural frequency observed in the laboratory testing may be due to changes in the boundary conditions.

6.9 Discussion

In general, the updating of a FE model produced results that compared well with the observed behaviour from the experimental testing. By looking at the changes in the parameters, Figure 6-27 and Figure 6-28, it can be seen that the progressive failure of the deck is captured by the reduction of stiffness in certain areas in a sequential manner. In most cases, the values of the updated

parameters changed in a way that was expected when compared to the damaged locations and crack lengths and sizes.

Longitudinal cracking in the slab often corresponded to a similar reduced stiffness in the updated FE models for both decks, indicating that this type of cracking produced a consistent effect on the stiffness of the slab.

Using the updated FE models to predict the dynamic behaviour of the decks at load levels not measured gave good correlation between the results up to approximately half the ultimate load of the decks. It was possible to observe the increases in natural frequencies found in the experimental testing by examining a FE model with changing support stiffnesses, indicating that this is a possible cause of the variation found in the measured natural frequency trends.

However, there are several limitations to the application of this method to the assessment of a real bridge. Firstly, it must always be remembered that the updating procedure is based on attempting to construct a FE model that successfully matches the natural frequencies obtained with those found experimentally. There will always be some error in the experimental results, and this should be considered when interpreting the results of the updated model.

An inherent limitation of the modelling is due to the fact that the parameter to be updated must cause a change in the natural frequencies to be correlated. If the cracking does not influence the natural frequencies enough, it is not possible to update the material successfully, particularly when several parameters are updated simultaneously. This, however, may indicate that the cracking itself is not significant in the actual specimen.

Thirdly, the method employed requires knowledge of the damaged locations in order that a separate Young's modulus can be assigned to this area in order to maintain the physical significance of the updated parameters. A solution to this problem could be found depending on the implementation of the method. From the point of view of the UK Highways Agency, the monitoring period would be instigated after an inspection determines that bridge has marginally

passed or failed, to investigate how quickly the bridge is deteriorating by looking at changes in the modal properties.

Due to the fact that the bridge would previously have been inspected, there will be a record of the areas in which the bridge was deemed to be unsatisfactory and the reasons for the failure of the inspection. This information could then be incorporated into a FE model updating procedure. It would also be possible to select the dynamic properties that are expected to be most sensitive to the anticipated deterioration and perform the monitoring to study these parameters. However, this would require more investigation to build up knowledge of the effects of various types of degradation on the dynamic characteristics of bridges.

It should also be noted that although the FE model updating performed in this study appears to be successful, the degree of damage to the decks in the form of structural cracking was significant due to the load steps used in the static testing. Therefore, any small errors in the modal parameters found experimentally would be small compared to the change in the property due to the increased damage. This may not be the case when applied to a real bridge, and would require careful determination of how significant the change in the dynamic properties needs to be before action is taken, when compared to any variation due to environmental effects.

At the current stage, it is unlikely that the method can be applied to a bridge without having *a priori* knowledge of the expected areas of deterioration. Also, it is still unclear as to the effects of environmental changes on the dynamic properties and whether the changes in bridge condition can be distinguished from these.

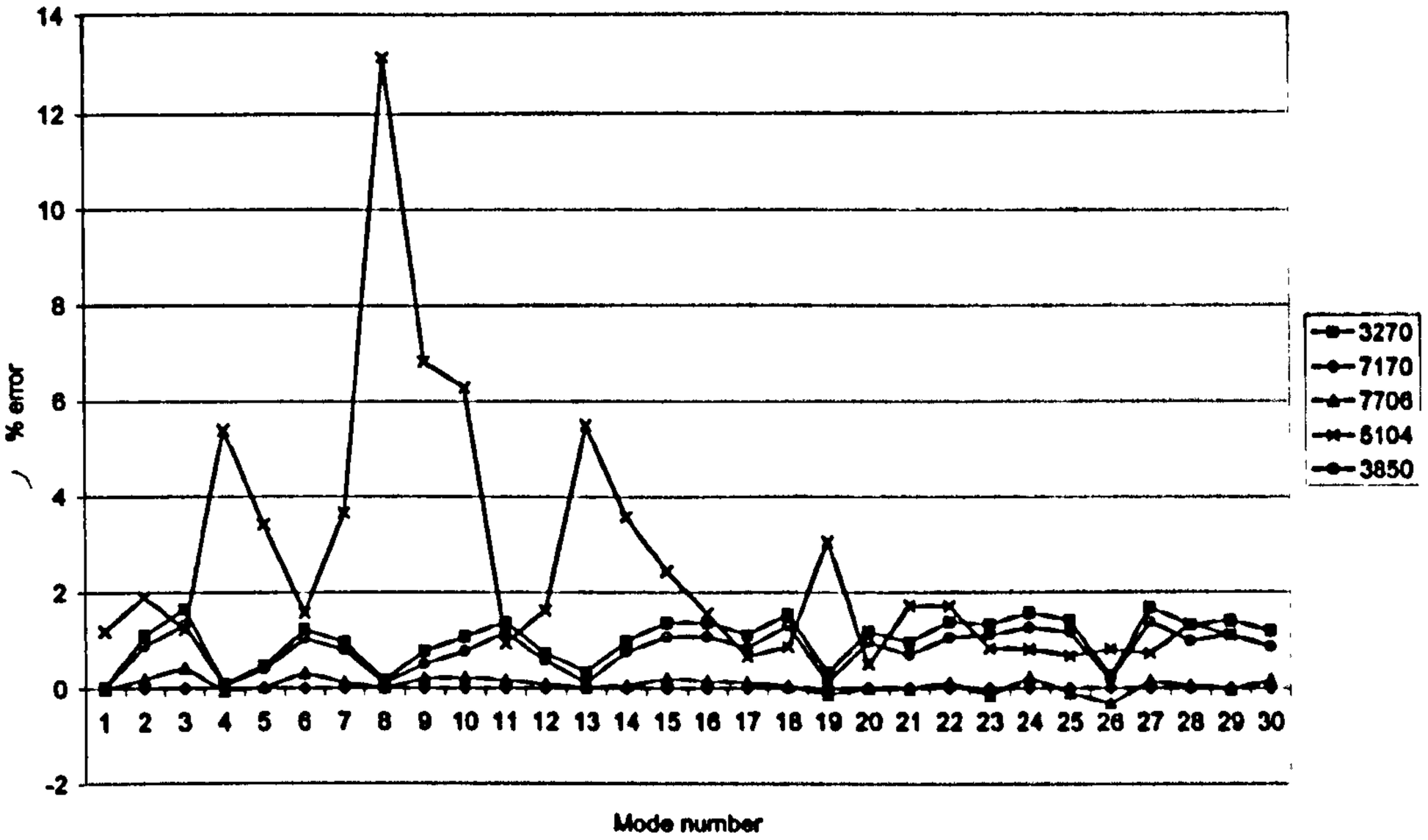

Figure 6-1: Percentage error in the natural frequencies of the first thirty modes from different models with respect to the finest symmetric model

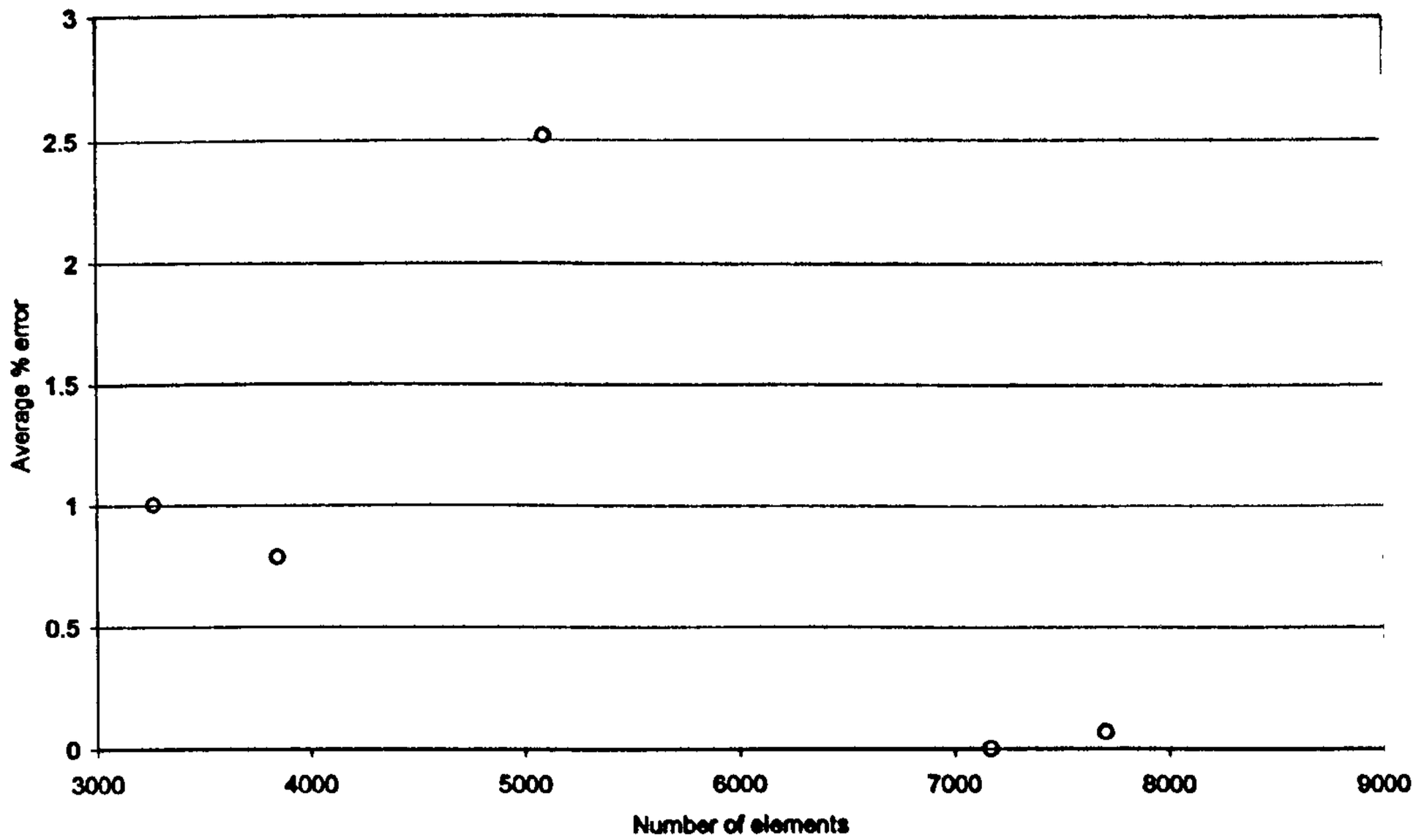

Figure 6-2: Average error in the first thirty modes for different numbers of elements

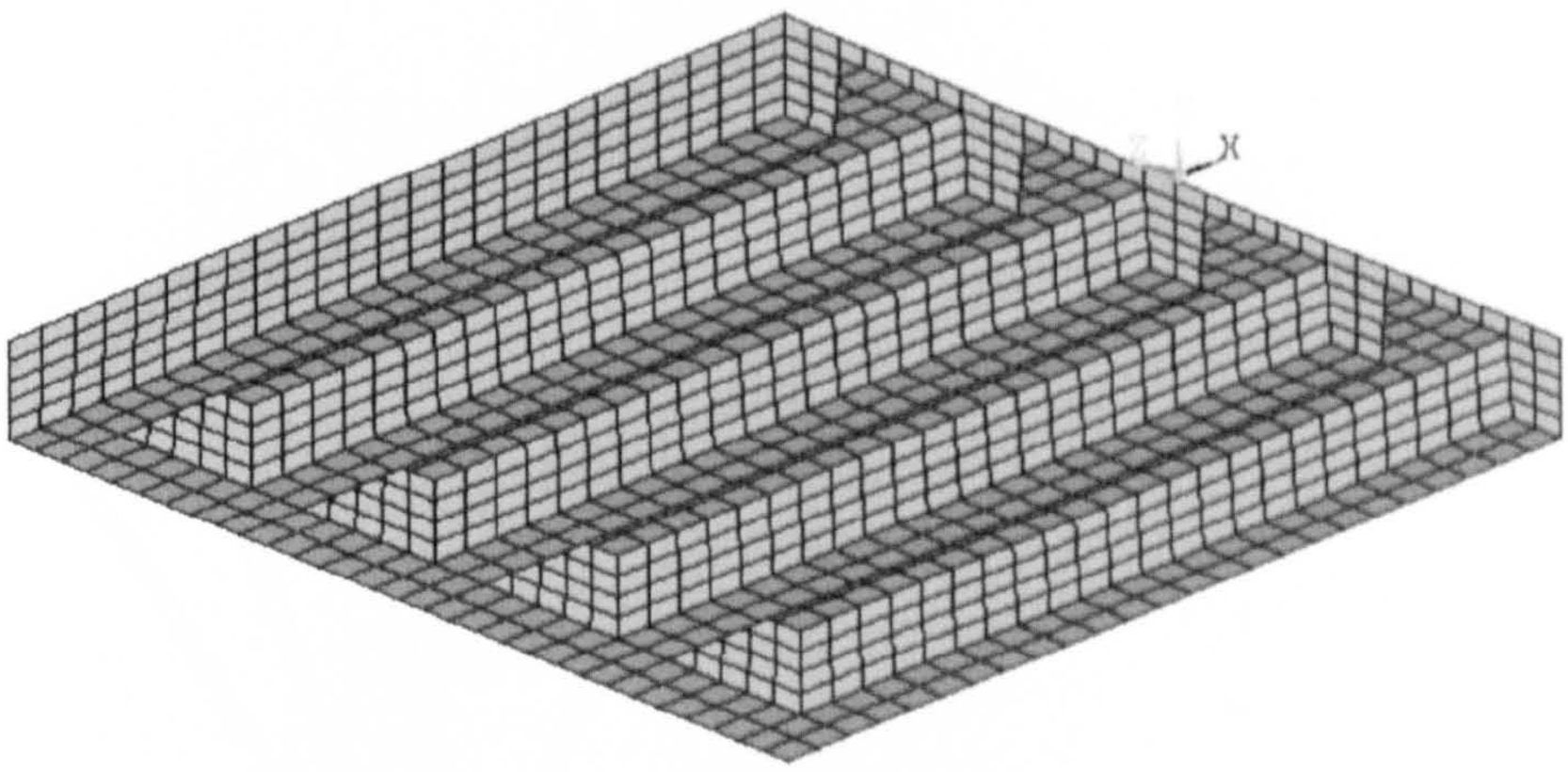

Figure 6-3: Finite element model of the deck, showing the longitudinal beams

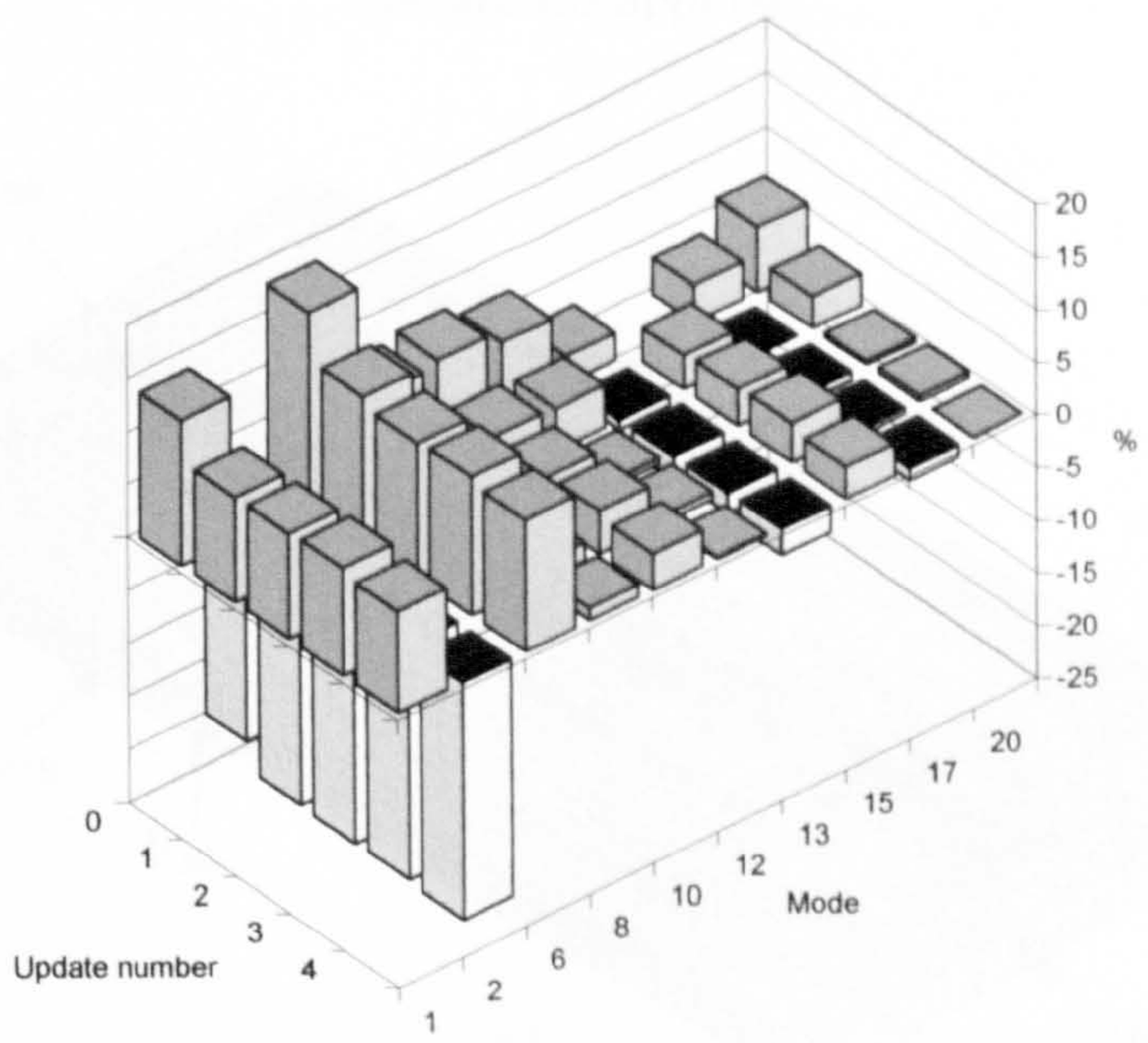

Figure 6-4: Percentage error between FEM updates and measured natural frequencies of deck 6

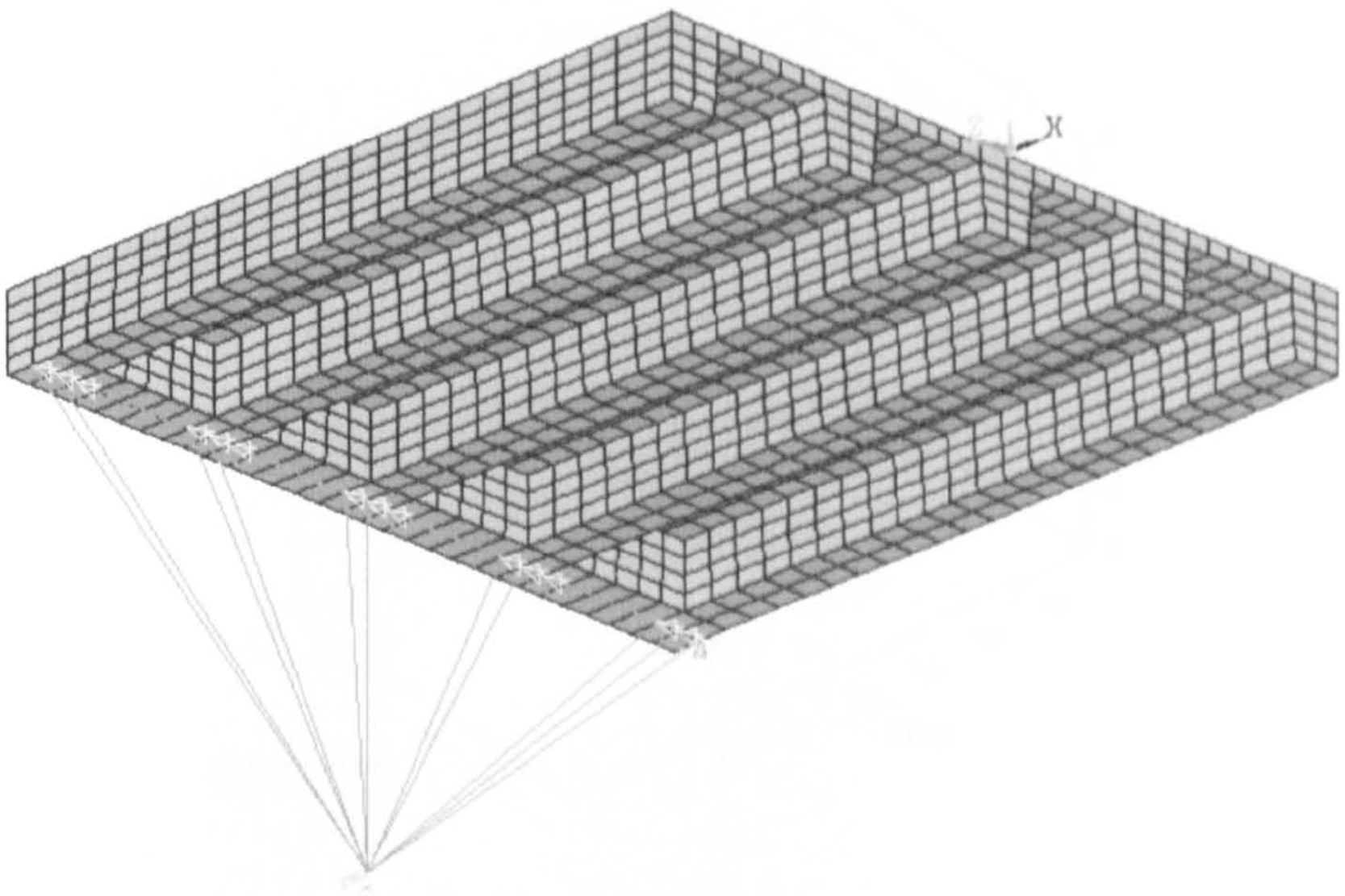

Figure 6-5: Finite element model of the deck showing boundary conditions and constraints applied

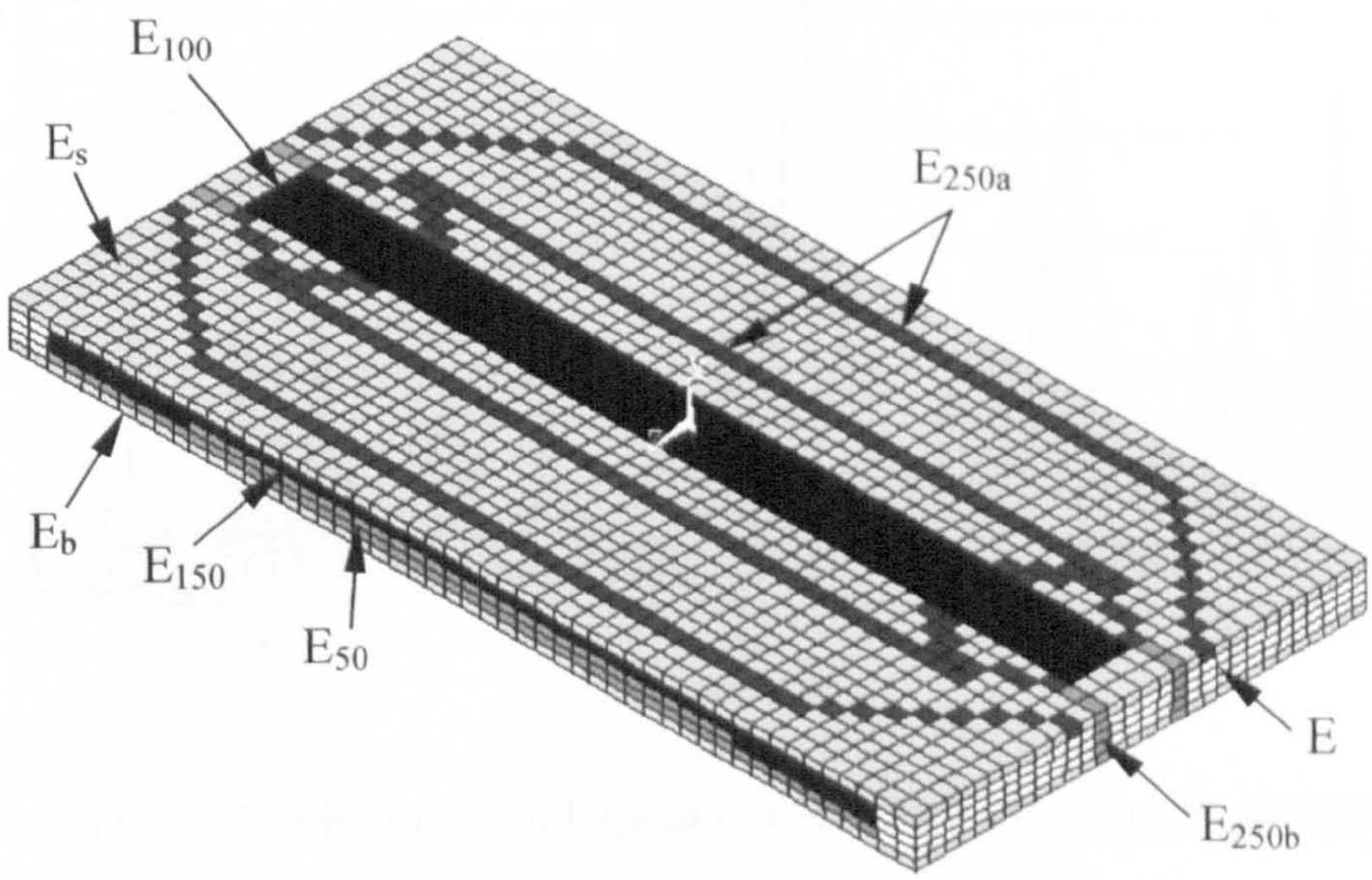

Figure 6-6: Areas assigned different material properties to model a symmetrically damaged deck up to 250kN

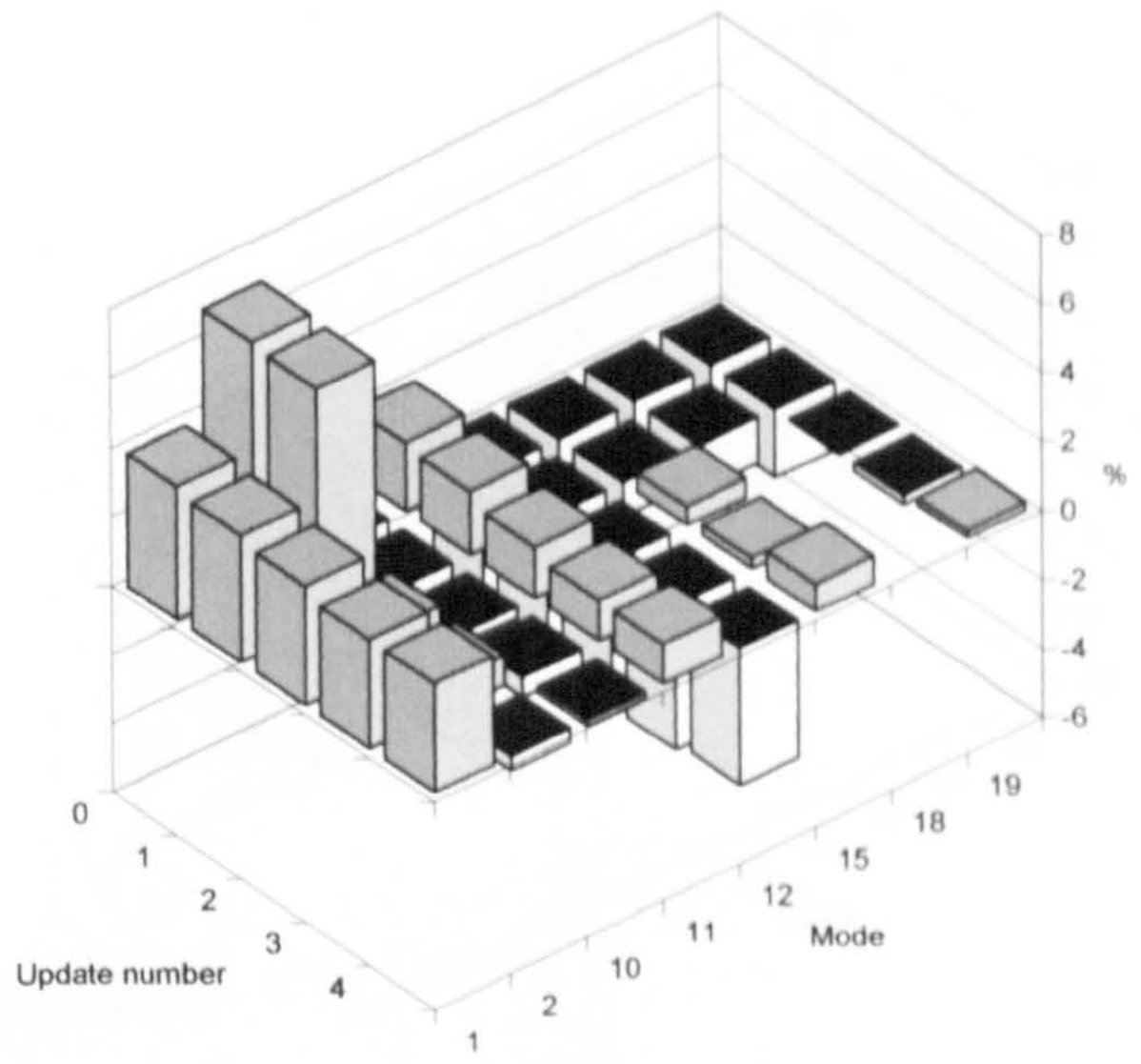

Figure 6-7: Percentage error between FEM updates and measured natural frequencies of deck 8 at 0kN

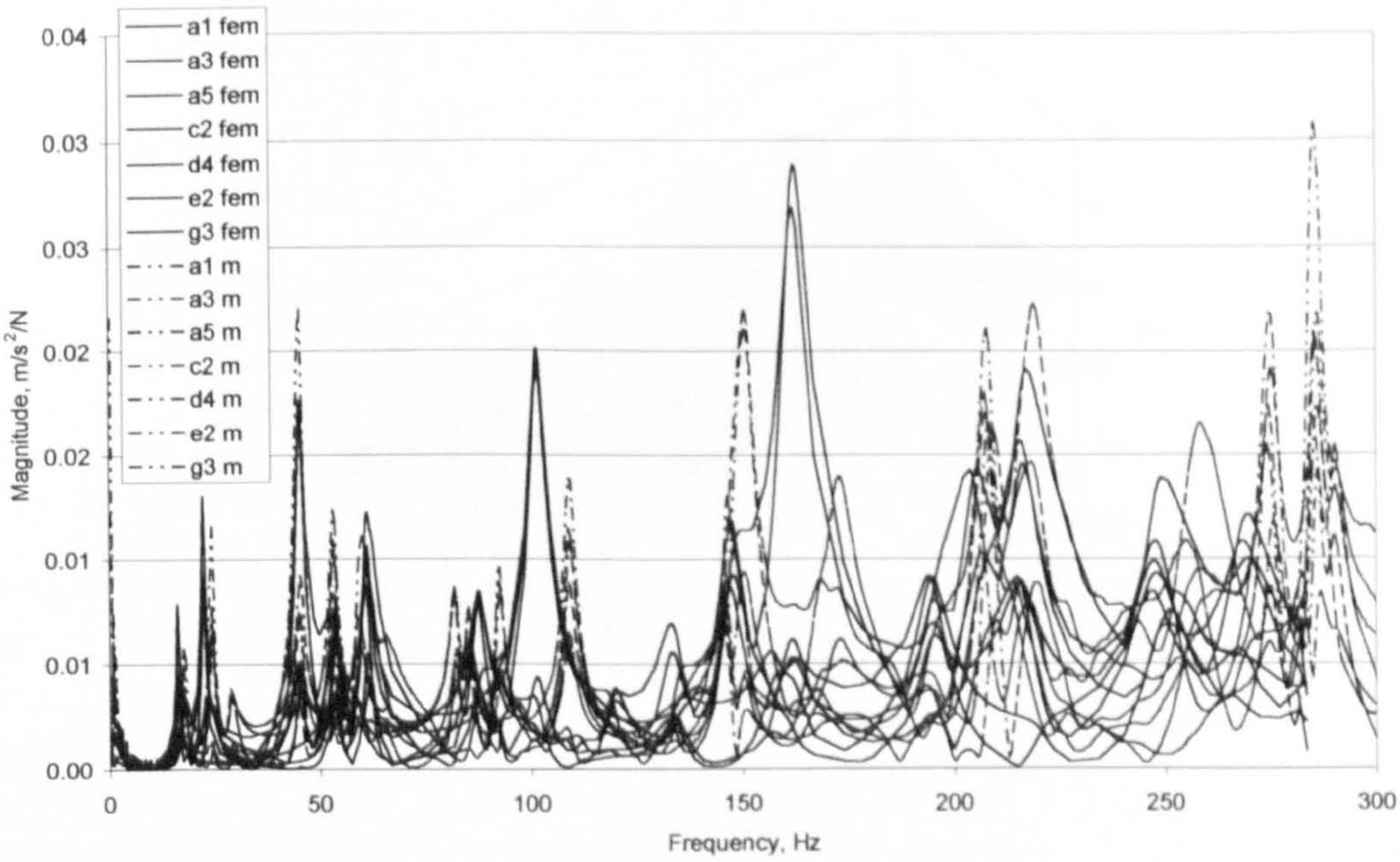

Figure 6-8: Measured and updated FEM FRFs for deck 8 at 0kN

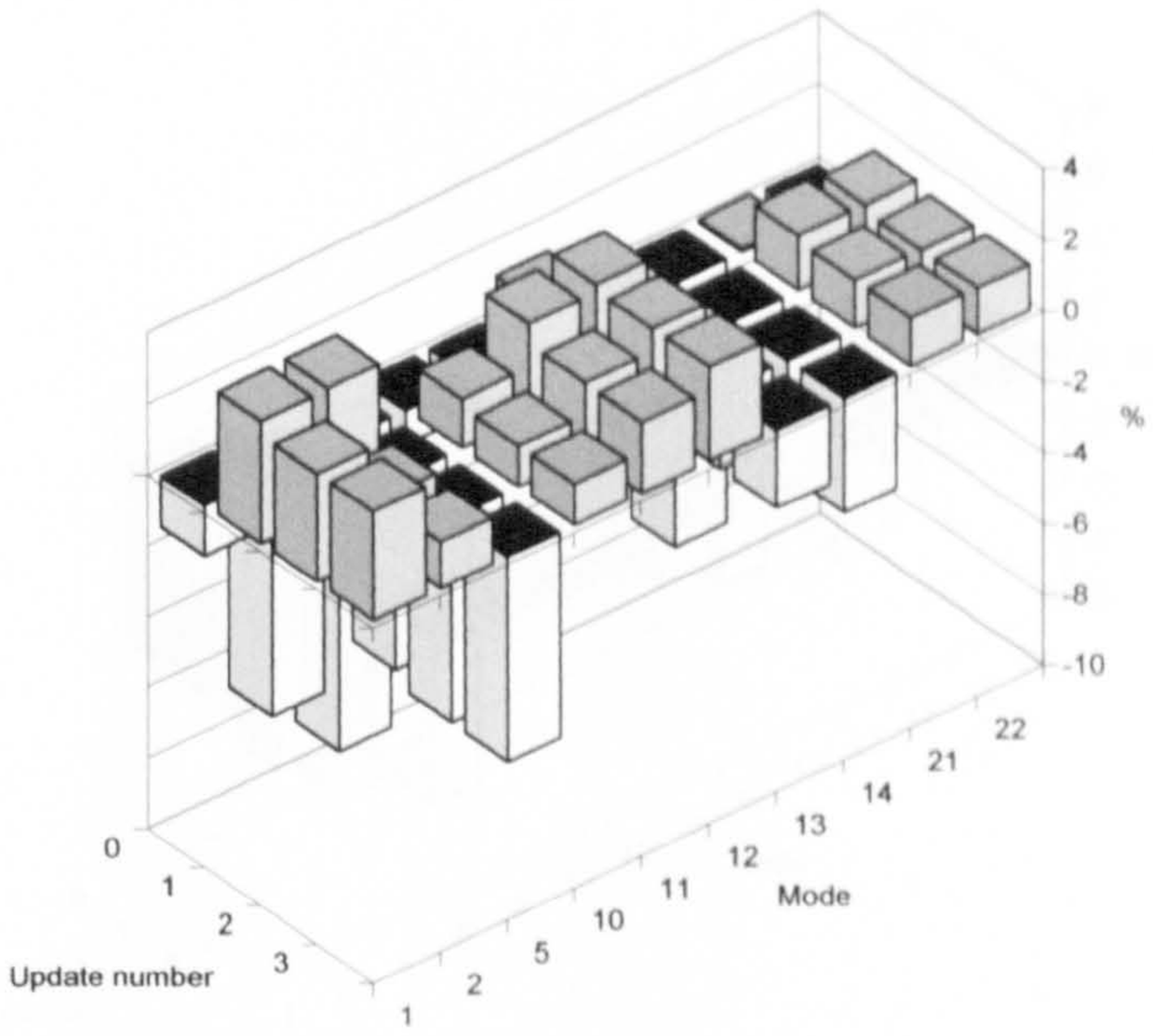

Figure 6-9: Percentage error between FEM updates and measured natural frequencies of deck 8 at 50kN

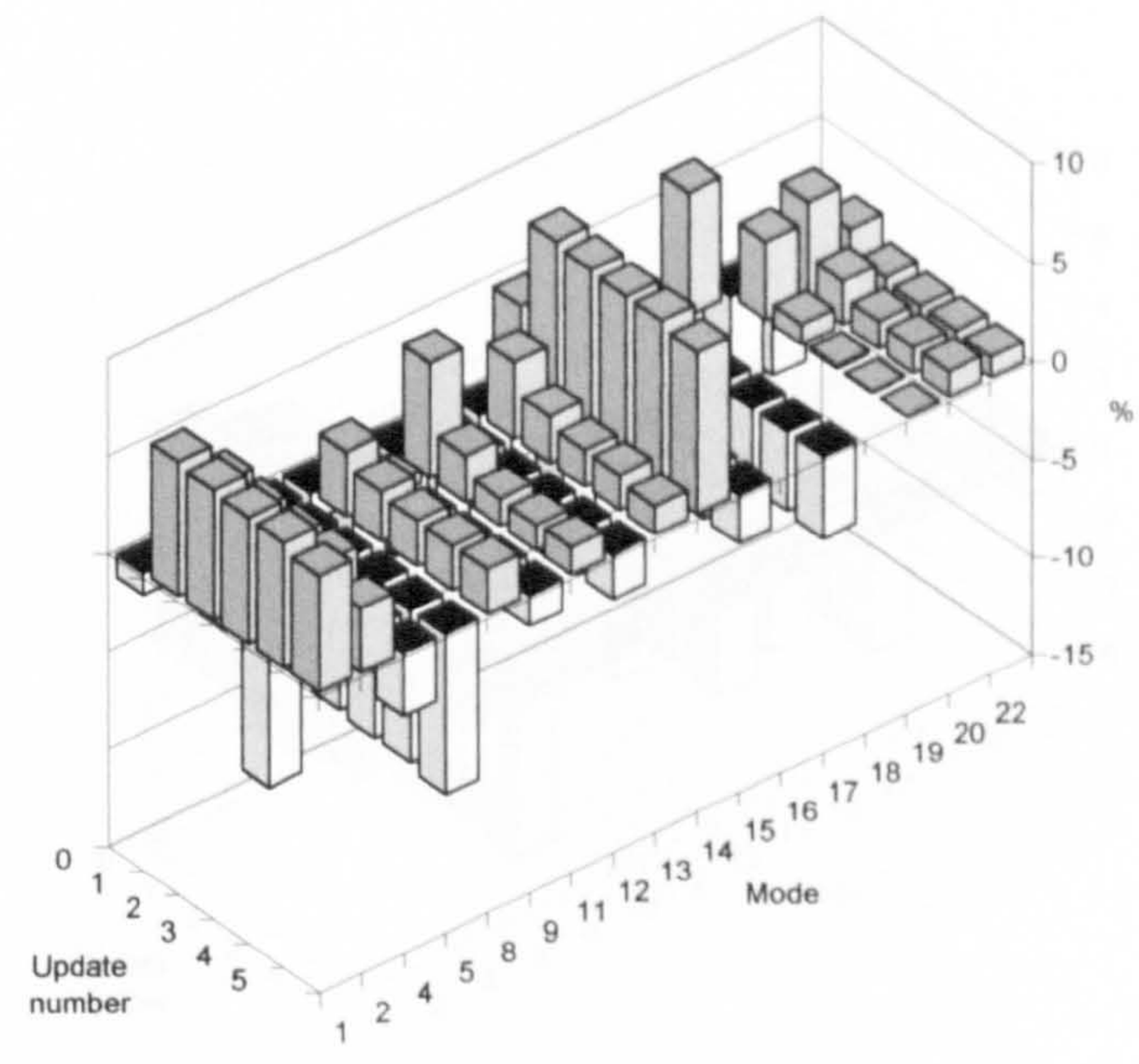

Figure 6-10: Percentage error between FEM updates and measured natural frequencies of deck 8 at 100kN

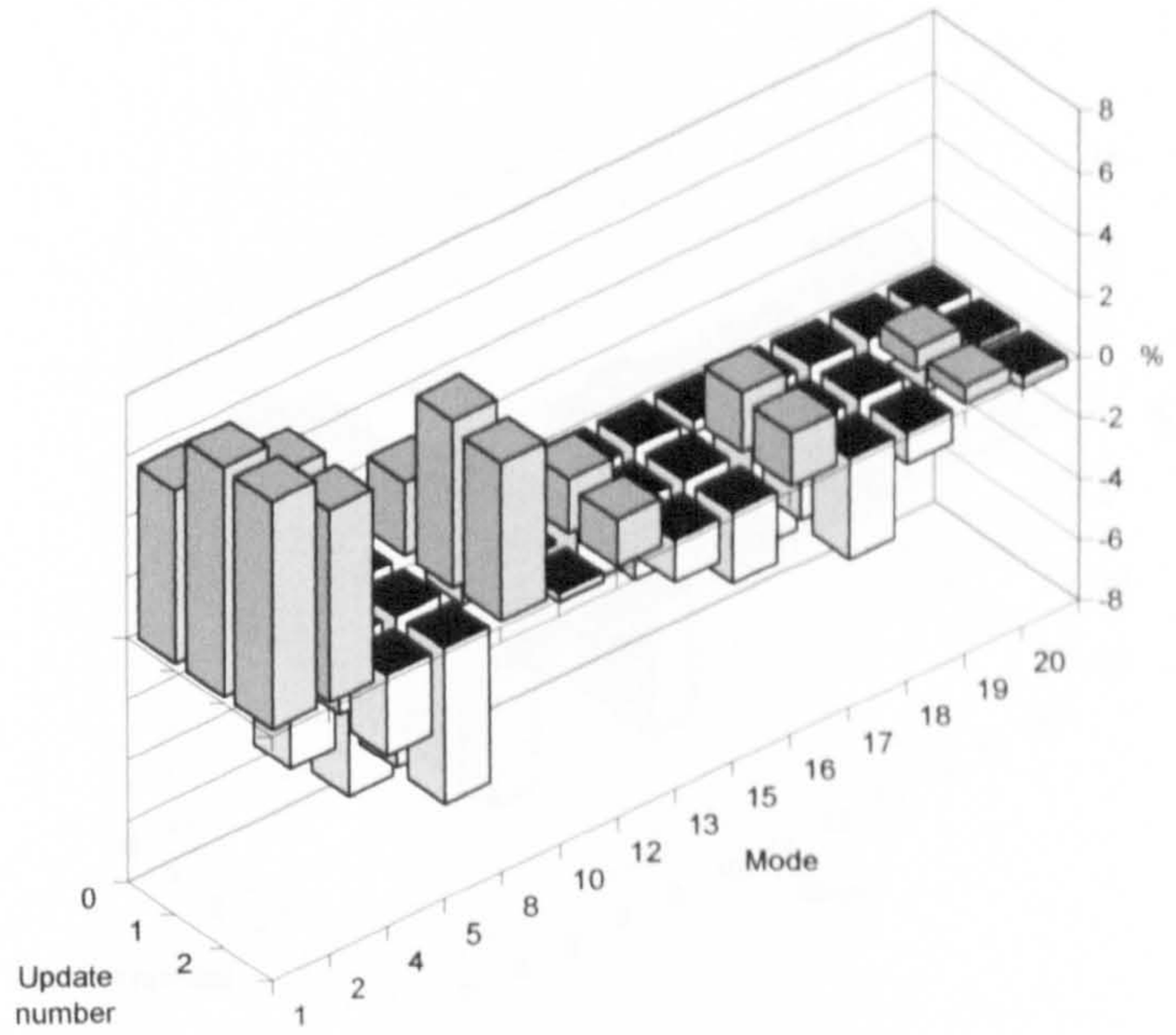

Figure 6-11: Percentage error between FEM updates and measured natural frequencies of deck 8 at 150kN

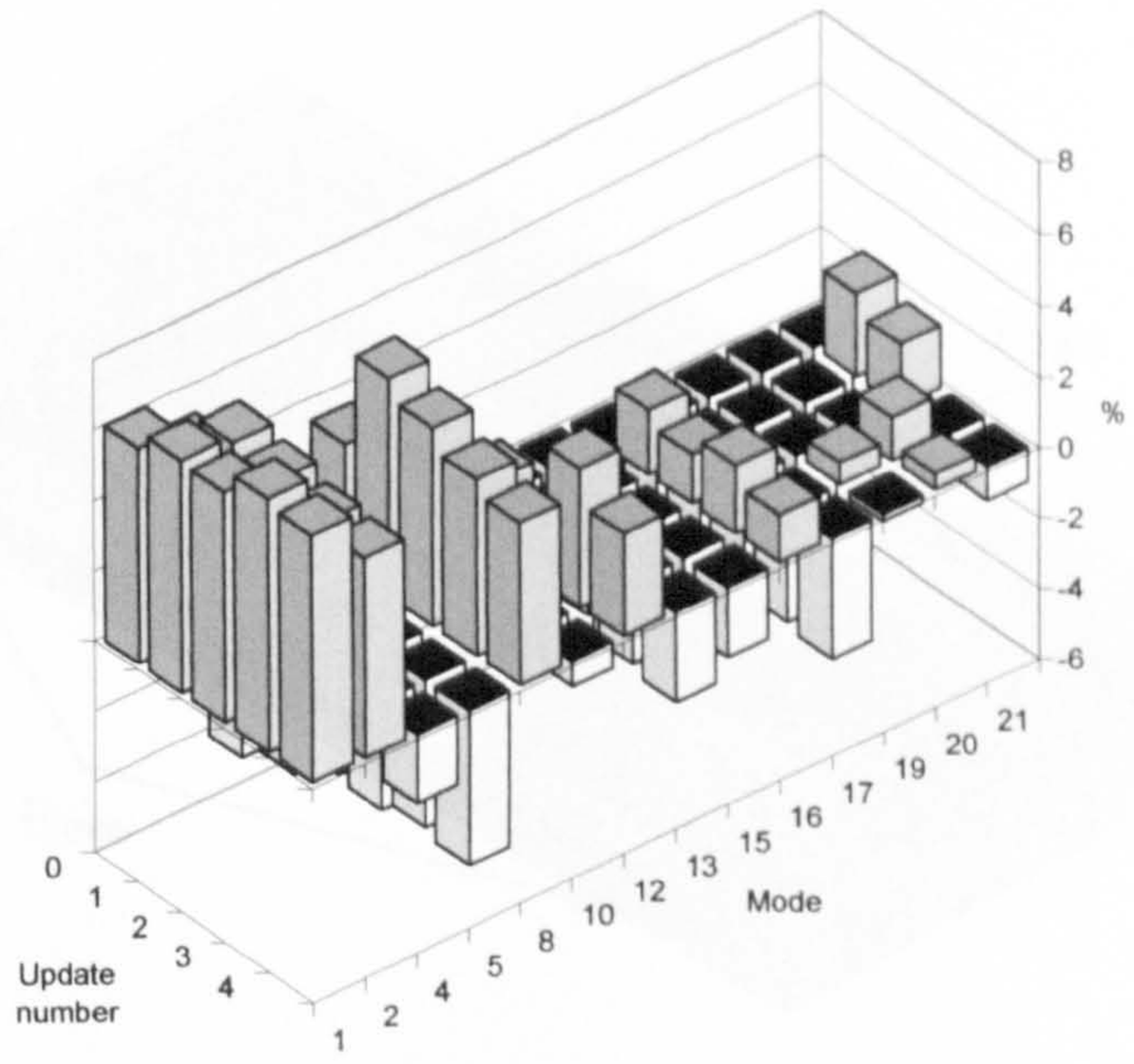

Figure 6-12: Percentage error between FEM updates and measured natural frequencies of deck 8 at 200kN

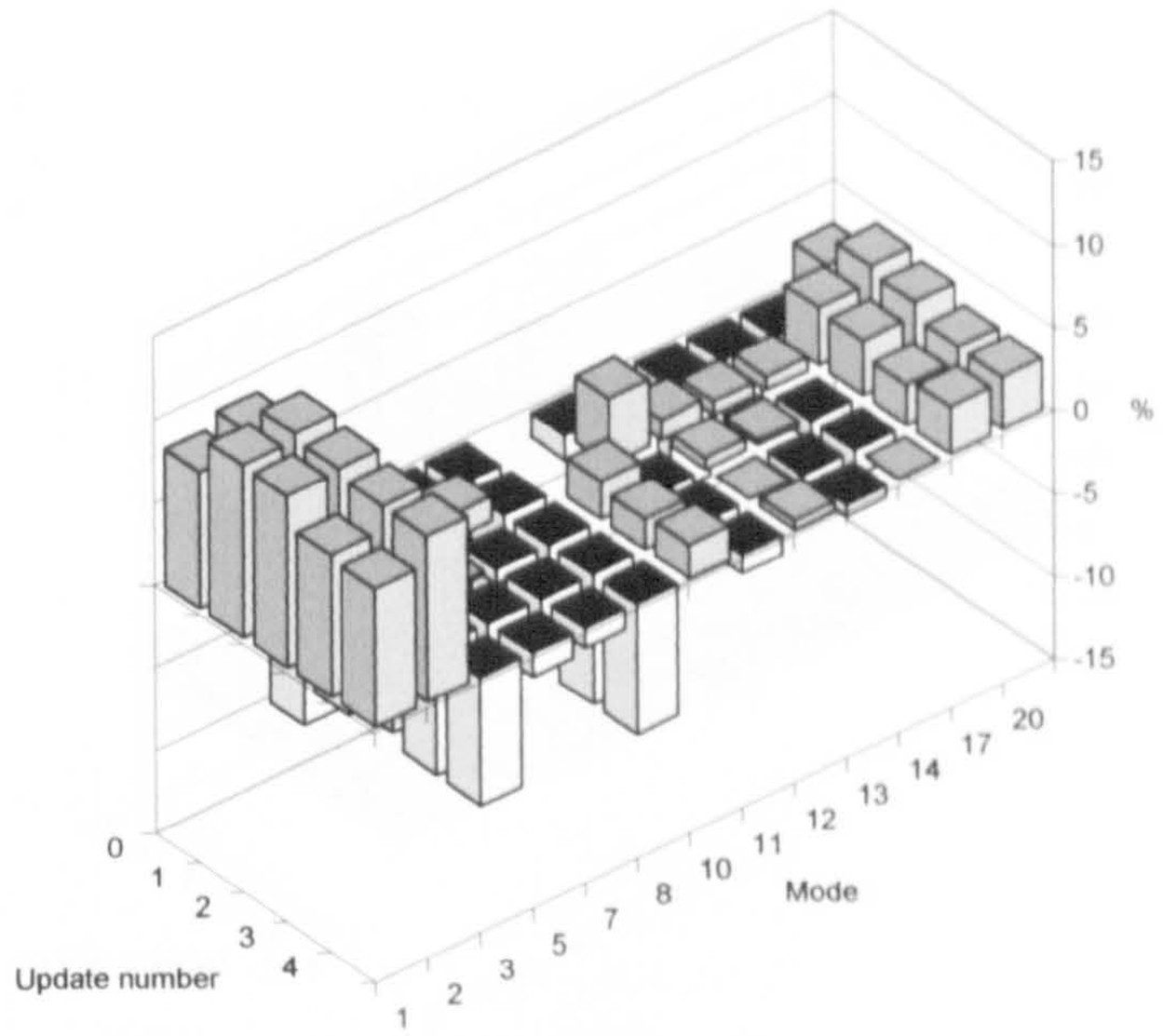

Figure 6-13: Percentage error between FEM updates and measured natural frequencies of deck 8 at 250kN

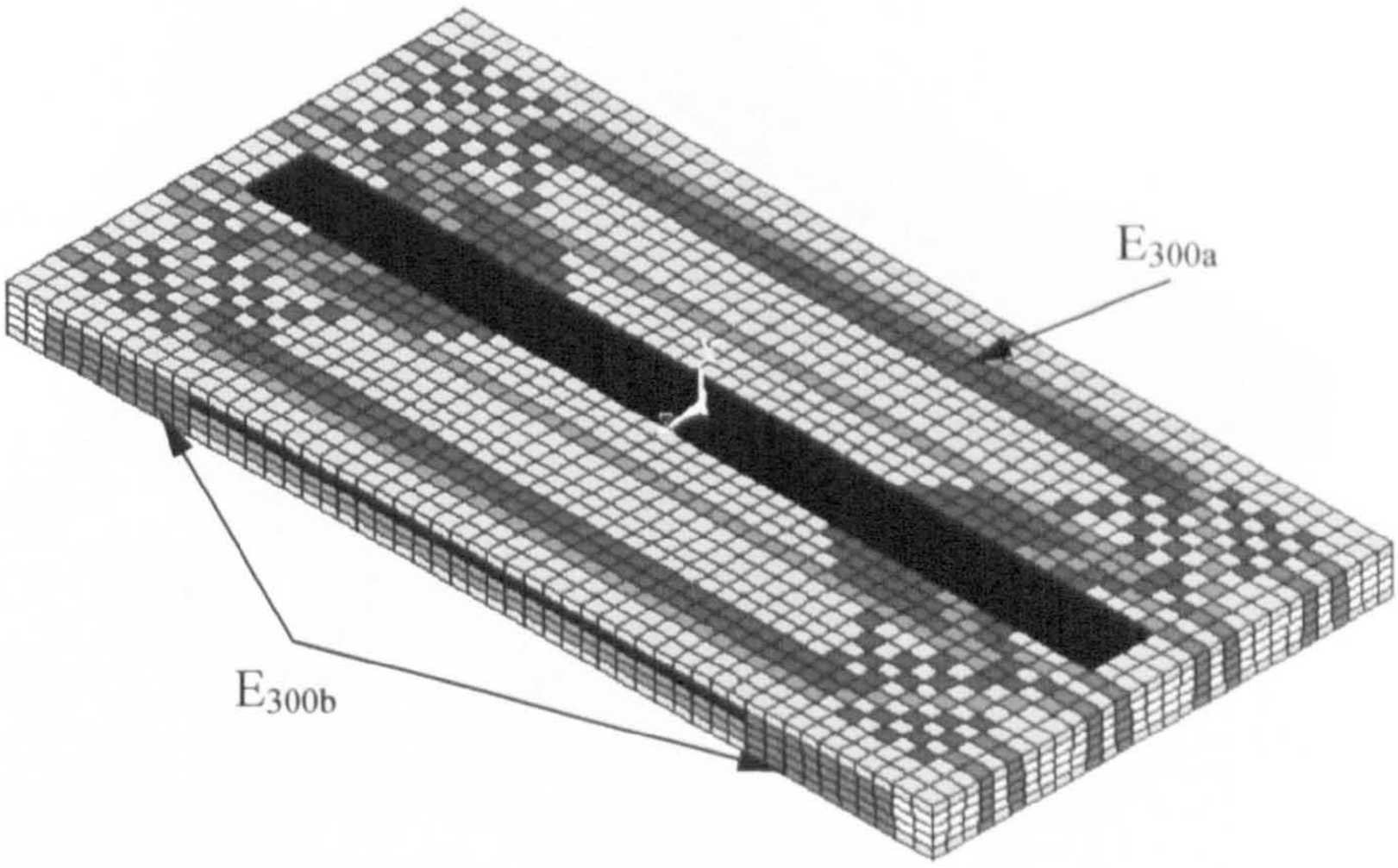

Figure 6-14: Areas assigned different material properties to model a symmetrically damaged deck at 300kN

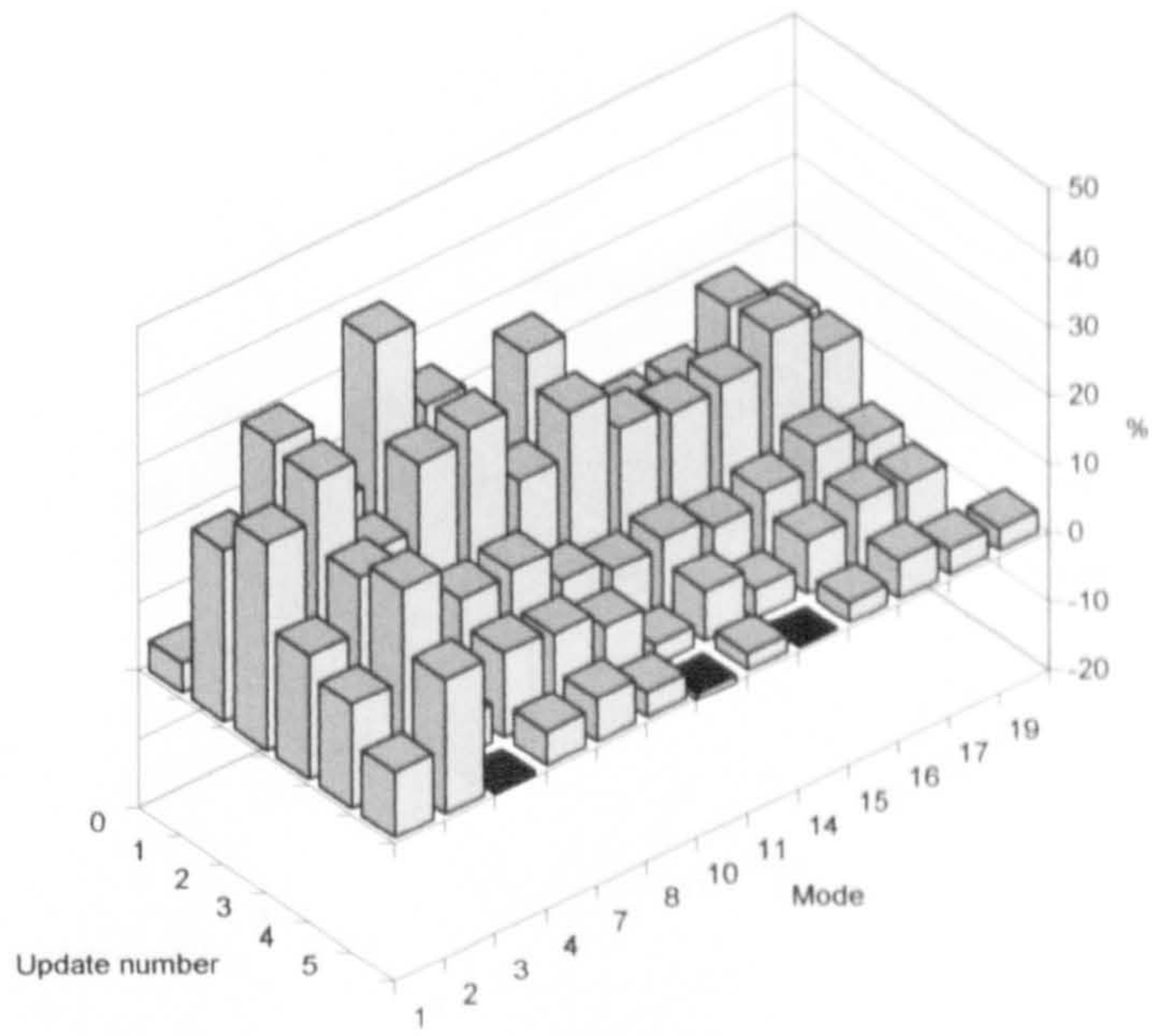

Figure 6-15: Percentage error between FEM updates and measured natural frequencies of deck 8 at 300kN

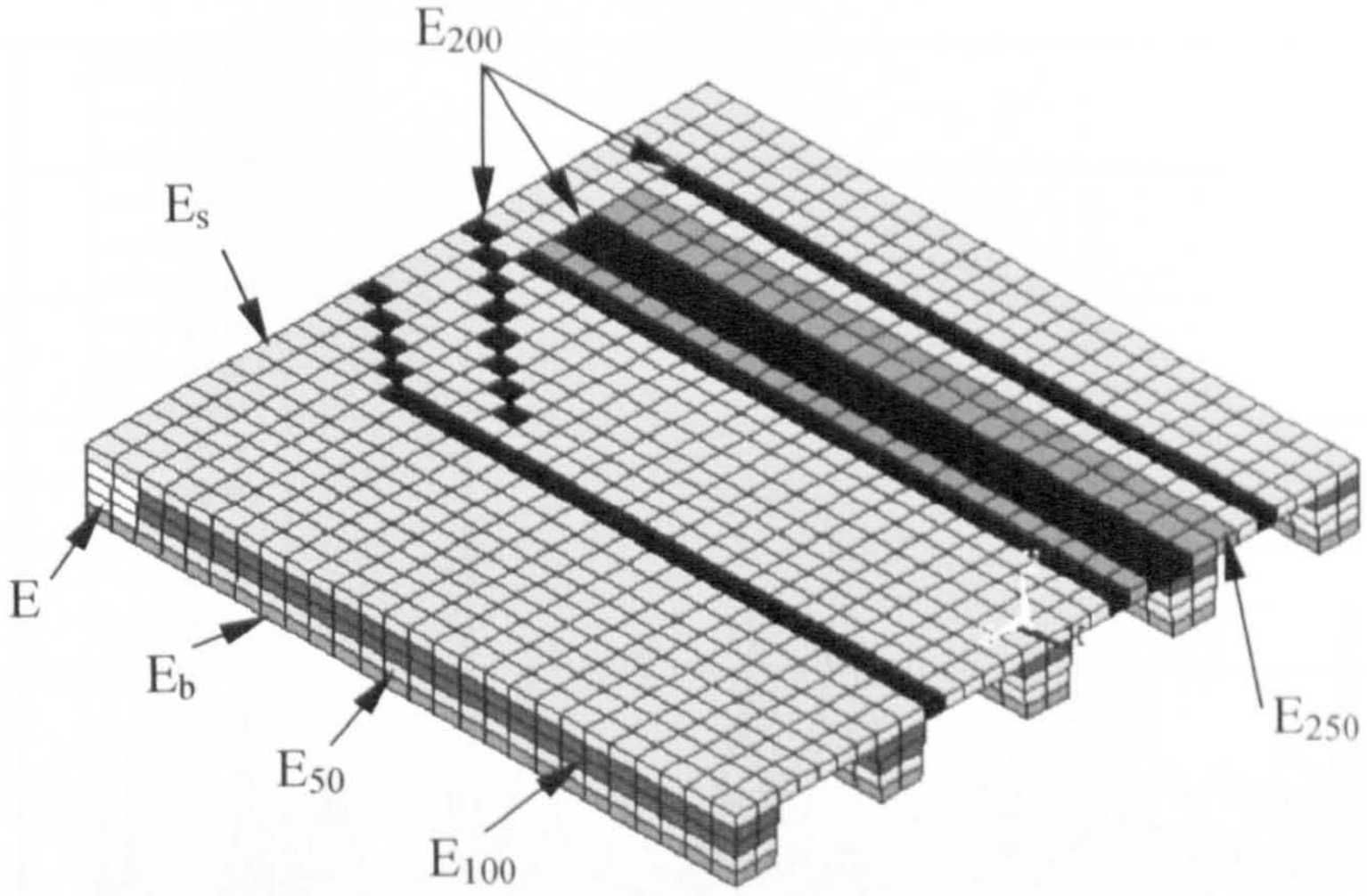

Figure 6-16: Areas assigned different material properties to model the damage in a HB loaded deck up to 250kN, showing the variation in the beams

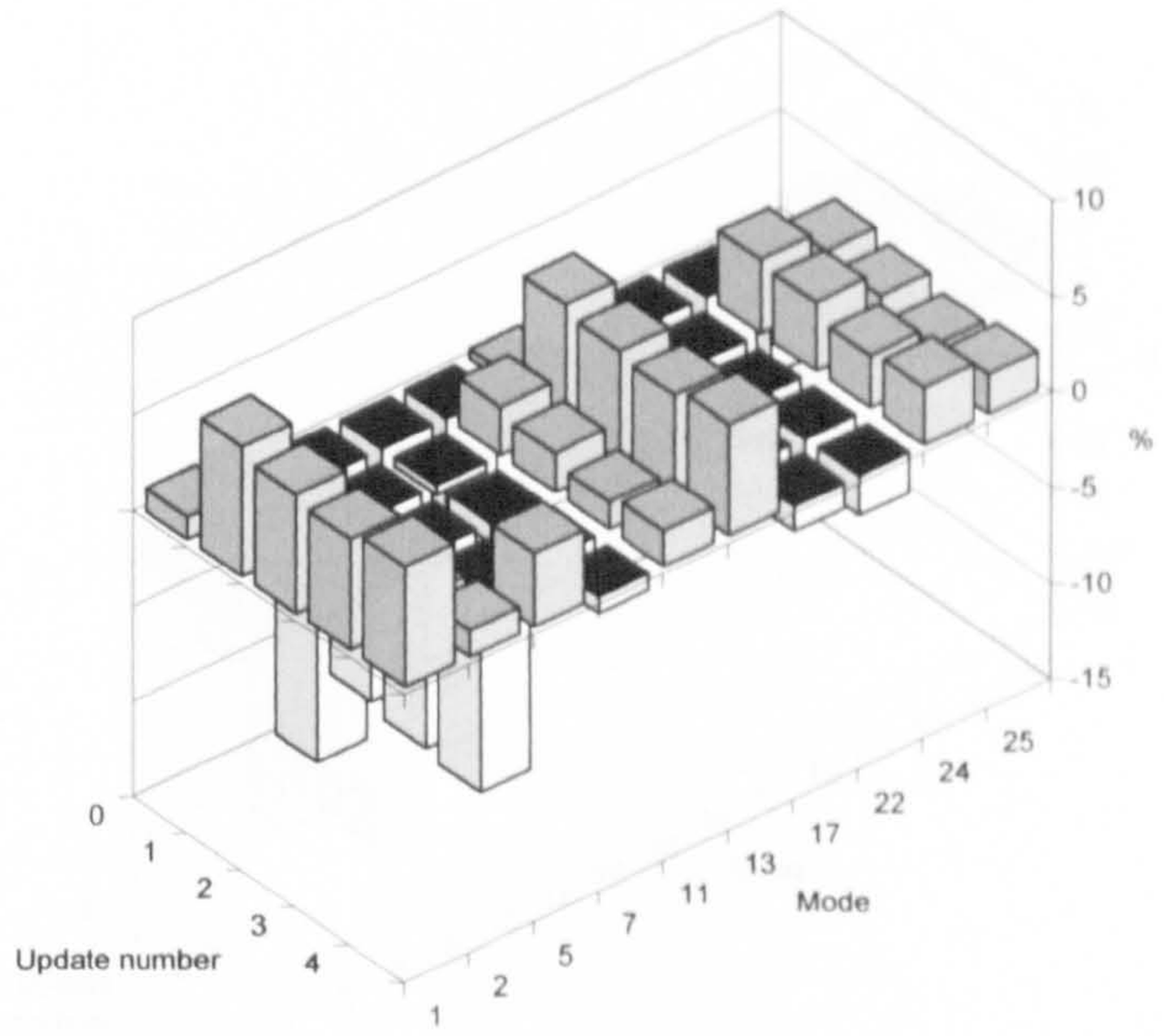

Figure 6-17: Percentage error between FEM updates and measured natural frequencies of deck 9 at 0kN

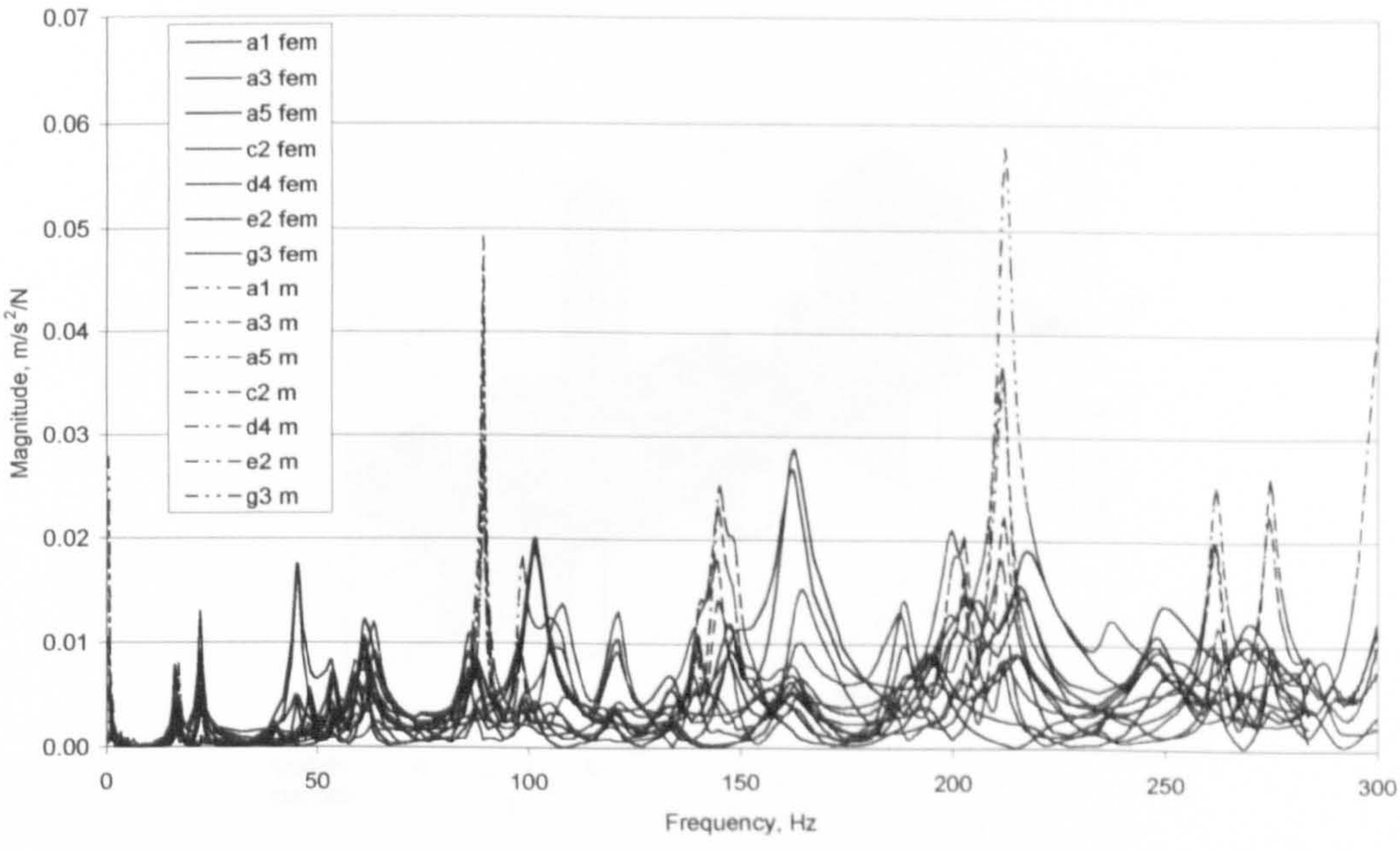

Figure 6-18: Measured and updated FEM FRFs for deck 9 at 0kN

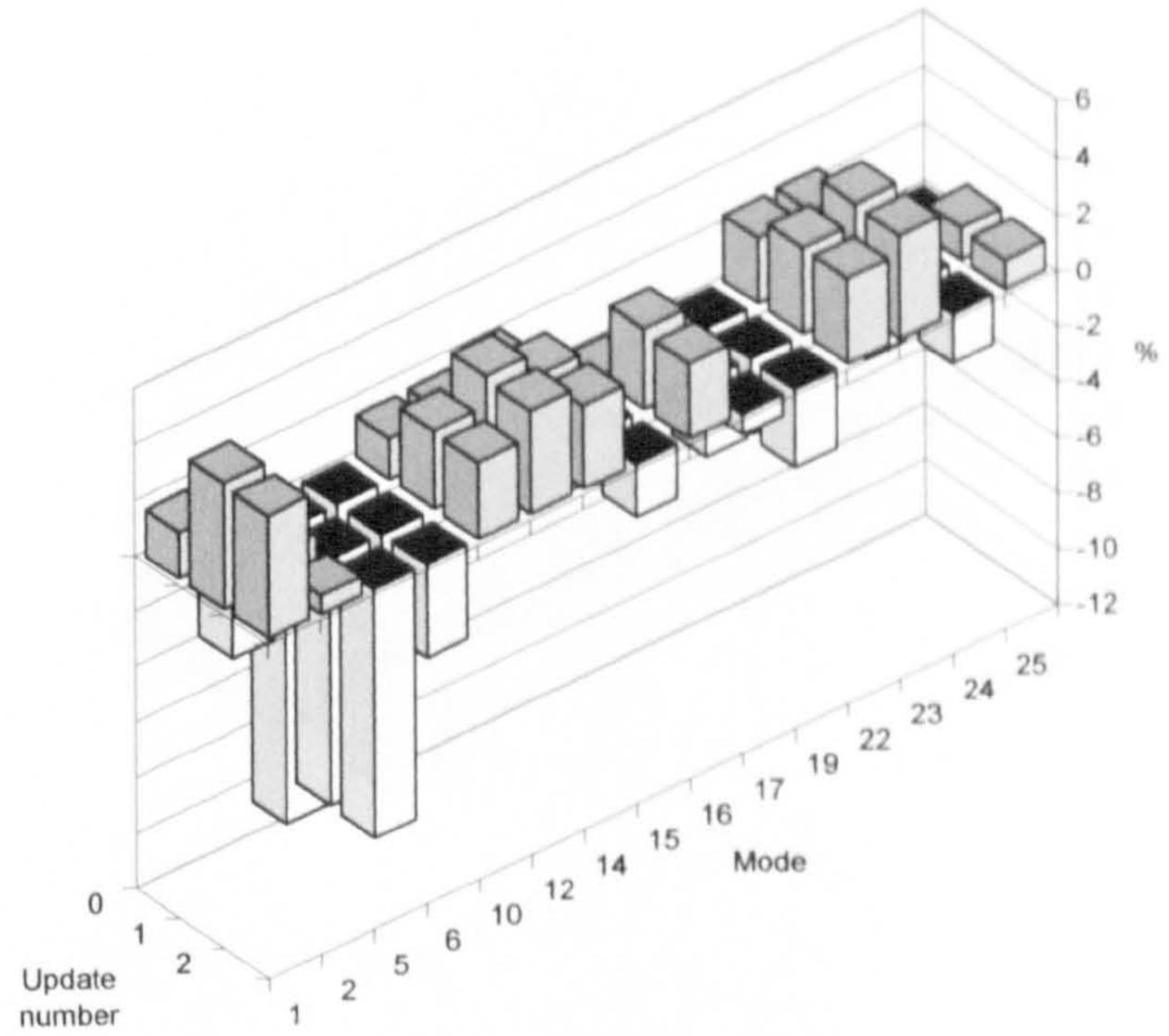

Figure 6-19: Percentage error between FEM updates and measured natural frequencies of deck 9 at 50kN

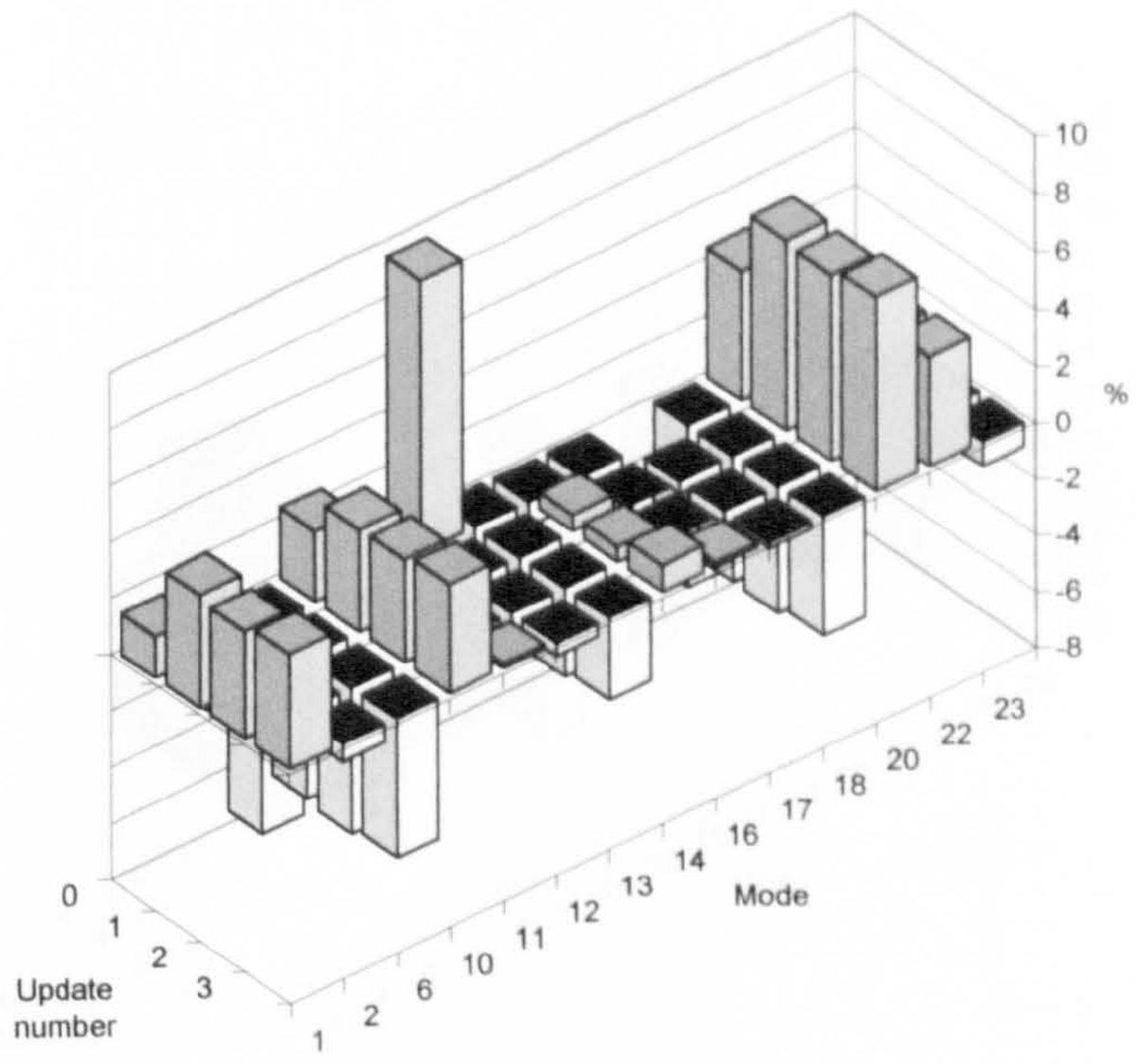

Figure 6-20: Percentage error between FEM updates and measured natural frequencies of deck 9 at 100kN

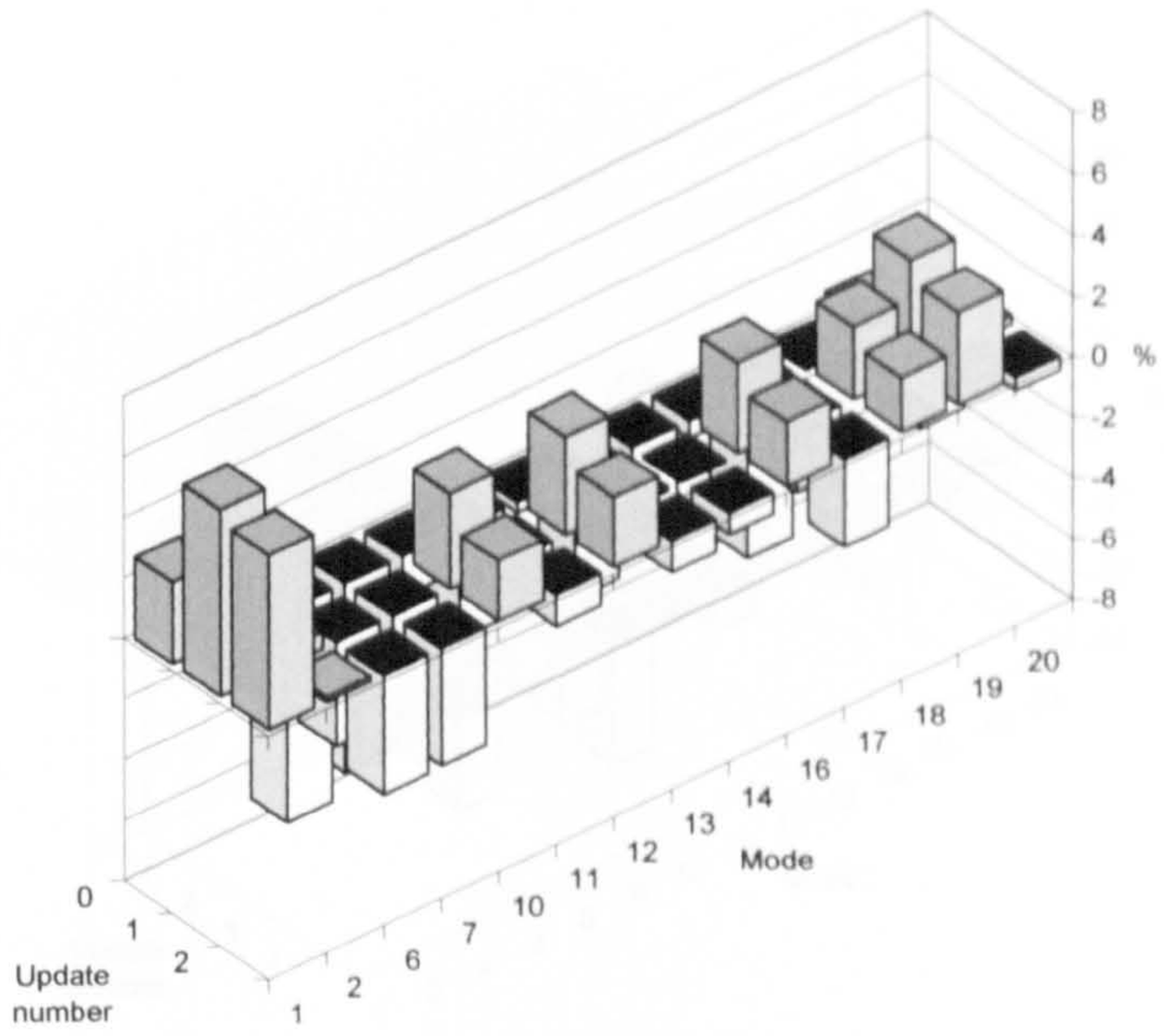

Figure 6-21: Percentage error between FEM updates and measured natural frequencies of deck 9 at 150kN

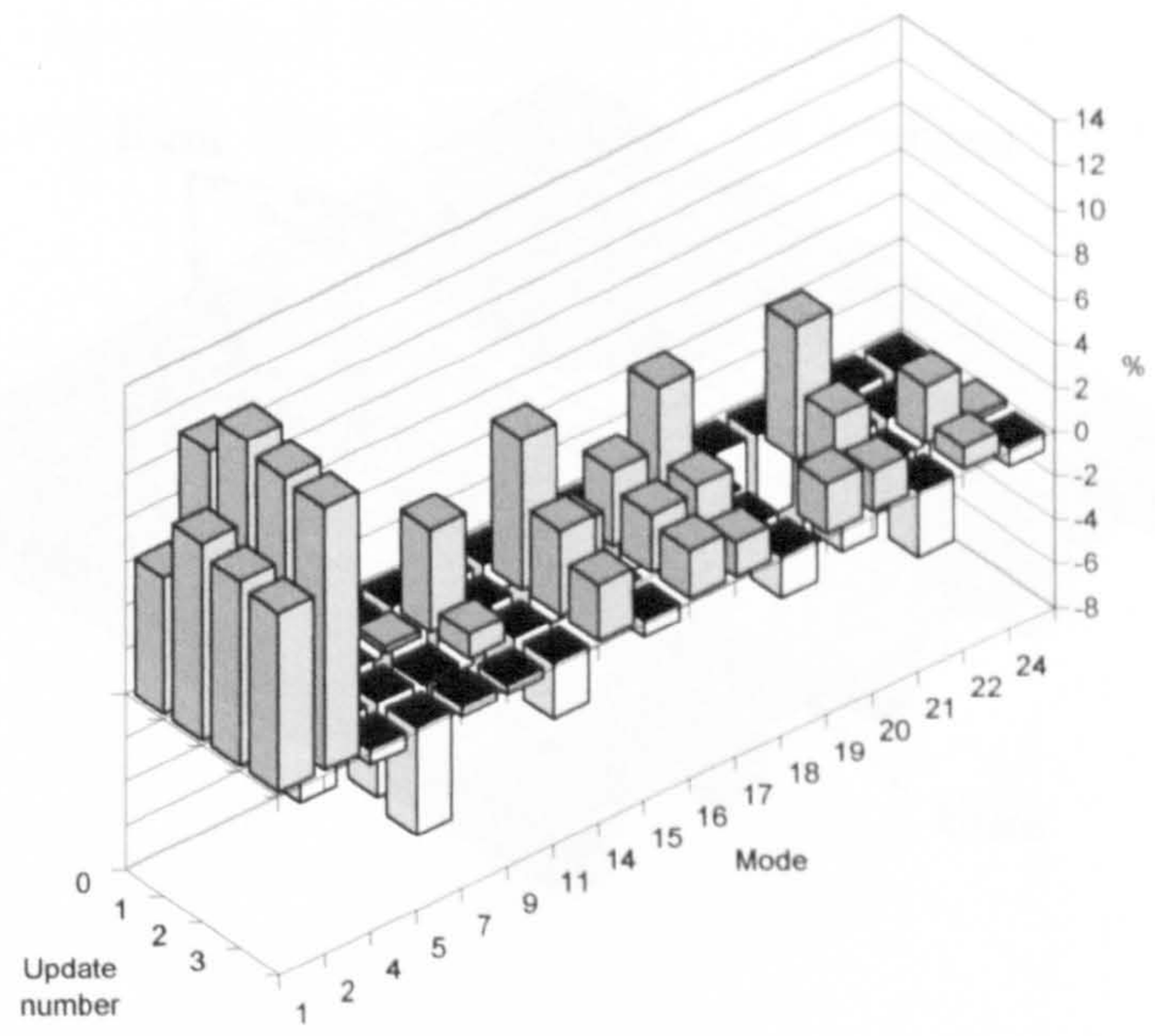

Figure 6-22: Percentage error between FEM updates and measured natural frequencies of deck 9 at 200kN

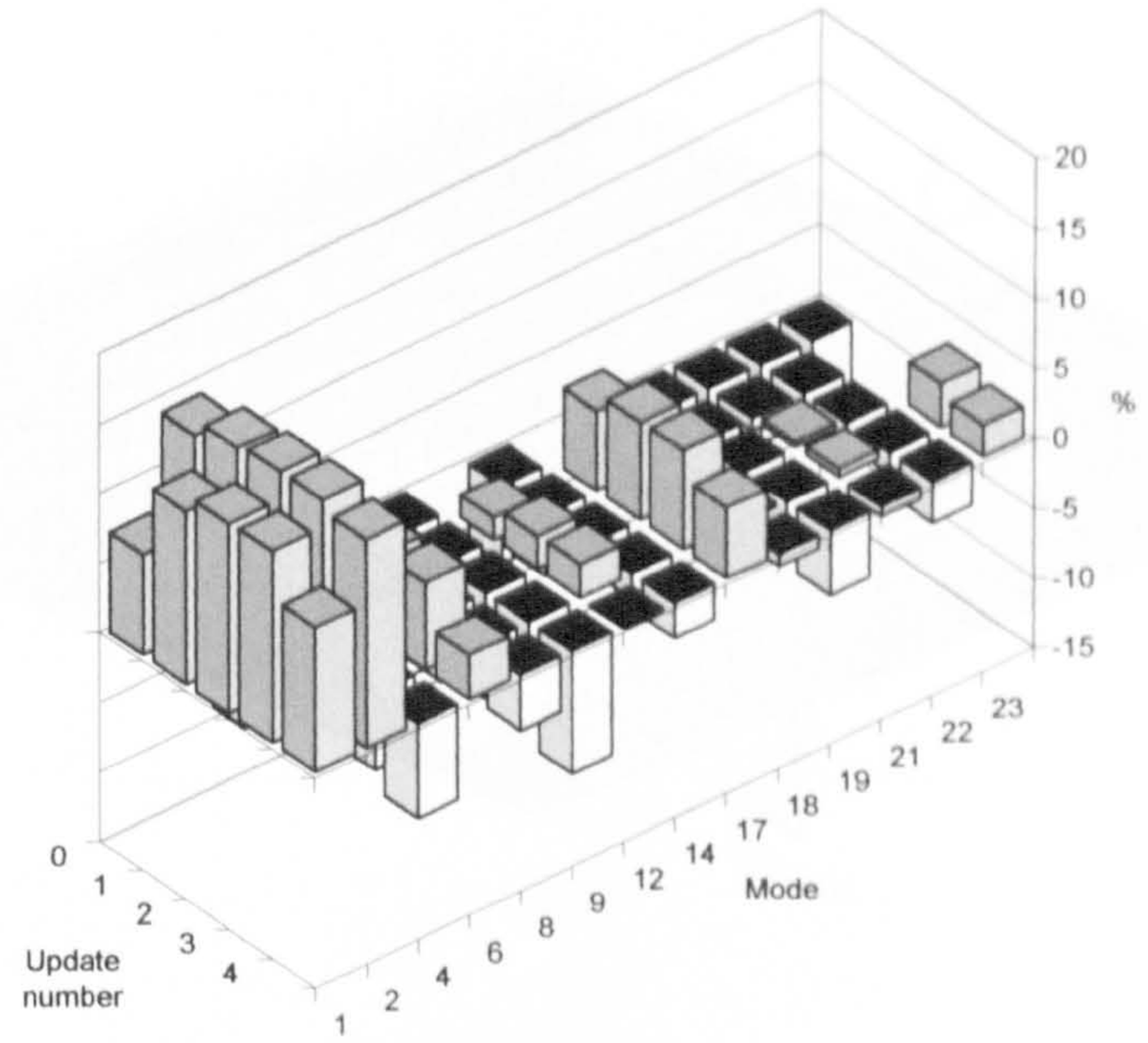

Figure 6-23: Percentage error between FEM updates and measured natural frequencies of deck 9 at 250kN

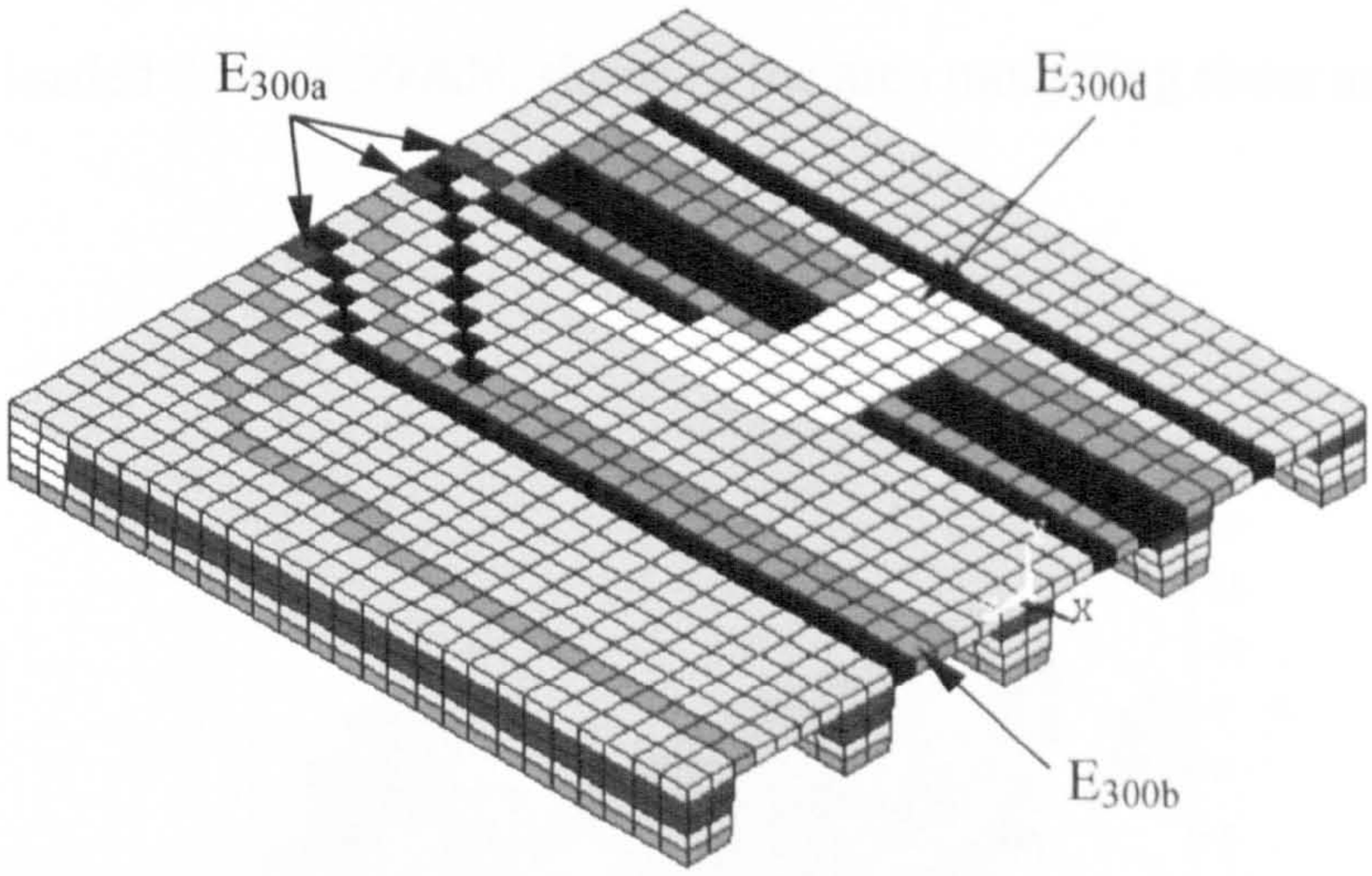

Figure 6-24: Areas assigned different material properties to model the damage in a HB loaded deck at 300kN, showing the variation in the beams

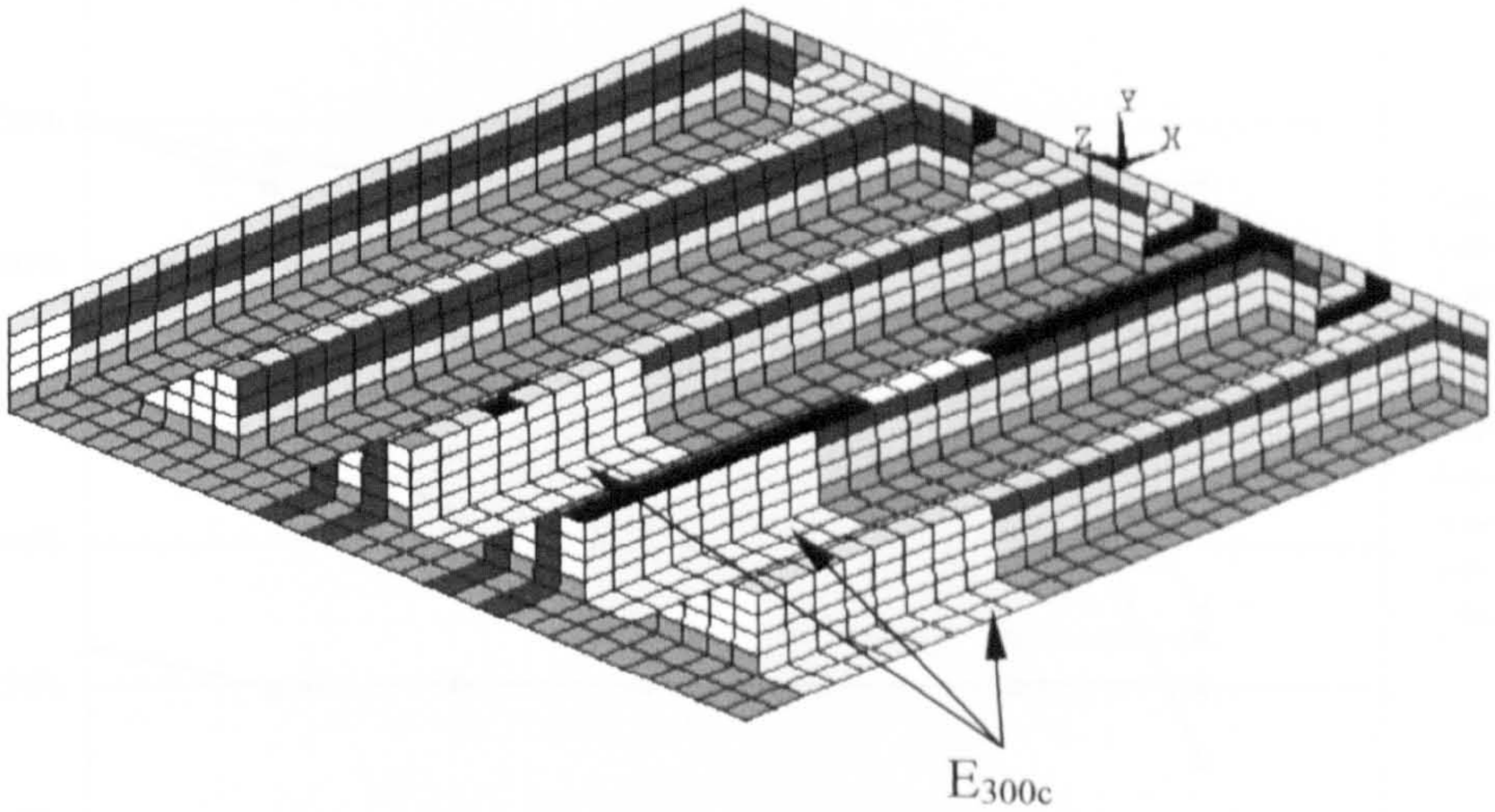

Figure 6-25: Areas assigned different material properties to model the damage in a HB loaded deck at 300kN, showing the area modelling shear and torsion cracking

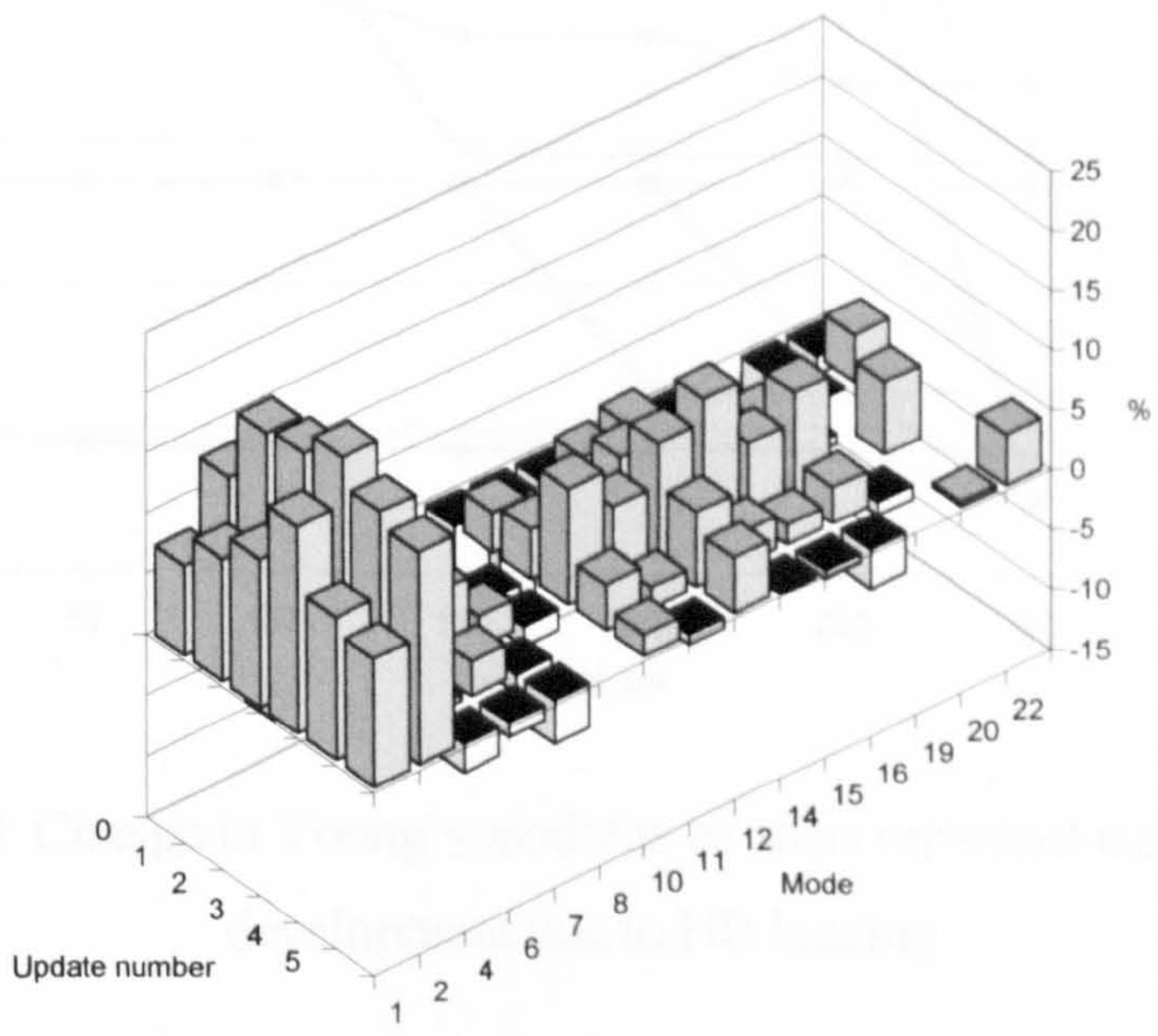

Figure 6-26: Percentage error between FEM updates and measured natural frequencies of deck 9 at 300kN

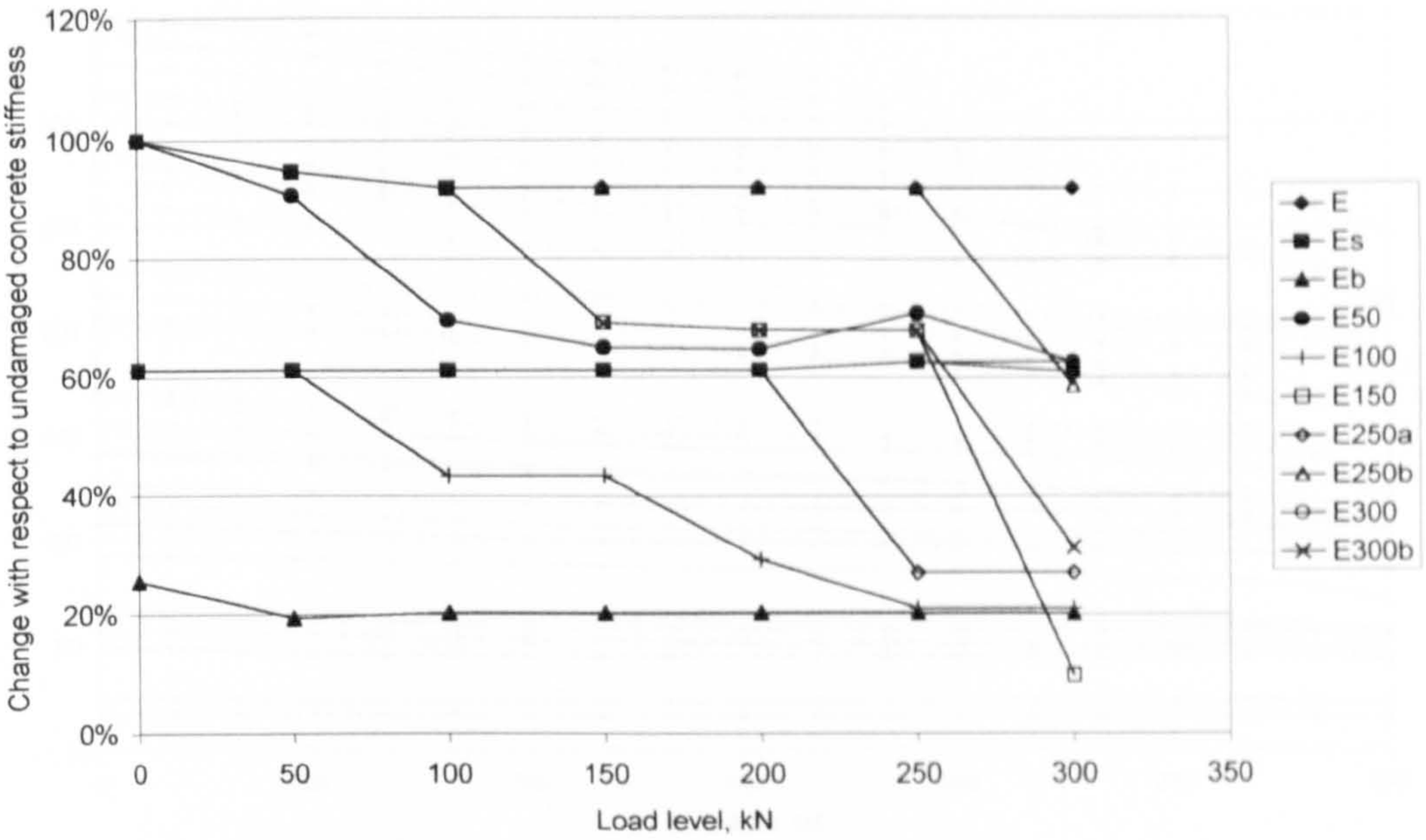

Figure 6-27: Change in Young's modulus of areas representing symmetrical damage development

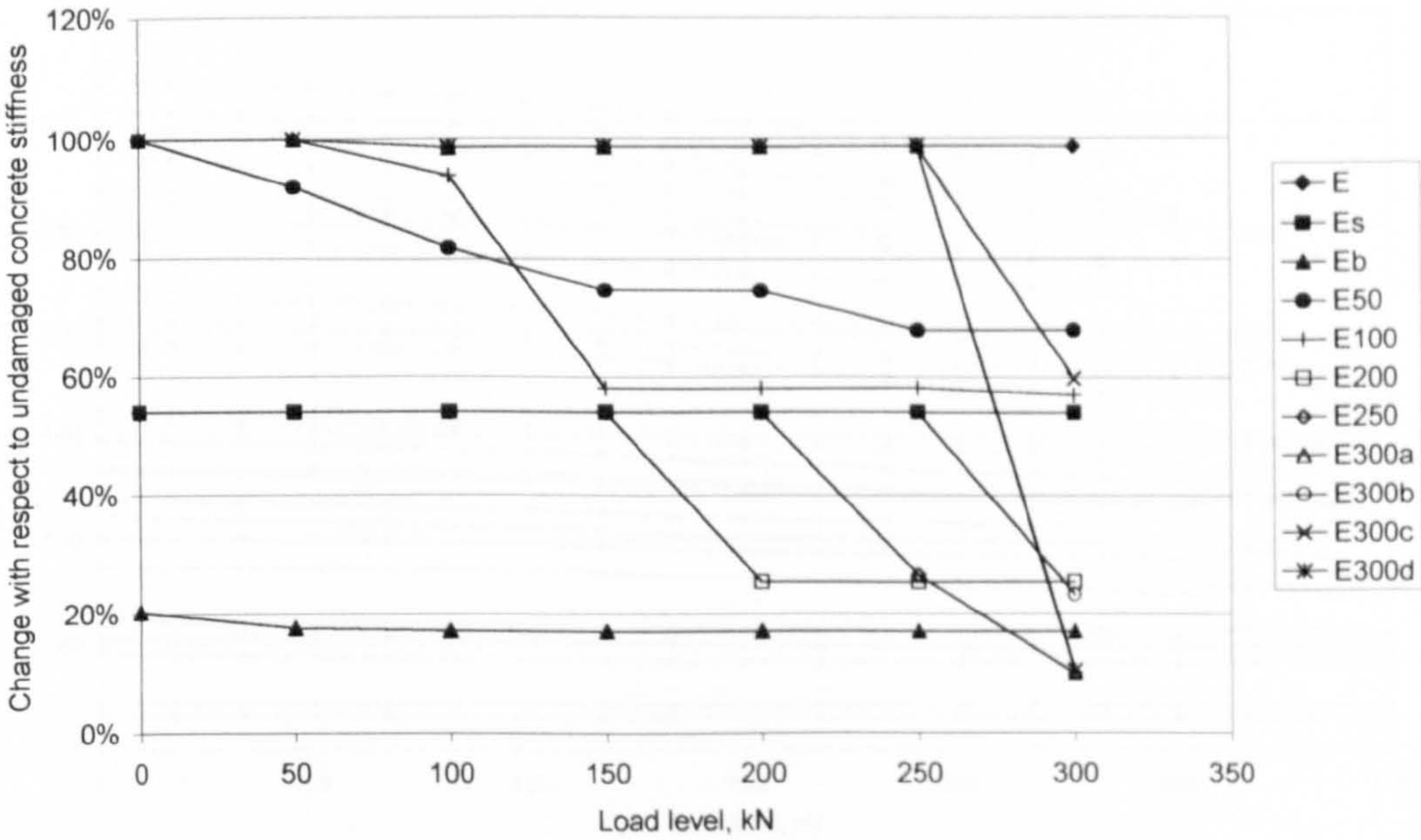

Figure 6-28: Change in Young's modulus of areas representing the damage development due to HB loading

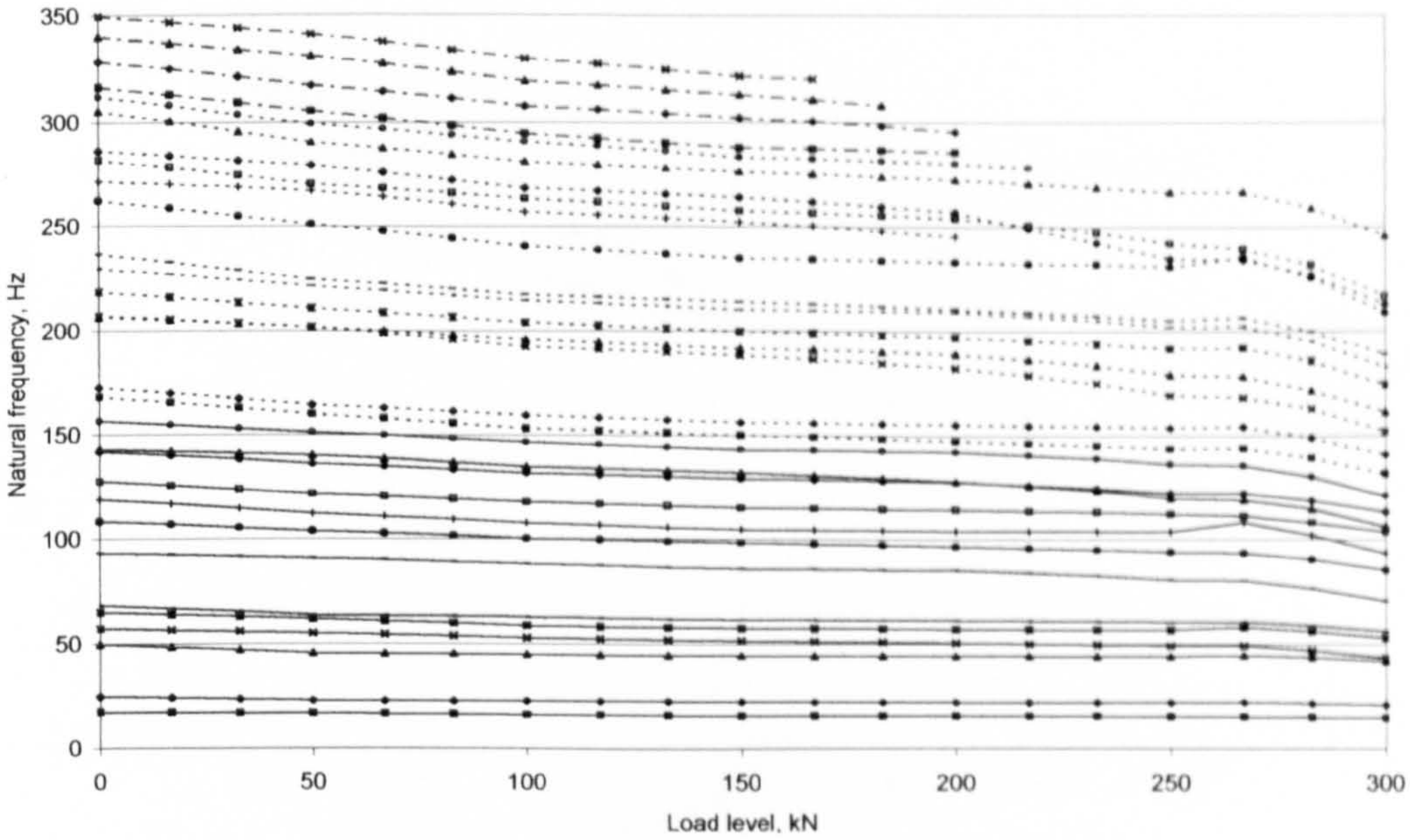

Figure 6-29: Natural frequencies of modes predicted by the FEM updated on deck 8

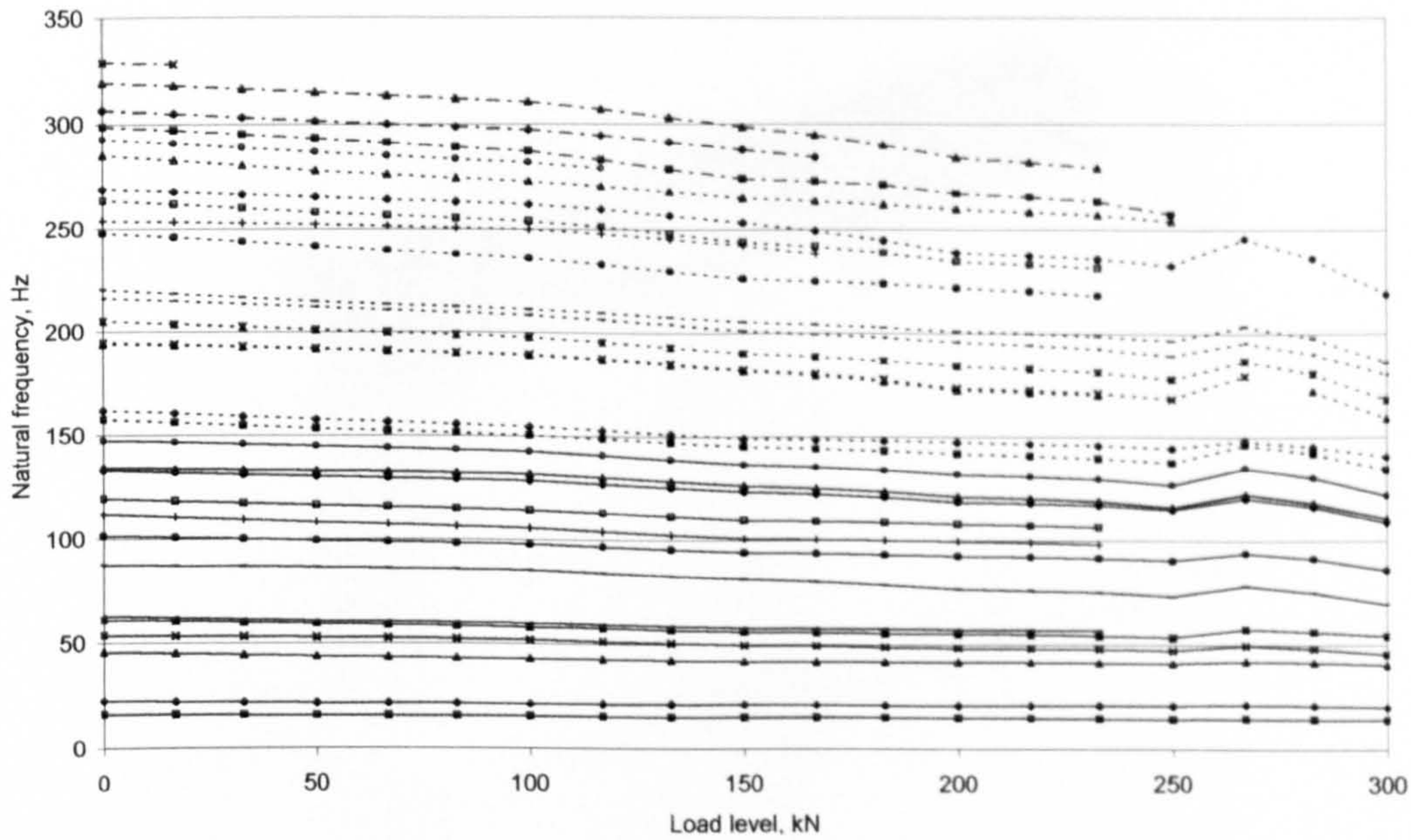

Figure 6-30: Natural frequencies of modes predicted by the FEM updated on deck 9

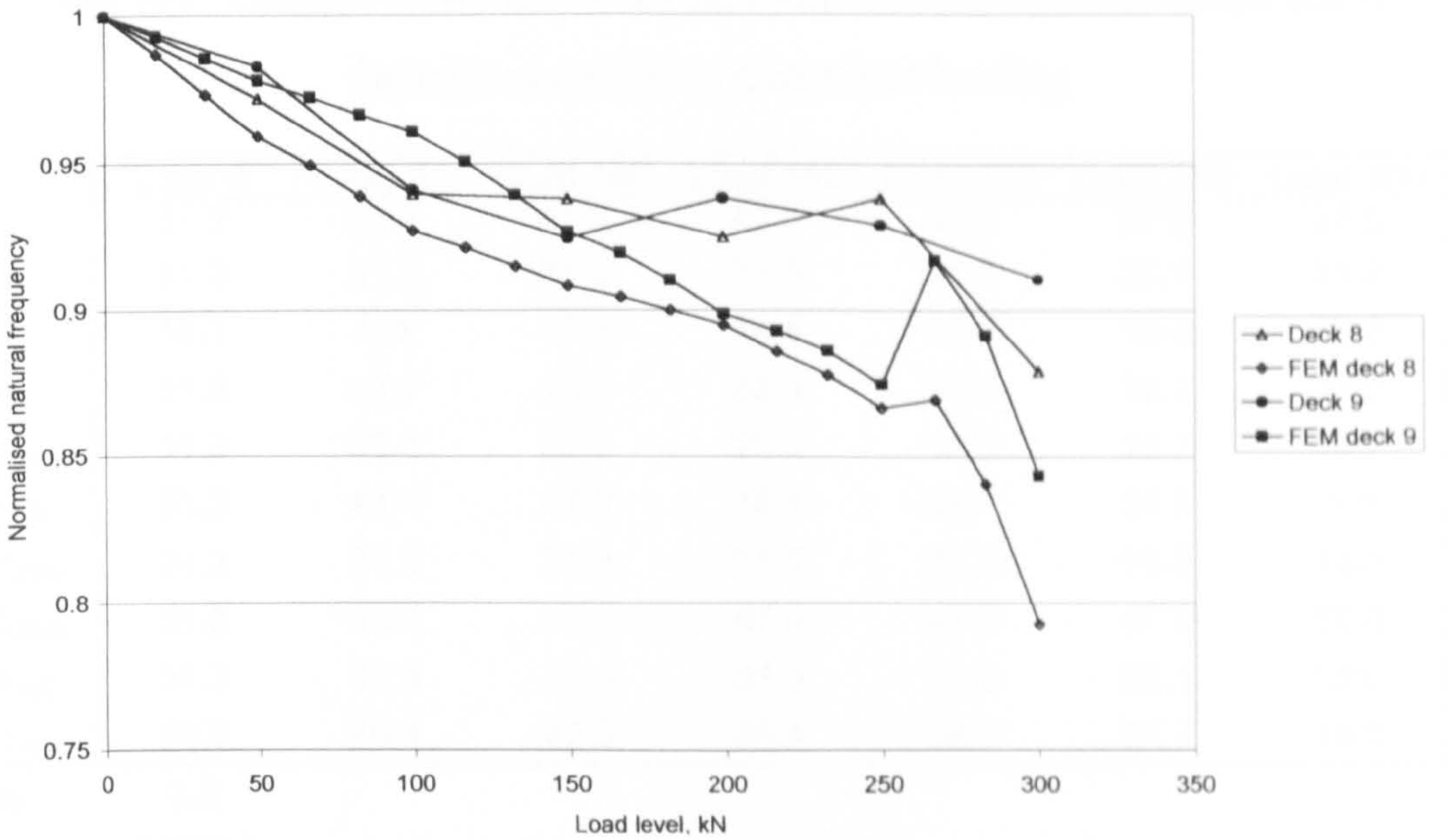

Figure 6-31: Average variation in natural frequencies found experimentally and by finite element modelling

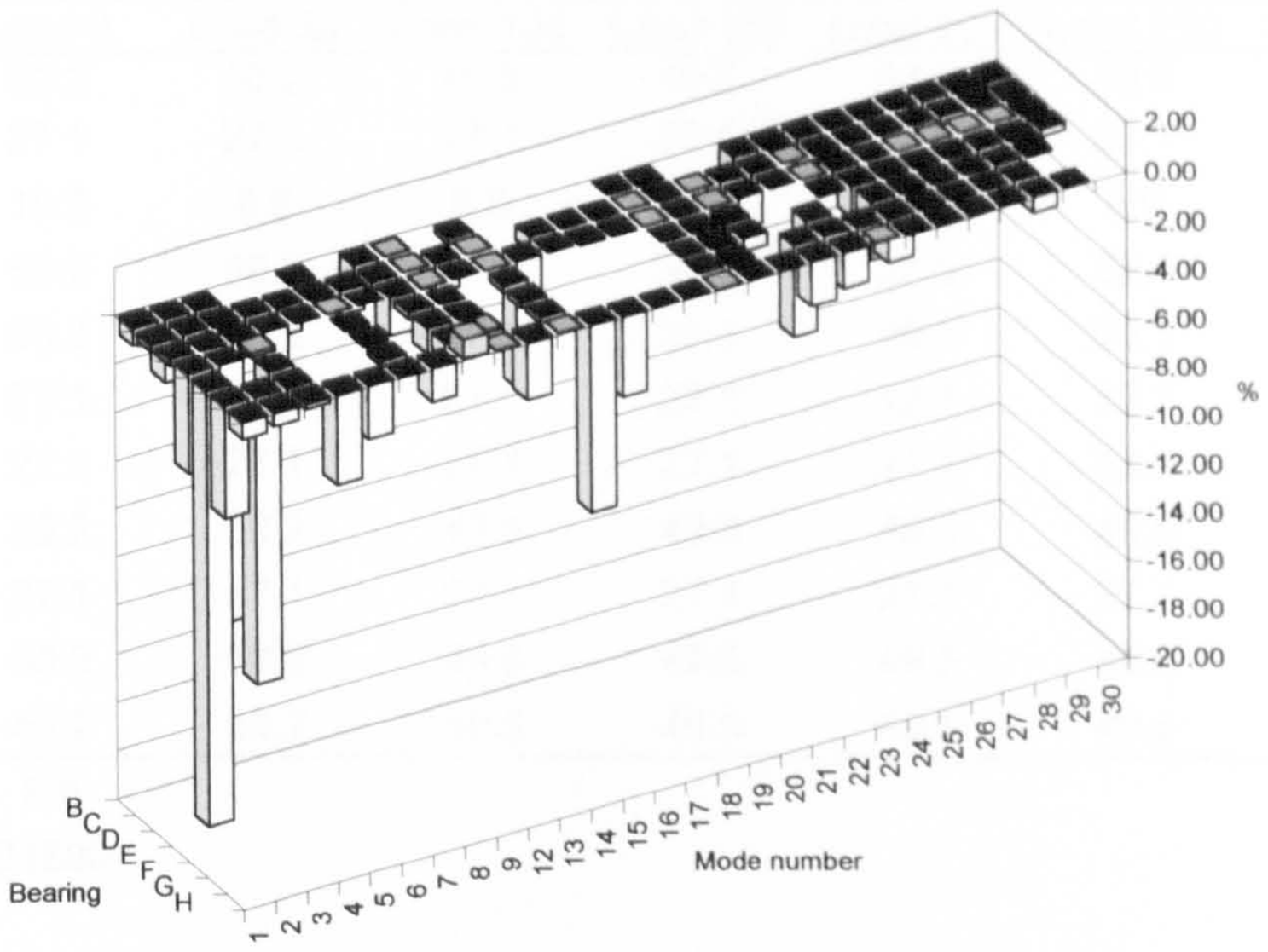

Figure 6-32: Percentage change in natural frequencies of modes found using different support conditions

Table 6-1: Young's modulus values (kN/mm^2) of the deck materials due to damage caused by symmetrical loading

	Load 0	Load 50	Load 100	Load 150	Load 200	Load 250	Load 300
E	51.2	48.4	47.0	47.0	47.0	47.0	47.0
E_s	31.3	31.3	31.3	31.3	31.3	32.1	31.2
E_b	13.1	9.9	10.4	10.4	10.4	10.4	10.3
E_{50}	51.2	46.4	35.7	33.3	33.1	36.2	32.0
E_{100}	31.3	31.3	22.2	22.2	14.9	10.7	10.7
E_{150}	51.2	48.4	47.0	35.4	34.7	34.7	5.0
E_{250a}	31.3	31.3	31.3	31.3	31.3	13.8	13.8
E_{250b}	51.2	48.4	47.0	47.0	47.0	47.0	30.0
E_{300}	31.3	31.3	31.3	31.3	31.3	32.1	32.0
E_{300b}	51.2	48.4	47.0	35.4	34.7	34.7	16.0
k_B	8.9						
k_T	492000						

Table 6-2: Young's modulus values (kN/mm^2) of the deck materials due to damage caused by HB loading

	Load 0	Load 50	Load 100	Load 150	Load 200	Load 250	Load 300
E	50.2	50.2	49.5	49.5	49.5	49.5	49.5
E_s	27.1	27.1	27.1	27.1	27.1	27.1	27.0
E_b	10.2	8.8	8.6	8.6	8.6	8.6	8.6
E_{50}	50.2	46.2	41.1	37.5	37.5	34.1	34.1
E_{100}	50.2	50.2	47.1	29.1	29.1	29.1	28.5
E_{200}	27.1	27.1	27.1	27.1	12.7	12.7	12.7
E_{250}	27.1	27.1	27.1	27.1	27.1	13.3	5.0
E_{300a}	50.2	50.2	49.5	49.5	49.5	49.5	5.0
E_{300b}	27.1	27.1	27.1	27.1	27.1	27.1	11.7
E_{300c}	50.2	50.2	49.5	49.5	49.5	49.5	30.0
E_{300d}	50.2	50.2	49.5	49.5	49.5	49.5	5.3
k_B	9.8						
k_T	21500						

Table 6-3: Bearing configurations (o indicates full stiffness, * indicates negligible stiffness)

Bearing number	Bearing configuration							
	A	B	C	D	E	F	G	H
1	o	*	o	o	*	*	*	o
2	o	o	*	o	*	*	*	*
3	o	o	o	*	o	*	o	o
4	o	o	o	o	o	o	o	*
5	o	o	o	o	o	o	o	o
6	o	o	o	o	o	o	o	o
7	o	o	o	o	o	o	o	o
8	o	o	o	o	o	o	o	o
9	o	o	o	o	o	o	*	o
10	o	o	o	o	o	o	*	o

Table 6-4: Percentage change in natural frequencies of modes found using different support conditions

		Bearing configuration						
		B	C	D	E	F	G	H
Mode number	1	-0.70	-0.33	-0.31	-4.09	-18.02	-4.69	-0.76
	2	-2.63	-0.34	0.00	-10.73		-11.93	-0.59
	3	-1.23	-0.09	-0.47	0.16	-0.84	-0.62	-0.25
	4		-1.69	-1.49				-3.78
	5		-1.25	-0.01				-2.24
	6	-0.05	-0.04	0.00	-0.06	-0.06	-0.22	-0.06
	7		-1.09	-0.01				-1.43
	8	-1.01	-0.30	-1.64	-0.29	-1.10	-0.67	0.84
	9	0.02	0.01	0.01	-0.02	-0.03	0.10	0.01
	12		-1.18	-0.01				-2.43
	13	-0.25	0.00	0.00	-0.27	-0.27	-0.27	0.00
	14			-5.27				-7.81
	15		-0.62	-0.01				-3.38
	16		-0.01	-0.11				-0.01
	17		-0.01	-0.08				-0.02
	18	-0.01	0.00	0.00	-0.01	-0.01	-0.01	0.00
	19	-0.04	-0.01	-0.02	-0.04	-0.06	-0.14	-0.01
	20		0.00	0.00	-0.18	-0.54		-0.01
	21		-1.27	-1.27			-3.79	-1.87
	22	-0.86	-0.44	-0.01		-1.27	-1.99	-1.50
	23	-0.06	0.00	0.00	-0.08		-0.42	0.00
	24	-1.10	-0.05	-0.76	-1.28	-2.41	-1.86	-0.08
	25	-0.03	-0.01	0.00	-0.04	-0.05	-0.07	-0.03
	26	-0.04	-0.01	0.00	-0.04	-0.04	-0.05	-0.02
	27	-0.02	0.00	0.00	-0.02	-0.02	-0.03	-0.01
	28	-0.68	-0.32	0.00	-0.88	-0.89	-0.91	-0.68
	29	-0.08	-0.02	0.00	-0.09	-0.09		-0.03
	30	-0.21	-0.08	-0.11	-0.29			

CHAPTER 7

CONCLUSIONS AND FURTHER WORK

7.1 Conclusions

In the introduction, it was reported that the UK Highways Agency are currently aiming to introduce more monitoring into the bridge inspection programme to develop more efficient management procedures. This study is concerned with the feasibility of using vibration characteristics as a structural health-monitoring tool and aims to evaluate the sensitivity of the dynamic behaviour of a realistic simply supported reinforced concrete bridge deck specimen to damage caused by static loading.

This chapter is a summary of the work presented in the thesis and discusses the issues raised with regard to testing a realistic bridge deck specimen and the importance of these factors in the implementation of the method on real bridges.

The testing was performed on a one-quarter-scale reinforced concrete bridge deck, designed to be typical of bridges constructed in the 1960s as these structures are now suffering from significant deterioration. Two reinforcement arrangements were investigated, type A (full flexural and shear provision) and type B (deficient in shear reinforcement) to study the development of different failure mechanisms and the effect on the vibration characteristics of the decks.

Three loading regimes were used to cause damage to the decks in the form of specific types of cracking and failure. These were symmetric, asymmetric 4-point bending and HB loading, designed to cause the failure of a single beam, multiple beams and mimic vehicle overloading, respectively. Static loading

was used to enable close control of the cracking and failure mechanisms that developed, and the produce cracking typical of that observed in bridges.

The vibration characteristics of the decks were measured at a number of load increments throughout the loading history of the decks to determine the sensitivity of the dynamic properties to damage. Three support conditions were investigated for the dynamic testing of the decks: ten steel bearings, three steel bearings and ten rubber bearings. Ten steel bearings were used to maintain the realistic nature, permitting some of the issues with regard to the application of the method to real bridges. Three bearings allowed the vibration characteristics of the deck to be measured without contamination of the results from the indeterminate supports. Using ten rubber bearings gave improved measurement of natural frequencies and mode shapes, but this was limited by the highly non-linear behaviour of the material.

Finite element model updating based on the modal properties of one deck loaded symmetrically and one loaded under the HB arrangement was performed to systematically investigate the flexural stiffness reduction as the deck was damaged. The results, in particular the cracking patterns, of the static loading of the decks were used to determine the areas that should exhibit a loss of stiffness due to cracking. The Young's modulus in these regions was modified using the eigen-sensitivity matrix to obtain better correlation with the natural frequencies measured in the laboratory.

Finite element modelling was also used to predict the dynamic properties of the decks at load levels not measured in the laboratory testing. This was achieved by interpolating the updated Young's modulus values found previously, and, in order to investigate the effect of changes in the support conditions, by reducing the stiffness of spring supports modelling the bearings.

The main findings can be summarised as follows:

- The different loading regimes produced distinctive cracking patterns and load-deflection curves, and caused the growth of certain types of cracks in several stages, indicating that the deck failed in a progressive collapse

- The slab of the deck contributed significantly to the ultimate load capacity and ductility by spreading the load applied to all the longitudinal beams, providing significantly more ductile behaviour in the type A decks than the type B decks

- Type A decks exhibited cracking consistent with flexural failure of the beams until application of the final load increment, when failure was by shear, torsion or excessive deflection of a beam

- Type B decks displayed some flexural cracking, but ultimate failure was due to insufficient shear reinforcement causing a sudden shear or torsion failure of the beams

- Cracking patterns produced by loading the type A decks were consistent with yield-line patterns found in slabs, and the application of yield-line theory produced a good correlation with ultimate load when membrane action was taken into account

- A consistent trend in the change of natural frequencies of the bridge decks when undergoing progressively more severe cracking was found

- There was a significant spread in the natural frequency reductions for each deck making the comparison of results difficult. This variation was caused by several factors, including the stiffness distribution and boundary conditions

- The changes in the mode shapes are not consistent when measured using the MAC algorithm, and were only affected significantly when highly localised damage occurred

- Changes in the natural frequency of some modes appeared to be more sensitive to the cracking introduced than others, depending on the nature of the cracks

- From the three support conditions investigated, the effects of indeterminate boundary conditions led to a significant change in the dynamic behaviour

- Significant changes in stiffness of the decks and slightly altered boundary conditions between each load increment created considerable problems in tracking modes through the loading histories
- Finite element model updating provided a suitable method to determine possible changes in the structure due to damage using the natural frequencies, although judgement and prior knowledge of the changes in the system were required
- The regions to be updated were based on observations of the cracking due to static loading, but, for real bridges could be provided by the results of the inspection procedure that determined the bridge should be monitored
- Whilst trends in the changes to natural frequency were observed, this was often only consistent for the decks supported on three bearings. Maintaining realistic boundary conditions of the decks introduced considerable variation in the dynamic properties as these appeared to be highly sensitive to the support conditions
- This could be a significant issue if the method is employed on real bridges, as deterioration of the bearings is one of the more common problems encountered and, from this investigation, could lead to unexpected changes in the vibration properties measured
- If the effects of variations in the bearing condition can consistently be found, it may be possible that the method could also be used to indicate the condition of the bearings as well as the structural condition of the bridge

7.2 Further work

Several of the issues raised in this study carry important implications for the application of interrogating vibration characteristics for structural health monitoring of bridges. It has been demonstrated that there is potential in using dynamic properties for detecting damage of complex structures, although there remain several areas warranting further investigation.

- A more comprehensive and systematic study is necessary to investigate the effects of the bearing conditions on the vibration characteristics, as well as other deterioration mechanisms that would compromise the maintainability of the bridge
- The effects of more common types of deterioration need to be determined, by performing tests involving accelerated freeze-thaw action and sulphate and chloride attack
- An investigation is required into the sensitivity of the vibration characteristics and finite element model updating for smaller degrees and different types of deterioration
- Full-scale and field tests are required in order to determine the feasibility of implementing this monitoring procedure in terms of the cost/benefit compared to the existing inspection methods
- Other types of construction need to be investigated, for example composite and prestressed, to examine the applicability of dynamic testing to monitoring these structures
- Due to the difficulties experienced in interpreting modal properties as damage increases and the variability found, other methods based on a more statistical approach should be investigated

Preliminary tests on decommissioned bridge beams (Owen et al, 2002) indicated that there is significant potential in using methods based on utilising the complete FRF measured, even when the modal properties do not provide conclusive results, as shown in Figure 7-1. The beams were tested under field-testing conditions and exhibited three general classes of structural integrity: light damage, heavy damage and modified using carbon fibre plate bonding.

It was observed that the FRFs of the different beams contained different numbers of modes and each class of beam produced a distinctive shape of FRF. By examination of these FRFs, it was possible to determine to which class the beam belonged. To permit an objective investigation into the classification of the beams using the FRFs, the study employed principal component analysis. This has the effect of reducing the quantity of data by representing the FRFs

using a number of principal components. It was possible to distinguish the state of the beams using only a two-dimensional feature vector, Figure 7-2.

By reducing the quantity of data, it was possible to use more components in conjunction with a neural network, where it was found that it was possible to successfully classify the beams according to their damage state, as given in Table 7-1. However, the number of beams tested and their relatively well-spaced damage states limited this study, and it is therefore necessary to improve the reliability and applicability of this method by studying more damage cases and real bridge structures.

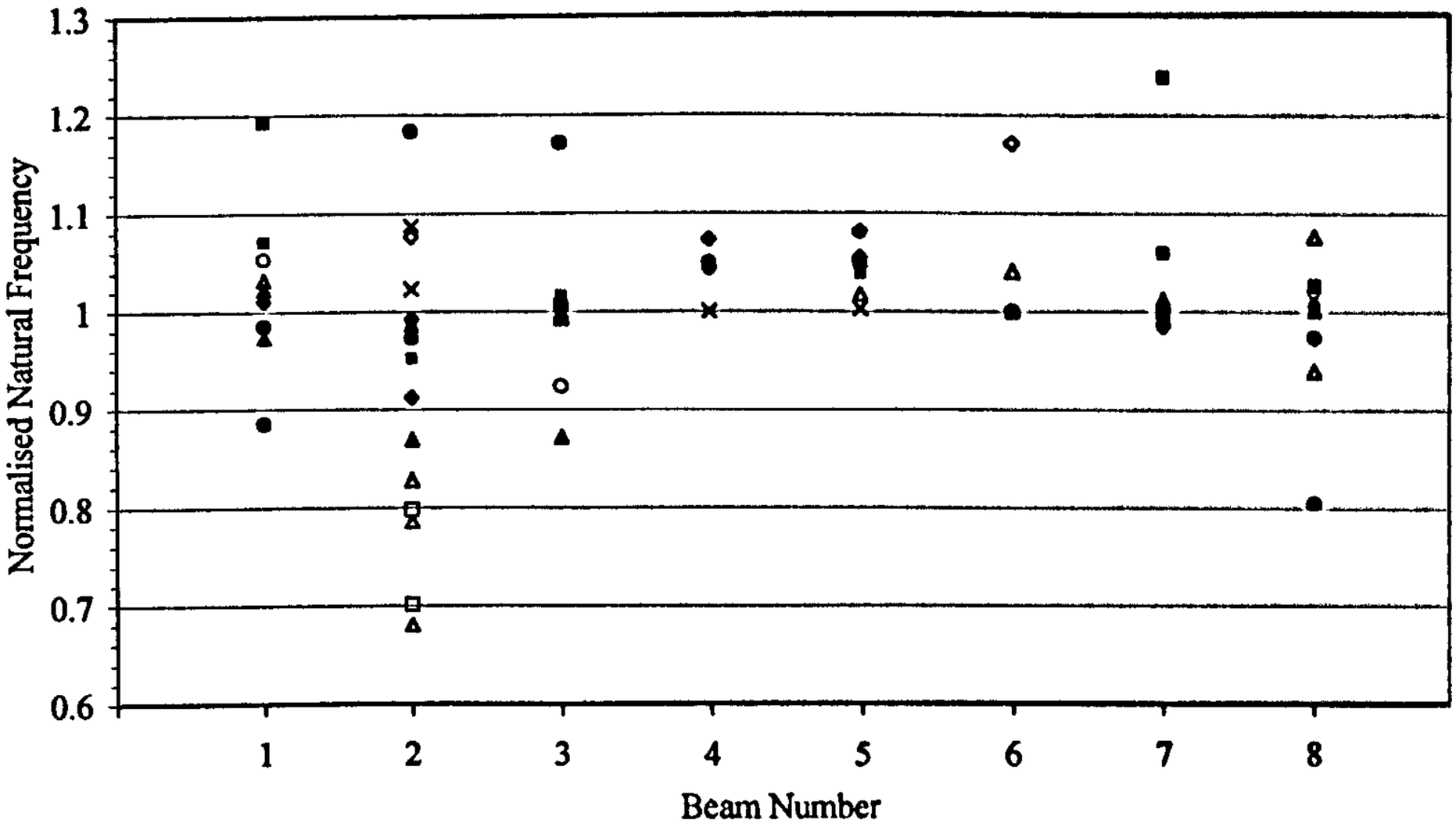

Figure 7-1: Normalised natural frequency change against beam type for all modes identified (Owen et al, 2002)

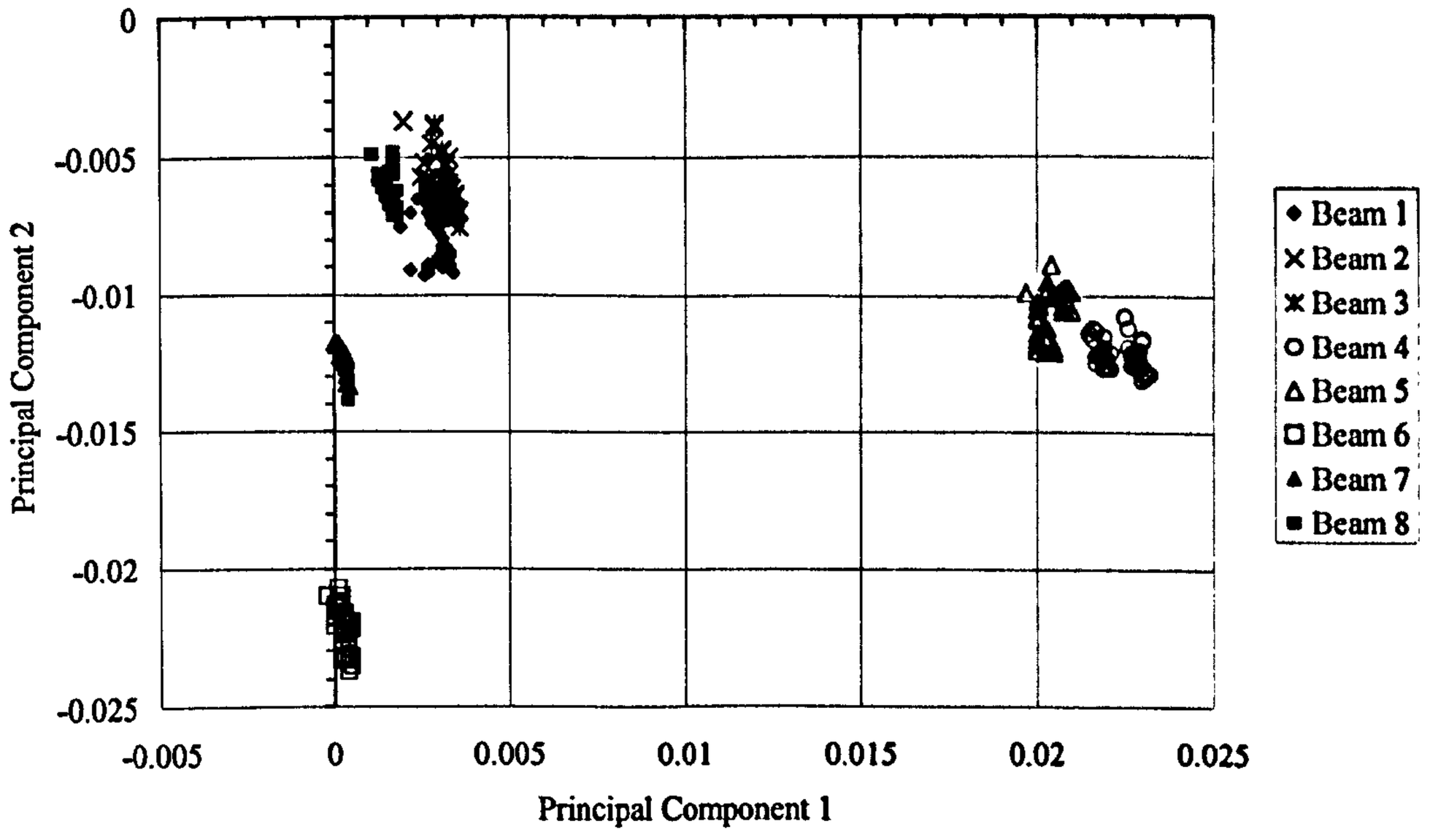

Figure 7-2: Feature vectors using first two principal components (Owen et al, 2002)

Table 7-1: Confusion matrices for neural network classifier (Owen et al, 2002)

		Training data			Test data			
		Predicted class						
			Class 1	Class 2	Class 3		Class 1	Class 2	Class 3
True class	Class 1	Class 1	90	0	0	Class 1	30	0	0
	Class 2	Class 2	0	60	0	Class 2	0	20	0
	Class 3	Class 3	0	0	90	Class 3	0	0	30

REFERENCES

Adams, D.E. (2002) "Frequency domain ARX model and multi-harmonic FRF estimators for non-linear dynamic systems", Journal of Sound and Vibration, 250(5), pp935-950

Adams, D.E. and Allemang, R.J. (1999) "Demonstration of multiple degree of freedom nonlinear system identification using time and frequency domain methods", Proceedings of the 17th International Modal Analysis Conference, Vol. 1, pp315-322

Aktan, A.E. et al (1997) "Objective global condition assessment", Proceedings of the 15th International Modal Analysis Conference, Vol. 1, pp364-373

Baker, C. (1999) "Wavelets in wind engineering", Workshop on Novel Data Analysis Techniques in Wind Engineering, December

BD 63/94 (1993) (Design Manual for Roads and Structures 3.1.4.), Inspection of Highway Bridges and Structures, Highways Agency, UK, January

Bendat, J.S. and Piersol, A.G. (1971) "Random Data: Analysis and Measurement Procedures", John Wiley & Sons Inc., USA

Brincker, R., Anderson, P., Kirkegaard, P.H. and Ulfkjaer, J.P. (1995) "Damage detection in laboratory concrete beams", Proceedings of the 13th International Modal Analysis Conference, pp661-667

Brown, B.J. (2000) "Nature and causes of failure in concrete bridges", Seminar on Assessment and Maintenance of Concrete Highway Bridges, University of Dundee, Scotland, 11-12 April

Brownjohn J.M.W., Dumanoglu A.A., Severn R.T. and Taylor C.A. (1987) "Ambient vibration measurements of the Humber Suspension Bridge and comparison with calculated characteristics" Proceedings of the Institution of Civil Engineers, Part 2, September, Vol. 83, pp561-600

Brownjohn, J.M.W., Xia, P-Q. Hao, H. and Xia, Y. (2001) "Civil structure condition assessment by FE model updating: methodology and case studies", Finite Elements in Analysis and Design 37, pp761-775.

BS1881-118, (1983) "Testing Concrete – part 118: method for determination of flexural strength", British Standards Institution, London

BS5400-2, (1978) "Steel, concrete and composite bridges – part 2: specification for loads", British Standards Institution, London

Casas, J.R. and Aparicio, A.C. (1994) "Structural damage identification from dynamic test data", ASCE Journal of Structural Engineering, Vol. 120, No. 8, August, pp2437-2450

Catbas, F.N., Lenett, M., Atkan, A.E., Brown, D.L., Helmicki, A.J. and Hunt, V. (1999) "Modal analysis as a bridge monitoring tool", Proceedings of the Seventeenth International Modal Analysis Conference, Volume 2, pp1230-1236

Cawley, P. and Adams, R.D. (1979) "The location of defects in structures from measurements of natural frequencies", Journal of Strain Analysis, Vol. 120(8), pp2437-2450

Chen, G., Yang, X., Alkhrdaji, T., Wu, J. and Nanni, A. (1999) "Condition assessment of concrete structures by dynamic signature tests", Proceedings of the 13th ASCE Engineering Mechanics Speciality Conference, Baltimore, MD, June 13-16, CD-ROM

Chiang, D-Y. and Cheng, M-S. (1999) "Modal parameter identification from ambient response", American Institute of Aeronautics and Astronautics AIAA Journal, Vol. 34, No. 4, pp513-515

Chui, K.C. (1992a) "An Introduction to Wavelets", Academic Press Inc., San Diego, USA

Chui, K.C. (1992b) "Wavelets: a Tutorial in Theory and Applications", Academic Press Inc., San Diego, USA

Creed, S.G. (1987) "Assessment of large engineering structures using data collected during in-service loading", Structural Assessment, (edited by Garas, F.K., Clarke, J.L. and Armer, G.S.T.), Butterworths, London, pp55-62

Crespo, P., Ruotolo, R. and Surace, C. (1996) "Non-linear modelling of a cracked beam", Proceedings of the 14th International Modal Analysis Conference, Vol. 2, pp1017-1022

Das, P.C., Owen, J.S., Eccles, B.J., Woodings, M.A. & Choo, B.S. (1997) "The role of dynamic testing in the assessment of bridges", Transport Research Record, Part 2: Structures 1594, pp115-124

Doebling, S.W., Farrar, C.R. and Cornwell, P.J. (1997) "DIAMOND: A Graphical User Interface Toolbox for Comparative Modal Analysis and Damage Identification", Proc. of Sixth International Conference on Recent Advances in Structural Dynamics, Southampton, UK, July 1997, pp399-412.

Ebert, M., Zabel, V. and Bucher, C. (1999) "Changes of dynamic structural parameters with progressive structural damage", Proceedings of the 13th ASCE Engineering Mechanics Speciality Conference, Baltimore, MD, June 13-16, CD-ROM

Eccles, B.J. (1999) "The Use of Non-Linear Vibrations in the Health Monitoring of Reinforced Concrete Structures", PhD thesis, School of Civil Engineering, University of Nottingham, UK.

Eriksson, P-E. (1991) "Modal analysis of a pre-cast concrete floor element", Proceedings of the 9th International Modal Analysis Conference, Vol. 1, pp430-434

Ewins, D.J. (2000) "Modal Testing: Theory, Practice and Application", Research Studies Press, Baldock, Hertfordshire, England

Farrar, C.R. and James III, G.H. (1997) "System Identification from Ambient Vibration Measurements on a Bridge", Journal of Sound and Vibration, 205(1), pp1-18

Fasana, A., Garibaldi, L., Giorcelli, E., Marchesiello, S. and Ruzzene, M. (1999) "Evaluation of a road bridge dynamic response to ambient excitation by wavelet and other estimation techniques", Proceedings of the 17th International Modal Analysis Conference, Vol. 2, pp1726-1736

Fasana, A., Garibaldi, L., Giorcelli, E., Ruzzene, M. and Sabia, D. (1997) "Analysis of a motorway bridge under random traffic excitation", Proceedings of the 15th International Modal Analysis Conference, Vol. 1, pp293-300

Feldman, M. (1997) "Vibration analysis of non-symmetric elastic force systems via the Hilbert Transform", Proceedings of the 15th International Modal Analysis Conference, Vol. 1, pp1017-1022

Feldman, M. and Braun, S. (1997) "Description of free responses of SDOF systems via the phase plane and Hilbert Transform: The Concepts of Envelope and Instantaneous Frequency", Proceedings of the 15th International Modal Analysis Conference, Vol. 1, pp973-979

Fladung, B. (1997) "Windows used for Impact Testing", Proceedings of the 15th International Modal Analysis Conference, Vol. 2, pp1662-1666

Fregolent, A., D'Ambrogio, W. and Sesteri, A. (1996) "Correlating a finite element model with tests from a set of sample structures", Structural Dynamics Modelling, Vol. 2, pp53-64

Friswell, M.I. and Mottershead, J.E. (1995) "Finite element model updating in structural dynamics", Kluwer Academic Publishers, Dordrecht

Friswell, M.I. and Penny, J.E.T. (1997) "Is damage location using vibration measurements practical?", EUROMECH 365 International Workshop: DAMAS '97, Structural Damage Assessment Using Advanced Signal Processing Procedures, Sheffield, UK.

Fugate, M.L., Sohn, H. and Farrar, C.R. (2001) "Vibration-based damage detection using statistical process control", Mechanical Systems and Signal Processing, Vol. 15, part 4, pp707-722

Gade, S. and Herlufsen, H. (1991) "The use of the impulse response function for modal parameter estimation", S V Sound and Vibration, Vol. 25, No. 3, March, pp22-28

Garcia, G.V., Osegueda, R. and Meza, D. (1999) "Damage detection comparison between damage index method and ARMA method", Proceedings of the 17th International Modal Analysis Conference, Vol. 1, pp593-598

Hamamoto, T. and Kondo, I. (1993) "Preliminary experiments for damage detection of offshore structures", Proceedings of the Third International Offshore and Polar Engineering Conference, pp685-692

Haritos, N. (1995) "Experimental modal testing of reinforced concrete bridges", European Seismic Design Practice, Rotterdam

Harris, C.M. ed (1996) "Shock and Vibration Handbook", McGraw-Hill Book Company

Hearn, G. (1996) "NDE in bridge management systems", Structural Reliability in Bridge Engineering, Boulder, CO., October 1996, pp60-71

Hon, A., Taplin, G. and Al-Mahaidi, R. (2001) "Investigating the behaviour of T-beam bridge decks in flexure", Australasian Structural Engineering Conference, Gold Coast, Australia

Hover, K.C. (1996) "Special problems in evaluating the safety of concrete bridges and concrete bridge components", Construction and Building Materials, Vol. 10, No. 1, pp39-43

James III, G.H., Zimmerman, D.C. and Mayes, R.L. (1998) "Experimental study of Frequency Response Function (FRF) based damage assessment tools", Proceedings of the Sixteenth International Modal Analysis Conference, Volume 1, pp151-157

James, G., Mayes, R., Carne, T. and Reese, G. (1994) "Damage detection and health monitoring of operational structures", Proceedings of the 1994 International Mechanical Engineering Congress and Exposition, pp371-380

Johnstone, R. (2000) "Maintenance and Assessment Policy", Seminar on Assessment and Maintenance of Concrete Highway Bridges, University of Dundee, Scotland, 11-12 April

Kim, J-T., Ryu, Y-S., Cho, H-M. and Stubbs, N. (2003) "Damage identification in beam-type structures: frequency-based method vs. mode-shape-based method", Engineering Structures, 25, pp57-67

Kullaa, J. (2001a) "A vibration-based structural health monitoring system", Proceedings of the International Conference on Structural System Identification, Kassel, Germany, 5-7 September, Vol. 1, pp263-272

Kullaa, J. (2001b) "Health monitoring of the Z24 bridge using control charts", Proceedings of the International Conference on Structural System Identification, Kassel, Germany, 5-7 September, Vol. 1, pp539-548

Lamonaca, B.G., Valente, C. and Brancaleoni, F. (1997) "Crack identification in nonlinear vibrating beams", Proceedings of the 15th International Modal Analysis Conference, Vol. 2, pp1808-1814

Law, S.S., Waldron, P. and Taylor, C. (1992) "Damage detection of a reinforced concrete bridge deck using the frequency response function", Proceedings of the 10th International Modal Analysis Conference, Vol. 1, pp772-778

Lee, U. and Shin, J. (2002) "A frequency response function-based structural damage identification method", Computers and Structures, 80, pp117-132

Ljung, L. (1999) "System Identification: Theory for the User, 2nd Ed", Prentice-Hall Inc., New Jersey, USA

Lu, C-J. and Hsu, Y-T. (1999) "Application of wavelet transform to structural damage detection", Proceedings of the 17th International Modal Analysis Conference, Vol. 1, pp908-914

Mannan, M.A, McHargue, P. and Richardson, M.H. (1994) "Continuous monitoring of modal parameters to quantify structural damage" Proceedings of the 12th International Modal Analysis Conference, Vol. 1, pp 59-65

Marwala, T. (2000) "Damage identification using committee of neural networks", Journal of Engineering Mechanics, Vol. 126, No. 1, January, pp43-50

Maunsell (1989) "The performance of concrete bridges. Supplementary Reports, literature review: deterioration of concrete", G. Maunsell and Partners, a report prepared for the Department of Transport, London

Mickelborough, N.C. and Pi, Y.L. (1989) "Modal parameter identification using Z-Transforms", International Journal for Numerical Methods in Engineering, Vol. 28, pp2307-2321

Mitra, S.K. and Kaiser, J.F. (1993) "Handbook for Digital Signal Processing", John Wiley & Sons Inc., New York, USA

Modena, C., Sonda, D. and Zonta, D. (1999) "Damage localization in reinforced concrete structures by using damping measurements", Key Engineering Materials, Vols. 167-168, pp132-141

Mottershead, J.E. and Friswell, M.I. (1993) "Model updating in structural dynamics: A survey", Journal of Sound and Vibration, Vol. 167(2), pp347-375

Moy, S.J. (1996) "Plastic methods for steel and concrete structures", Macmillan, Basingstoke, UK

Ndambi, J-M., Vantomme, J. and Harri, K. (2002) "Damage assessment in reinforced concrete beams using eigenfrequencies and mode shape derivatives", Engineering Structures, 24, pp501-515

Ni, Y.Q., Ko, J.M. and Zhou, X.T. (2002) "Damage region identification of cable-supported bridges using neural network-based novelty detectors", Structural Health Monitoring, Stanford, CA., pp449-458

Nield, S.A. (2001) "Using Non-Linear Vibration Techniques to Detect Damage in Concrete Bridges", PhD thesis, Department of Science, University of Oxford, UK

Nield, S.A., Williams, M.S. and McFadden, P.D. (2002) "Non-linear behaviour of reinforced concrete beams under low-amplitude cyclic vibration loads", Engineering Structures, Vol. 24, pp707-718

Owen, J.S., Eccles, B.J., Choo, B.S. and Woodings, M.A. (2001) "The application of auto-regressive time series modelling for the time-frequency analysis of civil engineering structures", Engineering Structures, Vol. 23, No. 5, pp521-536

Pandey, A.K., Biswas, M. and Samman, M.M. (1991) "Damage detection from changes of curvature mode shapes", Journal of Sound and Vibration, Vol. 145(2), pp321-332

Paz, M. (1997) "Structural Dynamics: Theory and Computation, 4th Ed", Chapman & Hall, New York, USA

Petro, S.H., Chen, S-E., GangaRao, H.V.S. and Venkatappa, S. (1997) "Damage detection using vibration measurements", Proceedings of the 15th International Modal Analysis Conference, Vol. 1, pp113-119

Prime, M.B. and Shevitz, D.W. (1996) "Linear and nonlinear methods for detecting cracks in beams", Proceedings of the 14th International Modal Analysis Conference, Vol. 2, pp1437-1443

Raghavendrachar, M. and Aktan, A.E. (1992) "Flexibility by multi-reference impact testing for bridge diagnostics", ASCE Journal of Structural Engineering, Vol. 118(8), pp2186-2203

Ramey, G.E. and Wright, R.L. (1997) "Bridge deterioration rates and durability/longevity performance", Practice Periodical on Structural Design and Construction, August, pp98-104

Rao, S.S. (1995) "Mechanical Vibrations, 3rd Ed", Addison-Wesley Publishing Company Inc., USA

Razak, H.A. and Choi, F.C. (2001) "The effect of corrosion on the natural frequency and modal damping of reinforced concrete beams", Engineering Structures 23, pp1126-1133

Red-Horse, J.R., Alvin, K.V., Mignolet, M.P. and Robertson, A.N. (1996) "An investigation of three major time-series data analysis techniques", Proceedings of the 14th International Modal Analysis Conference, Vol. 2, pp1600-1607

Richardson, M.H. (1986) "Global frequency and damping estimates from frequency response measurements", Proceedings of the 4th International Modal Analysis Conference

Richardson, M.H. and Formenti, D.L. (1982) "Parameter estimation from frequency response measurements using rational fraction polynomials", Proceedings of the 1st International Modal Analysis Conference

Richardson, M.H. and Formenti, D.L. (1985) "Global curve fitting of frequency response measurements using the rational polynomial method", Proceedings of the 3rd International Modal Analysis Conference

Rohrmann, R.G., Sachse, R. and Limberger, E. (2001) "Damage distribution of a RC footbridge evaluated by neural networks and classical update procedures", presented in the International Conference on Structural System Identification, Kassel, Germany, 5-7 September

Ruotolo, R., Surace, C. and Worden, K. (2000) "Application of two damage detection techniques to an offshore platform", Shock and Vibration Digest, Vol. 32, No. 1, January, pp30-31

Rytter, A. (1993) "Vibration Based Inspection of Civil Engineering Structures", PhD thesis, Department of Building Technology and Structural Engineering, Aalborg University, Denmark

Salane, H.J. and Balwin Jr, J.W. (1990) "Identification of modal properties of bridges", ASCE Journal of Structural Engineering, Vol. 116, No. 7, July, pp2008-2021

Salane, H.J., Baldwin Jr, J.W. and Duffield, R.C. (1981) "Dynamics approach for monitoring bridge deterioration", Transportation Research Record 832, Transportation Research Board National Academy of Sciences, pp21-28

Salawu, O.S. (1997) "Detection of structural damage through changes in frequency: a review", Engineering Structures, Vol. 19(9), pp718-723

Salawu, O.S. and Williams, C. (1995) "Bridge assessment using forced-vibration testing" ASCE Journal of Structural Engineering, Vol.121, No. 2, February, pp161-173

Salawu, O.S. and Williams, C. (1997) "Theoretical and experimental vibration analysis of a reinforced concrete bridge", Proceedings of the 15th International Modal Analysis Conference, Vol. 1, pp278-285

Samman, M.M. and Biswas, M. (1994a) "Vibration testing for nondestructive evaluation of bridges. II: results" ASCE Journal of Structural Engineering, Vol. 120, No. 1, January, pp290-306

Samman, M.M. and, Biswas, M. (1994b) "Vibration testing for nondestructive evaluation of bridges I: theory", ASCE Journal of Structural Engineering, Vol. 120, January, pp269-289

Schulz, M.J., Ahmad, S.N., Pai, P.F., Linville, M.S. and Chung, J. (1997) "Detecting structural damage using transmittance functions", Proceedings of the 15th International Modal Analysis Conference, Vol. 1, pp638-644

Schwarz, B.J. and Richardson, M.H. (1999) "Experimental Modal Analysis", CSI Reliability Week, Orlando, FL

Shelley, S.J., Freudinger, L.C. and Allemang, R.J. (1993) "Development of an on-line modal state monitor", Proceedings of the Eleventh International Modal Analysis Conference, Volume 2, pp1581-1586

Sohn, H., Czarnecki, J.A. and Farrar, C.R. (2000) "Structural health monitoring using statistical process control", Journal of Structural Engineering, Vol. 126, No. 11, November, pp1356-1363

Staszewski, W.J. and Chance, J.E. (1997) "Identification of Nonlinear Systems using Wavelets – Experimental Study", Proceedings of the 15th International Modal Analysis Conference, Vol. 1, pp1012-1016

Staszewski, W.J. and Giacomin, J. (1997) "Application of the Wavelet based FRFs to the Analysis of Nonstationary Vehicle Data", Proceedings of the 15th International Modal Analysis Conference, Vol. 1, pp425-431

Tajalli, S.M.A. and Rigden, S.R. (2000) "Partially and non-destructive testing of 40 concrete bridges", Proceedings of the Institution of Civil Engineers, Structures and Buildings, 140, February, pp25-38

Tan, C.M. (2003) "Non-Linear Vibrations of Cracked Reinforced Concrete Structures", PhD thesis, School of Civil Engineering, University of Nottingham, UK

Tan, C.M., Owen, J.S. and Choo, B.S. (2000) "The nonlinear vibrations of RC beams with distributed cracks", Proceedings of the 4th International Conference on Modern Practice in Stress and Vibration Analysis, September, pp273-284

Tomlinson, G.R. (1994) "Linear or nonlinear – that is the question", Proceedings of the 19th International Seminar on Modal Analysis; Tools for Noise and Vibration Analysis, 12-14 September, Leuven, Belgium, Vol. 1, pp11-32

Uzgider Z., Sanli A.K., Piroglu F. and Caglayan D.B. (1993) "Identification of Railway Bridges Using Locomotive-Induced Vibrations", Bridge Management 2, edited by Harding, J.E., Park, G.A.R. and Ryall, M.J., Thomas Telford, London, pp833-841

Vandiver, J.HK. (1975) "Detection of structural failure of fixed platforms by measurement of dynamic response", Journal of Petroleum Technology, March, pp305-310

Wahl, F., Schmidt, G. and Farrai, L. (1999) "On the significance of antiresonance frequencies in experimental structural analsyis", Journal of Sound and Vibration, 219(3), pp379-394

Wakeman, T. (2001) "M1 motorway bridges – 40 years on", Concrete, The Concrete Society, November/December, Vol. 35, No. 10, pp38-42

Wang Z., Lin R.M. and Lim M.K. (1997) "Structural damage detection using measured FRF data", Computational Methods in Applied Mechanical Engineering, 147, pp187-197

Wang, W., Hu, N., Fukunaga, H. and Yao, Z.H. (2001) "Structural damage identification using static test data and changes in frequencies", Engineering Structures, 23, pp610-621

Wardle, R., Worden, K. and King, N.E. (1997) "Classification of nonlinearities using neural networks", Proceedings of the 15th International Modal Analysis Conference, Vol. 1, pp980-986

Williams, C. and Salawu, O.S. (1997) "Damping as a damage indication parameter", Proceedings of the 15th International Modal Analysis Conference, Vol. 2, pp1531-1536

Williams, E.J., Messina, A. and Payne, B.S. (1997) "A frequency-change correlation approach to damage detection", Proceedings of the 15th International Modal Analysis Conference, Vol. 1, pp652-657

Wood, M.G., Bailey, M., Friswell, M.I., Penny, J.E.T. and Purkiss, J.A. (1991) "Damage location in reinforced concrete beams using vibration responses", Proceedings of the 9th International Modal Analysis Conference, Vol. 1, pp139-144

Woodward, R.J. (2000) "Issues surrounding current UK bridge stock", Seminar on Assessment and Maintenance of Concrete Highway Bridges, University of Dundee, Scotland, 11-12 April

Worden, K. (1998) "Random Vibrations of a Multi Degree-of-Freedom Nonlinear system", Proceedings of the 16th International Modal Analysis Conference, Vol. 1, pp711-717

Worden, K. and Manson, G. (1997) "Random vibration analysis of a nonlinear system", Proceedings of the 15th International Modal Analysis Conference, Vol. 1, pp1003-1011

Xia, Y., Hao, H., Brownjohn, J.M.W. and Xia, P-Q. (2002) "Damage identification of structures with uncertain frequency and mode shape data", Earthquake Engineering and Structural Dynamics, 31, pp1053-1066

Zang, C. and Imregun, M. (2001) "Structural damage detection using artificial neural networks and measured FRF data reduced via principal component projection", Journal of Sound and Vibration, 242(5), pp813-827

Zhang, Q.W., Chang, C.C. and Chang, T.Y.P. (2000) "Finite element model updating for structures with parametric constraints", Earthquake Engineering and Structural Dynamics, 29, pp927-944

Ziebarth, H. and Baumgartner, R.J. (1981) "Early detection of cross-sectional rotor cracks by turbine shaft vibration monitoring techniques", American Society of Mechanical Engineers, 1981

Zonta, D. and Modena, C. (2001) "Observations on the appearance of dispersive phenomena in damaged structures", Journal of Sound and Vibration, 241(5), pp925-933

APPENDIX A

EXPERIMENTAL MODAL ANALYSIS

This appendix contains a brief overview of the wide-ranging subject known as experimental modal analysis (EMA), and a more comprehensive discussion can be found in Ewins (2000) and Schwarz and Richardson (1999). EMA is the term used for determining experimentally the modal properties of a system. In many cases, the modal properties are considered to be in the form of a modal model, i.e. consisting of the modal frequencies, modal damping and the mode shapes. In other cases, it is more beneficial to describe the system by a mass, damping, stiffness model.

Modal frequencies are the frequencies at which the system's resonances occur, i.e. when the system's response becomes large when compared to the input. At this frequency, the system will vibrate with a particular shape, unique to this frequency, known as the mode shape. This resonance will also have a value of damping, which when related to the critical damping, is known as the damping ratio. This combination of frequency, damping and deflected shape is known as a mode of the system, hence modal analysis is the investigation into the modes of a system.

There are three main stages involved in experimental modal analysis. Firstly, the data from the system must be gathered in a process termed modal testing and transformed into a form suitable for further processing. The data then has to be analysed to determine the modal properties required; this stage is known as modal parameter estimation. The methods by which experimental modal analysis is conducted are described in the following sections. The next section outlines the first stage, modal testing, concentrating mainly on the practical

issues involved. The theoretical background of the processing of the raw data from the modal testing stage is given in section A.2. Section A.3 describes a range of techniques that have been developed for the determination of the modal properties of a system, which is the final stage of experimental modal analysis.

A.1 Modal testing

Modal testing involves measuring the response, usually acceleration, velocity or displacement, of a system to some form of excitation. In the case of modal testing of structures, there are three main alternative techniques that may be used, classified in terms of the excitation method. These can be categorised as forced vibration, free vibration or ambient vibration.

Forced vibration testing involves attaching a mass to the structure that can be vibrated in a controlled manner, usually by some form of electrodynamic shaker. This allows accurate regulation of the input force to the structure, and consequently a more controlled output measurement. The input force can be controlled both in terms of the force level and the frequency of excitation. It is also usual that the input waveform shape can be selected from a wide range of functions.

When using forced vibration testing, it is possible to produce a wide variety of different input signals, such as chirp or sine sweep. These different inputs allow a much more detailed understanding of the structure to be obtained, and are vital in the study of structures that are non-linear due to the consistency with which the input can be applied. However, it is often impractical for modal testing not conducted in the laboratory to employ the use of a shaker. This is due to the fact that the shaker must be attached to the structure to be tested, which, in the case of bridges, is not convenient because of the inevitable disruptions to the normal use of the bridge, both from attaching the shaker to the bridge and the actual testing which should not be influenced by the traffic.

Testing a structure using free vibration is often a much simpler process to carry out than forced vibration testing. The excitation of the structure lasts for a short duration, and the structure is then allowed to vibrate in an unforced state, eventually decaying back to its rest state. Two main methods of excitation are

used in this type of testing, either impact or quick release. In the testing of bridges, it is uncommon that the technique of quick release will be used, as this involves causing a deformation in the structure and then releasing it suddenly so the structure vibrates. The methods of achieving this are not practical when considering bridge testing. Impact testing is usually accomplished by hitting the structure with a mass, most commonly either a hammer or a dropped mass. The control of the input force is not as good as that when conducting forced testing but can be regulated to some extent, particularly by dropping a constant mass from a constant height. The type of material used to impact the bridge can also be used to control the frequency content of the excitation. When testing structures using impact testing, it is necessary to be confident that the structure will behave in a linear fashion, or to maintain a constant level of excitation.

The third method of exciting the structure is by use of ambient forces. In the case of bridge testing, this type of excitation arises from the effects of the wind and traffic applying forces to the bridge. Due to the nature of the excitation, it is not possible to control the input force unless a specific vehicle is used and the bridge closed to all other traffic. As the excitation is not applied at discrete points, it is usually impractical to accurately measure this input, although measures of wind speeds and direction may be taken for indicative purposes.

Due to the fact that the bridge does not have to be closed to traffic in order to perform the testing, this method of excitation is popular among researchers and would be particularly beneficial if dynamic testing were to be used as a health monitoring procedure.

For any testing conducted on bridges in the field, it is true to say that the results will always be subjected to some ambient excitation, particularly from the wind. However, the level of excitation attainable by ambient forces alone is usually small compared to that using forced or transient excitation.

The measurement of the response of the bridge is achieved by the use of suitable sensors. Most common is the use of accelerometers, which are attached to the structure by means of a screw fixing, magnets or adhesive wax. Usually these will be attached to a stable platform, which is in turn fixed to the

bridge to avoid problems associated with fastening the accelerometer to the deck itself.

A.2 Signal processing

This section describes the mathematical background of the processing techniques that are required to obtain a more meaningful representation of the system from the data collected in the modal testing phase. This involves categorising the data in terms of its statistical behaviour, allowing a number of well-developed procedures to then be applied.

The processing of the data obtained from the modal testing phase can often be simplified by categorising the data into one of a number of types. For this, a number of conditions need to be applied to the data in order that it can be categorised and subsequently processed in the correct manner. These involve the determination of the first and second order statistical properties, usually considered to be the mean and correlation, where correlation is a measure of the dependence of the data in two time histories.

For a single time history record, x, the mean is defined as;

$$\mu_x(t_1,k)=\frac{1}{T}\int_{t_1}^{t_1+T} x_k(t)dt \qquad \text{Equation A-1}$$

The correlation between two data records, known as cross-correlation, is calculated by multiplying the coordinates of two records, $x(t)$ and $y(t)$, at times t and $t+\tau$ respectively, and computing the average over all values of t. Mathematically, this may be written;

$$R_{xy}(t_1,t_1+\tau,k)=\frac{1}{T}\int_{t_1}^{t_1+T} x_k(t)y_k(t+\tau)dt \qquad \text{Equation A-2}$$

Correlation can also be found for a single data record. This correlation between values for the same sample at time t and time $t+\tau$ is known as autocorrelation, and may be expressed mathematically as;

$$R_x(t_1, t_1+\tau, k) = \frac{1}{T}\int_{t_1}^{t_1+T} x_k(t)x_k(t+\tau)dt \qquad \text{Equation A-3}$$

If the correlation and mean do not vary significantly as t_1 varies for the same sample, the sample record is categorised as weakly stationary. If all the statistical properties, of which there are an infinite number, do not vary with time then the record is strongly stationary. Usually, it is sufficient to confirm weak stationarity for the record to be termed stationary. If the time-averaged properties of the sample records do not vary between sample functions, the process is ergodic. Only a stationary process can be ergodic. Most of the theory developed for the processing of data is based upon the assumption that the process is both stationary and ergodic (Bendat and Piersol, 1971).

Two different types of data also exist, deterministic and random. For most cases, the data is assumed to be random and stationary. This in turn leads to an alternative definition of autocorrelation, due to the fact that the absolute time t is unimportant, and autocorrelation is therefore only dependent upon the separation τ. From equation A-2, it can be seen that the autocorrelation for a stationary random process may be redefined as;

$$R_x(\tau) = \lim_{T\to\infty}\frac{1}{T}\int_0^T x(t)x(t+\tau)dt \qquad \text{Equation A-4}$$

The cross-correlation can also be redefined to be independent of the absolute time;

$$R_{xy}(\tau) = \lim_{T\to\infty}\frac{1}{T}\int_0^T x(t)y(t+\tau)dt \qquad \text{Equation A-5}$$

A.2.1 Spectral functions

Any periodic function can be represented as a Fourier series, i.e. by sine and cosine terms of successive multiples of a fundamental frequency. The coefficients of the sine and cosine terms are calculated by the integration of the periodic function multiplied by sine or cosine terms over one period. The response of the system is then obtained by superposition of the response for each of the Fourier series terms of the excitation function, essentially reconstructing the original function by addition of sine and cosine waves. Fourier series may be expressed mathematically as;

$$F(t) = a_0 + \sum_{n=1}^{\infty} \{a_n \cos n\omega t + b_n \sin n\omega t\} \qquad \text{Equation A-6}$$

or

$$F(t) = \sum_{n=-\infty}^{\infty} c_n e^{in\omega t} \qquad \text{Equation A-7}$$

However, not all functions are periodic. The theory of Fourier series can be extended to non-periodic functions by means of Fourier integrals, which can then be developed to produce Fourier transforms. The Fourier integral is the limiting case of the Fourier series as the period tends to infinity, assuming the data will eventually become periodic. The theory of Fourier transforms allows the representation of non-periodic processes in terms of the frequencies they contain, by describing the amount of energy that each sine and cosine term can represent. The (integral) Fourier transform may be expressed mathematically as (Paz, 1997);

$$F(t) = \frac{1}{2\pi} \int_{-\infty}^{\infty} \left\{ \int_{-\infty}^{\infty} F(\tau) e^{-i\omega\tau} d\tau \right\} e^{i\omega\tau} d\omega \qquad \text{Equation A-8}$$

This can be written in two parts, giving a Fourier transform pair;

$$C(\omega)=\frac{1}{2\pi}\int_{-\infty}^{\infty}F(t)e^{-i\omega\tau}dt$$
$$F(t)=\int_{-\infty}^{\infty}C(\omega)e^{i\omega\tau}d\omega$$

Equation A-9

This relationship may also be written in terms of the frequency, f, rather than the angular frequency, ω, using the relation that;

$$f=\frac{\omega}{2\pi}$$

Equation A-10

The Fourier transform may be written in an equivalent form to equation A-9 as (Harris, 1996):

$$C(f)=\int_{-\infty}^{\infty}F(t)e^{-i2\pi ft}dt$$
$$F(t)=\int_{-\infty}^{\infty}C(f)e^{i2\pi ft}df$$

Equation A-11

The Fourier transform is a complex valued quantity; the real part of the Fourier transform is associated with the cosine terms, whilst the imaginary part is connected to the sine terms. Using a frequency representation of a function produces the spectrum of the function.

The spectral function of a signal is given by the contributions of the various frequency components of the signal to its mean square value. Spectral analysis expresses the mean square value in terms of the coefficients of the Fourier series when the signal is periodic, or by the Fourier transform when the signal is not periodic.

The representation of a single signal in terms of its frequency components is known as the autospectral density function (or power spectral density function). This describes the frequency composition of a single sample of data

in terms of the spectral density of its mean square value. The autospectral density function is related to the autocorrelation function by a Fourier transform. Obtaining the autospectral density function by means of a Fourier transform of the autocorrelation gives a two-sided power spectrum defined for frequencies between -∞ and ∞. Applying a Fourier transform to the autocorrelation of sample *x*, equation A-4, the power spectral density function may be written mathematically as;

$$S_x(f) = \int_{-\infty}^{\infty} R_x(\tau) e^{-j2\pi f\tau} d\tau \qquad \text{Equation A-12}$$

Taking the inverse Fourier transform of the power spectral density function will obtain autocorrelation, due to the fact that these are a Fourier transform pair (Bendat and Piersol, 1971);

$$R_x(\tau) = \int_{-\infty}^{\infty} S_x(f) e^{j2\pi f\tau} df \qquad \text{Equation A-13}$$

The autospectral density function obtained in practice is formed by filtering procedures, and will give a one-sided autospectral density function, existing between 0 and ∞. The magnitude of the one-sided autospectral density function is twice that of the two-sided, and may be expressed as;

$$G_x(f) = 2\int_{0}^{\infty} R_x(\tau) e^{-j2\pi f\tau} d\tau \qquad \text{Equation A-14}$$

The formation of the autospectral density above using the input data *x* can accordingly be used to produce the autospectral density function of the output variable *y*.

The production of cross-spectral density functions evolves directly from the cross-correlation function by means of the Fourier transform, equivalent to the

production of autospectral density functions. However, as the cross-correlation is not an even function, the cross-spectral density function is a complex valued quantity. Again, the cross-spectral density function can be produced both in a one- or two-sided form. The two-sided cross-spectral density function may be written as;

$$S_{xy}(f) = \int_{-\infty}^{\infty} R_{xy}(\tau) e^{-j2\pi f\tau} d\tau \qquad \text{Equation A-15}$$

The three relationships between $R_x(t)$, $R_y(t)$ and $R_{xy}(t)$, and $S_x(t)$, $S_y(t)$ and $S_{xy}(t)$ are known as the "Wiener-Khintchine" relations (Bendat and Piersol, 1971).

The above equations describe the spectral density functions in terms of frequency. However, it is also possible to describe these functions in terms of the angular frequency, ω, using the Fourier transform pair given in equation A-9.

Plots of the various spectral functions are often produced, and have specific names. A plot of the autospectral density function against frequency is known as a power spectrum, or autopower spectrum. A plot of the cross-spectral density function against frequency is known as the cross-spectrum.

The Fourier transform can be created using either a continuous or discrete representation. In the area of signal processing, the data is collected as a number of discrete values, so the spectral analysis is performed using the discrete Fourier transform (DFT), expressed mathematically as (Paz, 1997);

$$C_n = \sum_{j=0}^{N-1} F(t_j) e^{-2\pi(nj/N)}$$

$$F(t_j) = \sum_{n=0}^{N-1} C_n e^{2\pi(nj/N)} \qquad \text{Equation A-16}$$

The DFT is solved using numerical methods, which have lead to the development of an extremely efficient algorithm to evaluate the complex coefficients. This is known as the fast Fourier transform (FFT).

A.2.2 Frequency response function

A linear dynamic system with constant parameters may be expressed using a weighting function describing the output of the system to a unit impulse applied at a time τ before. For an arbitrary input $x(t)$, the system output $y(t)$ is given by the convolution integral (Rao, 1995);

$$y(t) = \int_{-\infty}^{\infty} h(\tau)x(t-\tau)d\tau \qquad \text{Equation A-17}$$

This equation is known as Duhamel's integral. The Laplace transform of $h(\tau)$ is the transfer function;

$$H(s) = \int_{0}^{\infty} h(\tau)e^{-s\tau}d\tau \qquad s = a + jb \qquad \text{Equation A-18}$$

If the system is stable, the dynamic characteristics can be described by the frequency response function (FRF) (Mitra and Kaiser, 1993), which is the Fourier transform of $h(\tau)$ or a special case of equation A-18 when $a=0$ and $b=2\pi f$;

$$H(f) = \int_{0}^{\infty} h(\tau)e^{-j2\pi f\tau}d\tau \qquad \text{Equation A-19}$$

It is possible to perform an inverse Fourier transform on the FRF to give the impulse response function (IRF). The IRF is a time domain representation of the system, which, due to the assumptions made in taking a Fourier transform of $h(\tau)$, is the response of the system when excited by a unit impulse. The IRF

is often used in the time-domain modal parameter estimation routines, as a result of the simplifying assumptions that can be made because of the unit impulse excitation.

A Fourier transform of the convolution integral given in equation A-17 may be found as;

$$Y(f) = H(f)X(f) \qquad \text{Equation A-20}$$

This is derived from the convolution theorem, which states that a convolution in the time domain is equivalent to multiplication in the frequency domain, and vice versa. This allows a much simpler formulation of the relationship between the input and output in the frequency domain than in the time domain. The FRF is a complex quantity.

For constant parameter linear systems, the FRF is only a function of the frequency. If the system were non-linear, the FRF would also be a function of the input sample, and if the parameters were not constant the FRF would be a function of time.

From equation 4-20, the FRF could theoretically be found by division of the Fourier transform of the output, *Y(f)*, by the Fourier transform of the input, *X(f)*. In practice, however, it is usual to calculate the FRF by use of the cross-spectrum of the input and output, and the autocorrelation function of either the input or the output. This leads to two alternative definitions of the FRF, H_1 and H_2 (Ewins, 2000);

$$H_1(f) = \frac{S_{yx}(f)}{S_y(f)} \qquad \text{Equation A-21}$$

$$H_2(f) = \frac{S_x(f)}{S_{xy}(f)} \qquad \text{Equation A-22}$$

These two alternative methods in calculating the FRF have different effects on the data. The H_1 estimate is the most common formulation used and tends to minimise the noise on the output, whilst the H_2 estimate minimises noise on the input. The H_2 estimate can be problematic as the cross-power spectrum can theoretically be zero at a point.

The power spectral density functions can also be used to form a useful measure of the quality of the FRF obtained from the data, in terms of the coherence function. The coherence function uses modulus of the two estimates of the FRF, H_1 and H_2, to quantify the effects of noise on the spectral functions. Using equations A-21 and A-22, the coherence function can be formulated as;

$$\gamma_{xy}^2(f)=\frac{|S_{xy}(f)|^2}{S_x(f)S_y(f)}=\frac{|G_{xy}(f)|^2}{G_x(f)G_y(f)} \qquad \text{Equation A-23}$$

The coherence function is a real-valued quantity, generating values between 0 and 1. A value of 1 indicates complete correlation between the two estimates of the FRF, and implies a high degree of confidence in the FRF at that frequency. Values of less than 1 suggest that noise is present in the data, the system is not linear and/or the output *y(t)* is due to more inputs than the only *x(t)*.

Several forms of the FRF exist depending on the particular variable measured as the output. If acceleration is used, the FRF is known as accelerance, when velocity is measured, the term mobility is used and for displacement FRFs, the term used is receptance. Due to the fact that the FRF is a complex-valued function, two graphs are necessary in order to display all the information of the FRF. The FRF can be expressed either in a magnitude and phase form or in a real and imaginary form. Graphical representations of the FRF are usually produced either as two plots of magnitude against frequency and phase against frequency, or as two plots of real part against frequency and imaginary part against frequency. It is also common to produce another type of plot,

consisting of a single graph of real part against imaginary part, known as a Nyquist plot. This however causes a loss of the frequency information.

A.2.3 Signal processing considerations

The Fourier transform in its discrete form is evaluated at multiples of a fundamental frequency. This is known as the frequency resolution. For a signal that is not exactly at one of these multiples of the fundamental frequency, the DFT cannot transform the time domain signal into the frequency domain accurately. Instead, the signal will be smeared between the frequencies adjacent to its actual frequency. This source of error in the transform from the time to frequency domain is called leakage. The same problem can be found for signals that are not periodic, or are not completely observed in the sampling process. The DFT assumes the signal is a periodic function and therefore introduces discontinuities between the records, affecting the evaluation of the Fourier transform.

In order to combat leakage due to samples that are not completely observed, it is good practise to apply a window to the time history. A wide range of window functions exists, but the most generally used types for impact testing are the exponential and force windows, and for forced vibration testing a tapered cosine bell window is often used. For impact testing, these windows also help to minimise or eliminate errors due to electronic noise after the signal has decayed, and for forced vibration testing the signal is forced to be periodic, thus complying with the requirement of the DFT.

For forced vibration testing, the same windows should be applied to both the input and the output waveforms. Impact testing requires the force window to only be applied to the input signal, whilst the exponential window should be applied to both the input and output signals. This is so the resulting windowed input and output waveforms are both functions of the same variable and will therefore produce an FRF of the correct variable (Fladung, 1997).

Another import consideration in modal testing is that of the filter frequency. A low pass filter at the correct frequency must be used to avoid problems of aliasing. Aliasing occurs when a signal contains a frequency that is too high compared to the sampling frequency. This causes too few of the points to be

observed in the time domain and, when the DFT is applied to the data, the frequency is distorted. This distortion is manifested by "wrap around" of the FRF above this critical frequency.

It can be shown that the maximum frequency signal that can be transformed correctly into the frequency domain is equal to half the sampling frequency. This maximum frequency at which a signal can be correctly transformed into the frequency domain is known as the Nyquist frequency. It is therefore essential to filter out the signals above the Nyquist frequency, so a low pass filter should be used at or below this frequency.

Another source of error in the FRF measurements is that of bias. This arises due to the fact that the DFT acts as a set of narrow band-pass filters, selecting narrow frequency bands to be evaluated. If the spectral density of the signal is rapidly changing within this narrow frequency band, then the spectral estimate will not represent the correct sharpness of the peak as the spectral estimate is averaged over the frequency band. The bias error is the difference between the true value of the spectral variable and that given for the centre frequency. For a resonance peak, the degree of bias error depends on the frequency resolution and the damping (Brownjohn et al, 1987).

A.3 Modal parameter estimation

Experimental modal analysis or modal parameter estimation is used to determine the system's modal properties. It can be thought of as an equivalent process to modal analysis for an analytical system, although this involves a root-finding or eigensolution exercise, whilst modal parameter estimation requires a curve-fitting procedure.

Modal parameter estimation is a special case of system identification where the model to be fitted to the data is known to be in the form of modal parameters. The modal parameters used to form the model are usually the complex-valued modal frequencies, modal vectors and modal scaling. Most parameter estimation algorithms also provide estimates of the modal participation vectors and residue vectors (Harris, 1996).

Parameter estimation is a curve fitting process used to represent a set of measured data points by an assumed analytical function. This curve fitting also operates as a data compression technique, representing the large number of experimental data points by a much smaller number of modal parameters.

A.3.1 Single degree-of-freedom modal analysis

All single degree-of-freedom (SDOF) modal identification algorithms are an approximation to the real modal parameters due to the fact that all systems in reality are multiple degree-of-freedom (MDOF). These methods all assume the total response at or near a resonant frequency is dominated by the mode whose natural frequency is closest. It is possible in some methods to assume the contribution of other modes can be represented by a simple approximation.

The use of SDOF algorithms can be very successful for modes that are not close in frequency and do not have a significant effect on each other. It is possible to constrain a MDOF algorithm to only identify a single mode, which will give a greater accuracy. The major advantage of SDOF algorithms is their speed and ease of use, usually requiring little data manipulation.

One of the simplest methods used for extracting the modal parameters from a FRF curve is by peak-picking or peak-amplitude. However, due to the simplifying assumptions made by the SDOF algorithm, the results can no longer strictly be thought of as modal parameters. For this reason, the results are referred to as operating vectors (rather than modal vectors). For a single dominant mode, the operating vector and the modal vector will be approximately equal. This simple method is useful for complex cases where a reasonable initial estimate of the modal properties is required to speed up subsequent curve fitting algorithms.

Peak-picking is limited by the fact that it requires very accurate measurements of the response at resonance. Therefore it should not be used for lightly damped structures where measurements at resonance are difficult to obtain accurately, or for heavily damped structures where the modes are strongly influenced by each other. The accuracy of this method can be improved by using the real part of the FRF to find the maximum magnitude, and a more

refined estimate of the modal frequency can be found from the mid-distance between the maximum and minimum imaginary part.

Another SDOF method uses the fact that the complex plot in the vicinity of resonance is circular, as the behaviour is dominated by a single mode. From the circle fit, the modal frequency can be found where the distance between the data points along the curve is greatest. The damping and modal constant (residual) can also be found from this circle fit.

The circle fit method can be used successfully to identify closely spaced modes. However, it does suffer from an inability to locate poorly excited modes in particular FRFs.

An alternative to the circle fit method described above is the inverse method, which utilises the fact that the reciprocal of the circle in the complex (Nyquist) plane will be a straight line. A plot of the reciprocal of receptance is used, and a least squares best-fit straight line is determined. A second least squares operation is then performed on the real part of the FRF data and the real part of the theoretical model to give the mass and stiffness parameters.

A.3.2 Multiple degree-of-freedom modal analysis

MDOF algorithms attempt to find the modal properties of several modes at the same time. This involves minimising the total error between the measured and a theoretically predicted curve. This is achieved by differentiating the total error with respect to each unknown in turn to give the same number of equations as unknowns. However, the equations formed from this are not linear so various algorithms have been developed to obtain estimates of the unknowns. The different algorithms apply a range of simplifications and assumptions to these equations and most then proceed in an iterative manner, but rely on reasonable initial estimates of the parameters to be found.

The domain in which they are applied often divides these methods. The time domain algorithms are most usually applied to the impulse response function (IRF) as a unit impulse can then be assumed, yielding simpler algorithms. Also, data is not often stored in the form of time histories but as FRFs, which require an inverse Fourier transform to be used, giving an IRF.

It has been found that many of the time-domain methods may be applied to the cross correlation function in order to determine the modal parameters of closely spaced modes (Farrar, and James III, 1997). Time-domain algorithms are, however, sensitive to any non-linearity or noise present in the data, as they rely on the eigenvalues being constant throughout the test (Catbas et al, 1999). Several time domain methods exist such as the complex exponential algorithm, the Ibrahim time domain method and autoregressive moving average based methods.

The complex exponential algorithm does not rely on initial estimates of the modal parameters in order to obtain a good solution. The method solves the time domain data set by constructing an eigenvalue problem to give the complex modal frequencies. From this, the natural frequencies and modal constants for the system can be found.

The least squares complex exponential (LSCE) algorithm is the first to use more than a single IRF measurement to obtain a global estimate of the modal frequency. This method is a high-order algorithm and consequently requires more time domain information than the lower order algorithms. Limitations of the use of high-order algorithms are cases of high damping. However, the complex exponential algorithm requires error terms for accurate estimation of parameters in the case of lightly damped systems (Gade and Herlufsen, 1991).

The Ibrahim time domain method does not curve-fit or analyse a single IRF at a time, but processes all the data at once. The response of the structure is measured at several points and at several time instants from which a set of equations can be formed. A second set of data is then used to form a second set of equations. The eigenvectors from both sets are actually related by a "system matrix", found using a least squares solution. The eigenvalues of the system matrix are then used to find the natural frequencies, damping and mode shape vectors (Chiang and Cheng, 1998). This algorithm is a low-order method and requires very few time points due to the increased use of the spatial information.

A different parametric representation of the input/output relationship can be found using the autoregressive moving average with exogenous inputs

(ARMAX) models (Red-Horse et al, 1996, Mickelborough and Pi, 1989). These models are based on assuming the measured data can be found to satisfy a recurrence relation. The coefficients of the model are evaluated by a maximum likelihood function or by minimisation of the error. Further processing of the parameters obtained is required to attain the modal parameters of the structure. The ARMA model approach determines the coefficients used in the model directly from the time history data, from which the modal parameters are found (Garcia et al, 1999).

Frequency-domain models are often used to take advantage of the speed of the fast Fourier transform. Using data in the frequency domain also allows data averaging operations to be performed on the cross and auto power spectra. As with all data analysis in the frequency domain, limitations arise due to the effects of leakage and aliasing as a result of the use of the discrete Fourier transform. Again, several modal parameter estimation methods have been developed, including the rational fraction polynomial method.

This MDOF method fits the rational fraction polynomial form of the FRF to the measured data. The fit is performed on the basis of a least squares error method. One major advantage of the RFP method is its unique handling of the effects of out-of-band modes. Whilst most other methods require the use of computational modes to compensate for unmeasured modes, the RFP methods allows extra numerator terms, maintaining accurate estimation of the modal parameters (Richardson and Formenti, 1985).

The RFP method, including the power polynomial (PP) and orthogonal polynomial (OP) (Richardson and Formenti, 1982), are high-order algorithms. These methods suffer from limitations due to poor numerical characteristics when not used for narrow frequency bands and a limited number of modes. For this reason, it is more effective to use low-order algorithms.

A.3.3 Multi-curve fit (global)

The simplest approach to modal parameter estimation is done in the "local" sense. In this, each measurement is individually fitted and the modal parameters estimated for each mode in the measurement. This will result in a large number of parameters being fitted at any time and can lead to errors.

As the modal properties of a structure should be the same for the whole structure, it would be sensible to obtain estimates of the modal parameters using all the information available. This leads to multi-curve fitting where several FRF curves are analysed simultaneously to find "global" parameter estimates (Richardson, 1986).

There are several limitations to obtaining global estimates. This method requires significant computing power for the curve fitting procedure (Schwarz and Richardson, 1999). There are also considerations to be noted in general when obtaining global parameters. Averaging any differences between individual measurements may not be appropriate and will not remove systematic errors.

The algorithms used for parameter estimation will usually enforce the criteria that the modal parameters found are treated as global properties of the system. Most current algorithms estimate the modal frequencies and damping in a global sense, but very few use a global method for estimating the modal vectors.

It is usual for the fitting process to be separated into two steps. The first is used to estimate the modal frequencies and damping parameters. The second step estimates the residue assuming the parameters found in the former stage are correct. This leads to a more accurate estimation of the residues as they are closely linked to the damping, which is assumed fixed (Harris, 1996).

APPENDIX B

BENDING CAPACITY OF T-BEAM

Material properties of deck

$$f_y = 460N/mm^2$$

$$f_{yv} = 460N/mm^2$$

$$f_{cu} = 61.9N/mm^2$$

$$A_s = 2\times\frac{20^2}{4}\pi = 628.3mm^2$$

$$A_s^{'} = 2\times\frac{10^2}{4}\pi = 157.1mm^2$$

$$A_s^{''} = 2\times\frac{6^2}{4}\pi\left(\frac{160+425}{200}\right) = 82.7mm^2 \text{ / T - beam}$$

Calculation of tensile force in steel

$$T = f_y A_s = 460\times 628.3 = 289018N$$

Equate compressive force in concrete and tensile force in concrete

$$C = T = 289018N$$

Calculation of compressive force

$$C = 0.67 f_{cu}\times 0.9x\times b$$

$$289018 = 0.67\times 61.9\times 0.9x\times 585$$

Depth of stress block

$$x = 13.2mm$$

Moment of resistance of beam

$$z = 217 - 0.45\times 13.2 = 211mm$$

$$M = 289018 \times 211 = 61.0 kNm$$

APPENDIX C

CALCULATION OF FLEXURAL STIFFNESS OF DECK

Second moment of area of deck

$$(2500\times 50+800\times 200)\bar{y}=2500\times 50\times 225+800\times 200\times 100$$

$$\bar{y}=154.8mm$$

$$I=\frac{2500\times 50^3}{12}+2500\times 50(225-154.8)^2+$$
$$\frac{800\times 200^3}{12}+800\times 200(100-154.8)^2$$

$$I=1656\times 10^6 mm^4$$

Deflection under four-point bending

$$\delta=\frac{PL^3}{6EI}\left(\frac{3a}{4L}-\left(\frac{a}{L}\right)^3\right)$$

$$\frac{P}{\delta}=\frac{6EI}{L^3\left(\frac{3a}{4L}-\left(\frac{a}{L}\right)^3\right)}$$

$$E=9.1f_{cu}^{1/3}=9.1\times 61.9^{1/3}=36kN/m^2$$

$$a=1400mm$$
$$L=4800mm$$

Approximate flexurally uncracked stiffness of deck

$$\frac{P}{\delta} = 16.6 kN/mm$$

APPENDIX D

YIELD LINE CALCULATION

Moment of resistance of beam

$$M_p = 61.0kNm$$

Hogging moment of resistance of slab

$$T = 460 \times \frac{6^2}{4}\pi \times \frac{1000}{200} = 65030N$$

$$C = T = 65030 = 0.67 \times 61.9 \times 0.9x \times 1000$$

$$x = 1.74mm$$

$$M_p^{S'} = 65030(50 - 15 - 3 - 1.74 \times 0.45) = 2.03kNm/m$$

Sagging moment of resistance of slab

$$x = 1.74mm$$

$$M_p^{S} = 65030(50 - 23 - 3 - 1.74 \times 0.45) = 1.51kNm/m$$

Torsion capacity of end beam, v_t=5.0N/mm^2 maximum ×1.25 partial safety factor

$$M_p^B = \tfrac{1}{2} v_t h_{\min}^2 \left(h_{\max} - \frac{h_{\min}}{3} \right)$$

$$M_p^B = \tfrac{1}{2} \times (5.00 \times 1.25) \times 200^2 \left(250 - \frac{200}{3} \right) = 23kN$$

For Figure 4.21, work done by beams and slab

$$W_1 = M_p + 2M_p^B + 2\times 0.425\beta M_p^S$$

$$\beta = \frac{1}{1.3}$$

$$M_p + 2M_p^B + 2\times \frac{0.425}{1.3} M_p^S$$

Work done by sagging and hogging in slab

$$W_2 = 4.6\gamma M_p^S + 4.6\gamma M_p^{S'}$$

$$\gamma = \frac{1}{0.425}$$

$$W_2 = \frac{4.6}{0.425} M_p^S + \frac{4.6}{0.425} M_p^{S'}$$

Total work done,

$$2\left(M_p + 2M_p^B + 2\times \frac{0.425}{1.3} M_p^S \right) + 2\left(\frac{4.6}{0.425} M_p^S + \frac{4.6}{0.425} M_p^{S'} \right) = W \times 1$$

$$M_p = 61.0kNm$$

$$M_p^B = 23.0kNm$$

$$M_p^S = 1.51kNm/m$$

$$M_p^{S'} = 2.03kNm/m$$

$$W = 2\left(61.0 + 2\times 23.0 + 2\times \frac{0.425}{1.3} \times 1.51 \right) + 2\left(\frac{4.6}{0.425} \times 1.51 + \frac{4.6}{0.425} \times 2.03 \right)$$

$$W = 292.6kN$$

APPENDIX E

TABULATED CHANGE IN NATURAL FREQUENCY

Table E-1: Normalised natural frequency for deck 3 supported on three bearings

	Load level, kN						
	0	50	100	150	200	250	316
Mode	1.00	0.94	0.88	0.89	0.90	0.87	0.80
	1.00	0.89	0.80	0.99	1.03	1.00	0.84
	1.00	0.94	0.87				
	1.00	0.97					
	1.00	0.96	0.89	0.93	0.96	0.92	0.81
	1.00	0.93	0.81	0.92	0.90	0.87	0.70
	1.00	0.99	0.96				
	1.00	0.96	0.83	0.94			
	1.00	0.98	0.95	0.83	0.88	0.84	0.81
	1.00	0.98	0.94				
	1.00	0.98					
	1.00	0.99	0.96				

Table E-2: Normalised natural frequency for deck 4 supported on three bearings

	Load level, kN				
Mode	0	50	100	150	180
	1.00	0.94	0.88	0.85	0.85
	1.00	1.05	1.03	1.00	0.97
	1.00	1.00			
	1.00	1.01			
	1.00	0.97	0.93	0.90	0.86
	1.00	0.99	0.96	0.93	0.91
	1.00	0.98	0.94	0.91	0.85
	1.00	0.97			
	1.00	0.97	0.89	0.88	0.84
	1.00	0.99	1.00	0.97	0.95
	1.00	1.01	0.97		
	1.00	0.95			
	1.00	0.98			
	1.00	0.98	0.94		

Table E-3: Normalised natural frequency for deck 5 supported on three bearings

	Load level, kN				
Mode	0	50	100	150	200
	1.00	1.01	0.92	0.94	0.90
	1.00	0.95	0.89	0.86	0.84
	1.00	0.98	0.97	0.96	0.93
	1.00	0.98	0.95	0.91	
	1.00	0.97	0.94	0.92	
	1.00	0.96	0.92	0.89	0.86
	1.00	0.98	0.95	0.91	0.87
	1.00	0.99	0.96	0.91	0.85
	1.00	0.95	0.91		
	1.00	0.98	0.94	0.91	0.88
	1.00	0.99	0.98	0.83	
	1.00	0.99	0.95	0.87	0.79
	1.00	0.98	0.96	0.91	0.87
	1.00	0.97	0.95		
	1.00	0.98			
	1.00	0.97	0.91	0.92	0.82
	1.00	0.98	0.95	0.89	0.81
	1.00	0.99	0.95	0.92	0.87
	1.00	0.97	0.94		
	1.00	0.98			

Table E-4: Normalised natural frequency for deck 6 supported on three bearings

	Load level, kN					
	0	50	100	150	185	210
Mode	1.00	1.00	0.96			
	1.00	0.96	0.88	0.85	0.85	0.83
	1.00	1.01	1.02			
	1.00	1.01	1.01	1.01	0.97	0.91
	1.00	0.97	0.90	0.87		
	1.00	0.97	0.94	0.91	0.88	0.86
	1.00	0.96	0.90	0.86	0.85	0.79
	1.00	0.97	0.94	0.90	0.87	0.83
	1.00	0.99	0.96	0.92	0.85	0.67
	1.00	0.96	0.93			
	1.00	0.90	0.88	0.87	0.88	
	1.00	0.96	0.88	0.83	0.79	0.64
	1.00	0.97	0.94	0.90	0.85	0.73
	1.00	0.98				
	1.00	0.95	0.86	0.82	0.81	
	1.00	0.96	0.89	0.84		
	1.00	0.97	0.94	0.92		
	1.00	1.00				
	1.00	0.96				
	1.00	0.97	0.91			

Table E-5: Normalised natural frequency for deck 7 supported on three bearings

	Load level, kN					
	0	40	120	160	200	235
Mode	1.00	0.89	0.81	0.79	0.78	0.78
	1.00	1.00	0.98	0.97	0.96	0.93
	1.00	0.99	0.92	0.88	0.85	0.79
	1.00	0.98	0.91	0.88	0.87	0.83
	1.00	0.98	0.91	0.87	0.86	0.79
	1.00	0.98	0.93	0.90	0.88	0.82
	1.00	0.99				
	1.00	0.98	0.91	0.88	0.86	0.83
	1.00	0.98				
	1.00	0.99	0.94	0.92	0.91	
	1.00	0.97	0.90	0.90	0.88	
	1.00	0.99	0.95	0.92	0.92	
	1.00	0.98	0.94	0.92	0.90	
	1.00	0.99				
	1.00	0.99	0.94	0.92	0.91	
	1.00	0.98				
	1.00	0.99				

Table E-6: Normalised natural frequency for deck 8 supported on three bearings

	Load level, kN							
	0	50	100	150	200	250	300	315
Mode	1.00	0.98	0.95	0.92	0.90			
	1.00	0.96	0.91	0.88	0.88	0.88	0.87	0.93
	1.00	0.99	1.01	0.99	0.99	0.99	0.94	0.90
	1.00	0.98	0.95	0.91	0.90	0.89	0.85	
	1.00	0.98	0.96	0.94	0.93	0.92	0.88	0.81
	1.00	0.98	0.95	0.91	0.91	0.88	0.84	0.80
	1.00	0.97						
	1.00	0.98	0.96	0.94	0.93	0.90	0.85	0.81
	1.00	0.99	0.98	0.96	0.94	0.92	0.87	0.84
	1.00	0.97	0.95					
	1.00	0.96						
	1.00	1.01	1.01	1.00	0.96			
	1.00	0.98	0.95	0.93				
	1.00	0.96	0.92	0.90	0.85			
	1.00	0.97	0.96	0.93	0.91	0.88	0.82	0.79
	1.00	0.99						
	1.00	0.96	0.93	0.90	0.89	0.86	0.79	
	1.00	0.98	0.96	0.95	0.94	0.87	0.80	0.72

Table E-7: Normalised natural frequency for deck 9 supported on three bearings

	Load level, kN							
	0	50	100	150	200	250	300	337
Mode	1.00	1.00	0.95	0.95	0.91	0.88	0.94	
	1.00	0.96	0.90	0.90	0.89	0.88	0.86	0.67
	1.00	1.01	1.01	1.01	0.99	0.98	0.96	0.73
	1.00	0.95	0.91	0.90	0.88	0.88	0.87	
	1.00	0.98	0.94	0.92	0.90	0.89	0.86	0.69
	1.00	0.98	0.95	0.93	0.90	0.88	0.84	0.68
	1.00	1.00	0.96	0.94	0.86	0.81	0.76	0.55
	1.00	0.96	0.92	0.91	0.89	0.87	0.85	0.64
	1.00	0.99	0.96					
	1.00	1.03	1.02	1.03				
	1.00	1.00	0.99	0.94	0.89	0.82	0.79	
	1.00	1.00						
	1.00	0.99						
	1.00	0.99						
	1.00	0.99						
	1.00	0.98	0.94	0.93	0.90	0.88	0.85	
	1.00	0.99	0.96	0.96				
	1.00	0.97	0.94	0.92	0.91			
	1.00	1.01						
	1.00	0.95						

Table E-8: Normalised natural frequency for deck 10 supported on three bearings

	Load level, kN						
	0	50	100	150	200	250	340
Mode	1.00	0.99	0.94	0.94	0.90	0.87	0.66
	1.00	0.95	0.89	0.89	0.88	0.87	0.75
	1.00	1.01					
	1.00	1.00	0.99	0.99	0.97	0.96	0.83
	1.00	0.99	0.96	0.94	0.89	0.86	
	1.00	0.98	0.94	0.93	0.92	0.90	
	1.00	0.97	0.93	0.92	0.90	0.88	0.78
	1.00	0.98	0.96	0.93	0.91	0.89	0.76
	1.00	0.99					
	1.00	0.97	0.91	0.88	0.81	0.78	0.63
	1.00	0.96	0.91	0.91	0.90	0.89	0.75
	1.00	0.99	0.97	0.97	0.99		
	1.00	1.00	1.00	0.99			
	1.00	1.00	0.98	0.95			
	1.00	0.99					
	1.00	0.98					
	1.00	0.97	0.90	0.89	0.88	0.87	
	1.00	0.99					
	1.00	0.98					
	1.00	0.98	0.95	0.94			
	1.00	0.98	0.95	0.94	0.89	0.87	0.71
	1.00	1.00					
	1.00	0.97	0.93	0.92	0.89	0.88	0.78
	1.00	1.00	0.94				

Table E-9: Normalised natural frequency for deck 2 supported on ten bearings

	Load level, kN						
	0	50	100	150	250	300	345
Mode	1.00	0.93	0.88	0.86	0.87	0.85	0.87
	1.00	1.02	0.98	0.96	0.94	0.91	0.88
	1.00	0.99	0.96	0.92	0.89	0.82	0.74
	1.00	1.01	0.94	0.91	0.91	0.90	
	1.00	1.00	0.96	0.94	0.92		
	1.00	0.99	0.96	0.94	0.92		
	1.00	0.99	0.96	0.94	0.93	0.90	
	1.00	0.98	0.94	0.91	0.89	0.84	
	1.00	0.97					
	1.00	0.99	0.95	0.92	0.90	0.78	
	1.00	0.99	0.95	0.92	0.90		

Table E-10: Normalised natural frequency for deck 6 supported on ten bearings

	Load level, kN					
Mode	0	50	100	150	185	210
	1.00	0.96	0.88	0.85	0.85	0.86
	1.00	0.96	0.83	0.79	0.83	0.80
	1.00	0.99	0.97			
	1.00	0.99				
	1.00	0.99	0.93	0.90	0.91	0.96
	1.00	0.96	0.95			
	1.00	0.95	0.84	0.81	0.82	
	1.00	0.99	0.97	0.94	0.86	0.67
	1.00	0.98	0.90	0.86	0.79	
	1.00	0.99	0.97	0.93	0.87	0.78
	1.00	0.95	0.90			
	1.00	0.97	0.93	0.88	0.85	0.80
	1.00	0.95	0.83	0.79	0.78	
	1.00	0.96	0.88			
	1.00	0.97	0.91	0.86	0.81	
	1.00	0.99				

Table E-11: Normalised natural frequency for deck 6 supported on ten bearings obtained from impact testing

	Load level, kN					
Mode	0	50	100	150	185	210
	1.00	0.94	0.87	0.84	0.84	0.90
	1.00	0.94	0.84	0.81	0.84	0.85
	1.00	0.94				
	1.00	0.94	0.86	0.83	0.85	0.86
	1.00	0.98	0.94	0.91	0.89	1.00
	1.00	0.95	0.95	0.93	0.93	0.62
	1.00	0.94	0.85	0.82	0.81	
	1.00	0.98	0.96	0.93	0.84	0.69
	1.00	0.90				
	1.00	0.95	0.88	0.84	0.78	0.63
	1.00	0.96	0.92	0.90	0.84	
	1.00	0.92				
	1.00	0.95	0.89	0.84	0.79	
	1.00	0.97				
	1.00	0.94	0.91	0.88	0.84	
	1.00	0.88				
	1.00	0.86				

Table E-12: Normalised natural frequency for deck 7 supported on ten bearings

	Load level, kN						
	0	40	80	120	160	200	235
Mode	1.00	1.03	1.00	0.96	0.96	0.96	0.98
	1.00	1.04	1.01	0.98	0.99	0.97	1.09
	1.00	1.01	1.01	1.01	0.99	0.98	
	1.00	1.04	1.01	1.00	1.00	0.99	0.95
	1.00	0.97	0.93	0.92	0.88	0.88	0.94
	1.00	0.93	0.91	0.89	0.89	0.89	0.90
	1.00	0.99	0.98	0.98	0.97	0.95	0.81
	1.00	0.95					
	1.00	0.96					
	1.00	0.98	0.95	0.94	0.92	0.89	
	1.00	1.01	0.97	0.97			
	1.00	0.98					
	1.00	0.98	0.95	0.94	0.92		
	1.00	0.95					
	1.00	0.98	0.94				
	1.00	1.02	0.99	0.97			

Table E-13: Normalised natural frequency for deck 8 supported on ten bearings

	Load level, kN							
	0	50	100	150	200	250	300	315
Mode	1.00	0.96	0.93	0.93	0.91	0.93	0.90	0.88
	1.00	0.94	0.95	0.96	0.95	0.99	0.98	0.88
	1.00	0.96						
	1.00	0.95	0.96	0.99	0.99	1.00	0.92	0.83
	1.00	0.98						
	1.00	0.96	0.90	0.91	0.91	0.93	0.93	0.89
	1.00	0.99	0.95	0.98	0.97	0.99	0.91	
	1.00	0.97	0.94	0.95	0.95	0.97	0.90	0.75
	1.00	0.99	0.97	0.97	0.96			
	1.00	0.97	0.90	0.87	0.85			
	1.00	0.99	0.95	0.94	0.92	0.90	0.84	
	1.00	0.97	0.95	0.93	0.90	0.86	0.75	0.64
	1.00	0.98						
	1.00	0.98	0.93	0.90	0.89	0.88	0.79	
	1.00	0.99	0.95	0.93	0.90			
	1.00	0.99						

Table E-14: Normalised natural frequency for deck 9 supported on ten bearings

Mode	Load level, kN							
	0	50	100	150	200	250	300	337
	1.00	0.96	0.93	0.92	0.92	0.91	0.89	0.68
	1.00	0.95	0.92	0.92	1.02	1.04	1.03	0.77
	1.00	0.98	0.96	0.96	1.03			
	1.00	1.00	0.95	0.94				
	1.00	0.95	0.91	0.89	0.91	0.91		
	1.00	0.97	0.96	0.96	1.03	1.06		
	1.00	1.05						
	1.00	1.00						
	1.00	0.96	0.91	0.88	0.90	0.91	0.92	
	1.00	0.98	0.95	0.94	0.91			
	1.00	0.96	0.93	0.89	0.90	0.90		
	1.00	0.97	0.94	0.93	0.92			
	1.00	0.99						
	1.00	1.00	0.99	0.96	0.90	0.86		
	1.00	1.00						
	1.00	0.98	0.92	0.90	0.90	0.84	0.79	0.57
	1.00	1.01						

Table E-15: Normalised natural frequency for deck 10 supported on ten bearings

Mode	Load level, kN						
	0	50	100	150	200	250	340
	1.00	0.98	0.94	0.98	0.98	0.96	0.83
	1.00	1.04	1.07	1.15	1.19	1.15	1.04
	1.00	1.01	1.02				
	1.00	1.03	1.07	1.21			
	1.00	1.01	1.02	1.11	1.11	1.14	
	1.00	0.98	1.02				
	1.00	0.97	0.97	0.99			
	1.00	1.01	0.99	0.97	0.93	0.89	
	1.00	0.99					
	1.00	0.98					
	1.00	0.99					
	1.00	1.00	0.98	0.95	0.88	0.85	
	1.00	0.98	0.97	0.94	0.91	0.88	0.75
	1.00	0.98	0.94	0.92			

APPENDIX F

TABULATED MAC VALUES

Table F-1: MAC for deck 2

Mode	MAC between load levels					
	0-50	50-100	100-150	150-250	250-300	300-345
	0.99	1.00	0.99	1.00	1.00	1.00
	0.99	1.00	1.00	1.00	1.00	0.99
	0.99	0.99	0.99	1.00	0.99	0.96
	0.89	0.98	0.96	0.99	0.93	
	0.95	0.83	0.87	0.95	0.82	
	0.87	0.92	0.93	0.94		
		0.83	0.99	0.97		
	0.80	0.98	0.98	0.99	0.74	
	0.80	0.93	0.83	0.94	0.88	0.70
		0.84				
	0.90	0.87	0.97			
		0.54	0.97	0.79	0.43	
	0.56	0.58	0.92			
			0.94	0.89		
			0.87	0.70	0.44	
				0.91		
				0.83		
				0.81		
				0.57	0.54	
					0.41	

Table F-2: MAC for deck 6 supported on ten bearings

Mode	MAC between load levels				
	0-50	50-100	100-150	150-185	185-210
	0.99	0.97	0.90	0.90	0.93
	0.99	0.98	0.94	0.93	0.95
	0.88	0.65			
	0.83				
	0.93	0.85	0.87	0.89	0.75
	0.92	0.85			
	0.88	0.94	0.98	0.91	
	0.95	0.88	0.92	0.60	0.47
	0.93	0.93	0.96	0.82	
	0.85	0.86	0.95	0.89	0.68
	0.73	0.57			
	0.84	0.83	0.96	0.84	0.52
	0.62	0.78	0.92	0.69	
	0.60	0.77			
	0.67	0.67	0.56	0.61	
	0.50				
		0.53	0.41		
		0.85	0.98		
			0.65		
				0.82	0.69

Table F-3: MAC for deck 6 supported on three bearings

Mode	MAC between load levels				
	0-50	50-100	100-150	150-185	185-210
	0.74	0.97	0.63	0.59	0.70
	0.99	0.99	0.98	0.96	0.96
	0.90	0.92	0.69	0.56	0.89
	0.88	0.95	0.49		
	0.98	0.97	0.79	0.69	0.88
	0.98	0.98	0.99	0.93	0.88
	0.99	0.98	0.99	0.98	0.87
	0.97				
	0.91	0.43	0.87	0.65	0.88
	0.93	0.97	0.98	0.74	
	0.98	0.98	0.96	0.96	0.80
	0.99	0.71	0.60	0.84	0.43
	0.78	0.67	0.88	0.79	
	0.95	0.90	0.92		
	0.83				
	0.76				
	0.63	0.81	0.80		
	0.57				
	0.65				
	0.52	0.51			
		0.63	0.87		
		0.80			
			0.58		
			0.79		
			0.81	0.86	
				0.60	
					0.63
					0.56

APPENDIX G

TABULATED FE UPDATING ERROR

Table G-1: Percentage error between FEM updates and measured natural frequencies of deck 6

		Update number				
		0	1	2	3	4
Mode	1	13.74	9.86	9.89	10.15	9.54
	2	-19.48	-21.96	-22.13	-21.98	-22.28
	6	18.17	13.66	12.83	13.10	12.47
	8	7.37	3.78	1.52	1.74	1.21
	10	7.96	4.18	3.82	4.05	3.43
	12	6.84	4.00	0.58	0.74	0.23
	13	2.62	-0.95	-2.20	-1.97	-2.53
	15		3.23	3.50	3.73	3.05
	17	3.58	-0.01	-0.78	-0.55	-1.14
	20	6.19	3.06	0.38	0.56	0.04

Table G-2: Percentage error between FEM updates and measured natural frequencies of deck 8 at 0kN

		Update number				
		0	1	2	3	4
Mode	1	3.87	3.69	3.49	3.18	3.15
	2	6.98	6.87	1.08	0.88	-0.41
	10	-1.58	-1.72	-0.34	-0.60	-0.18
	11	1.98	1.83	1.47	1.19	1.16
	12	-4.50	-4.65	-3.98	-4.25	-4.01
	15	-0.89	-1.02	0.55	0.31	0.81
	18	-1.21	-1.31			
	19	-1.88	-1.98	-0.04	-0.27	0.23

Table G-3: Percentage error between FEM updates and measured natural frequencies of deck 8 at 50kN

Mode	Update number 0	1	2	3
1	-1.45	3.44	3.04	3.05
2	-6.88	3.47	1.47	1.31
5	-8.74	-5.37	-5.79	-5.80
10	-0.98	1.38	1.15	1.15
11	-1.78	2.61	2.02	1.99
12	1.17	2.81	2.66	2.66
13	-4.95	-1.88	-2.20	-2.21
14	-7.44	-2.54	-3.19	-3.22
21	0.09	1.54	1.37	1.37
22	-0.70	1.48	1.31	1.32

Table G-4: Percentage error between FEM updates and measured natural frequencies of deck 8 at 100kN

Mode	Update number 0	1	2	3	4	5
1	-1.14	6.89	6.67	6.46	6.43	5.95
2	2.65	4.77	4.56	4.47	4.46	3.31
4	-5.03	-1.95	-2.07	-2.15	-2.16	-3.23
5	-14.08	-7.38	-7.64	-7.83	-7.86	-8.24
8	-1.52	3.34	2.55	2.29	2.26	2.31
9	-6.57	0.62	-0.92	-1.38	-1.43	-1.65
11	-5.23	5.93	2.39	1.41	1.31	1.38
12	-6.21	-1.56	-2.02	-2.21	-2.23	-2.30
13	-4.86	3.96	2.40	1.88	1.83	1.43
14	4.58	9.04	8.87	8.75	8.73	8.34
15	-9.84	1.90	-1.42	-2.39	-2.49	-2.50
16	-3.98					
17	-7.92	-3.68	-3.97	-4.11	-4.13	-4.28
18	6.19					
19	-6.37	3.92	1.01	0.15	0.06	0.02
20	-5.05	4.95	2.21	1.39	1.30	1.32
22	-3.13	2.52	1.39	1.18	1.16	1.02

Table G-5: Percentage error between FEM updates and measured natural frequencies of deck 8 at 150kN

	Mode	Update number 0	1	2
	1	5.72	7.56	7.51
	2	5.06	6.45	6.32
	4	-5.25	-2.37	-2.65
	5	-7.04	-5.03	-5.12
	8	2.41	5.49	5.17
	10	-2.52	-0.13	-0.32
	12	-0.65	1.79	1.53
	13	-3.74	-1.19	-1.43
	15	-4.40	-2.12	-2.35
	16	-0.43	1.95	1.73
	17	-5.20	-3.13	-3.31
	18	-2.85	-0.89	-1.08
	19	-1.09	0.75	0.56
	20	-2.63	-0.23	-0.41

Table G-6: Percentage error between FEM updates and measured natural frequencies of deck 8 at 200kN

	Mode	Update number 0	1	2	3	4
	1	6.14	6.63	6.55	7.20	7.01
	2	5.29	6.43	6.19	5.82	5.68
	4	-4.07	-1.62	-2.15	-1.25	-1.96
	5	-5.23	-4.38	-4.53	-4.20	-4.41
	8	3.49	6.22	5.63	5.02	4.62
	10	-1.43	0.22	-0.12	-0.52	-0.75
	12	-0.36	1.92	1.42	3.95	2.92
	13	-3.43	-1.31	-1.76	-2.32	-2.60
	15	-5.12	-3.10	-3.55	-1.07	-2.00
	16	-0.13	1.82	1.40	1.93	1.35
	17	-4.08	-2.48	-2.83	-3.23	-3.43
	19	-2.99	-1.28	-1.66	0.62	-0.21
	20	-2.16	-0.46	-0.84	1.23	0.46
	21	-1.76	2.34	1.76	-0.62	-1.00

Table G-7: Percentage error between FEM updates and measured natural frequencies of deck 8 at 250kN

		Update number				
		0	1	2	3	4
Mode	1	8.27	10.48	10.42	8.62	8.36
	2	9.10	10.92	10.55	10.10	10.10
	3	-10.05	-7.66	-6.93	-7.70	-7.75
	5	-1.94	0.37	0.24	-1.36	-1.50
	7	-6.14	1.46	-0.91	-1.61	-1.20
	8	-10.26	-7.45	-7.16	-7.93	-7.95
	10			2.30	1.83	2.06
	11	-1.53	3.97	-0.57	-1.43	-1.19
	12	-4.98	1.23	0.72	0.03	0.54
	13	-6.57	0.82	0.31	-0.66	-0.70
	14	-3.16	0.84	-1.24	-1.59	0.04
	17	-1.28	3.52	3.28	2.42	2.87
	20	2.79	4.57	4.12	3.19	3.15

Table G-8: Percentage error between FEM updates and measured natural frequencies of deck 8 at 300kN

		Update number					
		0	1	2	3	4	5
Mode	1	4.38	25.11	30.26	18.06	15.08	9.45
	2	8.13	37.23	36.19	26.05	28.58	19.53
	3	-15.92	24.64	22.10	9.58	5.52	-0.62
	4	-4.58	45.03	31.46	15.94	12.24	4.83
	7	-6.73	32.39	32.94	16.70	11.48	6.25
	8	-11.45	17.38	22.09	11.68	9.05	3.69
	10	-11.50	32.82	28.50	9.71	2.97	-1.05
	11	-11.18	18.91	22.66	10.77	7.36	2.36
	14	-10.62	17.35	21.28	8.96	4.14	-0.14
	15	-11.33	17.83	22.14	10.66	7.78	2.84
	16	-6.77	25.70	26.29	13.94	9.91	5.55
	17	-11.80	20.02	20.07	11.00	9.18	3.68
	19						3.12

Table G-9: Percentage error between FEM updates and measured natural frequencies of deck 9 at 0kN

		Update number				
		0	1	2	3	4
Mode	1	1.21	6.80	6.23	5.83	6.33
	2	0.04	1.22	0.89	1.11	1.39
	5	-14.85	-9.78	-10.25	-10.61	3.88
	7	-5.20	-0.49	-1.04	-1.37	-0.88
	11	-4.98	2.51	2.03	1.43	1.84
	13	0.53	6.28	5.77	5.38	5.83
	17	-7.20	-0.78	-1.25	-1.75	-1.34
	22	-7.58	-1.59	-2.07	-2.51	-2.10
	24	-6.05	3.92	3.65	2.76	2.99
	25	-5.69	2.79	2.37	1.72	2.08

Table G-10: Percentage error between FEM updates and measured natural frequencies of deck 9 at 50kN

		Update number		
		0	1	2
Mode	1	1.69	4.54	4.44
	2	-3.80	1.16	0.66
	5	-10.62	-8.87	-8.97
	6	-6.03	-3.30	-3.40
	10	1.48	2.81	2.75
	12	1.53	3.87	3.71
	14	2.08	3.02	2.98
	15	-3.50	-1.85	-1.94
	16	0.07	2.86	2.68
	17	-1.92	-0.68	-0.74
	19	-4.62	-2.72	-2.82
	22	2.39	3.13	3.09
	23	2.44	3.78	3.73
	24	-3.76	-1.65	-1.79
	25	-0.71	1.14	1.06

Table G-11: Percentage error between FEM updates and measured natural frequencies of deck 9 at 100kN

		Update number			
		0	1	2	3
Mode	1	1.47	4.01	3.79	4.05
	2	-2.06	-1.53	-1.53	-0.63
	6	-7.33	-5.00	-5.17	-4.92
	10	2.49	3.63	3.67	3.88
	11	-1.40	-0.20	-0.23	0.15
	12	9.63	-0.75	-0.80	-0.48
	13	-4.40	-3.19	-3.20	-2.95
	14	-0.89	0.60	0.54	0.94
	16	-1.14	-0.04	-0.03	0.15
	17		-0.44	-0.48	-0.22
	18	-5.75	-4.48	-4.53	-4.24
	20	4.55	6.69	6.57	6.88
	22		3.72	3.71	3.89
	23	-2.71	-1.10	-1.13	-0.88

Table G-12: Percentage error between FEM updates and measured natural frequencies of deck 9 at 150kN

		Update number		
		0	1	2
Mode	1	2.71	6.18	5.77
	2	-1.19	0.57	0.16
	6	-7.02	-3.43	-3.93
	7	-6.29	-3.18	-3.87
	10	-1.35	3.13	2.01
	11	-3.64	-0.34	-1.07
	12	-0.35	3.20	2.31
	13	-4.08	-0.14	-1.08
	14	-3.41	-0.08	-0.70
	16	-0.60	2.98	2.12
	17	-5.43	-2.20	-2.90
	18	-0.11	2.40	1.79
	19	0.74	3.71	3.03
	20	-3.85	0.29	-0.45

Table G-13: Percentage error between FEM updates and measured natural frequencies of deck 9 at 200kN

		Update number			
		0	1	2	3
Mode	1	6.22	8.94	8.41	8.12
	2	10.97	12.66	12.16	11.93
	4	-1.54	-0.22	-0.57	-0.74
	5	-6.99	-3.19	-4.35	-4.88
	7	-2.13	0.31	-0.20	-0.48
	9	-6.23	4.65	1.13	-0.43
	11	-4.35	-1.28	-2.16	-2.56
	14	-1.56	6.82	3.83	2.59
	15	-4.13	1.77	0.01	-0.80
	16	-0.07	3.42	2.59	2.16
	17	-3.52	6.26	2.97	1.56
	18	-4.54	-0.15	-1.39	-1.97
	19	-5.40			2.28
	20	-4.02	6.08	3.20	1.85
	21	-6.17	-5.17	-2.12	-3.05
	22	-1.78	-2.09	2.60	1.02
	24	-5.60		0.29	-0.88

Table G-14: Percentage error between FEM updates and measured natural frequencies of deck 9 at 250kN

		Update number				
		0	1	2	3	4
Mode	1	7.29	12.48	13.66	13.77	10.40
	2	14.16	15.30	15.68	15.72	14.96
	4	-8.74	-6.71	-5.59	-5.45	-6.79
	6	0.30	5.16	6.21	6.31	3.17
	8	-7.10	-5.39	-3.19	-2.89	-4.04
	9	-10.57	-8.58	-7.66	-7.55	-8.86
	12		1.56	2.33	2.41	-0.15
	14	-5.55	-4.37	-2.11	-1.81	-2.59
	17		5.68	6.98	7.11	5.09
	18	-3.23	-1.54	0.07	0.27	-0.87
	19	-7.30	-5.05	-3.43	-3.23	-4.71
	21	-2.89	-0.84	0.43	0.58	-0.76
	22	-5.61	-3.37	-1.70	-1.50	-3.00
	23	-6.51			3.13	2.20

Table G-15: Percentage error between FEM updates and measured natural frequencies of deck 9 at 300kN

		Update number					
		0	1	2	3	4	5
Mode	1	7.37	10.06	12.21	17.06	11.75	10.52
	2	12.87	18.73	19.23	21.07	18.72	17.54
	4	-8.95	-2.44	1.18	4.42	0.61	-2.44
	6	-9.76	-0.50	3.32	6.30	2.86	-1.21
	7	-11.04	-4.34	-1.50	2.58	-1.55	-3.62
	8			-4.91	-1.68		
	10	-5.76	3.27	4.06	9.62	3.79	1.81
	11	-8.70	-2.43	1.51	6.28	1.79	-0.87
	12	-4.98	4.37	6.48	9.82	6.21	4.56
	14	-7.70	5.24	5.53	11.72	2.75	-0.14
	15	-11.45	-1.82	1.89	6.25	1.64	-0.69
	16	-3.14	0.81	4.35	8.77	2.98	-3.34
	19			-0.85		-1.13	
	20	-7.45	-0.19		6.13		0.41
	22	-1.55	3.94				4.24

APPENDIX H

EXAMPLE DATA PROCESSING

The following presents a sample of the data collected and the processing performed.

The time data is transformed into the frequency domain by applying a Fourier Transform (FT):

$$F(t)=\frac{1}{2\pi}\int_{-\infty}^{\infty}\left\{\int_{-\infty}^{\infty}F(\tau)e^{-i\omega\tau}d\tau\right\}e^{i\omega\tau}d\omega$$

The relationship between the output and input in the frequency domain is known a the frequency response function (FRF), given by:

$$Y(\omega)=H(\omega)X(\omega)$$

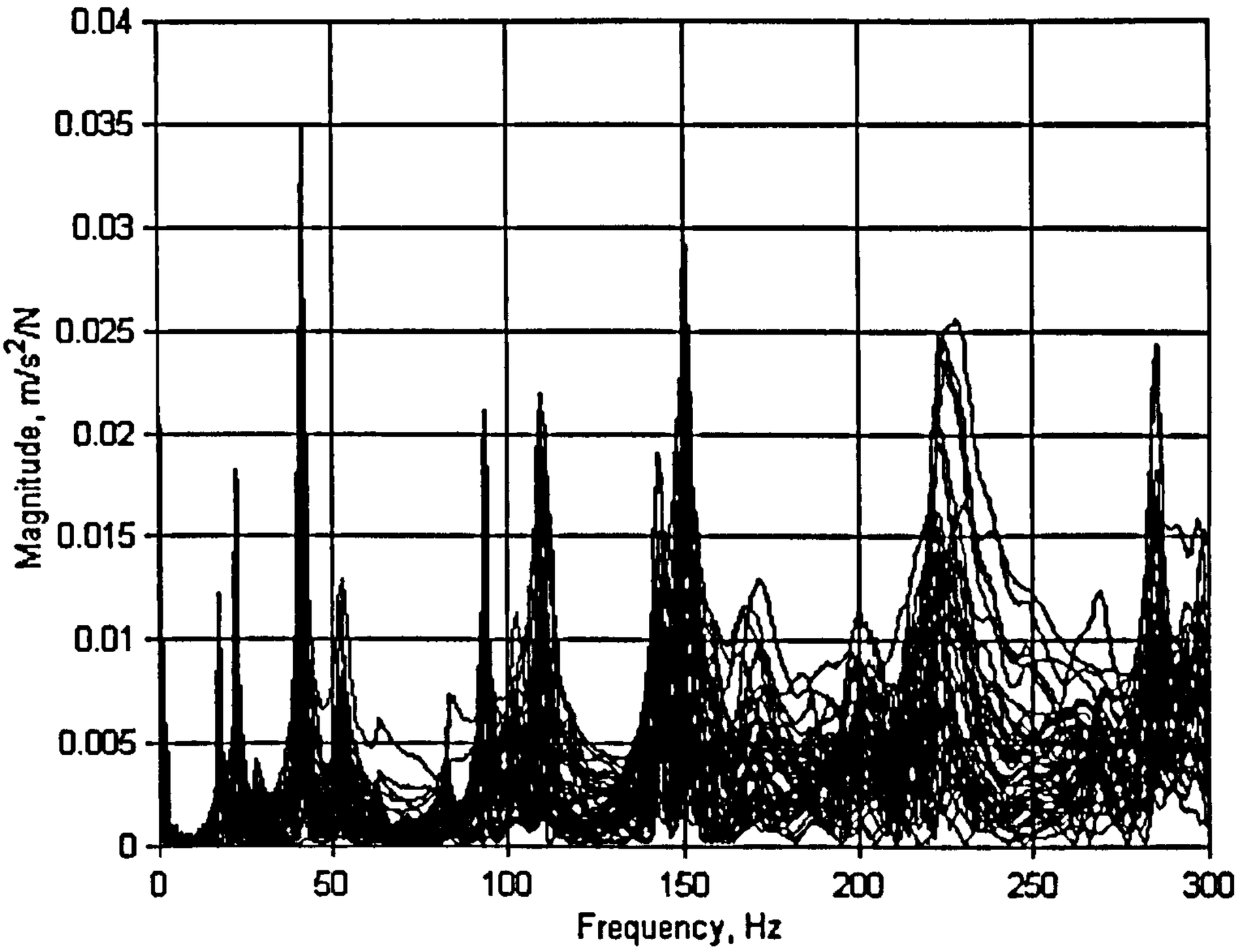

Figure H-1: FRF produced from FFT of time data

Using a combination of the Complex Mode Indicator Function and a visual inspection of the FRFs, initial values of the natural frequencies of the deck are estimated. These are then used in a rational polynomial curve fit routine;

$$H(\omega) = \frac{\sum_{k=0}^{m} a_k j\omega^k}{\sum_{k=0}^{n} b_k j\omega^k}$$

This is performed by curve fitting around the peaks in a given window, as shown in the figure below.

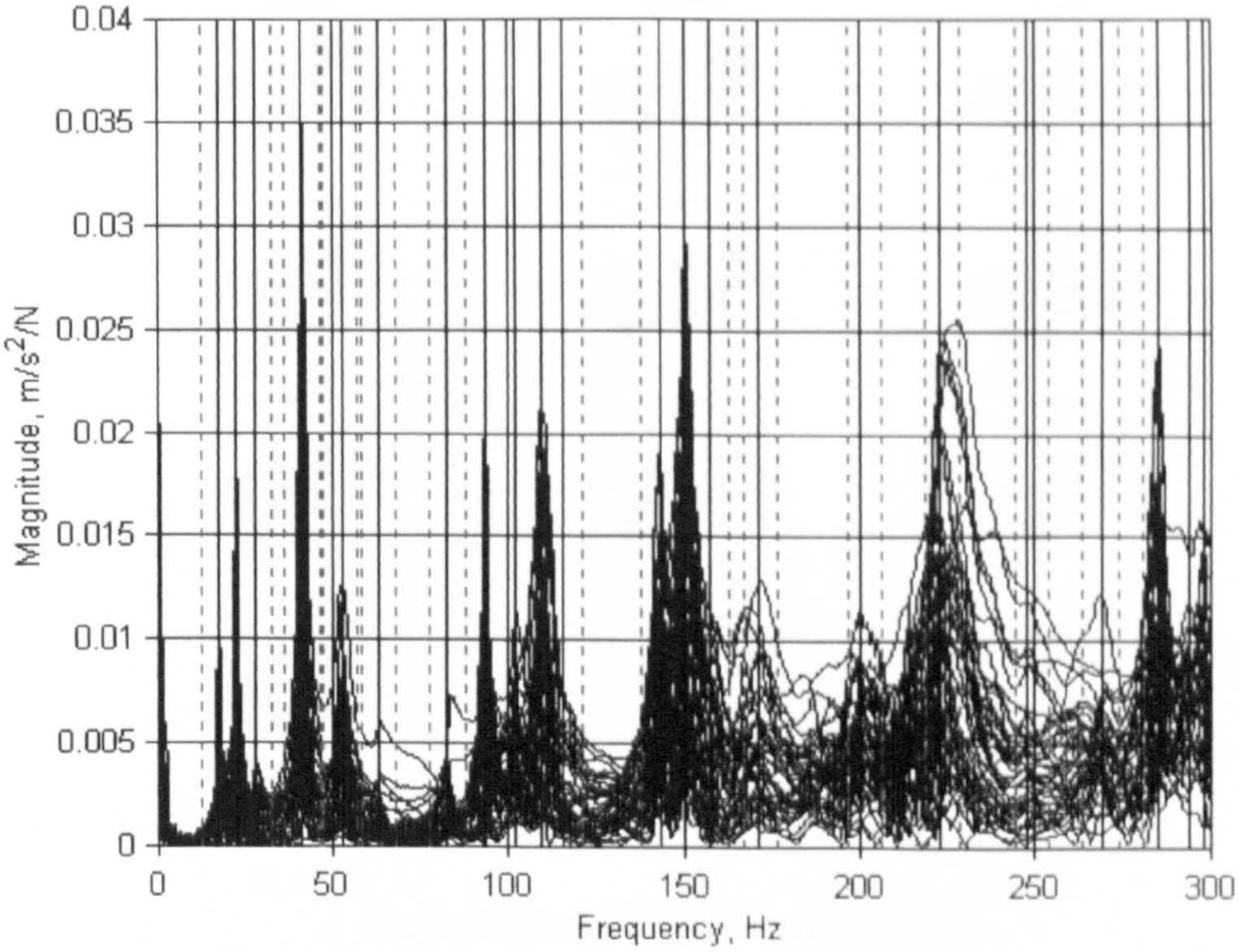

Figure H-2: Upper and lower curve fit values around peaks

This outputs a number of modes, described by their natural frequency, mode shape and modal damping.

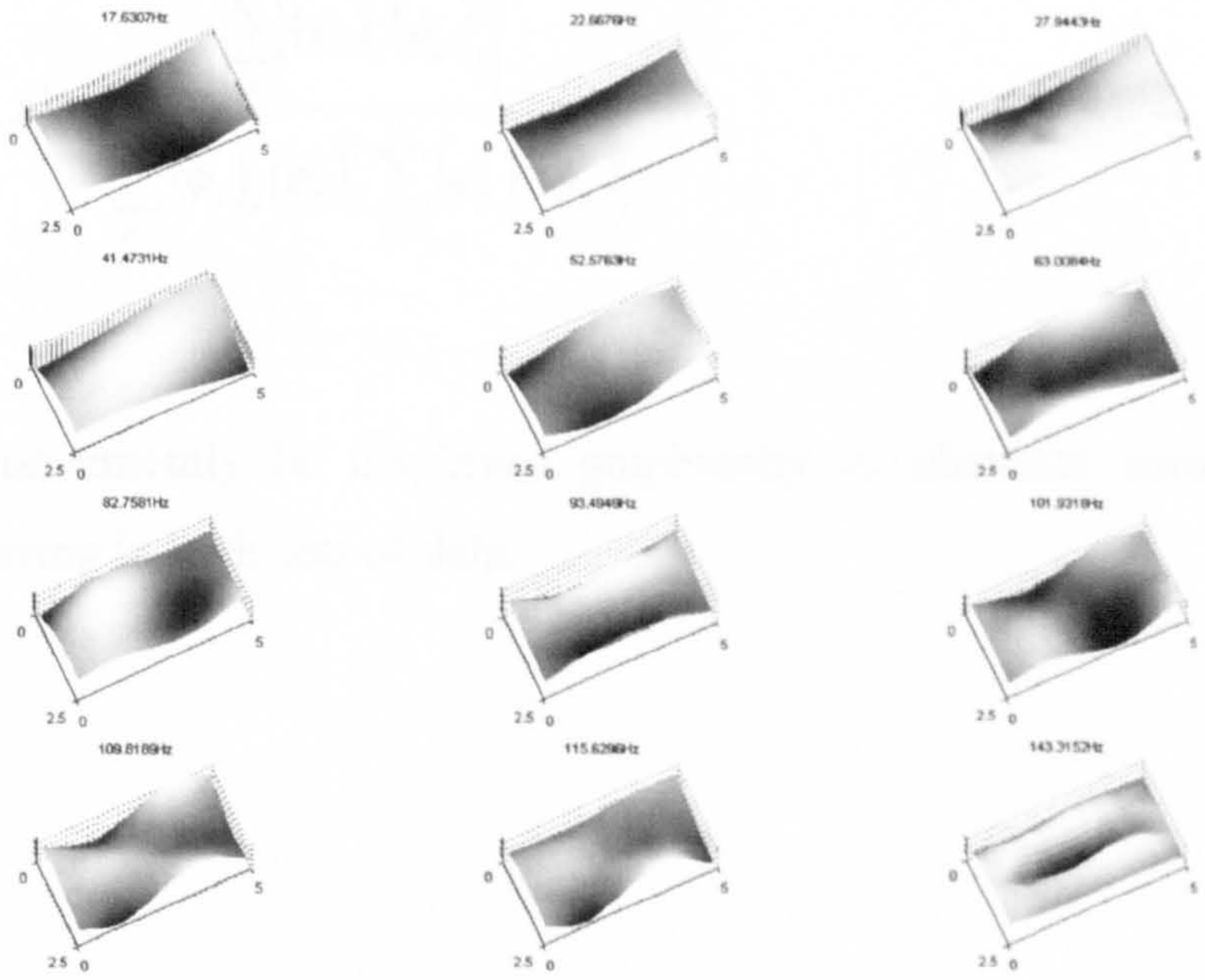

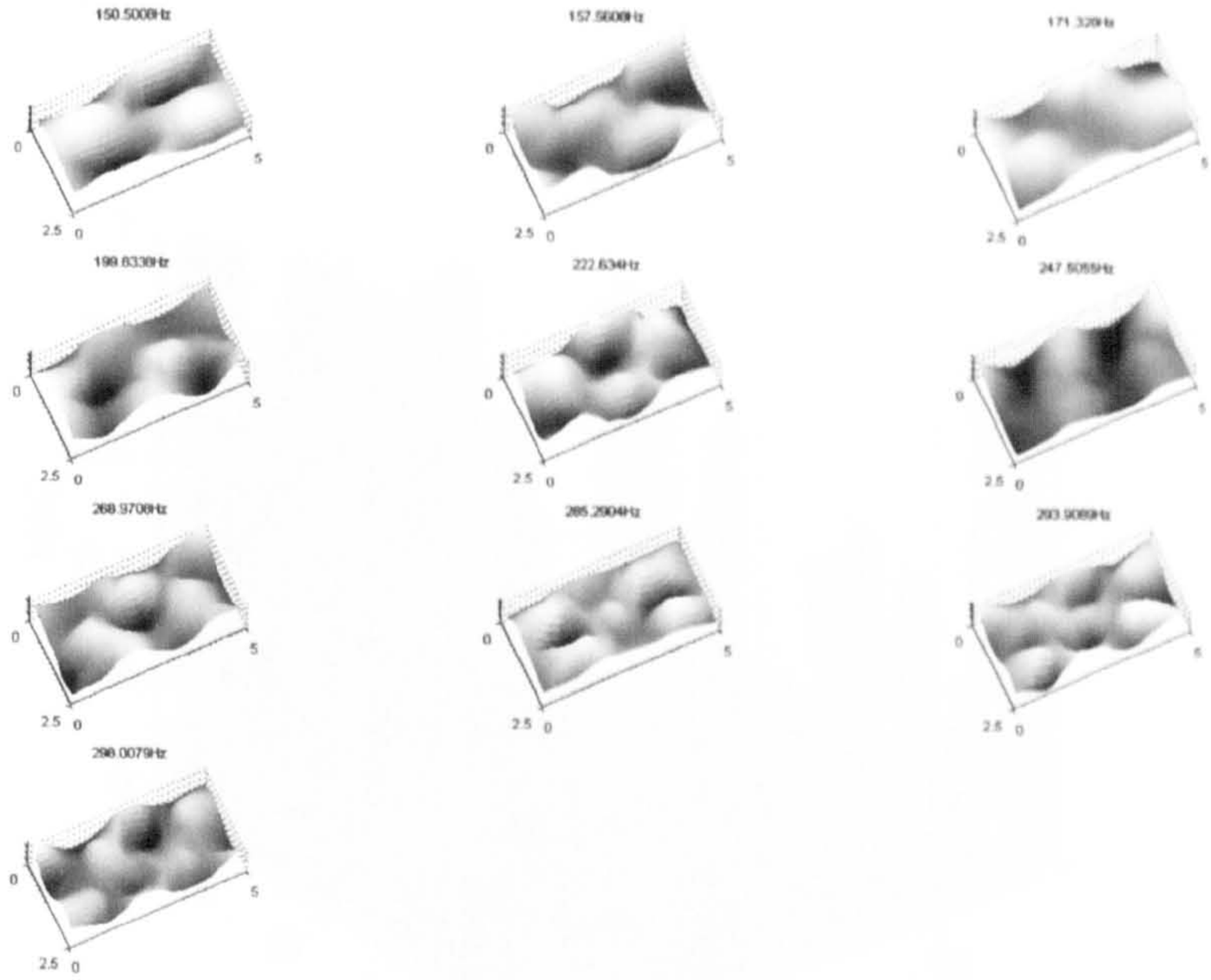

Figure H-3: Example mode shapes

A popular method for comparing sets of mode shapes is by use of the modal assurance criterion (MAC) algorithm:

$$MAC(p,x)=\frac{\left|\sum_{j=1}^{n}(\phi_x)_j(\phi_p)_j^T\right|^2}{\sum_{j=1}^{n}(\phi_x)_j(\phi_x)_j^T\sum_{j=1}^{n}(\phi_p)_j(\phi_p)_j^T}$$

This can conveniently be displayed graphically to illustrate similar shape modes occurring in both sets of data.

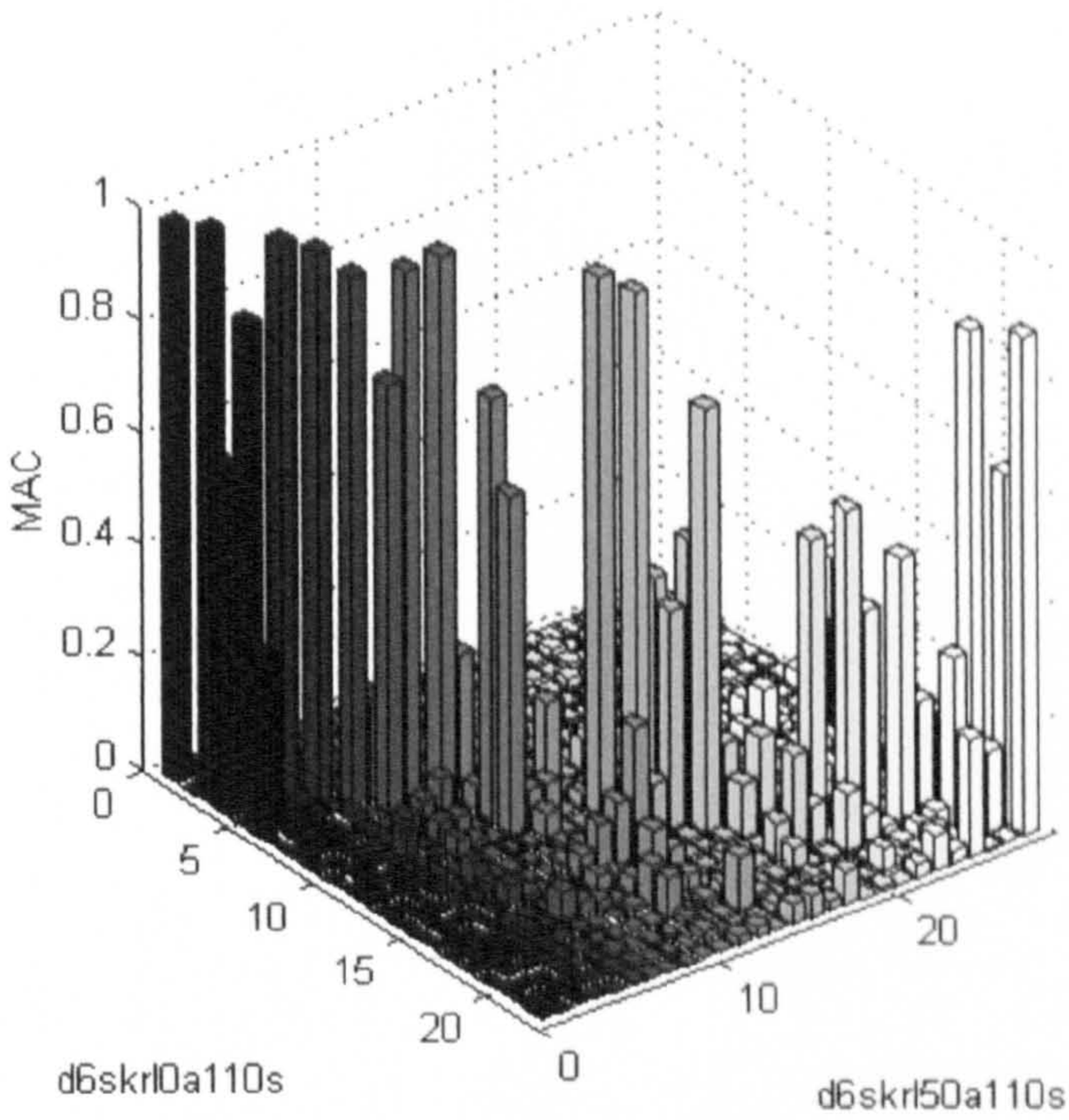

Figure H-4: MAC values between two sets of mode shape data